

NATIONAL NUCLEAR ENERGY SERIES
Manhattan Project Technical Section

Division I - Volume 5

THE CHARACTERISTICS OF ELECTRICAL
DISCHARGES IN MAGNETIC FIELDS

THE CHARACTERISTICS OF ELECTRICAL DISCHARGES IN MAGNETIC FIELDS

Edited by

A. GUTHRIE, Ph. D.

Radiation Laboratory, Department of Physics
University of California

and

L. K. WAKERLING, Ph. D.

Radiation Laboratory, Department of Physics
University of California

First Edition

New York · Toronto · London
McGRAW-HILL BOOK COMPANY, INC.

1949

THE CHARACTERISTICS OF ELECTRICAL
DISCHARGES IN MAGNETIC FIELDS

Copyright, 1949, by the
McGraw-Hill Book Company, Inc.

Printed in the United States of America

Copyright assigned, 1949, to the General Manager
of the United States Atomic Energy Commission.
All rights reserved. This book, or parts thereof,
may not be reproduced in any form without per-
mission of the Atomic Energy Commission.

Lithoprinted
by
Edwards Brothers, Incorporated
Ann Arbor, Michigan

FOREWORD

The United States program of development of atomic energy has been described by Major General L. R. Groves, who, as Commanding General of the War Department's Manhattan Project, directed the program from mid-1942 until December 31, 1946, as "a generation of scientific development compressed into three years." The tremendous scope of the Manhattan Project Technical Section of the National Nuclear Energy Series, which has been in preparation since 1944, is a tribute to the unprecedented accomplishments of science, industry, government, labor, and the Army and Navy working together as a team. These volumes can be a firm foundation for the United States atomic energy program which, in the words of the Atomic Energy Act of 1946, is "... directed toward improving the public welfare, increasing the standard of living, strengthening free competition in private enterprise, and promoting world peace."

David E. Lilienthal, Chairman
U. S. Atomic Energy Commission

ACKNOWLEDGMENT

The Manhattan Project Technical Section of the National Nuclear Energy Series embodies results of work done in the nation's wartime atomic energy program by numerous contractors, including Columbia University. The arrangements for publication of the series volumes were effected by Columbia University, under a contract with the United States Atomic Energy Commission. The Commission, for itself and for the other contractors who contributed to this series, wishes to record here its appreciation of this service of Columbia University in support of the national nuclear energy program.

PREFACE

This volume is one of a series which has been prepared as a record of the research work done under the Manhattan Project and the Atomic Energy Commission. The name Manhattan Project was assigned by the Corps of Engineers, War Department, to the far-flung scientific and engineering activities which had as their objective the utilization of atomic energy for military purposes. In the attainment of this objective, there were many developments in scientific and technical fields which are of general interest. The National Nuclear Energy Series (Manhattan Project Technical Section) is a record of these scientific and technical contributions, as well as of the developments in these fields which are being sponsored by the Atomic Energy Commission.

The declassified portion of the National Nuclear Energy Series, when completed, is expected to consist of some 60 volumes. These will be grouped into eight divisions, as follows:

- Division I — Electromagnetic Separation Project
- Division II — Gaseous Diffusion Project
- Division III — Special Separations Project
- Division IV — Plutonium Project
- Division V — Los Alamos Project
- Division VI — University of Rochester Project
- Division VII — Materials Procurement Project
- Division VIII — Manhattan Project

Soon after the close of the war the Manhattan Project was able to give its attention to the preparation of a complete record of the research work accomplished under Project contracts. Writing programs were authorized at all laboratories, with the object of obtaining complete coverage of Project results. Each major installation was requested to designate one or more representatives to make up a committee, which was first called the Manhattan Project Editorial Advisory Board, and later, after the sponsorship of the Series was assumed by the Atomic Energy Commission, the Project Editorial Advisory Board. This group made plans to coordinate the writing programs at all the installations, and acted as an advisory group in all matters affecting the Project-wide writing program. Its last meeting was held on Feb. 9, 1948, when it recommended the publisher for the Series.

The names of the Board members and of the installations which they represented are given below.

Atomic Energy Commission Public and Technical Information Service	Alberto F. Thompson
Technical Information Branch, Oak Ridge Extension	Brewer F. Boardman
Office of New York Operations	Charles Slessor, J. H. Hayner, W. M. Hearon *
Brookhaven National Laboratory	Richard W. Dodson
Carbide & Carbon Chemicals Corporation (K-25)	R. B. Korsmeyer, W. L. Harwell, D. E. Hull, Ezra Staple
Carbide & Carbon Chemicals Corporation (Y-12) †	Russell Baldock
Clinton Laboratories ‡	J. R. Coe
General Electric Company, Hanford	T. W. Hauff
General Electric Company, Knolls Atomic Power Laboratory	John P. Howe
Kellex Corporation	John F. Hogerton, Jerome Simson, M. Benedict
Los Alamos	R. R. Davis, Ralph Carlisle Smith
National Bureau of Standards	C. J. Rodden
Plutonium Project Argonne National Laboratory	R. S. Mulliken, H. D. Young
Iowa State College	F. H. Spedding
Medical Group	R. E. Zirkle
SAM Laboratories §	G. M. Murphy
Stone & Webster Engineering Corporation	B. W. Whitehurst
University of California	R. K. Wakerling, A. Guthrie
University of Rochester	D. R. Charles, M. J. Wantman

* Represented Madison Square Area of the Manhattan District.

† The Y-12 plant at Oak Ridge was operated by Tennessee Eastman Corporation until May 4, 1947, at which time operations were taken over by Carbide & Carbon Chemicals Corporation.

‡ Clinton Laboratories was the former name of the Oak Ridge National Laboratory.

§ SAM (Substitute Alloy Materials) was the code name for the laboratories operated by Columbia University in New York under the direction of Dr. H. C. Urey, where much of the experimental work on isotope separation was done. On Feb. 1, 1945, the administration of these laboratories became the responsibility of Carbide & Carbon Chemicals Corporation. Research in progress there was transferred to the K-25 plant at Oak Ridge in June, 1946, and the New York laboratories were then closed.

Many difficulties were encountered in preparing a unified account of Atomic Energy Project work. For example, the Project Editorial Advisory Board was the first committee ever organized with representatives from every major installation of the Atomic Energy Project. Compartmentation for security was so rigorous during the war that it had been considered necessary to allow a certain amount of duplication of effort rather than to permit unrestricted circulation of research information between certain installations. As a result, the writing programs of different installations inevitably overlap markedly in many scientific fields. The Editorial Advisory Board has exerted itself to reduce duplication in so far as possible and to eliminate discrepancies in factual data included in the volumes of the NNES. In particular, unified Project-wide volumes have been prepared on Uranium Chemistry and on the Analysis of Project Materials. Nevertheless, the reader will find many instances of differences in results or conclusions on similar subject matter prepared by different authors. This has not seemed wholly undesirable for several reasons. First of all, such divergencies are not unnatural and stimulate investigation. Second, promptness of publication has seemed more important than the removal of all discrepancies. Finally, many Project scientists completed their contributions some time ago and have become engrossed in other activities so that their time has not been available for a detailed review of their work in relation to similar work done at other installations.

The completion of the various individual volumes of the Series has also been beset with difficulties. Many of the key authors and editors have had important responsibilities in planning the future of atomic energy research. Under these circumstances, the completion of this technical series has been delayed longer than its editors wished. The volumes are being released in their present form in the interest of presenting the material as promptly as possible to those who can make use of it.

The Editorial Advisory Board

UNIVERSITY OF CALIFORNIA PROJECT FOREWORD

The existence of adequate experimental equipment, in particular the two operating cyclotrons of the Radiation Laboratory and the large 184-inch unit under construction, together with a nucleus of trained personnel, made it inevitable that work in connection with the war effort would be prosecuted vigorously at the University of California. Prior to the fall of 1941, studies of the properties of the transuranic elements were carried out and artificial radioactive materials were produced in the cyclotrons for use in various laboratories. This work was done informally and primarily on university funds. The importance of the studies of transuranic elements cannot be overestimated since the results formed a basis for the Plutonium Project.

Although the mass spectrographic method of separating uranium isotopes had been under consideration prior to the fall of 1941, there was no unanimity of opinion among physicists regarding the ultimate success of the method, owing to the space-charge effects. The feeling prevailed in the Radiation Laboratory of the University of California that in spite of this uncertainty the method should be pushed vigorously. The first concrete step in this direction was taken in November 1941, when a group was assigned to convert the 37-inch cyclotron to study this method of separating uranium isotopes. At about the same time two other groups started work on other electromagnetic separation schemes, namely, the ionic centrifuge and the radial magnetic separator. All this work was undertaken with the full support of the Uranium Committee but under no formal contract. The first formal contract designed to further work along these lines was entered into between the university and the Office of Scientific Research and Development in late December 1941, with the Laboratory Director as Project Leader.

The work on the mass spectrographic method, now called the "calutron process," proceeded so satisfactorily that by the early fall of 1942 plans were being formulated for a production plant. Also, owing to the very gratifying results obtained with this method, it was decided to discontinue work on the other methods. From the fall of 1942 to the end of hostilities in 1945 the Berkeley project was concerned primarily with the design and testing of prototype units for the plant, in addition to the necessary training of personnel. For a good portion of the time Radiation Laboratory personnel was stationed at Oak Ridge

to assist directly in putting the plant into operation. It was on May 1, 1943, that the Berkeley project came directly under the jurisdiction of the Manhattan District. This move, however, did not affect the organizational setup of the Radiation Laboratory in any way, and the development work proceeded without any break.

Perhaps the outstanding factor with regard to the entire electromagnetic separation project lies in the general smoothness with which the work proceeded. It was necessary to build a large development laboratory from a relatively small university research laboratory in a matter of months. This involved greatly multiplying the personnel and increasing the physical facilities and necessary experimental equipment appropriately. In spite of the rapid expansion, personnel and organizational difficulties were inconsequential. The entire laboratory organization was characterized by a minimum of formal procedure consistent with the nature of the work. It is indeed remarkable that the scientific and technical personnel of the Radiation Laboratory, many of whom had been accustomed to the academic freedom of educational institutions, could adjust themselves so readily to the necessary security, governmental regulations, and group action of the project. It must also be kept in mind that the work was predominately of a developmental rather than research nature. The form of laboratory organization was such as to allow a maximum of individual expression with regard to the various problems encountered, which undoubtedly contributed considerably to a maximum of cooperation. The fact that the first unit of the Oak Ridge plant was built and put into operation successfully within a matter of two years from the time that the first mass spectrographic unit was built attests to the close cooperation maintained among all people concerned—the Office of Scientific Research and Development, Manhattan District officials, Radiation Laboratory personnel, and the manufacturing and operating companies. It would not be fair to say that the organization used would have been adopted if the project had been built up on a long-range basis. However, in view of the haste with which the project had to be carried through, it worked extremely well.

In preparing the report on the work done at the Radiation Laboratory, the major emphasis has been placed on those subjects of most interest to people working in related fields. The engineering aspects have been minimized in view of the fact that this phase of the project will be treated elsewhere in this series. A number of papers dealing with the chemical problems of the project have been prepared and will be incorporated in other volumes of the series.

It is impossible to pay proper tribute to the many individuals—scientific, technical, and nontechnical—who participated in the Berkeley project. A cross section of scientific and technical personnel is

contained in these volumes, as authors of the various chapters and in the lists of references at the ends of the chapters. Others are referred to in the text. However, the names of many persons who contributed substantially to the progress of the project do not appear in these volumes.

The Office of the Director takes pleasure in expressing its deep appreciation to the project personnel for their unfailing loyalty and confidence; to the university as a whole for its support and cooperation; to the Area Engineer's Office for its very effective expediting of all matters pertaining to the rapid development of the Project; to the plant construction contractor, Stone and Webster Engineering Corporation; to the operating company, Tennessee Eastman Corporation; and to the major manufacturing contractors, Allis-Chalmers Company, Westinghouse Electric and Manufacturing Company, and many others for their close cooperation and effective handling of the engineering and operations problems.

E. O. Lawrence
Professor of Physics
Director, Radiation Laboratory
University of California

June, 1949

The Manhattan Project Technical Section of the National Nuclear Energy Series is intended to be a comprehensive account of the scientific and technical achievements of the United States program for the development of atomic energy. It is not intended to be a detailed documentary record of the making of any inventions that happen to be mentioned in it. Therefore, the dates used in the Series should be regarded as a general temporal frame of reference, rather than as establishing dates of conception of inventions, of their reduction to practice, or of occasions of first use. While a reasonable effort has been made to assign credit fairly in the NNES volumes, this may, in many cases, be given to a group identified by the name of its leader rather than to an individual who was an actual inventor.

VOLUME EDITORS' PREFACE

This volume has been prepared in an effort to collect the results of studies carried out at the University of California Radiation Laboratory under contract with the Manhattan District on the characteristics of electrical discharges in magnetic fields, particularly for the case of discharges in the vapors of uranium compounds. Unfortunately, when the preparation of this volume was started, many of the personnel who had contributed to the studies made at Berkeley were not available for contributions. Consequently the volume does not cover all the investigations carried out at the Radiation Laboratory, although it is believed that the most significant studies are reported.

The majority of these papers are based on reports written for use within the Manhattan Project. Only minor changes were made in these reports, primarily to satisfy the rules for declassification. Wherever possible the papers were submitted to the authors for comment. Three of the papers, included here as Chapters 1, 8, and 10, were written specifically for this volume.

Over half of this volume covers work carried out at Berkeley by members of a British scientific mission under the direction of Prof. H. S. W. Massey. Because the authors concerned were residing in England at the time this volume was started, it was not feasible to have them review the papers. Consequently Prof. Massey agreed that the original reports should be used with only minor changes. This procedure accounts for the fact that some of these papers include a great deal of detail. Some of this detail and a certain amount of repetition throughout the volume are imperfections in the form of presentation. However, this should not detract from the value of the scientific contribution.

The necessity for speed in putting the electromagnetic separation plant at Oak Ridge into operation precluded the possibility of making fundamental studies of the nature of gaseous discharges in vapors. Consequently, it was not until the plant was in operation that any concentrated effort could be applied to the study of the mechanism of gas discharges in a magnetic field. This work was undertaken with a view to eventually improving plant operation. The program was never completed, although a good deal of useful information was acquired. It is the purpose of this volume to summarize the studies made in the Radiation Laboratory.

It would be a difficult task to give due credit to all the personnel engaged in this program. However, special emphasis must be placed on the efforts of Prof. H.S.W. Massey, who had the responsibility for drawing up the program and for directing its progress. Many of the personnel involved are listed as authors of the papers and in other cases are included in the lists of references.

A. Guthrie
R. K. Wakerling

June, 1949

CONTENTS

	Page
Foreword	v
Preface	vii
University of California Project Foreword	xi
Volume Editors' Preface	xv

CHAPTER 1

Qualitative Description of the Arc Plasma in a Magnetic Field . .	1
By D. Bohm	

CHAPTER 2

The Use of Probes for Plasma Exploration in Strong Magnetic Fields	13
By D. Bohm, E. H. S. Burhop, and H. S. W. Massey	

CHAPTER 3

Minimum Ionic Kinetic Energy for a Stable Sheath	77
By D. Bohm	

CHAPTER 4

Theoretical Considerations Regarding Minimum Pressure for Stable Arc Operation	87
By D. Bohm	

CHAPTER 5

Experimental Investigation of Threshold Pressure for Stable Operation of Arcs	107
By E. H. S. Burhop, H. S. W. Massey, and G. Page	

CHAPTER 6

Measurements of the Absolute Values of the Cross Sections for Ionization of Uranium Tetrachloride and Uranium Hexafluoride by Electrons.	127
By W. E. Berkey, E. H. S. Burhop, J. D. Craggs, J. Keene, and H. S. W. Massey	

CHAPTER 7

The Ionization and Dissociation of Uranium Tetrachloride and Uranium Hexafluoride by Electron Impact	145
By E. H. S. Burhop, H. S. W. Massey, and C. Watt	

CHAPTER 8

The Rate of Ion Production by an Electron Beam	166
By T. L. Hill and L. H. Aller	

CHAPTER 9

A Study of the Arc Plasma.	173
By D. Bohm, E. H. S. Burhop, H. S. W. Massey, and R. W. Williams	

CHAPTER 10

Discharge Cathodes	334
By W. E. Parkins	

CHAPTER 11

Theory and Operation of a Philips Ionization Gauge Type Discharge	345
By J. Backus	

Index	371
-----------------	-----

Chapter 1

QUALITATIVE DESCRIPTION OF THE ARC PLASMA IN A MAGNETIC FIELD

By David Bohm

1. INTRODUCTION

In the course of the fundamental investigations of electrical discharges in strong magnetic fields, to be described in this volume, a general qualitative theory of the behavior of the arc plasma in a magnetic field was worked out. Although the details of this theory are not as yet very precise, the main features are probably substantially correct. It is hoped that a more quantitative theory will soon be published. Because the phenomena to be described in this volume involve so many different, but related, aspects of a subject that is both new and enormously complex, it is believed that the presentation of this qualitative theory as an introduction will help provide a unifying framework, with the aid of which subsequent material may be given some order.

2. EXPERIMENTAL RESULTS

It will be helpful to begin with a brief description of the conditions under which observations were made and of those results which throw the most light on the theoretical interpretation of the behavior of the system. Although a few experiments were performed in nitrogen, oxygen, chlorine, sulfur hexafluoride, and other gases, most of the fundamental studies were made with argon discharges. Argon was chosen primarily because its physical constants, such as cross sections, are known, and secondarily because it forms neither chemical compounds nor negative ions, either of which would greatly complicate the interpretation of results. The pressures used varied from 5×10^{-4} to 5×10^{-3} mm Hg, with most of the observations being taken at 2×10^{-3} mm. A description of the apparatus used for investigation

of plasma behavior is given in Chap. 9. The arc was run inside a graphite box, into which probes of various types could be inserted at positions that were externally adjustable. Electrons emitted from a filament entered the box through a small collimating slot at the top. They were collected at the bottom of the box, which thus served as an anode. The filament was usually run about 150 volts negative relative to the box, and the separation between filament and collimating slot was about $\frac{1}{8}$ in. Emission currents of the order of a few amperes were usually used. The electrons emitted from the filament and passing through the collimating slot will hereafter be referred to as "primary electrons."

The magnetic field was in the same direction as the motion of the primary electrons and will hereafter be referred to as the "Z direction." It varied from a few hundred to 10,000 gauss, although most of the observations were made at 3,000 gauss. With fields of these strengths the primary electrons were effectively collimated into a beam with a width equal to that of the collimating slot. When a small hole was cut in the box, the beam of primary electrons could be seen as a sharply delineated but very bright glow, surrounded by a more faintly glowing plasma extending perhaps 1 in. across the magnetic field. Because the mean free path for stopping the primary electrons is of the order of 50 cm at these pressures and because the box was 10 cm long, the primary electrons do not lose a large fraction of their energy before they are collected at the anode. The character of the discharge is therefore essentially that of a negative glow. Because the electrons are quite energetic and the pressure is so low, the negative glow extends the full length of the arc instead of the short distance usually required in arc discharges for the primary electrons to lose most of their energy. This system is illustrated in Figs. 1.1 and 1.2.

It should be emphasized that discharges in magnetic fields of these high strengths have not hitherto been studied in great detail. Previous investigations have shown that in magnetic fields of a few hundred gauss the discharge tends to constrict in the direction normal to the field. The main effect of the magnetic field is to cause electrons to move in rather small circles in the direction normal to the field. The Z motion is, of course, substantially unchanged. In fields of the order of a few thousand gauss the electronic radius of curvature is usually less than 10^{-2} mm, whereas even the ions have radii of the order of about 0.2 cm. Probe measurements showed that the plasma discharge surrounding the column of fast primary electrons did actually become more constricted as the magnetic field was increased. At fields of a few thousand gauss, for example, the density of arc plasma died off

more or less exponentially with distance from the central ionizing column, with a characteristic distance of decay of about 1 cm. At 10,000 gauss the decay distance was about half as great (see Chap.9). Yet the main problem is not why the discharge is constricted, but

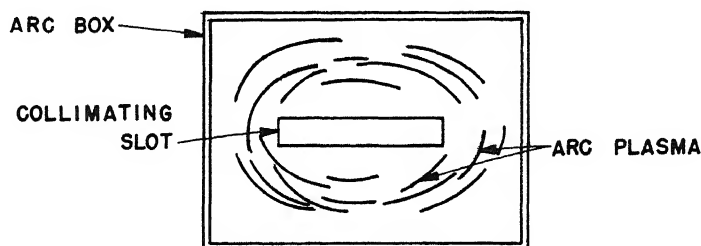


Fig. 1.1—Cross-sectional top view along magnetic field.

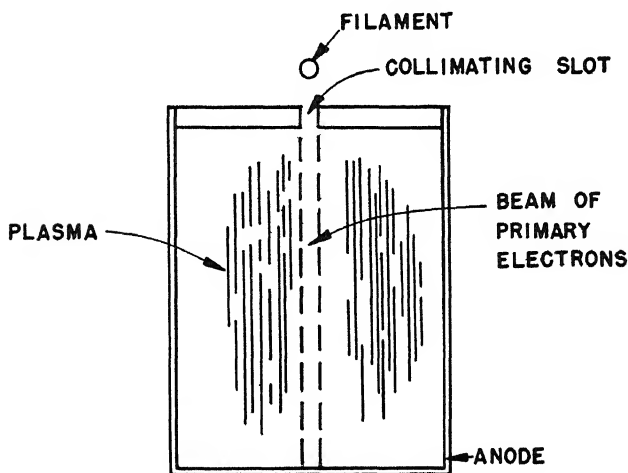


Fig. 1.2—Cross-sectional side view normal to field.

rather, in accordance with the small electron Larmor radius, why it was not constricted a great deal more. It seemed clear that a hitherto unsuspected mechanism was causing electrons to move across the field more easily than expected. That electrons were really moving across the field and were not simply trapped at great distances from

the source was proved by the large electron currents that could be collected on slightly positive probe wires placed some distance away from the beam of primary electrons. Many different experiments described in Chap. 9 also verify the existence of unexpectedly high electron mobility.

It was thought at first that collisions were responsible for this phenomenon, since they can move the center of an electron orbit in a random direction. Calculations showed, however, that the number of collisions was totally inadequate to account for the observed currents, being deficient by several orders of magnitude. The possibility that electrons attached to electronegative atoms to form negative ions was also considered. These negative ions would, of course, be heavy enough to move across the field with a fairly large Larmor radius. However, experiments in highly purified argon with a special out-gassed arc chamber (Chap. 9) gave the same results. Since argon forms no negative ions, it was concluded that negative ions could not account for the results. Other mechanisms, such as photoelectric emission, were also unable to explain the high mobility of electrons transverse to the field.

It was then suggested by Backus (see Chap. 11) that fluctuating electric fields in the plasma might cause electrons to drift fairly rapidly normal to both electric and magnetic fields, as a result of the well-known cycloidal motion of charged particles in such crossed fields. That the plasma fields were actually fluctuating was evident from the time variation of currents to probes, as observed on the oscillograph. The main questions were (1) whether these fluctuations were large enough to account for the observed electronic mobilities and (2) whether there was any special instability of a plasma in a magnetic field that could lead to such fluctuations. Subsequent work, which will be described shortly, answered both questions in the affirmative and thus showed that this is very probably the correct explanation. In the light of these facts the conclusion is reached that the average distribution of charge in a plasma in a strong magnetic field is determined primarily by the way in which the fields and particle densities fluctuate, so that this average can be understood only in terms of the dynamic behavior of the system.

3. THEORETICAL INTERPRETATION

A qualitative theoretical interpretation of the most important processes occurring in the arc is given below.

3.1 Ion Production. The main source of plasma electrons and ions is ionization of neutral atoms by the beam of fast primary electrons.

(This problem is treated in detail in Chap. 8.) For arc currents so low that the fraction of neutral atoms ionized is small, the rate of formation R of ions per unit volume within the beam of primary electrons is

$$R = J_e \sigma_r N_0 \quad (1)$$

where J_e is the current density (of primary electrons), σ_r is the ionization cross section, and N_0 is the density of neutrals.

As a function of electron energy, σ_r starts at zero for electron energy equal to the ionization potential, rises to a maximum at about

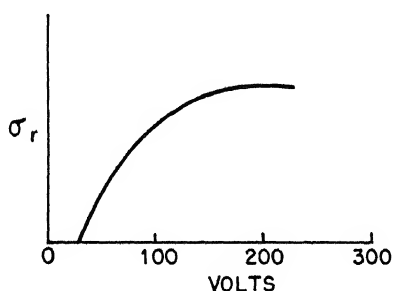


Fig. 1.3—Typical curve of the variation of ionization cross section with electron energy.

100 volts, and falls off slowly thereafter. The general shape of curves is similar for most gases, but the numerical values of the cross section vary widely. For argon the maximum is $\sigma_r = 4 \times 10^{-16}$ sq cm. A typical curve for σ_r is shown in Fig. 1.3. Arc voltages of from 100 to 200 volts provide the highest probability of primary ionization.

Secondary electrons, liberated in the process of ionization, come off with appreciable energies, which increase with cathode voltage drop. In hydrogen, for example, for primary electrons of 100 volts the mean energy of secondaries is 15 volts, whereas for primary energies of 300 volts the mean energy of secondaries has risen to 30 volts. Electron collisions cause these energies to be "shuffled" rapidly among the plasma electrons, which then dissipate the energy in the processes of excitation and ionization. Thus an appreciable fraction of all ionization may come from plasma electrons, which obtain their energy from the secondaries. In fact, probe measurements (see Chaps. 2 and 9) show a rise of ion density by a factor of 1.3 when the arc voltage is raised from 150 to 400 volts and everything else is kept

constant. Along with this rise occurs a rise in electron temperature of from 2.5 to 4 volts, indicating that plasma electrons obtain more energy from the secondaries. Present results indicate that total ionization by plasma electrons is about one-third as important (in argon) as primary ionization at an arc voltage of 200 volts.

Normally, arc currents are so great that the fraction of neutrals ionized is no longer small, thus destroying the validity of the simple Eq. 1. To estimate the fraction of neutrals ionized, a treatment by Hill will be used here.

If each individual neutral atom is followed through the column of primary electrons, the probability that it will be ionized may be expressed in terms of the cross section, arc-current density, and the time it spends in the column. Let l be the path length of a neutral in the column and V_n its velocity, so that it spends a time $T = l/V_n$ inside the column. Then the theory of probability shows that the chance of ionization P is

$$P = 1 - \exp \frac{-J_e \sigma_r l}{V_n} \quad (2)$$

From the above expression it can be seen that as J_e is increased indefinitely the probability of ionization approaches 1. Furthermore, P is a function only of the product $l J_e T$, which is equal to the primary current per unit length of collimating slot. The effect of ionization by plasma electrons, however, is to cause the effective value of J_e to increase.

To find the rate of production of ions, P is multiplied by the total number of neutral atoms entering the ionizing column per second. Because of their random directions, these neutrals have varying path lengths depending on the shape and size of the beam of primary electrons. Hill and Aller (Chap. 8) have worked out the average value by summing over all possible path lengths. The rate of ionization is then given by

$$R = \frac{N_0 V_n}{4} P(J) \quad (3)$$

where $P(J)$ is the average of P and must be tabulated graphically for each geometry, and J is the primary electron current per unit length of collimating slot; $N_0 V_n / 4$ is, of course, the mean current of neutrals through the column. For the dimensions used in these studies, $P(J)$ begins to show signs of saturation at 2 or 3 amp, at which current $P(J)$

is of the order of 0.25. Therefore it is seen that an appreciable fraction of neutral atoms entering the beam of primary electrons is ionized under normal operating conditions.

3.2 Plasma-balance Processes in Absence of Magnetic Field. A summary of the plasma-balance processes occurring in the absence of a magnetic field will be given first. This will not only provide a basis of comparison with what happens in the field but will also give a generally correct description of those plasma-balance processes which result from motion of plasma along the magnetic field.

In the absence of the field, the steady state of ion distribution can be understood with the aid of a method first developed by Tonks and Langmuir.¹ The process of ionization is more or less the same as that described in Sec. 3.1. Electrons are liberated with several volts of kinetic energy, ions with practically none. Because of their small mass and high energy, electrons rapidly leave the region in which they are liberated and collect on the walls, charging them negatively relative to the plasma. The charge has two effects: (1) it repels electrons, and (2) it attracts positive ions, which fall freely to the walls as a result of electric fields in which they happen to find themselves upon liberation. As for the electrons, they make so many collisions that a Maxwellian distribution of velocities is rapidly established among them. The temperature is usually 2 or 3 volts but varies with conditions. A steady state is finally reached in which ions are attracted to the walls at a rate equal to the number produced. As for the electrons, just enough are repelled so that the remaining few with sufficient energy to scale the sheath at the walls will be equal to the total number produced. In such a steady state the walls run about 10 volts negative relative to the space inside.

The main body of the arc is filled with an approximately equal number of positive ions and electrons, called a "plasma." Because of the enormous potentials resulting from even the slightest failure of space-charge neutralization, a plasma is characterized by enforced neutrality. The maximum potential drop that can be sustained in a plasma is about one-half the electron temperature, because greater drops would cause space charge to redistribute itself until they were neutralized.

Near a highly negative electrode, however, there must be a region containing only positive ions, since the plasma electrons do not have sufficient kinetic energy to reach the electrode. Such a region, called a "sheath," is usually quite small, because prevailing ion densities are great enough to sustain enormous potential drops in short distances. Normally the sheath is of the order of 0.1 mm in thickness,

although with high sheath voltage, or low ion density, it may become considerably larger.

Remembering that positive ions acquire kinetic energies from plasma electric fields of the order of one-half the electron temperature T_e , it is seen that they usually arrive at the sheath edge with kinetic energies of about 1 volt. In Chap. 3 it is shown that no sheath can be stable unless the ions arriving there have an energy of about one-half the electron temperature. Thus, if n_+ is the ion density at the sheath edge, the ion-current density is given by

$$J_+ = n_+ \sqrt{\frac{kT_e}{m_+}} \quad (4)$$

It is important to note that the ion current at the sheath edge is determined by electron temperature. The reason is, of course, that the plasma electric fields producing ionic velocities are limited by electron temperature.

3.3 Effect of Magnetic Field. The main effect of the magnetic field is to hinder motion of electrons (and of ions to a lesser extent) across the field while leaving their motion along the field unhindered. Thus, to describe Z motion, substantially the same picture as in the absence of a field may be used. Because Z motion is so free, variations of density in this direction may to a first approximation be neglected, so that we shall work in terms of the density, n , as a function of x and y only. The mean velocity of Z motion of electrons is of the order of 10^8 cm/sec, so that the electron strikes the sheaths at the top and bottom of the arc about once every 10^{-7} sec (the length is 10 cm). As it moves up and down, the collisions with other electrons will occasionally transfer to it enough energy to make it go over the sheath and be collected. There is therefore a process of continual collection of electrons at the top and bottom of the arc. Ions are attracted to the top and bottom electrodes, as in the absence of a field, so that they too are being collected to a great extent at the top and bottom of the arc.

With regard to motion normal to the field the main problem is, as has already been stated, to understand how electrons can move thousands of Larmor radii across the magnetic field. An explanation that has been suggested is that the electrons are drifting in cycloidal motion at right angles both to electric fields in the plasma and to the magnetic field.

Of course, the normal type of electron drift is caused by externally produced electric fields rather than by plasma fields themselves. The velocity of such drift is

$$V_d = \frac{cE}{H} \quad (5a)$$

where E is the electric field in e.s.u., H is the magnetic field in gauss, and c is the velocity of light. In other units,

$$V_d = \frac{10^5 E}{H} \quad (5b)$$

Static fields of several volts per centimeter have been observed in the plasma, and they are, in fact, expected on the basis of the plasma-balance theory, since they are needed to pull the ions out of the plasma. Assuming 3 volts per centimeter, with $H = 3,000$ gauss,

$$V_d = 10^5 \text{ cm/sec} \quad (6)$$

Along the magnetic field a 2.5-volt electron has a velocity of

$$V = 10^8 \text{ cm/sec} \quad (7)$$

Thus the mean drift velocity in the static fields is about 1/1,000 that of free motion along the field. This drift velocity is comparable to that of ions of a few volts kinetic energy.

The first step is to see to what extent such static fields might account for the observed rate of motion of electrons across the magnetic field. In general, there are two qualitatively different possible arrangements of the static fields in the plasma. In one of these the equipotentials surround the column of primary electrons, and in the other they cut through it. Examples of the two types of distribution are given in Figs. 1.4 and 1.5, which are cross sections viewed along the magnetic field.

As has already been pointed out, the direction of electron drift is normal to the electric field, or along an equipotential. If the equipotentials surround the primary column, as in Fig. 1.4, the electron drift results merely in an unbroken circulation of electrons without bringing them any closer to the wall sheath. If the equipotentials go through the primary column, however, as in Fig. 1.5, the drift process can bring a secondary or plasma electron out near the wall sheath.

Of course, the electron can eventually drift back into the primary column, but collisions meanwhile may cause it to cross the relatively short distance to the wall sheath and be collected before it can return. Besides, it repeatedly strikes the sheath at the top and bottom of the

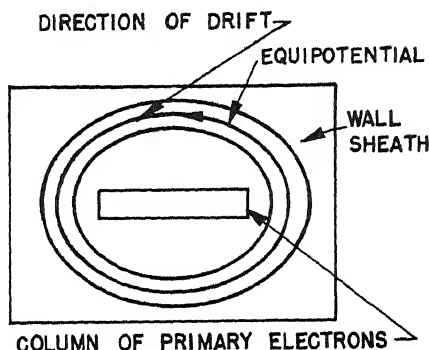


Fig. 1.4—One qualitatively distinct possible arrangement of the static fields in the plasma.

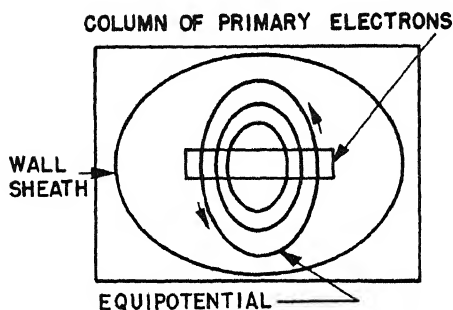


Fig. 1.5—The other qualitatively distinct possible arrangement of the static fields in plasma.

arc (as a result of Z motion), and there is a good chance that it may happen to strike the sheath with enough energy to be collected. Static fields may therefore be important in getting electrons away from the primary column, where most of them are liberated, and in causing them to be collected at some distance from this column.

It is significant that the equipotentials in Fig. 1.5 will result in an asymmetrical plasma distribution, since electrons will tend to leave the primary column in the directions shown by the arrows. This asymmetry has been observed, and the direction of maximum density is in agreement with that predicted by the distribution of potentials shown in Fig. 1.5 if it is assumed that the central equipotentials are the most positive, as would be necessary if ions were to be thrown out toward the walls (see Chap. 9).

In an unpublished study of the dynamic behavior of plasma in a magnetic field it was found that any system of plasma flow that is directed, i.e., that has a definite direction at each point, is unstable. If, for example, a small plasma oscillation should get started by chance, it has been shown that it will grow in amplitude with time, being limited only when the amplitude gets so large that the initial assumption of small oscillations breaks down. This phenomenon is similar to that of turbulent flow of fluids, which arises when certain conditions involving the Reynolds numbers are exceeded. A plasma in a magnetic field is always in a state of turbulent flow. Backus (Chap. 11) has obtained direct experimental evidence for such turbulence in a Philips-ionization-gauge-type discharge. This turbulence will result in a rapidly fluctuating electric field at any point,* which will cause an electron drift, the magnitude and direction of which undergo correspondingly rapid fluctuations. The net effect will be to produce a random drift of electrons that is equivalent to a form of diffusion. The ions will also drift in these fields but to a lesser extent because of their larger radii of curvature.

In actual practice, potential distributions of both types given in Figs. 1.4 and 1.5 may exist. The type given in Fig. 1.4, however, is associated with more turbulence, because the electrons can cross the magnetic field only as a result of such turbulence for this case. These potential distributions are, of course, now to be regarded only as averages, which can be measured on a probe. The exact form of the average potential and the associated degree of turbulence are determined by boundary conditions in a very complex way that has not yet been given a successful mathematical treatment. It is possible, however, to make a rough estimate of the effective diffusion coefficient

* In our discharges, random fluctuations in probe currents, as measured on an oscillograph, were always observed. The local potential seemed to fluctuate by a few volts at times varying from $1\ \mu\text{sec}$ to $1\ \text{msec}$. Shorter times were not observable on the oscillograph. The further the probe was from the center of the discharge, the greater was the fractional fluctuation of probe current.

resulting from the maximum turbulence expected on the basis of the theory. This diffusion coefficient D_e is

$$D_e = \frac{10^4 T_e}{H} \quad (8)$$

where T_e is the electron temperature in volts, and H is the magnetic field strength in thousands of gauss. This is in reasonable agreement with estimates based on probe measurements (see Chaps. 2 and 9). The value of D_e is intrinsically uncertain within an order of magnitude because of the dependence of fluctuation amplitudes on boundary conditions.

4. SUMMARY

On the basis of the above ideas, a general picture of the internal state of the arc may be given. Electrons and ions are produced mainly in the column of fast electrons and must diffuse either to the top and bottom or to the walls, where they are collected and recombine. Diffusion across the magnetic field may be brought about in static fashion by drift of electrons along equipotentials passing through the central column and dynamically by the self-excited fluctuating fields associated with turbulent flow, which produce a random diffusion. Along the magnetic field, electrons and ions move freely, and the ions gain a kinetic energy of half the electron temperature before they are collected at the sheath edge. Electrons, however, are repelled by the sheath to such an extent that only those with unusually high kinetic energies are collected. The rate at which ion density falls off with distance from the central column is determined by competition between outward diffusion and upward motion, although if negative ions are present, recombination must also be considered. The more rapid the diffusion across the field, the farther ions will travel before they strike the top and bottom, or recombine. Meanwhile the continual loss of ionization to the top and bottom electrodes causes the density to drop with distance from the central column. In Chap. 9 this drop is shown to be roughly exponential, with a decay distance of the order of 1 cm.

REFERENCE

1. L. Tonks and I. Langmuir, Phys. Rev., 33: 195 (1929).

Chapter 2

THE USE OF PROBES FOR PLASMA EXPLORATION IN STRONG MAGNETIC FIELDS

By David Bohm, E. H. S. Burhop, and H. S. W. Massey

1. INTRODUCTION AND SUMMARY

The Langmuir-type probe, consisting of a small collecting electrode inserted into a plasma to which various potentials may be applied and corresponding collected currents measured, is invaluable for the investigation of plasma conditions. However, for a study of a plasma such as that prevailing in an arc chamber in the presence of a uniform strong magnetic field, the usual Langmuir theory employed for interpretation of the probe current-voltage characteristics cannot be accepted, and it is the purpose of this chapter to show what modified procedure must be adopted to obtain the maximum useful information. This can be summarized briefly as follows.

In a plasma in the absence of a magnetic field, provided the probe is small compared with the mean free path of the electrons and ions, the characteristic has the general shape illustrated in Fig. 2.1. When large negative potentials are applied to the probe all electrons are repelled and only positive ions collected. This collected current reaches a saturation value J_+ at a sufficiently large negative potential V . With increasing V the higher-energy electrons begin to be collected, thus reducing the net positive-ion current to the probe. Eventually a value V_f of V is reached at which there is zero net current to the probe. V_f is known as the "floating potential," because it is that potential assumed by the probe when allowed to float. Further increase of probe potential leads to a rapid rise in negative currents collected until a value V_s , the space potential at the location of the probe, is reached, beyond which the increase is much slower. Beyond V_s there is negligibly small collection of positive ions, owing to their small energy spread and the repulsive potential of the probe toward

them. To determine V_s with reasonable accuracy from the characteristics it is customary to assume that the electrons have a Maxwellian distribution of energy with a temperature T_e . A logarithmic plot of $J - J_+$ against V shows then a nearly linear portion up to V_s but exhibits a break there. The location of this break determines V_s . The probe current at $V = V_s$ is denoted by J_e .

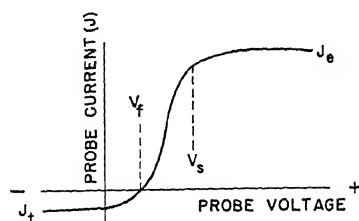


Fig. 2.1 —Probe characteristic in absence of magnetic field.

The electron temperature T_e , in volts, and the electron density n_e are then given by

$$T_e = \left[\frac{d}{dV} \ln (J - J_+) \right]^{-1} \quad (1)$$

$$n_e = \frac{J_e}{A} \sqrt{\frac{2\pi m_e}{kT_e}} \quad (2)$$

where A is the area of the probe, m_e the electron mass, and k is Boltzmann's constant. Assuming that the plasma is electrically neutral in the macroscopic sense, $n_e = n_0$, the positive-ion density in the plasma. The relation of n_0 to J_+ has not been discussed in detail by previous workers. For reasons described below, a detailed analysis of this relation is now presented (see Sec. 3). Because of penetration into the plasma of the electric field surrounding the probe, it may be shown (Sec. 3) that it is the same as if the ions have a mean random energy nearly equal to one-half that of the electrons, i.e.,

$$J_+ = 0.40 n_0 \sqrt{\frac{2kT_e}{m_+}} A \quad (3)$$

where A is the collecting area of the probe. This means that the ratio J_e/J_+ should be close to $\sqrt{m_+/m_e}$, where m_+ is the mass of a positive ion and m_e that of an electron.

Before considering the effect of a strong magnetic field, note the effect of the presence of a considerable concentration of negative ions in the plasma. This concentration would be manifested by a reduction of the ratio J_e/J_+ well below the value $\sqrt{m_+/m_e}$. Thus, if the negative ions of mass m_- are present to a concentration n_- ,

$$n_0 = n_e + n_-$$

so that J_e/J_+ is reduced approximately in the ratio $(1 - n_-/n_0)$ to 1 by the finite value of n_- . Owing to the large ratio of m_- to m_e , the negative saturation current is usually greater than the positive, even for a plasma in quite strongly electronegative vapors. Typical characteristics of this type are described by Spencer-Smith¹ for a glow discharge in iodine. Under these circumstances T_e , n_e , V_s may still be determined with sufficient accuracy, but n_0 cannot be found from them. To determine it, use must be made of J_+ and the theory developed in Sec. 3. This theory shows how n_0 may be found approximately from a knowledge of J_+ and T_e (see Eq. 3), provided the negative-ion current is small compared with that of the electrons. Even if it is not, n_0 may still be found to be at least one order of magnitude from J_+ . The uncertainty in this case arises from the need to substitute for T_e in Eq. 3 some quantity involving the mean energies of the positive and negative ions. This would have the effect of changing T_e to some quantity between T_e and T_g , the gas temperature. For most cases T_e/T_g is between 10 and 100, and therefore the uncertainty in n_+ is at most one order of magnitude, even when n_e is negligible. When n_0 has been found, n_- follows from the relation

$$n_0 = n_- + n_e$$

When a probe is used in a magnetic field of such strength that the Larmor radius of the electrons is smaller than the probe dimensions, and under conditions where no negative ions are present, it is found that J_e/J_+ is much less than the ratio $\sqrt{m_+/m_e}$ prevailing in the absence of the field. The reason for this is discussed in Sec. 4, where it is shown that the effect arises from the reduction of electron mobility in directions perpendicular to the magnetic field. This then reduces J_e below the value given by Eq. 2 to an extent depending on the transverse diffusion coefficient of the electrons. As this quantity cannot be predicted theoretically, for reasons elaborated in Sec. 5, J_e can no longer be used to determine n_e . Instead it becomes necessary to use J_+ to determine n_0 , Eq. 3 still holding until such magnetic fields are reached that the Larmor radius for the positive ions be-

comes smaller than the probe dimensions. For this reason the detailed analysis of positive-ion collection by probes has been worked out in Sec. 4. After n_0 has been determined, n_e is obtained from the condition of space-charge neutralization throughout the plasma. The values for T_e and V_s are obtained as before from the slope of the characteristic, but, as it has not proved possible to develop a detailed theory for this part of the characteristic in a strong magnetic field, it is not quite certain that the latter determinations are as reliable as in the absence of magnetic field. The theory developed in Sec. 5 for the electron collection shows that information concerning the diffusion coefficients of the electrons can be obtained from J_e .

Table 2.1

Magnetic field	None	None	Large	Large
Negative ions	None	Present, but $\frac{n_-}{n_e} < \sqrt{\frac{m_-}{m_e}}$	None	Present, but $\frac{n_-}{n_e} < \sqrt{\frac{m_-}{m_e}}$
$\frac{d}{dV} (\log J - J_+)$	T_e, V_s	T_e, V_s	T_e, V_s	T_e, V_s
J_+	n_0 ($n_0 = n_e$)	n_0 ($n_0 = n_e + n_-$)	n_0 ($n_0 = n_e$)	n_0 $n_0 = n_e + n_-$
J_e	Checks n_0	n_e	J_e gives information on electron diffusion coefficients	To separate n_- and n_e use J_e and assume electron diffusion coefficients the same as for a plasma where $n_- = 0$

When negative ions are present in a magnetic field, n_0 is determined approximately as before, but now n_e and n_- cannot be found separately unless the electron diffusion coefficients are known. These cannot be calculated, but, if the assumption is made that they do not differ very much from, say, plasma in argon and in chlorine, then knowing J_e/J_+ from the argon observations and assuming the same for chlorine, n_e and n_- may be estimated for the latter case, n_- being zero for argon.

Table 2.1 shows, by way of summary, how information may be derived from probe characteristics for different circumstances. The application of these methods of analysis of characteristics for probes in a strong magnetic field is described in Chap. 9.

2. EXPERIMENTAL STUDY OF PROBE CHARACTERISTICS IN STRONG MAGNETIC FIELDS

In this section the experimental study of probe characteristics in strong magnetic fields is described. The results will be discussed here only in connection with the light they shed on the correct interpretation of the characteristics. A description of the information found concerning ion and electron densities, electron temperatures, and space potentials in the types of arcs used will be given in Chap. 9.

2.1 Description of Apparatus. Some studies of probe characteristics in arcs in longitudinal magnetic fields have been carried out by Rokhlin² and by Spivak and Reichrudel,³ but no reference to any systematic work has been found. Measurements were therefore begun in the 2- by 2- by 7 1/2-in. arc chamber described in Chap. 9. The collimating slot was centrally placed in one end of the arc chamber. The gases used were argon and nitrogen. This arc was used with a magnet referred to as the "Annex magnet," which could provide fields as high as 4,600 gauss. A large number of measurements were also made in the two arc chambers (3/4 by 5/8 in. and 3 by 2 1/2 in.) in the 37-in. cyclotron magnet, again for argon. In these two chambers, fields up to 12,000 gauss could be obtained (for more details see Chap. 9).

The following types of probe were employed:

1. Probes used in 2- by 2- by 7 1/2-in. arc chamber in Annex magnet.

(a) Wire filament with insulator support. This is illustrated, with dimensions given, in Fig. 2.2a. The wire was of tungsten, and the insulator material was steatite. This probe could be rotated about its axis in such a way that the orientation of the filament relative to the magnetic field could be changed. The orientation in which the plane of the filament is parallel to the field is referred to as the "parallel position." This orientation favors the collection of electrons in a direction perpendicular to the field. In the perpendicular position, collection can take place in a direction parallel to the field.

(b) Wire filament with shielded support. This differed from (a) only in having a metal shield over the insulator as shown in Fig. 2.2b. In one set of observations the shield was kept at the wire potential, in others at the space potential as estimated from hot-probe measurements.

(c) Metal disk with insulated support. This is illustrated, with dimensions, in Fig. 2.2c. For this as for the other probes, the disk

could be rotated so that its plane could be set at any desired orientation to the magnetic field.

In all these cases the probe could be removed in the direction AB relative to the center of the electron column, as shown in Fig. 2.3; the range that could be covered was from 2 mm at the edge of the column to 25 mm at the inside edge of the arc block.

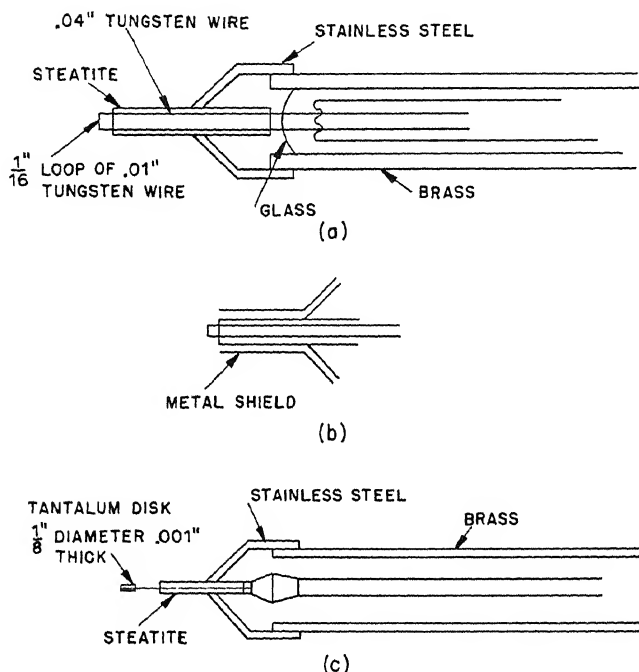


Fig. 2.2—Types of probes used in Annex magnet.

2. Probe used with arcs in 37-in. magnet (disk probe). This was the final standard form of probe used for ion-density measurements. It consisted of a disk of molybdenum, $\frac{1}{8}$ in. in diameter, spot-welded to a tungsten wire 0.030 in. in diameter. The construction is illustrated in Fig. 2.4. The glass-shield construction illustrated in the drawing was adopted to prevent tungsten evaporated from the filament from depositing on the glass near the tungsten seal and thus increasing the effective area of collection of the probe. In all measurements carried out with these probes the plane of the disk was parallel to the magnetic field. Unlike the arrangements in the Annex arc the probes in the arcs used with the 37-in. magnet could be moved either toward or parallel to the column in a plane parallel to the anode block as

shown in Fig. 2.5. Three probes were often used simultaneously to enable measurement to be made at three different distances from the anode.

2.2 Description of Results. (a) Arc in the Annex Magnet. Typical probe characteristics found are illustrated in Figs. 2.6 to 2.12. Figure 2.6 shows two characteristics obtained in argon at a pressure of

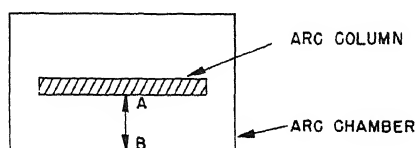


Fig. 2.3—Motion of probes with respect to arc column (Annex magnet).

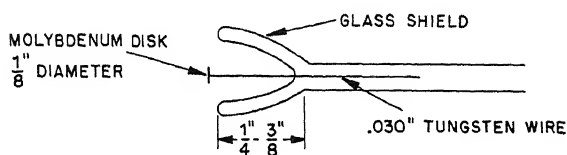


Fig. 2.4—Type of probe used in 37-in. magnet.

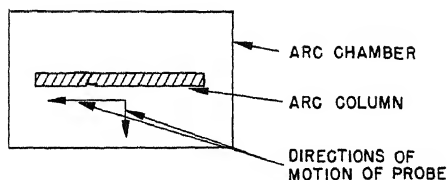


Fig. 2.5—Motion of probes with respect to arc column (37-in. magnet).

2.2×10^{-3} mm Hg with a magnetic field of 1,500 gauss, using the wire-filament probe with unshielded insulator support. One is with the front of the probe 4 mm from the center of the column, the other at 8 mm distance. In both cases the outstanding feature is the low ratio of the electron saturation current J_e (indicated on the figure) to that of the J_+ (also indicated on the figure). Reference to the preceding remarks shows that this ratio should be, for a normal argon plasma, about 280 to 1 instead of the observed 8 to 1. In both cases

in Fig. 2.6 the plane of the probe was perpendicular to the field, but measurements taken in the parallel orientation gave essentially similar results, except that there was a less clearly marked electron saturation, and the electron current was reduced by a factor between

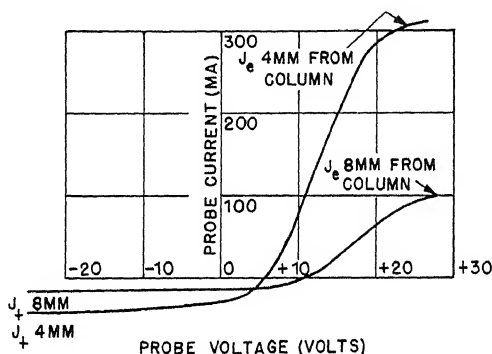


Fig. 2.6—Probe characteristics in argon showing variation with distance from column. Pressure, 2.2×10^{-3} mm Hg; magnetic-field strength, 1,500 gauss.

1.5 and 2. No change was observed in J_+ . Figures 2.7 and 2.8 provide a comparison of parallel and perpendicular orientation by filament (with unshielded insulator) and disk probes, again for fields of 1,500 gauss in nitrogen at 3×10^{-3} mm Hg at distances stated on the figure.

In all these cases the ratio J_e/J_+ is seen to be much below the value expected from the ordinary probe theory (280 for A^+ , 240 for N_2^+ , 170 for N^+). This was found to be so in a wide variety of other circumstances. Thus at a particular distance from the column, in a gas at fixed pressure, the characteristic always presented a low value of J_e/J_+ as the magnetic field was increased past 1,000 gauss, although the variation was often not monotonic, exhibiting maxima and minima at different fields but always well below the expected value. A study was also made in this range of magnetic field of the variation of J_e/J_+ with distance from the center of the column. In general, with high magnetic fields, the ratio remained roughly constant as the distance increased until the edge of the arc block was nearly reached, at which point there was a tendency for the ratio to increase considerably and then drop off to a value as low as 2 or less, indicating possibly that the probe was then within the positive-ion sheath. Figure 2.9 illustrates a typical case of this effect for nitrogen.

Owing to the lack of lateral definition of the incident electron in the absence of a magnetic field, with resultant presence of fast electrons

throughout the plasma, it was not possible to check the fact that normal ratios of J_e/J_+ are obtained in such circumstances. However, characteristics were taken with a low magnetic field of 120 gauss to check whether the ratio had begun to increase toward the zero field

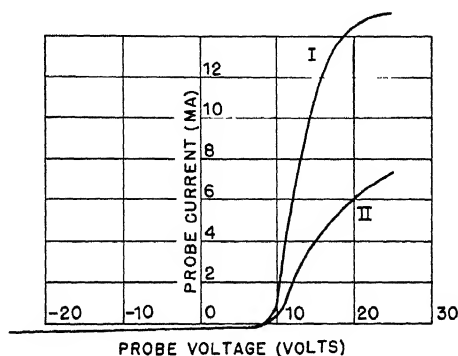


Fig. 2.7—Probe characteristics in nitrogen showing variation with orientation of the probe. Curve I, probe perpendicular to magnetic field; curve II, probe parallel to magnetic field.

value. This was found to be the case with both gases, particularly so for nitrogen, as may be seen by reference to Fig. 2.9, in which are compared characteristics under the same circumstances at magnetic fields of 120 gauss and 155 gauss, respectively. Thus the ratio J_e/J_+ has already attained a value of between 30 and 60 for the lower field in the cases illustrated as against values of 10 or less for the larger field.

(b) With Arcs in the 37-in. Magnet. The probe characteristics with these arcs were all obtained using the disk probe described above. The performance of this type of probe was very satisfactory and made possible the determination of accurate characteristics. This work was previously directed to obtaining systematic data concerning ion densities, electron temperatures, and space potentials in the arcs, but the results can also be used to check a theory of probe collection in a magnetic field, as they cover such a wide range of conditions of arc current, arc voltage, probe position, magnetic field, and gas pressure. In general they agree with those obtained with the arc in the Annex magnet if it is remembered that in all cases they refer to probe collection perpendicular to the magnetic field. As these data are used extensively in the comparison of theory and experiment given in Sec. 6, only a few illustrative results are given here.

Figure 2.10 compares two characteristics obtained in the smaller rc with argon and chlorine, respectively. The pressure, electrical conditions, and position of the probe relative to the electron column were nearly the same for both. It will be seen that, whereas the ratio

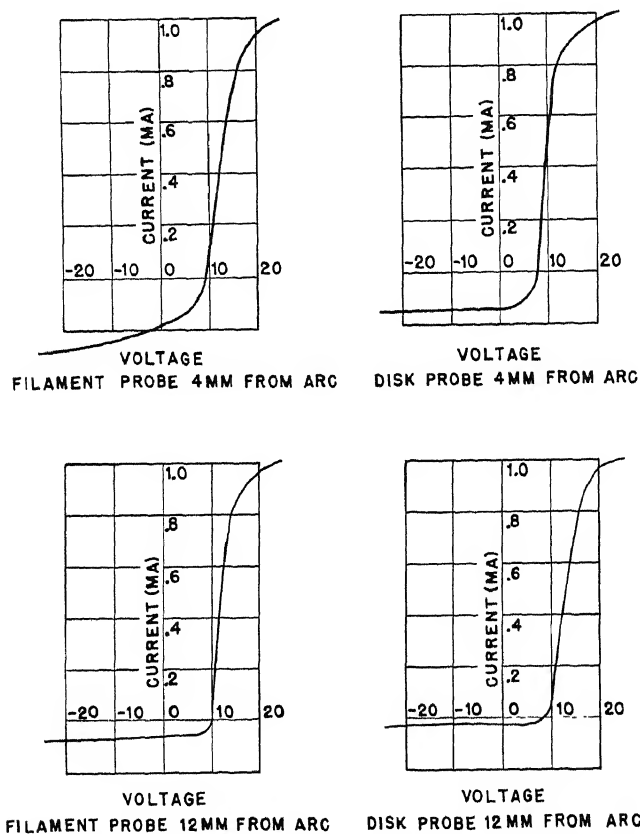


Fig. 2.8 —Probe characteristics for filament and disk probes.

of negative to positive saturation current is about 16 to 1 for the characteristic obtained in argon, it is nearly 1 to 1 for chlorine. This is due to the fact that the negative charge density in the latter is nearly all in the form of negative ions at the position in the plasma where the probe is located, and it is clear from the comparison of the two characteristics that the reduction of electron saturation current by the magnetic field is still not so large as to obscure the observation of a high density of negative ions when such are present.

2.3 Alternative Explanations of Low Negative Current Collection.

It has been stated in Sec. 1 that the low ratio of electron to positive-ion saturation current in an inert gas such as argon is due to decrease of electron mobility transverse to the magnetic field, and in Sec. 5

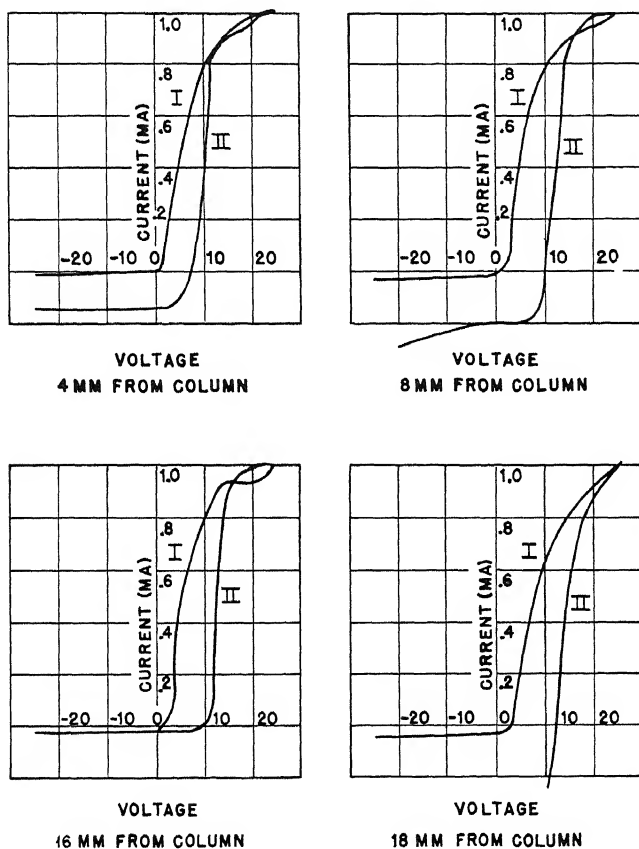


Fig. 2.9—Probe characteristics showing the variation of J_e/J_+ with distance from the arc. Curve I, magnetic field 155 gauss; curve II, magnetic field 120 gauss.

the theory of this effect is presented. It is important, however, to see if any alternative explanation exists, and indeed two possibilities are suggested.

The first concerns the effect of metastable atoms. The impact of these on the probe will release secondary electrons, giving rise to an apparent positive-ion collection. If they are present in such quantity that they release a secondary electron current that is comparable

with m_-/m_e times the true positive-ion saturation current, the effect on the characteristics would be much as observed. However, it is extremely unlikely that such large secondary emission due to metastable atoms could occur. They move with velocities comparable with the

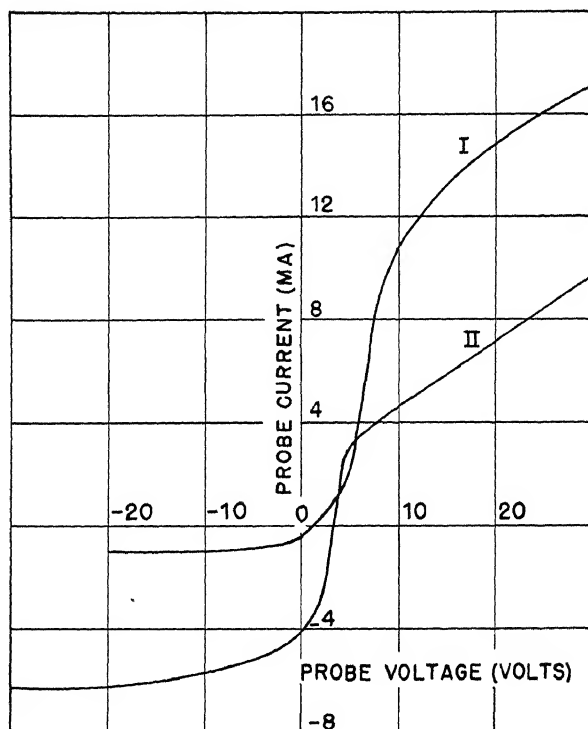


Fig. 2.10—Probe characteristics in small arc. Curve I, argon; curve II, chlorine. Pressure, 1×10^{-3} mm Hg; magnetic-field strength, 3,700 gauss.

positive ions and eject at most one electron per impact. To give the observed effect in, say, argon they would therefore have to be present in a concentration 280 times that of the positive ions. As their rate of formation is not likely to be much greater than that of the ions and as they will reach the walls at about the same speed, a concentration proportionately so much greater can be excluded.

The second concerns negative ions. It is also possible to interpret a characteristic of the type found in argon in a strong magnetic field as due to the presence of negative ions. In the experiments described above it is not possible to ensure freedom of the argon from electro-negative impurities, and, while the arc is running, they may be pres-

ent to a very considerable proportion. It is also possible that their effect may be increased by the presence of the magnetic field, for an electron reaching a point outside the ionizing column must make a great number of collisions in so doing, owing to its slow diffusion

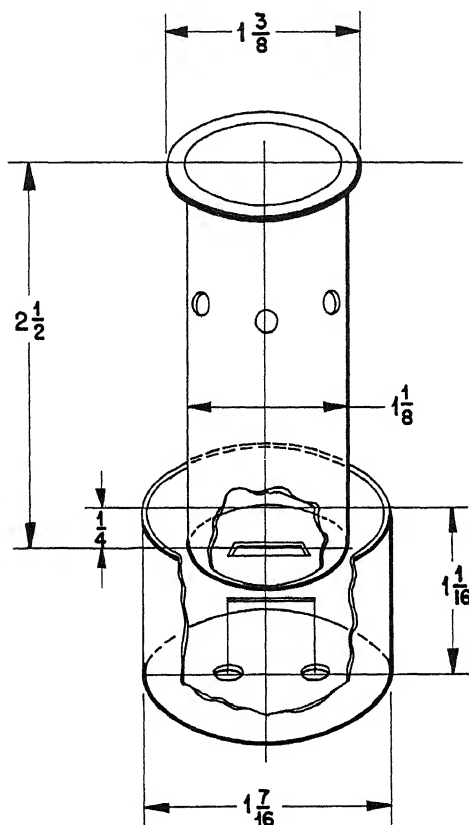


Fig. 2.11—Small glass-enclosed arc chamber designed to reduce effect of electro-negative impurities.

rate. Hence, it would have an increased chance of attaching to an electronegative atom or molecule of impurity. To investigate this possibility some experiments were carried out in a small model arc under conditions where the effect of electronegative impurities was reduced to negligible proportions.

This arc was constructed so that it could be run in pure argon under conditions in which extraneous substances had been so effectively eliminated that the chance of negative-ion formation was neg-

ligible. To this end the arc chamber was enclosed in a glass envelope, the whole of which could be baked so thoroughly that the entire apparatus could be run hot at a pressure greater than 10^{-6} mm Hg.

The construction of the arc chamber that was employed is shown in Fig. 2.11. This chamber was cylindrical in section, and $1\frac{1}{8}$ in. in

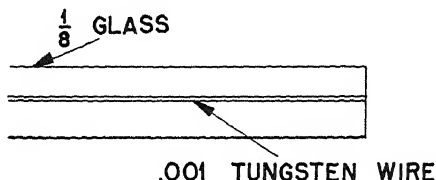


Fig. 2.12—Probe used in glass-enclosed arc chamber.

diameter and constructed of stainless steel, $\frac{1}{32}$ in. in thickness. The ends consisted of tungsten disks, and the dimensions of the collimating slot were $\frac{1}{2}$ by $\frac{1}{32}$ in. The filament itself was of tantalum, 0.040 in. in diameter. Attached to one side of the filament lead was a stainless-steel heat shield, as shown in Fig. 2.11. This shield overlapped, without touching, the arc chamber and protected the glass walls of the outer envelope from becoming coated with metal evaporated from the cathode. The arc chamber itself was supported by three stainless-steel strips spot-welded to a stout tungsten lead held in the same glass pinch as that used to bring in the leads to the filament. In the cylindrical walls of the arc chamber three holes $\frac{1}{4}$ in. in diameter were drilled. One of these enabled the arc column to be viewed. The other two enabled, respectively, a hot-filament-type probe and a cold-disk-type probe to be inserted. The glass envelope surrounding the arc chamber was wound on the outside with a coil of nichrome wire, which enabled the whole apparatus in the neighborhood of the arc chamber to be thoroughly outgassed by heating to a temperature just below the softening point of the glass.

The argon was obtained from a commercial cylinder of stated 99.7 per cent purity and, before entering the apparatus, was passed through a phosphorus pentoxide drying tube and a tube that contained copper heated to a red heat, in order to remove all trace of oxygen. The pressure was measured by means of a McLeod gauge, capable of measuring pressures of the order of a few times 10^{-7} mm Hg. The pump used to evacuate the apparatus was a two-stage glass mercury diffusion pump backed by a Megavac. A tap in the pumping line ensured that the apparatus never came in contact with mercury vapor

from the pump in the absence of liquid air in the cold trap. The magnetic field was supplied by a pair of water-cooled Helmholtz coils, which produced a uniform field of up to 700 gauss in the region of the arc.

Probe measurements were carried out using a shielded probe of the form and dimension shown in Fig. 2.12 so collection could take place parallel to the magnetic field. The characteristics obtained

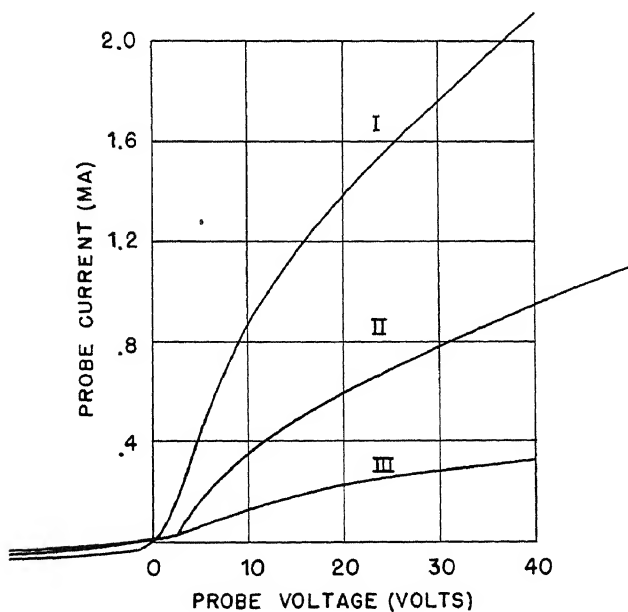


Fig. 2.13—Probe characteristics in argon in small glass-enclosed arc showing the variation with magnetic-field strength. Curve I, 1,550 gauss; curve II, 1,750 gauss; curve III, 2,200 gauss. Pressure, 5×10^{-3} mm Hg; arc current, 0.4 amp; arc voltage, 150 volts.

again exhibited a small ratio of negative to positive current, and in Figs. 2.13 and 2.14 a number of observed results are illustrated. However, it must be mentioned that the model-arc results differed in certain other respects from those obtained in the Annex and 37-in. experiments. The floating potential in almost all cases was found to be negative (see Fig. 2.14), in some cases by as much as 20 volts or more. Further, measurements of space potential carried out by a small hot probe gave negative space potentials. It is difficult to explain this except by supposing that strong oscillations exist in the arc, which oscillations, because of the nonlinear form of the probe char-

acteristic, throw the mean floating and space potentials to negative values. Hash* observations up to frequencies of 1 megacycle did not indicate the presence of particularly strong oscillations in that range of frequency, and therefore it is likely that much higher frequencies (of the order of the electron plasma frequency, 10^9 to 10^{10} cycles) were responsible.

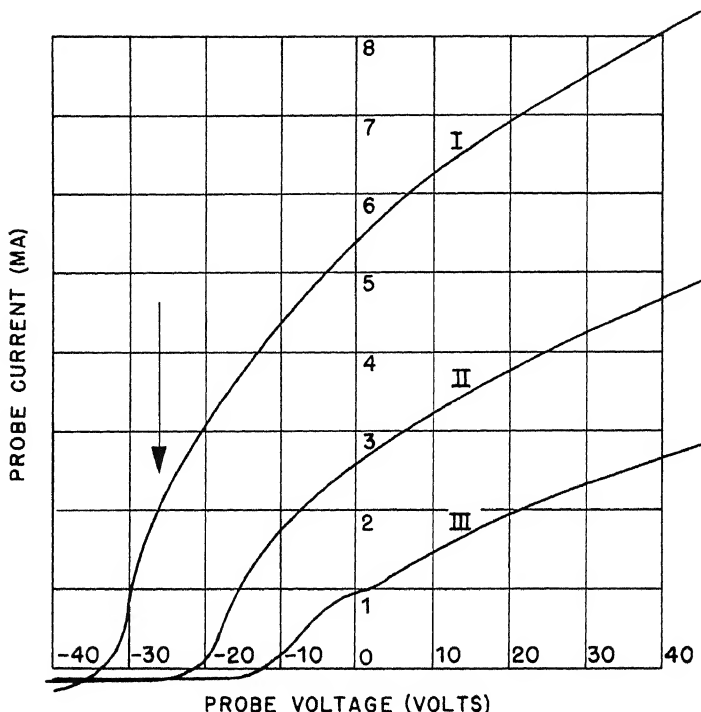


Fig. 2.14—Probe characteristics in argon in small glass-enclosed arc showing the variation with arc current. Curve I, 1.5 amp; curve II, 1.0 amp; curve III, 0.5 amp. Pressure, 4×10^{-3} mm Hg; magnetic field, 1,500 gauss; arc voltage, 150 volts; vertical line, space potential obtained by hot probe.

Another feature of the model-arc-probe characteristics was the poor saturation exhibited by the electron current. This was probably partly due to the form of the probe but may also have arisen from the presence of abnormal numbers of faster electrons, due to the intense high-frequency oscillations. It was verified by a calculation that at the position of the probe a negligible proportion of primary electrons

*See Chap. 9 for a definition and discussion of hash.

could have diffused to the probe by successive collisions. As the oscillations of velocity and frequency characteristic of the arc plasma will depend on geometrical conditions, it is quite possible that in the model arc these were particularly suited to the excitation of the high-frequency plasma oscillations.

Although it is unfortunate that these effects were so strong in the model arc, the fact that the ratio of electron to positive-ion collection remained small despite the presence of considerable numbers of fast electrons provides strong evidence that the small ratios observed in the other arcs were not due to the presence of negative ions.

In view of this result it seems clear that the effect of the magnetic field on the electron diffusion is the important factor, and the theory of this effect is developed in Sec. 5 and compared with the observed results in Sec. 6. It follows from the theory that, if the probe dimensions are small compared with the Larmor radius of the electrons, the characteristics should be normal. An unsuccessful attempt to verify this was made using a probe consisting of a wire 0.001 in. in diameter sealed through a glass tube, the exposed face of glass and wire being ground flat in order that no dimension of exposed metal would be greater than 0.001 in. (see Fig. 2.12). As the Larmor radius of a 1-volt electron is 0.0026 in. for a field of 500 gauss, it was hoped that more nearly normal characteristics would be obtained with this probe. However, when it was tried in the model arc, it was found that deposition of conducting material on the glass occurred to such an extent that the effective collecting area soon became much greater than that of the wire section, and the typically low ratios of negative to positive saturation current were again obtained. The deposition occurred so quickly that, even if the probe was not introduced into the arc chamber until just before taking a measurement, the characteristics usual for probes of larger dimensions were obtained.

3. INTRODUCTION TO THE THEORY OF PROBES IN A MAGNETIC FIELD

Since the ion and electron current collected by a probe is determined in part by conditions in the neighboring plasma, the probe has enjoyed wide application as a tool to investigate the properties of such plasmas. Unfortunately, the factors controlling probe characteristics are usually very complex. A partial list of the processes and conditions governing the actual current reaching the probe follows:

- Ion densities and velocities near the probe.

- Electric field set up by the probe.

- Collisions between electrons, ions, and gas molecules.

- Ultraviolet rays and metastable atoms striking the probe.

Plasma oscillations.

Effect of removal of ions by probe from surrounding plasma.

In the absence of a magnetic field, probe characteristics are so well understood that they can safely be used to furnish information about the plasma. Before the data can be interpreted unambiguously, however, it is necessary that the following conditions be satisfied:

1. Probe small compared with mean free path.
2. Sheath small compared with probe.
3. Ionization in sheath and secondary emission from probe both negligible.
4. Plasma oscillations absent.

Under the above conditions, probe currents are simply the sum of random thermally diffusing ion and electron currents that strike the probe with enough energy to be collected. Because these currents are controlled by simple kinetic theoretically determined factors, their interpretation in terms of electron and ion densities and temperatures is easily obtained. Thus the probe may be used to investigate plasma conditions, in a way described in Sec. 1.

In the presence of a magnetic field, the above simple picture is no longer true. The principal effect of a strong magnetic field is to confine the electrons within a Larmor radius, $r_L = eHv/mc$, where e is the charge on the electron, H is the magnetic-field strength, v is the velocity of the electron, m is its mass, and c is the velocity of light. This usually turns out to be about 0.001 cm in the cases here considered. The circle of motion can be changed only by collision with other particles or by plasma electric fields. As a result, the effective free path is reduced to a Larmor radius, and condition 1 is no longer satisfied, since most probes are at least 1 mm in diameter. When the probe is large compared with a mean free path, it collects so many electrons that the surrounding space is depleted more rapidly than can be made up by diffusion from the distant regions in which the electrons are created. Electron collection by a positive electrode is thus considerably reduced in the presence of a magnetic field. The precise manner in which it is reduced is very complex, because motion along the magnetic field is unaffected, whereas motion normal to the magnetic field is greatly impeded. The final result is a compromise, in which electrons are collected by the probe from regions quite distant along the magnetic field but not far away in a direction normal to the field. The formula for electron collection by a probe is worked out in Sec. 5 under the assumption that collisions and plasma electric fields are the cause of electron motion normal to the magnetic field. The result shows that the electron collection depends in a rather complicated way on electron temperature, ion energies, probe radius,

magnetic field, ion density, and hash conditions. Because it depends on so many factors beyond our control, the electron current is not of very much use as a tool in investigating plasma conditions. In this chapter it will be satisfactory merely to try to understand the factors that determine it.

Because the process of electron collection is so complex, a great deal more weight must be placed on the relatively simply determined positive-ion currents. In most cases ($H = 3,000$ gauss) the Larmor radius for positive ions is considerably larger than the probe radius, and consequently we may neglect the magnetic field in computing ion collection. Even if the magnetic field may be neglected, however, the collection of ions by a probe is by no means a simple process. For example, it is necessary to charge the probe highly negatively in order to repel electrons. To what extent does the resulting electric field around the probe influence positive-ion collection? In Sec. 1 it is shown that when the electron temperature is greater than the ion temperature the electric fields penetrating beyond the sheath surrounding the probe are determined entirely by the electron temperature. These electric fields are normally so powerful that they drag in many positive ions that would otherwise miss the probe. Thus it turns out that positive-ion current striking the probe is determined primarily, not by the mean ionic energy in the plasma, but by the mean electron temperature instead.

4. COLLECTION OF POSITIVE IONS BY PROBES

When a probe is inserted into a plasma, it collects positive ions at a rate determined, first, by the random thermal currents existing in the plasma and, second, by electric fields that direct this current toward or away from the probe. Because the thermal currents and the electric fields affect each other through the space-charge distribution, the problem is very complex. Therefore, in order to simplify discussion of the factors involved, the gas kinetic effects and the electrical effects will first be considered separately in Secs. 4.1 and 4.2, respectively, and then in combination in Sec. 4.3. The most important result will occur in Sec. 4.3, where it will be shown that under conditions occurring in practice the positive-ion collection is determined not by the positive-ion temperature but mainly by the electron temperature.

4.1 Gas Kinetic Effects. When a probe is at space potential, all electric fields vanish, and the rate of collection is determined solely by the random straight-line motion of the ions in the neighborhood. In the most elementary treatment of this problem it is assumed that the probe is struck by the same current that would strike an equal

element of area in the undisturbed gas. If n_0 is the gas density, \bar{v} the mean velocity, and A the probe area, kinetic theory shows that this current is

$$J = \frac{n_0 \bar{v} A}{4} \quad (4)$$

If Eq. 4 is to be valid, it is obviously necessary that the probe cause a negligible disturbance in the ion distribution. In order to estimate the magnitude of this disturbance, let us consider a spherical

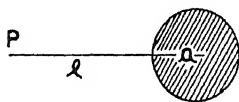


Fig. 2.15—Figure for discussion of gas kinetic effects (Sec. 4.1).

collector of radius a , immersed in a gas whose mean free path is \bar{l} . It is evident that ions striking the probe originate from collisions occurring at an average distance \bar{l} . When the probe is absent, collisions taking place at P (Fig. 2.15) involve ions coming from all directions, including those which pass through the space that is later to be occupied by the probe. When the probe is present, however, ions striking the probe cannot reach the point P . It is evident that the effect of the disturbance introduced by the probe is to decrease the density of ions at P in the ratio of the fraction of all of the solid angle subtended by the probe at P , namely, $\pi a^2 / 4\pi \bar{l}^2 = a^2 / 4\bar{l}^2$. This means that when a/\bar{l} is small, i.e., when the probe is small compared with a mean free path, the simple theory yielding Eq. 4 will be valid.

In order to calculate the probe current when \bar{l} is large, we may go to the opposite extreme and assume that all ionic motion takes place by diffusion. According to kinetic theory, the diffusion coefficient is $\bar{l}\bar{v}/4$. Hence, if n is the concentration of ions, the current density j is

$$j = -\frac{\bar{l}\bar{v}}{4} \operatorname{div} \vec{n} \quad (5)$$

Since ions are conserved, $\operatorname{div} j = 0$, and hence $\nabla^2 n = 0$ (Laplace's equation).

The value n is therefore a solution of Laplace's equation approaching plasma density n_0 at infinity, and approaching some definite value n_1 at the probe surface. To determine the magnitude of n_1 it is necessary to use the fact that the current is carried across the last mean free path, not by diffusion, but by free motion. Thus, the actual current collected by the probe is

$$J = \frac{n_1 \bar{v} A}{4} \quad (6)$$

But Eq. 5 gives another expression for probe collection, i.e.,

$$J = - \int \frac{\bar{v}}{4} \nabla n \cdot \vec{ds} \quad (7)$$

where the integration is over a surface one mean free path away from the probe. Since n is a solution of Laplace's equation, an analogy with electrostatics can be used in order to simplify the evaluation of the above integral. Thus

$$\phi = CV$$

where ϕ = charge = $(1/4\pi) \int \nabla \phi \cdot \vec{ds}$ (Gauss's theorem), C is the capacity of the electrode, and V is the potential.

If a formal analogy is made between ϕ and n ,

$$\int \nabla \phi \cdot \vec{ds} = 4\pi\phi = 4\pi C (V_0 - V_1) \quad (8)$$

where V_0 is potential at infinity, V_1 is potential at electrode, and

$$\int \nabla n \cdot \vec{ds} = \frac{4J}{\bar{v}} = 4\pi C (n_0 - n_1)$$

Note that C refers to the capacity of a surface that is one mean free path away from the probe, since this is the surface bounding the region in which the diffusion equations are applied.

The value of n_1 is found by equating the currents given in Eqs. 6 and 8. Thus

$$n_1 = \frac{4\pi C \bar{l} n_0}{4\pi C \bar{l} + A} \quad (9)$$

and

$$J = \frac{\bar{v} n_1 A}{4} = \frac{A n_0 \bar{v}}{4} \left(\frac{4\pi C \bar{l}}{4\pi C \bar{l} + A} \right) \quad (10)$$

For a spherical electrode the area is $4\pi a^2$, and the capacity of a sphere of radius $(a + \bar{l})$ is $(a + \bar{l})$. The radius $(a + \bar{l})$ is chosen because current collection is determined by the diffusion to a surface one mean free path from the probe. The final result, using this value of the capacity, is

$$J = \frac{n_0 v}{4} A \frac{\frac{\bar{l}}{a} \left(1 + \frac{\bar{l}}{a} \right)}{\left(1 + \frac{\bar{l}}{a} + \frac{\bar{l}^2}{a^2} \right)} \quad (11)$$

If $\bar{l} \ll a$, the current is reduced below that of the long-mean-free-path case by a factor of approximately \bar{l}/a . On the other hand, if $\bar{l} \gg a$, the collection approaches that given in Eq. 4. This provides additional verification of the result that the simple theory is valid when $(\bar{l}/a) \ll 1$.

For positive ions, \bar{l} is usually of the order of several centimeters, whereas the probe radius is usually a millimeter or less. Thus the above criterion is easily satisfied. Of course, the magnetic field cuts down the mean free path by confining the ions to a Larmor radius, which is often only a few millimeters. But unless the Larmor radius drops below the probe radius, there is no appreciable correction required for the simple theory.

4.2 Effects of Electric Fields. In Sec. 4.1 positive-ion collection has been studied when the probe is at space potential. Since positive-ion currents are in practice observed when the probe is highly negative, it is necessary now to consider how collection can be affected by the resulting electric fields. For the present, the theory will be confined to spherical and cylindrical probes, which are the only shapes simple enough to be handled. The main purpose of this work is to derive a number of quantitative relations between ion collection and potential distributions, which will be of use in Sec. 4.3. For the present, consideration is limited to the effects of arbitrary fields; in

Sec. 4.3 it will be narrowed to the actual space-charge-produced fields.

To find the effect of electric fields on probe currents, it is necessary to study the way in which the orbits of impinging ions are affected. In Fig. 2.16 a typical orbit APBC is shown, in which the ionic

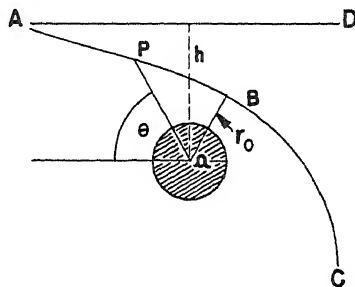


Fig. 2.16—Effect of electric fields on probe currents (Sec. 4.2).

path is curved by the attracting negatively charged probe. Let the straight line AD, which is h cm distant from the probe center, indicate the direction of motion of the particle before it is deviated. The distance h is called the collision parameter. An ion will be collected when r_0 , the distance of closest approach, is less than or equal to the probe radius, a . With the aid of the laws of conservation of energy and of angular momentum about the probe center, a relation may be derived between r_0 and h .

$$\text{Angular momentum:} \quad mr^2\dot{\theta} = L = \text{constant} \quad (12)$$

$$\text{Energy:} \quad \frac{m}{2}(\dot{r}^2 + r^2\dot{\theta}^2) - V(r) = E = \text{constant} \quad (13)$$

In the present case it is assumed that the potential is attracting, or that $V(r)$ is positive.

Since the angular momentum of an ion is conserved, it remains equal to its initial value at an infinite distance from the probe.

$$L = mv_0h = mr^2\dot{\theta} = h \sqrt{2E/m}$$

Eliminating $\dot{\theta}$ from Eq. 13,

$$E = \frac{m\dot{r}^2}{2} + \frac{Eh^2}{r^2} - V(r) \quad (14)$$

The distance of closest approach r_0 is found by setting $\dot{r} = 0$

$$E \left(\frac{h^2}{r_0^2} - 1 \right) = V(r_0) \quad (15)$$

or

$$h = r_0 \sqrt{1 + \frac{V(r_0)}{E}}$$

If $V(r_0)$ is the probe voltage,

$$h = r_0 \sqrt{1 + \frac{V_p}{E}} = a \sqrt{1 + \frac{V_p}{E}} \quad (16)$$

This result shows that the probe collects particles with collision parameter greater than r_0 by a factor $\sqrt{1 + V_p/E}$. To find out how great a current increase this produces, suppose that the velocities are distributed in random directions. In any direction corresponding to a given element of solid angle $d\Omega$, the mean current density will be $n_0 \bar{v} d\Omega/4\pi$. The amount of this current striking the probe is obviously equal to that striking a circle of radius h , namely,

$$dJ = \frac{n_0 \bar{v}}{4\pi} \pi h^2 d\Omega = \frac{n_0 \bar{v}}{4} h^2 d\Omega \quad (17)$$

since we are dealing with a spherical probe. Integrating over the solid angle gives

$$J = \frac{n_0 \bar{v}}{4} 4\pi h^2 = \frac{n_0 \bar{v}}{4} 4\pi a^2 \left(1 + \frac{V_p}{E} \right) \quad (18)$$

If there were no potential on the probe, the collection would be

$$J = \frac{n_0 \bar{v}}{4} 4\pi a^2 \quad (19)$$

so that the collection is thus increased by a factor of $(1 + V_p/E)$.

For a cylindrical probe, a similar treatment shows that the current is increased by the factor $\sqrt{1 + V_p/E}$.

Although Eq. 18 is completely general, it does not necessarily yield the correct value of the probe current. For certain types of field distribution it may happen that over some surfaces outside the probe the current predicted by Eq. 18 is less than that predicted at the

probe itself. The current collected will then be the minimum predicted over any surface surrounding the probe. The minimal surface thus becomes an effective probe boundary. This is elaborated in the following paragraphs.

Equation 18 is merely an upper limit to the current collected at a given electrode potential. This upper limit can be realized only if additional conditions are satisfied. The increase of current must be brought about by that part of the force which extends a long way out and draws in particles that otherwise would miss the probe. If the potential is so distributed that practically all the drop occurs very close to the probe, e.g., when a sheath is present, then there will be no long-range forces, and the increase in probe current will be much less than that predicted by Eq. 18. But because the force across the sheath is so great now on account of the concentration of potential drop, every particle striking the sheath will be drawn in until it is collected. Thus, when a sheath is present, the collection is increased only to the extent that the sheath increases the effective size of the probe. For potential distributions in which part of the drop is confined to a sheath and part penetrates into the plasma, intermediate behavior is to be expected.

It is possible to give an exact mathematical expression for probe collection with arbitrary shape of potential. From Eq. 15 we find the maximum collision parameter that a particle may have if it is to penetrate to a radius r .

$$h_{\max}^2 = r^2 \left[1 + \frac{V(r)}{E} \right] \quad (20)$$

If a particle is to reach a given r , it is necessary not only that h be less than h_{\max} for that value of r but also for all greater values of r . Otherwise the particle will be turned back at that larger value of r for which $h = h_{\max}$. Hence Eq. 18 gives the probe current correctly only if

$$\frac{dh_{\max}}{dr} = \frac{r}{h_{\max}} \left\{ 2 \left[1 + \frac{V(r)}{E} \right] + \frac{r}{E} \frac{\partial V}{\partial r} \right\} \geq 0 \quad \text{for } r \geq a \quad (21)$$

If, on the other hand, there is a point $r = r_1$ for which $dh_{\max}/dr = 0$ and if $dh/dr < 0$ when $r < r_1$, and $dh/dr > 0$ when $r > r_1$, then a different behavior occurs. As long as $dh/dr > 0$, the number of particles reaching a given value of r is given by

$$J = \frac{n_0 \bar{v}}{4} 4\pi r^2 \left[1 + \frac{V(r)}{E} \right]$$

in accordance with the reasoning used in deriving Eq. 18. But when dh/dr becomes negative, all particles that reach $r = r_1$ can also reach radii less than r_1 , because h_{\max} is now increasing with decreasing r . Physically this means that at $r = r_1$ the field has become so intense that it captures all particles that penetrate this far. From this we may conclude that the effective radius of the probe is r_1 , and that the current collected is

$$J = \frac{n_0 \bar{v}}{4} 4\pi r_1^2 \left[1 + \frac{V(r_1)}{E} \right] \quad (22)$$

The above equation shows that probe collection depends not only on probe potential but also on the distribution of potential drop in the space around the probe. The specific distribution has its effect through the determination of r_1 , which is found with the aid of Eq. 21.

4.3 Effects of Space Charge. In Sec. 4.2 it has been shown that the probe current depends not only on the probe potential but also on the precise form of the electric field in the surrounding space. In order to calculate the form of this electric field, which is determined by space-charge distribution, it is necessary to solve the problem of space-charge motion in a self-created electric field. With the aid of reasonable approximations this problem is solved, and it is found that the fields reaching into the plasma beyond the sheath are so large that they are the primary factor in determining positive-ion collection whenever the electron temperature is greater than the positive-ion temperature.

The solution of this otherwise hopelessly complex problem is made possible by two principal simplifying features: (1) the inability of the plasma to sustain a large potential drop; (2) the inability of electrons to reach the highly negative probe. To some extent these two factors are related, since the inability of a plasma to sustain large potential drops is due to the fact that neither the electrons nor the ions have more than a few volts of kinetic energy. Thus, if an electrode is made 20 volts negative, very few electrons can be present over most of the region of potential drop, which therefore takes the form of a positive-ion sheath surrounding the electrode and shielding the plasma from most of the potential drop.

To calculate the size of the sheath we use the fact that it contains only those positive ions which diffuse or drift into it from the inte-

rior of the plasma. To the extent that the electron penetration into the sheath is negligible, we may use the usual equation for space-charge flow for positive ions only. The approximate boundary condition is that at the plasma edge the field is zero, for if it were not, electrons would be repelled until this condition became satisfied. The size of the sheath then follows from the well-known equation for space-charge flow in one dimension

$$x = \frac{V^{\frac{3}{4}}}{(9\pi \sqrt{m/2e} j_e)^{\frac{1}{2}}} \quad (23)$$

where V is the probe potential in electrostatic units, m is the ionic mass, and j_e is the current density in electrostatic units. In a typical case for argon, occurring in arc investigations, $j_e = 20$ ma per sq cm, $m = 40 \times 1.6 \times 10^{-24}$ g, and the sheath width then becomes 5.7×10^{-3} cm. Since the sheath is so small, it might be thought that it shields the plasma completely from probe potentials. Because the electrons have several volts of kinetic energy, however, they can penetrate potential drops of several volts and thus permit correspondingly large residual potentials to penetrate into the plasma. These potentials, although not very great, are still large enough to draw in ions much more rapidly than would be done by ionic thermal velocities alone. It is for this reason that the assumption of zero field and zero voltage at the sheath edge is only correct to the extent that electron energies are small compared with total potential drop across the sheath.

Since electrons are not absorbed by the probe, they remain in equilibrium in its neighborhood, and their density is therefore given by the Maxwell-Boltzmann relation

$$n_e = n_0 e^{-eV/kT_e} \quad (24)$$

where n_0 is plasma density, V is the potential, k is Boltzmann's constant, and T_e is electron temperature. Poisson's equation, which governs the potential, becomes $\nabla^2 V = -4\pi e(n_e - n_+)$, where n_e is electron density and n_+ is ion density. Inserting in Eq. 24,

$$\nabla^2 V + 4\pi e n_0 e^{-eV/kT_e} = 4\pi e n_+ \quad (25)$$

Before Eq. 25 can be solved it is necessary to have another relationship between n_+ and V . Using a wide variety of assumptions for

this relationship under different conditions, Langmuir and Tonks⁴ have investigated this equation and have found in all cases that the solution splits into two parts, a plasma region and a sheath. In the plasma region the fields are weak; n_e is approximately equal to n_+ , so that $\nabla^2 V$ is negligible. But in the sheath V is large, $n_e = n_0 e^{-eV/kT_e}$ is small, and only positive ions are present in substantial quantity. The break between the two regions occurs at about $eV/kT_e \approx \frac{1}{2}$, since beyond this point the electron density rapidly becomes negligible. Physically, this happens because few electrons have enough kinetic energy to reach higher potentials. Thus the sheath forms, not at $V = 0$ as previously assumed, but at $V = kT_e/2e$. Until the sheath forms, the plasma must be almost neutral, so that $n_e \approx n_+$.

Because of this potential drop between the plasma and the sheath edge, current collection by the probe is greatly increased. It is of interest to compute the maximum current that can be attracted into the sheath by this residual potential. To do this, it must be noted that there is no infinitely sharp break between sheath and plasma but only a very rapid change, which takes place in the neighborhood of $V = kT_e/2e$. In the following equations the voltage at the edge of the sheath is denoted by V , the ion temperature by T_+ , and the mean ion velocity at the sheath edge by \bar{v}_+ . The current density at the sheath edge is $n_+ \bar{v}_+$, where n_+ is the ionic density at the sheath edge. Because the ion thermal velocities are randomly divided, approximately one-third of their energy will be directed normal to the sheath. This means that

$$\bar{v}_+ = \sqrt{\frac{2}{m}} \sqrt{\frac{kT_+}{3} + eV}$$

while $n_+ = n_0 e^{-eV/kT_e}$, since $n_e \approx n_+$. Thus

$$j_+ = \sqrt{\frac{2}{m}} n_0 e^{-eV/kT_e} \sqrt{\frac{kT_+}{3} + eV}$$

To maximize j_+ , set $dj_+/dV = 0$.

Then

$$eV = \frac{kT_e}{2} - \frac{kT_+}{3}$$

and

$$(j_+)_{\max} = n_0 \frac{2}{m} \sqrt{\frac{kT_e}{2}} e^{-\frac{1}{2} + T_+/3T_e} \quad (26)$$

If T_+ is small, j_{\max} occurs at $V = kT_e/2e$, which is just about the maximum potential a plasma can sustain without forming a sheath. As long as $T_+ < T_e$, it is evident from Eq. 26 that collection does not depend strongly on T_+ . For example, even if $T_+ = T_e$, collection is only 1.4 times as great as when T_+ is very small. It must be emphasized, however, that this calculation is somewhat rough. A better estimate, embodied in Eqs. 40 and 41, will be made presently.

Equation 26 gives merely the maximum current that can flow at the sheath edge. It might be thought that currents smaller than this may actually occur. However, it has been shown that a sheath can be stable only if this maximum current flows (see Chap. 3). It might be concluded therefore that Eq. 26 gives the current density at the probe surface in all cases. In order to verify that the residual fields actually do cause this current to be collected, the special case of a spherical probe will now be studied in detail. Since Eq. 26 is a somewhat rough approximation, the more precise calculation of the spherical probe will also serve as a check.

In order to simplify the discussion it may be assumed that all ions have the same energy E rather than a Maxwellian distribution. This does not introduce a serious error, since the collection is actually not very strongly dependent on E . Because the potential must be found only up to the sheath edge, it may be said that $n_e \approx n_+$, as shown in the discussion following Eq. 25. Since

$$\begin{aligned} n_e &= n_0 e^{-eV/kT_e} \\ n_+ &\approx n_0 e^{-eV/kT_e} \end{aligned} \quad (27)$$

The next step is obviously to express n_+ as a function of V by some other method. To do this, consider the current density directed within the element of solid angle $d\Omega$ at an infinite distance from the probe. Then

$$dj = n_0 \sqrt{\frac{2E}{m}} \frac{d\Omega}{4\pi}$$

The total quantity of this current with collision parameter less than h is obviously equal to that striking a circle of radius h , or

$$dJ = n_0 \sqrt{\frac{2E}{m}} \frac{\pi h^2 d\Omega}{4\pi}$$

Integrating over the solid angle yields

$$J = n_0 \sqrt{\frac{2E}{m}} \pi h^2 \quad (28)$$

From Eq. 14 the following expression can be derived for the collision parameter of a particle that reaches a given radius r , with a radial velocity \dot{r} . It is

$$h^2 = r^2 \left[1 + \frac{v(r)}{E} \frac{-m\dot{r}^2}{2E} \right] \quad (29)$$

Putting this in Eq. 28 yields

$$J = n_0 \sqrt{\frac{2E}{m}} \pi r^2 \left[1 + \frac{v(r)}{E} \frac{-m\dot{r}^2}{2E} \right] \quad (30)$$

In order to find the density n_+ from the current, it is necessary to analyze the current as a function of the radial velocity of its elements. The expression for that part of the current with radial velocity between \dot{r} and $\dot{r} + \delta\dot{r}$ is

$$\delta J = \delta n_+ \cdot 4\pi r^2 \dot{r} \quad (31)$$

which is found by integrating the current density over a spherical surface of radius r . By differentiating Eq. 30 with respect to \dot{r} partially, we can obtain another expression for that part of the current whose radial velocity lies between \dot{r} and $\dot{r} + \delta\dot{r}$. It is

$$\delta J = n_0 \sqrt{\frac{2E}{m}} \pi r^2 \frac{m\dot{r}}{E} \delta\dot{r} \quad (32)$$

(The minus sign may be dismissed if only the absolute value of current is desired.) Equating Eqs. 31 and 32 for δJ , we get

$$n_+ = \frac{n_0}{4} \sqrt{\frac{2m}{E}} \delta\dot{r} \quad (33)$$

To find the density of particles, it is necessary only to integrate Eq. 33 over the values of \dot{r} permissible at a given value of r . It is necessary to be careful, however, since, as shown in Sec. 4.2, particles entering the critical radius r_1 are all caught, whereas those

which do not reach this radius miss the probe. Particles that are caught pass a given radius only once, but those which miss pass it twice and therefore contribute twice to the density. At each point there is a critical value of \dot{r} , denoted here by \dot{r}_c , below which a particle is rejected and above which it is caught. This value is simply the smallest value of \dot{r} that will permit a particle to reach $r = r_1$. It is found by setting the collision parameter equal to the maximum that will allow the particle to reach $r = r_1$, which is, according to Eq. 20,

$h_c^2 = r_1^2 \left[1 + \frac{V(r_1)}{E} \right]$. Putting this value for h_c into Eq. 29 gives the following value for the critical \dot{r} , namely,

$$\begin{aligned} \dot{r}_c &= \sqrt{\frac{2E}{m}} \sqrt{1 + \frac{V(r_1) - h_c^2}{E r^2}} \\ &= \sqrt{\frac{2E}{m}} \sqrt{1 + \frac{V(r) - r_1^2}{E r^2} \left[1 + \frac{V(r_1)}{E} \right]} \quad (34) \end{aligned}$$

In integrating Eq. 33 for the density, it is necessary to consider separately the cases where $r > r_1$ and $r < r_1$.

Case I: $r > r_1$

In this case all particles with $\dot{r} > \dot{r}_c$ contribute only once to the density, since they are collected, while particles with $\dot{r} < \dot{r}_c$ contribute twice. The minimum value of \dot{r} is zero, since this is the value for a particle that is just being rejected, as it reaches the value of r under consideration.

Integration of Eq. 33 now yields

$$n_+ = \frac{n_0}{4} \sqrt{\frac{2m}{E}} [(\dot{r}_{\max} - \dot{r}_c) + 2(\dot{r}_c - \dot{r}_{\min})] = \frac{n_0}{4} \sqrt{\frac{2m}{E}} (\dot{r}_{\max} + \dot{r}_c) \quad (35)$$

\dot{r}_{\max} is found by setting $h = 0$ in Eq. 29. Its value is

$$\dot{r}_{\max} = \sqrt{\frac{2E}{m}} \sqrt{1 + \frac{V(r)}{E}}$$

Thus

$$n_+ = \frac{n_0}{2} \left\{ \sqrt{1 + \frac{V(r)}{E}} + \sqrt{1 + \frac{V(r) - r_1^2}{E r^2} \left[1 + \frac{V(r_1)}{E} \right]} \right\} \quad (36)$$

use II: $r < r_1$

In this case all particles contribute only once. Hence integration of 1.33 yields

$$n_+ = \frac{n_0}{4} \sqrt{\frac{2E}{m}} (\dot{r}_{\max} - \dot{r}_{\min})$$

n_{\max} is the same as in case I. The value of \dot{r} corresponding to a particle that can barely reach $r = r_1$ is \dot{r}_{\min} . This is equal to \dot{r}_c by definition. Thus

$$n_+ = \frac{n_0}{2} \left\{ \sqrt{1 + \frac{V(r)}{E}} - \sqrt{1 + \frac{V(r) - r_1^2}{E r^2} \left[1 + \frac{V(r_1)}{E} \right]} \right\} \quad (37)$$

To finish this problem, set $n_+ = n_0 e^{-eV/kT}$ and solve for r as a function of V . In cases I and II this yields

$$\left[1 + \frac{V(r_1)}{E} \right] \frac{r_1^2}{r^2} = 4e^{-eV/kT} \left[\sqrt{1 + \frac{V(r)}{E}} - e^{-eV/kT_e} \right] \quad (38)$$

$V(r_1)$ is found by setting $r = r_1$ in Eqs. 36 or 37. We get

$$e^{-eV(r_1)/kT_e} = \sqrt{1 + \frac{V(r_1)}{E}} \quad (39)$$

The single unsettled point remains as to what is the potential at the sheath edge (where $r = a$). This is determined by a method first used by Tonks and Langmuir.⁴ It is characteristic of the solutions of plasma equations of this type that, by use of the approximation $n_e \approx n_+$ or $\nabla^2 V = 0$, potentials are obtained for which $\nabla^2 V$ is actually very small until we reach a critical point, after which it grows rapidly. This critical point may be regarded as the breakdown of the plasma approximation and the beginning of the sheath approximation. It is shown in the paper of Tonks and Langmuir that to a fair degree of accuracy this point is located by finding the point at which $dV/dr = \infty$, as calculated with the aid of the assumption that $n_e = n_+$. A rough justification for this procedure is that the neglected $\nabla^2 V$ becomes large only very near this point.

Equation 38 will be solved for two cases, namely, $eE/kT_e = 0.01$ and $eE/kT_e = 0.5$. The comparison of these two cases will show the relative unimportance of ion energy in determining ion collection. The first step is to find $V(r_1)$. This is done in each case by solving Eq. 39. In case I, $V(r_1) = 2.8E$, and in case II, $V(r_1) = 0.79E$. Next it is necessary to locate the sheath edge by finding the potential at which $dV/dr = \infty$ or $dr/dV = 0$, if we assume that the sheath edge is located at $r = a$. This is done with aid of Figs. 2.17 and 2.18, in which r_1^2/a^2 is plotted against eV/kT and the maximum value is found, thus locating the point at which $dr_1/dV = 0$ when $r = a$. In case I $(r_1/a)_{\max}^2 = 4.2$ and in case II it is 1.17. This means that, when $E = 0.01kT_e/e$, the effective probe radius is increased by the factor $\sqrt{4.2} = 2.1$, whereas when $E = 0.5kT_e/e$, it is increased by only the factor $\sqrt{1.17} = 1.08$.

With the above values for r_1 and $V(r_1)$, Eq. 40 may be used to plot r against V , or equivalently V against r . These are plotted in Figs. 2.19 and 2.20, respectively. It can be seen that the potential is rather flat for large values of r but steepens rapidly as the sheath edge is approached. Very close to the sheath the approximation breaks down, so that the slope does not actually become infinite but goes instead to a large but finite value.

In order to compute the probe current Eq. 22 is used:

$$J = \frac{n_0 \bar{v}}{4} 4\pi r_1^2 \left[1 + \frac{V(r_1)}{E} \right]$$

with

$$\bar{v} = \sqrt{\frac{2E}{m}}$$

In case I, using values of r_1 and $V(r_1)$ obtained above,

$$J = 0.40n_0 \sqrt{\frac{2kT_e}{m}} (4\pi a^2) \quad (40)$$

In case II,

$$J = 0.38n_0 \sqrt{\frac{2kT_e}{m}} (4\pi a^2) \quad (41)$$

It is interesting to compare these results with those of Eq. 26, which were very crudely derived.

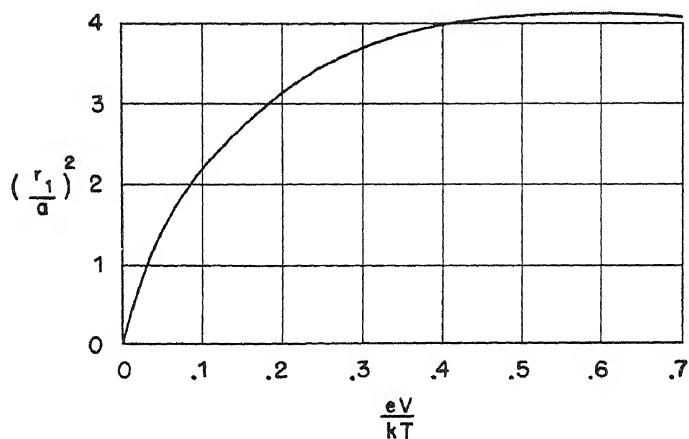


Fig. 2.17—Variation of r_1 with potential $eE/kT = 0.01$ (see Sec. 4.3).

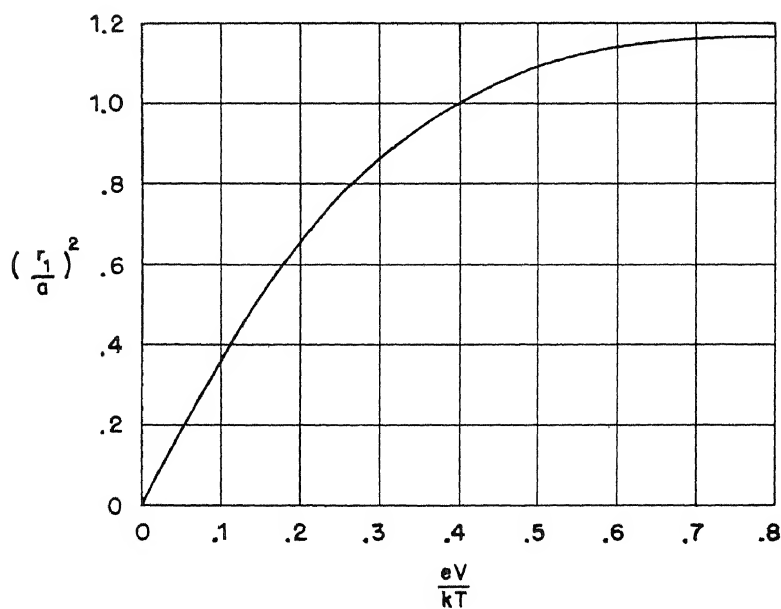


Fig. 2.18—Variation of r_1 with potential $eE/kT = 0.5$ (see Sec. 4.3).

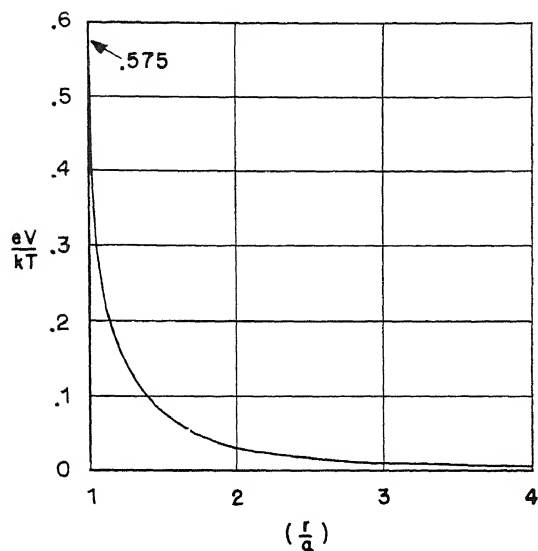


Fig. 2.19—Space potential near probe of radius a as a function of r ($eE/kT = 0.01$).

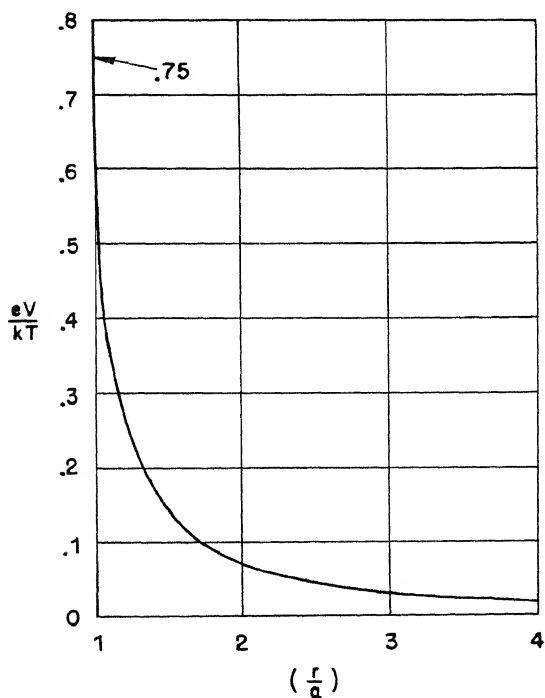


Fig. 2.20—Space potential near probe of radius a as a function of r ($eE/kT = 0.5$).

Case I:

$$J = 0.43n_0 \sqrt{\frac{2kT_e}{m}} (4\pi a^2) \quad (42)$$

Case II:

$$J = 0.50n_0 \sqrt{\frac{2kT_e}{m}} (4\pi a^2) \quad (43)$$

Equations 40 and 41 not only show no great change in probe collection as the ion temperature is raised from 0.01 of the electron temperature to 0.5 of the electron temperature, but there is actually a slight decrease. The decrease is probably characteristic of the approximations used. For the low-temperature case there is fairly good agreement between the crude treatment and the more accurate treatment, as shown by the approximate equality of the results in Eqs. 40 and 42.

The most important conclusion of this work is that ion collection is independent of the positive-ion temperature, within a factor of 20 per cent, as long as the ion temperature is smaller than the electron temperature.

The expression yielding ion collection in terms of ion density is

$$J = 0.40n_0 \sqrt{\frac{2kT_e}{m}} A$$

where A is the probe area (Eq. 3). The criterion for the validity of this result is that the effective probe radius is smaller than a mean free path. Since probes are seldom more than 0.15 cm in radius and since the effective radius r_1 is never more than twice the actual radius, the above results are correct as long as the mean free path is longer than 3 mm. Very rarely is the collision mean free path actually shorter than 1 cm. If a strong magnetic field (10,000 gauss) is present, however, the Larmor radius may go below 1 mm for argon ions with electron thermal energies. Whether this would invalidate the results just obtained is not yet clear, since compensating factors, such as the production of hash, may help overcome the effect of the magnetic field.

The conclusions derived in this section greatly simplify the interpretation of positive-ion probe currents. When positive ions are created, they have only the thermal energy of the neutral gas. In the static and fluctuating plasma electric fields, they may acquire ener-

gies comparable with, but usually somewhat smaller than, electron temperatures. Hence at any point the mean ion temperature is more or less unknown. But since the probe current depends mainly on electron temperatures that can be measured from the difference between floating and space potentials, it is now possible to interpret positive-ion currents in terms of plasma density. There remains some ambiguity as to the probe potential at which the ion density is to be measured. If all the conditions referred to in the introduction were satisfied, there would be complete saturation of the positive-ion current with highly negative probe potentials. Unfortunately these conditions are satisfied only approximately, and the saturation is not quite complete. This failure of complete saturation is probably due to the steadily increasing thickness of the sheath, which increases the effective size of the probe. Secondary emission may also set in at highly negative probe potentials down to the space potential. Ion density should thus be measured from the ion current extrapolated to space potential in this manner.

5. ELECTRON COLLISION IN A MAGNETIC FIELD—MAGNETIC DIFFUSION

Because electrons and ions in a magnetic field are constrained to move in circles, which can be changed only by collision with other particles or by electric fields, the current striking an electrode in a magnetic field is reduced. For electrons, whose Larmor radius lies between 10^{-3} and 10^{-2} cm, the collection process must, in fact, resemble that of a probe, which is much larger than a mean free path, so that as shown in Sec. 4.1 the electron current should be reduced in the ratio of the effective free path to the probe radius. Since the ion Larmor radii are, in most cases, somewhat larger than the probe radius, the ion currents are, on the other hand, reduced appreciably only in the strongest magnetic fields (over 3,000 gauss). In fact, it is because the ion currents are so little affected that they have been selected as a measure of ion density.

The most striking results of probe measurements are that the ratio of electron to ion saturation current is reduced from its normal value of 200 or more down to something between 10 and 20. To the extent that ion currents are not greatly affected, this represents a real decrease in electron current. In order to account for this decrease, it is necessary to consider not only the fact that motion transverse to the field is hindered but also the fact that motion along the field is normal. As a result of the ease with which electrons move along the field, they are collected from a long distance in this direction, where-

as they are greatly hindered in their transverse motion. The net result of this combination of slow transverse and rapid longitudinal diffusion is to increase the effective size of the probe along the field and to cause current collection to be a sort of geometric mean between its normal value and the value it would have if it depended on transverse diffusion alone. The theory of this effect is treated in Sec. 5.1. To calculate the transverse diffusion coefficient that must be used in the theory of electron collection, it is necessary to have detailed knowledge of the processes involved. Of all possible causes of diffusion, collisions are the first to suggest themselves, since they obviously cause ions to move by displacing the centers of their circular orbits on the average by a Larmor radius. When the diffusion coefficient resulting from all known collision processes is calculated, it turns out to be about one-millionth of the normal value in the absence of a magnetic field. Because the effective length of the probe is increased as a result of ease of collection of electrons moving along the magnetic field, the total current is not reduced in the ratio of this diffusion coefficient, but instead it is reduced only as r_0/a , where r_0 is the Larmor radius, and a is the probe radius. In actual practice, r_0 is usually about 0.15×10^{-2} cm, and a is 0.15 cm. Thus the expected ratio of electron to ion current is reduced from 200 to $200r_0/a$, or approximately 2, which is only about one-tenth of the observed value. This discrepancy suggests that causes of diffusion other than collision are operating. At present the most likely cause is thought to be the fluctuating electric fields associated with hash. In Sec. 5.2, where diffusion coefficients are derived, the entire question of the cause of electron diffusion is discussed at greater length.

5.1 Electron Collection. To calculate electron collection in this section, the basic assumption will be made that electronic motion is determined entirely by diffusion processes. Since electronic motion transverse to the field is much more hindered than that along the field, it is necessary to assume that there are two diffusion coefficients, D_{\perp} and D_z , where D_{\perp} is the transverse coefficient and D_z is the longitudinal coefficient. Normally, $D_{\perp} \ll D_z$. Let us define $D_{\perp}/D_z = \alpha$. Then $\alpha \ll 1$. This ratio will be determined in Sec. 5.2. The validity of the assumption that all electronic motion occurs by means of diffusion alone is unquestionable for transverse motion. For longitudinal motion, however, the free path is so long (about 1 cm) that the assumption becomes somewhat doubtful. In order to try to take this point into account, at least partially, the diffusion equations will be used only up to one free path away from the probe in the field direction, and up to one Larmor radius away from the probe in the

transverse direction. Closer than this, it will be assumed that the motion is free. Because the result is not critically dependent on the precise point at which the break in treatment occurs, some confidence may be placed in this procedure.

In order to make the equations solvable, it is necessary to restrict the treatment to the case where only electrons are collected and where all positive ions are repelled. This introduces the simplifying feature that the ions are in equilibrium, so that their density is given by the Boltzmann expression:

$$n_+ = n_0 e^{-eV/kT_+} \quad (44)$$

where T_+ is ion temperature, and V is the space potential relative to the plasma. As in the theory of ion collection, it may be assumed that in the plasma $n_e \approx n_+$ and that the point where this assumption fails defines the sheath edge. Thus

$$n_e \approx n_0 e^{-eV/kT_+} \quad (45)$$

Differentiation of Eq. 45 gives

$$\frac{\partial n_e}{\partial x} = \frac{-en_0}{kT_+} e^{-eV/kT_+} \quad \frac{\partial V}{\partial x} = \frac{-e}{kT_+} n_e \frac{\partial V}{\partial x} \quad (46)$$

The next step is, of course, to express n_e as a function of V in a different way. To do this the diffusion equations, which provide an additional relation between n_e and V , must be used. According to a well-known result, discussed in Chap. 9, these equations are

$$j_{ez} = -D_z \left(\frac{\partial n_e}{\partial z} - \frac{e}{kT_e} n_e \frac{\partial V}{\partial z} \right) \quad (47)$$

$$j_{e\perp} = -D_\perp \left(\vec{\nabla}_\perp n_e - \frac{e}{kT_e} n_e \vec{\nabla}_\perp V \right) \quad (48)$$

where j_{ez} is the current density in the Z direction, $j_{e\perp}$ is the current-density vector normal to the Z direction, and $\vec{\nabla}_\perp$ denotes the gradient normal to the Z direction, the direction of the magnetic field. Equations 46 and 47 take into account electron diffusion due to concentration gradient, electron drift brought about by the electric field.

Applying Eq. 46 to Eqs. 47 and 48,

$$j_{ez} = -D_z \left(1 + \frac{T_+}{T_e} \right) \frac{\partial n_e}{\partial z} \quad (49)$$

$$j_{e\perp} = -D_\perp \left(1 + \frac{T_+}{T_e} \right) \vec{\nabla}_\perp n_e \quad (50)$$

Since electrons are conserved, $\text{div } \vec{j}_e = 0$. Replacing the components of \vec{j}_e by the values given in Eqs. 49 and 50,

$$\frac{\partial^2 n_e}{\partial z^2} + \alpha \left(\frac{\partial^2 n_e}{\partial x^2} + \frac{\partial^2 n_e}{\partial y^2} \right) = 0 \quad (51)$$

Evidently, n_e is a solution of an equation resembling that of Laplace. To bring the equation exactly to Laplacian form, make the substitution, $\zeta = \sqrt{\alpha} z$. This yields

$$\frac{\partial^2 n_e}{\partial x^2} + \frac{\partial^2 n_e}{\partial y^2} + \frac{\partial^2 n_e}{\partial \zeta^2} = 0 \quad (52)$$

Thus n_e satisfied Laplace's equation in a highly flattened space.

In order to compute the total probe current, integrate the current density around a surface surrounding the probe. If a cylindrical surface surrounding the probe and extending an infinite distance up and down in the Z direction is chosen, the evaluation of this integral is greatly facilitated. For in this case the current crossing the surface flows perpendicularly to the field, therefore the following expression for the total current may be written:

$$\begin{aligned} J &= \int \vec{j}_\perp \cdot \vec{ds} = \left(1 + \frac{T_+}{T_e} \right) D_\perp \int \vec{\nabla} n \cdot \vec{ds} \\ &= \left(1 + \frac{T_+}{T_e} \right) \alpha D_z \int \vec{\nabla} n \cdot \vec{ds} \end{aligned} \quad (53)$$

Since n_e is a solution of Laplace's equation in (x, y, ζ) space, it is convenient to express Eq. 53 in these coordinates. Noting that the surface of integration is a cylinder with its axis in the Z direction, we may write $\vec{ds} = d\vec{z} \times d\vec{p}$ where $d\vec{z}$ is a displacement in the Z direction, and $d\vec{p}$ is a displacement normal to the Z direction but in the surface. Replacing z by its value in terms of ζ ,

$$ds = \frac{d\vec{\zeta} \times d\vec{p}}{\sqrt{\alpha}} \quad (54)$$

and

$$J = \left(1 + \frac{T_+}{T_e}\right) \sqrt{\alpha} D_z \int \nabla_{\vec{\zeta}} n \cdot d\vec{s}_{\vec{\zeta}} \quad (55)$$

where $\nabla_{\vec{\zeta}} n$ is now the gradient in ζ space, and $ds_{\vec{\zeta}}$ is the element of area in ζ space.

With the aid of the electrostatic analogy between n and the electrostatic potential ϕ , developed in Sec. 4.1,

$$J = \left(1 + \frac{T_+}{T_e}\right) \sqrt{\alpha} D_z 4\pi C(n_0 - n_1) \quad (56)$$

where n_0 is the plasma density, n_1 the density at the surface defined by the last mean free path before the probe is hit, as described in the beginning of this section, and C is the electrostatic capacity of the same surface, but transformed into ζ space.

To evaluate n_1 it is necessary to consider further the processes involved in the collection of electrons by their free motion across the last mean free path. This is done as in Sec. 4.1 by equating the total probe current to the random current flowing across the last mean free path.

$$J = \frac{n_1 \bar{v} A}{4} \quad (57)$$

where A is the probe area and \bar{v} is the mean velocity.

By equating the J 's found in Eqs. 56 and 57, the value of n_1 is obtained; because of the hindrance to diffusion offered by the magnetic field, this may be considerably less than n_0 .

$$n_1 = \frac{4\pi C D_z \left(1 + \frac{T_+}{T_e}\right) \sqrt{\alpha} n_0}{\frac{\bar{v} A}{4} + 4\pi C D_z \left(1 + \frac{T_+}{T_e}\right) \sqrt{\alpha}} \quad (58)$$

Since $D = \bar{l}\bar{v}/4$ (see Sec. 5.2), this becomes (\bar{l} is mean free path in Z direction)

$$n_1 = \frac{4\pi C n_0 \bar{l} \left(1 + \frac{T_+}{T_e}\right) \sqrt{\alpha}}{A + 4\pi \bar{l} C \left(1 + \frac{T_+}{T_e}\right) \sqrt{\alpha}} \quad (59)$$

The final value for the current is found by inserting this value of n_1 into Eq. 57

$$J = \frac{n_0 \bar{v} A}{4} \left[\frac{4\pi C \bar{l} \left(1 + \frac{T_+}{T_e}\right) \sqrt{\alpha}}{A + 4\pi \bar{l} C \left(1 + \frac{T_+}{T_e}\right) \sqrt{\alpha}} \right] \quad (60)$$

$n_0 \bar{v} A/4$ is, of course, the current that would be collected in the absence of a magnetic field. This is modified by the factor in brackets. When, as is usually the case, $4\pi \bar{l} C \left(1 + \frac{T_+}{T_e}\right) \sqrt{\alpha} \ll A$, then the probe current is given approximately by

$$J = \frac{n_0 \bar{v} A}{4} \left[\frac{4\pi C \bar{l} \left(1 + \frac{T_+}{T_e}\right) \sqrt{\alpha}}{A} \right] \quad (61)$$

The correction factor in the brackets decreases only as $\sqrt{\alpha} = \sqrt{D_\perp}/D_z$.

Thus the probe current does not decrease as rapidly as the transverse diffusion coefficient but only as its square root. To understand this physically, it is necessary only to refer to the beginning of this section, where it was pointed out that on account of the free motion of electrons along the field the effective length of the probe in the Z direction is greatly increased. In fact, by noting that $n = n(x, y, \zeta) = n(x, y, \sqrt{\alpha} z)$, we can get a better idea of what these solutions imply. Since $n(x, y, \zeta)$ is a solution of Laplace's equation, the surfaces of constant density tend to approach spheres in ζ space, far away from the probe. However, in Z space, since $z \gg \zeta$, these spheres become long needle-shaped ellipsoids, extending far up and down the magnetic field. The effective shape of the probe is thus transformed into a long needle-shaped object, with the result that electron collection drops only with the square root of the transverse diffusion coefficient.

Collection by Probes of Different Shapes. Because the effective length of the probe along the field is increased so markedly, it is

evident that probe collection is much less critically dependent on the z dimensions of the probe than on the transverse dimensions. In order to illustrate this point, let us first calculate the collection for a disk-shaped probe of radius a and then compare it with that to be expected from a needle-shaped ellipsoid of revolution with semiminor axis a and semimajor axis $(a/\sqrt{\alpha}) - \bar{l}$.

To obtain the current striking a disk-shaped probe, we need the capacity of a surface that is a Larmor radius r_0 away from the disk in the transverse direction, and a mean free path \bar{l} away in the longitudinal direction. Although the exact shape of this surface cannot be known very definitely, the assumption of an ellipsoid of revolution cannot be far wrong. In any case, the result does not depend critically on the shape. This surface is now transformed to ζ space, in which it becomes an ellipsoid of revolution of radius $a + r_0$ and height $\bar{l}\sqrt{\alpha}$. Since $r_0/a \ll 1$ the radius may be approximated by a itself. Electron mean free paths in a plasma are of the order of 1 cm, and in Sec. 5.2 it will be shown that $\sqrt{\alpha}$ must be somewhere between 0.01 and 0.001. Since the probe radius is 0.15 cm, we evidently have in (x, y, z) space an ellipsoid of radius 0.15 cm and height lying between 0.01 and 0.001 cm. It can be shown that the capacity C of such an ellipsoid differs inappreciably from that of a disk of radius a , which is, according to Smythe,⁵

$$C = \frac{2a}{\pi}$$

By inserting this in Eq. 61, the current going to a disk oriented perpendicular to the magnetic field is determined.

$$J_{\text{disk}} = \frac{n_0 \bar{v}}{4} \bar{l} \sqrt{\alpha} \left(1 + \frac{T_+}{T_e} \right) 8a \quad (62)$$

To find the ratio of disk current to ellipsoid current, use is made of the fact, evident from Eq. 61, that the ratio of currents to two electrodes A and B is

$$\frac{J_A}{J_B} = \frac{C_A}{C_B} \quad (63)$$

To find the capacity of the ellipsoid first add \bar{l} to its height, obtaining an ellipsoid of radius a and height $a/\sqrt{\alpha}$. On transformation to (x, y, ζ) space, this becomes a sphere of radius a and capacity a . Thus the ratio of ellipsoid current to disk current is

$$\frac{J_{\text{ellipsoid}}}{J_{\text{disk}}} = \frac{\pi}{2} \quad (64)$$

Hence the only result of elongating the probe in the Z direction to $1/\sqrt{\alpha}$ times its transverse dimension is to increase the current by 50 per cent. This striking result ought to be tested experimentally.

A ratio that has actually been measured, however, is that between the current collected by a disk oriented, respectively, perpendicular and parallel to the magnetic field. Because of the relatively free motion of electrons along the field, the perpendicular orientation should catch more current than the parallel orientation. On account of the fact that depletion of electrons above the probe must in both cases be made up by transverse diffusion, the difference between the two probes is not very great.

To obtain the ratio it is necessary to compute C_{\parallel} , the capacity of the parallel oriented disk in (x, y, ζ) space. In (x, y, z) space the effective height must be increased by \bar{l} , the mean free path. On transformation to x, y, ζ space, this yields an ellipsoidal disk of semimajor axis a and semiminor axis $(a + \bar{l})\sqrt{\alpha}$.

According to Smythe⁵, the capacity of such an ellipsoid is

$$C = \frac{2}{\int_0^\infty \frac{d\theta}{(a^2 + \theta)^{\frac{1}{2}} [(a + \bar{l})^2 \alpha + \theta]^{\frac{1}{2}} \theta^{\frac{1}{2}}}} \times \frac{\bar{l}}{a} \sqrt{\alpha}$$

This is an elliptic integral. When $(\bar{l}/a)\sqrt{\alpha}$ and $\sqrt{\alpha}$ are small, this integral may be approximated quite well by

$$C_{\parallel} = \frac{a}{\ln \left[\left(1 + \frac{\bar{l}}{a} \right) \sqrt{\alpha} \right]}$$

From Eq. 63, it is evident that

$$\frac{J_{e\perp}}{J_{e\parallel}} = \frac{-2}{\pi} \ln \left(1 + \frac{\bar{l}}{a} \right) \sqrt{\alpha} \quad (65)$$

The factor $\ln [(1 + \bar{l}/a)\sqrt{\alpha}]$ is very insensitive to its argument. Thus the result will not depend critically on the value of \bar{l} , for example. It is evident that the ratio cannot be much larger than unity, because of the logarithmic dependence on $(1 + \bar{l}/a)\sqrt{\alpha}$.

Another result of interest is to calculate the ratio of electron to ion current for the disk probe in the perpendicular orientation. To do this, refer to Eq. 3 of Sec. 1, derived in Sec. 4.

$$J_+ = \frac{n_0}{4} \sqrt{\frac{2kT_e}{m_+}} A(1.6) = \frac{1.6n_0\bar{v}}{4} \sqrt{\frac{m_e}{m_+}} 2\pi a^2$$

With the aid of Eq. 62, this becomes

$$\frac{J_{e\perp}}{J_+} = \frac{4 \frac{\bar{l}}{a} \sqrt{\alpha} \left(1 + \frac{T_+}{T_e}\right) \sqrt{\frac{m_+}{m_e}}}{1.6\pi} \quad (66)$$

Because electron collection does not saturate when the probe is more positive than space potential, we must obtain from the theory a unique potential at which electron current is to be measured. Since the theory demands that both sheath thickness and positive-ion collection be negligible, it is evident that the probe potential must be as close as possible to space potential, yet still positive enough to repel all positive ions. If the probe is 1 or 2 volts positive relative to space, sheath thickness is still quite small; and positive-ion collection is negligible on account of the smallness of ionic energies.

In principle it is possible to solve the diffusion equations for negative values of the probe potential and thus to predict theoretically the rapidly decreasing portion of electron characteristics. In practice, however, the labor involved in doing this is much greater than is justified by the value of the result. Although the steep portion of the electron characteristic is therefore without theoretical interpretation, self-consistency of experimental results indicates that the electron temperature is probably still given as in the case of no magnetic field, by the slope of the logarithmic plot of electron current against voltage (see Sec. 2).

In the case of highly positive probe potentials no attempt has been made to interpret their effects in a quantitative way. The failure of saturation is due probably to the increase of sheath thickness and of hash amplitude as the probe potential is made more positive. Because there are no theories of either sheath thickness in a strong magnetic field or of hash amplitude, it is not yet possible to investigate this problem.

5.2 Mechanism of Electron Diffusion in a Magnetic Field. In Sec. 5.1 electron collection by a probe slightly positive relative to surrounding space has been investigated theoretically. In terms of the

empirically defined diffusion coefficients D_{\perp} , and D_z we have expressed the characteristic ratios $J_{e\perp}/J_+$ and $J_{e\perp}/J_{e\parallel}$, which are, respectively, the ratio of electron to ion saturation current and the ratio of electron currents in probe orientations perpendicular and parallel to the magnetic field.

In order to apply the results of Sec. 5.1, it is necessary to obtain independent estimates of D_z and D_{\perp} . Fortunately D_z can be calculated quite readily by taking into account the mean free path for electrons colliding both with neutral atoms and with plasma electrons and ions. As for D_{\perp} , however, the theory is still in a state of incomplete development. Two important mechanisms for diffusion transverse to the magnetic field are being considered. The first of these is collision, which moves the center of the Larmor radius in a random direction. The second of these is the presence of oscillating electric fields in a plasma, which cause random drift in an arbitrary direction. Already, measurements of ion density in the arc plasma strongly support the latter theory. Because probe results also furnish evidence to enable a choice to be made between the two theories, the ratios J_{e+}/J_+ and $J_{e\parallel}/J_{e\perp}$ predicted by these theories will be worked out and each then compared with the experiment in Sec. 6. The results of this comparison will show that drift diffusion must be the actual process mainly responsible for moving electrons across the magnetic field, a result in good agreement with observations on arc-ion density.

(a) Diffusion by Collision. Although Hill and Aller have written a complete chapter on collision diffusion (Chap. 8), a brief qualitative account is given here for the sake of continuity.

An electron in a magnetic field moves in a circle with a Larmor radius, $r_0 = (mc/eH)v$, where v is the electron velocity, c is the velocity of light, and H is the magnetic field. Evaluating these constants, $r_0 = 3.3 \times 10^{-3} \sqrt{V/H}$, where r_0 is in centimeters, V is in volts, and H is in thousands of gauss.

For a typical electron energy of 3 volts and a field of 3,000 gauss,

$$r_0 = 1.9 \times 10^{-3} \text{ cm}$$

The electron is thus held practically in one spot, unless it undergoes collision with other particles. If there is a collision, the electron subsequently starts a new circular orbit, with its center displaced by an amount depending on the change in direction of motion occurring during a collision. For the special case where all collision angles are equally probable, it is evident from Fig. 2.21 that the center of the new circle is displaced by an average distance r_0 .

Because the deviations occur in a random direction, the problem resembles that of the random walk or of Brownian motion. It has been shown in Chap. 8 that such a process results in the following diffusion coefficient:

$$D_{\perp} = \frac{\bar{v}}{4\bar{l}} r_0^2$$

where \bar{v} is the mean velocity, r_0 is the Larmor radius, and \bar{l} is the mean free path. We see that D_{\perp} decreases rapidly with decreasing r_0 , hence with increasing H . Furthermore, a short mean free path

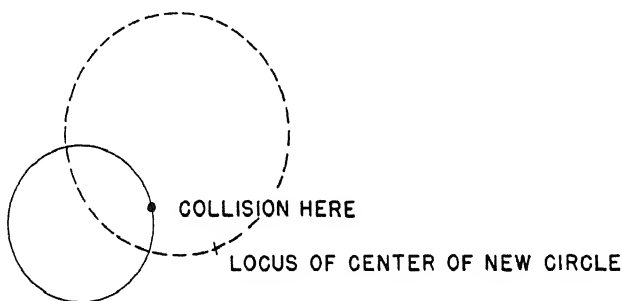


Fig. 2.21 —Case for collision angles equally probable.

and therefore a high pressure produce large D_{\perp} . This behavior is the opposite of that present in normal diffusion, where a low pressure encourages diffusion. The reason is obvious, since diffusion in a magnetic field occurs only because of collision.

The ratio D_{\perp}/D_z is interesting. Since $D_z = \bar{l}\bar{v}/4$, we have $\alpha = D_{\perp}/D_z = r_0^2/\bar{l}^2$. To estimate α , in a typical case, the data are: ($H = 3,000$ gauss, $T_e = 3$ volts, $r_0 = 1.9 \times 10^{-3}$ cm, and $\bar{l} = 1$ cm, whence $\alpha = 4 \times 10^{-6}$). This striking decrease of diffusion perpendicular to the magnetic field indicates that, if collision were the main source of electron diffusion, there would be practically no chance for an electron to leave the ionizing column where it is formed. The possibility of other diffusion mechanisms is discussed later in this section.

If we wish to apply these formulas, it is necessary to obtain expressions for the mean free path. Because most of the scattering is due to plasma electrons and ions, this is not a straightforward problem, since Coulomb scattering results in an infinite number of deflec-

tions through very small angles. It is therefore necessary to weight the importance of collisions as a function of the angular deflection in some physically reasonable way. The proper weighting arises very naturally in the Fokker-Planck-Einstein method. The results obtained by this method are as follows:

$$D_{\perp} = \frac{4.3 \times 10^2 n_0}{H^2 \sqrt{T_e}} \quad (67)$$

where n_0 is in units of 10^{12} particles per cubic centimeter, H is in units of thousands of gauss, and T_e is temperature in electron volts.

$$D_z = \frac{10^7 T_e^{\frac{5}{2}}}{n_0} \quad (68)$$

In order to facilitate comparison with experiment, express the principal quantities of interest, namely, $J_{e\perp}/J_+$ and $J_{e\perp}/J_{e\parallel}$, in terms of the diffusion coefficients predicted by the foregoing diffusion theory. To obtain first $J_{e\perp}/J_+$, Eq. 62 of this section is used.

$$J_{e\perp} = \frac{n_0 \bar{v}_e}{4} \bar{l} \sqrt{\alpha} \left(1 + \frac{T_+}{T_e} \right) 8a$$

Now, since $\bar{l} \bar{v}_e / 4 = D_z$ and $\alpha = D_{\perp} / D_z$,

$$J_{e\perp} = \sqrt{D_z D_{\perp}} \left(1 + \frac{T_+}{T_e} \right) 8an_0$$

To find J_+ , refer to Eq. 3 of Sec. 1

$$J_+ = 0.4n_0 (2\pi a^2) \sqrt{\frac{2kT_e}{m_+}}$$

Thus we get

$$\frac{J_{e\perp}}{J_+} = \frac{\sqrt{D_z D_{\perp}} \left(1 + \frac{T_+}{T_e} \right) 8a}{0.4 (2\pi a^2) \sqrt{\frac{2kT_e}{m_+}}} \quad (69)$$

If numerical values for D_{\perp} and D_z are inserted, the equation becomes

$$\begin{aligned}
\frac{J_{e\perp}}{J_+} &= \sqrt{\frac{10^7 T_e^{\frac{5}{2}}}{n_0} \times \frac{4.3 \times 10^2 n_0}{T_e^{\frac{1}{2}}}} \left(\frac{8}{2\pi} \times \frac{1}{0.4} \right) \frac{\left(1 + \frac{T_+}{T_e}\right)}{aH} \left(\frac{271}{6 \times 10^7 \sqrt{T_e}} \right) \\
&= T_e \frac{6.55 \times 10^4 \times 8}{\sqrt{T_e} aH \times 10^7 \times 2\pi} \left(\frac{1}{0.4} \right) \left(\frac{271}{6} \right) \left(1 + \frac{T_+}{T_e} \right) \\
\frac{J_{e\perp}}{J_+} &= \frac{0.95 \left(1 + \frac{T_+}{T_e} \right) \sqrt{T_e}}{aH} \quad (70)
\end{aligned}$$

To obtain $J_{e\perp}/J_{e\parallel}$, under the assumption that collision with electrons and ions is the main source of diffusion, Eqs. 67 and 68 are applied to Eq. 65.

$$\frac{J_{e\perp}}{J_{e\parallel}} = \frac{-2}{\pi} \ln \left(1 + \frac{\bar{l}}{a} \right) \sqrt{\alpha}$$

Since $\bar{l} > 1$ cm and a is ~ 0.1 cm, the approximate equation is

$$\frac{J_{e\perp}}{J_{e\parallel}} = \frac{-2}{\pi} \ln \frac{\sqrt{\alpha} \bar{l}}{a}$$

Now $\bar{v}_e \bar{l}/4 = D_z$; hence $\bar{l} = 4D_z/\bar{v}_e$. Therefore

$$\frac{J_{e\perp}}{J_{e\parallel}} = \frac{-2}{\pi} \ln \left(\sqrt{\frac{D_\perp}{D_z}} \cdot \frac{4D_z}{a\bar{v}_e} \right) = \frac{-2}{\pi} \ln \frac{4}{a\bar{v}_e} \sqrt{D_z D_\perp} \quad (71)$$

But $\sqrt{D_z D_\perp} = 6.55 \times 10^4 (T_e/H)$ (see Eqs. 67 and 68), and

$$v_e \approx 10^8 \sqrt{T_e}$$

so that

$$\frac{J_{e\perp}}{J_{e\parallel}} = \frac{-2}{\pi} \ln \frac{4}{a} \sqrt{T_e} \frac{6.55 \times 10^4}{H 10^8} = \frac{-2}{\pi} \ln \frac{2.6 \times 10^{-3} \sqrt{T_e}}{aH} \quad (72)$$

We see that this ratio is only weakly dependent on parameters like T_e , a , and H , since they occur within the logarithm. A quantity also

of interest is $\frac{J_{e\parallel}}{J_+}$, which is $\frac{J_{e\perp}}{J_+} \frac{J_{e\parallel}}{J_{e\perp}}$. This becomes

$$\frac{J_{e\parallel}}{J_+} = \frac{0.95 \left(1 + \frac{T_+}{T_e}\right) T_e}{aH \left(\frac{-2}{\pi} \ln \frac{2.6 \times 10^{-3} \sqrt{T_e}}{aH}\right)} \quad (73)$$

Comparison with the experiment is made in Sec. 6.

(b) Diffusion by Motion Transverse to Electric and Magnetic Fields.

Because collision diffusion is too small to account for the observed electron collection rates, additional mechanisms of electron motion across the magnetic field are now being investigated. Of those considered so far, the most promising appears to be the cycloidal motion of electrons perpendicular to both electric and magnetic fields. Such motion has already been met with in the form of "drain." In a plasma the problem of drain is much more complex than it is in free space, because the electric fields are created by the space charge itself, whose distribution is determined in turn by the rate of drain of electrons in the same electric fields.

It is well known that, in the presence of crossed electric and magnetic fields, electrons move in cycloidal paths, which result in an average drift perpendicular to both electric and magnetic fields, with a velocity given by $v = cE/H$, where E is the electric field in electrostatic units and c is the velocity of light. Changing to volts and putting H in thousands of gauss, the equation becomes

$$v = \frac{10^5 E}{H}$$

To estimate the order of magnitude of drain velocities in a plasma, note that fields of several volts per centimeter are commonly observed. Assuming 3 volts per cm and $H = 3,000$ gauss,

$$v = 10^5 \text{ cm/sec}$$

This is about the same order of magnitude as that of ionic velocities in a plasma. In some cases one can see how this mechanism operates directly in a static fashion to move electrons away from the ionizing

column where they are formed, and out to the wall. For example, in Fig. 2.22 we have a cross section of an arc in which the magnetic field is perpendicular to the plane of the paper. If the equipotentials adjust themselves diagonally with respect to the collimating slot, as in Fig. 2.23, the electric field will cause electrons to drain to the wall. There remains the problem of finding whether such a field is consistent with the equations for space-charge motion.

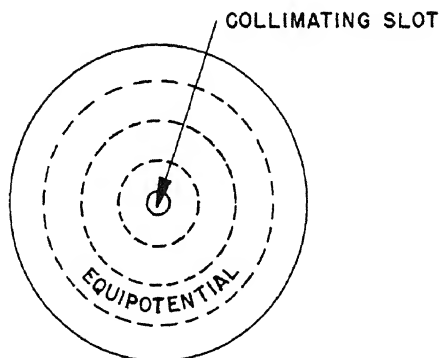


Fig. 2.22—Cross section of arc with magnetic field perpendicular to plane of paper.

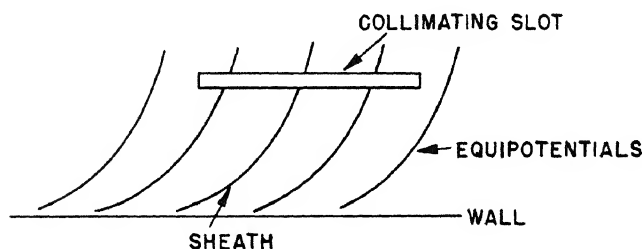


Fig. 2.23—Equipotentials adjusted diagonally with respect to collimating slot.

With a cylindrically symmetrical arc, however, this drain mechanism cannot function in a static way, since the equipotentials will now be circles, which do not intersect the source. The drain will thus confine itself to circular motion, which cannot dispose of the electrons continually being produced below the collimating slot. It has been found, however, that a static distribution of this type is unstable and that it tends to break up into an oscillating distribution, with

waves traveling around the center. These waves create electric fields transverse to the radius, which cause electrons to drain both inward and outward. But since the density falls as we go out to the wall, the average drain is outward.

Such plasma oscillations, which are usually associated with certain types of hash, have actually been observed in the arc (see Chap. 9). With the aid of probes inserted into the arc, plasma oscillations have been observed with magnitudes increasing progressively as the probe is brought further from the slot, and with frequencies between 2×10^5 and 4×10^4 cycles. Because these particular oscillations are only weakly correlated with hash in the arc current, it seems likely that they are the ones that move the electrons across the magnetic field.

It may be shown quite readily that oscillations of not unreasonable magnitude are far more effective than collisions in getting electrons out to the wall. Because static fields of several volts per centimeter have often been observed in the arc, it is not at all unlikely that the fluctuating components of the field have about the same strength. With 3 volts/cm and a field of 3,000 gauss, the drain velocity is 10^5 cm/sec. To estimate the distance that an electron can go with this velocity, note that an electron will move in a given direction until the field reverses. Such reversals take place twice during each period. The distance covered by an electron is thus $10^5 T/2$, where T is the period of the oscillation. Assuming a frequency of 2.5×10^5 , an electron moves 0.2 cm before the field reverses. Since the Larmor radius is only 0.019 cm under these conditions, the electron moves 100 Larmor radii at a time. It therefore crosses the magnetic field much more readily with the aid of plasma oscillations than by collision.

Because plasma oscillations cause electrons to drain back and forth in a random direction, their effect is to increase the rate of diffusion of electrons across the magnetic field. In order to predict the increase of D_{\perp} brought about in this fashion, it is necessary to have a theory that takes into account time variation of plasma density. Although such a theory is now being developed, for the present we shall content ourselves with a brief account of the results that have already been obtained.

By investigating the dynamic theory of the plasma, it has been shown that when electrons move across the magnetic field by collision diffusion the plasma is unstable. If a small deviation from the steady state is accidentally produced, the system does not return to its initial condition but instead begins to oscillate with an amplitude increasing exponentially with time. Of course, the amplitude of these oscillations is ultimately limited by new processes that first become appreciable at large oscillation amplitudes. The most important of

these processes is precisely the electron drain brought about by the oscillating electric fields, which rapidly increases the diffusion coefficient D_{\perp} . It may be shown mathematically, and the result is very reasonable physically, that diffusion tends to damp plasma waves. Thus at a certain mean amplitude the diffusion coefficient will provide just enough damping to stop the exponential increase, and the system will oscillate in a steady state. With the aid of the theory the value of D_{\perp} at which this balance occurs can be calculated. It is

$$D_{\perp} \approx \frac{10^5}{16H} \left(\frac{kT_e}{e} \right) \quad (74)$$

where H is in thousands of gauss and kT_e/e is in volts. The exact value of D_{\perp} is uncertain within a factor of 2 or 3.

As might be expected, the rate of drain diffusion varies as $1/H$, in contrast to that of collision diffusion, which varies as $1/H^2$. On the whole, this type of diffusion is much more rapid than collision diffusion. A comparison of the three coefficients for diffusion along the field, perpendicular to the field by drain, and perpendicular to the field by collision, respectively, appears below for a mean free path of 1 cm, a field of 3,000 gauss, and an electron of 3 volts.

Along magnetic field	2.5×10^7
Perpendicular to magnetic field	
Drain diffusion	0.6×10^4
Collision diffusion	100

By use of the diffusion coefficient given in Eq. 74, the ratios $J_{e\perp}/J_+$ and $J_{e\perp}/J_{e\parallel}$ may be calculated using Eq. 69.

$$\frac{J_{e\perp}}{J_+} = \frac{\sqrt{D_z D_{\perp}} \left(1 + \frac{T_+}{T_e} \right) \frac{8a}{0.4}}{a^2 \sqrt{\frac{2kT_e}{m_+}} 2\pi}$$

with $D_z = 10^7 T_e^{5/2} / n_0$ and $D_{\perp} = 10^5 T_e / 16H$, where H is in thousands of gauss and T_e is in electron volts. This is now the coefficient of drain diffusion.

$$\frac{J_{e\perp}}{J_+} = \frac{1}{4} \sqrt{\frac{T_e^{7/2} \times 10^7 \times 10^5}{n_0 H T^4}} \times \frac{8}{2} \times \frac{271}{0.4 \times 6 \times 10^7} \quad (75)$$

$$\frac{J_{e\perp}}{J_+} = \frac{1}{4} \frac{10^6 T_e^{\frac{5}{4}}}{a \sqrt{H n_0}} \times \frac{271}{10^7} = 3.65 \frac{T_e^{\frac{5}{4}}}{a \sqrt{H n_0}} \quad (76)$$

Note that the dependence of T_e is somewhat stronger than it was in the case of drain diffusion. The dependence on H is, however, inversely as the square root of H , and the density of plasma no longer cancels out. Instead we have the ratio inversely proportional to the square root of n_0 . Finally, the most important difference is that the ratio is about ten times as large as that predicted by collision diffusion.

The ratio $J_{e\perp}/J_{e\parallel}$ is calculated according to Eq. 71.

$$\frac{J_{e\perp}}{J_{e\parallel}} = \frac{-2}{\pi} \ln \frac{4}{a \bar{v}_e} \sqrt{D_z D_\perp}$$

As we have seen,

$$\sqrt{D_z D_\perp} = \sqrt{\frac{T_e^{\frac{7}{2}}}{n_0 H}} \frac{10^6}{4}$$

$$\bar{v}_e \approx 10^8 \sqrt{T_e}$$

and therefore

$$\frac{J_{e\perp}}{J_{e\parallel}} = \frac{-2}{\pi} \ln \frac{4}{a \times 10^8 \sqrt{T_e}} \times \frac{10^6}{4} \sqrt{\frac{T_e^{\frac{7}{2}}}{n_0 H}} = -\frac{2}{\pi} \ln \frac{a}{10^2} \sqrt{\frac{T_e^{\frac{5}{2}}}{n_0 H}} \quad (77)$$

Finally

$$\frac{J_{e\parallel}}{J_+} = \frac{3.65 T_e^{\frac{5}{4}}}{a \sqrt{H n_0}} \frac{1}{\left(-\frac{2}{\pi} \ln \frac{a}{10^2} \sqrt{\frac{T_e^{\frac{5}{2}}}{n_0 H}} \right)} \quad (78)$$

6. COMPARISON OF THEORY AND EXPERIMENT

The objective in comparing theoretical predictions for $J_{e\perp}/J_+$ and $J_{e\perp}/J_{e\parallel}$ with the observed values of these ratios is mainly to account for their general order of magnitude, without too much concern for their detailed variation with arc conditions. Because these ratios depend on many quantities such as ion density, electron temperature,

and ion temperature, each of which is subject to fairly large uncertainties in measurement, the cumulative effects of errors in all these measurements may create wide deviations in any individual measurement. Considering also that the rate of drain diffusion depends on the amount of hash present, it is evidently unlikely that the precise values of these ratios have more than statistical significance. Hence the order of magnitudes will be used primarily to decide between the alternative theories of drain diffusion and collision diffusion. Secondly an effort will be made to determine whether there is a statistical correlation of the ratios in the same general direction as that predicted by theory.

6.1 Order of Magnitude. Experiments in the Annex arc disclose that the ratio of electron current in the perpendicular orientation to that in the parallel orientation varies from 1.5 to 2. The general order of magnitude for $J_{e\perp}/J_+$ is about 20 to 35, and the general order of magnitude of $J_{e\parallel}/J_+$ varies from 10 to 20. The 37-in. arc usually showed somewhat lower ratios than the Annex arc.

(a) Collision-diffusion Theory. For collision diffusion the predicted ratio of $J_{e\perp}/J_{e\parallel}$ is given by Eq. 72,

$$\frac{J_{e\perp}}{J_{e\parallel}} = \frac{-2}{\pi} \ln \left(\frac{2.6 \times 10^{-3} \sqrt{T_e}}{aH} \right)$$

The probe radius a is 0.15 cm; a typical magnetic field is 3,000 gauss, and a typical electron temperature is 3 volts. Because of the logarithmic dependence on all quantities involved, the ratio varies so little with arc conditions that the above typical values may be used in practically any situation likely to be met with in practice. For example,

$$\left(\frac{J_{e\perp}}{J_{e\parallel}} \right)_{\text{collision}} = 2.85 \quad (79)$$

The predicted ratio is thus somewhat too large. Because of the logarithmic dependence on the parameters involved, a small error in the ratio indicates a large error in diffusion coefficients.

The ratio $J_{e\perp}/J_+$ predicted by collision-diffusion theory is given by Eq. 70, Sec. 5.

$$\frac{J_{e\perp}}{J_+} = \frac{0.95 \left(1 + \frac{T_+}{T_e} \right) \sqrt{T_e}}{aH}$$

Using the same values of T_e , a , and H , and assuming the reasonable value for T_+ of 1 volt,

$$\left(\frac{J_{e\perp}}{J_+} \right)_{\text{collision}} = 4.8 \quad (80)$$

This ratio is about five or six times less than the experimentally observed ratios.

With the ratio for $J_{e\parallel}/J_+$, the disparity between theory and experiment is even greater. Thus

$$\left(\frac{J_{e\parallel}}{J_+} \right)_{\text{collision}} = 1.68 \quad (81)$$

The theoretical predictions using collision diffusion alone are thus about ten times too low. Since the low values of $J_{e\parallel}/J_+$ arise from the very low rate of diffusion across the magnetic field by collision alone, the actual diffusion must be brought about mainly by processes much more effective than collision.

(b) Drain-diffusion Theory. For drain diffusion, the predicted ratio $J_{e\perp}/J_{e\parallel}$ is given by Eq. 77:

$$\left(\frac{J_{e\perp}}{J_{e\parallel}} \right)_{\text{drain}} = \frac{-2}{\pi} \ln \left[\frac{10^{-2}}{a} \frac{T_e^{\frac{5}{4}}}{(n_0 H)^{\frac{1}{2}}} \right]$$

Using the typical values of T_e and a , and assuming $n_0 = 3 \times 10^{12}$, a more or less typical value,

$$\left(\frac{J_{e\perp}}{J_{e\parallel}} \right)_{\text{drain}} = 1.55 \quad (82)$$

The predicted ratio is thus of the correct order of magnitude. To find $J_{e\perp}/J_+$, use Eq. 76,

$$\left(\frac{J_{e\perp}}{J_+} \right)_{\text{drain}} = \frac{3.65 T_e^{\frac{5}{4}} \left(1 + \frac{T_+}{T_e} \right)}{a H^{\frac{1}{2}} n_0^{\frac{1}{2}}}$$

With the typical values of parameters and with T_+ negligible,

$$\left(\frac{J_{e\perp}}{J_+} \right)_{\text{drain}} = 26.3 \quad (83)$$

This is actually of the order of magnitude found in the Annex arc.

Finally,

$$\left(\frac{J_{e\parallel}}{J_+} \right)_{\text{drain}} = 16.8 \quad (84)$$

Once again the correct order of magnitude is obtained with the drain-diffusion theory.

In summary it can be said that the order of magnitude of the observed ratios $J_{e\parallel}/J_+$ and $J_{e\perp}/J_{e\parallel}$ agrees satisfactorily with the drain-diffusion theory, but collision diffusion gives results that are too small.

(c) Variation with Plasma Conditions. A study of the data indicates that the plasma condition undergoing widest variation in our series of measurements of $J_{e\perp}/J_+$ was the ion density. Since collision diffusion suggests that $J_{e\perp}/J_+$ is independent of ion density, whereas the drain-diffusion theory predicts a dependence as $1/\sqrt{n_+}$, the first study was made by plotting $J_{e\perp}/J_+$ against $1/\sqrt{n_+}$ for the pressures of 4, 8, 20, and 200 μ a. There was so little variation between 4 and 8 μ a results that they are included on the same graph. Because of the variability of the electron temperature and hash conditions, we do not expect a definite curve. However, we do expect a general tendency for the ratio $J_{e\perp}/J_+$ to increase with increase of $1/\sqrt{n_+}$ and therefore with decrease of n_+ . This increase is due to the increase of the mean free path in the Z direction with a drop in the plasma density. In order to take into account the effect of electron temperature, all points for which the temperature is above average are plotted with circles, and those below average, with triangles. If the probe theory is correct, there should be a statistical tendency for the circle points to be above the triangle points, at a given value of $1/\sqrt{n_+}$.

In Figs. 2.24, 2.25, and 2.26, the ratio $J_{e\perp}/J_+$ is plotted against $1/\sqrt{n_+}$ for pressures of 4 to 8×10^{-4} mm Hg in Fig. 2.24, 2×10^{-3} mm Hg in Fig. 2.25, and 2×10^{-2} mm Hg in Fig. 2.26. In Figs. 2.24 and 2.25, a general tendency is seen for the ratio to fall off as $1/\sqrt{n_+}$ goes to zero. In Fig. 2.26 this tendency is not present. As will be seen later, the flat behavior at 200 μ a is due to the fact that the neutral atoms are as important as the ions in scattering. Meanwhile in accordance with theory it will be noted that the circle points tend to be above the triangle points for a given value of $1/\sqrt{n_+}$. Thus the

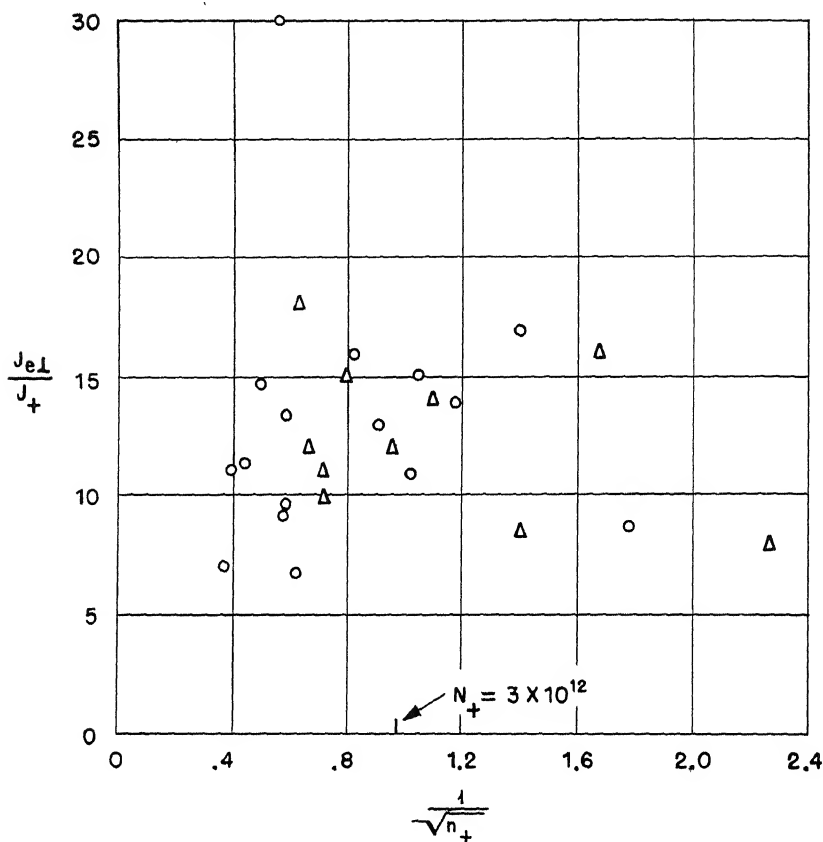


Fig. 2.24—Plot of $J_{e\perp}/J_+$ vs. $1/\sqrt{n_+}$, small arc (argon). Pressure, 4 to 8×10^{-4} mm Hg; \circ , $T_e \geq +3$; \triangle , $T_e \leq +3$.

correlations between $J_{e\perp}/J_+$ and n_+ and T_e are at least qualitatively in agreement with the theory. The theoretically predicted tendency of the ratio to rise with decreasing ion density accounts for the main part of the observed rise of the ratio as the probe is moved away from the arc column (see Sec. 1).

In Figs. 2.27 and 2.28, $J_{e\perp}/J_+$ is again plotted against $1/\sqrt{n_+}$, but this time in order to find correlations with arc current. The squares represent arc currents of 3 amp, the triangles 1.5 amp, and the circles 0.5 amp. We see a general tendency for the high arc currents to be above the low arc currents for a given $1/\sqrt{n_+}$. This is quite reasonable, since a high arc current is likely to be associated with more hash, and thus with an increase of drain diffusion, which gets the electrons to the probe.

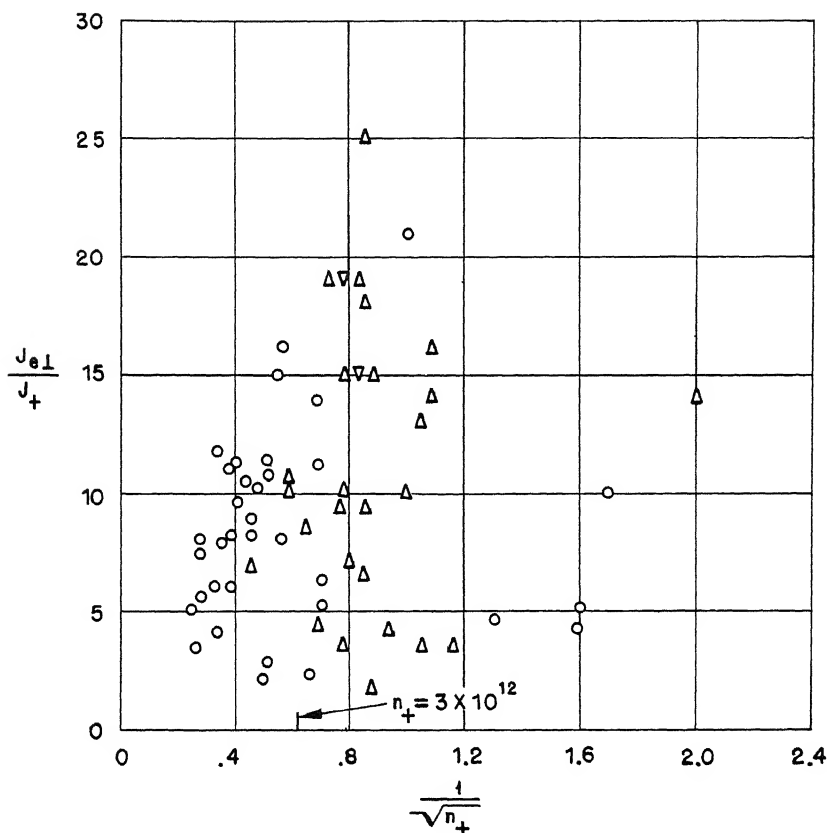


Fig. 2.25—Plot of $J_{e\perp}/J_+$ vs. $1/\sqrt{n_+}$, small arc (argon). Pressure, 2×10^{-3} mm Hg; O, $T_e \geq 2.4$; Δ , $T_e \leq 2.4$.

Although the ratios are subject to so much error in measurement and so much unpredictability arising from hash that their precise values cannot be compared within a factor of 2, it is nevertheless interesting to see whether Eq. 76 predicts the correct general variation of ratio with plasma conditions, at least statistically. For this reason an effort has been made to test for the constancy of the ratio

$$Q = \frac{J_{e\perp}}{J_+} \times \frac{aH^{\frac{1}{2}}n_0^{\frac{1}{2}}}{T_e^{\frac{5}{4}} \left(1 + \frac{T_+}{T_e}\right)}$$

According to the above-mentioned equation, drain-diffusion theory predicts that this ratio is constant. There are some difficulties in

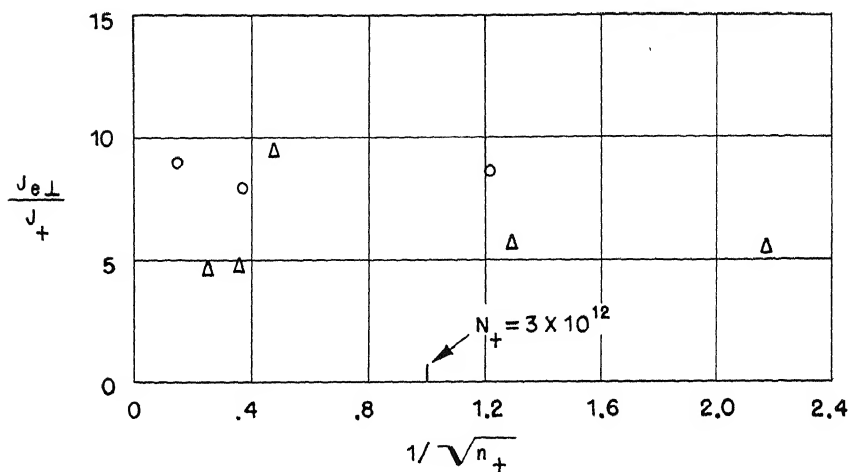


Fig. 2.26—Plot of $J_{e\perp}/J_e$ vs. $1/\sqrt{n_+}$, small arc (argon). Pressure, 2×10^{-2} mm Hg; O, $T_e \geq 0.6$; Δ , $T_e \leq 0.6$.

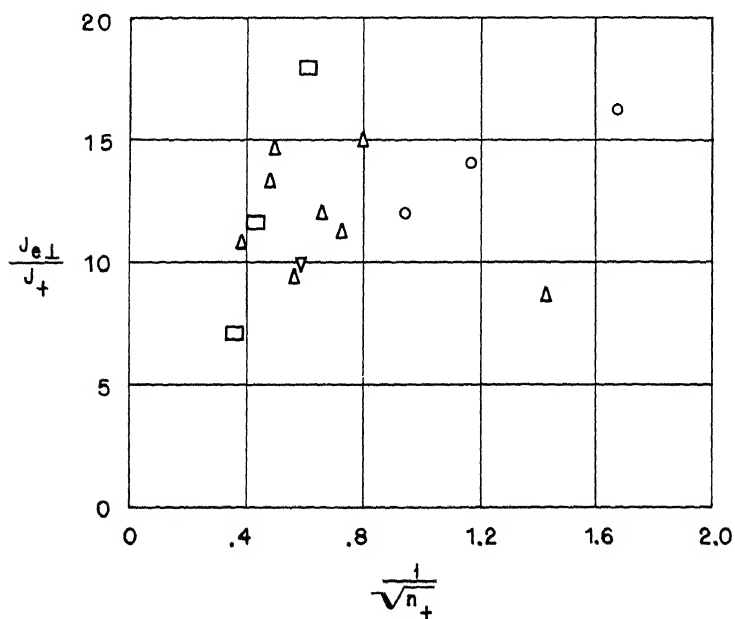


Fig. 2.27—Plot of $J_{e\perp}/J_e$ vs. $1/\sqrt{n_+}$, small arc (argon). Pressure, 8×10^{-4} mm Hg; magnetic field, 3,700 gauss; arc current: \square , 3 amp; Δ , 1.5 amp; O, 0.5 amp.

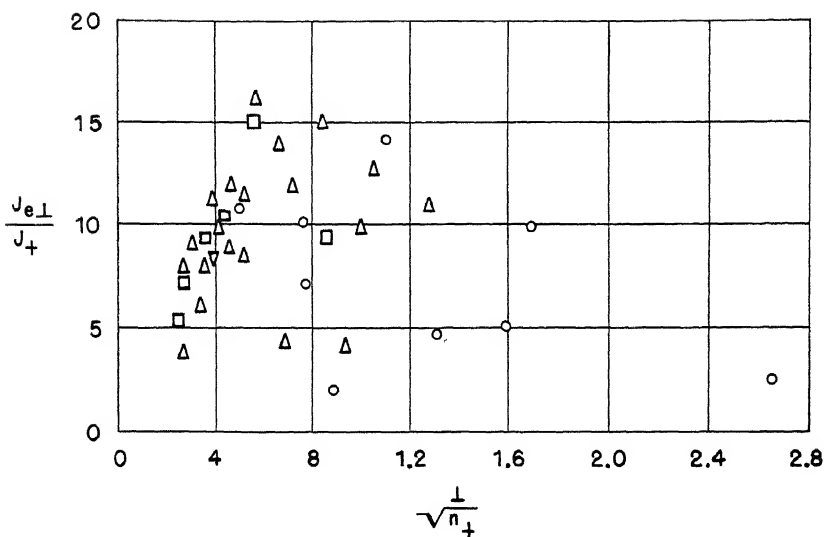


Fig. 2.28—Plot of $J_{e\perp}/J_e$ vs. $1/\sqrt{n_+}$, small arc (argon). Pressure, 2×10^{-3} mm Hg; magnetic field, 3,700 gauss; arc current: \square , 3 amp; \triangle , 1.5 amp; \circ , 0.5 amp.

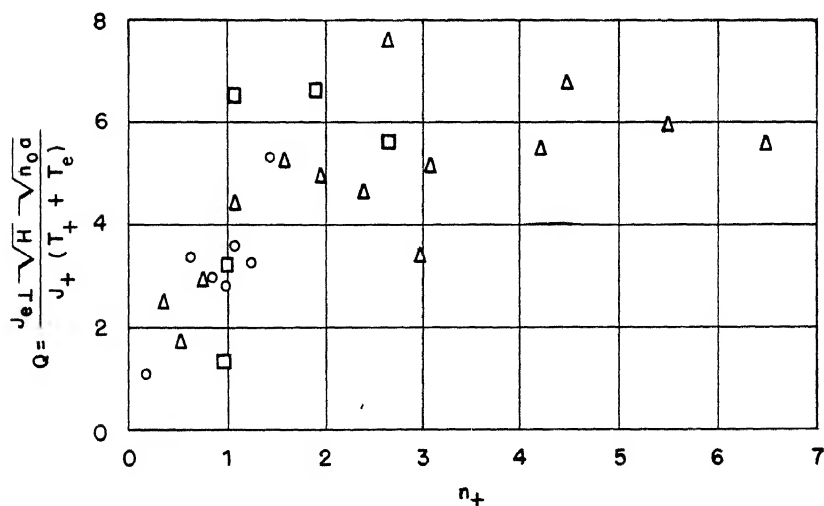


Fig. 2.29—Plot of Q vs. n_+ , small arc (argon). \circ : pressure, 4×10^{-4} mm Hg; magnetic field, 3,700 gauss. \triangle : pressure, 8×10^{-4} mm Hg; magnetic field, 3,700 gauss. \square : pressure, 8×10^{-4} mm Hg; magnetic field, 11,000 gauss.

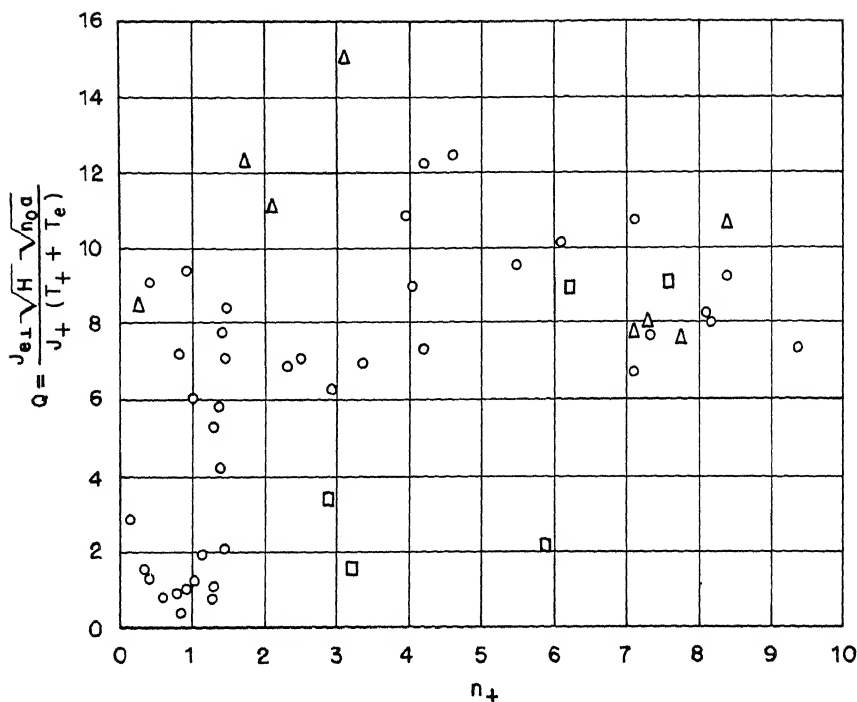


Fig. 2.30—Plot of Q vs. n_+ , small arc (argon). \circ : pressure, 2×10^{-3} mm Hg; magnetic field, 3,700 gauss. Δ : pressure, 2×10^{-3} mm Hg; magnetic field, 11,400 gauss. \square : pressure, 2×10^{-2} mm Hg; magnetic field, 3,700 gauss.

evaluating Q , since we do not know T_+ . We have assumed that T_+ is equal to the kinetic energy gained by an ion in falling from the arc column to the point at which the probe is located. This is obtained as the difference in space potentials at the two points. Because of the difficulty of exact measurement of space potential, the average over a large number of measurements was taken, and the same average used at a given probe position in all individual cases. Furthermore, because the measurement of T_e is rough, $T_e^{\frac{5}{4}}$ was replaced by T_e , since the effect of $T_e^{\frac{1}{4}}$ could hardly have been noticed. In Fig. 2.29, Q is plotted against n_+ for pressures of $4 \mu a$ and $8 \mu a$, and in Fig. 2.30, Q is plotted for pressures of $20 \mu a$.

The scattering of points is not too bad in Fig. 2.29, but in Fig. 2.30 there is very little definite behavior of any kind. Let us therefore look at Fig. 2.29 first. If the theory is correct, Q should be constant. Actually it approaches constancy at high ion densities, falling off as the ion density drops below 5×10^{12} . Before it falls, the results begin

to scatter. Apparently the simple drain-diffusion theory is adequate at high ion density but inadequate at too low a density. There are several possible reasons. First the electron sheath around the probe may become so large that electron collection across the field is greatly impeded, thus bringing $J_{e\perp}/J_+$ and hence Q down. The electron sheath around the probe is about forty times as large as the ion sheath. It is interesting that at an ion density of 5×10^{12} this sheath becomes about as large as the probe (see Eq. 23 in Sec. 4). Secondly the hash mechanism for drain diffusion may fail at too low an ion density.

With these considerations some order can be brought into the chaos appearing in Fig. 2.30. Evidently, for high n_+ , Q approaches a more or less constant value, which is about the same as that approached in Fig. 2.29. At low density the hash mechanism for electron diffusion is probably unreliable and very variable. Because of the known variability of drain diffusion with arc current alone, the points for Q would be expected to scatter considerably.

Finally, consider again Fig. 2.26, which shows an anomalous tendency for $J_{e\perp}/J_+$ to remain constant with n_+ . For the pressure of $200 \mu a$, at which these measurements were taken, the mean free path for electron collisions with neutral atoms becomes about equal to that for electron-electron and electron-ion collisions, namely, about 1 cm. Thus the plasma density no longer plays a critical role in determining the mobility in the Z direction. Since the pressure remains constant, the ratio should not vary much with plasma density.

7. CONCLUSION

The drain-diffusion theory gives a good account of the order of magnitude of electron currents to a probe in a magnetic field. Its detailed predictions, however, are only partially verified. The difficulty of accounting for the detailed variations of this ratio probably arise from the fact that it depends rather strongly on the state in which the arc is running, particularly with regard to the hash, which has a strong effect on the rate of diffusion of electrons across the magnetic field.

ACKNOWLEDGMENTS

The help and cooperation of the following persons made this work possible: Dr. J. Backus allowed the authors in their first measurements to use his experimental setup, with which he had already made the first probe measurements in an argon arc. H. Tomlinson, J. Morris, and D. Stanley afforded technical assistance, without which

the measurements would scarcely have been possible. R. Williams sorted and prepared some of the graphs and assisted in making observations. W. Berkey and Dr. L. Aller assisted in making some of the observations. A. Horn furnished mathematical assistance in the solution of several equations. Mrs. Jane Jones analyzed a great number of probe characteristics.

REFERENCES

1. J. L. Spencer-Smith, *Phil. Mag.*, 19: 806 (1935).
2. G. N. Rokhlin, *J. Phys. U.S.S.R.*, 1: 347 (1939).
3. G. Spivak and E. Reichrudel, *Tech. Phys. U.S.S.R.*, 5: 715 (1938).
4. L. Tonks and I. Langmuir, *Phys. Rev.*, 34: 876 (1929).
5. W. R. Smythe, "Static and Dynamic Electricity," pp. 111-112, McGraw-Hill Book Company, Inc., New York, 1939.

Chapter 3

MINIMUM IONIC KINETIC ENERGY FOR A STABLE SHEATH

By David Bohm

Characteristic of a plasma is its tendency to maintain itself in a neutral and field-free state in spite of any forces or processes tending to change it. A common example of this property is its ability to envelop any electrode not at plasma potential with a sheath that is able to shield the plasma region from the strong fields that would otherwise be caused by such an electrode. Although the shielding is so good that the sheath edge is very nearly at plasma potential, it is not quite perfect, and a small portion of the potential drop between electrode and plasma may penetrate beyond the sheath edge. In order to understand and predict ion distributions in an arc, it is evidently necessary to know just what determines the extent to which such penetration occurs. In this chapter it will be shown that the potential penetration must be such as to accelerate ions to a velocity corresponding to half the mean electron kinetic energy. This criterion is not exact, however, because it depends somewhat on the distribution of ionic velocities at the sheath edge. Yet, within 20 or 30 per cent it applies in practically all cases.

In order to derive the above criterion, it is helpful to consider in some detail the processes by which a steady state of electron and ion distribution in an arc is maintained¹ (see also Chaps. 2, 4, and 9). When a neutral atom is ionized, secondary electrons are liberated with many volts of kinetic energy and ions with practically none. Because of their rapid motion, electrons collect on the walls, charging them negatively. This negative charge has two effects: (1) it repels electrons; (2) it attracts ions, which fall to the wall as a result of the electric fields in which they happen to find themselves when they are formed. Meanwhile, by frequent collision, the electrons attain an approximately Maxwellian distribution with a temperature of 2 to 4 volts. In order to produce a steady state, ions and electrons must

reach the walls at a rate equal to that at which they are formed. This happens automatically with the ions, which simply fall into the walls quite steadily. As for the electrons, however, they strike the walls so often that the majority must be repelled if the distribution is to be steady. The potential of the wall finally adjusts itself to such a value that the number of electrons energetic enough to go over the barrier is equal to the number produced. This value is usually about 10 volts negative relative to the plasma. Most of this potential drop occurs not in the plasma but across the wall sheath. In fact, as shown later, potential drops much larger than half the electron temperature cannot usually exist stably in the plasma itself.

In the plasma region it is quite easy to see why no appreciable potential drops can occur, because if they did the electrons would soon redistribute themselves in such a manner that the potential drops would be destroyed. Potential changes that are not too large compared to the mean electron kinetic energy can be maintained, however, because these are not strong enough to bring about appreciable redistribution of electrons. But near a highly negative electrode, such as a wall or a negative probe, very few electrons have energy enough to penetrate. Here the ions are mostly positive, moving under the influence of their own space charge. Because the ion density is usually quite high, the entire potential drop between electrode and plasma can be sustained in a very small positive-ion sheath, usually less than a millimeter in thickness. The sheath thickness is obtained by using the well-known formula for the distance between two electrodes carrying a given space-charge-limited current, with the plasma considered as emitting electrode and the probe as collector.

$$x \sim \frac{V^{\frac{3}{4}}}{j^{\frac{1}{2}}} \quad (1)$$

where V is the potential between the electrodes, in volts; j is the space-charge-limited current, in amperes per square centimeter; and x is the electrode distance, in centimeters.

The above formula assumes that the potential and the electric field at the sheath edge are exactly zero. Actually it is known that some potential penetrates into the plasma, but not much. In order to find the exact magnitude and distribution of the fields that do penetrate, it is necessary to know what processes are involved in the production of ionization and in its diffusion to the walls. When the balance is expressed mathematically between ion production and diffusion, there is obtained what Langmuir¹ calls the "plasma-sheath" equation. The solutions of this equation contain an approximately neutral field-free

region, stretching over most of the container but changing with surprising rapidity into a sheath region at a distance from the wall given approximately by Eq. 1. In general, the potential resembles that shown in Fig. 3.1.

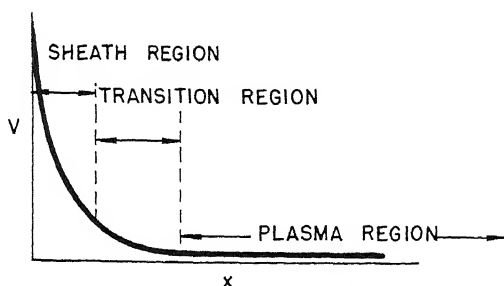


Fig. 3.1 — The variation of potential near the wall; V is the negative of the potential.

Within the plasma region a very gradual change in potential takes place. Although there is no precise point at which the sheath begins, there is a transition region in which the plasma region, characterized by the stability of the neutral state of zero field, is in a short distance replaced by the sheath region, characterized by negligible electron density.

Although the problem of potential penetration into the plasma can be treated exactly, such a treatment is always very complex. In order to obtain a simple and useful qualitative picture, the exceedingly complex processes actually occurring in the arc will be represented by a simplified model, which nevertheless retains all features important for the qualitative understanding of sheath stability. The simplified model retains the necessary features, owing to the fact that plasma fields, compared with sheath fields, are so small that they produce negligible changes of potential over distances many sheath thicknesses in extent. To a first approximation, therefore, it may be assumed that the plasma potential is constant, at least in so far as the processes involved in sheath formation are concerned. However, the plasma fields cannot be completely neglected, because over the long distances that they cover they are able to accelerate positive ions up to appreciable energies, of the order of the plasma electron temperature. In the approximation that is used here, however, the role of these fields may be taken into account by assuming that they provide ions at the sheath edge with some mean energy equal to eV_0 . Although there may actually be a distribution of energies, it will be

seen later that for qualitative purposes the distribution can be replaced by a stream of ions, all of which possess the mean energy of the distribution. There remains only a small uncertainty in V_0 , arising from the lack of exact definition of the sheath edge. This uncertainty is, however, quite unimportant, because of the smallness of plasma fields.

The problem is thus replaced by a considerably simpler one. If in Fig. 3.1 attention is fixed on a region not more than several sheath thicknesses in extent, a potential is obtained which resembles that shown in Fig. 3.2.

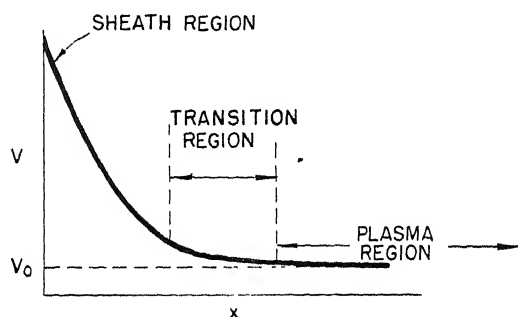


Fig. 3.2—Potential variation near the sheath.

To a first approximation, as pointed out in the previous paragraph, the change in plasma potential beyond the sheath edge may be neglected, assuming that deep inside the plasma the potential approaches V_0 and that the electric field approaches zero.

In deriving the plasma-sheath equation for this simple case, the first step is to put down Poisson's equation.

$$\nabla^2 V = 4\pi e(n_+ - n_e) \quad (2)$$

where n_+ is the ion density and n_e is the electron density. Since the electrons are approximately in thermal equilibrium,

$$n_e = n_0 \exp \frac{-e(V - V_0)}{kT_e} \quad (3)$$

where T_e is the electron temperature and k is Boltzmann's constant. The factor of $(V - V_0)$ in the exponential indicates that near the sheath edge, where $V = V_0$, the electron density is n_0 .

The value for n_+ is found from the current density by $J_+ = n_+ \times v_+$, where v_+ is the velocity of positive ions.

Since the ions have a kinetic energy eV , their velocity is

$$v_+ = \sqrt{\frac{2eV}{m_+}}$$

and their current density, which must be the same at all points, is

$$J_+ = n_+ \sqrt{\frac{2eV}{m_+}} = n_0 \sqrt{\frac{2eV_0}{m_+}}$$

so that

$$n_+ = n_0 \sqrt{\frac{V_0}{V}} \quad (4)$$

Equation 4 shows that ionic density drops as ions are accelerated. Substituting Eqs. 3 and 4 in Poisson's equation, gives

$$\frac{\partial^2 V}{\partial x^2} = 4en_0\pi \left[\sqrt{\frac{V_0}{V}} - \exp \frac{-e(V - V_0)}{kT_e} \right] \quad (5)$$

This is the plasma-sheath equation. Multiplying Eq. 5 by $\partial V / \partial x$ and integrating,

$$\frac{1}{2} \left(\frac{\partial V}{\partial x} \right)^2 = 4\pi n_0 e \left[2\sqrt{V_0 V} + \frac{kT_e}{e} \exp \frac{-e(V - V_0)}{kT_e} \right] + C \quad (6)$$

The constant of integration is obtained by setting $\partial V / \partial x = 0$ when $V = V_0$. Although there is no precise point at which the sheath begins, it is known that in the plasma near the sheath edge the fields are so small that the potential remains close to V_0 over a distance several sheath thicknesses in extent. Thus the simplified boundary condition is used; i.e., as the plasma is entered, the field disappears and the potential approaches V_0 . Equation 6 then becomes

$$\left(\frac{\partial V}{\partial x} \right)^2 = 8\pi n_0 e \left\{ 2V_0 \left(\sqrt{\frac{V}{V_0}} - 1 \right) + \frac{kT_e}{e} \left[\exp \frac{-e(V - V_0)}{kT_e} - 1 \right] \right\} \quad (7)$$

Because $(\partial V / \partial x)^2 \geq 0$, a condition can be found that V_0 must satisfy if plasma solutions of zero field are to be obtained as $V \rightarrow V_0$. When V is large, the right-hand side of Eq. 7 is obviously positive. To study the behavior of this member when V is close to V_0 , it is expanded as a power series in $\Delta V = V - V_0$. The first two terms vanish, and the third term is

$$\frac{1}{8\pi n_0 e} \left(\frac{\partial V}{\partial x} \right)^2 = \frac{1}{2} \left(\frac{e}{kT_e} - \frac{1}{2V_0} \right) (\Delta V)^2 \quad (8)$$

Evidently solutions are possible only if

$$\frac{e}{kT_e} \geq \frac{1}{2V_0}$$

or

$$V_0 \geq \frac{kT_e}{2e}$$

Thus it is shown mathematically that a stable sheath is possible only when ions reach the sheath with a kinetic energy at least half the electron temperature.

Leaving aside temporarily the physical significance of the above result, the exact solution to Eq. 7 may be considered. In Figs. 3.3 and 3.4, respectively, are graphs of V obtained by numerical integration of Eq. 7 for $V_0 = 1.5kT_e/2e$ and for the critical case of $V_0 = kT_e/2e$. The solution has been carried to $V = 104$ volts, with an assumed electron temperature of 4 volts and an ion density of 4×10^{12} ions per cubic centimeter.

It is characteristic of these solutions that within the plasma itself the penetration of sheath potential dies off rapidly in exponential fashion. As the sheath region is entered, however, the potential climbs rapidly, ultimately reaching an $x^{\frac{1}{2}}$ variation characteristic of unneutralized space-charge-limited current flow. In the transition region the electron density dies out rapidly. Thus in the first case it drops to practically zero in the region from 0.07 to 0.04 cm from the 100-volt electrode, whereas in the second case (Fig. 3.4) it does the same in the region from 0.08 to 0.04 cm. The transition between plasma and sheath is thus very sharp, extending only 0.3 to 0.4 mm.

In considering what happens when $V_0 < kT_e/2e$, the right-hand side of Eq. 5 maybe expanded as a power series in ΔV , keeping only the first power.

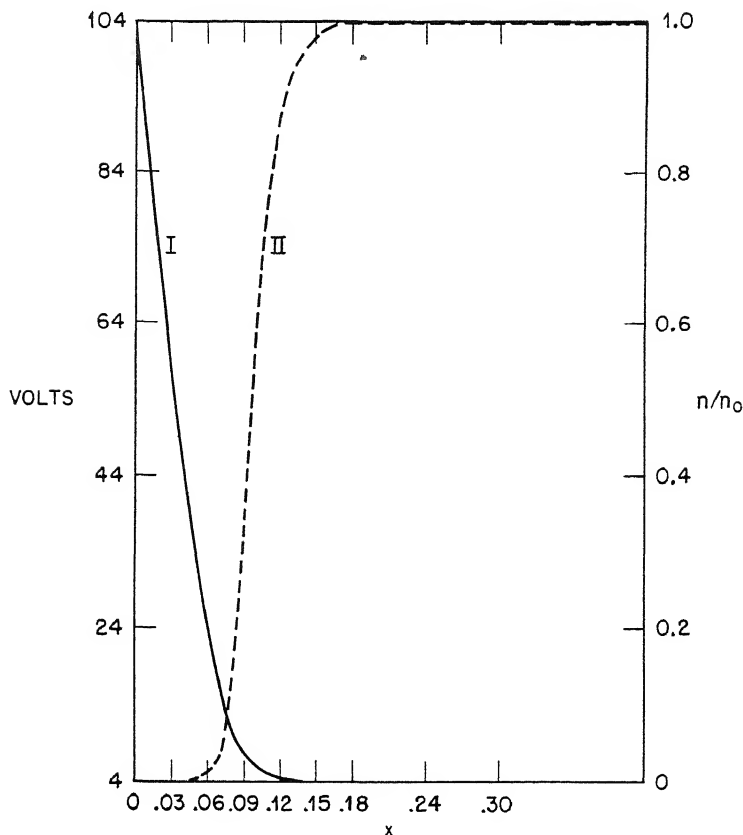


Fig. 3.3—Potential and electron density in sheath region and region joining sheath and plasma ($V_0 = 1.5kT_e/2e$). Curve I, potential vs. distance; curve II, electron density (n/n_0) vs. distance.

$$\frac{\partial^2(\Delta V)}{\partial x^2} \approx 4\pi n_0 e \left(\frac{e}{kT_e} - \frac{1}{2V_0} \right) \Delta V$$

When $V_0 < kT_e/2e$, the coefficient of ΔV is negative, and the solutions are oscillatory; but, if $V_0 > kT_e/2e$, the coefficient is positive, and the solutions are exponentials. If the solutions are oscillatory, it is impossible for the voltage to increase indefinitely, as would be required for sheath formation. With exponential behavior of ΔV , however, it is seen that ΔV can join onto a sheath solution when it becomes large. In fact, Figs. 3.3 and 3.4 show that for small ΔV the

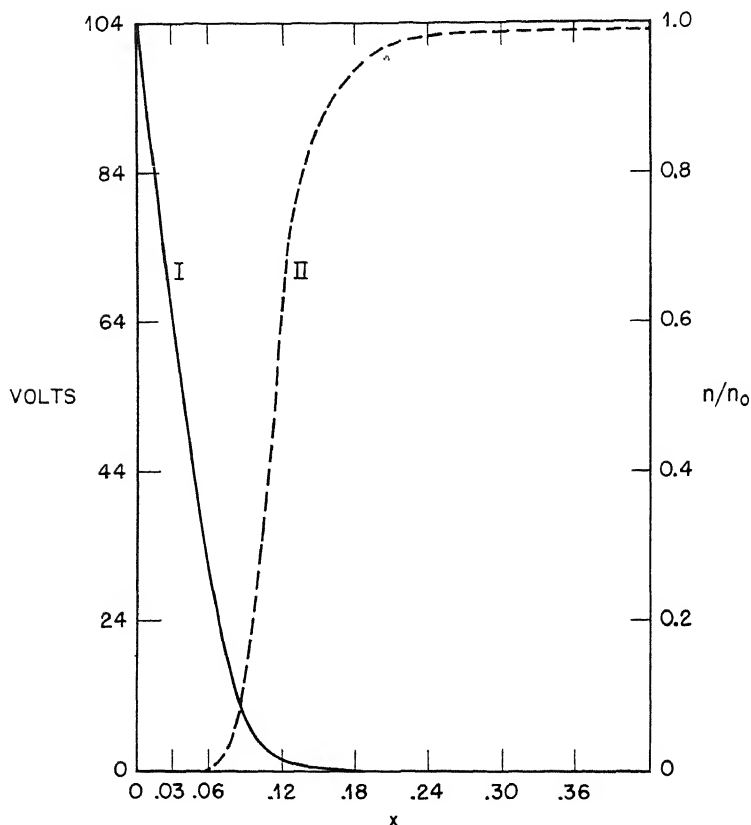


Fig. 3.4—Potential and electron density in sheath region and region joining sheath and plasma ($V_0 = kT_e/2e$). Curve I, potential vs. distance; curve II, electron density (n/n_0) vs. distance.

exact solution is approximately exponential and does join smoothly to a sheath.

It may be seen physically why the potential oscillates when $V_0 < kT_e/2e$. The electron charge density is $n_e = n_0 \exp [-e(V - V_0)/kT_e]$. Expanding for small ΔV , the equation becomes

$$n_e \approx n_0 \left(1 - \frac{e \Delta V}{kT_e} \right) \quad (9)$$

The ion density is

$$n_+ = n_0 \sqrt{\frac{V_0}{V}} = n_0 \sqrt{\frac{V_0}{V_0 + V}} \approx n_0 \left(1 - \frac{1}{2} \frac{\Delta V}{V_0} \right) \quad (10)$$

Their difference is

$$\rho = n_+ - n_e = n_0 \Delta V \left(\frac{e}{kT_e} - \frac{1}{2V_0} \right) \quad (11)$$

Thus, if an ion is accelerated so that it gains an energy ΔV , the electron density drops as shown in Eq. 10 because the forces that attract ions must repel electrons. The ion density also drops because ions speed up while ion current remains constant. When $V_0 < kT_e/2e$, the ion density drops more than the electron density, thus causing an excess of negative charge to develop whenever positive charges are accelerated. The excess negative charge ultimately overcomes and reverses the initial accelerating force, giving rise to an oscillatory potential. To sum up, it might be said that the very ease with which slow ions are accelerated leads to an excess negative charge, which ultimately prevents further acceleration. If, however, $V_0 > kT_e/2e$, then the ion density drops less rapidly than electron density, and an accelerating potential may be built up.

On the basis of the above results the question may be raised as to what happens to ions at a sheath edge if $V_0 < kT_e/2e$. Aside from the possibility of oscillatory or unstable sheaths, the difficulty may be resolved by taking into account the small accelerating forces inside the plasma, which automatically adjust themselves to bring the ions up to at least the critical velocity given above. The reason such small accelerating forces may exist is that some additional processes are going on inside the plasma. These produce no appreciable effect near the sheath edge but over a long distance may add up to produce a large effect. For example, in the more complete Langmuir theory the fact that ionization is usually occurring in the body of the plasma is taken into account. With the aid of this ionization the excess negative space charge resulting from acceleration of positives can be neutralized. Because the rate of creation of ions is small, however, only small excesses may be neutralized in this manner, and the plasma fields must likewise be small. Another example is treated in Chap. 2, i.e., a small, highly negative probe that is able to draw in ions from great distances by means of the residual fields penetrating into the plasma. This process of concentrating the ions is able to supply enough excess positive charge to make up the deficit otherwise resulting from acceleration. In other situations, still other ways exist by which slow acceleration of plasma ions inside the plasma is made possible. In any case, however, these slow processes tend to adjust themselves in such a way that ions are brought up to about half the mean electron kinetic energy, after which a sheath is formed.

These results may be summarized from another viewpoint in order to make their meaning clearer. A plasma is characterized by an ex-

tremely great stability of the neutral state of zero field. This stability is brought about through the agency of electrical forces between the particles comprising the plasma, which forces normally operate in such a way as to oppose automatically any deviation from equilibrium conditions. As long as the positive ions have a mean kinetic energy less than half the electron temperature, these stabilizing forces, necessarily accompanying any effort to accelerate ions, are so strong that they can neutralize and reverse the accelerating fields in a short distance. Whether such attempts to destroy the plasma result from externally applied fields or from chance fluctuations, it has been shown that they cannot succeed when the ionic velocity is too low. To the extent that additional space charge is supplied slowly by such processes as ionization or concentration of ions into a small space, however, a slow but steady acceleration of ions may take place within the plasma region, which, nevertheless, retains its property of weak fields and approximate neutrality.

As soon as, by one means or another, the mean ionic energy has been brought up to half the electron temperature, a new condition prevails. No longer do electrostatic fields between charges tend to restore the system to the neutral field-free plasma state when it is disturbed, but instead these forces lead to instability. Thus a small fluctuation tending to increase the acceleration slightly will now produce an excess of positive charge, which causes the potential to increase still further. If V_0 becomes as large as $kT_e/2e$, the electron density drops even more rapidly with the voltage because it is exponential in its dependence. A small fluctuation therefore leads to a cumulative series of processes, all tending to increase the size of the fluctuation and lower the electron density even more rapidly. Within a short distance all electrons can thus be repelled, and a transition between plasma and sheath regions is brought about by self-multiplying actions that build up in almost explosive fashion.

Although the sheath edge cannot be given a precise definition, it is clear from the foregoing description that, once V_0 grows larger than $kT_e/2e$, a qualitative change takes place since the plasma behavior ceases to be stable, and instead the sheath behavior becomes stable. Because the electric forces are very large they are able to bring about in a short distance a change from plasma to sheath, once the plasma becomes unstable. Thus it may be said roughly that a sheath begins when $V_0 = kT_e/2e$, remembering that this means that beyond this point the potential begins to climb rapidly and the electron density to drop very rapidly.

REFERENCE

1. I. Langmuir, *Phys. Rev.*, 34: 876 (1929).

Chapter 4

THEORETICAL CONSIDERATIONS REGARDING MINIMUM PRESSURE FOR STABLE ARC OPERATION

By David Bohm

1. INTRODUCTION

Surrounding the filament is a double sheath containing ions drifting in from the plasma and electrons emitted thermally by the filament. The maximum electron current that can be drawn from this sheath is

$$J_e = \gamma \sqrt{\frac{m_+}{m_e}} J_+ \quad (1)$$

where m_+/m_e is the ratio of ionic to electronic mass, J_+ is the positive-ion current reaching the sheath from the plasma, and γ is a correction factor depending on the age of the filament and varying from $\frac{1}{3}$ to $\frac{2}{3}$.

Equation 1 provides an upper limit to electron emission from the filament. When the number of ions returning to the filament per electron emitted falls below this limit, the arc will become hashy or go out. Since the rate of generation of ions is proportional to pressure, there will be a minimum pressure below which the arc does not function properly because too few ions reach the filament sheath to satisfy the requirements of Eq. 1.

There are two factors determining the value of this minimum pressure: (1) the number of ions generated per electron, and (2) the fraction of these ions reaching the filament sheath. Any process increasing either of these quantities will decrease the pressure required for stable operation. A great deal of work, both theoretical and experimental, has been done on both factors mentioned above. In Secs. 3 to 5 of this chapter enough of the results of the detailed work are quoted to discuss the minimum operating pressure for the argon arc.

If the arc meniscus is brought closer than a certain critical distance d , which is specified in Sec. 6, it begins to rob the arc column of ions so rapidly that the fraction reaching the filament sheath is reduced, and the minimum operating pressure is raised.

At present the main factor determining minimum pressure of operation of an arc in a magnetic field is the appearance of "flopping hash," a form of instability resulting from the fact that the arc is on the verge of going out altogether. An important cause of such low-pressure instability is that the positive-ion density becomes too low for maintenance of a filament sheath. In this chapter the processes governing ion supply to the filament sheath are studied, and the minimum running pressure of the argon arc is accounted for in terms of known ion distributions in the plasma. Several methods for decreasing this minimum are suggested, among which are the reflecting anode, positive block potentials, increase in size of the filament, and, finally, feeding gas at high pressure into a gastight compartment surrounding the filament.

2. DOUBLE SHEATH AT FILAMENT

In order to illustrate better the origin of ion-supply limitation of the arc current at the filament sheath, consider first the problem of accelerating electrons when no plasma is present. The space-charge-limited current is given by the well-known formula

$$j = \frac{V^{\frac{3}{2}}}{9\pi x^2 \sqrt{m/2e}} = 0.00235 \frac{V^{\frac{3}{2}}}{x^2}$$

where j is current density in amperes per square centimeter, V is voltage in units of 100 volts, x is distance in centimeters to negative electrode, and m and e are, respectively, the electron mass and charge.

In a typical case it is desired to draw an electron current of about 5 amp/sq cm at about 100 volts. This gives a value of x equal to 2.17×10^{-2} cm. Clearly it is impracticable to construct a grid so close to the filament. Instead, advantage is taken of the ability of the plasma to surround a negative electrode with a sheath, which causes the plasma itself to become the accelerating electrode (Figure 4.1).

However, it will be shown that the maximum arc current that can be drawn when the plasma is used in this way is limited by the positive-ion current in the sheath. Qualitatively the source of this limitation can be understood with the aid of a somewhat more detailed analysis appearing below. At the plasma-sheath boundary the electric field

must be zero, since the plasma is not able to sustain appreciable potential drops. On the other hand, if a space-charge-limited electron current is drawn, the field is likewise zero at the filament surface. Because no lines of force enter or leave the sheath in this case there must be an equal number of electrons and ions in it. The electrons, however, are concentrated near the filament where they move the slowest, and the ions are similarly concentrated near the plasma boundary. Thus there is a sort of electron-ion double layer, as shown in Fig. 4.2.

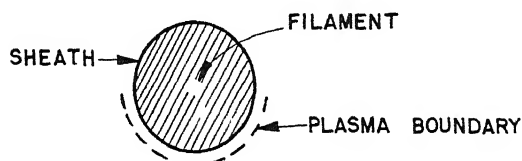


Fig. 4.1.

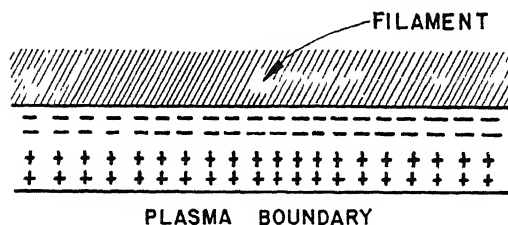


Fig. 4.2.

In this double layer, ions attract electrons and vice versa. Thus the strength of the field pulling out electrons is determined by the number of ions present. But the number of ions present is in turn affected by the number of electrons, because the electrons are pulling the ions in toward the filament. On account of their greater mass, the ions move more slowly than the electrons, and thus a smaller ionic current is required to give the same charge density. A simple calculation appearing below shows that the maximum possible electron current is given in terms of the ion current by Eq. 1. There is no reason, however, why less than the maximum electron current may not flow. In fact, if the filament is not hot enough to supply this max-

imum electron current, the double sheath will contain fewer electrons than ions, a nonzero field will exist at the filament surface, and the ratio of ion current to electron current may be quite large. It is only when operating at the critical pressure that the electron current is equal to the upper limit specified in Eq. 1.

In order to treat the problem mathematically, let n_+ = positive-ion density in sheath; n_e = electron density; J_+ = positive-ion current density; J_e = electron current density; V = negative of potential, $V = 0$ at plasma boundary, and $V = V_1$ at filament surface; m_e = electron mass; and m_+ = ion mass. By Poisson's equation

$$\frac{\partial^2 V}{\partial x^2} = 4\pi e(n_+ - n_e)$$

Now

$$n_+ = J_+ \sqrt{\frac{m_+}{2eV}}$$

and

$$n_e = J_e \sqrt{\frac{m_e}{2e(V_1 - V)}}$$

so that

$$\frac{\partial^2 V}{\partial x^2} = 4\pi \sqrt{\frac{e}{2}} \left(J_+ \sqrt{\frac{m_+}{V}} - J_e \sqrt{\frac{m_e}{V_1 - V}} \right)$$

Multiplying by $\partial V / \partial x$ and integrating,

$$\left(\frac{\partial V}{\partial x} \right)^2 = 16 \sqrt{\frac{e}{2}} \left(J_+ \sqrt{m_+} \sqrt{V} + J_e \sqrt{m_e} \sqrt{V_1 - V} + K \right)$$

To choose the constant of integration, note that $\partial V / \partial x = 0$ at the plasma boundary, where $V = 0$. Thus

$$\left(\frac{\partial V}{\partial x} \right)^2 = 16\pi \sqrt{\frac{e}{2}} \left[J_+ \sqrt{m_+} \sqrt{V} + J_e \sqrt{m_e} (\sqrt{V_1 - V} - \sqrt{V_1}) \right] \quad (2)$$

a rearrangement of terms gives

$$J_e \sqrt{m_e} (\sqrt{V_1} - \sqrt{V_1 - V}) = J_+ \sqrt{m_+} \sqrt{V} - \frac{(\partial V / \partial x)^2}{16\pi} \sqrt{\frac{2}{e}}$$

If V_0^1 = electric field at filament surface, the desired result can be obtained by setting $V = V_1$ in the above equation. This becomes

$$J_e = J_+ \sqrt{\frac{m_+}{m_e}} - \frac{(V_0^1)^2}{16\pi\sqrt{m_e} V_1} \sqrt{\frac{2}{e}}$$

To obtain the maximum possible value of J_e , V_0^1 must be set equal to zero; i.e., there must be zero field at the origin with resulting space-charge limitation. This gives

$$\frac{J_e}{J_+} \leq \sqrt{\frac{m_+}{m_e}}$$

In practice, it has been found by Langmuir,¹ who first presented the theory of the double sheath, that on account of irregularities in the filament the ratio cannot be brought above a fraction of the theoretical value. This fraction depends on the state of the filament and varies between $\frac{1}{3}$ and $\frac{2}{3}$.

The empirical correction to the theory is denoted by writing $J_e \leq \gamma \sqrt{m_+/m_e} \times J_+$, where γ is a fraction varying from $\frac{1}{3}$ to $\frac{2}{3}$.

For argon, $\sqrt{m_+/m_e} = 275$, so that with $\gamma = \frac{1}{3}$ about 100 electrons per ion can be drawn.

Size of Sheath. To obtain the size of the sheath, Eq. 2 is solved for dx/dV and integrated over V . This gives

$$x = \frac{1}{4\sqrt{\pi}} \left(\frac{2}{e}\right)^{\frac{1}{2}} \int_0^{V_1} \frac{dV}{\left[J_+ \sqrt{m_+} \sqrt{V} + J_e \sqrt{m_e} (\sqrt{V_1 - V} - \sqrt{V_1}) \right]^{\frac{1}{2}}} \quad (3)$$

If J_e were zero, the usual formula for a single positive-ion sheath would result. The effect of the term multiplying J_e is thus to increase the integrand. Hence the sheath thickness is greater than it would be for a sheath containing positive ions only. Physically the reason for the increase is that the effective space-charge density of positive ions is reduced by the electrons present so that a greater thickness is required to contain enough ions to absorb the full potential drop. When the maximum possible electron current is flowing, this thickness is increased over that of a single sheath with the same positive-ion current by a factor of 1.36, obtained by numerical integration of Eq. 3.

The actual sheath thickness is given by

$$x = \frac{\beta V^{\frac{3}{4}}}{(9\pi \sqrt{m/2e})^{\frac{1}{2}} j^{\frac{1}{2}}} \quad (4)$$

where j is the density of ion current and β is a factor depending on the fraction of the maximum possible ion current that is flowing. β varies from 1 for no electron current to 1.36 for maximum electron current. In more convenient units,

$$x = 3\beta \times 10^{-2} \frac{V^{\frac{3}{4}}}{j^{\frac{1}{2}}} \text{ cm}$$

where V is voltage in units of hundreds of volts and j is current in amperes per square centimeter.

In a typical case a positive-ion current of 10 ma/sq cm is available. The sheath thickness becomes, for 100 volts, $x = 3 \times 10^{-2}\beta$ cm. Thus the sheath is somewhat over 0.3 mm thick, depending on the value of β .

3. ION PRODUCTION

The rate of ion production is determined by the arc current, pressure, and cross section for ionization. For arc currents so low that the fraction of neutrals ionized is small, the rate of formation of ions per unit volume of arc column by primary ionization is

$$R = J_e \sigma_1 N_0 \quad (5)$$

where J_e is the arc-current density, σ_1 is ionization cross section, and N_0 is density of neutrals.

As a function of arc voltage, σ_1 starts at zero for arc voltage equal to ionization potential, rises to a maximum at about 100 volts, and falls off slowly thereafter. The general shape of the curve is similar for most gases, but the numerical values of the cross section vary widely. For argon the maximum is $\sigma_1 = 4 \times 10^{-16}$ sq cm, and for UCl_4 it appears to be about five times as great. A typical curve for σ_1 is shown in Fig. 4.3. Clearly, if only primary electrons are effective, the best operating voltage is near 100 volts.

Secondary electrons liberated in the process of ionization come off with appreciable energies that increase with arc voltage. In hydrogen, for example, at an arc voltage of 100 volts, the mean energy of secondary electrons is 15 volts, but for an arc voltage of 300 volts, their mean energy has risen to 30 volts. Electron-electron collisions cause these energies to be shuffled rapidly among the plasma electrons, which dissipate this energy in the processes of excitation and ionization. Thus an appreciable fraction of all ionization may come from plasma electrons, which obtain their energy from the secondaries. In

fact, probe measurements in the 37-in. arc show a rise of ion density by a factor of 1.3 when the arc voltage is raised from 150 to 400 volts with everything else kept constant. Along with this rise occurs a rise in electron temperature of from 2.5 to 4 volts, indicating that the increase is due to increase of high-energy "tail" in the Maxwellian distribution of plasma electrons. Present indications are that ionization by plasma electrons is about one-third as important as primary ionization at an arc voltage of 200 volts in argon.

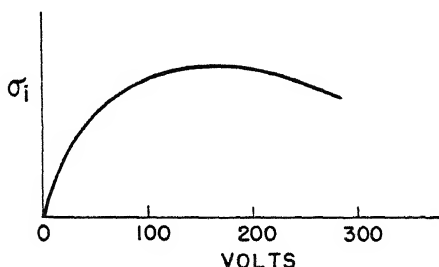


Fig. 4.3.

Normally, arc currents are so great that the fraction of neutrals ionized is no longer small, thus destroying the validity of the simple Eq. 5 for the rate of ionization. Hill and Aller have investigated this problem in detail; their results are quoted here from Chap. 8.

If each individual neutral is followed through the arc column, the probability that it will be ionized may be expressed in terms of the cross section, arc-current density, and time that it spends in the column. Let l be the path length of a neutral in the column, and v_N its velocity, so that it spends a time $T = l/v_N$ inside the column. Then the theory of probability shows that the chance of ionization is

$$P = \left(1 - \exp \frac{-J_e \sigma_i l}{v_N} \right)$$

From the above expression it can be seen that as the arc current is increased indefinitely the probability of ionization approaches 1. Furthermore P is a function only of the product $J_e l$, which is equal to the arc current per unit length of filament. Thus the thickness of the filament does not affect the probability of ionization for a given arc current. The effect of ionization by plasma electrons, however, is to cause an increase in the effective value of J_e .

To find the rate of production of ions, P is multiplied by the total number of neutrals passing through the arc column. Because of their random directions, these neutrals have varying path lengths, depending on size and shape of slot. Hill and Aller have worked out the average value of P by summing over all possible path lengths (Chap. 8). The rate of ionization is then given by

$$R = \frac{N_0 v_N}{4} P(J) \quad (6)$$

where $P(J)$ is the average of P , tabulated graphically in each case. $P(J)$ is proportional to the arc current J at low values but approaches saturation at high arc currents.

4. PLASMA-BALANCE PROCESSES DETERMINING FRACTION OF IONS REACHING FILAMENT

In order to predict the fraction of ions reaching the filament sheath, it is necessary to have a general understanding of what determines the relative motion of ions along the magnetic field and across it. In this chapter only a brief summary is given of the complex interplay of processes involved in bringing about the final steady state of the arc. Further information regarding this problem is found in Chap. 9.

In the absence of a magnetic field, the steady state of ion distribution can be understood with the aid of a method first developed in detail by Langmuir.² Electrons are liberated with several volts of kinetic energy, and ions with none. Because of their small mass and high energy, electrons rapidly leave the region in which they are liberated and collect on the walls, charging them negatively relative to the plasma. This charge has two effects: (1) it repels electrons; (2) it attracts positive ions, which fall freely to the walls as a result of electric fields in which they happen to find themselves upon liberation. As for the electrons, they make so many collisions that a Maxwellian distribution of velocities is rapidly established among them. A steady state is finally reached in which ions are attracted to the walls at a rate equal to the number produced. As for the electrons, just enough are repelled so that the remaining few with sufficient energy to scale the sheath at the walls will be equal to the total number produced. In such a steady state, the walls run about 10 volts negative relative to the space inside.

The main body of the arc is filled with a mixture containing approximately equal numbers of positive ions and electrons, called a "plasma." Because of the enormous potentials resulting from even the

slightest failure of space-charge neutralization, a plasma is characterized by enforced neutrality. The maximum potential drop that can be sustained in a plasma is about half the electron temperature, because greater drops would cause space charge to redistribute itself until it was neutralized.

Near a highly negative electrode, however, there must be a region containing only positive ions, since the plasma electrons do not have sufficient kinetic energy to reach the electrode. Such a region, called a "sheath," is usually quite small, because prevailing ion densities are great enough to sustain enormous potential drops in short distances. Normally the sheath is of the order of 0.1 mm in thickness, although with high sheath voltage or low ion density it may become considerably larger.

Remembering that positive ions acquire kinetic energies from plasma electric fields of the order of half the electron temperature, it can be seen that they usually arrive at the sheath edge with kinetic energies of about 1 volt. In Chap. 3 it is shown that no sheath can be stable unless the ions arriving there have an energy of about half the electron temperature. Thus if n_+ is the ion density at the sheath edge, the ion current density is given by

$$J_+ = n_+ \sqrt{\frac{kT_e}{m_+}} \quad (7)$$

It is important to note that the ion current at the sheath edge is determined by the electron temperature. The reason is, of course, that the plasma electric fields producing ionic velocities are limited by electron temperature.

Effect of Magnetic Field. The main effect of the magnetic field is to hinder motion of electrons (and of ions to a lesser extent) across the field, while leaving their motion along the field unhindered. Thus to describe motion parallel to the magnetic lines, substantially the same picture may be used as in the absence of a field. Because this type of motion is so free, variations of density in this direction may to a first approximation be neglected so that equations may be derived in terms of the density n as a function of x and y only.* Since the current density to the filament sheath is given by Eq. 7, the remaining problem is to find n_+ .

*The direction of the magnetic lines of force has been taken as the Z axis in a rectangular system of coordinates. The Y axis is then the direction of motion of ions leaving the arc slit when they are accelerated.

It is clear that the mean ionic density at the arc column is determined in part by the rate at which ions and electrons diffuse outward across the magnetic field. Since the electron Larmor radius is very small, of the order of 0.01 mm, it would appear at first sight that electrons cannot leave the arc column unless they undergo collisions that move the center of a circular orbit by a Larmor radius at a time. Yet calculations show that collisions are totally inadequate to account for the observed rate at which electrons do diffuse across the magnetic field. However, another source of electronic motion is usually overlooked, namely, drain at right angles to electric and magnetic fields. The drain velocity is

$$v_d = \frac{cE}{H} = \frac{10^5 E}{H}$$

where E is the electric field in volts per centimeter, H is the magnetic field in thousands of gauss, and c is the velocity of light.

Now fields of several volts per centimeter are not uncommon in the plasma. Assuming 3 volts per centimeter, with $H = 3,000$ gauss

$$v_d = 10^5 \text{ cm/sec}$$

Along the magnetic field a 2.5-volt electron has a velocity of

$$v \approx 10^8 \text{ cm/sec}$$

Thus the mean electronic velocity normal to the field is reduced about a thousand times to a value comparable with that of the positive ions.

Diffusion of electrons and ions across the field is discussed in Chap. 9 and is also treated qualitatively in Chap. 2. There are two possible ways in which electrons may drain across the magnetic field—statically, and by plasma oscillations. In Figs. 4.4 and 4.5, respectively, there are represented two possible arrangements of equipotentials within the arc, one of which is characteristic of oscillatory electron diffusion, and the other of static diffusion. These figures are cross sections of the arc viewed in the direction of the magnetic field.

In Fig. 4.4 the equipotentials surround the arc column so that drain merely causes an unbroken circulation of electrons around the column. In Fig. 4.5, however, the equipotentials go through the arc column, and drain can therefore bring an electron from the column to the wall sheath. The arrangement of potentials in Fig. 4.5 will result in an asymmetric distribution of ionization, since there will be a

tendency for electrons and ions to leave the arc column in the directions shown by the arrow. This asymmetry is in agreement with observations that show a high density on the antidrain* side as predicted by the assumption of equipotentials given in Fig. 4.5.

As for potentials of the type drawn in Fig. 4.4 these are unstable and tend to break up into plasma oscillations running around the filament. Since these oscillatory fields have components along the length of the arc column, they will cause alternate inward and outward drain of electrons that will in turn cause a random diffusion of ions tending to bring them to the walls.

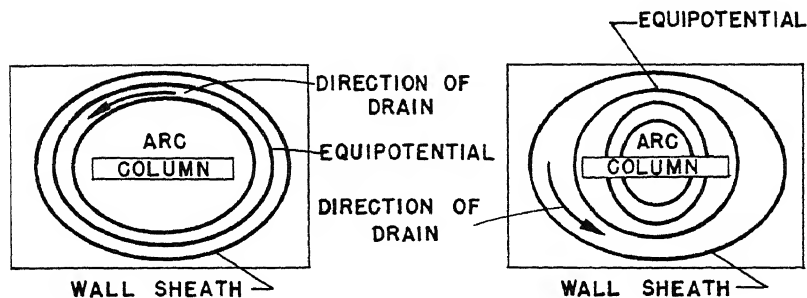


Fig. 4.4.

Fig. 4.5.

In actual practice, potential distributions of the types in both Figs. 4.4 and 4.5 are somewhat unstable, although Fig. 4.4 is more unstable. Thus there is normally a mixture of static drain diffusion and oscillatory diffusion. If the arc can function in the state shown in Fig. 4.5, it tends to do so; but if, as we shall see later, the ion supply to the filament should be inadequate in this state, it might go to the state illustrated in Fig. 4.4, where oscillatory drain is the only cause of electronic motion normal to the field. The oscillatory drain is so random in nature that it acts like an ordinary diffusion process. In fact, the diffusion coefficient resulting from this cause can be estimated theoretically and has been found to be

$$D_e = \frac{10^4 T_e}{H}$$

*Negatively charged particles accelerated toward the ion source from the region of the accelerating slits migrate to one side of the source, called the "drain side," due to the combination of electric and magnetic fields. The opposite side of the ion source is then referred to as the "antidrain side."

where T_e is electron temperature in volts and H is the magnetic field in thousands of gauss. This value is in good agreement with estimates based on probe measurements (see Chap. 2). The actual value of the oscillatory drain-diffusion coefficient is intrinsically uncertain to a factor of the order of 2 because of the variability of hash amplitudes.

As for ions, they have Larmor radii of the order of 0.2 cm for argon. Since the walls are normally farther out than 0.2 cm, ions also get out by a mixture of static drain diffusion and plasma oscillations.

On the basis of the above information, a general picture of the internal state of the arc may be given. Electrons and ions are produced in the arc column and must diffuse either to the top and bottom or to the walls, where they recombine. Diffusion across the magnetic field is brought about statically by drain in electric fields whose equipotentials pass through the arc column, and dynamically by self-excited plasma oscillations, producing on the average a random diffusion. Along the magnetic field, ions and electrons move freely, and the ions gain a kinetic energy of half the electron temperature by the time they reach the sheath edge. Electrons, however, are repelled by the sheath to such an extent that only those with unusually high kinetic energies are collected. The rate at which ion density falls off with distance from the arc column is determined by competition between outward diffusion and upward motion. The more rapid the diffusion transverse to the field, the farther ions will get before they are collected at top and bottom. Meanwhile, the continual robbing of the plasma by top and bottom electrodes results in a steady drop in ion density with distance from the arc column.

The quantitative theory of variation of ion density is treated in Chap. 9. Below, merely such results as are needed will be presented, without proof. Also, this section will be restricted to an arc with walls so far away that wall collection does not appreciably affect ion density at the column. This case is usually referred to as the "large arc." In Sec. 6 the effect of bringing walls or meniscus closer is investigated.

When the diffusion equations are solved, it turns out that an exponential decrease of ion density with distance from the arc column is predicted. That is,

$$n = n_0 e^{-y/d} \quad (8)$$

where n_0 is ion density at edge of the arc column and d is a characteristic distance in which n falls to $1/e$ of its value. The exponential fall is fairly well verified by probe experiments.

The term d is determined by the formula

$$d^2 = \frac{Dh}{2 \sqrt{kT_e/m_+}} \quad (9)$$

where D is a sort of average between electronic and ionic diffusion coefficients whose precise nature need not be gone into here, and h is the height of the arc. The value of D , however, depends on the state of the arc, being greater in the state shown in Fig. 4.5 than in that shown in Fig. 4.4. D also varies inversely as the magnetic field, because of the greater difficulty of ionic motion across the field at high field strengths.

The value of D has been estimated theoretically as pointed out previously. It is most convenient, however, to use the observed value of d , which can be found from probe measurements of ion density, to obtain D . At 3,000 gauss, experiments show that $d = 0.8$ cm when $h = 12$ cm (37-in. arc) and $T_e = 3$ volts. This gives $D = 4 \times 10^4$, which agrees in order of magnitude with the predicted theoretical value of $D \approx 10^5 T_e/H$ (see the detailed discussion on drain diffusion in Chaps. 2 and 9).

The next step is to use these diffusion coefficients to obtain the ion density at the arc column. The rate at which ions leave each square centimeter of arc column on both sides together can be expressed in terms of the ion density n_0 at the arc column; the electron temperature T_e ; the height of the arc, h ; and the characteristic distance d in which ion density falls to $1/e$ of its value. The expression, given here without proof, is

$$R_L = 4n_0 \frac{d}{h} \sqrt{\frac{kT_e}{m}} \quad (10)$$

The rate of loss is, as it should be, proportional to ion density at the edge of the arc column and to the square root of the electron temperature that determines the electric fields pulling ions out. The origin of the ratio d/h occurs in a mathematically roundabout fashion. Yet its significance is simply that if d/h is observed to be small, it can be concluded that ions are not leaving the arc column at nearly so great a speed as they are moving upward.

In order to obtain a balance the rate at which ions leave the arc column must be equated to the rate at which they are produced inside, minus the number that go to the top and bottom, before they have a

chance to reach the edge of the arc column. The rate of production is given by Eq. 6, which, however, must be multiplied by a factor of 2 to take into account the fact that neutral gas is entering the arc column from both sides, i.e.,

$$R = \frac{N_0 v_N}{2} P(J)$$

The rate at which ions strike the top and bottom per unit area is, by Eq. 7

$$J_+ = n_0 \sqrt{\frac{kT_e}{m_+}}$$

To find the total loss at top and bottom this must be multiplied by twice the area of the slot between the filament and the arc chamber, through which slot the electron stream from the filament must pass (collimating slot). Since this loss is distributed* over the height of the arc, h , the loss per unit volume is

$$L = 2n_0 \sqrt{\frac{kT_e}{m_+}} \frac{t}{h}$$

where t is the thickness of the collimating slot. Equating $R - L$ to R_L ,

$$4n_0 \frac{d}{h} \sqrt{\frac{kT_e}{m_+}} = \frac{N_0 v_N}{2} P(J) - 2n_0 \sqrt{\frac{kT_e}{m_+}} \frac{t}{h}$$

Solving for n_0 yields

$$n_0 = \frac{N_0 v_N}{8} \frac{P(J)}{\sqrt{kT_e/m_+}} \left(\frac{h}{d + t/2} \right) \quad (11)$$

The value of n_0 is proportional, as it should be, to gas density N_0 and probability of ionization $P(J)$. The ratio $v_N / \sqrt{kT_e/m_+}$ is the ratio of the velocity of neutrals to velocity of ions with energy equal to half the electron temperature. Its occurrence means that ion density is reduced below neutral density because ions move out of the arc col-

*The variation of ion density along the magnetic field is much smaller than its variation normal to the field. To a first approximation it may be assumed that the ion density along the field is uniform.

umn faster in the Z direction than neutrals. The ratio $h/(d + t/2)$ takes into account the fact that ionic motion across the magnetic field is hindered. The appearance of the factor $d + t/2$ in the denominator indicates that n_0 is not greatly affected by thickness of the collimating slot until $t/2$ becomes as great as d . This will occur for argon in the 37-in. arc at $t = 0.6$ in. In UCl_4 , however, this distance may be considerably shorter.

Having found the ion density, the current density of ions to the filament is obtained by multiplying n_0 by the ionic velocity at the sheath edge, or $v = \sqrt{kT_e/m_+}$ (see Eq. 7).

$$J_+ = n_0 \sqrt{\frac{kT_e}{m_+}} \frac{N_0 v_N}{8} P(J) \frac{h}{d + t/2} \quad (12)$$

To obtain the total positive current it is necessary to multiply by the area of the collimating slot, which is l , where l is the length of the filament. Then

$$J_+ = \frac{N_0 v_N}{8} P(J) \frac{htl}{d + t/2} \quad (13)$$

Equation 13 completes the objective of Sec. 4. It is now possible to predict the positive-ion current to the filament in terms of known quantities. $P(J)$ is obtained from curves calculated by Hill; d is obtained from probe measurements.

5. MINIMUM PRESSURE FOR ARC OPERATION

The minimum pressure at which the arc can operate can now be computed. According to Eq. 1,

$$J_+ \geq \sqrt{\frac{m_e}{m_+}} \frac{J_e}{\gamma}$$

Replacing J_+ by its value given in Eq. 13, the equation becomes

$$\frac{N_0 v_N}{8} \frac{htl}{d + t/2} P(J_e) \geq \frac{J_e}{\gamma} \sqrt{\frac{m_e}{m_+}}$$

or

$$P(J_e) \geq \frac{8(d + t/2)}{\gamma N_0 v_N htl} \sqrt{\frac{m_e}{m_+}} J_e$$

Setting

$$K = \frac{8 \left(d + \frac{t}{2} \right) \sqrt{\frac{m_e}{m_+}}}{\gamma N_0 v_N h t l}$$

the above inequality can be written $P(J_e) \geq KJ_e$. This means that the arc will not operate unless $P(J)$ is greater than KJ . In order to find the limiting conditions for arc operation, the curves $y = P(J)$, and

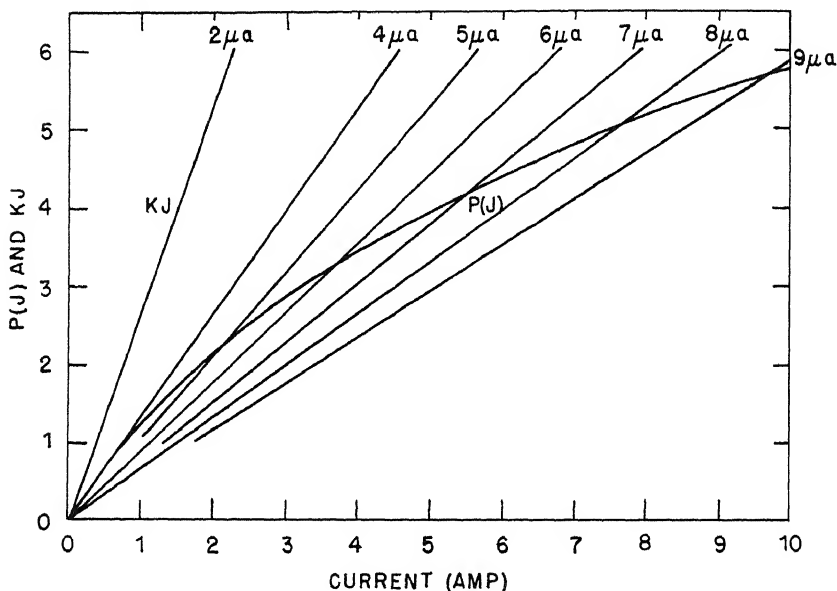


Fig. 4.6— $P(J)$ and KJ vs. arc current.

$y = KJ$ are plotted on the same sheet. Where $P(J)$ is above KJ , the arc can run. Limiting conditions are obtained where the two curves intersect. In Fig. 4.6, $P(J)$ is plotted for an argon arc with a filament $\frac{1}{2}$ in. long. The straight lines $y = KJ$ are also plotted for a range of pressures indicated on the graph. Where $P(J)$ lies above the straight line corresponding to a given pressure, the arc can run. Obviously the slope of the line is inversely proportional to the pressure, so that it is easier to obtain good running conditions at higher pressures.

If the pressure is reduced below the critical value, the arc may not go out but may fluctuate into the less stable state shown in Fig. 4.4,

in which the rate of diffusion is decreased. Since the diffusion coefficient D is reduced, Eq. 9 predicts an increase of d , therefore a decrease of K . Such a decrease in slope of the straight line may be sufficient to enable it to intersect the curve $y = P(J)$, even though it does not do so when the arc runs in the normal state. The gain available from such a change of state may permit a further reduction of pressure of the order of 30 to 40 per cent under suitable conditions.

In many cases such a readjustment of internal state is likely to lead to hash before the critical pressure is reached. The reason is that this critical pressure is calculated for a uniform steady arc. With nonuniform or unsteady conditions, the arc can run only if the ion supply is adequate in the region of weakest ionization. Thus, close to the critical pressure the arc will begin to go out if there is a slight fluctuation in ion density. Before going out, however, it may flop into a state of smaller outward diffusion and thus save itself. In the process of flopping, a plasma oscillation is created, whose inertia will transform a local deficiency of ions into an excess within a half period of an oscillation. When working close to the critical pressure, this temporary surplus resulting from the oscillation near the filament may be great enough to permit flopping back to the normal state for a short time. But when the plasma wave recedes, the arc must flop back again. Thus hash is created and maintained.

6. EFFECT OF ARC MENISCUS IN RAISING OPERATING PRESSURE

Thus far the investigation has been of minimum running pressure in an arc with walls so far away from the column that they have little effect on ion density at the column itself. As long as the walls are farther than the critical distance d , they remove so little current that they do not appreciably affect conditions in the column. If they are brought closer, however, they begin to withdraw ions so rapidly that the rate of diffusion outward is increased. In particular, if a meniscus is brought very close to the arc column, motion of ions to the meniscus becomes more rapid than motion to the back wall, which is relatively far away.* Detailed investigation shows that the fraction of ions leaving the arc column in the direction of the meniscus may be raised as high as 80 to 90 per cent in this fashion. In practice, however, this high fraction is unrealizable for two reasons: first because the more rapid removal of ions from the arc column raises the minimum

*Mean plasma electric field between column and meniscus is inversely proportional to the distance between them.

running pressure even more than it raises the ion output; second, because of nonuniformity of intensity of ionization in the arc column, a meniscus close to the weakest part of the plasma may be quite far from the strongest part.

For the present no effort will be made to work out in detail the precise effect of meniscus distance, mainly because of excessive complexity. Instead the minimum running pressure will be expressed in terms of a quantity denoted by f , which is the fraction of all ionization leaving the arc column in the direction of the meniscus. When the walls are at a distance greater than d , this fraction is, as we have seen, close to $\frac{1}{2}$, since the same ion current flows either way.

The ratio of current flowing to the back wall to ion density at the arc column is shown in Chap. 9 to be independent of the location of the meniscus. The following equation expresses the proportionality mentioned above:

$$J_{+b} = cn_+$$

where c is a constant determined from the diffusion equations, in a manner that need not be discussed here, and J_{+b} is ion current flowing backward.

If R is the total ion production, then, with distant meniscus, $R/2$ flows backward. As the meniscus is brought closer, and the fraction going backward decreases to $(1 - f)$, the density n_+ must drop. Thus,

$$\frac{n_+}{n_{0+}} = \frac{J_{+b}}{J_{+b0}}$$

where n_{0+} is ion density for distant meniscus and J_{+b0} is backward current for distant meniscus. Noting that

$$\frac{J_{+b}}{J_{+b0}} = 2(1 - f)$$

the above equation becomes

$$\frac{n_+}{n_{0+}} = 2(1 - f)$$

When $f < \frac{1}{2}$, there will be a drop in ion density and a reciprocal rise in minimum running pressure; therefore

$$\frac{p}{p_0} = \frac{1}{2(1 - f)}$$

That there is no advantage in increasing f beyond $\frac{1}{2}$ can be made evident by a numerical example. Thus, if f is increased to $\frac{3}{4}$,

$$\frac{p}{p_0} = 2$$

and the minimum running pressure is doubled, although the ion output is raised only 50 per cent.

When running close to the minimum pressure, the arc will go out if the accelerating voltage is raised high enough to bring the meniscus too close to the arc column. By raising the arc voltage, however, the arc can be saved. The explanation is that with increase in ionization by secondaries the number of ions returned to the filament per electron leaving is increased to such an extent that the arc can run at the lower ion density resulting from too close a meniscus. Experimental results in the 37-in. arc substantiate these conclusions in a qualitative way.

7. RECOMMENDATIONS FOR LOWERING OPERATING PRESSURE

All devices aimed at lowering the running pressure must result in increasing the number of ions returning to the filament per electron leaving. Two methods of accomplishing this objective are possible: first, the number of ions liberated per arc electron can be increased; second, the fraction of these ions reaching the filament may be increased.

The first objective may be accomplished with the reflecting anode, which causes each electron to be used many times. A rise in arc voltage will also increase the ionization per ampere of arc current, because the secondary electrons become more energetic and ionize more. With regard to the reflecting anode, it must be remembered that it too is surrounded by a double sheath, just like the one at the filament, so that the function of the reflecting anode may become unstable if too few ions reach it. In fact, because an electron is in the reflecting anode sheath twice as long as in the filament sheath (going in and coming out), twice as many positive ions are needed to maintain a sheath.

The most promising way to increase the number of ions reaching the filament is to surround the filament with a container that is gas-tight except for a very deep collimating slot. With proper dimensions it should be possible to maintain a high pressure near the filament and a negligible pressure outside. Thus there would be an auxiliary arc, able to run at a pressure independent of that in the main arc chamber.

As for the second method of running at low pressure, namely, increasing the fraction of ions reaching the filament, this usually has the disadvantage that it decreases the fraction reaching the meniscus and thus decreases the ion output. The most promising application of such a method is to use a thicker filament, which will enable more ions to reach it. Doubling the filament thickness should halve the running pressure with some decrease in the fraction of ions reaching the meniscus. It is of no use, however, to make the filament thicker than the characteristic distance of exponential drop in ion density d .

Increasing the magnetic field would be of help, since it holds ions in and favors their going to the filament; but it must be remembered that, conversely, a decrease of field will raise the minimum running pressure. According to theory, a fourfold decrease will double the running pressure required.

Block voltage also falls in this category, since it keeps ions away from the wall, driving them to the filament instead. However, it appears to do so at the expense of a decrease in ion output.

REFERENCES

1. I. Langmuir, Phys. Rev., 33: 954 (1929).
2. I. Langmuir, Phys. Rev., 34: 876 (1929).

Chapter 5

EXPERIMENTAL INVESTIGATION OF THRESHOLD PRESSURE FOR STABLE OPERATION OF ARCS

By E. H. S. Burhop, H. S. W. Massey, and G. Page

1. INTRODUCTION

A theoretical discussion of the factors determining the minimum pressure for stable arc operation is contained in Chap. 4. In this chapter are described some experiments directed toward testing the theory that ascribes the pressure limitation to the need for supply of sufficient ions to the filament to satisfy the Langmuir condition at the double sheath there. The arcs were run in argon, helium, and sulfur hexafluoride, and good general agreement with the theory was found in all three cases.

Summary of the Theory of the Threshold Pressure. If J_c is the arc current, j_+ the positive-ion current to the filament, m_+ the mean mass of the positive ions, and m_e the mass of an electron, then the Langmuir condition that must be satisfied for the arc to run stably is

$$\frac{j_+}{J_c} \geq \alpha \sqrt{\frac{m_e}{m_+}} \quad (1)$$

where α is a parameter of the order of 1.

Now j_+ may be written in the form

$$j_+ = f_K p \psi(J_c, J_v) \quad (2)$$

where p is the pressure in the arc column, $p \psi(J_c, J_v)$ is the rate of production of ions in the column, and f_K is the fraction of these ions reaching the filament. J_v is the arc voltage.

Combining Eqs. 1 and 2,

$$p \geq \alpha \sqrt{\frac{m_e}{m_+}} \frac{J_c}{f_K \psi(J_c, J_v)} \quad (3)$$

To proceed further it is necessary to inquire further into the form of $\psi(J_c, J_v)$. It may be written to a good approximation in the form

$$\psi(J_c, J_v) = ec(1 - e^{-aJ_c}) \quad (4)$$

where c is the total flux $A\bar{v}$ of neutral molecules through the column with mean speed \bar{v} , e is the charge on an ion formed, and $1 - e^{-aJ_c}$ is the chance that a molecule will be ionized in passing through the column. The parameter a will be inversely proportional to the mean speed \bar{v} of flow of the molecules through the column and directly proportional to the cross section $q(J_v)$ for ionization of the molecules by the electrons. The equation may therefore be written

$$\psi(J_c, J_v) = Ae\bar{v} \left\{ 1 - \exp \left[\frac{-kq(J_v)}{\bar{v}} J_c \right] \right\} \quad (5)$$

where k is some constant.

Substituting this in Eq. 3,

$$p \leq \alpha \sqrt{\frac{m_e}{m_+}} \frac{J_c}{Af_K e \bar{v} \left\{ 1 - \exp \left[\frac{-kq(J_v)}{\bar{v}} J_c \right] \right\}} \quad (6)$$

It is clear from the form of the variation of the right-hand side with J_c that the higher J_c , the greater the pressure required for stable operation. For small values of J_c , however, the right-hand side becomes constant, giving a threshold pressure

$$p_0 = \alpha \sqrt{\frac{m_e}{m_+}} \frac{1}{Af_K ekq(J_v)} \quad (7)$$

For a given geometry and magnetic field, A and k will be constant, and f is not likely to vary very much unless the arcs run in different modes, i.e., dispose of the secondary ionization differently. It is seen therefore that the ratio of the threshold pressures for two arc voltages J_v^1 , and J_v^2 should be

$$\frac{p_0(J_v^1)}{p_0(J_v^2)} = \frac{q(J_v^2)}{q(J_v^1)} \quad (8)$$

Change of magnetic field will change f_K so that, in general, for higher fields, a bigger fraction of ions reaches the filament. Hence for two magnetic fields H_1 and H_2

$$\frac{p_0(H_1)}{p_0(H_2)} = \frac{f_K(H_2)}{f_K(H_1)} \quad (9)$$

ignoring any effect of magnetic field on the filament.

For two different gases, G_1 and G_2 , at the same arc voltage and magnetic-field strength,

$$\frac{p_0(G_1)}{p_0(G_2)} = \sqrt{\frac{m_+(G_2)}{m_+(G_1)}} \frac{q(J_v, G_2)}{q(J_v, G_1)} \frac{f_K(G_2)}{f_K(G_1)} \quad (10)$$

The ratio of the f 's for the two gases is included here because the effectiveness of the magnetic field in concentrating the ion flow in the direction of the field will be greater the smaller the mass of the ion, i.e., f_K will be greater the smaller the mass m_+ . The effect of a change of geometry, other things being unaltered, will be to change A , f_K , and k . Such changes were not considered in this investigation.

Now consider the factors determining the minimum pressure at which a given arc current can be attained. From Eq. 3 it may be seen that

$$\frac{J_c(\max)}{p} = \frac{f_K}{\alpha} \sqrt{\frac{m_+}{m_e}} \psi(J_e, J_v) \quad (11)$$

It has been noted that ψ has the general form

$$\psi = \text{const} \times \left\{ 1 - \exp \left[\frac{-kq(J_v)}{\bar{v}} J_c \right] \right\} \quad (12)$$

so, if f_K were independent of J_c ,

$$\frac{J_c(\max)}{p} = \text{const} \times \left\{ 1 - \exp \left[\frac{-kq(J_v)}{\bar{v}} J_c \right] \right\} \quad (13)$$

In general, however, f_K must be expected to vary somewhat with J_c and possibly even to show sudden changes if a change in the mode of disposal of the secondary ionization occurs at some value of J_c . A change of mode that affects the temperature of the secondary electrons may also change $q(J_v)$ as it includes contributions to the ionization from these electrons.

The simplest assumption to make, however, is that $q(J_v)$ is just the cross section for primary ionization by the arc electrons of electron voltage J_v . For a given geometry of column, k may be calculated and the function ψ determined to this approximation. Calculations have been carried out in this way for the three gases investigated, using the ionization cross sections for argon and helium as measured by Smith¹ and that for sulfur hexafluoride recently measured in the 37-in. unit. The resulting function ψ^* is illustrated in Fig. 5.1. There are various reasons why, in practice, $J_c(\text{max})/p$ should depart in form from the appropriate functions illustrated in Fig. 5.1. Among these are

1. The fraction f_K of ions produced that reaches the filament may depend on arc current. This will be particularly marked at a change of state of the arc, but there may be a gradual variation of f_K with J_c in any case. This may involve either a decrease or increase with increasing J_c .

2. Ionization by secondary electrons may become important, particularly at higher arc voltages. This has the effect of increasing the apparent value of $q(J_v)$, and its importance may depend, through the electron temperature, on the arc current. It is also possible that, under conditions near the threshold, the plasma adjusts itself to produce sufficiently large potential gradients to increase the ionization by secondary electrons.

3. For a polyatomic molecule such as sulfur hexafluoride, the rate of production of ions is increased by the possibility of ionizing all the constituent atoms by multiple collisions. The curve of Fig. 5.1 for sulfur hexafluoride was obtained by taking for $q(J_v)$ just the cross section for ionization of SF_6 in a single impact, giving mainly SF_5^+ . As the arc current increases, the ionization proceeds by stages to give eventually $S^+ + SF^+$, thus augmenting the rate of ion production. The effective function ψ will therefore not saturate so quickly as that

*The form of the function depends somewhat on the angular distribution of the emission from the filament. The results illustrated in Fig. 5.1 are obtained on the assumption that the chance that the initial direction of motion of an electron makes an angle θ with the magnetic field is proportional to $\cos \theta$.

of Fig. 5.1 would indicate and will increase beyond 1, a single neutral molecule being capable at sufficiently high arc currents of producing not only one but up to seven ions.

To analyze the experimental results it will nevertheless be convenient to plot the observed $J_c(\text{max})/p$ as a function of arc current and compare with the curves of Fig. 5.1. The nature of the deviations will in some instances throw light on the phenomena involved.

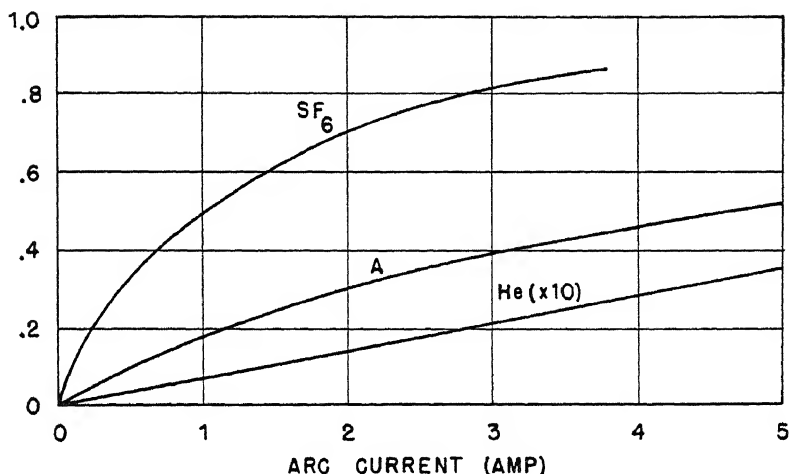


Fig. 5.1—The calculated probability of a neutral molecule being ionized on passing through the arc column as function of arc current in different cases. Secondary ionization is neglected.

2. ARGON, HELIUM, AND SULFUR HEXAFLUORIDE

2.1 Experimental Apparatus and Procedure. The arc chamber used is illustrated in Figs. 5.2 and 5.3. The arc chamber was of carbon, and anode, collimating plate, and filament were of tungsten. Pressure in the arc chamber was measured by a Western Electric ionization gauge for argon and helium and by a McLeod gauge for sulfur hexafluoride. The gas entered the arc chamber through the series of holes indicated in Fig. 5.2.

The procedure employed in making the measurements was to set the gas pressure to a particular value by means of an adjustable leak. The magnetic field and arc voltage were then set, and the filament current increased until the maximum arc current was attained under

these conditions. Attainment of the maximum was characterized either by saturation at a steady value with increase of filament current, or by the onset of a high degree of instability when any attempt was made to increase the arc current still further. These observations were repeated at different arc voltages, magnetic fields, and

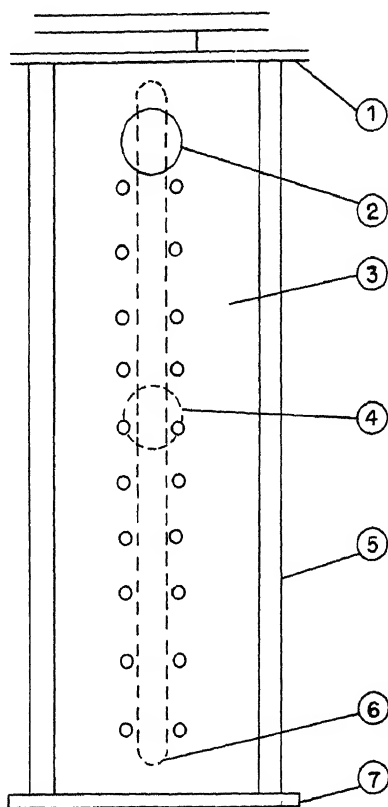


Fig. 5.2—Plan view of arc box: 1, arc chamber; 2, gas inlet; 3, connection to Western Electric or McLeod gauge; 4, collimating slot; 5, arc slit; 6, accelerating structure; 7, anode.

gas pressures, the latter being measured, with the arc off, before and after the complete set of measurements at the pressure concerned. The running of the arc introduces some change in the pressure, particularly for sulfur hexafluoride, with which it rises considerably with rise in arc current, owing to dissociation. In all cases, however, the pressure measured refers to that in the absence of the arc.

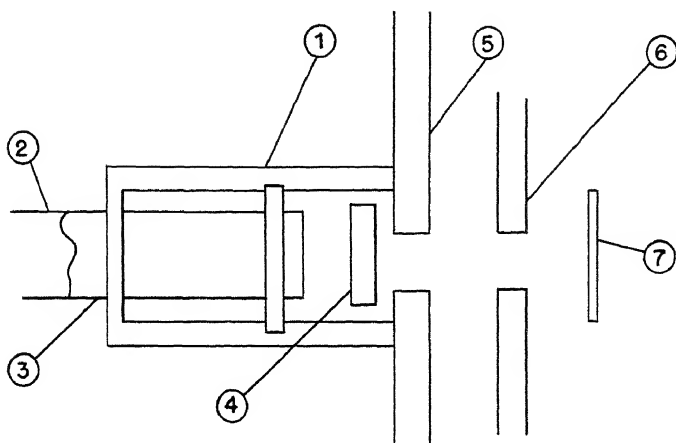


Fig. 5.3—Schematic plan of arc box: 1, arc chamber; 2, gas inlet; 3, connection to Western Electric or McLeod gauge; 4, collimating slot; 5, arc slit; 6, accelerating slit; 7, collecting plate.

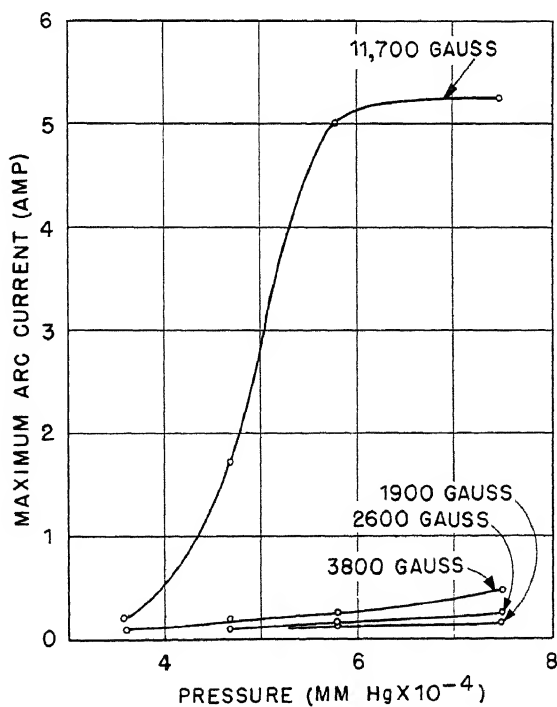


Fig. 5.4—Maximum arc current attainable with an arc in argon at various pressures and magnetic fields ($J_v = 100$ volts).

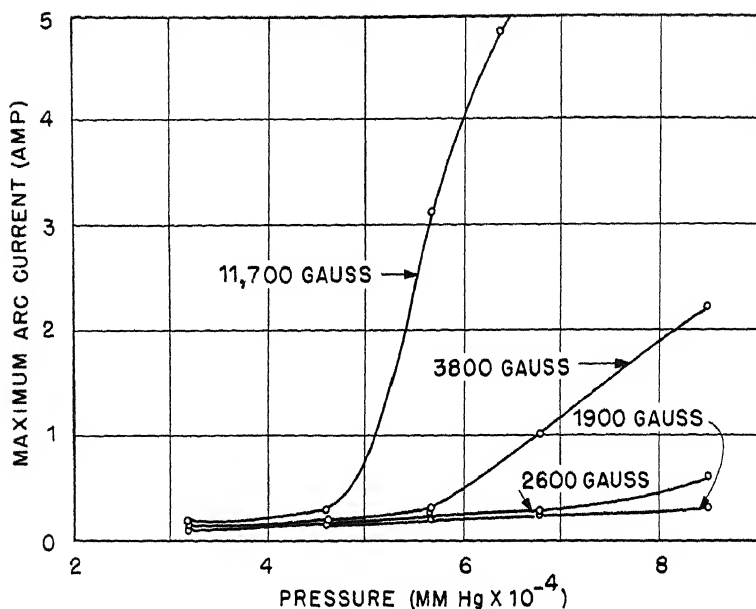


Fig. 5.5—Maximum arc current attainable with an arc in argon at various pressures and magnetic fields ($J_v = 200$ volts).

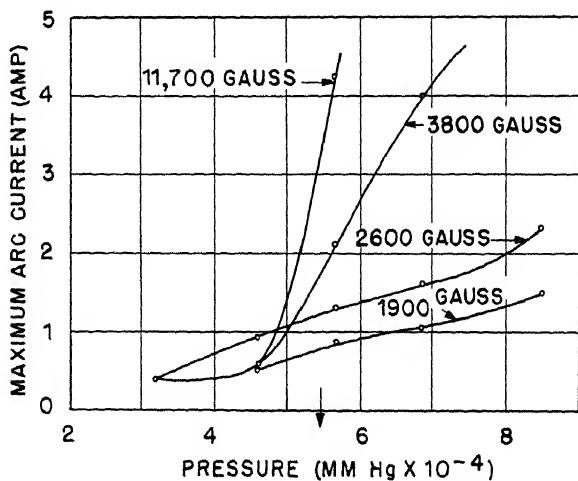


Fig. 5.6—Maximum arc current attainable with an arc in argon at various pressures and magnetic fields ($J_v = 500$ volts).

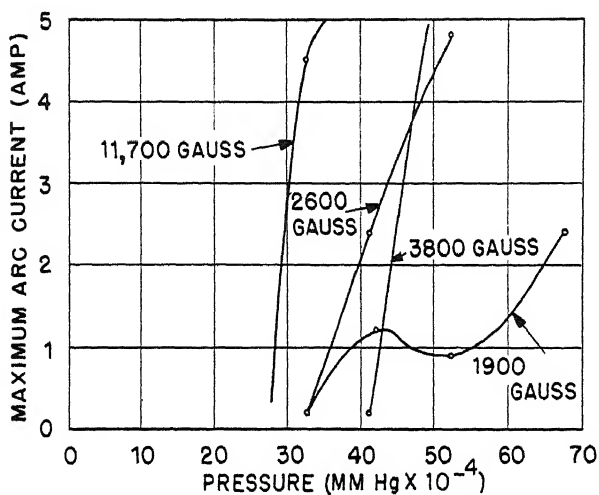


Fig. 5.7—Maximum arc current attainable with an arc in helium at various pressures and magnetic fields ($J_v = 200$ volts).

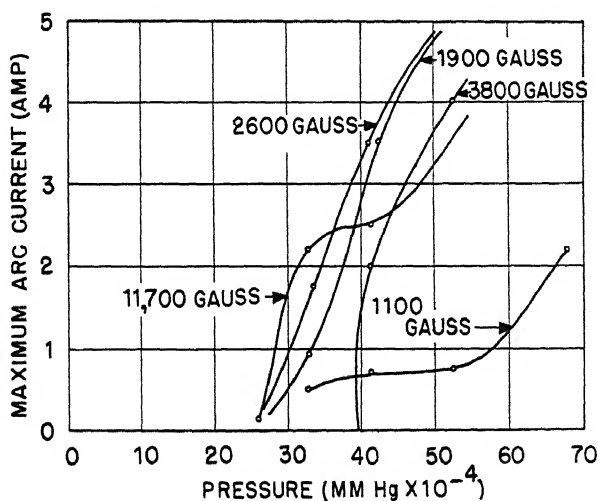


Fig. 5.8—Maximum arc current attainable with an arc in helium at various pressures and magnetic fields ($J_v = 500$ volts).

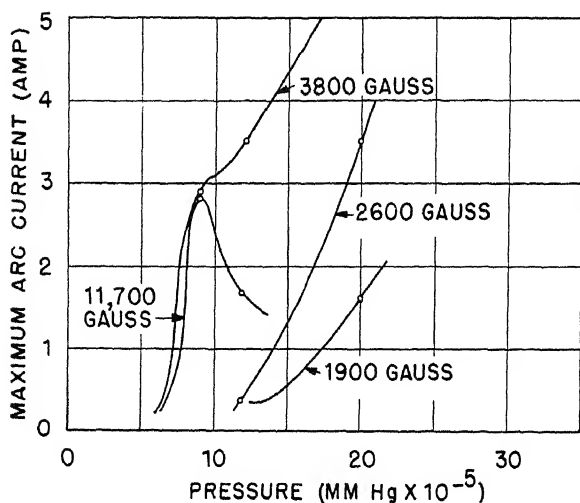


Fig. 5.9—Maximum arc current attainable with an arc in sulfur hexafluoride at various pressures and magnetic fields ($J_v = 200$ volts).

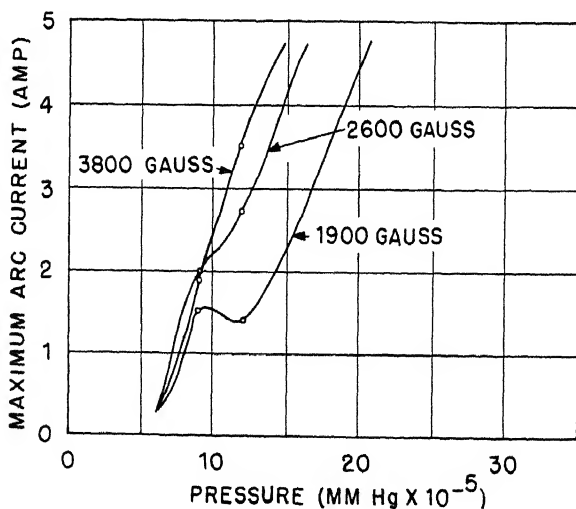


Fig. 5.10—Maximum arc current attainable with an arc in sulfur hexafluoride at various pressures and magnetic fields ($J_v = 500$ volts).

2.2 Experimental Results. (a) Variation of J_c (max) with Pressure, Magnetic Field, and Arc Voltage. Figures 5.4 to 5.10 inclusive show the observed variation of J_c (max) with pressure, magnetic field (H), and arc voltage (J_v) for the three gases. The results obtained can be summarized in the following manner:

1. The maximum obtainable value of arc current increases with pressure under almost all conditions. Exceptions are noted, however, in some cases, e.g., for helium at $J_v = 200$ volts, $H = 1,900$ gauss; and for sulfur hexafluoride at $J_v = 200$ volts, $H = 11,700$ gauss, and at $J_v = 500$ volts, $H = 1,900$ gauss and 2,600 gauss. These exceptions, as well as a number of others not shown on these curves, all occur in limited pressure ranges.

2. For argon and sulfur hexafluoride the attainable arc current at a given pressure increases with magnetic field, the difference leading also in many cases to a greater rate of increase with pressure. For helium, on the other hand, there are conditions in which the attainable arc current is least for intermediate as well as small magnetic fields. This can be seen by reference to Figs. 5.7 and 5.8. Thus in Fig. 5.8 it will be seen that the best operation of the arc, as regards attainable arc current, occurs in magnetic fields between 1,900 and 2,600 gauss.

3. In general, increase of arc voltage also increases J_c (max). For argon and sulfur hexafluoride this effect is more marked the lower the magnetic-field strength. This is also true to some extent for helium but is confused by the complicated variation with magnetic field described in Sec. 1.

In discussing these results further the relative threshold pressures are considered first, and then the form of J_c (max)/ p as function of J_c (max).

(b) Observed Threshold Pressures. From Figs. 5.4 to 5.10 the pressures at which a true arc can be regarded as struck may be derived. These are recorded in Tables 5.1 to 5.3 for argon, helium, and sulfur hexafluoride, respectively. The effects of change of arc voltage, magnetic-field strength, and nature of gas are considered separately.

1. Variation with arc voltage. There is relatively little variation with arc voltage at the higher magnetic fields and at voltages above 300 volts. Since $q(J_v)$ would decrease as J_v is increased above 200 volts for all three gases if it arose from primary ionization only, it is clear that ionization by secondary electrons becomes important at the higher arc voltages, an effect that becomes more pronounced the higher the magnetic field. It is of interest to note (Chap. 9) that some measurements have been given for threshold pressures for

argon arcs with arc voltage below 100 volts, and these could be represented very well over a considerable range (down to $J_v = 20$ volts) by the assumption of primary ionization only.

2. Variation with magnetic-field strength. At the higher arc voltages the effect of magnetic-field variations is small for both argon

Table 5.1—Threshold Pressures, Argon

Magnetic field, kilogauss	Arc voltage, volts	Threshold pressure, mm Hg $\times 10^{-4}$
11.7	500	4.65
	400	4.65
	300	4.6
	200	4.8
	100	5.0
3.8	500	4.8
	400	4.65
	300	4.65
	200	5.5
	100	6.8
2.6	500	5.0
	400	4.65
	300	4.6
	200	6.8
	100	> 8.0
1.9	500	4.6
	400	4.65
	300	4.6
	200	> 8.0
	100	> 8.5

and sulfur hexafluoride, but for helium the threshold pressure rises, as the field decreases, to a maximum at about 4,000 gauss, and then falls again to a minimum before rising again at very low fields. The effect of the magnetic field on f_k is therefore relatively small at the high arc voltages except for helium. At the lower voltages, where secondary ionization appears to be unimportant, the variation with magnetic-field strength is as expected for argon and sulfur hexafluoride, i.e., decrease of threshold pressure with increasing field.

3. Variation with type of gas. Taking J_v as 200 volts, at which secondary ionization appears not to be very important, and using

Table 5.2—Threshold Pressures, Helium

Magnetic field, kilogauss	Arc voltage, volts	Threshold pressure, mm Hg $\times 10^{-4}$
11.7	500	20.7
	400	20.3
	300	19
	200	21
3.8	500	30.2
	400	29.5
	300	31
	200	31.5
2.6	500	22.7
	400	21
	300	24.5
	200	24.5
1.9	500	23
	400	21.5
	300	22.5
	200	24.5
1.1	500	20
	400	36
	300	39.5
	200	

Table 5.3—Threshold Pressures, Sulfur Hexafluoride

Magnetic field, kilogauss	Arc voltage, volts	Threshold pressure, mm Hg $\times 10^{-4}$
3.8	500	0.65
	400	0.70
	300	0.60
	200	0.60
2.6	500	0.65
	400	0.70
	300	0.60
	200	1.20
1.9	500	0.65
	400	0.70
	300	0.60
	200	1.25

Eq. 10 and taking for q the cross sections for primary ionization, the equation becomes

$$p_0(\text{argon}) : p_0(\text{helium}) : p_0(\text{SF}_6) =$$

$$1 : \frac{30f_K(\text{argon})}{f_K(\text{helium})} : 0.13 \frac{f_K(\text{argon})}{f_K(\text{SF}_6)} \quad (14)$$

From Tables 5.1 to 5.3 the following values for the f_K ratios at different magnetic fields are therefore found:

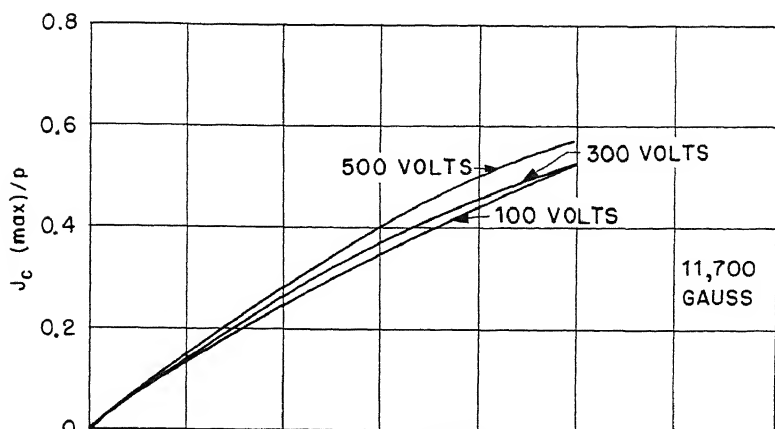
Table 5.4— f_K Ratios as a Function of Magnetic-field Strength

Magnetic field, kilogauss	$\frac{f_K(\text{argon})}{f_K(\text{helium})}$	$\frac{f_K(\text{argon})}{f_K(\text{SF}_6)}$
11.7	0.19	
3.8	0.25	1.0
2.6	0.16	2.0
1.9	< 0.13	1.2

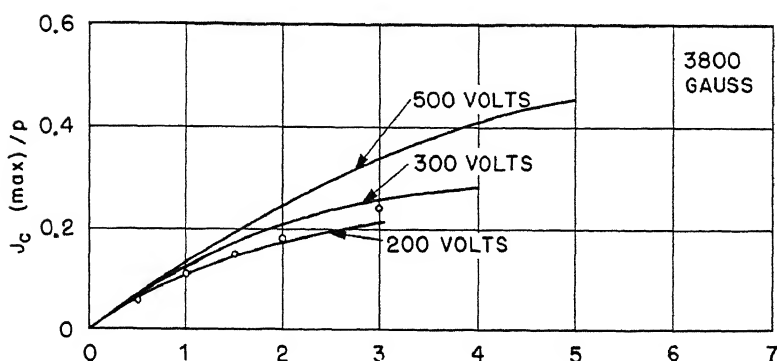
It would be expected that the lighter the mass of the ions the larger the value of f_K , as is found. A much wider variation would be expected in f_K in proceeding from argon to helium, owing to the large mass ratio, and therefore the f_K ratios found are not unreasonable. Also the effective mass of the ions in the case of SF_6 may well be rather smaller than for SF_5^+ ; therefore the f_K ratios in the third column of Table 5.4 may be somewhat too small.

4. Observed forms of $J_c(\text{max})/p$. In Figs. 5.11 to 5.13 the observed variation of $J_c(\text{max})/p$ with $J_c(\text{max})$ is illustrated for a variety of magnetic-field strengths, arc voltages, and types of gas.

For argon these curves were found to be smooth in all cases. If f_K were independent of J_c , and secondary ionization were not important, all the J_c/p curves should be superposable by a change of scale. This test was applied to the three curves for a 3,800-gauss magnetic field (Fig. 5.11), and it was found that the 200-volt curve tends to saturate earlier than the 500-volt curve. Unless there is assumed either a greater increase of f_K with J_c , or of secondary ionization and hence q , with J_c at the higher arc voltages, this result would not be explainable. Both these variations, which are not great, could well occur, an increase of electron temperature with arc currents being quite possible and leading to an increased secondary ionization, which is known from the threshold pressures discussed in paragraph 2, above,



(a)



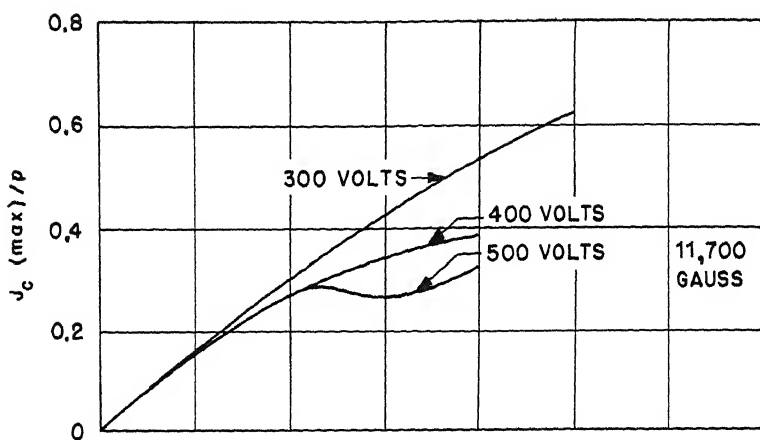
(b)

 J_c (AMP)

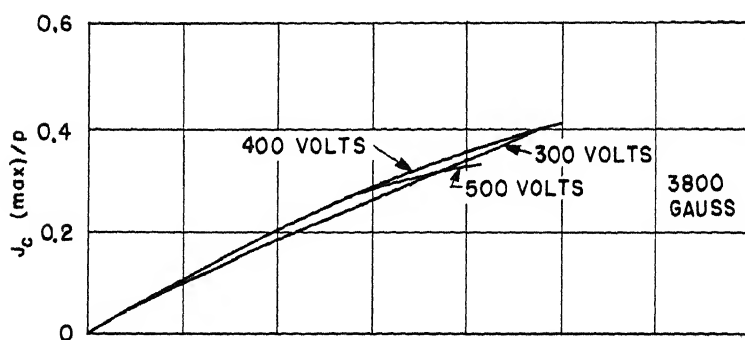
Fig. 5.11—Observed $J_c(\max)/p$ curves for argon. Calculated points, assuming primary ionization with scale chosen to give agreement at 1-amp arc current.

to be more important at the higher arc voltages. The shape of the 200-volt curve agrees well with the theoretical curve for argon shown in Fig. 5.1. (See Fig. 5.11, in which the scale of the theoretical curve has been adjusted to equality with the observed curve at $J_c = 1$ amp.) At the higher magnetic field the differences between the curves for different arc voltages are less apparent.

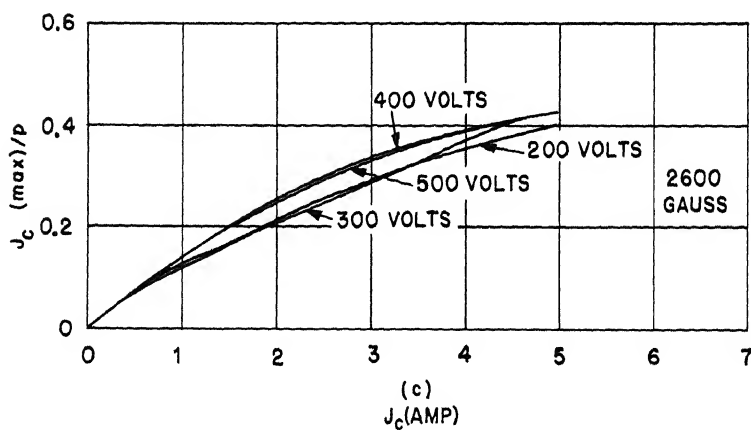
For helium the behavior of the $J_c(\max)/p$ curves for a magnetic field of 3,800 gauss (Fig. 5.12) most nearly follows the behavior expected on the elementary theory (primary ionization alone effective,



(a)

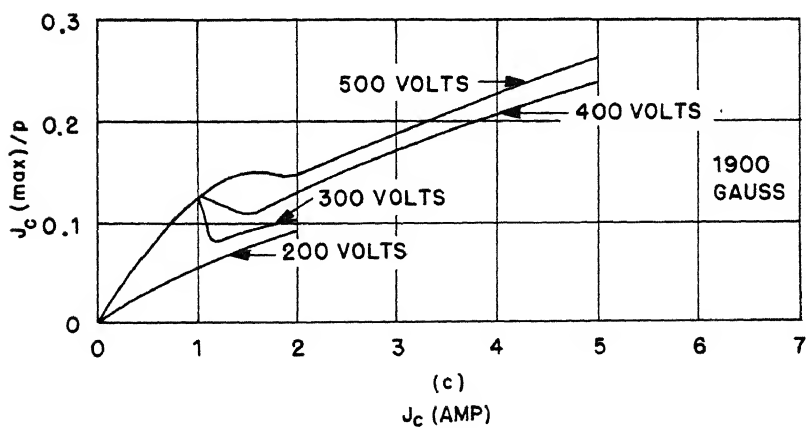
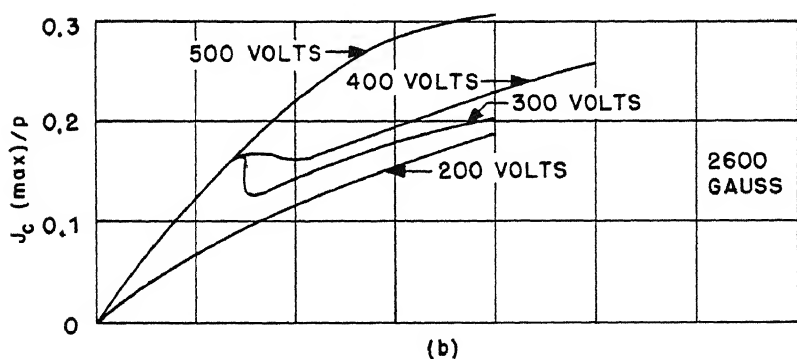
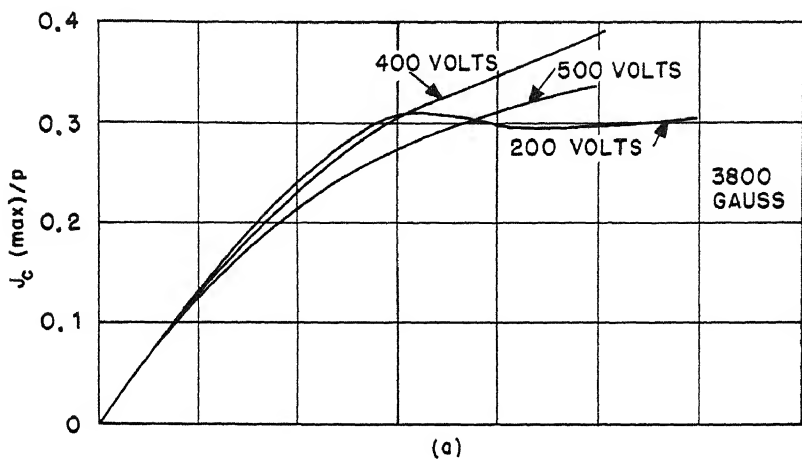


(b)



(c)

Fig. 5.12—Observed $J_c(\text{max})/p$ curves for helium.

Fig. 5.13—Observed $J_c(\text{max})/p$ curves for sulfur hexafluoride.

f_K nearly independent of J_c). This is particularly true of the curves for the lower arc voltages, which do not depart much from straight lines (compare with curve for helium in Fig. 5.1). The 500-volt curve is beginning to show a tendency toward saturation, but it is not very marked.

At the lower magnetic field of 2,600 gauss (Fig. 5.12) the curves are far from linear, indicating either a marked variation of f_K with J_c or a strong contribution from secondary ionization. The curves for the highest magnetic-field strength (11,700 gauss, Fig. 5.12) show clearly a case where a rather rapid variation of f_K with J_c occurs. This is for the 500-volt curve, indicating a change of state of the arc at an arc current of about 3 amp. The 400-volt curve does not show this effect to the same degree, but it does tend to flatten out rather markedly at arc currents above 2 amp. Further reduction of the voltage to 300 volts seems to remove the effect altogether in the range of arc currents up to 5 amp.

Cases of change of state at certain arc currents are most clearly exhibited by the $J_c(\text{max})/p$ curves for sulfur hexafluoride Fig. 5.13). It would appear that there are two states differing markedly either in f_K or the amount of secondary ionization. High arc voltage and high magnetic-field strength favor the first state, in which the ion current to the filament for a given arc current is the larger. Thus in Fig. 5.13 it will be seen that at the lowest magnetic-field strength (1,900 gauss) the transition occurs from the first to the second states when the arc currents are greater than 2, 1.5, and 1 amp, respectively, if $J_v = 500, 400$, and 300 volts, but for $J_v = 200$ volts the arc never runs in the first state at all. Increase of magnetic-field strength to 2,600 gauss raises the critical current to 1.5 amp for $J_v = 300$ volts, 2 amp for $J_v = 400$ volts, and 4 amp for $J_v = 500$ volts, but the arc still runs only in the second state for $J_v = 200$ volts. At the highest magnetic-field strength (3,800 gauss, Fig. 5.13) for all values of J_v observed, the arc runs in the first state up to an arc current of 3 amp, beyond which for $J_v = 200$ volts it begins to change over to the second state. For the higher J_v it remains in the first state up to $J_c = 5$ amp at least. None of the $J_c(\text{max})/p$ curves for either the first or second state saturates as quickly as would be expected if ions were being produced only by single-state primary ionization to SF_5^+ (compare with curve for SF_6 in Fig. 5.1, calculated on this assumption). As pointed out in the introduction, this is not surprising, since further stages of ionization that occur as the arc current is increased will increase the ion supply by providing F^+ as well as S^+ ions.

5. Effect of ion extraction by high voltage. To consider the effect of application of a high field at the arc slit that extracts ions from the

arc plasma, assume an arc running with maximum current at the pressure concerned before the field is applied.

It is to be expected that the effect of the field will not be pronounced until it is sufficiently large to drive the plasma boundary inside the arc slit, i.e., to form a concave meniscus. Then the reduced distance from the arc column to this boundary increases the gradient of potential within the plasma, which is responsible for the outward flow

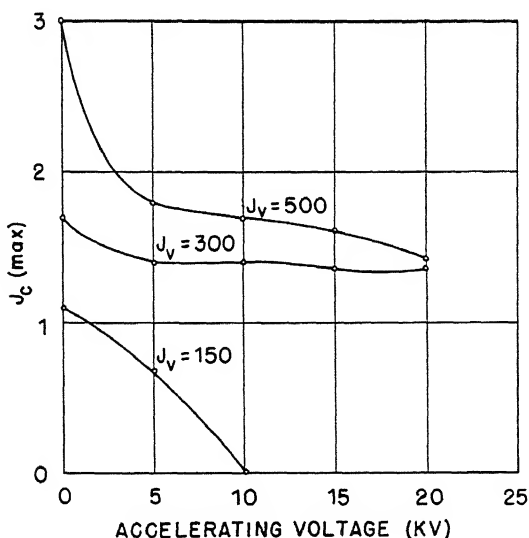


Fig. 5.14—Variation of maximum attainable arc current with accelerating voltage; argon arc, 3,800-gauss magnetic field. The accelerating voltage is the voltage between the arc slits and the accelerating slit. Pressure, 8.5×10^{-4} mm Hg.

of ions. The fraction of ions flowing upward to the filament is therefore reduced, and consequently lowers the maximum obtainable arc current. If no readjustment takes place within the arc to meet these changed circumstances, this decrease of maximum arc current should continue as the field increases until the arc flops out. On the other hand, readjustment of the potential distribution within the plasma may occur as the meniscus becomes more concave, tending to offset the increased ion drain outward.

Figure 5.14 illustrates some measurements that were made with the arc running with argon at a pressure of 8.5×10^{-4} mm Hg. The geometry of the electrode system over which the accelerating voltage was applied is shown in Fig. 5.3. It will be seen that, although at an

arc voltage of 150 volts the arc is unable to readjust itself to the application of the voltage and soon flops out, a considerable degree of adjustability is exhibited when the arc voltage is 300 volts or higher. This observation is in line with a number of other results discussed in preceding sections, which show that high arc voltage in general leads to a greater facility of the plasma to provide the necessary supply of ions to the filament under a variety of circumstances.

ACKNOWLEDGMENTS

The following persons contributed to the work of preparing this paper: J. Jungerman assisted in taking the observations; M. P. Edwards, J. Morris, and H. Tomlinson supplied technical assistance; and D. Bohm furnished many discussions of arc problems.

REFERENCE

1. P. T. Smith, Phys. Rev., 36: 1293 (1930).

Chapter 6

MEASUREMENTS OF THE ABSOLUTE VALUES OF THE CROSS SECTIONS FOR IONIZATION OF URANIUM TETRACHLORIDE AND URANIUM HEXAFLUORIDE BY ELECTRONS

By W. E. Berkey, E. H. S. Burhop, J. D. Craggs, J. Keene,
and H. S. W. Massey

1. INTRODUCTION

To gain an understanding of the performance of arcs run in vapors, it is important to obtain absolute values of the cross sections for ionization of these vapors. In the cases of gases such as argon, helium, and sulfur hexafluoride it had been expected theoretically (Chap. 4) and was confirmed by an experimental investigation (Chap. 5) that the threshold pressures for steady operation depend very markedly on the ionization cross sections. The work reported in this chapter is concerned with the measurements of the cross sections for ionization by electrons of uranium tetrachloride and uranium hexafluoride, for which no values have been reported in the literature. The dependence of threshold pressure on ionization cross section mentioned above would presumably apply in these cases also.

In the determination of ionization cross sections for electrons it is necessary to measure the absolute gas or vapor pressure. For the compounds discussed here the problem of measuring the pressure is of considerably greater difficulty than for most gases. The uranium tetrachloride has to be heated to several hundred degrees Centigrade to make the cross-section measurements, and the uranium hexafluoride is quite corrosive. Consequently the methods used for measuring the pressure are treated in some detail.

2. PRINCIPLE OF THE METHOD

The principle of the method employed is common to most previous work on rates of electron ionization. A beam of electrons of finite

energy, held together by a magnetic field, is accelerated from a hot cathode through a pinhole into the ionizing chamber in which the gas or vapor under investigation is maintained at a definite measurable pressure. The positive ions produced are all collected a short distance to the side of the beam by a plate to which a potential of -10 to -20 volts is applied relative to the ionization-chamber walls. If l is the path length of the electron beam before collection, p the gas or vapor pressure in millimeters of mercury (reduced to 0°C), i_1 the electron current, and i_2 the positive-ion saturation current, then Q_1 , the cross section for ionization, is given by

$$Q_1 = \frac{i_2}{i_1} \frac{760}{lp} \frac{1}{2.7 \times 10^{19}} \text{ sq cm} \quad (1)$$

To ensure that only ions formed by primary electron impacts are being measured, the current i_1 and the pressure must be such that i_2 is directly proportional to both. It is further necessary that a good saturation, at between -10 to -20 volts, is exhibited by the current characteristic of the positive-ion collector plate. To ensure this, the plate should extend over the whole length of the electron beam and be distant from it less than the mean Larmor radius of the ions in the magnetic field employed to hold the electron beam parallel. Further, in practice with an apparatus of this sort the path length l is not given by the geometrical distance the beam travels between entering and leaving the chamber. Many electrons present will not be moving initially in a direction parallel to the magnetic field and so will be executing spiral motions. On the average, this effect will not depend appreciably on the gas or vapor being ionized, and, therefore, before each experiment the apparatus was calibrated by using argon, for which the ionization cross section has been measured. Given below is a detailed discussion of the apparatus used and the procedures adopted to determine the pressure when using uranium tetrachloride and uranium hexafluoride, respectively.

3. DESCRIPTION OF APPARATUS

The electrons were supplied by a filament made from tungsten wire of 0.020 in. diameter. The beam was defined by a pinhole collimating slot, consisting of a hole $\frac{1}{32}$ in. in diameter in a tungsten sheet 0.020 in. thick, and was collimated by means of the magnetic field, which in these experiments was between $1,000$ and $2,000$ gauss. In the earlier experiments the arc current was controlled by varying the temperature of the filament, but with the low currents used in these experi-

ments the current tended to be unsteady and difficult to control accurately by this means. Later, a grid, consisting of another thin sheet of tungsten and a hole rather larger than the collimating slot, was placed between the filament and the collimating slot, and the current was controlled by applying a small negative potential to this grid. This provided a much steadier means of controlling the arc current. The collimating slot and arc chamber were connected together and maintained at earth potential, the filament itself being maintained at a negative potential that determined the energy with which the electrons passed through the collimating slot and into the arc chamber.

A section through the arc chamber is shown in Fig. 6.1. The chamber itself was made of copper that had been heavily nickel-plated. This was necessary, since uranium tetrachloride vapor will react with copper to produce a volatile chloride that is likely to upset the measurement of the total ionization cross section. The front of the arc chamber, A, consists of a nickel-plated copper plate $\frac{1}{2}$ in. thick. Inside the chamber and about $\frac{1}{4}$ in. from the front is placed the collecting electrode C, to which a small negative potential (10 to 20 volts) can be applied in order to collect positive ions produced by the electron beam E, which passes between the collector and the front wall A. The collector consists of a rectangular piece of nickel-plated copper shell, $2\frac{1}{2}$ in. long, $1\frac{5}{16}$ in. wide, and $\frac{1}{8}$ in. thick. A number of holes were drilled in the collector in order to facilitate the equalization of the pressure within the arc chamber.

The electron beam passed out of the arc chamber, through a hole $\frac{3}{4}$ in. in diameter, to the bottom and then fell upon the anode consisting of a disk of nickel-plated copper $\frac{3}{4}$ in. in diameter. The anode had to be kept well insulated from the arc chamber, since the minute current to the anode, of the order of 6×10^{-8} amp, had to be known accurately in order to calculate the ionization cross section. Normally a bias potential of about +20 volts was applied to the anode to prevent the injection of secondary electrons.

In order to carry out the measurements with uranium tetrachloride, the whole arc chamber had to be maintained at a temperature between 300 and 400°C. This was done by means of the cathode heater B. The temperature of the arc chamber was measured by a thermocouple embedded in one of the side walls, and this in turn controlled the temperature of the chamber by means of a Foxboro constant-temperature regulator. In the earliest experiments the anode was not separately heated, and the anode insulation failed, owing to the condensation of uranium tetrachloride around it. Subsequently, therefore, the anode was surrounded by a nichrome wire heater, and the temperature of the anode was measured by means of a thermocouple attached to it.

Normally the anode was maintained at a temperature of about 20°C above that of the arc chamber.

Also shown in Fig. 6.1 are details of the apparatus used when the ionization cross section in uranium tetrachloride vapor was being determined. D is a charge bottle (made from nickel), which could be

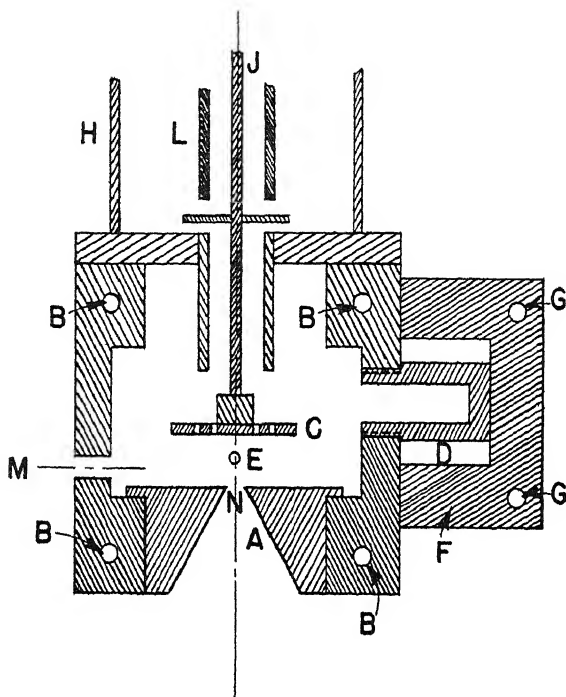


Fig. 6.1—Sectional view of the arc chamber.

screwed into the side wall of the arc chamber as shown. Three charge bottles were used in general, one above the other at different distances along the length of the chamber. The bottles were about two-thirds filled with uranium tetrachloride and sealed with thin foil to protect them from moisture. It was found necessary, in order to maintain the charge bottles at the same temperature as the arc chamber, to surround them with the copper shield F, which could itself be heated by means of the subsidiary calrod heaters G.

In general, it was found that the pressure of uranium tetrachloride in the arc chamber, estimated in the manner described below, was considerably lower than that which would be expected for the arc-chamber temperature from the vapor-pressure curve for uranium

tetrachloride. It was thus concluded that the total area of the evaporating surface was too small in comparison with the area of holes in the arc chamber through which the vapor could escape. Such a condition is rather serious for a measurement such as this, because it means that there will be large pressure gradients within the arc chamber itself. Accordingly, in the final run with this apparatus a shallow nickel container filled with uranium tetrachloride charge was placed on the bottom of the arc chamber. The total surface area of the charge in this container was many times greater than the evaporating surface area of the charge in the charge bottles. In the measurements made with uranium tetrachloride it is very important to avoid temperature gradients in the arc chamber, since these give rise to pressure gradients. Unfortunately, however, owing to the necessity of mounting the chamber, it was not possible to avoid temperature gradients altogether. The arc chamber was mounted about 3 in. away from a water-cooled brass plate by means of a stainless-steel tube H, which was turned very thin in order to reduce heat conduction.

When working with uranium hexafluoride or argon, the copper shield F was dispensed with, and the charge bottles were removed. One of the holes into which the charge bottles screwed was blocked up, and into a second hole was introduced a copper tube connected through a needle valve to a cylinder of uranium hexafluoride. At the same time a tube coming into the third hole could be connected to either a mercury McLeod gauge or an ionization gauge for the measurement of the arc-chamber pressure. The ion currents collected by the electrode C were conducted away through the conductor J and were measured by means of an FP54 electrometer tube with a d-c amplifier. Surrounding the lead J was the shield L, which was maintained at the collector-bias potential. In these experiments the collector current varied from 10^{-8} to 10^{-10} amp.

4. MEASUREMENT OF THE PRESSURE

The pressure of uranium tetrachloride in the arc chamber was determined by measuring the rate of effusion of uranium tetrachloride vapor through a hole of accurately known diameter. Provided the diameter of such a hole is small in comparison with the mean free path, the mass of gas of molecular weight M effusing per unit time through a hole of area A is given by

$$\text{Mass of gas} = \frac{pM^{\frac{1}{2}}}{(2\pi RT)^{\frac{1}{2}}} \quad (2)$$

where p is the pressure, T the absolute temperature, and R the gas constant per gram molecule. This expression holds for a hole of infinitesimal thickness. If the effusion occurs through a short tube instead, the mass rate of effusion given above has to be multiplied by a factor which can be calculated and which is less than 1.

Two holes, marked M and N in Fig. 6.1, were used in the effusion measurements. M is a cylindrical hole 0.098 in. in diameter and $\frac{1}{4}$ in. long. It is clear from the diagram that this hole is situated about 1 in. away from the electron beam at E, so that, if pressure gradients exist in the chamber, the pressure, as measured by effusion through the hole M, may not be the same as the pressure at E where the ionization actually takes place. Accordingly a second hole, N, was used in the front of the arc chamber near E. This was a tapered hole as shown, the minimum diameter being 0.098 in. and the angle of the taper 35 deg.

The type of collector used to condense the uranium tetrachloride vapor issuing through the holes M and N is shown in Fig. 6.2. It consists of a stainless-steel vessel P, $\frac{15}{16}$ in. in internal diameter and $1\frac{3}{8}$ in. long. The inside surface of this cylinder was roughened by sandblasting, since it was thought this might increase the fraction of uranium tetrachloride molecules that stick. The collecting cylinder was clamped to an outer brass cylinder Q through a rubber gasket R. Water was circulated in the space between P and Q to cool the collector P and thus prevent reevaporation of the uranium tetrachloride molecules from P. In order to test whether there was any reevaporation of the vapor after striking the water-cooled surface, the collector opposite M was fitted with a lid consisting of a thin stainless-steel disk that covered the opening of the collector except for a hole 0.150 in. in diameter in the center of the disk. It was not possible to place such a lid on the collector opposite the hole N, since the diameter of the outside of this conical hole was already equal to the diameter of the collector. A thermocouple was attached to the collector can to ensure that the temperature of the can did not rise appreciably.

The collectors were placed opposite the holes M and N, centered as accurately as possible relative to them, and about $\frac{1}{16}$ in. away from the outside surface of the arc chamber. A copper vane placed between the collectors and the holes M and N prevented material from entering the collector until the ion current collected by the electrode C of Fig. 6.1 had reached a steady value, thus indicating that any volatile impurities in the charge material had disappeared. These vanes were operated from outside the tank by means of rods passing through Wilson seals.

Two methods were used in the various runs for determining the amount of uranium tetrachloride deposited on the collectors. In the first method the mass was determined by direct weighing. The difficulty with this method was the very small masses involved. In order to get quantities sufficiently large to weigh by means of an ordinary chemical balance it was necessary to collect for many hours at a temperature considerably higher than that actually used in the experiment. Then, in order to estimate the pressure actually used when the

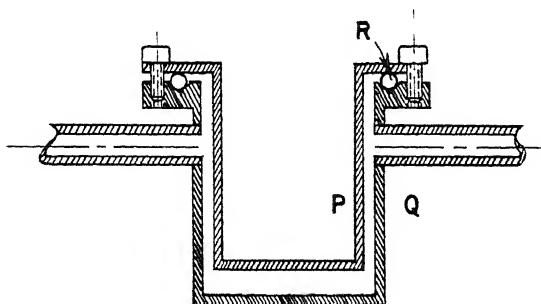


Fig. 6.2—Sectional view of water-cooled collector-can assembly.

total ionization determinations were made, recourse had to be made to the vapor-pressure curve for uranium tetrachloride. Furthermore, great care had to be taken to prevent the deposited material absorbing moisture from the atmosphere prior to the weighing. This was done by sealing up the opening to the collector P with paraffin immediately after letting down the vacuum. After the deposited sample had been weighed, a chemical analysis of it was carried out.

In the second method the uranium tetrachloride was dissolved out of the stainless-steel collector, and the uranium metal was recovered by electroplating, the amount of uranium present being determined by an alpha count. The accuracy obtainable with this method was usually of the order of 5 per cent. This method of uranium estimation was superior to the direct weighing method, since much smaller quantities could be used, and it was not necessary to collect for long periods at temperatures far above that for which the ion currents were measured. Further, the absorption of moisture by the uranium tetrachloride was a less important factor.

Knowing the mass rate of effusion of uranium tetrachloride and introducing an appropriate value for the factor γ to correct for the

shape of the holes used, Eq. 2 above was used to calculate the pressure.

The measurement of the pressure of uranium hexafluoride is difficult, owing to the readiness with which it reacts with the walls of the apparatus. Presumably, if all the surfaces were thoroughly outgassed this reaction rate would be very small. In practice, however, evidence has been found that considerable adsorption was occurring on the walls of the apparatus.

Two methods were used for the measurement of the pressure. In the first method a mercury McLeod gauge was used, connected to the arc chamber by means of a glass tube $\frac{1}{2}$ in. in diameter and about 6 ft in length. For the pressures used in this experiment and the compression ratio in the McLeod gauge, the pressure of uranium hexafluoride after compression is always much smaller than the vapor pressure, and therefore it is legitimate to apply Boyle's law for the compression of the vapor. In general there was no evidence, at the pressures dealt with in these measurements, of any action between the uranium hexafluoride vapor and the mercury in the McLeod gauge. A given sample of vapor was compressed and expanded several times in the McLeod-gauge bulb, but there was no evidence of any reduction in the indicated volume of the compressed vapor. With this method any adsorption of the uranium hexafluoride vapor on the walls of the arc chamber or of the tube connecting the arc chamber to the McLeod gauge would be expected to act in such a direction as to give too small a reading for the pressure.

The second method that was employed for the measurement of the uranium hexafluoride pressure depended on the use of a calibrated flowmeter. The uranium hexafluoride was introduced into the arc chamber by means of a needle valve and then passed through a copper tube 15 ft long and $\frac{1}{8}$ in. in internal diameter. The difference in pressure between the two ends of the tube was measured by means of a U-tube manometer that contained Litton oil as a working substance. Assuming conditions of hydrodynamical flow, the rate of flow of the vapor through the tube is connected with the pressures P_1 and P_2 at the ends of the tube by the relation

$$M = (p_1^2 - p_2^2)k \quad (3)$$

where k is a constant depending on the dimensions of the copper tube and the viscosity of the gas. Since, in these measurements, $p_1 \gg p_2$, we may write

$$M = kp_1^2 \quad (4)$$

The flow gauge was calibrated by measuring the loss of weight of a cylinder of uranium hexafluoride over a given period of time, with the needle valve set so as to maintain a constant reading of the manometer of the flow gauge over that period. In a typical calibration measurement the needle valve was adjusted so that the difference in height of the two columns of the flow-gauge manometer was 2 cm. The uranium hexafluoride was allowed to flow in for a period of about 6 hr. During this time the loss in weight of the uranium hexafluoride cylinder was about 20 g.

To estimate the arc-chamber pressure knowing the rate of flow of uranium hexafluoride, a subsidiary experiment was carried out using argon. By means of a Western Electric ionization gauge connected to the arc chamber, the pressure in the arc chamber was measured for argon as a function of the rate of flow of argon into the system. It was then assumed that for a given arc-chamber pressure the mass rate of flow through the arc chamber was proportional to the square root of the molecular weight of the gas flowing. In this way it was possible to obtain a calibration of the uranium hexafluoride pressure in the arc chamber as a function of the flowmeter readings.

The assumption made concerning the rate of flow through the arc chamber is correct provided there is no adsorption of the uranium hexafluoride on the walls of the arc chamber or of the tube leading from the flow gauge to the arc chamber. If there is adsorption on the walls, this method will indicate a value of the uranium hexafluoride pressure higher than the true value.

5. MEASUREMENT OF THE TOTAL IONIZATION CROSS SECTION

Before proceeding to measurements with uranium tetrachloride and uranium hexafluoride it was necessary to carry out a check measurement with argon for the reasons explained above. The arc chamber was filled with argon to a pressure of about 2×10^{-4} mm Hg as measured by the ionization gauge. A homogeneous electron beam of energy determined by the negative potential applied to the filament relative to the arc chamber (which was grounded) was then accelerated through the collimating slot. The magnitude of the beam striking the anode was measured and was usually about $0.1 \mu\text{a}$. The collecting electrode C was made about 10 volts negative relative to the arc chamber. Thus positive ions produced by the passage of the electron beam through the gas were collected at C. Then the total cross section could be determined from Eq. 1 above. The actual value of the negative-bias potential that had to be applied to C to ensure collection of all the ions was determined by measuring the collector current as a function of collector bias.

The curves obtained exhibited good saturation characteristics and indicated that virtually all the positive ions produced are collected by C with a bias of 10 volts. This is below the ionization produced by secondary electrons before reaching the grounded arc-chamber wall.

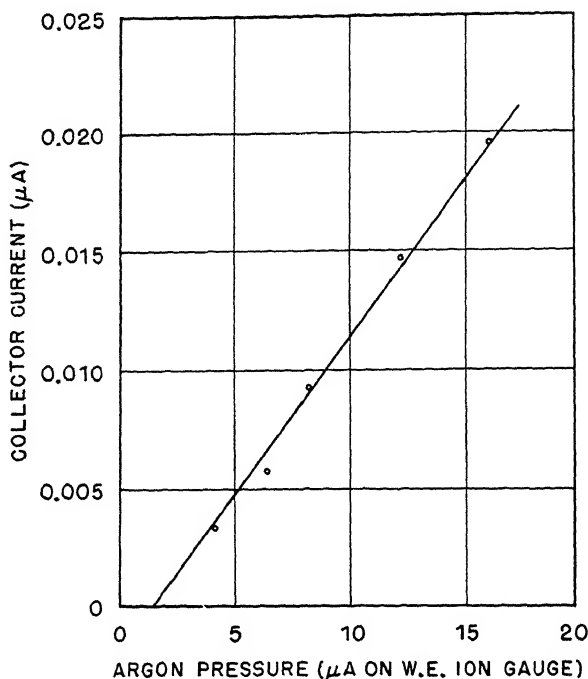


Fig. 6.3—Collector current vs. pressure for argon. Arc voltage, 200 volts; arc current, 0.03 μ a; magnetic-field strength, 1,000 gauss; collector bias, -20 volts.

In order to ensure that the pressure and currents at which these measurements were carried out were low enough to make certain that the conditions for each electron and atom undergoing not more than a single ionizing collision were satisfied, the collector current was measured as a function of arc current and of the pressure. Figures 6.3 and 6.4 indicate that a linear relationship exists between collector current and both pressure and arc current, thus satisfying the single-collision criterion. The fact that these currents do not pass exactly through the origin is not significant. It is due to zero errors in the measuring instruments.

Figure 6.5 shows the variation of total ionization cross section of argon with arc voltage. The absolute value of the cross section for

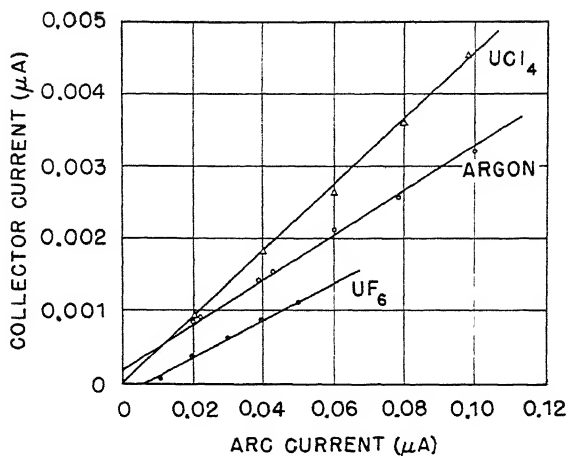


Fig. 6.4—Collector current vs. arc current; collector bias is -20 volts for all curves. For argon: arc voltage, 100 volts; pressure in arc chamber, 1.7×10^{-4} mm Hg; magnetic-field strength, $1,000$ gauss. For uranium tetrachloride: arc voltage, 100 volts; arc-block temperature, 350°C ; magnetic-field strength, $1,000$ gauss. For uranium hexafluoride: arc voltage, 200 volts; pressure in arc chamber, 2×10^{-3} mm Hg, magnetic-field strength, $2,000$ gauss.

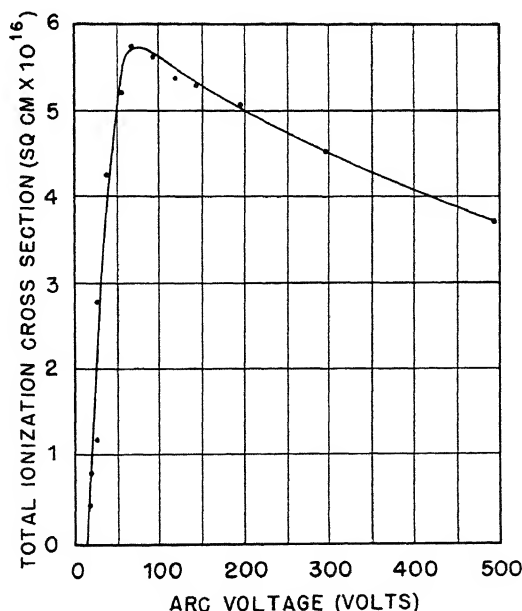


Fig. 6.5—Ionization cross section vs. arc voltage for argon. Arc current, $0.06 \mu\text{A}$; pressure in arc chamber, 1.7×10^{-4} mm Hg; magnetic-field strength, $1,000$ gauss; collector bias, -20 volts.

electrons of 100 volts energy is seen to be 5.70×10^{-16} sq cm. This is to be compared with the value given by Smith¹ of 4.44×10^{-16} sq cm. Thus the value obtained from the present apparatus is about 30 per cent too high. This seems reasonable in view of the uncertainty of the total electron-path length (see Sec. 2).

With uranium tetrachloride the measurements for the first two runs were carried out using a direct-weighing method for the determination of the uranium tetrachloride pressure, as described above. Both these runs suffered from various defects, primarily due to electrical difficulties.

In run 3 the counting method of determining the amount of uranium present as described above was used for the first time. It is pointed out above that this method requires a much shorter collection time than the direct mass-determination method. In this run the uranium tetrachloride was not baked sufficiently before starting to collect, and the current to the ion-collecting electrode fell continuously during the run. The value obtained for the ionization cross section was absurdly high, being about 190 times that for argon for electrons of 100 volts energy. In view of this disturbing result it appeared likely that in this run the impurities had never been eliminated, and the ionization was therefore produced in some material other than uranium tetrachloride vapor. In view of this, in the next run (run 4) the apparatus was set up with a mass spectrograph (see Chap. 7).

The arc chamber was heated to 400°C , and after about 30 min at this temperature a mass-spectrographic analysis was made. A bewildering collection of ion beams was found. UCl_3^+ was relatively weak, and two other ion beams were more than ten times as intense. One of these was identified as CuCl_2^+ . The other was a very heavy ion with a mass of about 540 and could conceivably have been UBr_4^+ . After baking overnight it appeared that the impurities had mostly disappeared, and the collection was started. The ionization current to the collecting electrode C was measured as a function of anode current both before and after collection. A check was also made of the collector current as a function of collector bias to determine the potential that had to be applied to the collector to ensure saturation. Figure 6.6 shows that the saturation was reasonable at -10 volts bias. In Fig. 6.4 is shown the variation of collector current with the anode current, and it can be seen that the curve obtained is linear. Figure 6.7 shows the variation of collector current with arc voltage. For given arc voltage and arc current it was found that the collector current did not change more than 2 per cent during the period of collection (about 3 hr). The collector on opposite M was now assayed for uranium by the counter method referred to above.

The following data were obtained for this run:

Mass of uranium metal collected by can	7.25×10^{-4} g
Mass of uranium tetrachloride collected by can	1.15×10^{-3} g
Temperature of collector	400°C
Time of collection	1.13×10^4 sec
Area of hole M	0.046 sq cm
Mass rate of effusion through hole at 400°C	2.21×10^{-6} g/sq cm/sec

From these data can be calculated the following:

Pressure of uranium tetrachloride at 400°C	4.16×10^{-5} mm Hg
Molecular density at 400°C	6.48×10^{11} molecules/cc
Anode current	6.0×10^{-8} amp
Arc voltage	100 volts
Collector current	2.0×10^{-9} amp
Length of arc column	6.4 cm
Total ionization cross section:	

$$\frac{2.0 \times 10^{-9}}{6.0 \times 10^{-8}} \times \frac{1}{6.4 \times 6.48 \times 10^{11}} = 8.0 \times 10^{-15} \text{ sq cm}$$

This value of the ionization cross section for uranium tetrachloride is $14 Q_a^i$, where Q_a^i is the cross section for argon. Measurements made at 380 and 360°C gave values for the ionization cross section of $12.5 Q_a^i$ and of $14.5 Q_a^i$, respectively, giving a mean value of $13.6 Q_a^i$.

In all the runs up until this one the hole M was tapered, the angle of taper being 45 deg. A rough estimate shows that the value of the ionization cross section deduced above should be reduced by about 10 per cent to allow for this taper. In order to reduce this uncertainty factor in subsequent runs, the hole at M was made cylindrical as shown in Fig. 6.1. For a cylindrical hole the correction due to finite length has been calculated accurately.

At a temperature of 400°C the vapor pressure of uranium tetrachloride is 5×10^{-3} mm Hg. In the results given above, however, it is seen that the measured pressure actually came to be 4.16×10^{-5} mm Hg, i.e., less than one one-hundredth of the vapor pressure. This undoubtedly arises from the small evaporation area of the uranium tetrachloride. In view of this difference between the estimated pressure and the known vapor pressure, it is important to examine whether pressure gradients occurring in the arc chamber could upset the results. The hole M was about 1 in. away from the electron beam E, and consequently the pressure measured at M may be quite different from the actual pressure at E. In order to check this, a second collector was placed opposite the hole M in run 5.

The results of run 5 were as follows:

Ionization cross section estimated from front collector, $10.2 Q_a^1$.

Ionization cross section estimated from side collector, $13.9 Q_a^1$.

It appears from this run, then, that, owing to pressure gradients in

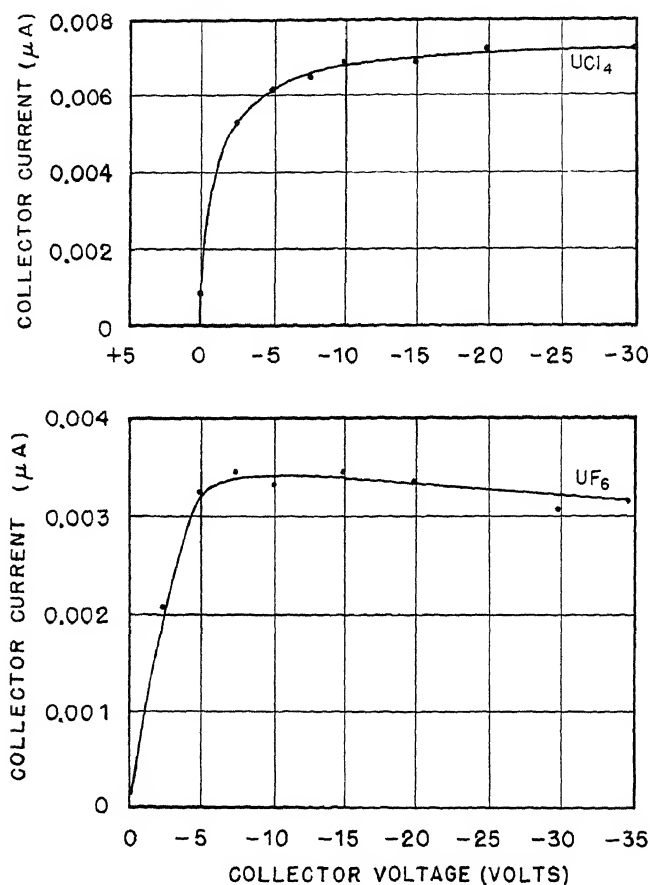


Fig. 6.6—Collector current vs. collector voltage; for both curves, arc voltage is 100 volts, and arc current is $0.06 \mu a$. For uranium tetrachloride: arc-block temperature, $350^\circ C$; magnetic-field strength, 1,000 gauss. For uranium hexafluoride: pressure in arc chamber, 9×10^{-4} mm Hg; magnetic-field strength, 2,000 gauss.

the arc chamber, the pressure near the electron column at E is about 35 per cent greater than the pressure as measured by effusion through the hole M.

In run 5 a lid with a hole in the middle was placed over the collector opposite M, as described in the section above on the measurement of

pressure. It was found that an inappreciable amount of uranium tetrachloride was deposited on the inside of the lid, thus indicating that practically all the uranium tetrachloride striking the water-cooled surface of the collecting can stuck to it.

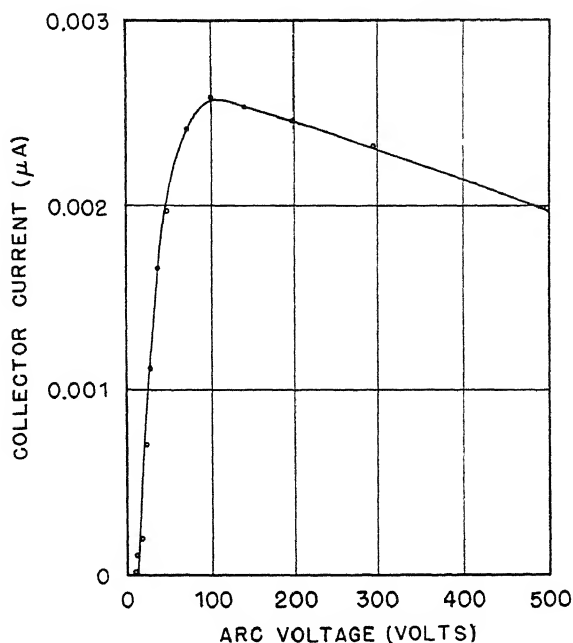


Fig. 6.7—Collector current vs. arc voltage for uranium tetrachloride. Arc current, $0.06 \mu\text{A}$; arc-block temperature, 350°C ; magnetic-field strength, 1,000 gauss; collector bias, -20 volts.

In the final run (run 6) an attempt was made to run under conditions at which the pressure of uranium tetrachloride was more nearly the vapor pressure at the temperature of the arc chamber. A subsidiary charge bottle in the form of a flat nickel disk about 2 by 1 cm was placed on the bottom of the arc chamber behind the collecting electrode C. In this run the measured arc-chamber pressure was about twenty-five times less than that estimated from the vapor pressure. The run appeared to be a good one, and the side collector (opposite M) gave a value of ionization cross section of about $16 Q_a^i$. In this case the hole in the lid of the collector was not directly opposite the hole M, and uranium tetrachloride was deposited on the outside of the lid. Although most of this was recovered, some was probably lost on the Parafilm that was used to cover the collecting-can orifice. Thus the

value of the cross section obtained would be expected to be high. For some reason, which is not clear, the result of the assay of the collecting can opposite N showed less uranium tetrachloride than the can opposite M. It is most difficult to understand how this could occur, since clearly the rate of effusion through the hole N of infinitesimal length should be much greater than through the cylindrical hole at M.

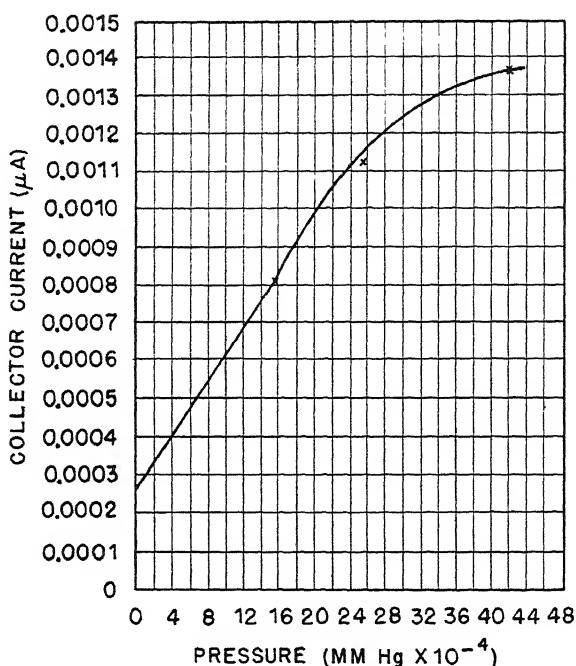


Fig. 6.8—Collector current vs. pressure in arc chamber for uranium hexafluoride. Arc current, $0.06 \mu a$; arc voltage, 200 volts; magnetic-field strength, 2,000 gauss; collector bias, -20 volts.

In this case the correction factor for the finite length of the hole M was 2.79. Moreover, if the pressure as indicated by the front can were correct, it would indicate an absurdly high ionization cross section of about $80 Q_a^i$. It seems reasonable, then, to neglect this one value and to suppose that some error crept into the measurement during this collection.

The evidence from the collector opposite M in the three good runs referred to above suggests a cross section of about $14 Q_a^i$. However, run 5 has indicated that the measured pressure at M is lower than the pressure near E by about 35 per cent. Thus, allowing for this, the

cross section of ionization of uranium tetrachloride by electrons of about 100 volts energy comes out at about ten times the ionization cross section for argon by electrons of the same energy. That is, $Q_{UCL_4} = 5 \times 10^{-15}$ sq cm for electrons of 100 volts energy.

The procedure for carrying out the measurement in uranium hexafluoride was essentially similar to that used for argon except that the pressure was determined by the two methods outlined above, namely, mercury McLeod gauge and flowmeter, instead of the ion-gauge determination used in the case of argon.

In Fig. 6.6 a typical collector characteristic curve for uranium hexafluoride appears, showing once again the existence of good saturation for bias voltages above 7 volts.

Figures 6.4 and 6.8 show the variation of collector current with arc current and with estimated pressure, respectively.

The absolute value of the total ionization cross section for the two methods of pressure determination varied so widely that it is difficult to draw any definite conclusion. Using the mercury McLeod gauge, the cross section for electrons of 100 volts energy came out to be twelve times the total ionization cross section for electrons of the same energy in argon.

Using the flowmeter method of pressure estimation, however, this value came to be only $0.6Q_a^i$. In view of the results found in the uranium tetrachloride case, it is difficult to believe the cross section for uranium hexafluoride could be as low as the latter value. This would seem to indicate that the McLeod-gauge pressure measurements were more reliable than those made with the flowmeter.

6. SUMMARY

The experimental investigation described above has indicated a value of about 5×10^{-15} sq cm for the ionization cross section of uranium tetrachloride for electrons of 100 volts energy. This is about ten times the value for argon for electrons of the same energy. There is some question regarding the accuracy of the pressure determination. However, it appears fairly certain that the ionization cross section for uranium tetrachloride is several times that for argon.

In the case of uranium hexafluoride, the disparity between the results obtained by the two methods of measuring pressure is so great that no value can be given for the ionization cross section. It does appear that the McLeod-gauge method of determining pressure would lead to more reasonable results. However, considerably more work will have to be done with this compound before a trustworthy value of the ionization cross section could be given.

ACKNOWLEDGMENTS

Thanks are due the following persons for contributions to this experiment: Dr. B. Peters, who designed the original apparatus; Dr. C. Watt and J. Jungerman, for assistance in making some of the observations; R. Lilly, for carrying out the numerous assays of the samples by the counting method; Dr. T. S. Pillsbury, for carrying out the chemical analysis in runs 1 and 2; Roy Krohn, for preparing the UCl_4 charge bottles; Dr. G. McWood, for preparing some specially pure charge material and for valuable discussions; M. P. Edwards and J. Morris, for valuable technical assistance; and S. Wild and B. Parker, for assistance with the electrical measurements.

REFERENCE

1. P. T. Smith, Phys. Rev., 36: 1295 (1930).

Chapter 7

THE IONIZATION AND DISSOCIATION OF URANIUM TETRACHLORIDE AND URANIUM HEXAFLUORIDE BY ELECTRON IMPACT

By E. H. S. Burhop, H. S. W. Massey, and C. Watt

1. INTRODUCTION

In the operation of uranium tetrachloride and uranium hexafluoride arcs a considerable proportion of the beam leaving the arc slits consists not of U^+ ions but of ions of UCl_n^+ , UF_n^+ , etc. As a first step in studying the relative intensities of these ion beams it is of fundamental interest to study the way in which uranium tetrachloride and uranium hexafluoride are dissociated and ionized by the impact of electrons under conditions in which the dissociation is produced by single impacts of electrons homogeneous in energy. In the present investigation the electron-current density is kept sufficiently low to ensure that the chance of a neutral molecule suffering collision with more than one electron is small. The pressure is so low that the chance of an electron suffering an ionizing collision with more than one neutral molecule is also small. Under such conditions the ionization is too weak to give rise to any marked plasma effects, and consequently the possibility that some of the ionization may be due to plasma electrons is small.

This investigation covers a study of the relative intensities of the ions UCl_n^+ , UCl_n^{++} , Cl^+ , Cl^- , UF_n^+ , UF_n^{++} , UF_n^- , F^+ , F^- , etc., produced by electron impact for different electron energies, current densities, and pressures, and we have also measured the appearance potentials for the various ions.

From a knowledge of the appearance potentials and of some of the chemical constants of UF_n and UCl_n it is possible to obtain some information on the processes in which the various ions are formed.

2. DESCRIPTION OF APPARATUS

The arc chamber in which the ionization and dissociation were produced has already been described in Chap. 6. A few modifications of this chamber were made, and a mass spectrometer was added so that the setup was as shown in Fig. 7.1. This figure shows a section through the apparatus perpendicular to the magnetic field.

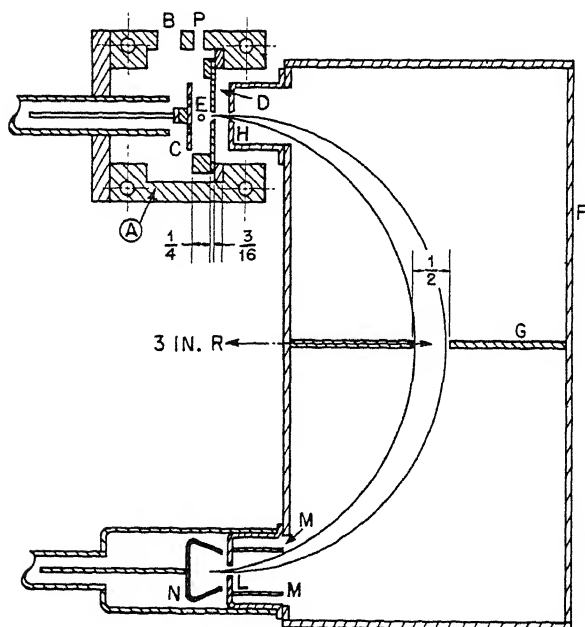


Fig. 7.1—Sectional view of arc chamber and analyzer.

The walls A of the arc chamber are made of nickel-plated copper, $\frac{1}{4}$ -in. thick with calrod heaters embedded in them. The uranium hexafluoride was introduced through the hole B in one of the side walls. For the uranium tetrachloride experiment three nickel charge bottles were screwed into the side of the chamber just as described in Chap. 6. The ionizing electron column was placed at position E in the chamber. It was defined by means of a tungsten collimating slot consisting of a hole $\frac{1}{32}$ in. in diameter in a thin tungsten plate, and the beam was collimated by the magnetic field. The anode was insulated from the collimating-slot electrode and the walls of the chamber and thus gave a true measure of the electron current. In general, a potential of

about +20 volts was maintained on the anode to prevent the emission of secondary electrons, but this potential was not applied when measurements were being made of the appearance potentials. In front of the electron column was placed the arc slit D, which in most of these experiments was 0.010 in. wide and $1\frac{1}{2}$ in. long. Behind the electron column was electrode C, upon which a positive potential was placed in order to accelerate the ions toward the arc slit. In general, the potential difference between C and D was about 10 volts. It has to be kept low to prevent ionization by the secondary electrons that are accelerated toward C. Both C and D are made of nickel-plated copper.

The box F, constructed from copper sheet, served as the mass spectrometer. The slit H was 0.030 in. wide and $1\frac{1}{2}$ in. long, and the clearance between the arc slit and the slit H was $\frac{3}{16}$ in. Thus the slits D and H defined a beam in an angular range of ± 4 deg. The beam was also defined within this angular range by means of the defining vane G in the 90-deg position. The collector slit L was 0.025 in. wide and 2 in. long, and the distance between the L and H slits was 6 in.; consequently the spectrometer operated on a 3-in. radius. On either side of the collector slit were two vanes M, placed in such a position that when the UF_4^+ beam was entering the collector slit the UF_3^+ and UF_5^+ beams fell outside these vanes.

The collector N was made of copper and was bent into the shape shown to prevent the escape of secondary electrons. The collector was completely surrounded by a metal shield at the potential of the H slit. The apparatus was set up in the 37-in. Berkeley magnet, and it was necessary to measure the very small currents collected by the collector M (somewhat of the order of 10^{-12} amp) at a distance of about 8 ft from the magnet in order to get the electrometer tube away from the magnetic field. A shielded lead of this length possesses a considerable capacity, and this means that, for a conventional type of circuit, the true constant of the impact to the electrometer tube will be long (of the order of some tens of seconds). In order to overcome this difficulty a d-c amplifier in which the effective time constant was a small fraction of a second was developed. This amplifier operated very satisfactorily in these experiments.

3. RESULTS OF EXPERIMENTS

3.1 Uranium Tetrachloride. (a) Relative Intensity of Ion Beams. Data on the ion beams that were observed following ionizing electron collisions with uranium tetrachloride are shown in Table 7.1; the relative intensities, under conditions where it would be expected that only single-collision processes are important, are shown for a num-

ber of different electron energies, the intensity of UCl_3^+ being taken as 100 in each case.

(b) Variation of Ion-beam Intensities with Voltage. Figure 7.2 shows the variation of intensity of the UCl_3^+ beam with voltage, taking the intensity as 100 at an electron energy of 100 volts. A type of voltage variation similar to this was observed for all the positively charged ions, although in the case of the doubly charged ions the intensity fell away more rapidly after passing through its maximum at about five times the appearance potential.

Table 7.1 — Relative Intensities of Ion Beams at Various Electron Energies
(Arc-current density = 1 ma/sq cm)

Ion	Electron energy				
	25 ev	50 ev	100 ev	200 ev	500 ev
UCl_4^+	13.5	13.2	14	12.9	13
UCl_3^+	100	100	100	100	100
UCl_2^+	47	38	30	26	25
UCl^+	26	40	40	31	29
U^+	0	28	37	36	34
Cl^+	0	40	84	91	94
Cl_2^+	0	0.9	1.8	1.4	1.4
UCl_4^{++}	0.5	1.1	2.0	1.1	1.0
UCl_3^{++}	0	1.6	3.5	1.9	1.1
UCl_2^{++}	0.5	4.2	13.8	9.3	5.0
UCl^{++}	0.1	4.7	17.9	11.5	5.4
U^{++}	1.5	4.2	16.6	11.7	7.6
UCl_4^-	2.6	3.0	4.4	5.4	3.8
UCl_3^-	15.5	30	62	95	76
UCl_2^-	2.0	1.5	2.3	2.4	9.5
Cl^-	49	41	18	3.8	2.7

In the case of the negative ion intensities the variation with arc voltage was far from regular. Curves for UCl_3^- , UCl_4^- , and Cl^- are shown in Figs. 7.2 and 7.3. The curve for UCl_4^- has the same general type of variation with arc voltage as in the case of UCl_3^+ and exhibits a definite appearance potential at about 15 volts, although the flat maximum of intensity appears to occur at somewhat higher potentials (from twelve to fifteen times the appearance potential) than was the case with the singly charged positive ions. The curve for UCl_3^- shown in Fig. 7.2 exhibits a definite subsidiary maximum at about 10 volts, and for the voltages below 2 volts its intensity was rapidly reaching a maximum for arc voltages near zero. It appears likely that this rise of UCl_3^- intensity with decreasing arc voltages near zero arises

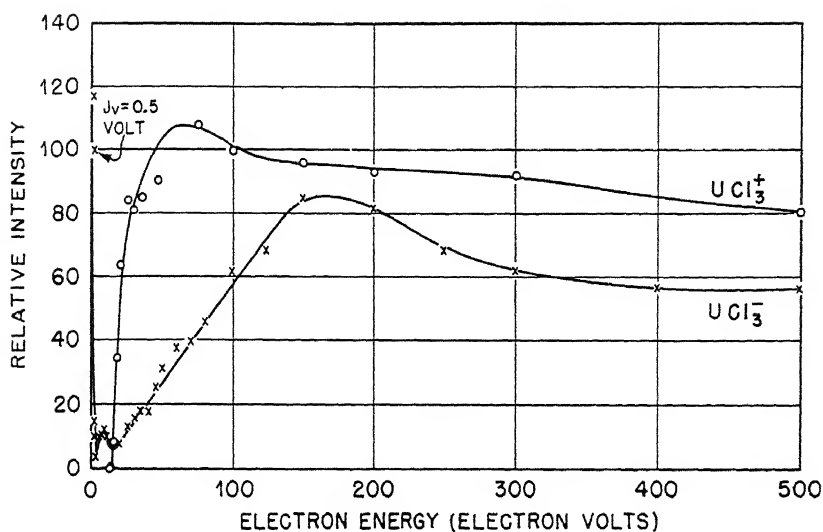


Fig. 7.2—Intensity as a function of electron energy for UCl_3^+ and UCl_3^- ions.

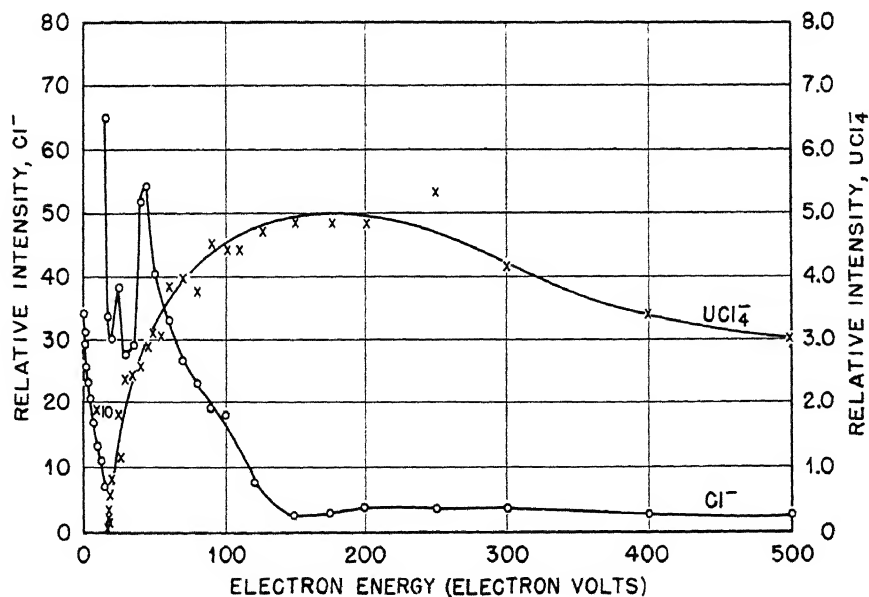


Fig. 7.3—Intensity as a function of electron energy for Cl^- and UCl_4^- ions.

from direct attachment to a neutral molecule. It would be expected that the chance of such attachment would increase rapidly with decrease of arc voltage near zero. Another possible factor giving rise to an increase in negative-ion intensity near zero voltages consists in the formation of negative ions by extraction of an electron from the hot tungsten filament by a neutral molecule at the surface. In accordance with Saha's equation, the chance of this happening would increase rapidly with increase of filament temperature. When running at low arc voltage there was always a tendency to run with the filament hotter in an attempt to push up the arc current, and consequently this effect may have become more important at low arc voltages.

The variation of Cl^- intensity with arc voltage is very complex, as shown in Fig. 7.3. Very large intensities of Cl^- were observed almost down to zero voltage. (The drop of potential across the filament would be such as to give an effective arc voltage of a couple of volts even when no further arc voltage was applied.) The Cl^- intensity reaches a minimum at about 20 volts and then passes through two distinct maxima, one at 25 volts and one at 42 volts, before it falls rapidly to small values. Above about 150 volts arc voltage there appears to be very little Cl^- produced in single impacts.

(c) Variation of Ion-beam Intensity with Arc Current. Figures 7.4 and 7.5 show the variation of intensity with arc current over a wide range of current for the ion beams UCl_3^+ , U^+ , UCl_2^{++} , and Cl^+ . In these curves a current of $100\ \mu\text{a}$ represents a current density of $10\ \text{ma/sq cm}$. Also the curves in Fig. 7.5 show the relative intensities of the ions Cl^+ , U^+ , and UCl_2^{++} . Except for UCl_3^+ , all these curves show a tendency to increase less rapidly for the higher arc currents as though some kind of saturation were beginning to become important. It is difficult, however, to see how any kind of saturation could be appearing at these low current densities.

For the negative ions the variation with arc current is anomalous. Figure 7.6 shows the variations of intensity of UCl_3^- with arc current for two arc voltages, 1 volt and 50 volts. In the latter case the intensity appears to increase faster than linear. This can probably be attributed to the formation of negative ions by extraction of electrons from the filament as has been discussed above. To obtain the higher arc currents the filament has to be run hotter, and therefore an overall increase of UCl_3^- intensity faster than linear might be expected. In the case of an arc voltage of 1 volt, however, the intensity-current curve shows a rapid saturation. Figure 7.7 shows similar curves for the variation of Cl^- intensity with arc current. In this case the curve corresponding to an arc voltage of 50 volts shows a marked decrease with increase of arc current. The explanation of this phenomenon is

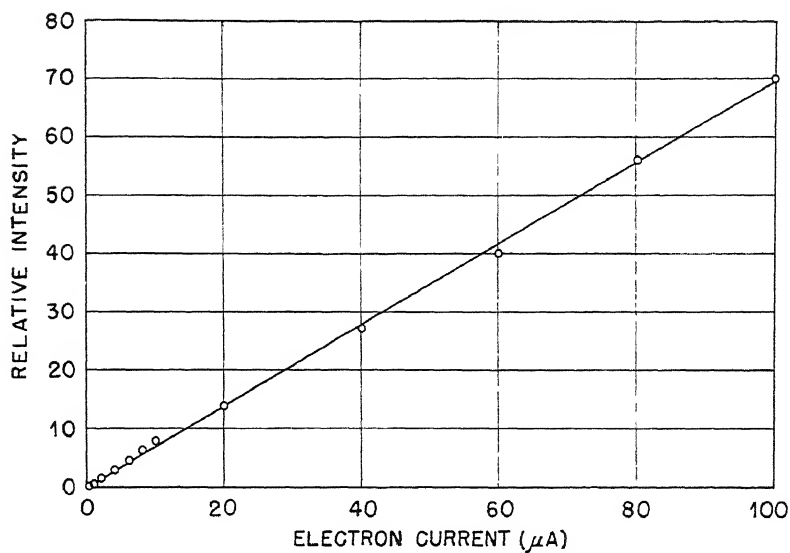


Fig. 7.4—Intensity as a function of electron current for the UCl_3^+ ion (electron energy = 100 ev).

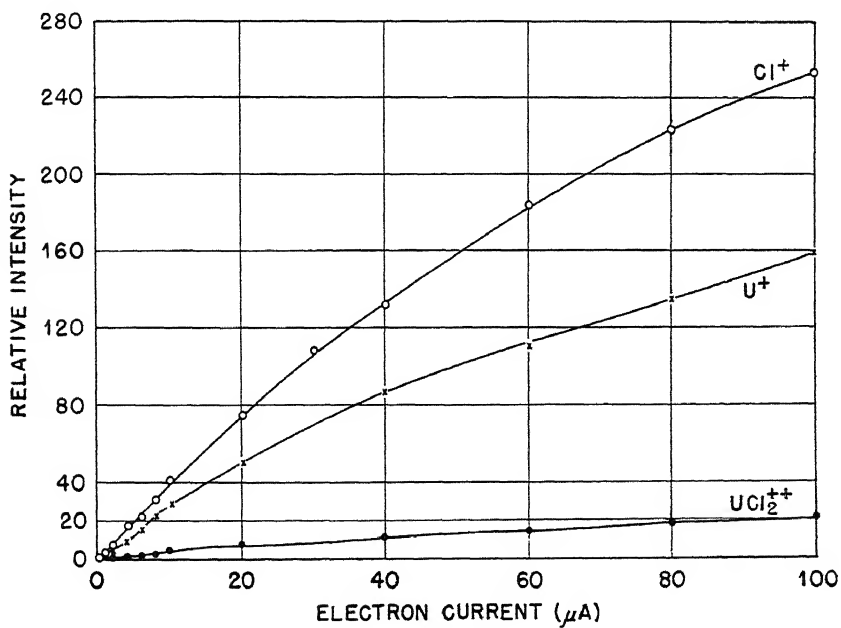


Fig. 7.5—Intensity as a function of electron current (electron energy = 100 ev).

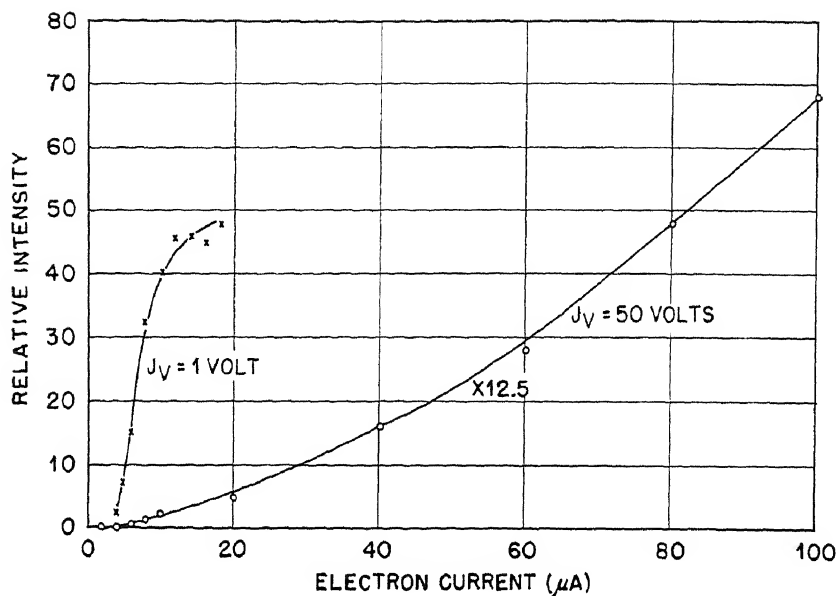


Fig. 7.6—Intensity as a function of electron current for the UCl_3^- ion.

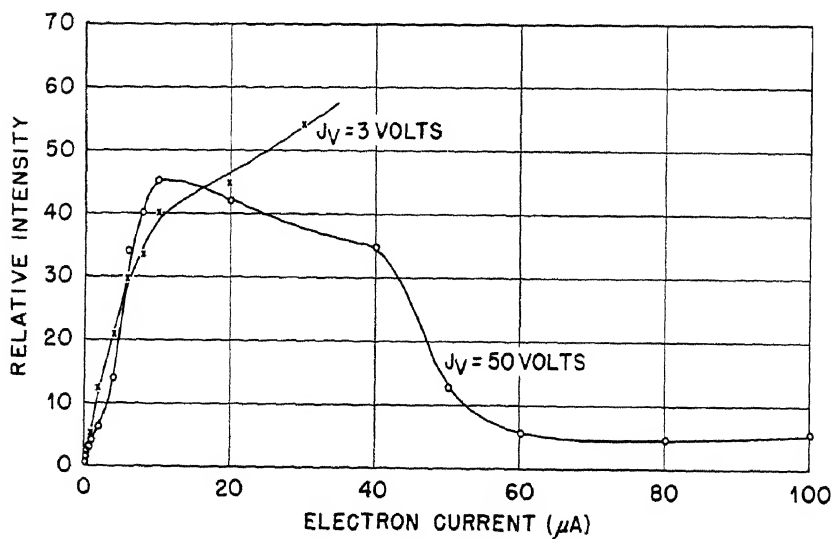


Fig. 7.7—Intensity as a function of electron current for the Cl^- ion.

not clear. It seems unsafe to draw conclusions from these curves about the production of negative ions in the dissociation of UCl_4 by electron impact, since such a process of formation is masked by the other processes discussed above.

(d) Appearance Potentials. The appearance potentials of the various ions have been determined by measuring the variation of intensity of the various ion beams with voltage for voltages near the appearance potential and extrapolating back to zero intensity. For this experiment a Leeds & Northrup potentiometer was used to measure the arc voltage. With the aid of this instrument, measurements of the ion-beam intensity were made for different arc voltages decreasing in steps of 0.1 volt near the appearance potential. To calibrate the apparatus and to make allowance for errors arising from contact potentials, the ionization potential of argon was first measured, and then the appearance potentials of the UCl_4 and UF_6 fragments were measured relative to the ionization potential of argon, which was taken to be 15.7 volts. The actual measured value of the argon ionization potential taken with the setup used for appearance-potential measurements was 15.0 volts, so that the correction to the observed results arising from calibration errors and contact-potential correction was only 0.7 volt.

Figure 7.8 shows a typical curve of the variation of intensity with arc voltage near the appearance potential for the UCl_3^+ ion. For comparison, a similar curve for A^+ is shown in the same figure. It is seen that the two curves have a different form near the appearance potential. In the case of A^+ the rise from zero intensity at the appearance potential is quite sharp. For UCl_3^+ the rise from zero intensity at the appearance potential is much less sharp. This form of curve near the appearance potential is typical of the ionization curves generally observed for molecules. It arises from the fact that at room temperature both the initial molecule and the molecular ion resulting from the ionization can exist as a number of closely spaced vibrational and rotational states. The lack of sharpness in the cutoff for these molecules makes it difficult to get the appearance potentials as accurately in the case of molecules as is the case for atomic ionizations.

Figure 7.9 shows the curve for ion-beam intensity against arc voltage in the case of the U^{++} ion. This type of curve is typical of those obtained in all cases for doubly charged ions and apparently arises from the fact that these ions can be produced either in a single impact or in two impacts.

Presumably, in Fig. 7.9 the point A represents the appearance potential corresponding to ionization occurring in two impacts, and

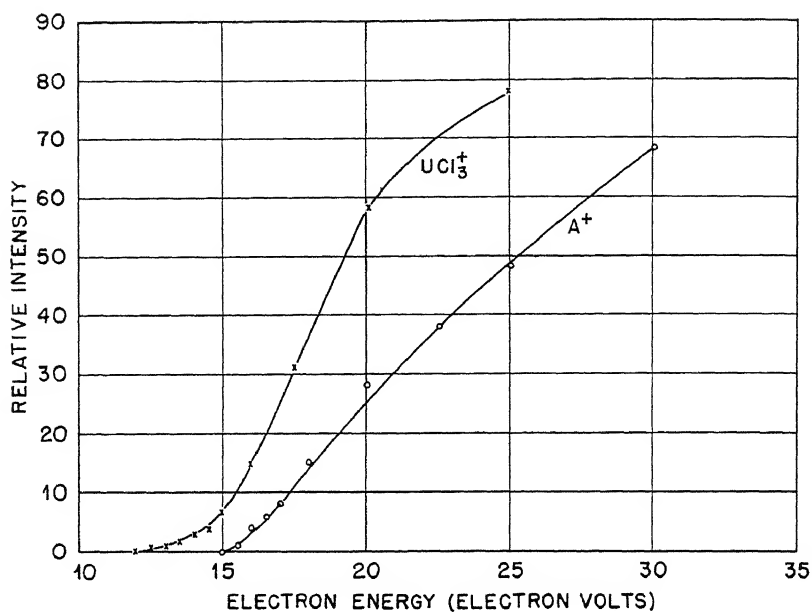


Fig. 7.8—Intensity as a function of electron energy near the appearance potential for A^+ and UCl_3^+ ions.

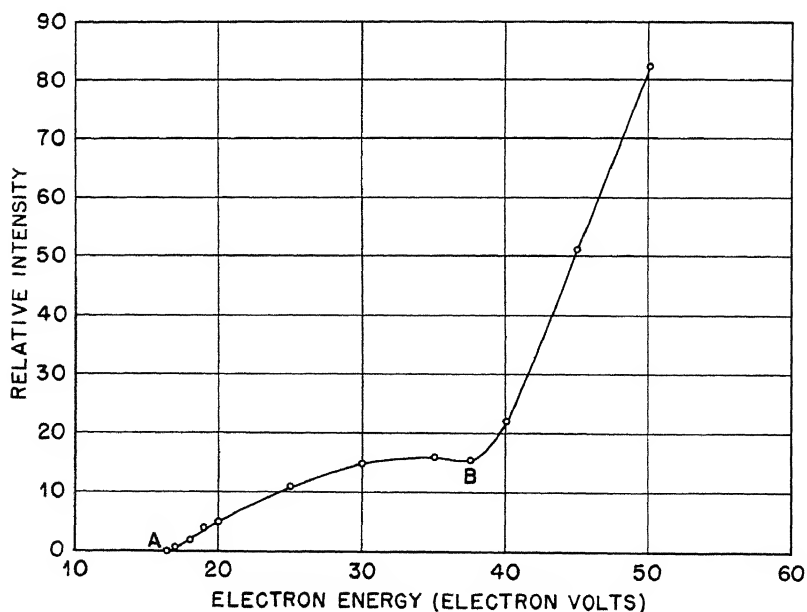


Fig. 7.9—Intensity as a function of electron energy near the appearance potential for U^{++} ion.

the point B represents the appearance potential corresponding to the ionization occurring in a single impact. In all cases the ionization in two stages was much less important than ionization in a single impact, thus indicating that in these experiments the arc-current density was sufficiently small to satisfy the single-impact criterion discussed earlier. Table 7.2 shows the observed appearance potentials in the case of UCl_4 . In the second column the appearance potentials given for the doubly charged ions represent the minimum potentials required for ionization in a single impact. The figures given in the third column represent the appearance potentials for production of the doubly charged ions in two stages.

Of the negative ions, only UCl_4^- had a definite appearance potential (15.0 volts). As has been mentioned above, all the other negative ions showed a characteristic increase of intensity as the arc voltage was decreased toward zero.

These appearance potentials should be accurate to within ± 4 volts.

3.2 Uranium Hexafluoride. (a) Relative Intensity of Ion Beams. Table 7.3 shows the relative intensity of the UF_6 ion beams for a number of different arc voltages. For comparison the relative intensity of the ion beams at one of the voltages as measured at Columbia University is also given. The agreement between the two observations is good in the case of the singly charged ion beams but not so good in the case of the doubly charged ions. It should be remembered, however, that the relative intensity of the doubly charged ions is more sensitive to arc current than is that of the singly charged ions, so that, if a higher current density were used in the Columbia experiment than in the experiments referred to here, the relative intensity of the doubly charged ions would be expected to be greater.

Table 7.4 shows the relative intensity of the ion beams for two different pressures. The most striking point about this table is the reduction of the relative intensity of the doubly charged ion beams at the higher pressure. It is difficult to account for this reduction in ion-beam intensity. It could arise from a process of charge exchange suffered by the doubly charged ions in the arc chamber before reaching the arc slits. Conceivably such a process could occur in which the doubly charged ion struck an electron from a neutral molecule, leaving two singly charged ions. However, the back of the arc chamber between the electron column and the arc slit is only about $\frac{1}{8}$ in., and in order to have a mean free path for this charge-exchange process of $\frac{1}{8}$ in. at a pressure of 3×10^{-4} mm Hg, a charge-exchange cross section of 6×10^{-14} sq cm would be needed for the process. This is very large. However, it should be remembered that the ions in the arc region are moving slowly, and in the experiments on the charge-exchange cross sections of singly charged UF_5^+ ions in UF_6 ,

Table 7.2—Appearance Potentials for UCl_4 Dissociation

Ion	Appearance potential	
	for single ionization, volts	for double ionization in two processes, volts
UCl_4^+	11.5	
UCl_3^+	12.5	
UCl_2^+	15.3	
UCl^+	18.6	
U^+	24.7	
Cl^+	23.0	
Cl_2^+	24.0	
UCl_4^{++}	22.0	12.5
UCl_3^{++}	27.4	
UCl_2^{++}	25.0	11.9
UCl^{++}	33.0	14.4
U^{++}	37.0	17

Table 7.3—Relative Intensities of UF_6 Ion Beams at Various Arc Voltages

Ion	Arc voltage					
	25 volts	50 volts	100 volts	200 volts	300 volts	100 volts*
UF_6^+						0.3
UF_5^+	100	100	100	100	100	100
UF_4^+	26	27	30	33	29	30
UF_3^+	18	22	23	35	28	21
UF_2^+		14	20	27	16.5	24
UF^+		4.8	14	15	9	15
U^+		0.8	10	11	5.5	9
UF_5^{++}		1	Uncertain			0.02
UF_4^{++}		2	3.7	4.1		9
UF_3^{++}		1.5	4.1	4.4		10.5
UF_2^{++}		0.6	4.1	4.0		7.2
UF^{++}		0.2	6.2	6.5		12.2
U^{++}		0.05	4.2	11		
F_2^+		0.25		0.25		
F^+		3.3		20		
UF_n^-		Comparable				
F^-		with UF_5^+				
F^-		Comparable				
		with UF_5^+				

* Results obtained in Columbia University experiment.

Table 7.4—Effect of Pressure on the Relative Intensity of UF_6 Ion Beams
(Arc voltage = 100 volts; arc-current density = 0.05 ma per sq cm)

Ion	Relative intensity	
	At 3×10^{-4} mm Hg	At 1.4×10^{-3} mm Hg
UF_5^+	100	100
UF_4^+	30	43
UF_3^+	23	24
UF_2^+	20	16
UF^+	14	8.5
U^+	10	5.2
UF_5^{++}		0.6
UF_4^{++}	3.7	1.0
UF_3^{++}	4.1	1.0
UF_2^{++}	4.1	1.2
UF^{++}	6.2	1.5
U^{++}	4.2	1.8

Table 7.5—Appearance Potentials for UF_6 Dissociation

Ion	Appearance potential	
	for single ionization, volts	for double ionization in two processes, volts
UF_6^+	17.7	
UF_4^+	21.7	
UF_3^+	21.7	
UF_2^+	25.2	
UF^+	26.1	
U^+	43.7	
UF_4^{++}	37	19.5
UF_3^{++}	37.5	24
UF_2^{++}	50	33
UF^{++}	52	34
U^{++}	52	37
F^+	32.5	
F_2^+	33	

cross sections of the order of 10^{-14} sq cm were obtained for ions of energy about 10 volts. Thus it is not impossible that the cross section for charge exchange of doubly charged UF_n^{++} ions should be of the order of magnitude to explain the observed intensity drop of the doubly charged ions with pressure.

(b) Appearance Potentials. Table 7.5 shows the appearance potentials observed in the case of UF_6 dissociation. These measurements were carried out in precisely the same manner as for UCl_4 , and the same type of phenomena were observed. The value of the appearance potential of UF_5^+ observed should be compared with the value 16 ± 1 volts obtained at Columbia.

It is of interest to note that in both UCl_4 and UF_6 there are several instances in which the appearance potential for a doubly charged ion in two processes is less than the appearance potential for the corresponding singly charged ion. This is true for UCl_2^{++} , UCl^{++} , and U^{++} in the case of UCl_4 and for U^{++} in the case of UF_6 . In all these cases the doubly charged ion must be produced by the ionization and dissociation of a singly charged ion containing a larger number of halogens than the final doubly charged ion. For instance, U^{++} could be produced by the ionization and dissociation of UF_5^+ , etc.

4. CHEMICAL-DISSOCIATION ENERGIES OF UCl_4 AND UF_6

It is convenient to investigate what light the observed appearance potentials throw on the particular processes in which the various ions observed are produced. But before doing this it is necessary to know something about the energies required for the chemical dissociation (without ionization) of the molecules UCl_4 and UF_6 . Unfortunately not all the chemical data are known, but estimates have been made in the cases where measurements have not been made. The following chemical data have been used in the subsequent discussion:

A. Uranium Tetrachloride

	Heat, kcal/mole
Heat of formation of UCl_4 (solid) from U (solid) and Cl_2	251
Heat of dissociation of Cl_2	58
Heat of sublimation of UCl_4	48
Heat of sublimation of UCl_3	55
Heat of vaporization of U	57.2*
Heat of vaporization of U	142*
Heat of formation of UCl_3 (solid) from U (solid) and Cl_2	212

* These are the results of two determinations. The uncertainty in this quantity is one of the biggest obstacles to making this analysis more complete.

To complete the information required the following quantities were estimated:

	Heat, kcal/mole
Heat of sublimation of UCl_2 and UCl	50
Heat of formation of UCl_2	158
Heat of formation of UCl	88

The following method was used to estimate the heat of formation of UCl_2 and UCl :

Known heat of formation of UCl_6 = 272 kcal/mole = 45.3 kcal/gram atom Cl
Known heat of formation of UCl_5 = 262 kcal/mole = 52.4 kcal/gram atom Cl
Known heat of formation of UCl_4 = 251 kcal/mole = 62.7 kcal/gram atom Cl
Known heat of formation of UCl_3 = 212 kcal/mole = 70.7 kcal/gram atom Cl

Using first differences of the heat of formation per chlorine atom gives, respectively, 7.1, 10.3, and 8.0, with a mean of 8.5. Assuming the same first differences for UCl_2 and UCl heats of formation per chlorine atom, the values of the heats of formation of UCl_2 and UCl given above are obtained.

B. Uranium Hexafluoride

The following known chemical data have been used:

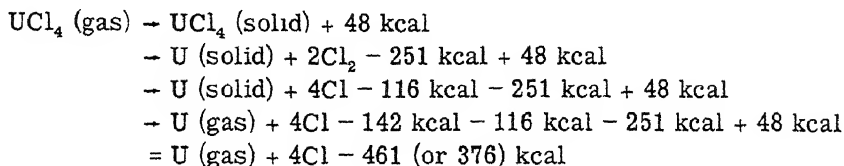
	Heat, kcal/mole
Heat of sublimation of UF_6	10
Heat of sublimation of UF_4	54
Heat of formation of UF_6	516
Heat of formation of UF_5	488
Heat of formation of UF_4	446
Heat of formation of UF_3	384
Heat of dissociation of F_2	63

To complete the information required, the following quantities were estimated in the same way as for UCl_4 :

	Heat, kcal/mole
Heat of formation of UF_2	292
Heat of formation of UF	166
Heat of sublimation of UF_5	25
Heat of sublimation of UF_3	55
Heat of sublimation of UF_2 , UF	60

From these data the energies required to dissociate UF_6 and UCl_4 in various ways have been calculated. The following example shows the kind of calculation involved:

To calculate the energy required for the reaction $\text{UCl}_4 \rightarrow \text{U} + 4\text{Cl}$:



In this way the dissociation energies are obtained in electron volts for the various types of dissociation of UCl_4 and UF_6 , shown in Table 7.6 (1 electron volt per molecule = 23.05 kcal/mole).

5. MODE OF FORMATION OF THE ION BEAMS

It is of interest to examine the data on the appearance potentials together with the chemical-dissociation data to see how far it enables us to discover the most probable reactions in which the various ion beams are formed. For example, consider the ion beam Cl^+ . The ionization potential of Cl is known to be 13.05 volts. In the present experiments the appearance potential was measured to be 23.0 volts. From an analysis of Table 7.6 it is seen that it is energetically possible to form Cl^+ in the reactions shown below. Alongside each reaction is listed the excess energy in volts available as a result of the reaction. In this list the electron affinity of Cl is taken to be 3.7 volts.

	Excess energy, electron volts	
$\text{UCl}_3 + \text{Cl}^+$	6.6	(1)
$\text{UCl}_2 + \text{Cl}^+ + \text{Cl}$	3.1	(2)
$\text{UCl}_2 + \text{Cl}^+ + \text{Cl}^-$	6.8	(3)
$\text{UCl} + \text{Cl}^+ + \text{Cl}_2$	1.2	(4)
$\text{UCl} + \text{Cl}^+ + \text{Cl} + \text{Cl}^-$	1.9	(5)

This list ignores possibilities associated with the formation of negative ions such as UCl_3^- , UCl_2^- , UCl^- . The anomalous type of variation of the Cl^- intensity with arc voltage and its lack of correlation with the voltage variation of any of the positive-ion beams make it appear probable that Cl^- is not formed in reactions such as these. If, then, reactions 3 and 5, which involve the production of Cl^- , are ignored, the reactions 1, 2, and 4, which are energetically possible, remain.

It is not possible to distinguish among these three reactions because it is not known with what energy the various fragments fly apart. In analyses similar to this made with simpler systems,¹ it is usually assumed that the reaction corresponding to the least excess energy

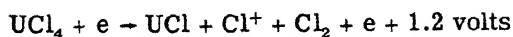
Table 7.6—Dissociation Energies for UCl_4 and UF_6

Dissociation energy, ev	
UCl_4	
$\text{U} + 4\text{Cl}$	20.0* or 16.3†
$\text{U} + \text{Cl}_2 + 2\text{Cl}$	17.5* or 11.3†
$\text{U} + 2\text{Cl}_2$	15.0* or 11.3†
$\text{UCl} + 3\text{Cl}$	11.2
$\text{UCl} + \text{Cl}_2 + \text{Cl}$	8.7
$\text{UCl}_2 + 2\text{Cl}$	6.8
$\text{UCl}_2 + \text{Cl}_2$	4.2
$\text{UCl}_3 + \text{Cl}$	3.3
UCl_4	0
UF_6	
$\text{U} + 6\text{F}$	36.2* or 32.6†
$\text{U} + \text{F}_2 + 4\text{F}$	33.7* or 30.1†
$\text{U} + 2\text{F}_2 + 2\text{F}$	30.7* or 27.1†
$\text{U} + 3\text{F}_2$	28.0* or 24.4†
$\text{UF} + 5\text{F}$	24.2
$\text{UF} + \text{F}_2 + 3\text{F}$	21.5
$\text{UF} + 2\text{F}_2 + \text{F}$	18.7
$\text{UF}_2 + 4\text{F}$	17.4
$\text{UF}_2 + \text{F}_2 + 2\text{F}$	14.6
$\text{UF}_2 + 2\text{F}_2$	11.9
$\text{UF}_3 + 3\text{F}$	11.8
$\text{UF}_3 + \text{F}_2 + \text{F}$	9.1
$\text{UF}_4 + 2\text{F}$	7.7
$\text{UF}_4 + \text{F}_2$	4.9
$\text{UF}_5 + \text{F}_2$	3.2

* Assuming heat of sublimation of U of 142 kcal/mole.

† Assuming heat of sublimation of U of 57 kcal/mole.

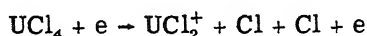
is the most probable one. If this were the case in the present investigation, it would be assumed that the reaction producing Cl^+ with an appearance potential of 23.0 volts is



In the case of most of the ion beams, however, the ionization potential is unknown, and it is not possible to continue the analysis as far as this. Thus, consider the ion beam UCl_2^+ . The observed appearance potential was 15.3 volts. If reactions involving negative ions are ignored, there are two possibilities:



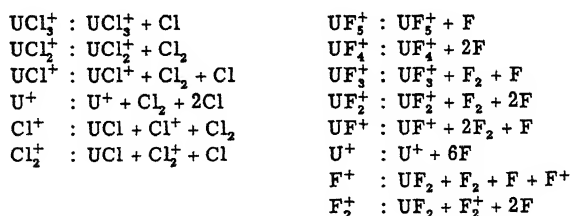
or



For the former to be energetically possible the ionization potential of UCl_2 cannot exceed 11.1 volts. For the latter to be energetically possible it cannot exceed 8.5 volts. This then gives an upper limit of 11.1 volts as the ionization potential of UCl_2 .

An analysis similar to this is carried out in Table 7.7 for the positively charged ion beams produced from UCl_4 and in Table 7.8 for the similar ion beams produced from UF_6 .

Making reasonable assumptions about the probable ionization potentials of the various ion beams and assuming the reactions in which the excess energy is least as the most probable, the following list is obtained of the most probable manner in which the various ion beams are formed:



6. AN ATTEMPT TO MEASURE THE IONIZATION POTENTIAL OF URANIUM METAL

By means of the apparatus shown in Fig. 7.1 an attempt was made to measure the first and second ionization potentials of uranium. A slot P, $1\frac{1}{2}$ in. long and $\frac{1}{8}$ in. wide, was cut in the side of the arc chamber, and opposite and parallel to it was mounted a tungsten wire, 0.100 in. in diameter. This was heated by means of a current of about 170 amp to a temperature sufficiently high to melt and evaporate uranium. With the tungsten wire hot, uranium wire was fed on to it

through a Wilson seal in the side of the tank. In this way an intense jet of vapor was produced in the space between the electrode C and the arc slit D. The electron stream E ionized this jet. In the resulting mass spectrum detected in the analyzer, an intense beam of U^+ ion

Table 7.7 — Positively Charged Ion Beams Produced from UCl_4

Ion beam	Appearance potential, volts	Possible reaction	Upper limit of ionization potential of ion beam, volts	Excess energy available, volts
UCl_4^+			11.5	
UCl_3^+	12.5	$\text{UCl}_3^+ + \text{Cl}$	9.2	
UCl_2^+	15.3	$\text{UCl}_2^+ + \text{Cl}_2$	11.1	
		$\text{UCl}_2^+ + 2\text{Cl}$	8.5	
UCl^+	18.6	$\text{UCl}^+ + \text{Cl}_2 + \text{Cl}$	9.9	
		$\text{UCl}^+ + 3\text{Cl}$	7.4	
U^+	24.7	$\text{U}^+ + 2\text{Cl}_2$	9.7 or 13.4*	
		$\text{U}^+ + \text{Cl}_2 + 2\text{Cl}$	7.2 or 10.9*	
		$\text{U}^+ + 4\text{Cl}$	4.7 or 8.4*	
Cl^+	23.0	$\text{UCl}_3 + \text{Cl}^+$	13.05	6.6
		$\text{UCl}_2 + \text{Cl}^+ + \text{Cl}$		3.1
		$\text{UCl} + \text{Cl}^+ + \text{Cl}_2$		1.2
Cl_2^+	24.0	$\text{UCl}_2 + \text{Cl}_2^+$	13	6.8
		$\text{UCl} + \text{Cl}_2^+ + \text{Cl}$		2.3

* The ambiguity in these cases arises from the uncertainty in the heat of evaporation of uranium.

was obtained. Several other beams which were evidently to be attributed to various oxides of uranium were also observed. The UO^+ beam had an intensity comparable with that of U^+ and was present right down to zero arc voltage. It appeared to arise from surface ionization at the hot tungsten wire.

The apparatus was first calibrated by introducing argon into the arc. A value of 15.15 volts was obtained for the ionization potential of argon as compared with the true value of 15.7 volts, indicating a correction for contact potential and calibration errors of +0.55 volt should be applied to ionization potentials measured by the apparatus.

The tungsten wire was then heated and the uranium melted on to it. A very intense U^+ beam was obtained, but when an attempt was made to measure its ionization potential, a value of 15.5 volts was obtained. No trace of U^+ beam could be detected for any value of the arc voltage below this.

It appears quite certain from other evidence that the ionization potential of uranium could not be nearly so high as this. The clue to the observation of this high value is probably to be found in the occurrence of peaks corresponding to various uranium oxide ions in some intensity. Evidently what is being observed is not the true ionization

Table 7.8—Positively Charged Ion Beams Produced from UF_6

Ion beam	Appearance potential, volts	Possible reaction	Upper limit of ionization potential of ion beam, volts	Excess energy available, volts
UF_5^+	17.7	$\text{UF}_5^+ + \text{F}$	14.5	
UF_4^+	21.7	$\text{UF}_4^+ + \text{F}_2$	16.8	
			14.0	
UF_3^+	21.7	$\text{UF}_3^+ + \text{F}_2 + \text{F}$	12.6	
		$\text{UF}_3^+ + 3\text{F}$	9.9	
UF_2^+	25.2	$\text{UF}_2^+ + 2\text{F}_2$	13.3	
		$\text{UF}_2^+ + \text{F}_2 + 2\text{F}$	10.6	
		$\text{UF}_2^+ + 4\text{F}$	7.8	
UF^+	26.1	$\text{UF}^+ + 2\text{F}_2 + \text{F}$	7.4	
		$\text{UF}^+ + \text{F}_2 + 3\text{F}$	4.6	
		$\text{UF}^+ + 5\text{F}$	1.9	
U^+	43.7	$\text{U}^+ + 3\text{F}_2$	15.7 or 19.3	
		$\text{U}^+ + 2\text{F}_2 + 2\text{F}$	13.0 or 16.6	
		$\text{U}^+ + \text{F}_2 + 4\text{F}$	10.0 or 13.6	
		$\text{U}^+ + 6\text{F}$	7.5 or 10.1	
F^+	32.5	$\text{UF}_5 + \text{F}^+$	17.3	12.0
		$\text{UF}_4 + \text{F} + \text{F}^+$		7.5
		$\text{UF}_3 + \text{F}_2 + \text{F}^+$		6.1
		$\text{UF}_3 + 2\text{F} + \text{F}^+$		3.4
		$\text{UF}_2 + \text{F}_2 + \text{F} + \text{F}^+$		0.6
F_2^+	33.0	$\text{UF}_4 + \text{F}_2^+$	17.8	10.3
		$\text{UF}_3 + \text{F}_2 + \text{F}$		6.1
		$\text{UF}_2 + \text{F}_2^+ + \text{F}_2$		3.3
		$\text{UF}_2 + \text{F}_2^+ + 2\text{F}$		0.6

potential of uranium but the appearance potential of the U^+ ion in the dissociation of one of the oxides of uranium by electron impact.

It is difficult to see how to avoid this and to determine the true ionization potential of uranium in an apparatus such as that at present being used. The uranium wire used, of course, had the usual oxide coating, but this coating appeared quite thin in comparison with the diameter of the wire ($\frac{1}{16}$ in.). Another possibility is that there was sufficient oxygen in the tank gases to convert a uranium atom to an

oxide molecule on its path between the tungsten wire and the electron stream. However, the base pressure in the tank had a normal value (10^{-5} mm Hg).

It would appear that to carry out this measurement it will be necessary to work with a glass apparatus that can be thoroughly baked, and it will be necessary actually to distil the uranium metal on to the tungsten wire inside the apparatus itself.

The appearance potential of the U^{++} ion was also measured under the conditions described above. It came to be about 22 volts.

ACKNOWLEDGMENTS

The authors of this chapter are indebted to Dr. G. E. MacWood for several discussions and for bringing to their attention the chemical data on UCl_4 and UF_6 used above; to R. C. Lilly for preparing the UF_6 used and to R. Krohn for preparing the UCl_4 charge bottles; to J. D. Gow for developing and constructing the d-c amplifier used in the measurements; to G. Page and J. Jungerman for assistance in taking some of the measurements; to J. Edwards, J. Morris, and H. Tomlinson for invaluable mechanical assistance; and to S. Wild and B. Parker for the setting up and maintenance of the electric circuits.

REFERENCE

1. L. G. Smith, Phys. Rev., 51: 263 (1937).

Chapter 8

THE RATE OF ION PRODUCTION BY AN ELECTRON BEAM

By Terrell L. Hill and Lawrence H. Aller

For a number of problems in connection with electrical phenomena in gases it is desirable to be able to estimate the rate of ion production when an electron current i_e passes through a gas. For small currents it has been customary to employ an expression of the form

$$i = n_0 Q_i s i_e \quad (1)$$

where i_e is the electron current, s is the path length of an electron in the gas, Q_i is the ionization cross section of the gas molecules for the particular electron energy being used, n_0 is the density of gas molecules, and i is the ion current produced. Ordinarily $n_0 Q_i s$ is small and may be thought of as the probability that a given electron will produce an ion in the distance s . There are, however, many experimental conditions of interest under which Eq. 1 is not at all satisfactory, and it is the purpose of the present paper to refine Eq. 1 accordingly. It should be emphasized that the treatment to be given here is still very crude indeed and should only be considered the next higher approximation over Eq. 1. An exact solution is possible in principle, but the mathematical problem is extremely complicated.

There are two essential ways in which Eq. 1 may break down as a good approximation:

(1) If either n_0 or s is too large, most electrons will make several ionizing collisions, with loss of energy and hence with a change in the value of Q_i . Also, other types of inelastic collision must be taken into account. In extreme cases, some electrons may lose enough energy by collisions so that the residual energy they possess is less than the ionization potential. Such electrons can no longer produce ions.

(2) If i is too large, the effective density of gas molecules in the electron beam itself is appreciably less than the density outside of

the beam, owing to the rapid rate at which molecules are converted into ions once they enter an electron beam with high i_e . In the extreme, every molecule that enters the beam is ionized, and hence the maximum rate of ion production is the rate at which molecules enter the beam.

An outline of the approximate treatment of the problem follows: Suppose that all electrons, after being emitted from the cathode, enter the enclosure containing the gas with energy V_0 . The origin of coordinates is taken at this entrance and the direction along which the electron beam is directed is taken as the Z axis. In general, at $z = 0$, all electrons will not be moving exactly parallel to the Z axis, but some will be entering the gas chamber making an angle θ_0 with the axis. A certain distribution is assumed in θ_0 , e.g., $F(\theta_0) = k \cos \theta_0$, where k is a constant. To prevent a random diffusion of electrons with consequent loss in beam intensity, a frequent experimental practice has been to introduce a homogeneous magnetic field, the lines of force of which are parallel to the direction of motion of the electrons. In this problem the uniform magnetic field will be directed along the Z axis. The magnetic field influences the rate of ionization only secondarily through this collimation effect. The electron trajectories will be circular helices in the magnetic field (assuming negligible electric fields), and, as is well known, the path lengths are the same as would be the case if no magnetic field were present.

The fundamental simplifications made are the following: (1) the collision processes occurring are treated as being continuous instead of discrete; (2) all free paths between collisions are assumed to be mean free paths; and (3) the change in $\cos \theta$ (θ is the angle between the Z axis and a tangent to the electron trajectory at any point) as a result of a collision is taken as the mean value, properly weighted (see below).

In general, several different types of collision must be taken into account. For each type, with an appropriate subscript, $I_j(\phi, V)$ is defined as the cross section for scattering into unit solid angle at ϕ (the angle of scattering) for electrons with energy V , and the total cross section $Q_j(V)$ for the process is defined as

$$Q_j(V) = 2\pi \int_0^\pi I_j(\phi, V) \sin \phi \, d\phi \quad (2)$$

If an electron with energy V and angle θ undergoes a collision characterized by ϕ and ω (the azimuthal orientation of ϕ), it is easy to show that the change in θ as a result of the collision is

$$\Delta(\cos \theta) = (\cos \theta)(\cos \phi - 1) + \sin \phi \cos \omega \sin \theta \quad (3)$$

We wish to make use of the mean value of $\Delta(\cos \theta)$, averaged over ϕ and ω , the weighting function being $I_j(\phi, V) \sin \phi d\phi d\omega$. Thus

$$\overline{\Delta(\cos \theta)} = (\cos \theta) \frac{A_j(V)}{Q_j(V)} \quad (4)$$

with

$$A_j(V) = 2\pi \int_0^\pi (\cos \phi - 1) I_j(\phi, V) \sin \phi d\phi \quad (5)$$

Now let the subscript i refer to ionizing* collisions and let 1, 2, ... refer to whatever other types of collisions are to be taken into account in the particular case being studied (e.g., excitation and elastic scattering). We consider a differential length of path, ds , for a given electron. If the mean gas density within the electron beam is n (the relation between n and n_0 , the density inside and outside the electron beam, respectively, will be considered later), then in ds the

$$\left. \begin{aligned} \text{Number of ionizing collisions} &= dj = nQ_i(V) ds \\ \text{Number of type 1 collisions} &= nQ_1(V) ds \\ \text{Number of type 2 collisions} &= nQ_2(V) ds \\ &\vdots \\ &\vdots \\ &\vdots \end{aligned} \right\} \quad (6)$$

where dj is the number of ions produced in ds by the electron. The change dx in $\cos \theta = x$ is

$$\begin{aligned} dx &= nQ_i(V) ds \cdot x \frac{A_i(V)}{Q_i(V)} + nQ_1(V) ds \cdot x \frac{A_1(V)}{Q_1(V)} + \dots \\ &= [A_i(V) + A_1(V) + A_2(V) + \dots] nx ds = A(V) nx ds \end{aligned} \quad (7)$$

having defined $A(V)$ by Eq. 7. If ΔV_j (taken as positive) is the loss in energy due to a single collision of a given type, then

$$\begin{aligned} -dV &= nQ_i(V) ds \Delta V_i + nQ_1(V) ds \Delta V_1 + \dots \\ &= [Q_i(V) \Delta V_i + Q_1(V) \Delta V_1 + \dots] n ds = P(V) n ds \end{aligned} \quad (8)$$

*Double ionization is neglected here, though it may easily be taken into account.

which defines $P(V)$. The following relation is also used:

$$dz = \cos \theta \, ds = x \, ds \quad (9)$$

Equations 6 to 9 may now be rewritten in the form of a system of differential equations.

$$\frac{dj}{ds} = nQ_i(V) \quad \text{or} \quad \frac{dj}{dz} = \frac{nQ_i(V)}{x} \quad (10)$$

$$\frac{dx}{ds} = nxA(V) \quad \text{or} \quad \frac{dx}{dz} = nA(V) \quad (11)$$

$$\frac{dV}{ds} = -nP(V) \quad \text{or} \quad \frac{dV}{dz} = -\frac{nP(V)}{x} \quad (12)$$

The initial conditions are $z = 0$, $j = 0$, $V = V_0$, $x = x_0 = \cos \theta_0$.

A convenient method of solving Eqs. 10, 11, and 12 is as follows: When Eq. 10 is divided by Eq. 12, it becomes

$$\frac{dj}{dV} = -\frac{Q_i(V)}{P(V)} \quad (13)$$

or

$$j(V) = \int_V^{V_0} \frac{Q_i(V)}{P(V)} \, dV \quad (14)$$

The function $j(V)$ starts out at zero for $V = V_0$ and increases as V decreases until V becomes equal to the ionization potential V_p . When $V = V_p$, $Q_i = 0$, and $j(V)$ attains its maximum value, $j(V_p)$. Next, if Eq. 11 is divided by Eq. 12, then

$$\frac{dx}{dV} = -\frac{x A(V)}{P(V)} \quad (15)$$

or

$$x(V) = x_0 e^{f(V)} \quad (16)$$

with

$$f(V) = \int_V^{V_0} \frac{A(V)}{P(V)} \, dV \quad (17)$$

It can be seen from Eq. 5 that $A(V)$ is never positive, and hence $f(V)$ is zero at $V = V_0$ and decreases as V decreases. Thus $x = x_0$ at $V = V_0$

and also decreases as V decreases. That is, θ starts at θ_0 and increases toward $\pi/2$ as V decreases. In order to relate the decrease in V to the increase in z , Eq. 12 is rearranged to read

$$dz = -\frac{x \, dV}{nP(V)} = -\frac{x_0 e^{f(V)} \, dV}{nP(V)} \quad (18)$$

and therefore

$$nz = x_0 \int_V^{V_0} \frac{e^{f(V)} \, dV}{P(V)} = x_0 g(V) \quad (19)$$

which defines $g(V)$. It will be convenient to retain nz as a variable in future equations.

Equation 19 gives $V(nz, x_0)$. Combining Eqs. 14 and 19 makes it possible to find $j(nz, x_0)$, which is the desired function. This gives the number of ions produced by an electron (which started with θ_0) by the time it reaches z .

It is clear from Eq. 19 that $g(V)$ increases as V decreases and attains a maximum value $g(V_p)$. The corresponding value of nz ,

$$nz(V_p) = x_0 g(V_p) \quad (20)$$

is that value beyond which no further ions are produced by an electron starting with x_0 . The electrons that produce ions furthest along z are those with $x_0 = 1$ ($\theta = 0$; electrons starting parallel to the Z axis). Thus the value of z, z_{\max} , beyond which no ions whatever are produced, is

$$z_{\max} = \frac{g(V_p)}{n} \quad (21)$$

This sharp cutoff is due to the crudity of the model; in particular, allowance has not been made for the distribution in free paths.

Finally, the mean value of $j(nz, \theta_0)$, averaged over θ_0 , is desired.

$$\overline{j(nz)} = \frac{\int_0^{\theta_0(V_p)} j(nz, \theta_0) F(\theta_0) \, d\theta_0 + j(V_p) \int_{\theta_0(V_p)}^{\pi/2} F(\theta_0) \, d\theta_0}{\int_0^{\pi/2} F(\theta_0) \, d\theta_0} \quad (22)$$

The mean number of ions produced per electron between $z = 0$ and z is now expressed as a function of nz . A more practical result would

be to have $\overline{j(n_0 z)}$ instead of $\overline{j(nz)}$, since n_0 is the experimentally measured density. Incidentally, it will be noted that the variation of n with z is neglected throughout and a mean value is used instead.

The number of molecules entering the electron beam per second between $z = 0$ and z is $\alpha n_0 z$, where $\alpha = \frac{1}{4} \bar{v} l$, \bar{v} being the average molecular velocity and l the length of the perimeter of the electron beam in the plane perpendicular to the Z axis. The number of ions produced per second between $z = 0$ and z is, as already seen, $\overline{j(nz)} i_e$. Hence the mean probability P that a molecule entering the electron beam between $z = 0$ and z will be ionized while passing through it is

$$P = \frac{\overline{j(nz)} i_e}{\alpha n_0 z} \quad (23)$$

where there is a functional relationship between n and n_0 in Eq. 23 (such that, for example, P never exceeds unity). The approximate form of this functional relationship is easily obtained in terms of P . Let the mean path length of molecules passing through the electron beam be represented by a . Then, from probability considerations, P may be expressed in the form

$$1 - P = e^{-ka} \quad (24)$$

where k is an averaged constant that need not be further specified for our purposes. Consider now the relative density of un-ionized molecules in going from $x = 0$ (molecules just entering electron column) to $x = a$ (molecules just leaving). The relative density is clearly unity at $x = 0$, e^{-ka} at $x = a$, and, in general, e^{-kx} at x . Hence the mean relative density of molecules in the electron column is

$$\frac{n}{n_0} = \frac{\int_0^a e^{-kx} dx}{\int_0^a dx} = \frac{1 - e^{-ka}}{ka} = \frac{P}{\ln \frac{1}{1 - P}} \quad (25)$$

If we substitute P from Eq. 23 into Eq. 25, there results

$$n_0 z = \frac{\overline{j(nz)} i_e}{\alpha \left\{ 1 - \exp \left[-\frac{\overline{j(nz)} i_e}{\alpha n z} \right] \right\}} \quad (26)$$

Thus, from Eq. 26, $n_0 z(nz, i_e)$ is derived, which, when combined with $\overline{j(nz)}$, gives $\overline{j(n_0 z, i_e)}$. Thus in place of Eq. 1, which may be written in the form

$$i = \frac{n_0 Q_1(V_0) z i_e}{\cos \theta_0} \quad (27)$$

where $\overline{\cos \theta_0}$ is obtained by averaging $\cos \theta_0$ using $F(\theta_0)$, the following somewhat more refined equation is derived:

$$i = \overline{j(n_0 z, i_e)} i_e \quad (28)$$

In practical calculations the order in which the various equations are used is as follows:

1. Calculate $Q_j(V)$ and $A_j(V)$ from Eqs. 2 and 5 for the processes being considered, using experimental data for the gas in question.
2. Obtain from these results $A(V)$ and $P(V)$ as defined in Eqs. 7 and 8.
3. Then find $j(V)$ from Eq. 14, $f(V)$ from Eq. 17, and $g(V)$ from Eq. 19.
4. Combine $g(V)$ and $\overline{j(V)}$ to obtain $j(nz, x_0)$.
5. Using $F(\theta_0)$, find $\overline{j(nz)}$ from Eq. 22.
6. Calculate $n_0 z(nz, i_e)$ by means of Eq. 26.
7. Combine $n_0 z(nz, i_e)$ with $\overline{j(nz)}$ to give $\overline{j(n_0 z, i_e)}$ and i by Eq. 28.

The calculation of ion production by the method outlined above is straightforward, although the fundamental collision data must be supplied by experiment. Detailed computations have been carried out for argon under varying conditions of gas density and electron current. The elastic-scattering curves $I(\phi, V)$ in this case were taken from the work of Arnot¹ for large scattering angles and computed by means of the Born approximation for small angles. The experimental and theoretical curves were then fitted together.

ACKNOWLEDGMENT

The authors of this chapter are indebted to H. S. W. Massey for his very helpful suggestions.

REFERENCE

1. F. L. Arnot, Proc. Roy. Soc., A133: 615 (1931).

Chapter 9

A STUDY OF THE ARC PLASMA

By D. Bohm, E. H. S. Burhop, H. S. W. Massey, and R. M. Williams

1. DESCRIPTION OF APPARATUS

1.1 The Arcs. In the course of these investigations three different arcs have been used. These are described below.

(a) Arc Designed by Backus. The earliest measurements were carried out in an arc designed by Backus. This consisted of a square-sectioned chamber constructed in carbon, having an internal breadth and depth of 2 in. The internal length of the arc was $7\frac{1}{2}$ in. Figure 9.1 shows the relevant dimensions of this arc. The opening, 2 by $1\frac{1}{4}$ in., in the front wall of the arc chamber permitted the insertion of various types of probes (described below) in the arc plasma. In the back wall of the chamber were drilled two $\frac{1}{4}$ -in. holes, one above the other, $3\frac{3}{4}$ in. apart. One of these brought in the gas with which the experiments were performed (in this case argon); the other was connected with an ionization gauge or McLeod gauge for the measurement of the pressure in the arc chamber.

The arc chamber was closed at either end by two copper plates, $\frac{1}{4}$ in. thick and $2\frac{1}{2}$ in. square, water-cooled and insulated from the arc block. Each plate carried a tungsten insert, 1 by 1 in., in the center. In the bottom plate, referred to subsequently as the "anode," this tungsten plate intercepted the negative-arc current. In the top plate, referred to subsequently simply as the "slot," the tungsten insert had a collimating slot $\frac{1}{2}$ by $\frac{3}{32}$ in. cut in it. In these experiments the collimating slot was placed centrally in the arc. The cathode filament consisted of a tungsten wire 0.145 in. in diameter placed $\frac{1}{8}$ in. above the collimating slot. With this arc it was possible to measure separately the current collected by the anode, slot, or side walls of the arc and to probe the arc plasma in the neighborhood of the central opening in the front wall.

This arc was mounted in a tank placed between the poles of the arc electromagnet. It was possible to carry out measurements with magnetic fields up to 4,000 gauss. The tank was sealed by means of rubber gaskets, using the normal technique, and was evacuated by means of oil diffusion pumps.

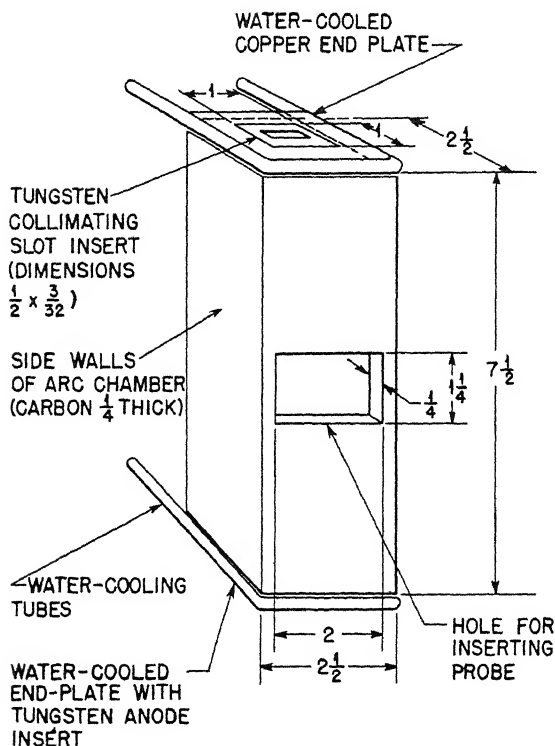


Fig. 9.1

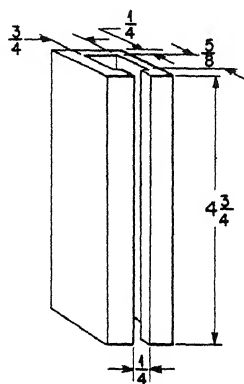


Fig. 9.2

Fig. 9.1—Arc chamber designed by Backus.

Fig. 9.2—The small arc.

(b) Arc Used in Measurements with 37-in. Magnet with Narrow Arc Chamber (Small Arc). The arc used in the measurements with the 37-in. magnet is sketched in Fig. 9.2. The arc chamber was constructed of carbon and had the dimensions shown in the figure. The ratio of length to depth was much greater than in the Backus arc, namely, 7.6 as compared with 3.75 for the Backus arc.

A vertical opening $\frac{1}{4}$ in. wide was cut down the front of the arc chamber, and hot and cold probes could be moved up and down this

slot and in and out of the arc chamber, so that probe measurements could be carried out over a much greater portion of the arc than was possible with the earlier arcs.

For some of the later experiments the front of the arc chamber shown in Fig. 9.2 was replaced by a carbon plate with three horizontal slots, each $\frac{1}{4}$ in. wide, cut in it. One of these slots was situated at the center of the plate. The second slot was $1\frac{1}{2}$ in. above the central plane, and the third one the same distance below it.

As in the case of the Backus arc, the slot and anode consisted of copper plates with tungsten inserts to carry the collimating slot and to intercept the main portion of the negative-arc current striking the anode. The slot and anode were insulated from the vertical side walls of the block. In most of the experiments the collimating slot was straight, was $\frac{1}{2}$ in. long by $\frac{1}{8}$ in. wide, and was symmetrically placed relative to the arc-chamber section. Some experiments were also carried out in which the collimating slot was placed either in front of or behind the central position. Other experiments were carried out in which the collimating slot was curved in the shape of the arc of a circle $\frac{1}{2}$ in. in diameter, subtending an angle of 120 deg at its center.

The filament consisted of tungsten wire 0.1 in. in diameter, mounted on water-cooled leads and capable of adjustment relative to the collimating slot in a direction perpendicular to its length. The length of the filament parallel to the collimating slot was 1 in. The clearance between the bottom of the filament and the top of the slot was $\frac{1}{8}$ in.

Between the slot and the block and between the anode and block were mounted two series of six tungsten wires 0.030 in. in diameter. These wires were fused through two glass rods placed 1 in. apart and mounted parallel to the collimating slot. Figure 9.3 shows the construction and spacings between the respective wires constituting one of these frames. The extreme wires were placed $\frac{1}{32}$ in. from the front and back of the arc chamber, respectively. By measuring the currents collected by these wires it was possible to obtain information on the disposition of currents in the arc under normal operating conditions. It was possible also to supply positive and negative voltages to the individual wires and also to the block. In this way the nature of the currents collected by the different wires and the block could be estimated. It also made possible a study of the effect on the arc plasma of the application of potentials to the wires and the block.

The gas employed was introduced into the arc chamber by means of a variable leak. Argon and chlorine were the gases used, the majority of the measurements being made with the former. Both were obtained from commercial cylinders, the argon being certified as containing 99.7 per cent argon gas. No attempt was made at further purification.

A third copper tube leading into the back of the arc block was connected to a vacuum gauge and enabled the pressure in the arc to be measured. In the earlier experiments with argon, both a McLeod gauge and a Western Electric ionization gauge were used for measurement of arc pressure. Later, however, with argon the McLeod

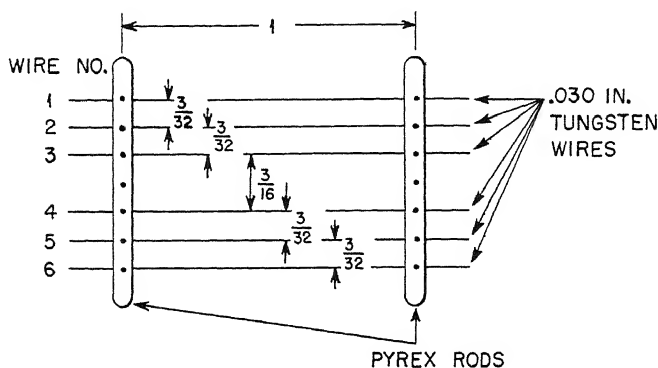


Fig. 9.3 — Construction of wire grid used with small arc.

gauge was dispensed with, and all measurements were carried out using the ionization gauge. It was noticed, when using this gauge, that when the arc was struck the apparent pressure, as registered by the ionization gauge, fell. With large arc currents this fall might amount to as much as 50 per cent of the total reading. No such fall of pressure appeared to be indicated by the McLeod gauge, although the investigations with the McLeod gauge were not very thorough. The reason for this anomalous behavior is obscure, but when the ionization gauge was used for pressure measurements the pressure was always determined prior to striking the arc.

When chlorine was used, the McLeod gauge was reconnected and found to be the most satisfactory means of measuring the chlorine pressure, the ionization gauge being dispensed with.

The arc chamber for the 37-in. magnet was mounted on one of the side walls of the 37-in. tank, and the whole was evacuated by means of the vacuum system installed with the tank. This consisted of two diffusion pumps in parallel, each of which has a speed of about 1,200 liters/sec. With the 37-in. magnet a whole range of fields extending up to 11,000 gauss was available.

(c) Arc Used in Measurements with 37-in. Magnet with Large Arc Chamber (Large Arc). The dimensions of this arc are shown in Fig. 9.4. It is the same length as the previous one but with transverse

dimensions four times greater. The Backus arc (Sec. 1.1a) thus represented a case intermediate between the two arcs used in the 37-in. magnet, as far as the ratio of length to transverse dimension was concerned, these ratios being 7.6 and 1.9 for the former two and 3.75 for the Backus arc.

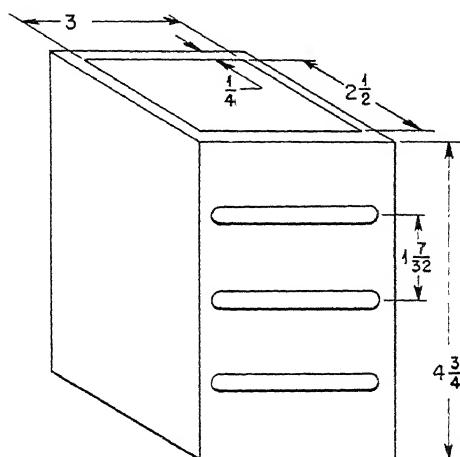


Fig. 9.4 — The large arc.

The collimating slot was placed in a central position and was of the same dimensions as for the smaller arc. By means of it, currents could be measured separately to the block, anode plate, and slot plate, and three probes could be inserted through horizontal slots in the front face, in the positions shown in Fig. 9.4. The distribution of current over the anode and slot plates was observed by measuring currents to wires as in the case of the narrower arc. The positions of these wires are illustrated in Fig. 9.5.

The gas employed was introduced into the arc chamber, as in the case of the narrower arc, by means of two copper tubes leading into the side walls of the chamber. The arc was connected in the same way as the narrower one. The majority of the measurements with this arc were carried out using argon, but a number were also obtained with chlorine.

1.2 The Probes. In most of the measurements described in this report two distinct types of probe were used.

(a) Cold Probe. The cold probe in general use consisted of a disk of molybdenum, $\frac{1}{8}$ in. in diameter, spot-welded to a tungsten wire 0.030 in. in diameter. The construction is illustrated in Fig. 9.6.

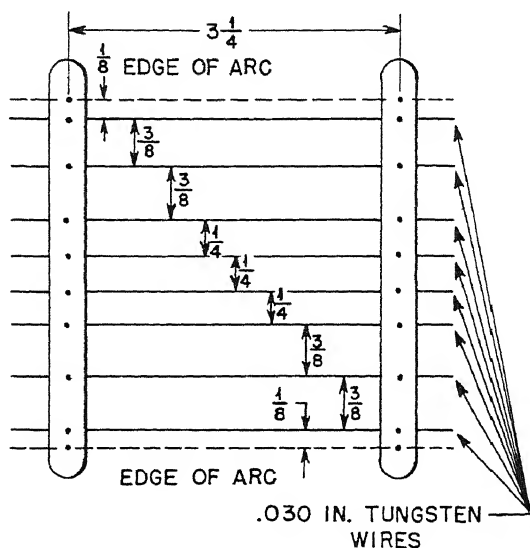


Fig. 9.5—Construction of wire grid used with large arc.

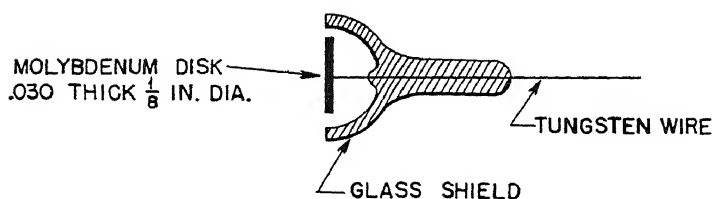


Fig. 9.6—Construction of cold probe.

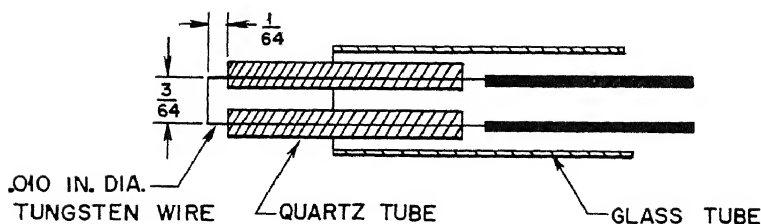


Fig. 9.7—Construction of hot probe.

The glass-shield construction, illustrated in the drawing, was adopted to prevent tungsten, evaporated from the filament, from depositing on the glass near the tungsten seal and thus increasing the effective area of collection of the probe. A great deal of difficulty from this source was encountered in earlier probe designs.

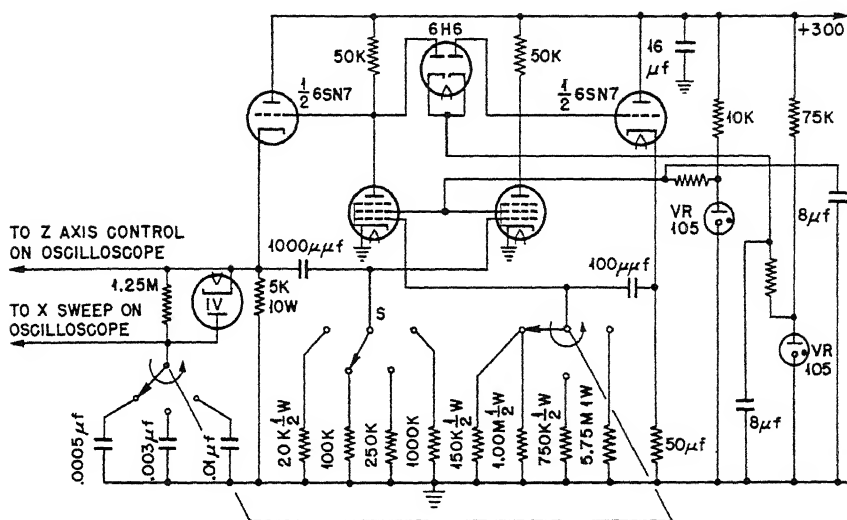


Fig. 9.8—Blackout circuit for cathode-ray tube for operating grid on Du Mont 208 oscillograph. It turns beam on for 1/500, 1/3,000, or 1/20,000 sec periodically, as determined by S. This will vary from every 1/20 sec to every 3 sec as determined by selector switch.

(b) Hot Probe. The hot-probe construction is illustrated in Fig. 9.7. The probe itself consisted of 0.010-in. tungsten wire bent into a rectangular loop $\frac{3}{4}$ in. by $\frac{1}{4}$ in. The wire was lead in through two quartz tubes, which fitted fairly tightly over the wire. These tubes were in turn held by means of a $\frac{1}{4}$ -in. pyrex tube collapsed around them. After passing through the quartz tubes, the 0.010-in. tungsten wire constituting the probe was spot-welded to two stouter tungsten leads that led out of the vacuum. Difficulty was experienced with this probe owing to evaporation of tungsten from the filament onto the quartz leads, which caused an increase in the effective collecting area. Although absolute measurements of ion density were not carried out with this probe, the gradual increase of effective collecting area made the hot-probe indications less and less sensitive.

1.3 Measurement of Hash.* Suitable resistances were placed in series with the arc supply, carbon block, anode, slot, collecting wires, and probe so that the wave form of the current collected by various parts of the chamber and the measuring electrodes in it could be investigated by applying the voltage drop across these resistances to the Y plates of a Du Mont type 208 oscilloscope.

An unbalanced multivibrator circuit designed by Baker and Anderson was fitted to the oscilloscope and was coupled to the Z axis and X sweep of the scope, thus enabling the trace to be blacked out after a single sweep for a period that could be adjusted. In this way it was possible to view the wave form of the hash associated with the current collected by the various parts of the arc chamber without confusion from subsequent traces, which normally prevent the wave form from being viewed, owing to the nonrecurrent nature of the hash pattern. The circuit used for this purpose is shown in Fig. 9.8. With this arrangement it was possible to select three linear sweeps of duration 0.002, 0.00033, and 0.00005 sec and to select periods of blackout between sweeps, ranging from 0.05 to 3 sec.

In practice this arrangement made it possible to obtain a rough estimate, not only of the order of magnitude of the frequencies present in the hash but also of their relative amplitudes.

2. INVESTIGATION OF THE ION-DENSITY DISTRIBUTION FOR DIFFERENT ARC CONDITIONS

2.1 Introduction and Summary. In Chap. 2 on probe measurements in a magnetic field, it was shown that the saturation positive-ion current measured by the probe provides a measure of the positive-ion density. This is so because the penetration of the probe field into the plasma is limited by the electron temperature, and consequently the positive ions are collected on the average from a region that is at a potential greater than that of the probe by an amount comparable with the electron temperature measured in volts. Variation of electron temperature with position in an arc plasma is not very rapid, therefore, to a first approximation, the saturation positive-ion current to the probe is proportional to the positive-ion density at the position of the probe. Absolute determination of the density is more difficult.

The probes employed were of the standard type described in Sec. 1.2 and illustrated in Fig. 9.7. According to Eq. 3 of Chap. 2, the ion density n_+ is given by

* The term "hash" refers to electrical fluctuations in the arc. It is applied to any time variation of the electrical properties of the arc not controlled by the regulator.

$$J_+^s = 0.40n_+ \sqrt{\frac{2kT_e}{m_+}} A \quad (1)$$

where J_+^s is the saturated positive-ion current collected by the probe, T_e is the electron temperature, m_+ is the ionic mass, k is Boltzmann's constant, and A is the effective probe area. For a probe of the shape used it is difficult to assign the correct value to A ; the reason for this is given in Chap. 2. It must, however, lie between that of the front face of the disk and the total area, including both faces of the disk and the surface of the lead wire up to the glass seal. Experiments have been carried out comparing ion collection currents on probes with and without the glass shield at the early stages of an experiment when coating of the glass has not been sufficient to increase the collecting area for the probe with the shield. These indicate that A should certainly be greater than the area of the front face of the disk, though probably not so great as the maximum possible area. For present purposes, A has been taken as the mean between the maximum and minimum areas. The mean electron temperature corresponding to a mean energy of 2 volts has also been assumed. This represents a reasonable average of the observed electron temperatures (see Figs. 9.82 to 9.85*).

A series of systematic observations of ion densities was made in argon plasmas using the arcs in the 37-in. magnet described in Sec. 1.1b and c. In the small arc, measurements were made with the collimating slot centrally placed, with it displaced $\frac{7}{64}$ in. toward the front, and with it displaced $\frac{7}{64}$ in. toward the back face of the arc chamber. Measurements were also made in the same arc, using the curved collimating slot described in Sec. 1.1b. In most of these measurements the slotted-carbon front plates of the arc chamber illustrated in Fig. 9.2 (small arc) and Fig. 9.4 (large arc) were used. A set of three equivalent probes mounted in the same vertical plane perpendicular to that of the arc column and equidistant from it could be inserted through the slots and moved as a whole either parallel to the slots (parallel to the width of the column) or in a perpendicular (in-and-out) direction. In this way the variation of ion density in three perpendicular directions could be obtained, the use of the three probes providing information on the variation parallel to the length of the column. The distribution of ion density obtained in this way was studied for a variety of magnetic fields, argon pressures, and arc currents and voltages. The points at which observations were taken by

* It will be seen that a somewhat higher value of 2.5 volts might have been preferred, but the accuracy of the remaining quantities hardly justified making the change.

the central probe are illustrated by network diagrams in Fig. 9.9, which include also, to scale, the position and shape of the column and of the arc walls.

Earlier measurements of the variation of ion density in a direction parallel to the narrow dimension of the column were taken with the Backus arc described in Sec. 1.1a, but, as they do not provide anything additional to the more extensive systematic series obtained with the 37-in. magnet, they are not included here.

In general, it can be said that in argon the ion density (1) is a maximum on the antidrain side* of the column, (2) decreases with distance from the column, and (3) tends to be greater at the anticathode rather than the cathode end. For detailed description, the transverse (parallel to the column, perpendicular to magnetic field), in-and-out (perpendicular to the column), and longitudinal (parallel to magnetic field) distributions will be considered separately.

2.2 Transverse Distribution of Ion Density. The important feature of this distribution is the asymmetry it exhibits. The maximum ion density in any line parallel to the side of the column and perpendicular to the magnetic field occurs always on the antidrain side. The effect may be clearly seen in the ion-density contour diagrams illustrated in Fig. 9.9.

In order to study the dependence of the degree of asymmetry under various conditions, it is necessary to define an asymmetry factor. This, referring to Fig. 9.9a, is the ratio of the sum of the ion-density measurements taken along the line AA to those taken along line BB.

As the most likely condition to be correlated with the asymmetry is the magnetic field, it is considered first. The first general result is that the sense of the asymmetry is determined by the sense of the magnetic field, as proved by reversing the field. It also increases with magnitude of the field as shown in Fig. 9.10, where the asymmetry ratio, as defined above, is illustrated as a function of magnetic field for each of the cases illustrated in Fig. 9.9 for standard arc current and voltage conditions as specified. In Fig. 9.10 it will be seen that the ratio falls well below 1 as the magnetic field is reversed, corresponding to the change in sense. Measurements of ion density carried out with the large arc in argon showed the same asymmetry as those observed for the small arc when made near the arc column. Thus the ion density was greatest on the antidrain side of the front edge of the arc column and least on the drain side. The ion-density contours for the large-arc case are shown in Fig. 9.9e.

*The drain side of the column is defined as the side toward which the electrons migrate in the magnetic field.

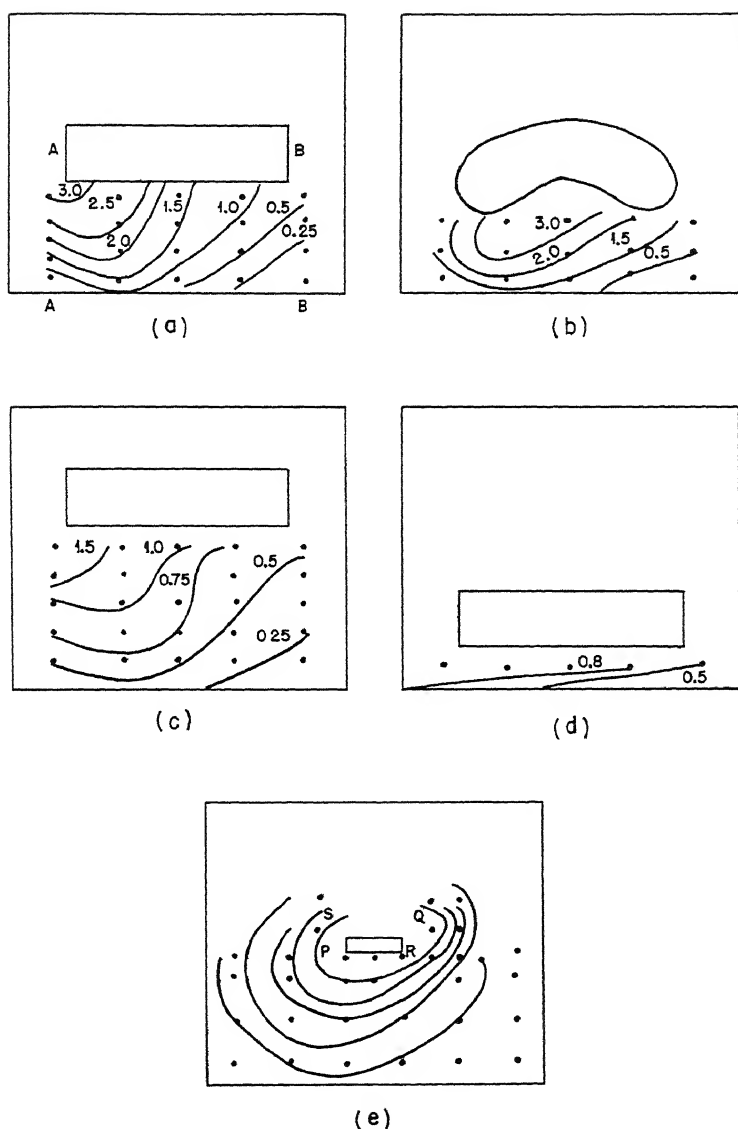


Fig. 9.9—Contours of equal ion density in argon. (a) Small arc (enlarged 4 \times), symmetrical collimating slot; (b) small arc, curved collimating slot; (c) small arc, collimating slot near back; (d) small arc, collimating slot near front; (e) large arc (full scale), symmetrical collimating slot. The contours are given in terms of milliamperes to the probe (at -15 volts below floating potential). The conversion factor to ion density is approximately 1.9×10^{12} . Contours taken in middle plane of arc. Pressure 8×10^{-4} mm Hg; magnetic field 3,700 gauss; arc voltage 150 volts; arc current 1.5 amp. Dots indicate points at which measurements were taken.

In this case it was possible to probe at points near the arc column but toward the back of the chamber. It was found that behind the column the asymmetry was in the reverse sense. Thus in Fig. 9.9e the maximum ion densities were measured at positions P and Q and the minimum ion density was measured at positions R and S.

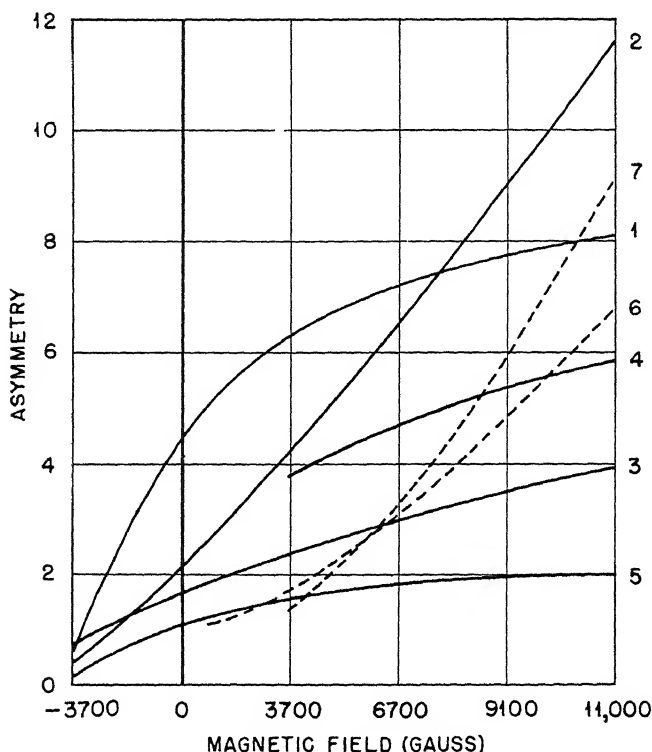


Fig. 9.10—Variation of asymmetry of ion distribution. Arc voltage 150 volts; arc current 1.5 amp for curves 1 to 5. Curve 1: symmetrical collimating slot; small arc; pressure 0.6×10^{-3} mm Hg. Curve 2: symmetrical collimating slot; small arc; pressure 1.4×10^{-3} mm Hg. Curve 3: collimating slot near face; small arc; pressure 0.6×10^{-3} mm Hg. Curve 4: collimating slot remote from face; small arc; pressure 0.6×10^{-3} mm Hg. Curve 5: curved collimating slot; small arc; pressure 0.6×10^{-3} mm Hg. Curve 6: large arc; pressure 1.4×10^{-3} mm Hg; arc voltage 150 volts; arc current 1.5 amp. Curve 7: small arc in chlorine.

Before proceeding to consider the relation of the asymmetry to arc current, voltage, and pressure it is necessary to note that it was found that the length of life of the filament was an important factor in determining the magnitude, though not the sense of the effect. It appears that the filament tends to wear in such a way as to reduce the

asymmetry. Evidence for this was obtained from the following experiment: With a fresh filament the ion-density distribution was measured at pressure 0.6×10^{-3} mm Hg, magnetic field 3,700 gauss, arc voltage 150 volts, and arc current 1.5 amp. After a series of measurements, some at a very high pressure, the measurements were repeated, and the asymmetry found to be approximately compensated by the filament wear. It would then be expected that reversal of the

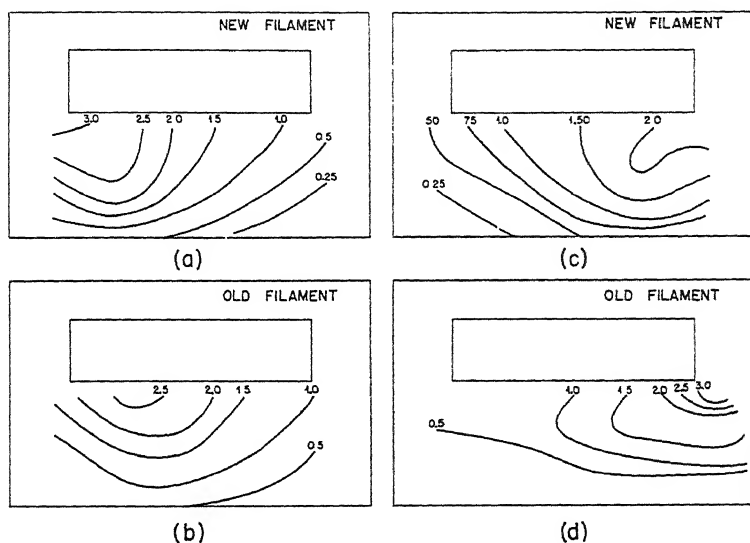


Fig. 9.11—Dependence of asymmetry on sense of magnetic field and filament wear. (a), (b) Pressure 0.6×10^{-3} mm Hg; magnetic field 3,700 gauss; arc voltage 150 volts; arc current 1.5 amp. (c), (d) Pressure 0.6×10^{-3} mm Hg; magnetic field -3,700 gauss (reversed); arc voltage 150 volts; arc current 1.5 amp.

magnetic field should reveal a more than normally great asymmetry in the reversed sense, for the filament would have worn in a sense to aggravate the asymmetry with reversed field. That this was indeed the case is revealed in Fig. 9.11, which illustrates the asymmetry for the three cases.

Figure 9.11 illustrates the effect of reversal of magnetic field and filament wear on the observed ion-density distribution. Figure 9.11a was taken with a new filament and with the following arc conditions: pressure 0.6×10^{-3} mm Hg, magnetic field 3,700 gauss, arc voltage 150 volts, and arc current 1.5 amp. Figure 9.11c illustrates the distribution obtained with the arc conditions maintained as above but with the magnetic field reversed, showing how the asymmetry is reversed also. After the measurements plotted in Fig. 9.11c were made,

the arc was run for some hours at a very high pressure of argon (7×10^{-3} mm Hg) and a high arc current. The measurements of Fig. 9.11a were then repeated with the result shown in Fig. 9.11b. It is seen that the asymmetry is reduced owing to the wear in the filament. Finally the field was reversed, and the measurements of Fig. 9.11c repeated with the result shown in Fig. 9.11d.

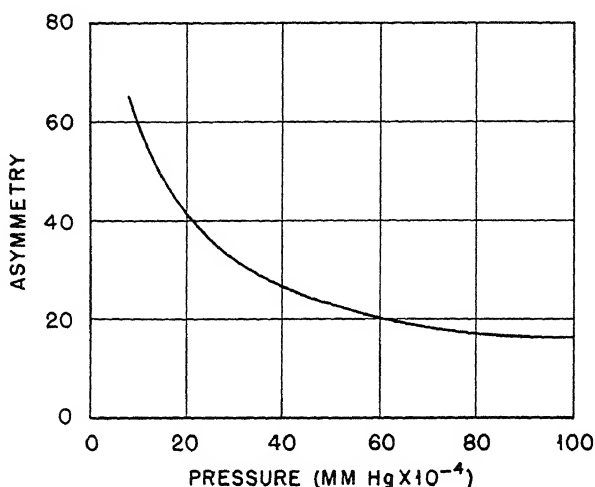


Fig. 9.12—Variation of asymmetry of ion distribution with pressure. Magnetic field 3,700 gauss; arc voltage 150 volts; arc current 1.5 amp.

Figure 9.12 shows the variation of the asymmetry (as defined above) with the pressure for the symmetrical small arc in argon under these conditions: magnetic field 3,700 gauss, arc voltage 150 volts, and arc current 1.5 amp. It is seen that the asymmetry decreases markedly as the pressure is increased.

Figure 9.13 shows the variation of the asymmetry with arc current. With the exception of one of the cases shown in this figure, it appears that this variation is not very marked.

Figure 9.14 illustrates a slight general tendency for the asymmetry to decrease with increase of arc voltage.

In all the cases described here the asymmetry is seen to be least for the case of the curved collimating slot or for the collimating slot near the front of the arc.

It has not yet been possible to account in detail for the asymmetrical ion distribution exhibited by the arc. However, there seems little doubt that the asymmetry is associated with the necessity that

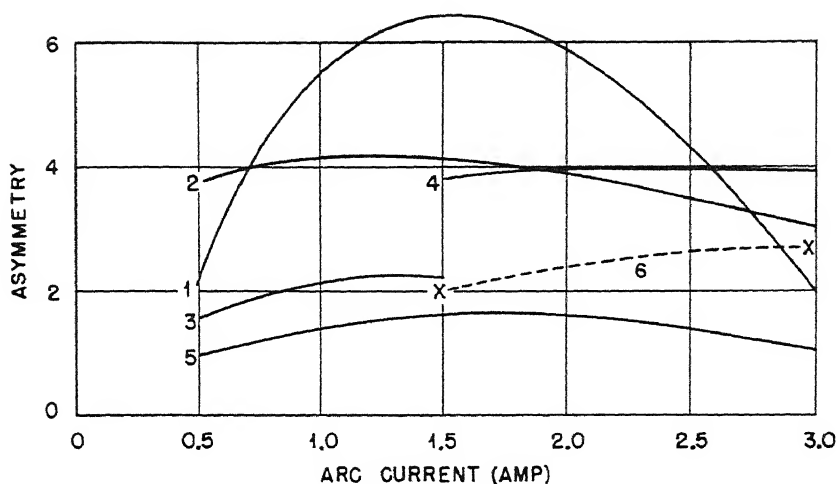


Fig. 9.13—Variation of asymmetry of ion distribution with arc current for small arc, magnetic field 3,700 gauss, arc voltage 150 volts. Curve 1: symmetrical collimating slot; pressure 6×10^{-4} mm Hg. Curve 2: symmetrical collimating slot; pressure 14×10^{-4} mm Hg. Curve 3: collimating slot near face; pressure 6×10^{-4} mm Hg. Curve 4: collimating slot remote from face; pressure 6×10^{-4} mm Hg. Curve 5: curved collimating slot; pressure 6×10^{-4} mm Hg. Curve 6: pressure 0.6×10^{-3} mm Hg.

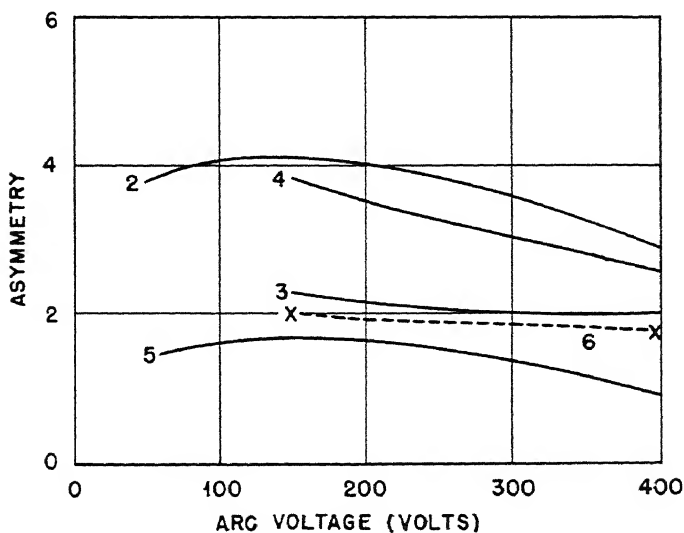


Fig. 9.14—Variation of asymmetry of ion distribution with arc voltage for small arc, magnetic field 3,700 gauss, arc current 1.5 amp. Curve 1: symmetrical collimating slot; pressure 6×10^{-4} mm Hg. Curve 2: symmetrical collimating slot; pressure 14×10^{-4} mm Hg. Curve 3: collimating slot near face; pressure 6×10^{-4} mm Hg. Curve 4: collimating slot remote from face; pressure 6×10^{-4} mm Hg. Curve 5: curved collimating slot; pressure 6×10^{-4} mm Hg. Curve 6: pressure 0.6×10^{-3} mm Hg.

ions be removed from the arc column, where they are formed, to the walls of the chamber in order for the arc to run stably. If the ion distribution were completely symmetrical, the plasma equipotentials would have the form shown in Fig. 9.15. Thus, under the action of the crossed magnetic and electric field, the ions and electrons would tend to drain around the equipotential surfaces without ever reaching

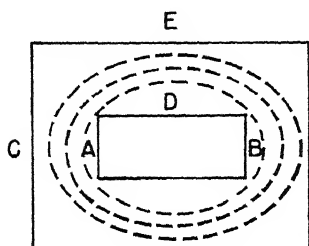


Fig. 9.15

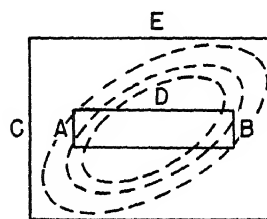


Fig. 9.16

Fig. 9.15—Plasma equipotentials for completely symmetrical ion distribution.

Fig. 9.16—Plasma equipotentials making ion drain possible.

the walls. This would tend to cause a piling up of ionization and a breakdown of the space-charge neutralization condition. Such a state of affairs might cause the onset of violent plasma oscillations and enable the ions to reach the walls owing to the action of the strongly oscillating plasma fields. Alternatively, the arc could pass over into another state in which the steady plasma equipotentials are such as to cause the transfer of ions from the arc column to the vicinity of the sheath. It is believed that the latter behavior is that which occurs when the arc runs in an asymmetrical state. Thus, if the equipotential distribution, instead of being that shown in Fig. 9.15, were that in Fig. 9.16, it would be possible for ions to drain out under the action of the steady electric and magnetic fields until they were quite close to the sheath (within a distance of the order of their Larmor radii from it), so that relatively few collisions would suffice to get them to the walls.

In general, for a uniform arc column, an asymmetrical distribution of potential would require an asymmetrical ion-density distribution; however, if filament wear during a run is important, it would be possible for the filament to wear in such a way that the arc column would not be uniform and an asymmetrical distribution of equipotentials could be produced by a symmetrical ion-density distribution.

Although the factors governing the precise shapes of the asymmetrical equipotentials are not clear,* the mechanism by which they might be set up can be understood in a qualitative way. If the geometric form of the arc were cylindrical and completely symmetrical, there would be no preferred direction for the asymmetry; therefore there would be no stable mode of getting ions and electrons to the walls. It can be shown that the piling up of space charge would then result in plasma oscillations, in whose fields the ions and electrons would drain to the walls. When the form is, as in our case, rectangular, certain preferred orientations of the equipotentials become more stable than others. In particular, as will be shown in the report on oscillations mentioned above, the symmetrical distribution appearing in Fig. 9.15 is less stable than the asymmetrical one appearing in Fig. 9.16. Other types of asymmetrical potentials are also possible (see Sec. 4). It can be shown that, in general, small potential gradients of the order of a few volts per centimeter, which originate in exceedingly slight deviations from perfect electrical neutrality, so adjust themselves as to move ions to the walls in the most rapid manner possible, since greater stability of the asymmetrical equipotentials is thus brought about by the greater speed with which they remove space charge to the walls. The question of the equipotentials will be discussed again in Sec. 4 under space-potential measurements.

2.3 Variation of Ion Density from Top to Bottom of the Arc. In general, it was found that the ion distribution was not uniform up and down the arc column but showed a marked tendency to increase from top to bottom. Figure 9.17 shows the ion distribution for the small arc in argon at three planes: the median plane, the plane at a height of $1\frac{1}{16}$ in. above it, and the plane $1\frac{1}{16}$ in. below it. The effect does not appear to change much with changing arc conditions, persisting up to very high pressures of 7×10^{-3} mm Hg. Furthermore, the ion distribution at the bottom section is more symmetrical than that at the top, as is seen in a typical example in Fig. 9.17. The reason for this variation of ion density along the arc length is not clear. Any effect due to absorption of the fast electrons by the gas in the arc would be expected to act in the reverse direction. It may be that some of these effects are to be attributed to the presence of secondary electrons produced by the impact of the arc column on the anode. Many of these electrons would have energies of some tens of volts and would be accelerated through the anode sheath into the plasma.

* The potential gradients must originate, however, in exceedingly slight deviations from neutrality, which so adjust themselves as to remove ionization to the walls in the most rapid manner possible.

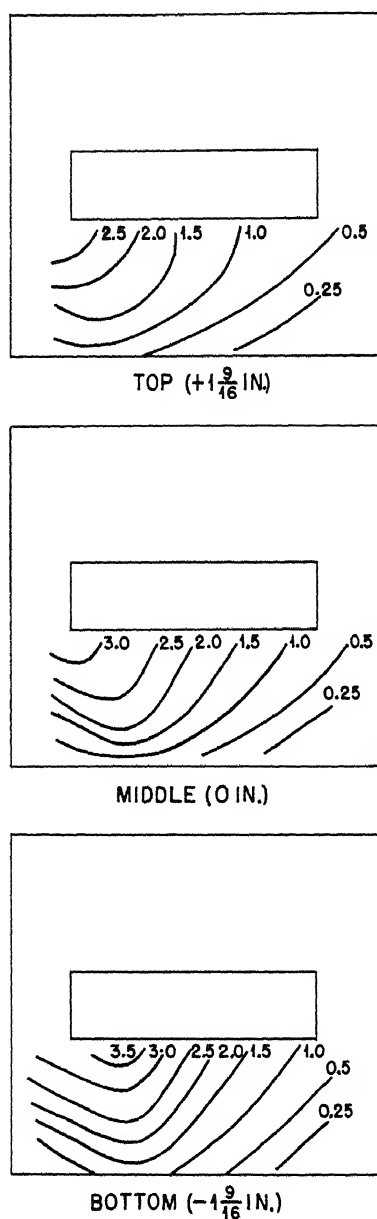


Fig. 9.17 —Contours of equal ion density, showing vertical variation for small arc in argon (enlarged $4\times$). Pressure 6×10^{-4} mm Hg; magnetic field 3,700 gauss, arc voltage 150 volts; arc current 1.5 amp.

It is possible, however, that the effect may be in the experimental arrangement and be due to inhomogeneity of the magnetic field near the position of the arc. Independent evidence was available to show that the column tended to run closer to the front of the chamber at the bottom than at the top.

2.4 Variation of Ion Density Transversely along Central Axis of the Arc. The variation of the ion density in the direction from the arc column along the central axis is a quantity of great importance

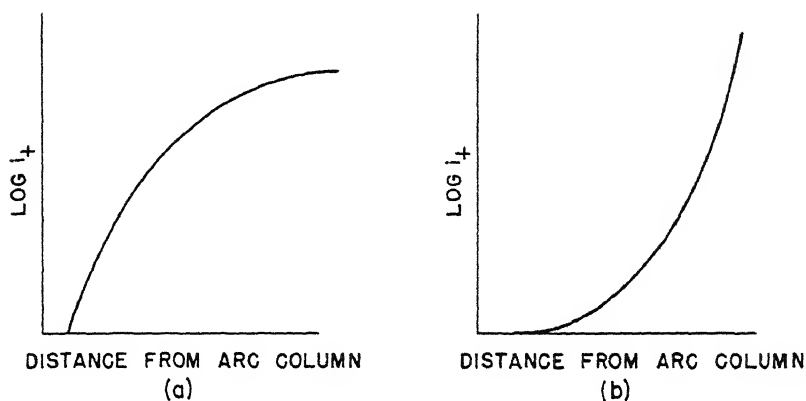


Fig. 9.18—Form of $\log i_+$ vs. distance curve for (a) small arc in argon; (b) large arc in argon.

from the point of view of the operation of an arc, since it gives a measure of the loss of ionization between the arc column and the meniscus by recombination, diffusion to the top and bottom of the chamber, etc.

The asymmetry of the distribution of ion density about the central axis complicates the study of the variation of current along it. Thus, if owing to filament wear or operation at high pressures the ion distribution is fairly symmetrical about the central axis, the distribution along it is exponential. If, however, the distribution shows considerable asymmetry, the distribution along the central axis is far from exponential. Since high magnetic fields lead to a markedly asymmetrical distribution, it is to be expected that in these cases the departure from exponential behavior would be most marked. In the small arc in argon the lack of symmetry for high fields leads, in general, to a curve of the form shown in Fig. 9.18a, i.e., $\log i_+$ vs. distance, while in the large arc the variation is of the form shown in Fig. 9.18b.

If instead of measuring the ion distribution along the central axis it is considered along an axis nearest to the axis of symmetry of the ion density, the distribution tends to become more nearly exponential. This effect is illustrated in Fig. 9.19 for the small arc in argon. In

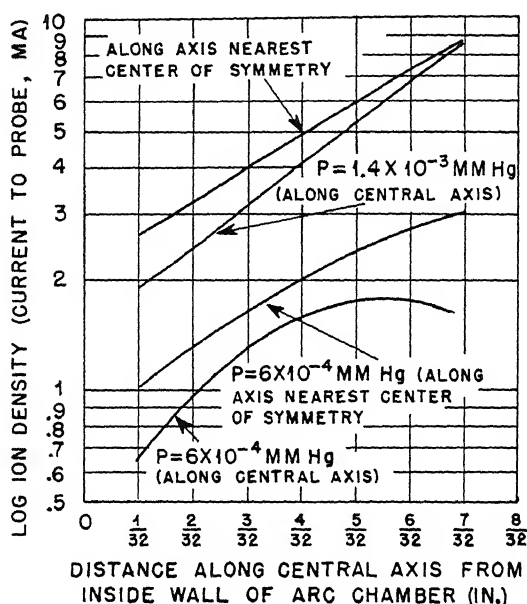


Fig. 9.19—Variation of ion density for small arc in argon. Magnetic field 3,700 gauss; arc voltage 150 volts; arc current 1.5 amp.

general, for convenience in this work the variation has been considered along the central axis. Figures 9.19 to 9.21 show the variation of the logarithm of the ion density along the central axis for the small and large arcs in argon. Figure 9.19 shows the effect of pressure on the ion distribution for the case of the small arc. The higher pressure (1.4×10^{-3} mm Hg) appears to give a more nearly exponential distribution than the lower pressure (0.6×10^{-3} mm Hg), but since, as has been pointed out above, the shape of the distribution is affected by the symmetry, which is in turn affected by filament wear, extraneous effects may mask the true variation with pressure. At points close to the wall of the arc chamber the ion density is seen from these curves to be roughly proportional to the pressure.

Figure 9.20 shows the variation of ion density along the central axis of the small arc for the case of a very high magnetic field. The curve shows the characteristic form for a high field described above.

Figures 9.21 and 9.22 show the ion distribution along the central axis of the large arc for different magnetic fields. Figure 9.21 shows a comparison for a pressure of 0.6×10^{-3} mm Hg at fields of 3,700 and 11,400 gauss. At the low field the distribution is approximately

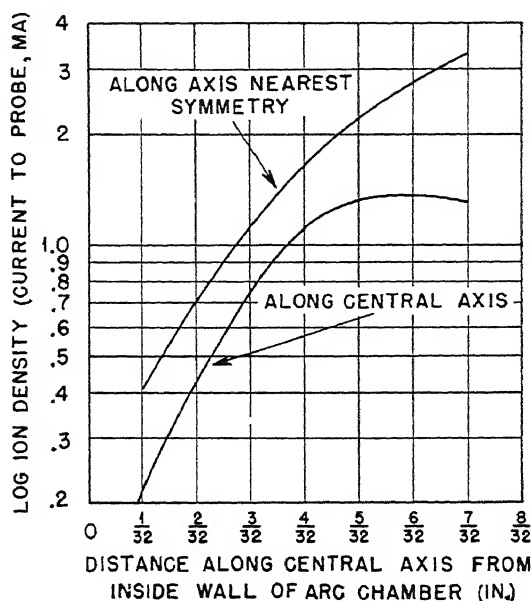


Fig. 9.20—Variation of ion density for small arc in argon. Pressure 6×10^{-4} mm Hg; magnetic field 11,400 gauss; arc voltage 150 volts; arc current 1.5 amp.

exponential, but for the high field the density falls off less rapidly in the direction away from the arc column. Figure 9.22 shows a similar comparison of the effect of magnetic field taken with a chamber pressure of 1.4×10^{-3} mm Hg for fields of 1,000, 3,700, and 11,000 gauss. These curves show that with the field of 1,000 gauss the ion density falls off less rapidly than for a field of 3,700 gauss, but there is little difference between the rate of fall-off in the direction away from the arc column between the fields of 3,700 and 11,000 gauss.

Figure 9.23 shows the effect of variation in arc current and voltage on the central-axis distribution for the large arc in argon. These results indicate that when the current is increased from 1.5 to 3.0 amp the rate of fall-off of the ion density is increased. No marked effect of arc voltage was observed, however.

To illustrate the effect of arc conditions on the ion-density distribution along the central axis, it is convenient to specify the distance

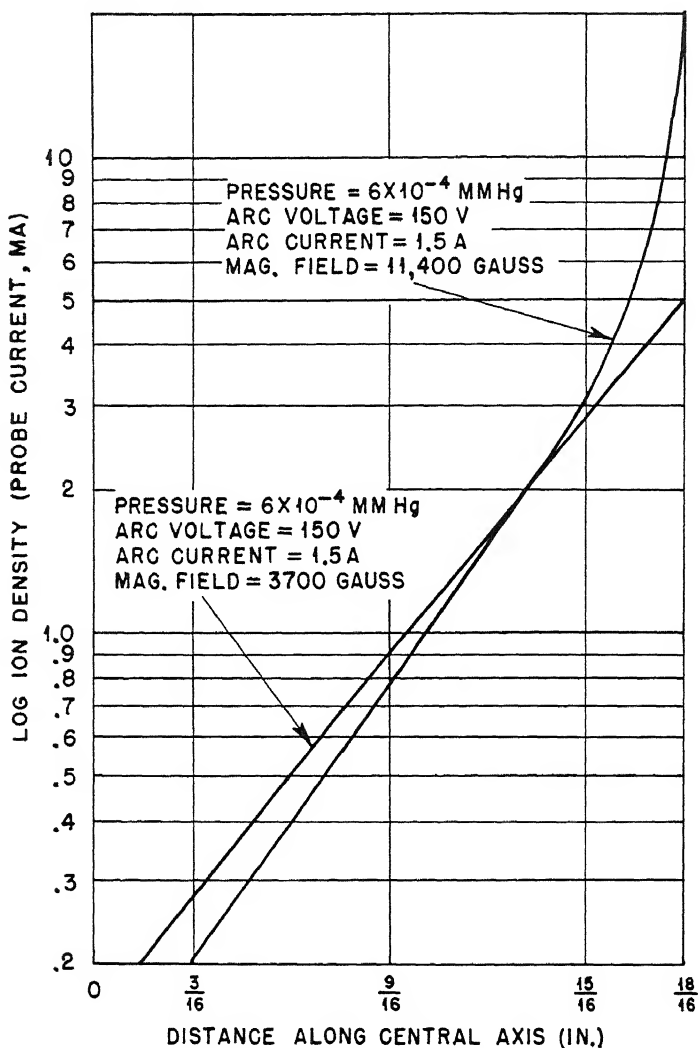


Fig. 9.21—Variation of ion density with distance along central axis for large arc in argon. Pressure 6×10^{-4} mm Hg; arc voltage 150 volts; arc current 1.5 amp.

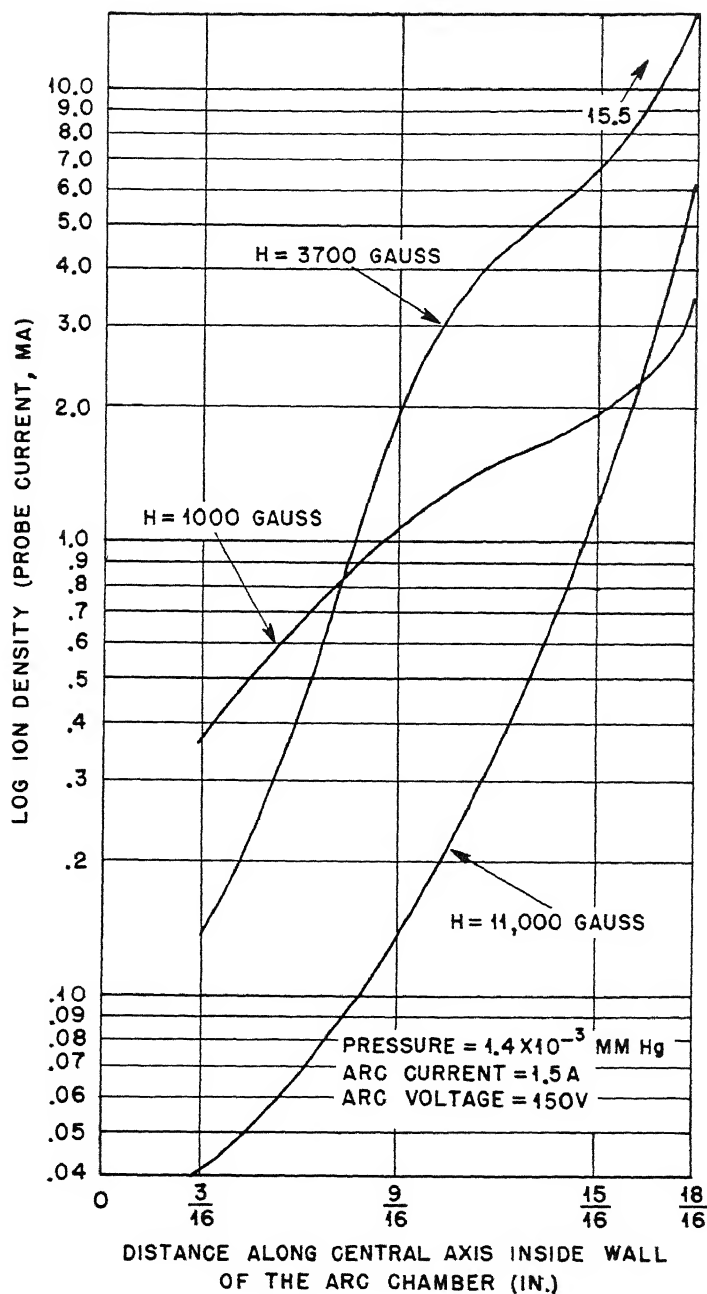


Fig. 9.22—Variation of ion density with distance along central axis for large arc in argon. Pressure 1.4×10^{-3} mm Hg; arc voltage 150 volts; arc current 1.5 amp.

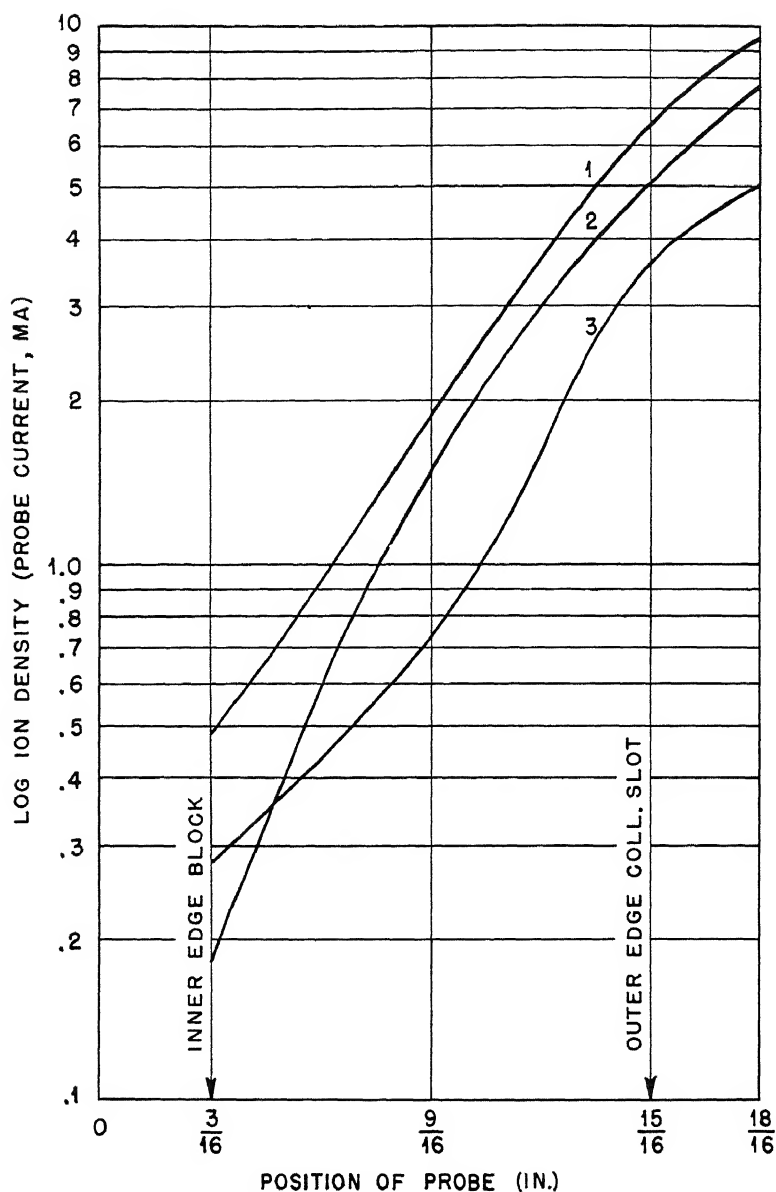


Fig. 9.23—Variation of ion density with distance along central axis for large arc in argon. Pressure 0.56×10^{-3} mm Hg. Curve 1: magnetic field 3,650 gauss; arc voltage 400 volts; arc current 1.5 amp. Curve 2: magnetic field 3,700 gauss; arc voltage 150 volts; arc current 3.0 amp. Curve 3: magnetic field 3,700 gauss; arc voltage 150 volts; arc current 1.5 amp.

in which the ion density falls to $1/e$ of its value. In view of the departure from an exponential distribution due to the effects of asymmetry about the central axis, as noted above, this quantity is difficult to specify accurately. Table 9.1 shows the best values for this distance obtained for a variety of arc conditions in the case of argon.

Table 9.1 — Distance for Ion Density to Fall to $1/e$ of Its Value

Type of arc	Pressure, mm Hg $\times 10^{-3}$	Magnetic field, gauss	Arc voltage, volts	Arc current, amp	Distance for ionization to be reduced to $1/e$ of its value, in.	Remarks
Small	1.4	3,700	150	1.5	$1/8$	Distribution
Small	0.6	3,700	150	1.5	$5/32$	exponen-
Small	0.6	11,400	150	1.5	$1/16$	tial at dis-
Large	1.4	900	150	1.5	$9/16$	tances a-
Large	1.4	3,700	150	1.5	$3/16$	bove $1/8$ in.
Large	1.4	11,400	150	1.5	$7/32$	from arc column
Large	0.6	3,700	150	1.5	$5/16$	Within $1/4$ in.
Large	0.6	11,400	150	1.5	$1/16$	from arc column
Large	0.6	11,400	150	1.5	$9/32$	Farther out
Large	0.6	3,700	150	3.0	$3/16$	than $1/4$ in.
Large	0.6	3,700	400	1.5	$5/16$	from arc column

This table indicates the following trends with arc conditions: The rate of fall-off of ion density in moving away from the arc column (1) increases as the magnetic field is increased, (2) increases as the arc current is increased, except at points close to the column, and (3) does not depend markedly on pressure and arc voltage over the range of variation investigated.

2.5 Diffusion Theory of Arc Plasma in Absence of Negative Ions.

The loss of ions (and electrons) to the ends by diffusion leads to an approximately exponential form for the ion density as a function of the distance from the arc column. For example, consider an elementary layer of the plasma parallel to the arc column, of unit width, of length equal to the arc length l , and of thickness dx . In this one-dimensional theory x is regarded as small relative to the width of the column.

The elementary portion of plasma gains and loses ions and electrons in the following ways:

1. It gains owing to the resultant drift current $j(x)$ across the boundary at x .
2. It loses owing to the resultant drift current $j(x + \delta x)$ across the boundary at $x + \delta x$.
3. It loses ions and electrons owing to the diffusion to the walls at the top and bottom of the arc.

$$\text{Net gain of electrons due to drift current} = -\frac{dj_e}{dx} l \delta x$$

$$\text{Net loss of electrons due to diffusion to the ends} = \gamma n_e \delta x$$

Assuming that this diffusion rate is proportional to the electron density n_e , then

$$\frac{dj_e}{dx} = -\frac{\gamma}{l} n_e \quad (2)$$

Similarly,

$$\frac{dj_+}{dx} = -\frac{\beta}{l} n_+ \quad (3)$$

where $\beta n_+ \delta x$ is taken to be the net loss of positive ions due to diffusion to the ends. In the expressions for the loss of electrons and ions to the ends, the assumption is made that the quantities γ and β are constant throughout the plasma. This, however, represents a very simplified picture. Thus, in the case of electron drain to the ends, the electron temperature as well as the electron density n_e determines the loss parallel to the field. In order to reach the anode or collimating slot, the electrons have to pass through the sheath, across which there exists a retarding potential of about 6 volts. Only those electrons at the high-energy end of the Maxwellian distribution will penetrate the sheath. Equation 2 will be valid only if the electron temperature is independent of x . It will be seen in Sec. 4 that the electron temperature tends to drop as the distance away from the arc column increases.

Similarly in Eq. 3 it is assumed that the energy with which the ions are collected is independent of x . However, since all ions that reach the sheath are collected, Eq. 3 is probably a closer approximation to the truth than Eq. 2.

More precise assumptions regarding the loss of electrons and ions to the ends would have made the equations unmanageable. Equations 2 and 3 probably give a reasonable general representation of the ion- and electron-density distribution in the argon arc, and deductions of a qualitative nature can be made from them. The expressions j_e and j_+ may be written in terms of the diffusion coefficients D_e , D_+ and the mobilities k_e , k_+ , where $k_e = D_e e / kT_e$, etc.

$$j_e = -D_e \frac{dn_e}{dx} + \frac{D_e e}{kT_e} n_e \frac{dV}{dx} \quad (4)$$

$$j_+ = -D_+ \frac{dn_+}{dx} - \frac{D_+ e}{kT_+} n_+ \frac{dV}{dx} \quad (5)$$

Thus, Eqs. 3 and 2 become

$$D_+ \frac{d^2 n_+}{dx^2} + \frac{D_+ e}{kT_+} \frac{d}{dx} \left(n_+ \frac{dV}{dx} \right) = \frac{\beta n_+}{l} \quad (6)$$

$$D_e \frac{d^2 n_e}{dx^2} - \frac{D_e e}{kT_e} \frac{d}{dx} \left(n_e \frac{dV}{dx} \right) = \frac{\gamma n_e}{l} \quad (7)$$

If there is space-charge neutralization, $n_+ \approx n_e$,* and dV/dx can be eliminated between these equations, giving

$$\frac{d^2 n_+}{dx^2} = \frac{\beta T_+ D_e + \gamma T_e D_+}{D_+ D_e (T_+ + T_e)} \frac{n_+}{l}$$

$$n_+ = A e^{\eta x} + B e^{-\eta x}$$

$$\eta = \sqrt{\frac{\beta T_+ D_e + \gamma T_e D_+}{D_e D_+ (T_e + T_+) l}} \quad (8)$$

If the wall of the arc chamber is sufficiently far from the arc column so that the first term can be neglected, then

$$n_+ = n_0^+ e^{-\eta x} \quad (9)$$

* Although $n_e \approx n_+$, there are very slight deviations from neutrality which permit $d^2 V/dx^2$ to be practically arbitrary. It requires a deviation of only a small fraction of 1 per cent to produce potentials of hundreds of volts. Thus, in the present approximation, $n_e \approx n_+$ in the diffusion equations but not in Poisson's equation.

indicating the exponential fall-off of ion density observed. The distance x_0 in which the density falls off to $1/e$ of its value is

$$x_0 = \sqrt{\frac{(T_e + T_+)l}{\frac{\beta T_+}{D_+} + \frac{\gamma T_e}{D_e}}} \quad (10)$$

As the magnetic field is increased, D_e will decrease markedly so that x will also decrease with increase of field, as observed.

In general, in the presence of a large magnetic field it would be expected that

$$\frac{\gamma T_e}{D_e} \gg \frac{\beta T_+}{D_+}$$

so that Eq. 10 may be written as

$$x_0 = \sqrt{\left(1 + \frac{T_+}{T_e}\right) \frac{l D_e}{\gamma}} \quad (11)$$

It was pointed out above that the distance x appears also to decrease as the arc current is increased. This may imply an increase in T_e , the electron temperature, as the arc current is increased.

Equation 11 shows that the distance x_0 in which the ion density falls to $1/e$ of its value increases proportionately to the square root of the length of the arc and to the square root of the diffusion coefficient D_e of electrons across the field. Since D_e would be expected to depend markedly on the magnetic field, decreasing with increase of field, it follows that x_0 would be expected to fall off with increase of field. Further, as would be expected, the distance x_0 increases as γ , the rate of collection to the top and bottom of the arc, decreases.

It is of interest to examine whether the value of D_e/γ , which is required in order that x_0 of Eq. 10 should agree with distance observed, is reasonable.

The term γ may be regarded as the mean velocity, parallel to the magnetic field, of those electrons which have sufficient velocity in the same sense to penetrate through the anode sheath to the anode. If V_0 is the potential drop across the sheath and T_e is the electron temperature, then

$$\gamma \approx \frac{v_e}{\sqrt{4\pi}} e^{-eV_0/kT_e}$$

where v_e is the electron velocity $\sqrt{2kT_e/m}$ corresponding to the electron temperature T_e . If typical values for a magnetic field of 4,000 gauss and a pressure of 10^{-3} mm Hg are substituted, namely, $kT = 2\text{ev}$ and $V_0 = 8$ volts, then $\gamma \approx 4 \times 10^5$ cm/sec. Taking 0.3 cm as a typical value of x_0 , then from Eq. 10, for an arc 12 cm in length,

$$D_e = 0.09 \gamma/l = 3 \times 10^3 \text{ sq cm/sec} \quad (12)$$

Now in Chap. 2 a discussion of the mechanism of electron diffusion was given. If the process is one of drain, then D_e was found to be approximately

$$D_e (\text{drain}) = \frac{10^5}{16H} \frac{kT_e}{e}$$

where H , the magnetic field, is in thousands of gauss and kT_e/e is in volts. On the other hand, for diffusion by collision

$$D_e (\text{collision}) = \frac{4.3 \times 10^{-10}}{H^2} \frac{n_e}{\sqrt{kT_e/e}}$$

where n_e is the number of electrons per cubic centimeter and is of the order 10^{12} . For this case

$$D_e (\text{drain}) = 3 \times 10^3 \text{ sq cm/sec}$$

$$D_e (\text{collision}) = 20 \text{ sq cm/sec}$$

When this is compared with Eq. 12 it is found that the whole theory is self-consistent if the main cause of the electron diffusion is by drain diffusion. It is of interest to note that the study of the probe characteristics in Chap. 2 also indicated that drain diffusion is the important mechanism for transporting electrons perpendicular to the magnetic field.

2.6 Variation of Ion Density with Arc Conditions. (a) Effect of Magnetic Field. Figure 9.24 shows the variation of ion density with magnetic field at a number of different distances from the arc column in the case of the large arc. The distances indicated on the curves are distances from the front chamber wall in the direction of the arc column. Close to the wall ($\frac{3}{16}$ in. distant) the ion density falls with increase of magnetic field from a field of 900 up to 11,000 gauss. As the distance from the arc column decreases, however, the curves of ion density vs. magnetic field show a characteristic maxi-

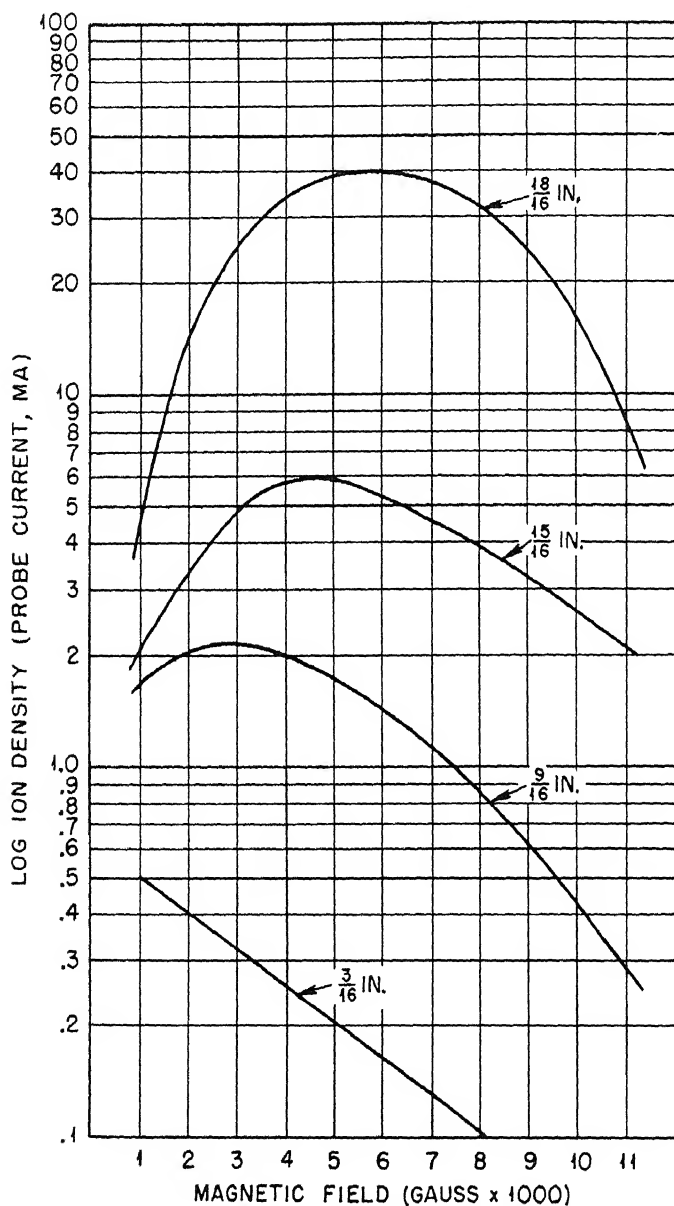


Fig. 9.24—Large arc in argon. Pressure 1.4×10^{-3} mm Hg; arc voltage 150 volts; arc current 1.5 amp. Figures on curves represent distances in inches from inside front wall of the arc chamber.

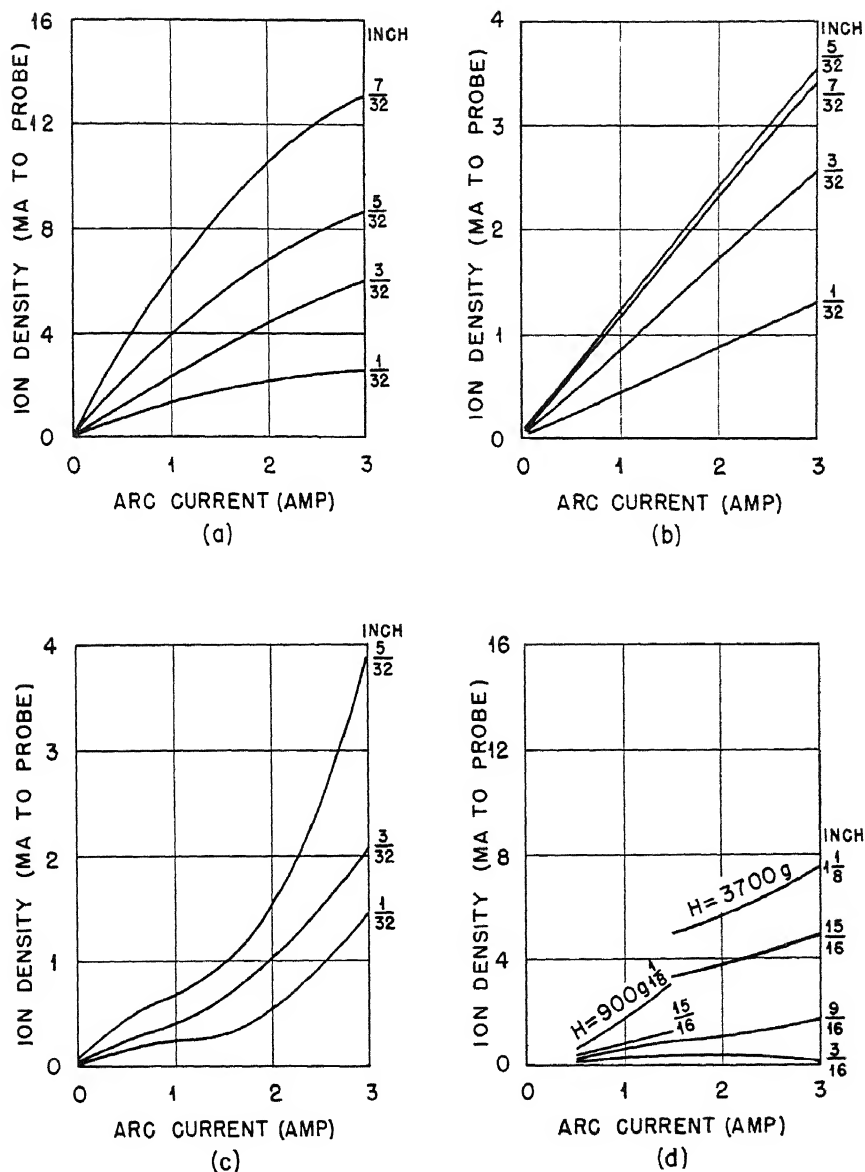


Fig. 9.25—Variation of ion density with arc current in argon. (a) Small arc; symmetrical collimating slot; magnetic field 3,700 gauss; arc voltage 150 volts; pressure 14×10^{-4} mm Hg. (b) Small arc; symmetrical collimating slot; magnetic field 3,700 gauss; arc voltage 150 volts; pressure 14×10^{-4} mm Hg. (c) Small arc; curved collimating slot; pressure 6×10^{-4} mm Hg; magnetic field 3,700 gauss; arc voltage 150 volts. (d) Large arc; symmetrical collimating slot; pressure 6×10^{-4} mm Hg; magnetic field 900 and 3,700 gauss; arc voltage 150 volts.

imum. The position of this maximum moves out toward higher magnetic fields as the column is approached. Thus, at $\frac{9}{16}$ in. from the walls the maximum occurs at about 2,500 gauss; at $\frac{15}{16}$ in., at about 4,500 gauss; and at $\frac{18}{16}$ in. (i.e., at $\frac{1}{16}$ in. from the arc column), at about 6,500 gauss. This form of behavior is what would be expected since at very low magnetic fields the positive ions and electrons are not held in by the field, and thus the ionization is spread out over the whole arc region. As the magnetic field is raised the ions and electrons are kept for a longer time close to the arc column. Thus for a given voltage, current, and pressure it would be expected that the ion density near the column would increase with magnetic field, while that far away from the column should decrease, as observed. At any given distance from the column, the existence of a critical field would be expected; above this field the ionization would decrease with increase of field and below it the ionization would increase with the field. This is exactly the behavior observed. The above argument may need modifying slightly because at higher magnetic fields a given arc current may produce more ionization on account of the longer total path of the electrons, but this effect probably would not modify the qualitative features to be expected.

(b) Effect of Arc Current. Figure 9.25 shows the variation of ion density with arc current in a number of cases. The curves in Fig. 9.25a and b refer to the small arc with the standard collimating slot; those in Fig. 9.25c refer to the small arc with a curved collimating slot; and those in Fig. 9.25d refer to the large arc. The numbers marked on these curves represent the distances of the probe from the inside front wall of the chamber at which the measurements were made.

The curves in Fig. 9.25a are of the conventional type, showing saturation effects at higher currents. However, anomalous curves, such as those in Fig. 9.25c, were often obtained. These could arise from variations in the degree of asymmetry as the current is raised.

(c) Effect of Pressure. Figure 9.26 shows the variation of ion density with pressure for different distances from the arc column with the small arc. The ion density is not proportional to pressure, as might have been anticipated, but increases less rapidly. Furthermore, the departure from linearity is just as great close to the column as it is farther out. One possibility is that the deviation from linearity with pressure results from recombination. The necessary value of the recombination coefficient required to explain the observed variation with pressure can be calculated. Thus

$$\frac{dn}{dt} = kp f(J_c) - \beta n - \alpha n^2 = 0$$

for steady conditions, where $kp f(J_c)$ is the rate of production of ions, which can be calculated for a given current from the known ionization cross section of argon; the term βn represents the rate of diffusion to the walls from unit volume; and αn^2 is the rate of recombination per unit volume. Assuming $n = 5 \times 10^{12}$ per cu cm at a pressure of 1.4×10^{-3} mm Hg and a current of 1.5 amp, and using the

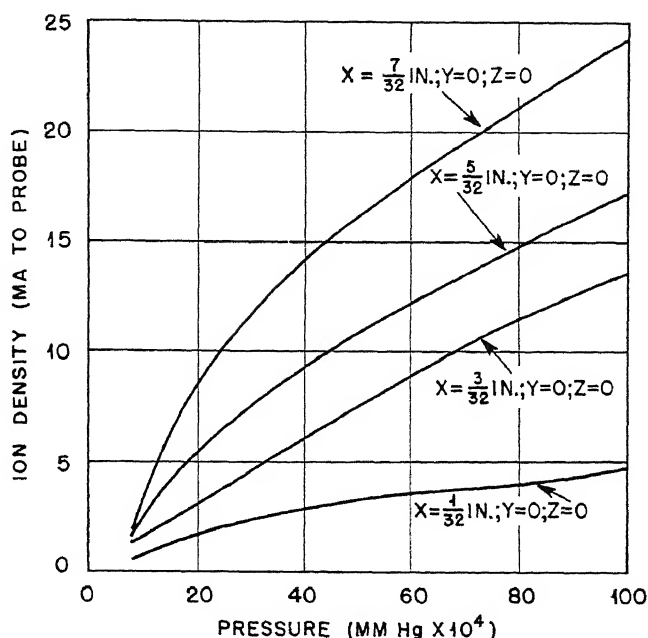


Fig. 9.26—Variation of ion density with pressure for small arc in argon.

variation of n with pressure obtained from Fig. 9.26, it can be calculated that for such a variation with pressure the required value of the recombination coefficient comes out to be 5×10^{-8} cu cm/sec, which seems an impossibly high value for electron-ion recombination.

An alternative explanation of the departure from linearity in the dependence of ion density on pressure is to be found in the possibility that an appreciable proportion of the ionization at the lower pressures is produced by plasma electrons. As will be shown in Sec. 4.3, the electron temperature decreases with increase of pressure. Thus ionization by plasma electrons would be expected to become less important as the pressure increases. If this explanation is correct, then at least 20 per cent of the observed ionization in argon at a pressure

of 1.4×10^{-3} mm Hg must arise from collisions involving plasma electrons.

A third possible explanation is that, with the drop in electron temperature attending increased transfer of energy from electrons to gas atoms by excitation and ionization, the probe current corresponding to a given density decreases (see Eq. 1). This decrease is due to

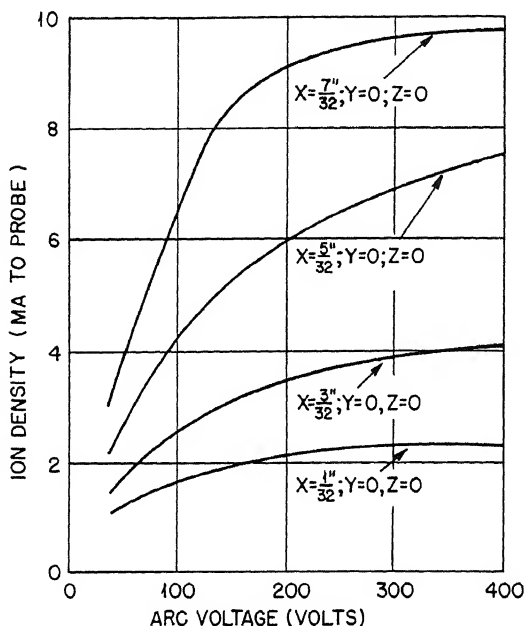


Fig. 9.27—Variation of ion density with arc voltage for small arc in argon.

a corresponding drop in residual fields penetrating into the plasma and pulling in positive ions. Therefore the full increase of ion density might not be properly recorded by the probe described in Sec. 2.1 if used with kT_e taken as 2 ev under all conditions.

(d) Effect of Arc Voltage. Figure 9.27 shows the variation of ion density with arc voltage in the small argon arc for different distances from the column along the central axis. The variation behaves as expected, showing a rapid increase with voltage up to 100 volts, followed by a slower rise extending up to at least 400 volts.

2.7 Investigation of Ion Densities in a Chlorine Arc. The qualitative features of the positive-ion distribution in a chlorine arc are similar to those in the case of argon. The distribution exhibits the

same features of asymmetry about the vertical axis of the arc with the maximum ion density on the antidrain side. The up-and-down variation of ion density is also similar to that in the case of argon, the maximum density occurring at the bottom. In the direction perpendicular to the magnetic field the variation along the central axis appears reasonably exponential in both the large and small arcs at the lower magnetic fields (up to 3,700 gauss), but in the case of high fields (up to 11,400 gauss) the deviation is again of the type observed in argon (see Fig. 9.18). The main feature that distinguishes the case of chlorine from that of argon lies in the existence of considerable densities of negative ions in the former case. These change markedly the form of the probe characteristics. Thus, although for argon the ratio of the saturation negative to saturation positive current varied from 10 to 60 (in the presence of a magnetic field), in the case of the chlorine arc the ratio was generally nearer to 1. This must be attributed to the presence of negative ions in the latter case. In fact, the observed probe characteristics can be used to estimate negative-ion density in the discharge. Thus, suppose that under certain conditions of magnetic field, etc., the ratio of saturation negative to saturation positive currents is given by "a" in the case of a gas such as argon, which does not form negative ions. Then under the same conditions in a gas such as chlorine, in which the electron and negative-ion densities are, respectively, n_e and n_- , the ratio is given by

$$\frac{i_-}{i_+} = \frac{an_e + bn_-}{n_+} = -(a - b) \frac{n_-}{n_+} \quad (13)$$

where the ratio of the mean energy of the negative ions to the mean energy of the positive ions is b^2 . The ratio of n_-/n_+ can then be calculated.

$$\frac{n_-}{n_+} = \frac{a - \frac{i_-}{i_+}}{a - b}$$

and

$$\frac{n_-}{n_e} = \frac{a - \frac{i_-}{i_+}}{\frac{i_-}{i_+} - b} \quad (14)$$

Unfortunately it is difficult to estimate the ratio n_-/n_e from this equation since the quantity b , determining the mean negative-ion

energy, is not known. In some cases ratios of i_-/i_+ as low as 0.14 were obtained. Even if all the negative current was due to negative ions, this would imply a ratio of negative-ion to positive-ion energy not greater than 0.02. If some of the negative current was due to electrons, this ratio would have to be even smaller.

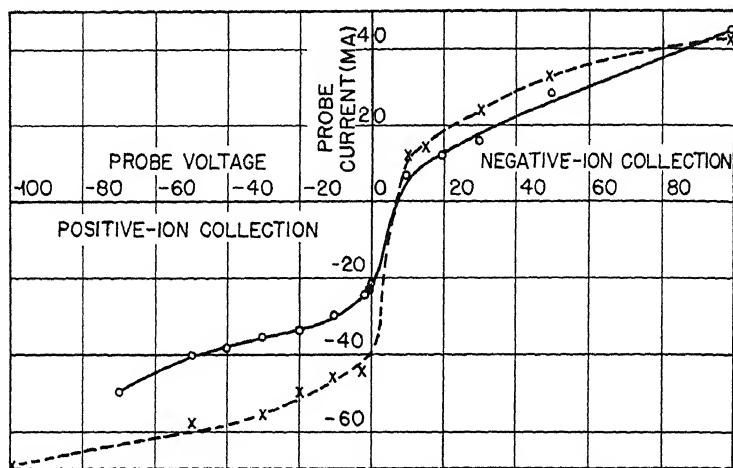


Fig. 9.28 — Typical probe characteristics in chlorine.

Low values of i_-/i_+ could also be caused by the poor saturation conditions exhibited by the negative currents. The so-called “saturation” positive and negative currents were taken as those currents measured at +30 volts above or below the floating potential. Figure 9.28 shows a typical probe characteristic curve obtained with a chlorine arc. It is believed, however, that bad saturation could not account for more than a small part of the anomalously low negative currents, so that the major part of the effect has to be attributed to low negative-ion energy.

Figures 9.29a and b show the distribution of positive and negative saturation currents to the probe, taken over the central transverse section of the arc in a number of cases for small arcs in chlorine. These curves exhibit the same asymmetry as in the case of argon and in the same sense, namely, the ion densities show a maximum on the antidrain side near the arc column. The negative-ion densities also show the asymmetry and in the same sense as the positive-ion distributions. As in the case of argon the asymmetry appears to depend markedly on the condition of the filament, and insufficient data were

obtained to exhibit systematic variation of the asymmetry with pressure, field, arc voltage, and current. In some cases asymmetry ratios (defined as the ratio of ion densities at the extreme ends of the column) as high as 16 were obtained for positive ions and 12 for negative ions. Generally, however, these ratios were closer to 2 or 3.

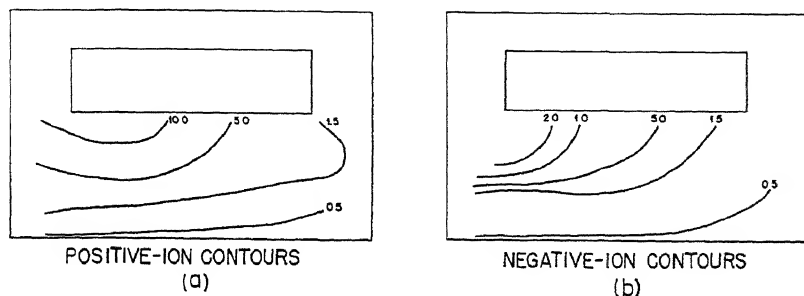


Fig. 9.29—Tests of small arc in chlorine. (a) Positive-ion contours; (b) negative-ion contours. Pressure 0.7×10^{-3} mm Hg; magnetic field 10,000 gauss; arc voltage 150 volts; arc current 1.5 amp.

Table 9.2 shows the variation of the asymmetry ratio for the chlorine arc under different conditions.

The case marked with an asterisk in Table 9.2 is the only one in all our measurements, in either argon or chlorine, in which the ion density was greatest on the drain side. The accuracy of these data was probably not high, however. It is clear there are no consistent trends of asymmetry with arc conditions. This may be due to the unknown factor of the effect of filament condition.

(a) Variation of Positive-ion Density with Arc Conditions. In the case of the chlorine arc the measurements were too few to yield much exact information on the variation of positive- and negative-ion densities with arc conditions, but a qualitative picture can be obtained from Table 9.3, which shows the positive and negative saturation currents at different positions along the central axis in the transverse median plane of the large arc.

In Table 9.3 the positive saturation currents give a measure of the positive-ion density. Qualitatively the features of the variation of positive-ion density are similar to those for argon. Thus, increasing the magnetic field from 3,700 to 11,400 gauss increases the positive-ion density near the arc column but decreases it further out.

Increase of arc current and voltage causes an increase in the ion density at all points.

The effect of pressure on the positive-ion density appears anomalous, although the data are very scanty. Thus, both at high and low magnetic fields the positive-ion density increases much less rapidly than linearly in the range of pressures from 1×10^{-3} to 2×10^{-3} mm

Table 9.2—Variation of Asymmetry Ratio

Type of arc	Pressure, mm Hg $\times 10^{-4}$	Magnetic field, gauss	Arc voltage, volts	Arc current, amp	Asymmetry ratio	
					Positive ions	Negative ions
Small	10	11,000	150	1.5	7	7
Small	10	3,700	150	1.5	1	1
Large	20	3,700	150	1.5	1.5	4
Large	20	11,000	150	1.5	2.2	2.2
Large	10	11,000	150	1.5	5.5	12
Large	10	3,700	50	1.5	10	12
Large	10	3,700	150	3.0	16	9
Large	10	3,700	150	0.5	1.3	0.5*
Large	10	3,700	150	1.5	1.5	2.0
Large	10	3,700	150	1.5	1.5	1.0

* The only measurement in both argon and chlorine in which the ion density was greatest on the drain side.

Table 9.3—Saturation Currents

Pressure, mm Hg $\times 10^{-4}$	Magnetic field, gauss	Arc voltage, volts	Arc current, amp	Saturation current, ma							
				$x = \frac{1}{2} \frac{1}{16}$ in.		$x = \frac{1}{2} \frac{1}{16}$ in.		$x = \frac{1}{16}$ in.		$x = \frac{1}{16}$ in.	
				Pos.	Neg.	Pos.	Neg.	Pos.	Neg.	Pos.	Neg.
20	3,700	150	1.5	7.3	6.5	1.6	0.35	0.38	0.12	0.07	0.04
20	11,400	150	1.5	8.2	1.1	1.4	0.35	0.10	0.05	0.04	0.04
10	11,400	150	1.5	5.5	1.3	1.0	1.5	0.08	0.03	0.03	0.02
10	3,700	150	1.5	5.0	35	2.0	1.6	0.37	0.22	0.07	0.06
10	3,700	50	1.5	1.6	4.6	0.7	0.7	0.20	0.22	0.06	0.07
10	3,700	150	3.0	10	85	12	100	1.1	1.2	0.27	0.35
10	3,700	150	0.5	3.5	12.5	1.2	1.0	0.18	0.20	0.05	0.05

Hg. This behavior should be compared with the similar behavior for the small arc in argon and with the variation of block current with pressure in the case of the chlorine arc mentioned in Sec. 3 of this chapter. In that case the positive current to the block decreased with increase in pressure. The explanation of the present change with pressure is probably to be ascribed to the same cause as for argon (Sec. 2.6c). At first sight the recombination hypothesis would seem probable for chlorine if not for argon, but the evidence from the

diffusion theory of Sec. 2.7f suggests that the value of the recombination coefficient for chlorine is too small to give rise to the observed effects. Thus a value of the order 5×10^{-8} cu cm/sec would be required, whereas the analysis of Sec. 2.7f suggests that the true value is only of the order 10^{-10} cu cm/sec.

(b) Variation of Ion Density from Top to Bottom of the Arc. As in the case of argon, the ion density measured by the probe at the bottom of the arc was considerably greater than the density as measured by the probe near the top. The same considerations that were discussed in the case of argon apply also in the case of chlorine. It appears quite likely that most of the effect arises from inhomogeneity of the magnetic field, causing the arc column to pass closer to the bottom probe than to the top probe.

(c) Variation of Positive-ion Density Transversely along the Central Axis of the Arc. As has been mentioned above, the positive-ion density along the central axis is approximately exponential in both the large and small arcs for small magnetic fields (of the order of 4,000 gauss), but at high fields (11,000 gauss) the distributions depart from the exponential and in the same direction as in the case of argon.

Figure 9.30 shows curves for positive-ion density for the large arc in magnetic fields of 3,700 and 11,400 gauss. Figure 9.31 shows similar curves for the small arc.

For the large arc the fall-off of ion density near the arc column becomes more rapid with increasing field strength, as in the case of argon. For the small arc there appeared to be no large tendency of this kind.

Figure 9.32 shows the positive-ion distribution in the case of the large arc in chlorine for three different arc currents: 0.5, 1.5, and 3.0 amp. These curves do not show markedly the tendency revealed in the case of argon for higher arc currents to correspond to a greater rate of fall-off of ion density in the direction away from the column.

Table 9.4 shows how the distance required for the positive-ion density to be reduced to $1/e$ of its value varies with arc conditions in chlorine.

(d) Proportion of Negative-ion and Electron Currents. As shown above, it is impossible to obtain evidence of the variation of the relative negative-ion and electron densities from measurements of the variation of saturation negative and positive currents. The smaller this ratio becomes, the smaller is the proportion of electron current relative to negative-ion current. The point at which this quantity attains the value 1 may be used as a measure of the effectiveness of negative-ion formation under different circumstances.

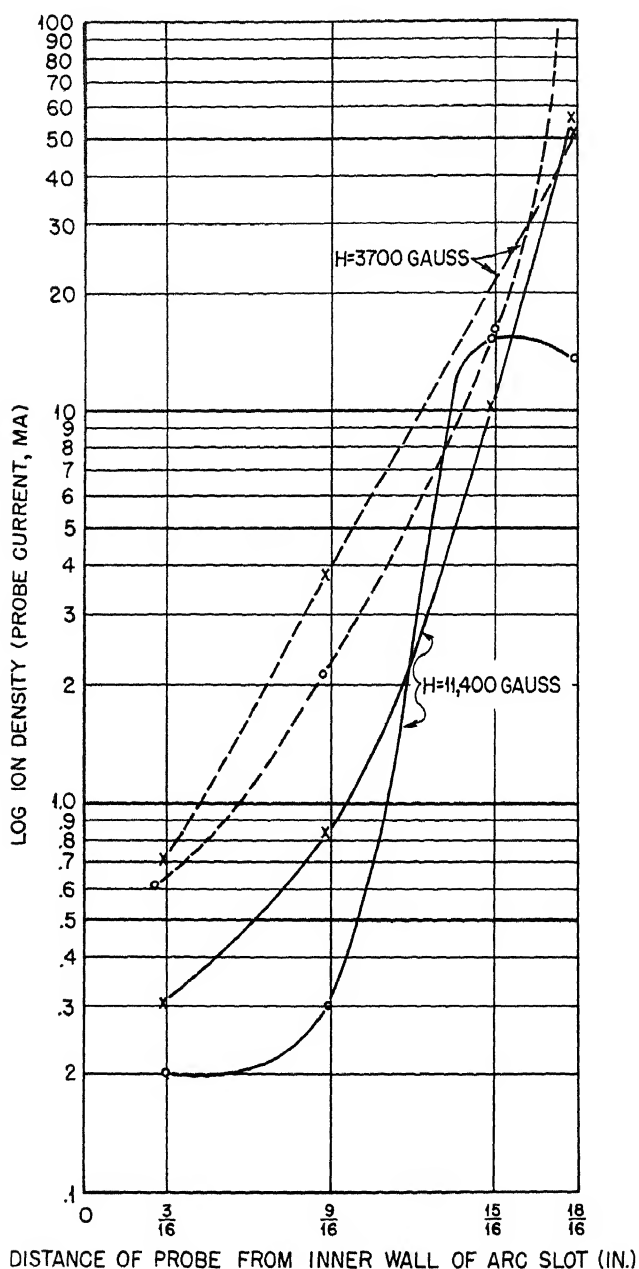


Fig. 9.30—Ion density vs. position of probe for the large arc in chlorine. Pressure 10×10^{-4} mm Hg; arc voltage 150 volts; arc current 1.5 amp. X represents positive ions; circles represent negative ions.

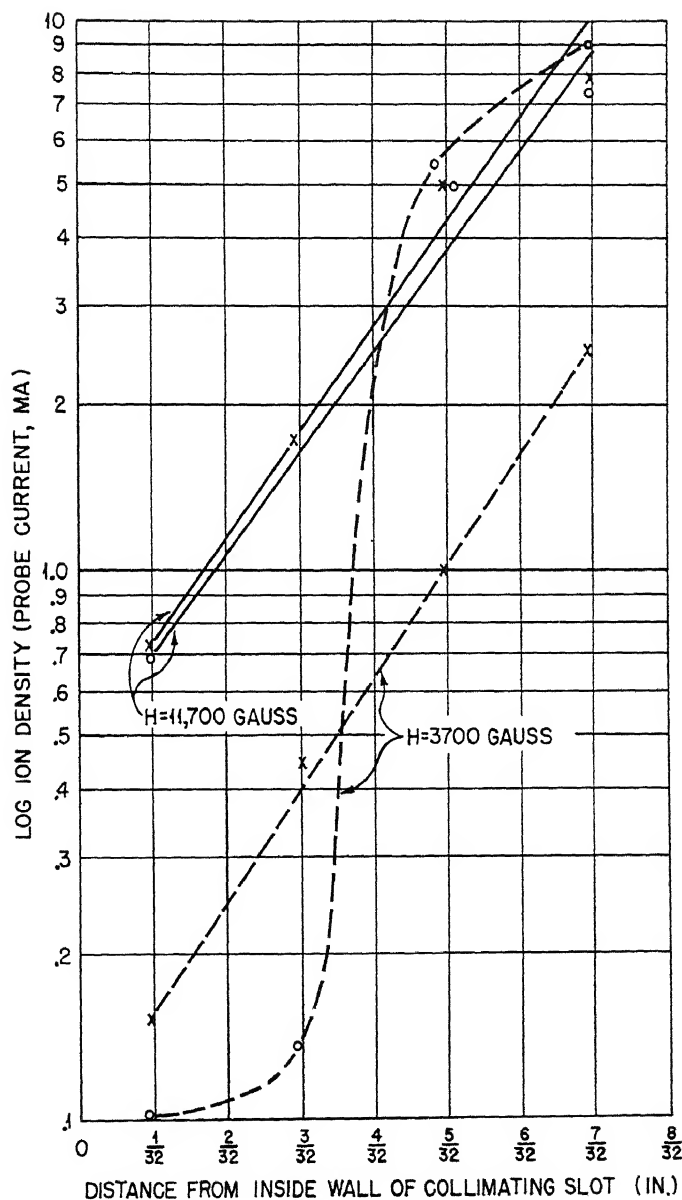


Fig. 9.31—Ion density vs. probe position for small arc in chlorine. Pressure 10×10^{-4} mm Hg; arc voltage 150 volts; arc current 1.5 amp. X represents positive ions; circles represent negative ions.

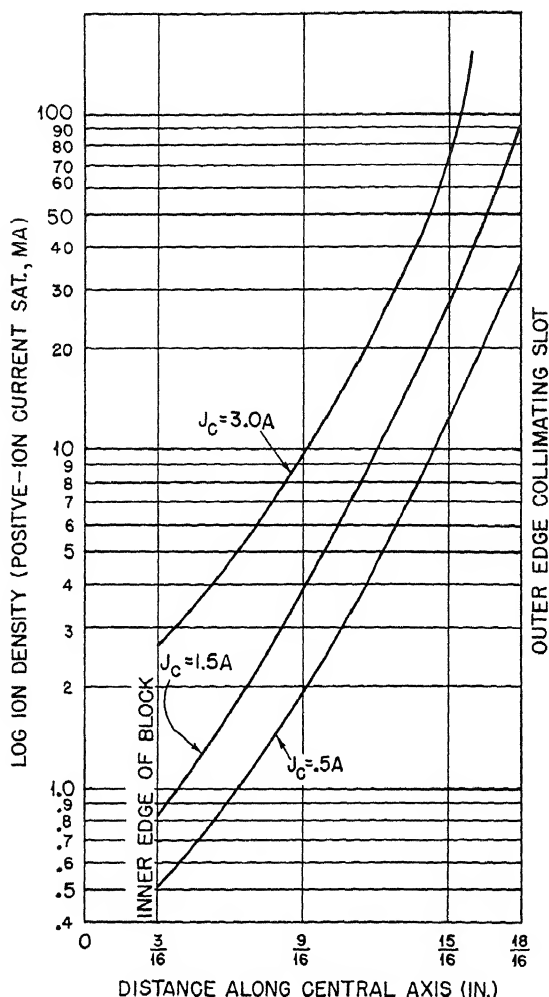


Fig. 9.32—Positive-ion distribution for large arc in chlorine. Pressure 10×10^{-4} mm Hg; magnetic field 3,700 gauss; arc voltage 150 volts.

Table 9.5 gives the distances out from the arc column at which this value of 1 is attained under various arc conditions. The main trends exhibited by this table are as follows:

1. Increase of arc current up to 3 amp increases markedly the distance from the arc column at which electron currents first make an inappreciable contribution to the negative current.
2. Increase of magnetic field up to 11,000 gauss decreases this distance.

3. Increase of pressure from 1×10^{-3} to 2×10^{-3} mm Hg appears to decrease this distance slightly.

(e) Interpretation of Effects Observed with the Chlorine Arc. It is not possible to derive a completely unambiguous picture of the chlorine arc (including negative ions) since insufficient information is available about some of the factors important in the operation of the arc.

Table 9.4

Type of arc	Magnetic field, gauss	Pressure, mm Hg $\times 10^{-4}$	Arc voltage, volts	Arc current, amp	Distance for ionization to be reduced to 1/e of its value, in.	Remarks
Small	3,700	10	150	1.5	5/64	Marked difference between top and bottom
Small	11,400	10	150	1.5	9/128	
Large	3,700	10	150	1.5	7/32	Near center
Large	11,400	10	150	1.5	3/32	
Large	11,400	10	150	1.5	3/8	Near outside of arc
Large	3,700	10	150	0.5	1/4	
Large	3,700	10	150	1.5	1/4	
Large	3,700	10	150	3.0	7/32	

Table 9.5

Pressure, mm Hg $\times 10^{-4}$	Magnetic field, gauss	Arc voltage, volts	Arc current, amp	Distance at which i_-/i_+ first reaches 1, sixteenths of an inch
10	3,700	150	0.5	2.3
10	3,700	150	0.5	2.5
10	3,700	150	3.0	9.3
10	3,700	50	1.5	3.0
10	11,400	150	1.5	1.5
20	3,700	150	1.5	2.0
20	11,400	150	1.5	1.0

Negative ions are formed by attachment of electrons to neutral Cl_2 . In the collision between the electron and the Cl_2 molecule the latter is dissociated into a Cl atom and a Cl^- ion. The attachment energy of Cl^- is 3.7 volts. This energy, together with the initial electron energy, is used up in dissociating the Cl_2 molecule and in supplying the kinetic energy of the dissociated atom and ion. Either arc electrons or plasma electrons may be effective in the attachment, but the optimum energy for attachment is of the order of a few volts; since

there are many times more plasma electrons than arc electrons, it is the plasma electrons that are most effective in the production of negative ions. In the subsequent discussion the production of negative ions by arc electrons is ignored.

Negative ions may be destroyed in a variety of ways. Plasma electrons of energy greater than the attachment energy will be quite effective in detaching an electron from Cl^- . If the electron temperature is of the order of 1 volt, an appreciable fraction of the plasma electrons will have sufficient energy to produce detachment. Similarly, if a negative ion gets into the arc column, it may be destroyed by direct collision with an arc electron. It appears that the plasma electrons will be more effective in producing detachment on account of their greater numbers, but the arc electrons will be relatively more effective than was the case with attachment.

Negative ions may also be destroyed by recombination with positive ions at a rate proportional to $\alpha n_+ n_-$ at any point, where α is the recombination coefficient and n_+ and n_- are the positive-ion and negative-ion densities, respectively, at that point. The distribution of positive-ion and negative-ion densities is also determined by the drift currents arising from concentration and potential gradients in plasma and also by losses to the end of the arc. These drift currents will be such as to carry positive ions away from the arc column toward the walls, but the plasma fields are probably such as to cause negative ions to move in toward the arc column.

The possibility of loss of energy of plasma electrons in detaching an electron from a negative ion will probably cause the electron temperature in the chlorine arc to be less than that in the argon arc. At the same time the plasma fields, which are determined by the electron temperature, would be expected, correspondingly, to be less than in the case of the argon arc.

The following picture of the behavior of negative ions in a chlorine arc is thus obtained: The negative ions are formed mostly outside the arc column by the plasma electrons and when formed tend to drift toward the column. They are either destroyed on their way by collision with plasma electrons, are lost through recombination with chlorine positive ions, or are destroyed by fast arc electrons in the column. Some will move to the top and bottom of the arc, where they will be collected.

As for the plasma electrons, which are formed in the column and diffuse outward, their distribution is determined by all the factors operating in the absence of an electronegative gas, and in addition by the process of attachment. Thus the electrons may now be disposed of either by collection at the top and bottom electrodes or by attach-

ment, and the characteristics of the electron density will be determined by competition between the two modes of disposal. In general, it appears that attachment is rapid enough to remove practically all the electrons within a very short distance from the arc column, usually of the order of $\frac{1}{8}$ in. (see Table 9.3), but varying with conditions of pressure, arc current, and magnetic field. This is inferred from the fact that the ratio of electron to ion current collected by a probe drops from a value of the order of 10 (comparable with that of argon) near the arc column to 1 or less within $\frac{1}{8}$ in. of the column. Since the mean distance for electron density to drop to $1/e$ of its value in the absence of an electronegative gas is of the order of $\frac{3}{16}$ in., it may be concluded that most electrons formed in the column will attach before they are collected at the top and bottom electrodes. This is discussed in greater detail later.

Consider now the over-all balance of these processes occurring in the arc. For simplicity consider the arc column.

Let n_+ , n_- , and n_e be, respectively, the mean positive-ion, negative-ion, and electron densities in the column; let p be the pressure, J_c the arc current, and $f(J_c)$ the number of ions produced in the column by the arc current. Assume that n_+ , n_- , and n_e are uniform throughout the region considered. Then

$$\frac{dn_+}{dt} = \underbrace{k_1 p f(J_c)}_{\text{Rate of production of positive ions}} - \underbrace{k_2 \alpha n_+ n_-}_{\text{Rate of loss of positive ions by recombination}} - \underbrace{k_3 n_+}_{\text{Rate of loss of positive ions by diffusion, etc.}} \quad (15)$$

$$\frac{dn_-}{dt} = \underbrace{k'_1 \sigma p n_e}_{\text{Rate of production of negative ions by attachment of plasma electrons}} - \underbrace{k_2 \alpha n_+ n_-}_{\text{Rate of loss of negative ions by recombination}} - \underbrace{k'_3 n_-}_{\text{Rate of loss of negative ions by diffusion, etc.}} - \underbrace{k'_4 n_- J_c}_{\text{Rate of destruction of negative ions by arc electrons}} - \underbrace{k'_5 n_- n_e}_{\text{Rate of destruction of negative ions by plasma electrons}} \quad (16)$$

Neglecting α and writing

$$n_e = n_+ - n_- \quad (17)$$

then in the steady case when

$$\frac{dn_+}{dt} = \frac{dn_-}{dt} = 0 \quad (18)$$

the mean positive-ion density becomes

$$n_+ = \frac{k_1 \text{pf}(J_c)}{k_3} \quad (19)$$

and Eqs. 15 and 16 yield for n_- the relation

$$k'_5 n_-^2 - n_- (k'_3 + k'_4 J_c + k'_1 \sigma p + k'_5 n_+) + k'_1 \sigma p n_+ = 0 \quad (20)$$

There are two possible limiting cases to be considered:

1. The destruction of negative ions due mainly to plasma electrons so that k'_4 is small.

2. The destruction of negative ions due mainly to arc electrons so that k'_5 is small.

In both cases it is assumed that the loss of negative ions by diffusion from the column is small, and therefore k'_3 may be considered equal to zero.

Consider case 1. If $k'_4 = 0$, then

$$n_- = \frac{k'_1 \sigma p}{k'_5} \quad (21)$$

or $n_- = n_+$. The second solution is trivial, and consequently the solution required for small k'_4 is that which reduces to Eq. 21 when $k'_4 = 0$. This solution is

$$n_- = \frac{k'_1 \sigma p}{k'_5} \left(1 + \frac{k'_4 J_c}{k'_1 \sigma p - k'_5 n_+} \right) \quad (22)$$

or

$$\frac{n_-}{n_+} = \frac{k'_1 \sigma k_3}{k'_1 f(J_c)} \left(1 + \frac{k'_4 J_c}{k'_1 \sigma p - k'_5 n_+} \right) \quad (23)$$

Consider now case 2. If $k'_5 = 0$, then

$$\frac{n_-}{n_+} = \frac{k'_1 \sigma p}{k'_1 \sigma p + k'_4 J_c} \quad (24)$$

The solution of case 2 required for small k'_5 is then

$$\frac{n_-}{n_+} = \frac{k'_1 \sigma p}{k'_1 \sigma p + k'_4 J_c + \frac{k'_4 J_c \times k'_5 n_+}{k'_4 J_c + k'_1 \sigma p}} \quad (25)$$

which reduces to Eq. 24 when $k'_5 = 0$

(1) Effect of Pressure on n_-/n_+ . In case 1 Eq. 23 shows that, as the pressure increases, n_-/n_+ also increases, since

$$k'_1 \sigma p < k'_5 n_+ \quad (26)$$

The relationship in expression 26 follows from the fact that $n_- \leq n_+$. Thus the second term of Eq. 23 is negative, and consequently n_-/n_+ rises slowly with increase of pressure.

In case 2 the same conclusion is reached, since from Eq. 25 n_-/n_+ will increase with increase of pressure. The effect should be greater in this case, however, since $k'_4 J_c$ is of the same order of magnitude as $k'_1 \sigma$.

(2) Effect of Arc Current on n_-/n_+ . In case 1, n_-/n_+ clearly decreases as the current increases, owing to the occurrence of $f(J_c)$ in the denominator of Eq. 23. Similarly in case 2, n_-/n_+ decreases as the arc current increases, owing to the appearance of $k'_4 J_c$ in the denominator of Eq. 25. Thus in both cases n_-/n_+ (and therefore n_-/n_e) increases with increase of pressure and decreases with increase of arc current.

These results are in agreement with the observation on the large arc in chlorine. Thus Eq. 13 indicates that i_-/i_+ decreases as n_-/n_+ increases. A decrease of i_-/i_+ would be predicted with an increase of pressure, and an increase of i_-/i_+ would be predicted with increase of arc current at points near the column.

Table 9.3 shows that this dependence on pressure and arc current does, in fact, occur. Thus at the position $x = 1\frac{1}{16}$ in., the nearest point to the column for which measurements were taken in the case of the large arc, i_-/i_+ decreases from 7.0 at a pressure of 1×10^{-3} mm Hg to 0.9 at a pressure of 2×10^{-3} mm Hg for a field of 3,700 gauss; and for a field of 11,400 gauss it decreases from 0.24 at 1×10^{-3} mm Hg to 0.14 at 2×10^{-3} mm Hg.

With increase of arc current at the position $x = 1\frac{1}{16}$ in., Table 9.3 indicates that the ratio i_-/i_+ shows a marked increase. Thus, at a magnetic field 3,700 gauss and a pressure of 1×10^{-3} mm Hg this

ratio is 3.5 for a current of 0.5 amp, 7.0 for a current of 1.5 amp, and 8.5 for a current of 3.0 amp. This means that n_-/n_+ (and thus n_-/n_e) decreases as the arc current increases, as was predicted above.

(f) Diffusion Theory with Negative Ions Present. In principle it should be possible to treat the motion of charged particles in a chlorine arc including negative ions in a similar way as in the simpler case of argon without negative ions, which led to Eqs. 6 and 7. When the effects of negative ions are included, however, the equations become difficult to handle.

As before, consider an elementary layer of the plasma parallel to the arc column, of unit width, of length equal to the arc length l , and of thickness dx . Then this elementary portion of plasma gains and loses positive ions in the following ways:

1. It gains $-\frac{dj_+}{dx} l \delta x$ owing to the drift current across the boundaries at x and at $x + \delta x$.

2. It loses $\beta_+ n_+ \delta x$ owing to loss of positive ions to the ends.

3. It loses $\alpha n_+ n_- l \delta x$ owing to recombination with negative ions.

At the same time this elementary portion gains and loses negative ions in the following ways:

1. It gains $-\frac{dj_-}{dx} l \delta x$ owing to the drift current across the boundaries at x and at $x + \delta x$.

2. It loses $\beta_- n_- \delta x$ owing to loss of negative ions to the ends.

3. It loses $\alpha n_+ n_- l \delta x$ owing to recombination with positive ions.

4. It gains $\sigma' n n_e l \delta x$ owing to attachment of plasma electrons to neutral particles (density n per cubic centimeter).

5. It loses $\epsilon n_- n_e l \delta x$ owing to detachment by plasma electrons.

In the arc column there would be additional terms due to detachment by arc electrons.

The drift currents j_+ , j_- , and j_e will be given by the relations

$$j_+ = -D_+ \frac{dn_+}{kT_+} - \frac{D_+ e}{kT_+} n_+ \frac{dV}{dx} \quad (27)$$

$$j_e = -D_e \frac{dn_e}{dx} + \frac{D_e e}{kT_e} n_e \frac{dV}{dx} \quad (28)$$

$$j_- = -D_- \frac{dn_-}{dx} + \frac{D_- e}{kT_-} n_- \frac{dV}{dx} \quad (29)$$

so that the quantities n_+ , n_- , n_e , and V are connected by the following relations:

$$D_+ \frac{d^2 n_+}{dx^2} + \frac{D_+ e}{kT_+} \frac{d}{dx} \left(n_+ \frac{dV}{dx} \right) = \frac{\beta_+ n_+}{l} + \alpha n_+ n_- \quad (30)$$

$$D_- \frac{d^2 n_-}{dx^2} - \frac{D_- e}{kT_-} \frac{d}{dx} \left(n_- \frac{dV}{dx} \right) = \frac{\beta_- n_-}{l} + \alpha n_+ n_- + \epsilon n_e n_- - \sigma' n_e n \quad (31)$$

$$D_e \frac{d^2 n_e}{dx^2} - \frac{D_e e}{kT_e} \frac{d}{dx} \left(n_e \frac{dV}{dx} \right) = \frac{\gamma n_e}{l} + \sigma n_e n - \epsilon n_e n \quad (32)$$

In addition, in the plasma $n_+ = n_e + n_-$. These equations are not suited for general solution owing to their complexity and nonlinearity. However, it is possible to work with them if the following assumptions are made:

1. The major part of the electronic motion across the field arises from the diffusion term $D_e \frac{d^2 n_e}{dx^2}$.

2. The major part of the ionic motion across the field arises from the mobility terms $\frac{D_+ e}{kT_+} \frac{d}{dx} \left(n_+ \frac{dV}{dx} \right)$ and $\frac{D_- e}{kT_-} \frac{d}{dx} \left(n_- \frac{dV}{dx} \right)$.

3. The destruction of negative ions by plasma electrons is unimportant so ϵ may be neglected.

4. The electron density is small compared with the ion density so n_+ may be written n_- .

Under these circumstances V can be eliminated from the equations, and the following equations are obtained:

$$D_e \frac{d^2 n_e}{dx^2} = \frac{\gamma n_e}{l} + \sigma' n_e n \quad (33)$$

$$\frac{T_+}{D_+} \left(\frac{\beta_+ n_+}{l} + \alpha n_+^2 \right) + \frac{T_-}{D_-} \left(\frac{\beta_- n_+}{l} + \alpha n_+^2 \right) = \frac{T_-}{D_-} \sigma' n n_e \quad (34)$$

$$n_+ = n_- \quad (35)$$

Equation 33 gives

$$n_e = n_{e0} e^{-\eta x} \quad (36)$$

where

$$\eta = \sqrt{\left(\frac{\gamma}{l} + \sigma' n\right) \frac{1}{D_e}} \quad (37)$$

Equation 34 could be solved for n_+ . If, however, l is sufficiently long, it is probably legitimate to neglect β_+/l , β_-/l and write also $D_+ = D_-$. Then

$$n_+ = n_- = \sqrt{\left(\frac{\sigma' n n_e}{\alpha}\right) \left(\frac{T_-}{T_+ + T_-}\right)} \quad (38)$$

$$n_+ = n_- = \sqrt{\left(\frac{\sigma' n n_{e0}}{\alpha}\right) \left(\frac{T_-}{T_+ + T_-}\right) e^{-\eta x/2}} \quad (39)$$

The following deductions can be made from Eqs. 37, 38, and 39.

1. The fall-off in positive- and negative-ion density should be exponential. An exponential fall-off was found approximately experimentally, although, as has been pointed out above, this was somewhat masked by the asymmetry of the ion distribution. This theory is based on the assumption of symmetry of the distribution.

2. The rate of fall-off of the electron density with distance from the arc column should be much greater than the rate for the positive and negative ions. The distance in which the electron density falls to $1/e$ of its value, x_{ne} should be about half the corresponding distance for the positive and negative ions, x_{n+} . The greater rapidity with which the electron density falls off, as compared with the ion density, has been remarked above. Thus Table 9.3 shows how the ratio between the negative saturation current and the positive saturation current decreases as one moves away from the arc column.

3. From Eq. 39 it is seen that

$$\frac{n_{+0}}{n_{e0}} = \sqrt{\left(\frac{\sigma' n}{\alpha n_{e0}}\right) \left(\frac{T_-}{T_+ + T_-}\right)}$$

At a pressure of 10^{-3} mm Hg we have

$$n \approx 3 \times 10^{13} / \text{cu cm}$$

$\sigma' = \frac{1}{4} v \sigma$ where σ is the cross section for attachment of electron of velocity v cm/sec to Cl_2 . For 1-volt electrons, $v = 5 \times 10^7$ cm/sec and $\sigma = 2 \times 10^{-18}$ sq cm; therefore σ' is 2.5×10^{-11} .

If we write $T_+ \approx T_-$, the factor $T_-/(T_+ + T_-) \approx 1/2$. Suppose the value $n_{e0} = 10^{12}/\text{cu cm}$. For α no values are available, but if it were assumed too large it would lead to a low value of n_{+0}/n_{e0} in conflict with the observations. We shall take for the value $10^{-10} \text{ cu cm/sec}$. Then $n_{+0}/n_{e0} \approx 2$. This value appears fairly reasonable and consequently it provides some evidence for a value of α of the order of magnitude assumed, namely, $10^{-10} \text{ cu cm/sec}$.

4. The ratio

$$\frac{n_{+0}}{n_{e0}} = \sqrt{\left(\frac{\sigma' n}{n_{e0}}\right) \left(\frac{T_-}{T_+ + T_-}\right)}$$

(a) decreases with increase of arc current, since n_{e0} will increase with current (as seen from Table 9.3, this is just what is observed); (b) decreases with increase of arc voltage, since n will increase with voltage (again in agreement with the observations recorded in Table 9.3); (c) increases with increase of pressure, since n is proportional to pressure (also borne out by Table 9.3, where increase of pressure is seen to produce a marked decrease in this ratio).

With this solution it is of interest to investigate the form of the function V . If Eqs. 37, 38, and 40 are substituted in expression 30 and β_+/l is neglected,

$$\frac{d}{dx} \left(n_{e0} e^{-\eta x} \frac{dV}{dx} \right) = \frac{1}{2} \sigma' n n_{e0} e^{-\eta x} \times \frac{kT_+}{D_+ e}$$

provided $T_+ \approx T_-$, and therefore

$$\frac{dV}{dx} = -\frac{kT_+}{D_+ e} \frac{\sigma' n}{2\eta} + C e^{\eta x} \quad (40)$$

$$V = -\frac{kT_+}{D_+ e} \frac{\sigma' n x}{2\eta} + \frac{C}{\eta} e^{\eta x} \quad (41)$$

One would like to make $dV/dx = 0$ when $x = 0$, but if this were done d^2V/dx^2 would be positive and V would increase with increase of x . In order to find a solution that will fit smoothly on the solution at the sheath it is necessary to choose a negative value of C so that d^2V/dx^2 will be negative. Suppose the sheath begins at $x = b$, and choose C such that

$$V(b) - V(0) = -\frac{kT_e}{2e}$$

that is,

$$\frac{C}{\eta} (e^{\eta b} - 1) = -\frac{kT_e}{2e} + \frac{kT_+}{2e} \frac{\sigma' n}{D_+ \eta} b$$

$$\therefore C = -\frac{k}{2e(e^{\eta b} - 1)} \left(\eta T_e - \frac{T_+ \sigma' nb}{D_+} \right) \quad (42)$$

and consequently Eq. 40 becomes

$$\frac{dV}{dx} = -\frac{kT_+}{D_+ e} \frac{\sigma' n}{2\eta} - \frac{ke^{\eta x}}{2e(e^{\eta b} - 1)} \left(\eta T_e - \frac{\sigma' nb}{D_+} T_+ \right) \quad (43)$$

and Eq. 41 becomes

$$V = -\frac{kT_+}{D_+ e} \frac{\sigma' nx}{2\eta} - \frac{ke^{\eta x}}{2\eta e(e^{\eta b} - 1)} \left(\eta T_e - \frac{\sigma' nb}{D_+} T_+ \right) \quad (44)$$

Such a solution cannot, of course, lead to $dV/dx = 0$ at $x = 0$ as one would expect physically, but this arises from the fact that the original equations (30, 31, and 32) are valid only outside the arc column. No account is taken in them of production occurring inside the column.

With the value of dV/dx given by Eq. 43, the magnitude of the term

$\frac{D_e e}{kT_e} \frac{d}{dx} \left(n_e \frac{dV}{dx} \right)$ in Eq. 32 may now be calculated. We have

$$\frac{D_e e}{kT_e} \frac{d}{dx} \left(n_e \frac{dV}{dx} \right) = \frac{D_e T_+}{T_e D_+} \frac{\sigma' n n_{e0}}{2} e^{-\eta x}$$

and

$$D_e \frac{d^2 n_e}{dx^2} = D_e \eta^2 n_{e0} e^{-\eta x}$$

so that the ratio

$$\frac{\frac{D_e e}{kT_e} \frac{d}{dx} \left(n_e \frac{dV}{dx} \right)}{D_e \frac{d^2 n_e}{dx^2}} = \frac{T_+ \sigma' n}{2 T_e D_+ \eta^2} = \frac{D_e T_+}{D_+ T_e} \frac{1}{2 \left(1 + \frac{\gamma}{l \sigma' n} \right)}$$

But $D_e \ll D_+$ and $T_+ < T_e$. The ratio $\gamma/(\lambda\sigma'n)$ measures the relative importance of drain to the ends of the arc and electron attachment in removing electrons from the plasma. It is clear then that the assumption made above neglecting

$$\frac{D_e e}{kT_e} \frac{d}{dx} \left(n_e \frac{dV}{dx} \right)$$

in comparison with $D_e d^2 n_e / dx^2$ is consistent with the solution obtained. Increase of magnetic field decreases D_e/D_+ and increases $\gamma/(\lambda\sigma'n)$, consequently the validity of the assumption is greater at high magnetic fields. On the other hand $\gamma/(\lambda\sigma'n)$ decreases with increase of pressure, so that the approximation is less valid at high pressures.

3. DISTRIBUTION OF CURRENTS IN THE ARC PLASMA

In this apparatus the magnitude and nature of the current flow in different parts of the arc plasma could be determined. Thus, since the anode, block, and slot were insulated from each other, the flow of current to each of these could be measured separately. Furthermore, the twelve wires placed at the top and bottom of the arc at different distances from the column made it possible to distribute the current at different distances from the column to be determined (see Figs. 9.3 and 9.4). By applying potentials to the wires or block it was possible to measure the saturation positive-ion current to these electrodes and thus to sort out the nature of current flow to these parts.

3.1 The Currents to Anode, Collimating Slot, and Block. Let J_c be the total arc current as measured by the arc-current meter and i_A , i_S , i_B be the currents recorded by the anode, collimating-slot plate, and block, respectively. Then we must have

$$J_c = i_A + i_S + i_B \quad (45)$$

Further, if we distinguish that portion of i_A and i_S arising from the primary electron beam from that portion arising from secondary ionization by writing i'_A , i'_S for the latter, then

$$i'_A + i'_S + i'_B + j'_S = 0 \quad (46)$$

where j'_S is the secondary current passing through the collimating slot that does reach the slot plate. Unfortunately it was not possible to measure i'_A and i'_S directly, but some evidence of their magnitude

was obtained in some cases by integrating the current to the wires at the top and bottom of the arc.

(a) Variation of i_A , i_S , and i_B with Magnetic Field. Figure 9.33 shows variation of the block current with magnetic field for a number of different arc currents in the case of an argon arc run in the

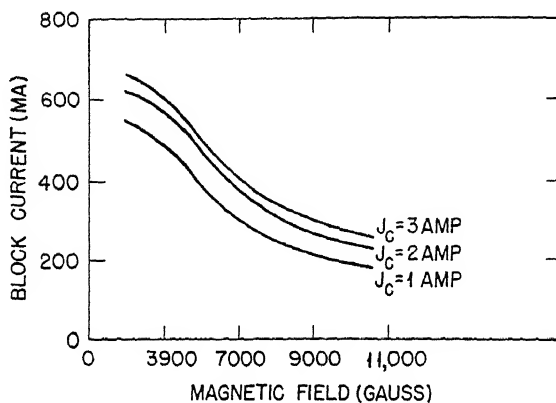


Fig. 9.33—Block current vs. magnetic-field strength for small arc in argon. Pressure 3.5×10^{-3} mm Hg; arc voltage 150 volts.

small chamber. The current collected by the wall is in all cases a positive current, and, as would be expected, its magnitude decreases markedly as the field is increased from 2,000 to 11,000 gauss; this corresponds to the fact that more of the ions are lost to the ends before reaching the walls as the magnetic field increases. The current to the wall is predominantly positive because of the greater ease with which the positive ions move across the field in comparison with the electrons.

As the block current decreases, the (negative) currents to collimating slot and anode also decrease. This type of effect is shown in Fig. 9.34. In this figure and unless otherwise specified in subsequent figures the currents are expressed as ratios of the arc current.

For the large arc block the behavior with increasing magnetic field is shown in Fig. 9.35. For low magnetic fields the block current fell rapidly with increase of magnetic field. With the higher magnetic fields (above about 4,000 gauss), the block current decreased to a very small value. This probably corresponds to the fact that above this field practically all the ionization has been drained to the top and bottom before reaching the wall. The lateral dimensions of the large arc block were just four times those of the small arc chamber. Thus

one might expect the block current in the case of the large block to be comparable with that observed for the small block with a magnetic field about four times as great. Figures 9.34 and 9.35 show that this comparison does not work out very well. Thus the block current at a field of 11,000 gauss for the small arc is much greater than that at

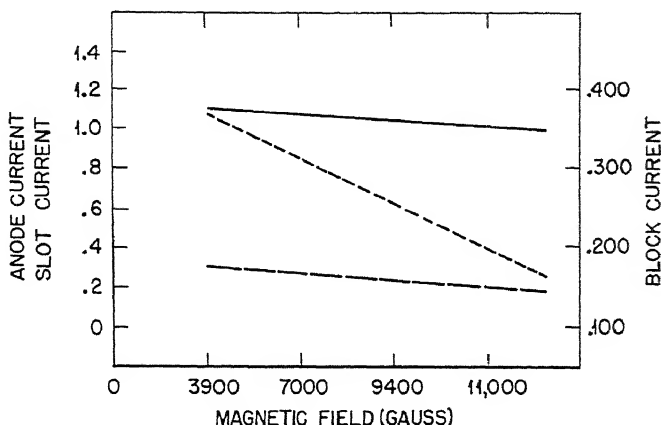


Fig. 9.34—Slot, anode, and block currents vs. magnetic-field strength for small arc in argon. Pressure 1.4×10^{-3} mm Hg; arc voltage 300 volts; arc current 1.5 amp. Unless otherwise specified, the currents are expressed as fractions of the arc current.

2,750 gauss for the large arc. In the case of the large arc in argon for high magnetic fields and large arc curves, it was sometimes observed that the arc ran in a state in which the block current was negative. The conditions under which this occurred are discussed in Sec. 5.1a on hash.

For the large arc operating in chlorine the variation of the currents with magnetic field is shown in Fig. 9.36. Qualitatively the block-current behavior is very similar to that for the large arc in argon. For a field of 4,000 gauss the block currents in the two cases are about the same, but as the field is decreased the block current increases more rapidly in the case of chlorine than in the case of argon. Such differences as there are between the two arcs are no doubt to be ascribed to the presence of chlorine negative ions in the one case. For low magnetic fields the anode current decreases and the collimating-slot current increases in the case of the chlorine arc but this may have arisen from bad filament and collimating-slot alignment.

(b) Variation of i_A , i_S and i_B with Pressure. In the case of each of the three types of arc, data were obtained at three pressures. Typical

results are listed in Table 9.6. By increasing the collision frequency, increase of pressure makes it easier for charged particles to reach the walls. Thus the effect of increase in pressure might be expected

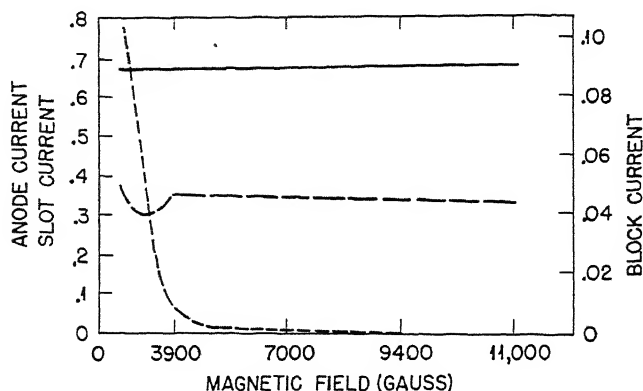


Fig. 9.35—Slot, anode, and block currents vs. magnetic-field strength for large arc in argon. Pressure 1.4×10^{-3} mm Hg; arc voltage 150 volts; arc current 1.5 amp. Unless otherwise specified, the currents are expressed as fractions of the arc current.

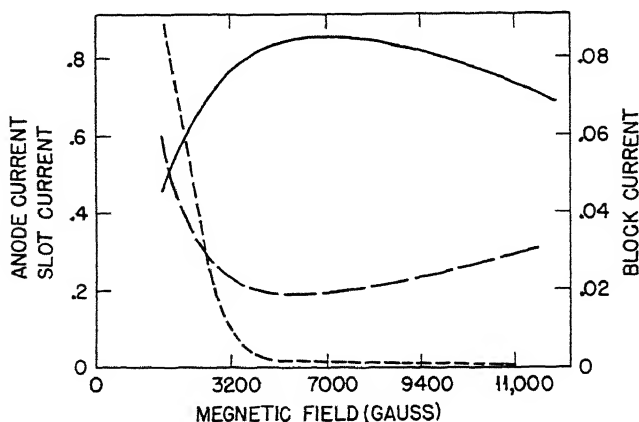


Fig. 9.36—Slot, anode, and block currents vs. magnetic-field strength for large arc in chlorine. Pressure 7×10^{-4} mm Hg; arc voltage 150 volts; arc current 1.5 amp. Unless otherwise specified, the currents are expressed as fractions of the arc current.

to be somewhat similar to the effect of decrease in magnetic field. Consequently i_B might be expected to increase at a rate that is more than proportional to pressure.

In Table 9.6 it is seen that for the small arc in argon this is indeed the case for low arc currents or low arc voltages, i.e., under conditions where the relative degree of ionization is small. However,

Table 9.6

Pressure, mm Hg $\times 10^{-4}$	Magnetic field, gauss	Arc voltage, volts	Arc current, amp	i_A , amp	i_S , amp	i_B , amp
For small arc in argon						
5.6	3,900	150	1.5	1.5	0.30	0.25
14	3,900	150	1.5	1.77	0.35	0.57
5.6	3,900	150	0.5	0.51	0.02	0.04
14	3,900	150	0.5	0.66	0.07	0.20
5.6	3,900	150	3.0	2.76	0.74	0.50
14	3,900	150	3.0	3.0	0.72	0.70
5.6	3,900	50	1.5	1.20	0.39	0.045
14	3,900	50	1.5	1.59	0.22	0.34
5.6	3,900	300	1.5	1.44	0.38	0.39
14	3,900	300	1.5	1.65	0.45	0.55
For large arc in argon						
5.6	3,900	150	1.5	1.00	0.50	0.008
14	3,900	150	1.5	1.00	0.53	0.012
For large arc in chlorine						
8.5	800	150	1.5	0.60	0.98	0.15
27	800	150	1.5	0.75	0.75	0.053
8.5	800	150	0.5	0.30	0.25	0.05
27	800	150	0.5	0.25	0.25	0.028
8.5	3,900	150	0.5	1.14	0.33	0.015
27	3,900	150	0.5	1.02	0.48	0.022
8.5	800	150	3.0	1.50	1.86	0.187
27	800	150	3.0	1.35	1.68	0.108

when the arc current or voltage is higher (3.0 amp, 300 volts) it appears that the increase in block current with pressure is less rapid. In the case of the large arc in chlorine the block current actually decreases with increase of pressure for low magnetic field (for the higher magnetic fields, little current reaches the block from the large arc and consequently, the comparison then has not a great deal of interest). This decrease persists up to high arc currents. These effects are probably related to the corresponding variation of ion density with pressure discussed in Secs. 2.6c and 2.7a and arise from the same cause. For reasons given in Secs. 2.6c and 2.7a this is

probably not volume recombination but the reduction of electron temperature with pressure increase; this would have the effect of (1) reducing the mean velocity of the ions and (2) reducing the contribution to the ionization by plasma electrons.

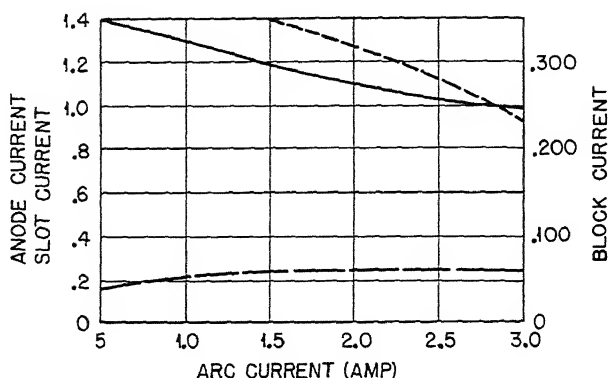


Fig. 9.37—Slot, anode, and block currents vs. arc current for small arc in argon. Pressure 1.4×10^{-3} mm Hg; magnetic field 3,900 gauss; arc voltage 150 volts. Currents are expressed as fractions of the arc current.

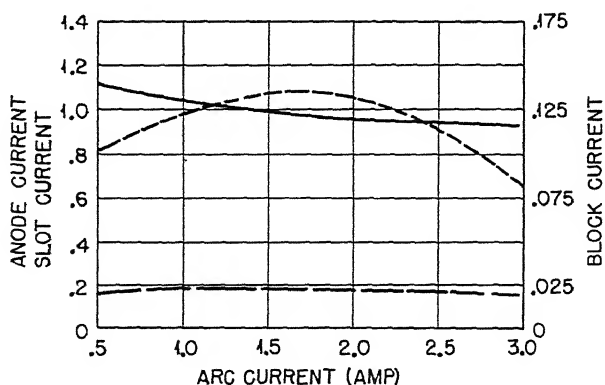


Fig. 9.38—Slot, anode, and block currents vs. arc current for small arc in argon. Pressure 0.6×10^{-3} mm Hg; magnetic field 3,900 gauss; arc voltage 150 volts. Currents are expressed as fractions of the arc current.

It might be expected that the increase in block current when the pressure is increased would cause an increase in slot and anode currents equal to half the increase in the block current. However, it is seen from the results with the small arc in argon that the bulk of the

extra current appears to go to the anode. It is difficult to understand this effect. It may be that secondary electrons ejected from the anode produce more intense ionization at the anode end. Or it may be that

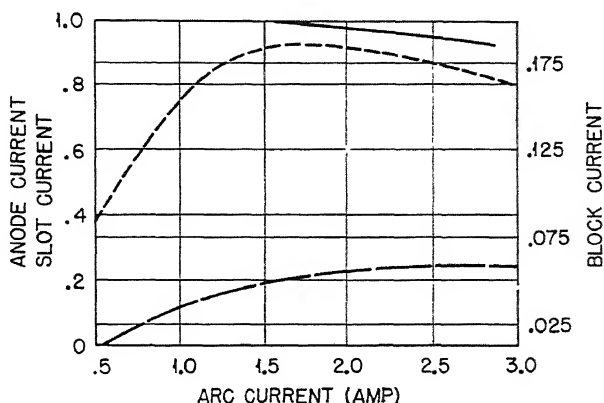


Fig. 9.39—Slot, anode, and block currents vs. arc current for small arc in argon. Pressure 1.4×10^{-3} mm Hg; magnetic field 11,000 gauss; arc voltage 150 volts. Currents are expressed as fractions of the arc current.

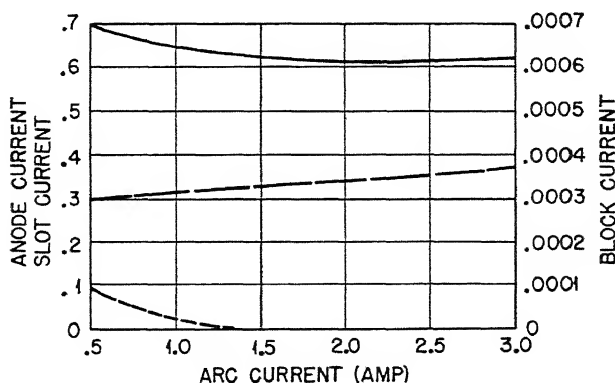


Fig. 9.40—Slot, anode, and block currents vs. arc currents for large arc in argon. Pressure 1.4×10^{-3} mm Hg; magnetic field 11,000 gauss; arc voltage 150 volts. Currents are expressed as fractions of the arc current.

the proportion of fast electrons striking the collimating slot changes with change of pressure.

(c) Variation of i_A , i_S , and i_B with Arc Current. (1) Small Arc in Argon. Figures 9.37, 9.38, and 9.39 show the currents i_A , i_S , and i_B

expressed as ratios of the arc current, plotted as a function of arc current for different conditions of magnetic field and pressure. In each case the block current shows a tendency to saturation at high arc

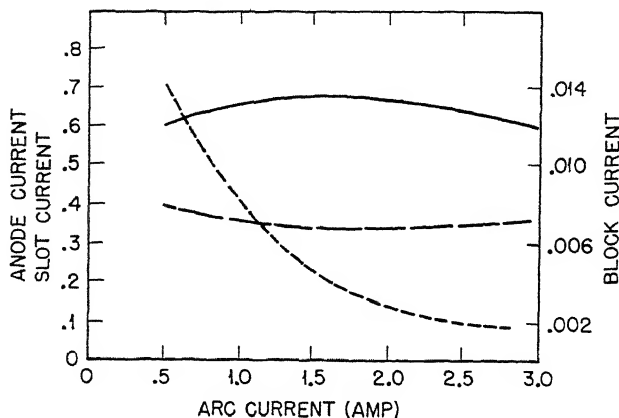


Fig. 9.41—Slot, anode, and block currents vs. arc current for large arc in argon. Pressure 1.4×10^{-3} mm Hg; magnetic field 3,900 gauss; arc voltage 150 volts. Currents are expressed as fractions of the arc current.

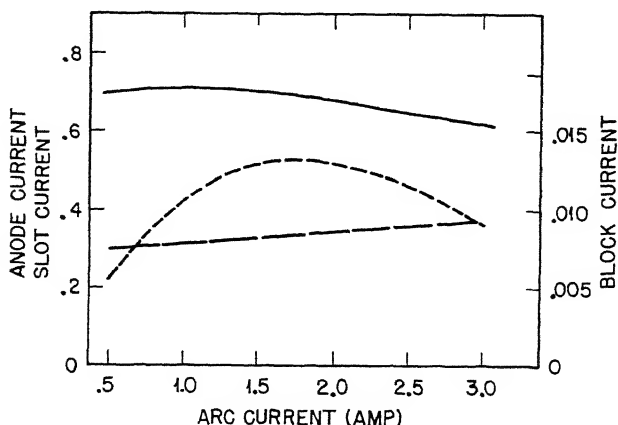


Fig. 9.42—Slot, anode, and block currents vs. arc current for large arc in chlorine. Pressure 25×10^{-4} to 29×10^{-4} mm Hg; magnetic field 4,600 gauss; arc voltage 150 volts. Currents are expressed as fractions of the arc current.

currents when there is a high degree of ionization in the column. In two cases (higher magnetic field and lower pressure) the wall current is seen to increase at a rate faster than linear for low arc cur-

rents. It is difficult to account for this without knowing how the block current is divided between positive-ion and electron currents.

For high arc currents the fraction of current going to the anode

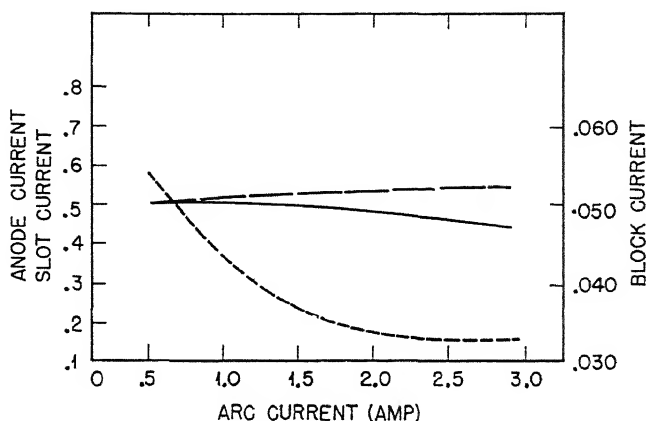


Fig. 9.43—Slot, anode, and block currents vs. arc current for large arc in chlorine. Pressure 25×10^{-4} to 29×10^{-4} mm Hg; magnetic field 1,000 gauss; arc voltage 150 volts. Currents are expressed as fractions of the arc current.

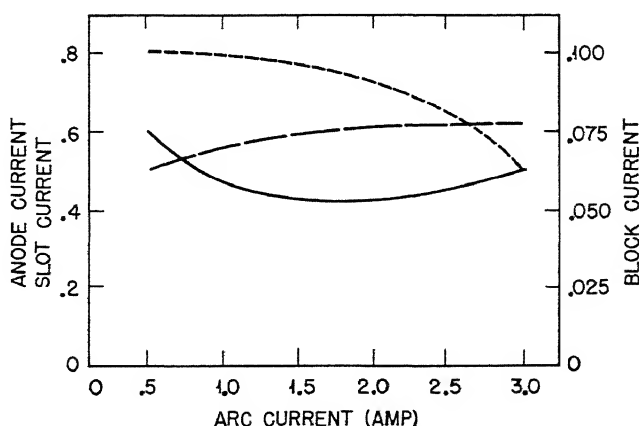


Fig. 9.44—Slot, anode, and block currents vs. arc current for large arc in chlorine. Pressure 7×10^{-3} mm Hg; magnetic field 1,000 gauss; arc voltage 150 volts. Currents are expressed as fractions of the arc current.

tends to drop, and the fraction to the collimating slot tends to rise slightly.

(2) Large Arc in Argon. Figures 9.40 and 9.41 show the ratios of i_A , i_S , and i_B to arc current as a function of arc current for the

case of the large arc in argon. The main feature of these currents is the rapid fall of the block-current to arc-current ratio with increasing arc current. In these cases, however, the block current is so small that it probably does not bear any strong direct relation to the ionization produced in the column. Figure 9.40 illustrates a case in which the block current becomes negative for large magnetic fields as the arc current is increased.

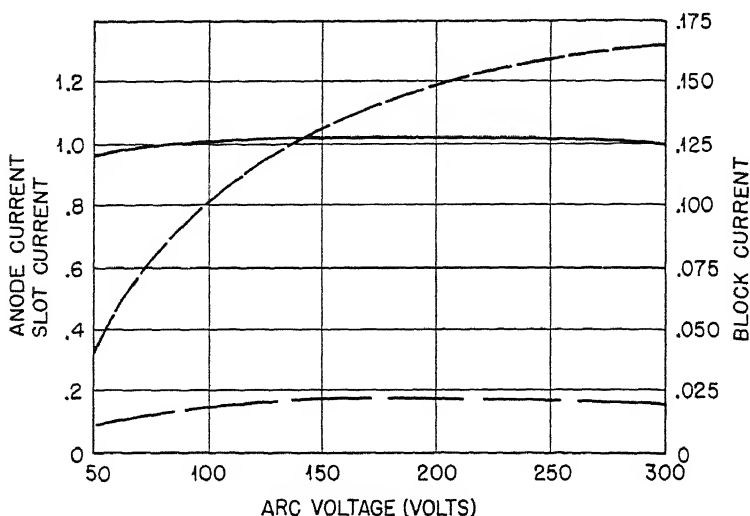


Fig. 9.45—Slot, anode, and block currents vs. arc voltage for small arc in argon. Pressure 1.4×10^{-3} mm Hg; magnetic field 11,000 gauss; arc current 1.5 amp. Currents are expressed as fractions of the arc current.

(3) Large Arc in Chlorine. The variation of the ratios of i_A , i_S , and i_B to arc current as a function of arc current seems complicated in the case of the large arc in chlorine and difficult to interpret. Typical curves are shown in Figs. 9.42, 9.43, and 9.44. The complicated behavior of the block current probably arises from the possibility of electron attachment in the case of chlorine. In general, the fraction of current going to the anode tends to decrease, and the fraction to the collimating slot tends to increase with increase of arc current.

(d) Variation of i_A , i_S , and i_B with Arc Voltage. In all cases the block current increases with arc voltage. Figure 9.45 shows the variation in the case of the small arc in argon.

For the larger arcs both in argon and chlorine there are not sufficient data to give the actual shape of the curve, but it shows a general increase.

3.2 Currents to Wires at the Top of the Arc. Figure 9.46a shows the general shape of curve obtained for currents collected to the wires in the small arc in argon. Most of the distributions are asymmetrical, which is probably to be associated with lack of symmetry of

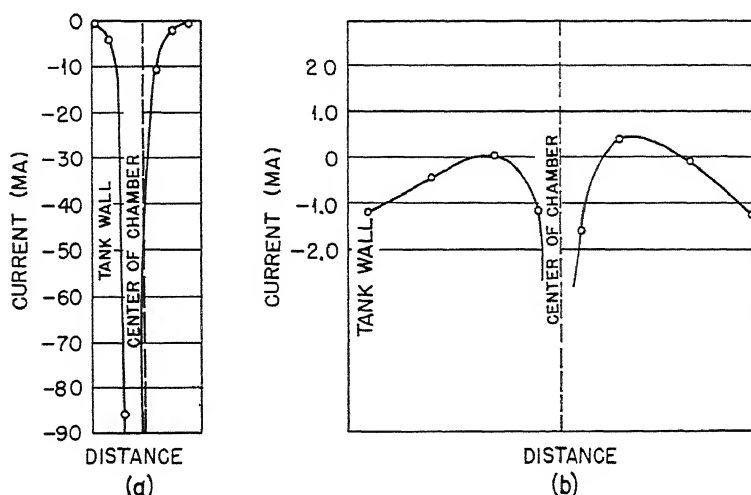


Fig. 9.46—Distribution of current to collimating-slot plate in argon. Pressure 0.6×10^{-3} mm Hg; magnetic field 3,900 gauss; arc voltage 150 volts; arc current 1.5 amp. (a) Small arc. (b) Large arc.

collimating slot relative to the arc chamber. In general, the resultant current was a negative current. As is seen in the section on the ion distribution in the arc, these currents fall off much more rapidly as one moves away from the column than was the case with ion density. Equations 6 and 7 of the previous section, however, yield a solution in which the current to the wires at different distances x from the column would be expected to fall off exponentially as $e^{-\eta x}$ where η is given by Eq. 8. The marked departure of the observed current distribution from that predicted by the simple theory of the previous section, which successfully accounted for many of the features of the ion-density distribution, arises from the inadequate treatment in that theory of the diffusion of ions and electrons to the ends of the arc. The quantities β and γ of Eqs. 6 and 7 have been treated as constants,

but this is valid only so long as the energy distribution of the ions and electrons is independent of x . As a matter of fact it will be shown in Sec. 4 that the electron temperature of the ions tends to decrease with distance from the arc column. On a simple picture of the arc plasma this could be regarded as due to the fact that the fastest moving electrons penetrate the sheath and reach the anode and collimating-slot electrodes close to the arc column, whereas the slower moving electrons are unable to penetrate the sheath, remain in the plasma, and diffuse out toward the walls, thus causing the effective electron temperature to drop in moving away from the column. But the electron collection to the top and bottom of the arc will fall off exponentially with decrease of electron temperature, owing to the field in the sheath repelling electrons back into the plasma. Thus one would expect the electron currents to the top and bottom of the arc to fall off much more rapidly than the electron density in moving away from the arc column, just as is observed in the measurements of the currents to the wires.

Other factors are also present, tending to make the distribution of current to the top and bottom of the arc a steeper function of distance from the column. Thus the positive ions collected for larger values of x will tend to come from nearer the middle of the column than those collected at small values of x , which will tend to come from the ends of the column. Then, since the maximum plasma potential occurs at the middle of the column, the positive ions will tend to be collected with greater energy as one moves away from the column. Hence the positive-ion current will tend to decrease less rapidly than the exponential rate corresponding to Eq. 8.

Furthermore, a study of the diffusion equations in two dimensions might disclose the possibility of the relative rate of diffusion of electrons across and parallel to the field being itself a function of x .

It seems likely, however, that the most important factor in producing the more rapid fall-off of the current to the wires is the decrease of electron temperature with distance from the arc column.

The analysis of the nature of the currents going to the wires reported in Sec. 3.4, which shows a rapid fall-off in the electron current as x increases, lends support to such an interpretation.

Figure 9.46b shows the type of current distribution characteristic for the large arc in argon plotted to the same horizontal scale as the small-arc distribution. It is seen that close to the arc column the wires register a negative current as in the case of the small arc. With increasing distance away from the column, however, the sign of the current changes; at still greater distances out a resultant negative current is again registered. The reason for the latter behavior

is difficult to determine. The effects of variation of arc current and voltage, magnetic field, and pressure on the wire distribution are discussed below.

(a) Small Arc in Argon. (1) Variation with Arc Current. Figure 9.47 shows the effect of varying arc current on the distribution of currents to the wires. The distribution remains similar in form for the different arc currents, but the magnitude of the respective currents increases markedly with increase of arc current.

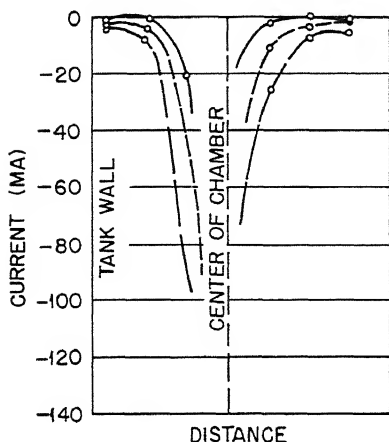


Fig. 9.47

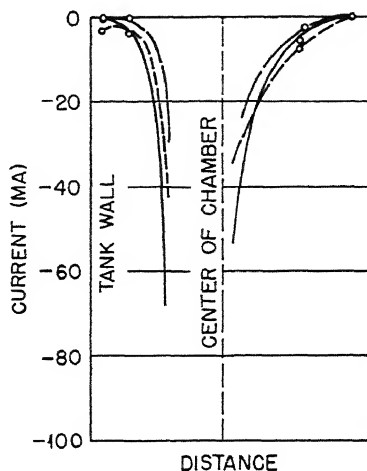


Fig. 9.48

Fig. 9.47—Distribution of current to collimating-slot plate for small arc in argon. Pressure 0.6×10^{-3} mm Hg; magnetic field 3,900 gauss; arc voltage 150 volts; arc current: solid line, 0.5 amp; short dashes, 1.5 amp; long dashes, 3.0 amp.

Fig. 9.48—Distribution of current to collimating-slot plate for small arc in argon. Pressure 0.6×10^{-3} mm Hg; magnetic field 3,900 gauss; arc current 1.5 amp; arc voltage: solid line, 300 volts; long dashes, 150 volts; short dashes, 50 volts.

(2) Variation with Arc Voltage. Figure 9.48 shows the effect of varying arc voltage. The general effect of increase of voltage appears to be to increase the magnitude of the wire currents near the center and to sharpen the distribution of currents. The currents to the outer wires appear to decrease with increase of arc voltage.

(3) Variation with Pressure. Figure 9.49 shows the distribution of currents at two pressures. It is difficult to draw general conclusions from these curves. The currents appear greater in the case of the higher pressure, but the data do not permit any quantitative relationship to be obtained.

(4) Variation with Magnetic Field. Figure 9.50 shows the effect of changing the magnetic field. At the higher field the currents to the wires near the center appear to be increased, but the currents farther out are decreased. This is in line with the general picture of the arc plasma developed above. Increase in magnetic field increases the difficulty of motion of electrons across the field and thus gives rise to larger electron currents to the wires near the arc column.

These curves are difficult to interpret since the composition of the currents to the wires is not known; furthermore it was not possible

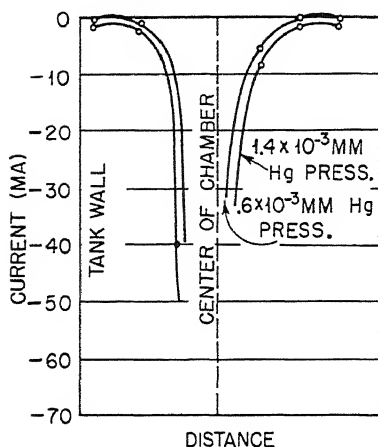


Fig. 9.49

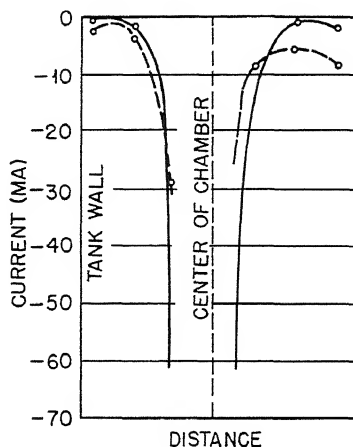


Fig. 9.50

Fig. 9.49—Distribution of current to collimating-slot plate for small arc in argon. Magnetic field 3,900 gauss; arc voltage 150 volts; arc current 1.5 amp.

Fig. 9.50—Distribution of current to collimating-slot plate for small arc in argon. Pressure 1.4×10^{-3} mm Hg; magnetic field: dash line, 3,700 gauss; solid line, 11,000 gauss; arc voltage 150 volts; arc current 1.5 amp.

to place wires actually in the arc column to obtain the current distribution at the center. An attempt was made in the following way to calculate the current that would have been collected by a similar wire placed at the center of the column:

It was assumed that the ionization up and down the arc was uniform, and that consequently the random currents collected by the collimating slot and anode were equal. From Eq. 46 above, each of these currents would then be equal in magnitude to half the block current. But the current density at different distances across the arc chamber can be calculated from the measurements of the currents to the wires,

provided the value to be chosen for the effective collecting area of the wire is known. Then the integrated current density assumed across the chamber should equal the current to the slot or anode. The random current A_0 at the center of the chamber then has to be such that this equality is satisfied. The current that would have been collected by a wire placed at the center of the arc column has been calculated, using a number of assumptions regarding the effective collecting area of the wires, ranging from the area of the diametral

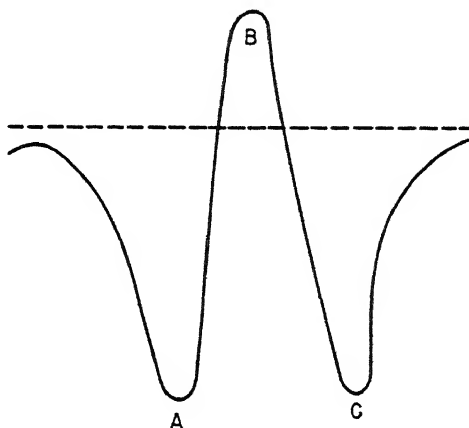


Fig. 9.51—Current distribution for large positive values of A_0 .

plane to an area greater than the total surface area, but the values of A_0 do not show any regular behavior. The apparent values of A_0 are all much smaller than the currents collected by the nearest wires; in fact, these calculations often lead to large positive values of A_0 , which would point to a current distribution of the type shown in Fig. 9.51. However, since no points on the portion of the curve between A, B, and C have ever been observed and since the evidence for curves of this shape is only indirect, it does not seem safe to attach much importance to the estimated values of A_0 .

A possible explanation for the positive currents deduced for the region inside the arc column can, however, be offered. Although the random electron current probably exceeds the random ion current within the column, it must be remembered that electrons cannot be collected in the region covered by the collimating slot, since the filament is 150 volts negative. On the other hand, ions going through the collimating slot are collected by the filament and filament shield. Therefore, even if the random electron and ion currents were equal,

there would be a large excess ion current collected from the region inside the arc column. In fact, as long as the random electron current was less than twice the random ion current, balance conditions of the type used here would show an excessive ion current for the region inside the column. Secondary emission of electrons from the filament, which may be appreciable, would make the effect even larger. Similar remarks apply to the distribution obtained for Cl_2 and argon in the large arc.

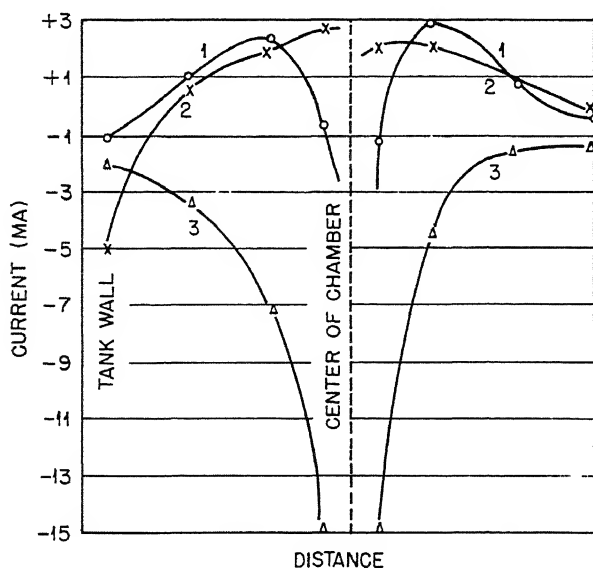


Fig. 9.52—Distribution of current to collimating-slot plate for large arc in argon. Pressure 0.6×10^{-3} mm Hg. Curve 1: magnetic field 1,000 gauss; arc voltage 150 volts; arc current 1.5 amp. Curve 2: magnetic field 3,900 gauss; arc voltage 150 volts; arc current 0.5 amp. Curve 3: magnetic field 3,900 gauss, arc voltage 205 volts; arc current 3.0 amp.

(b) Large Arc in Argon. (1) Variation with Arc Current. Figure 9.52 shows a typical set of curves for different arc currents with the large arc in argon. An interesting feature of these curves is the positive wire currents collected in the case of low arc current.

(2) Variation with Arc Voltage. Figure 9.53 shows the variation of wire currents with arc voltage.

(3) Variation with Pressure. Figure 9.54 shows current distributions in two cases of pressures 0.6×10^{-3} mm Hg and 1.4×10^{-3} mm Hg. There appears to be surprisingly little difference between the curves in these two cases.

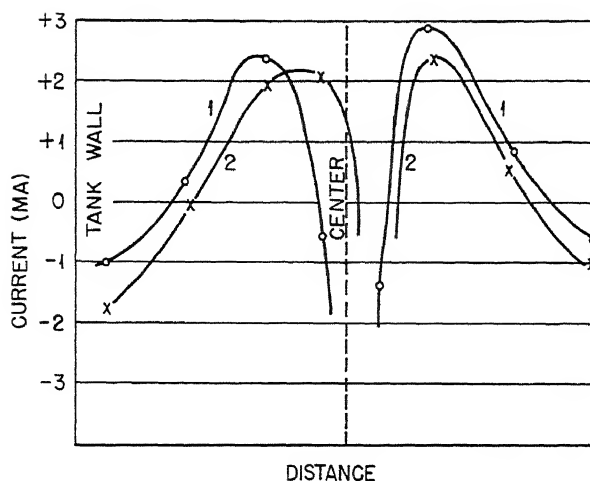


Fig. 9.53—Distribution of current to collimating-slot plate for large arc in argon. Pressure 1.4×10^{-3} mm Hg; magnetic field 3,900 gauss; arc voltage 150 volts (curve 1), 400 volts (curve 2); arc current 1.5 amp.

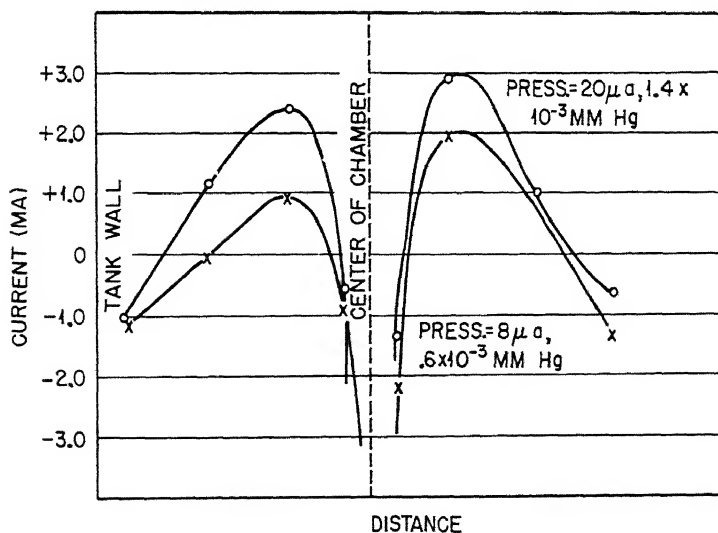


Fig. 9.54—Distribution of current to collimating-slot plate for large arc in argon. Magnetic field 3,900 gauss; arc voltage 150 volts; arc current 1.5 amp.

(4) Variation with Magnetic Field. Figure 9.55 shows the effect of variation of magnetic field on the wire-current distributions.

(c) Large Arc in Chlorine. The current distributions in the case of the large arc in chlorine show marked differences from the argon case. Presumably this is to be associated with the high probability of the formation of negative ions in the chlorine case, i.e., for high field

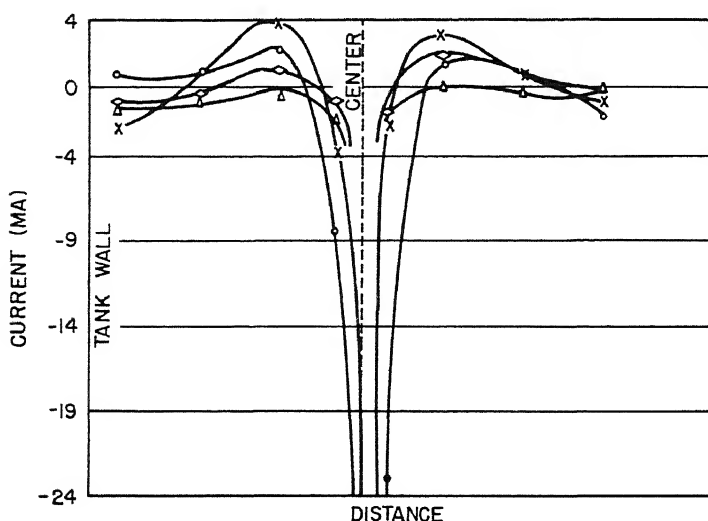


Fig. 9.55—Distribution of current to collimating-slot plate for large arc in argon. Pressure 0.6×10^{-3} mm Hg. Curve X: magnetic field 3,000 gauss; arc voltage 150 volts; arc current 1.5 amp. Curve O: magnetic field 2,000 gauss; arc voltage 200 volts; arc current 1.1 amp. Curve <: magnetic field 11,000 gauss; arc voltage 150 volts; arc current 1.5 amp. Curve Δ: magnetic field 3,900 gauss; arc voltage 150 volts; arc current 1.5 amp.

and high arc current one finds a distribution of the type shown in Fig. 9.56a, which is very similar to the large-arc distribution in the case of argon. For low fields and low arc currents, however, the opposite behavior is observed, the currents being always positive* and the distribution of the form shown in Fig. 9.56b. This behavior should be compared with that reported in Sec. 2 on the ion density in the chlorine arc. There it was shown that in general the ratio of the saturation negative current to the saturation positive current to a probe

* In order that the current balance be satisfied, it is of course necessary that in these cases the current must reverse at points near the arc column. All that the observations show is that this reversal takes place within the region between the two wires placed nearest the column.

outside the arc column was often less than 1 and tended to decrease in the direction away from the column. This was interpreted as evidence that the negative-ion temperature was somewhat less than the positive-ion temperature.

In the case of the wire currents, the wires, being kept at anode potential, will have around them a positive-ion sheath, and consequently negative ions will tend to be repelled. Thus both the lower negative-ion temperature and the positive-ion sheath around the wire would tend to produce a resultant positive current to the wire.

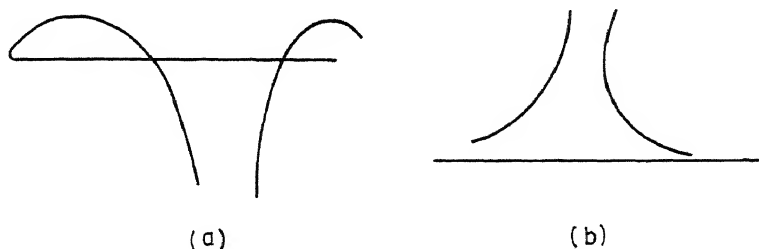


Fig. 9.56—Current distributions in large arc in chlorine. (a) High field and high arc current; (b) low field and low arc current.

When the arc current is increased, however (see Sec. 2), the ratio of the saturation currents to a probe becomes considerably greater than 1 near the arc column and falls off in the direction away from the column. Evidently a greater proportion of the negative currents in the arc is carried by electrons in the case of high arc currents, and this proportion falls off in the direction away from the column. This would produce just the type of effect observed.

In line with our picture of the arc this can probably be interpreted in the following way: A high arc current means a high degree of positive ionization, and thus, since most of the neutrals are ionized, the chance of formation of negative ions near or in the column is reduced. Accordingly with high arc currents one would expect a more normal type of distribution approaching that for argon.

Similarly the effect of high magnetic field could be explained on the ground that a high field has the effect of keeping the plasma electrons in regions where there is a high degree of positive ionization, and accordingly there is less chance of formation of negative ions and a more normal arc.

(1) Variation with Arc Current. Figure 9.57 shows the effect of changing the arc current on the current distribution as the arc current is increased.

(2) Variation with Arc Voltage. Figure 9.58 illustrates the effect of change of arc voltage on the current distribution. Both these distributions are of the anomalous "low-current, low-field" type.

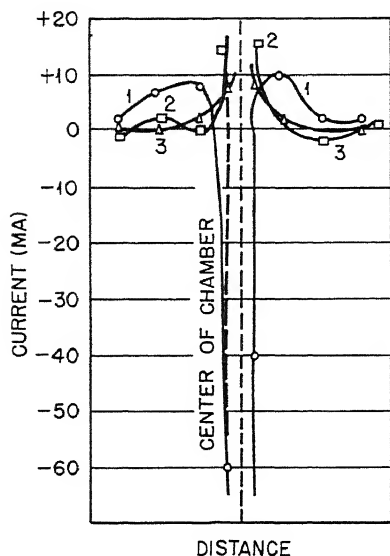


Fig. 9.57

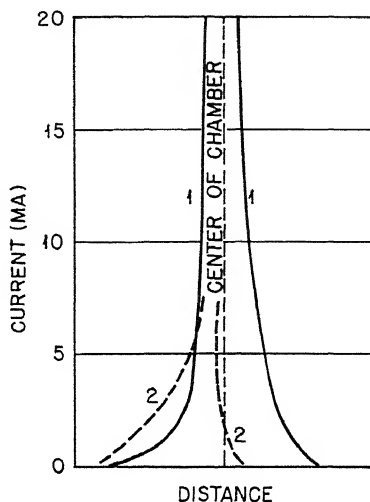


Fig. 9.58

Fig. 9.57—Distribution of current to collimating-slot plate for large arc in chlorine. Pressure 22×10^{-4} to 29×10^{-4} mm Hg; magnetic field 4,500 gauss; arc voltage 150 volts; arc current 3.0 amp (curve 1), 1.5 amp (curve 2), 0.5 amp (curve 3).

Fig. 9.58—Distribution of current to collimating-slot plate for large arc in chlorine. Magnetic field 4,600 gauss; arc voltage 150 volts (curve 1), 50 volts (curve 2); arc current 1.5 amp.

(3) Variation with Pressure. Figure 9.59 shows the effect of pressure change on the distribution. It is seen that the (positive) wire currents are reduced as the pressure is increased.

(4) Variation with Magnetic field. Figure 9.60 shows the effect of variation of magnetic field on the current distribution, illustrating the change from the anomalous to the normal current distribution with increase of magnetic field.

There appears, however, to be an anomaly between the effect of magnetic field on the probe measurements with the chlorine arc reported in Sec. 2 and the effect on the wire currents reported in this section. Thus in the previous section the ratio of the saturation negative to saturation positive probe currents decreases with increase

of magnetic field close to the arc column, indicating a decrease of the ratios of electron density to negative-ion density with increase of magnetic field. Thus negative current to wires 3 and 4 for low magnetic fields and positive currents for high magnetic fields might have

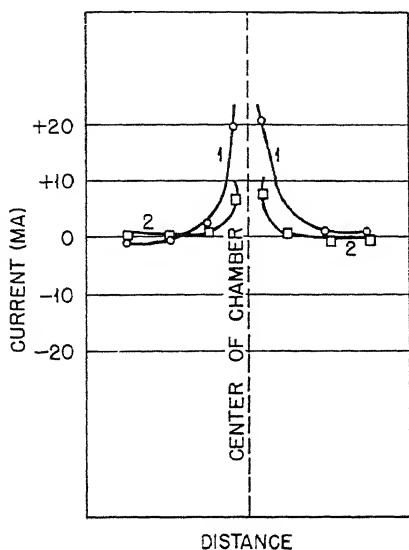


Fig. 9.59

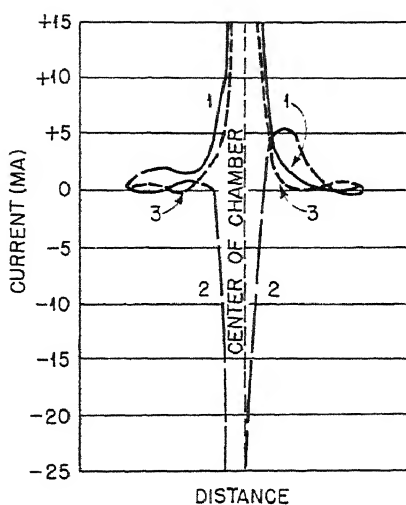


Fig. 9.60

Fig. 9.59—Distribution of current to collimating-slot plate for large arc in chlorine. Pressure 7×10^{-4} mm Hg (curve 1), 22×10^{-4} to 24×10^{-4} mm Hg (curve 2); magnetic field 4,600 gauss; arc voltage 150 volts; arc current 1.5 amp.

Fig. 9.60—Distribution of current to collimating-slot plate for large arc in chlorine. Pressure 22×10^{-4} to 29×10^{-4} mm Hg; magnetic field 4,600 gauss (curve 1), 11,000 gauss (curve 2), 1,000 gauss (curve 3); arc current 1.5 amp.

been expected instead of the opposite behavior observed. The reason for this anomaly is far from clear. It may arise from instrumental causes.

3.3 Saturation Block Current. In a number of cases, mostly for the small arc in argon, the block current has been measured as a function of potential applied to the block, and the saturation positive-ion current to the block has been determined. The results of these measurements are shown in Figs. 9.61 to 9.64.

Figure 9.61 shows the variation of the saturation positive-ion current to the block as a function of arc current for small arc currents. It is seen that over the range of arc currents studied the variation is appreciably linear.

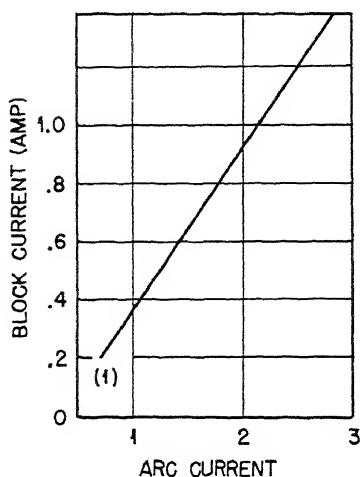


Fig. 9.61

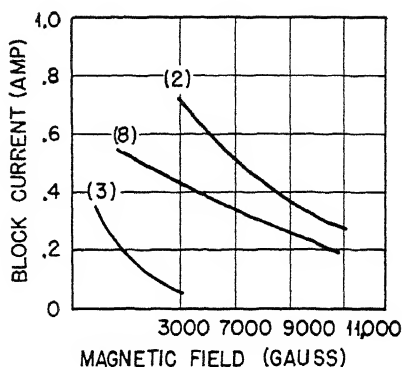


Fig. 9.62

Fig. 9.61—Variation of saturation block current with arc current (extrapolated to anode potential). See Table 9.7.

Fig. 9.62—Variation of saturation block current with magnetic field (extrapolated to anode potential). See Table 9.7.

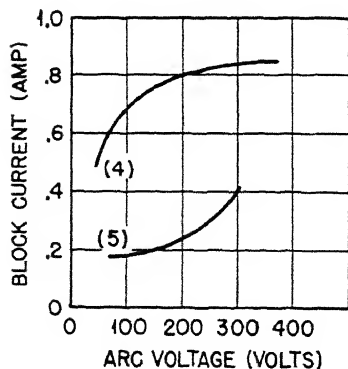


Fig. 9.63

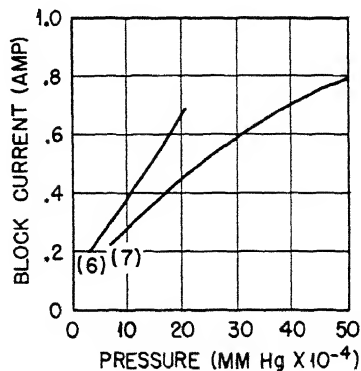


Fig. 9.64

Fig. 9.63—Variation of saturation block current with arc voltage (extrapolated to anode potential). See Table 9.7.

Fig. 9.64—Variation of saturation block current with pressure (extrapolated to anode potential). See Table 9.7.

Figure 9.62 shows the variation of saturation block current with magnetic field. As would be expected, this current decreased markedly as the field is increased.

Figure 9.63 shows the variation of saturated block current with arc voltage. It shows a slow increase in general with voltage.

Figure 9.64 shows the variation of saturated block current with pressure.

Table 9.7*

Curve No.	Type of arc	Pressure, mm Hg $\times 10^{-3}$	Magnetic field, gauss	Arc voltage, volts	Arc current, amp
1	Small	1.4	3,900	150	
2	Small	1.4		150	1.5
3	Large	1.4		150	1.5
4	Small	1.4	3,900		1.5
5	Small	1.4	4,600		1.0
6	Small	1.4	3,900	150	1.5
7	Small	1.4	3,900	150	1.5
8	Small	1.4		150	1.5

* The blanks indicate that the quantity was varied.

Table 9.8*

Wire No.	Distance from center of arc, in.	Positive-ion current, ma	Electron current, ma
1	+9/32	2.0	-2.0
2	+3/16	10.0	-11.0
3	+3/32	18.0	-46.0
4	-3/32	19.0	-25.0
5	-3/16	8.0	-8.0
6	-9/32	2.5	-3.5

* Pressure 1.4×10^{-3} mm Hg; magnetic field 3,900 gauss; arc voltage 150 volts; arc current 0.5 amp.

Table 9.7 shows the conditions under which the various curves of Figs. 9.61 to 9.64 were taken.

3.4 Saturation Current to Wires. In one case for the small arc the nature of the currents going to the wires was analyzed by measuring the saturated positive-ion current in the various cases. The results are shown in Table 9.8.

Under the same conditions the current going to the block was made up of 300 ma positive-ion current and 110 ma electron current. It is

seen that the positive-ion current in this case was reduced to about $1/e$ of its value in moving $\frac{3}{32}$ in. from the column. This should be compared with the values of ion density of Table 9.1, where under similar conditions (except for a higher arc current of 1.5 amp) the ion density fell to $1/e$ of its value in a distance of $\frac{1}{8}$ in. It was then assumed that the actual positive-ion current reaching the wires when they were maintained at anode potential was equal to the saturation current, and consequently the actual electron current when the wires were maintained at anode potential could be obtained by adding the saturation positive-ion current to the observed total current.

4. INVESTIGATION OF SPACE POTENTIAL AND ELECTRON TEMPERATURE IN THE ARC

4.1 General Considerations. Systematic measurements have been made of the space potential and electron temperature in the arc, using both hot and cold probes.

A drawing of the hot probe used is shown in Fig. 9.7 of Sec. 1. With such a probe the normal type of characteristic curve shown by the full curve in Fig. 9.65 is obtained when the probe is run cold. However, when the probe is heated to a temperature sufficiently high to give rise to thermionic emission, the characteristic curve is changed. So long as the potential of the probe is positive relative to the surrounding space, thermionic emission is prevented. But if the probe potential is now decreased until it becomes negative relative to the space potential, thermionic emission occurs, and consequently the net negative current reaching the probe when the probe is hot is less than when it is cold. Thus the probe-characteristic curve for a hot probe would be expected to follow the dotted line of Fig. 9.65. By measuring the probe potential at which heating the probe to a temperature sufficient for thermionic emission just fails to make any change in the probe current, an estimate of the space potential was obtained.

Several sets of measurements were carried out using the hot-probe technique, but unfortunately the measurements were made difficult by the very short lifetime of the probe when operating in the arc plasma. Accordingly most of the systematic measurements of space potential were made by analyzing cold-probe characteristics. This method also has the advantage that the same analysis yields the electron temperature.

Figure 9.66 illustrates the method of carrying through the analysis for the cold-probe case. A plot is made of $\ln(J + |J_+|)$ against voltage V , where J is the probe current when the probe potential is V and J_+ is the saturation positive-ion current. The point A is taken as the

position of the space potential. It is the intersection of the two lines CA and BA defined by the portion of the curve corresponding to joint electron and ion collection and the portion corresponding to saturation electron collection. In most of the curves the position of the space potential, defined by the point A, seemed quite definite to within about 1 volt.

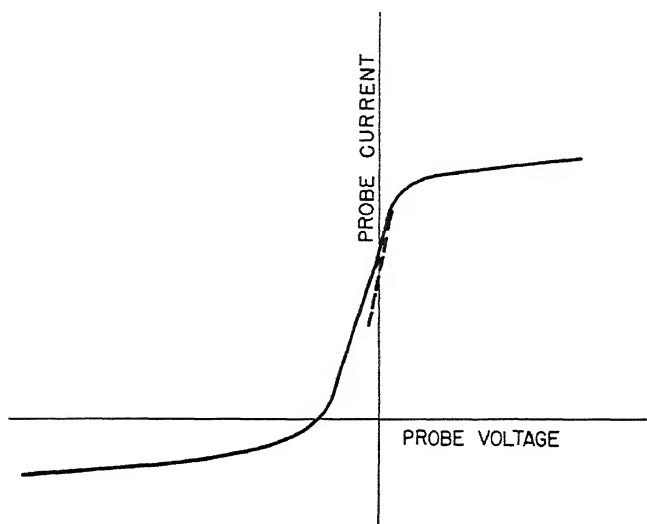


Fig. 9.65—Hot-probe characteristic.

The electron temperature is given by the relation

$$T_e = \left[\frac{d \ln (J + |J_+|)}{dV} \right]^{-1} \quad (47)$$

where T_e is in volts. Thus the inverse slope of the line AC of Fig. 9.66 gives a measure of the electron temperature.

In the case of the hot-probe measurements it was not possible to derive the electron temperature accurately. However, some idea of the slope of the portion of the probe characteristic that determines the electron temperature was obtained by measuring the difference between the space potential (estimated by the hot-probe method) and the floating potential. In investigations of the variation of electron temperature with arc conditions it seems reasonable to assume that the difference between space and floating potential is proportional to the electron temperature.

Care has to be taken, however, in interpreting the space-potential and electron-temperature values deduced by these methods on account of the possibility that plasma oscillations will have a major influence on the results. To illustrate the effect of plasma oscillations in influencing the probe characteristics, consider a probe characteristic as shown by the full curve in Fig. 9.67 and suppose that the plasma potential near the probe is oscillating by an amount represented by the length of arrow drawn in the figure. Then, owing to the greater

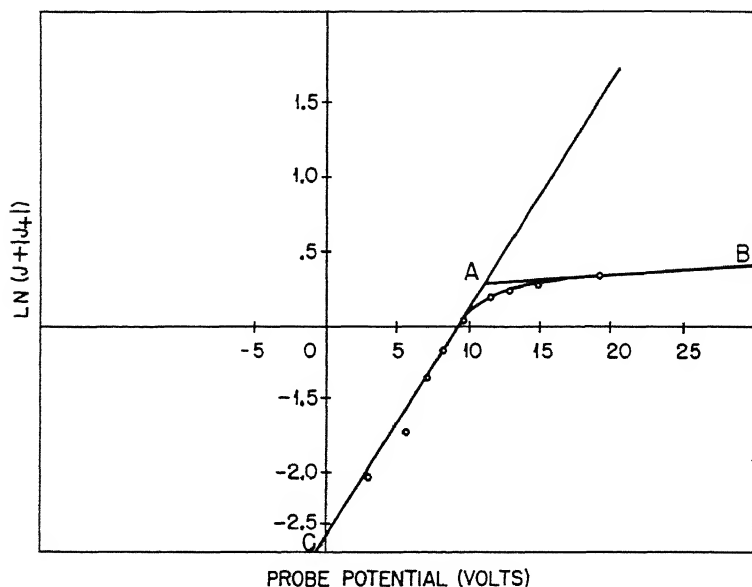


Fig. 9.66—Cold-probe characteristic for large arc in argon. Pressure 1.4×10^{-3} mm Hg; magnetic field 3,700 gauss; arc voltage 150 volts; arc current 1.0 amp.

ease with which electrons are collected compared with ions, the resultant observed probe characteristic would be expected to be of the form given by the broken-line curve of the figure. Both the apparent floating potential and the space potential would be more negative than the true value, owing to the presence of the oscillations, but the effect on the floating potential would be expected to be greater than on the space potential. As a result the apparent electron temperature is greatly increased.

In the case of the hot-probe measurements one might expect the presence of plasma oscillations to lead to an apparent value of the space potential more positive than the true value, since the presence

of the oscillations will cause the space to go positive relative to the probe and thus draw out thermal electrons when the probe potential corresponds to the point A on the diagram.

The above considerations apply only, however, if the frequency of the plasma oscillations is not too high and the electrons are therefore able to move away from the neighborhood of the sheath during the period of a complete plasma oscillation. However, if the oscillation frequency is so high (of the order of 10^9 oscillations per second or higher) that the electrons are unable to move away from the sheath

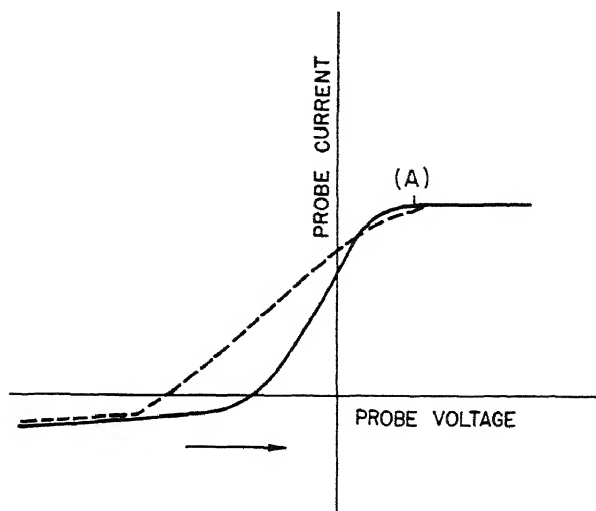


Fig. 9.67 — Effect of plasma oscillations on probe characteristic.

during such an interval, the effect of plasma oscillations would not be so marked on the observed space potential and floating potential. In such a case the simple picture used above breaks down, and it is difficult to predict the effect of the oscillations.

4.2 Space Potential. In the absence of magnetic field in a steady state of the arc plasma, the plasma potential runs about 10 volts positive relative to the walls. This arises from the fact that the electrons are produced with energies of several volts, whereas the positive ions are produced with much smaller energies. On account of their greater mobility the electrons reach the walls more easily than the positive ions. But approximate space-charge neutralization must be maintained in the plasma, and thus electric fields must be set up in the plasma in such a way as to force the ions to the walls. Thus

the plasma runs at a positive potential relative to the walls. The actual potential reached is just that which will make the rate of collection of positive ions and of electrons to the walls equal to the rate of production.

In an arc in which the ends of the arc are connected to the side walls, an essentially similar picture holds. Although the electrons now diffuse less readily than the ions across the field, the electron-collection rate to the top and bottom (along the field) will still be much faster than the ion-collection rate, and consequently once again the plasma will be forced to run at a positive potential relative to the walls in order to maintain an over-all balance of positive-ion and electron collection.

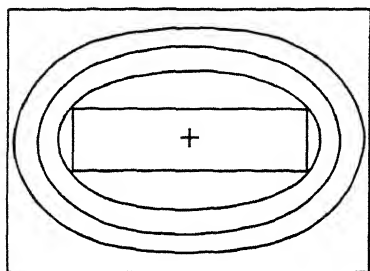


Fig. 9.68

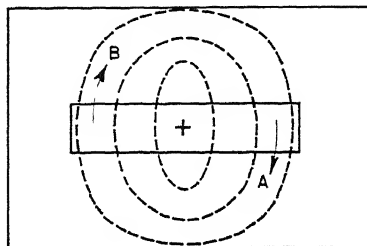


Fig. 9.69

Fig. 9.68—Symmetrical equipotential distribution providing no drain mechanism.

Fig. 9.69—Symmetrical equipotential distribution providing drain mechanism.

This general result was observed in the space potentials measured in this arc. In the case of the small arc the plasma potential was found to run about 8 volts positive relative to the walls. In the case of the large arc the plasma was forced to run about 12 volts positive relative to the walls.

The detailed distribution of space potential was difficult to interpret. One might at first sight have expected a gradual symmetrical falling off of space potential on moving away from the arc column, causing the equipotentials to be as shown in Fig. 9.68. Such a distribution would provide no drain mechanism, however, by which the electrons formed in the column could get into the surrounding space.

As has been shown in earlier sections of this chapter, electrons from the arc region do reach regions far from the column, and the rate at which they would be expected to do this owing to collisions is

far too small to account for the observed rates of diffusion across the field. Accordingly a drain mechanism has been suggested by Bohm (Chap. 2) to account for at least some of the electron motion across the field. But if the potential distribution were like that of Fig. 9.3, electrons would simply drain round the arc column without getting away from it.

A symmetrical equipotential distribution that would get electrons away from the column is shown in Fig. 9.69. Such a distribution would cause electrons and ions to drain out of the column in the directions indicated by the arrows. This would tend to cause a piling up of ion density in the regions A and B (i.e., on the antidrain side of the front of the column) as was observed in the positive-ion-density distributions actually observed.

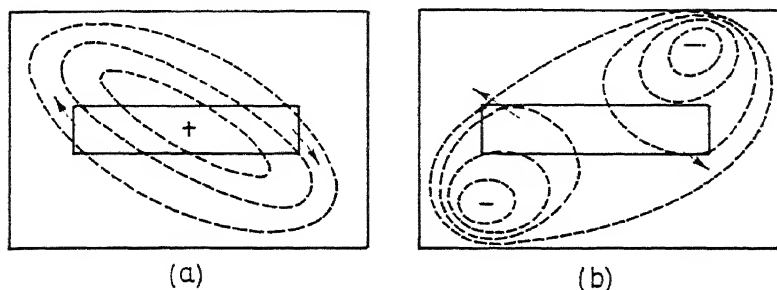


Fig. 9.70 — Alternative potential distributions providing for drain.

Other types of potential distribution, however, could be imagined in the arc column which would give rise to a concentration of ion density in the plasma on the antidrain side of the front of the column.

Thus Figs. 9.70a and b show such distribution.

Some typical observed ion distributions are shown in Figs. 9.71 to 9.74. Figure 9.71 shows a form of distribution similar to that predicted in Fig. 9.69; Fig. 9.72 shows a form similar to Fig. 9.70a; and Fig. 9.73 shows a form similar to Fig. 9.70b. The type of ion distribution shown in Fig. 9.74 does not seem to fall in any of these classes, and it is difficult to see how such a distribution would produce drain in the sense necessary to give rise to an ion-density distribution with a maximum on the antidrain side of the column. It is interesting to note, however, that this particular type of distribution was obtained for a very high pressure (7×10^{-3} mm Hg). In Sec. 2, on ion-density distribution, it is shown that at this pressure the asymmetry was almost absent, and consequently one would expect to obtain an ion-

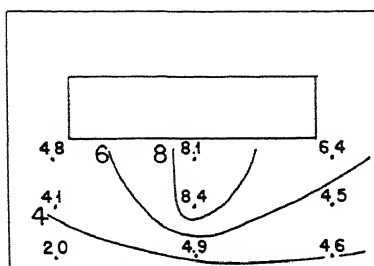


Fig. 9.71

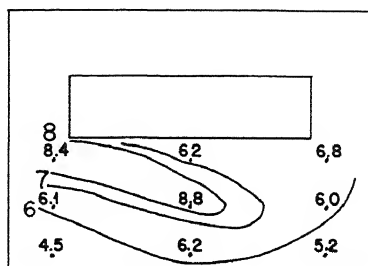


Fig. 9.72

Fig. 9.71—Contours of space potential relative to arc walls for small arc in argon. Pressure 1.4×10^{-3} mm Hg; magnetic field 11,000 gauss; arc voltage 150 volts; arc current 1.5 amp.

Fig. 9.72—Contours of space potential relative to arc walls for small arc in argon. Pressure 1.4×10^{-3} mm Hg; magnetic field 3,700 gauss; arc voltage 150 volts; arc current 1.5 amp.

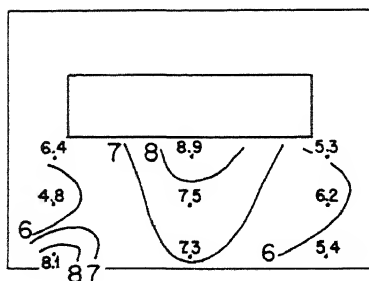


Fig. 9.73

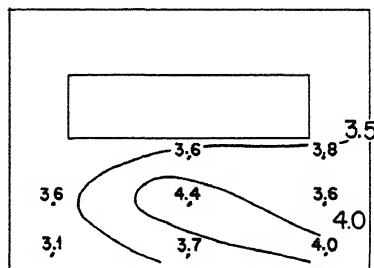


Fig. 9.74

Fig. 9.73—Contours of space potential relative to arc walls for small arc in argon. Pressure 1.4×10^{-3} mm Hg; magnetic field 3,700 gauss; arc voltage 400 volts; arc current 1.5 amp.

Fig. 9.74—Contours of space potential relative to arc walls for small arc in argon. Pressure 7.0×10^{-3} mm Hg; magnetic field 3,700 gauss; arc voltage 150 volts; arc current 1.5 amp.

density distribution different from that obtained in the other cases. At high pressures diffusion by collision might be great enough to make drain diffusion unnecessary.

Apart from this case of high pressures, there was no very clear correlation between the particular type of distribution observed and

the arc conditions. Thus Table 9.9 shows the arc conditions that have been observed to give rise to the various types of distribution.

The absence of correlation with arc conditions seems to indicate that the particular type of space-potential distribution is determined mainly by such effects as filament wear, etc., rather than by arc conditions.

Table 9.9

Pressure, mm Hg $\times 10^{-3}$	Magnetic field, gauss	Arc voltage, volts	Arc current, amp	Type of distribution
0.6	3,700	150	1.5	As in Fig. 9.69
0.6	11,000	150	1.5	As in Fig. 9.69
1.4	3,700	150	1.0	As in Fig. 9.69
1.4	11,000	150	1.5	As in Fig. 9.69
0.3	3,700	300	1.2	As in Fig. 9.70a
1.4	3,700	150	1.5	As in Fig. 9.70a
1.4	3,700	400	1.5	As in Fig. 9.70b
1.4	3,700	150	3.0	As in Fig. 9.70b
1.4	3,700	150	0.5	As in Fig. 9.70b
1.4	3,700	50	1.5	As in Fig. 9.70b
7.0	3,700	150	1.5	As in Fig. 9.74

The type of space-potential distribution obtained for the large arc in argon is shown in Fig. 9.75. Near the arc column the distribution shown in this case resembles that of Fig. 9.69 for the small arc, and consequently might be expected to lead to an asymmetric ion-density distribution near the column, as was in fact observed.

The above results all refer to measurements taken with the cold probe. A number of measurements at points along the central axis of the arc were taken, in the case of argon, with the hot probe. In some cases hot- and cold-probe measurements were taken at the same points in the small arc in argon and under the same arc conditions. A comparison of the space potentials obtained by the two methods of measurement is shown in Table 9.10. All these measurements were made along the central axis in the central transverse plane of the arc. The x coordinate is the distance from the inside wall of the chamber in the direction of the arc column.

In view of the uncertainties in the space-potential measurements pointed out above, the agreement to within a volt or so between measurements using hot and cold probes may be considered satisfactory.

Figures 9.77 to 9.82 show the results of measurements using the hot probe in the small arc in argon.

Figure 9.77 shows the variations of space potential along the central axis for three different transverse planes in the arc. The system of coordinates used is shown in Fig. 9.76. The origin 0 of the system is at the center of the inside front face of the arc chamber and the Z axis is in the inside front face parallel to the direction of the magnetic field.

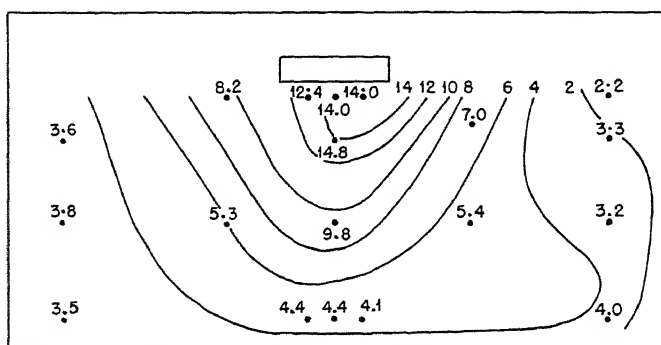


Fig. 9.75—Space potentials relative to arc-chamber walls for large arc in argon. Pressure 6×10^{-3} mm Hg; magnetic field 3,700 gauss; arc voltage 150 volts; arc current 1.5 amp.

Figure 9.78 shows the vertical variation of the space potential for given values of x . Figures 9.77 and 9.78 show that the space potential is highest near the arc column in the central plane. In the direction up and down from this plane or out toward the front face of the chamber the space potential drops a couple of volts in moving 2 in. in the vertical direction and about the same in moving away from the column to about the position of the sheath in the x direction. This drop in space potential between the center of the plasma and the sheath edge would be expected to be of the order of half the electron temperature (Chap. 2). Figures are given later in this section for the electron temperature (see Sec. 4.3). The observed variation of space potential within the plasma is in agreement with this expectation.

Figure 9.79 shows the variation of space potential with magnetic field at a point in the arc plasma. Curves are given for a pressure of 3.5×10^{-3} mm Hg at different positions in the plasma. The variation is not very marked. At low fields the space potential decreases with increase of field, but for fields above 5,000 gauss it is almost independent of field.

Figure 9.80 shows the variation with space potential as a function of pressure at different distances from the arc column. The space

potential appears, in general, to fall by about 2 volts between pressures of 0.6×10^{-3} mm Hg and 3.5×10^{-3} mm Hg. As will be seen later, there seems some evidence that the electron temperature decreases with increase of pressure. Thus the potential drop in the plasma necessary to get rid of the positive ions produced and therefore maintain space-charge neutralization would be expected to be smaller.

Table 9.10

Pressure, mm Hg $\times 10^{-3}$	Magnetic field, gauss	Arc voltage, volts	Arc current, amp	x, in.	Space potential, volts	
					Hot probe	Cold probe
0.6	3,700	150	1.5	0	6.5	8.3
				1/8	8	8
				1/4	8	8.5
0.6	11,000	150	1.5	0	4.5	5.3
				1/4	10.5	8.2
0.6	3,700	400	1.5	0	10.5	7
				1/4	13	10
0.6	3,700	150	0.5	0	6	5
				1/4	8.5	8
0.6	3,700	150	3.0	0	6	7.5

Figure 9.81 shows the variation of space potential with arc current, at a pressure of 3.5×10^{-3} mm Hg for two different positions in the plasma. The variation is seen to be very small in both cases.

Figure 9.82 shows the observed variation with arc voltage at pressures of 0.6×10^{-3} mm Hg and 3.5×10^{-3} mm Hg. At the lower pressure there appears to be an appreciable increase of space potential with arc voltage, but this effect is not marked at the higher pressure. One might have expected an increase in space potential with arc voltage, since a higher voltage would be expected to give rise to a higher initial energy of formation of the secondary electrons in the column and thus to a higher electron temperature.

The variation of space potential with arc conditions was also studied, using the cold-probe method. The results of this investigation are illustrated in Figs. 9.83a to 9.86b, where the space potential is plotted as a function of distance along the central axis of the chamber for different pressure, magnetic fields, arc voltage, and arc current. In general, the conclusions to be drawn from these measurements agreed with those obtained by the hot-probe method, namely, at a given position in the plasma the space potential relative to the walls

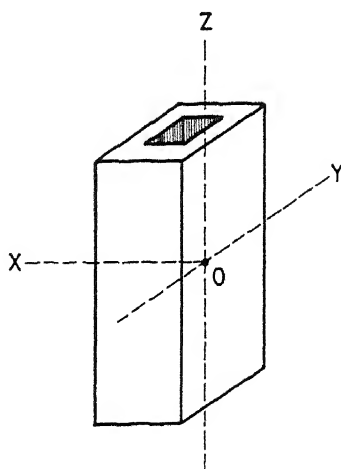


Fig. 9.76—System of coordinates for hot-probe measurements.

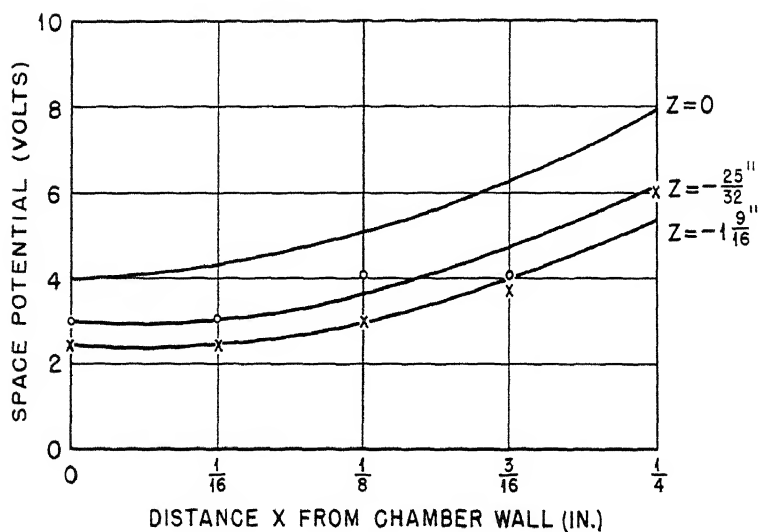


Fig. 9.77—Space potential relative to arc-chamber walls as a function of distance x of a probe from wall for different vertical distances z from central position. Pressure 3.5×10^{-3} mm Hg; magnetic field 3,700 gauss; arc voltage 150 volts.

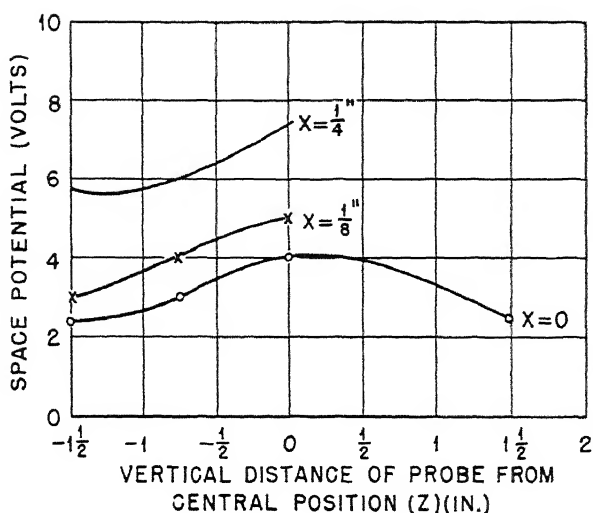


Fig. 9.78—Space potential relative to arc-chamber walls as a function of vertical distance z of probe above central position for different distances x from walls. Arc conditions as for Fig. 9.77.

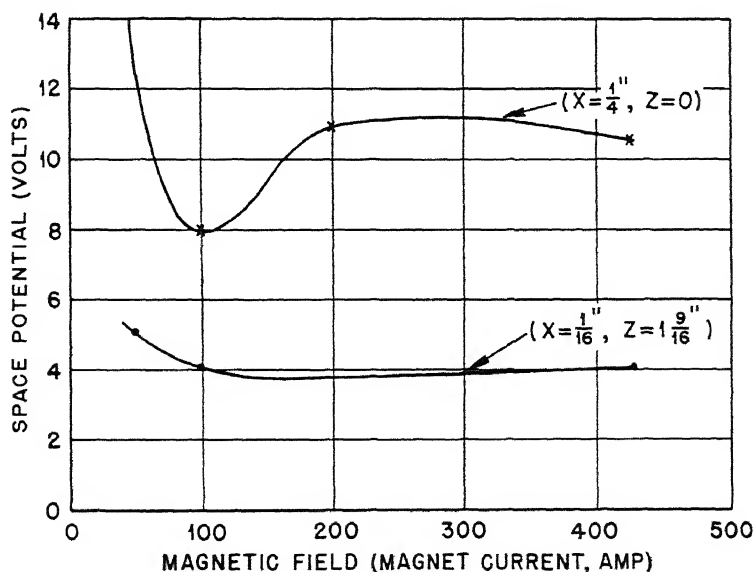


Fig. 9.79—Space potential relative to arc-chamber walls vs. magnetic field. Pressure 3.5×10^{-3} mm Hg; arc voltage 150 volts; arc current 1.5 amp. A magnetic current of 100 amp = magnetic field of 3,700 gauss; 400 amp = 11,000 gauss.

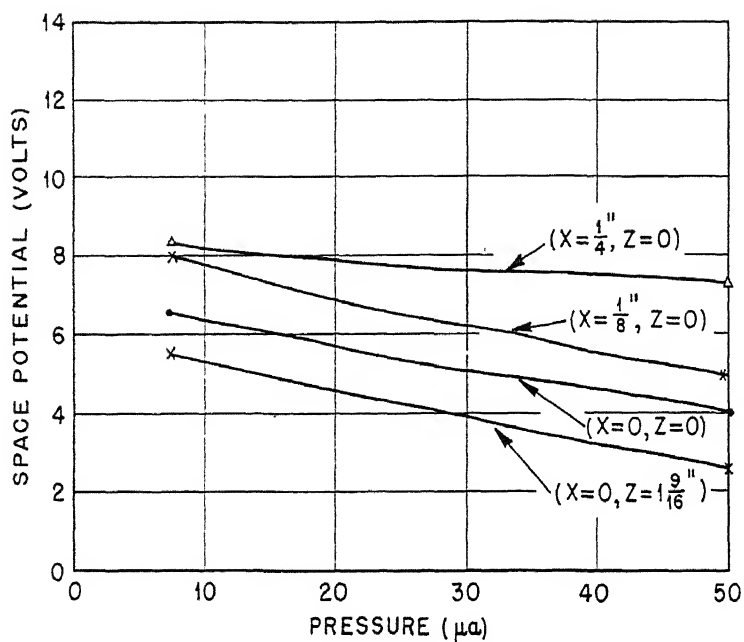


Fig. 9.80—Space potential relative to arc-chamber walls vs. pressure. Magnetic field 3,700 gauss; arc voltage 150 volts; arc current 1.5 amp. $1 \mu a = 0.7 \times 10^{-4}$ mm Hg.

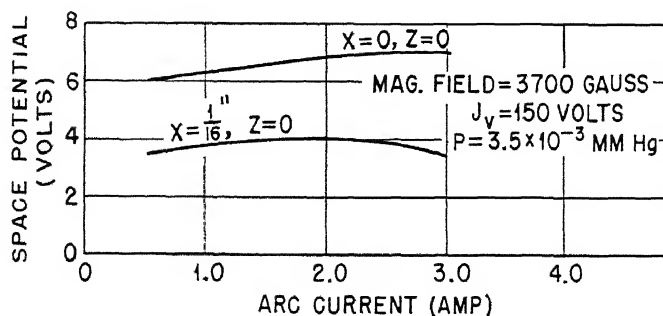


Fig. 9.81—Space potential relative to arc-chamber walls vs. arc current. Pressure 3.5×10^{-3} mm Hg; magnetic field 3,700 gauss; arc voltage 150 volts.

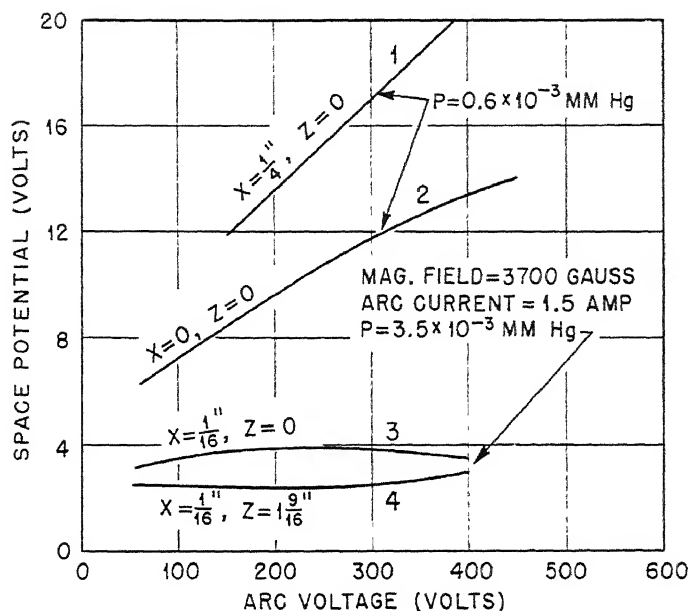


Fig. 9.82—Space potential relative to arc-chamber walls vs. arc voltage. Pressure 0.6×10^{-3} mm Hg (curves 1 and 2), 3.5×10^{-3} mm Hg (curves 3 and 4); magnetic field 3,700 gauss; arc current 1.5 amp.

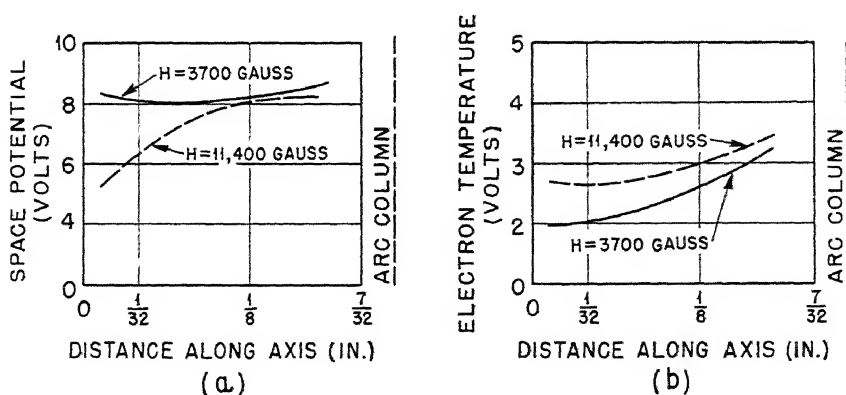


Fig. 9.83—Variation of electron temperature and space potential along central axis for the small arc in argon. (a) Arc current 1.5 amp; arc voltage 150 volts; pressure 8×10^{-4} mm Hg. (b) Arc current 1.5 amp; arc voltage 150 volts; pressure 6×10^{-4} mm Hg.

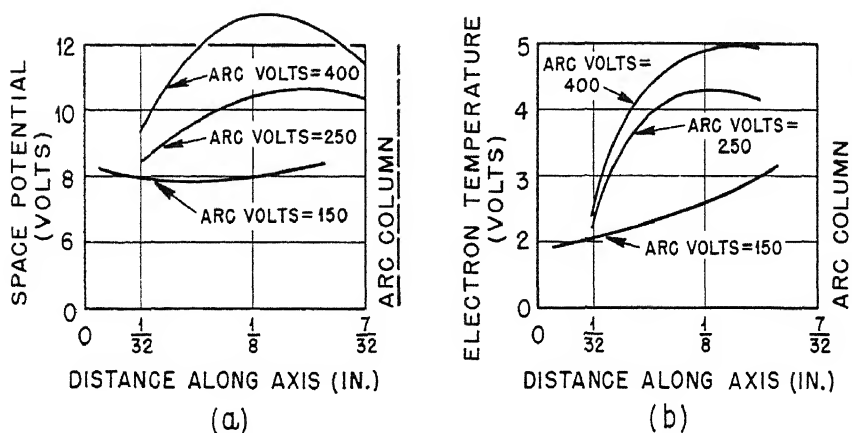


Fig. 9.84—Variation of electron temperature and space potential along central axis for small arc in argon. (a) Arc current 1.5 amp; magnetic field 3,700 gauss; pressure 8×10^{-4} mm Hg. (b) Arc current 1.5 amp; magnetic field 3,700 gauss; pressure 6×10^{-4} mm Hg.

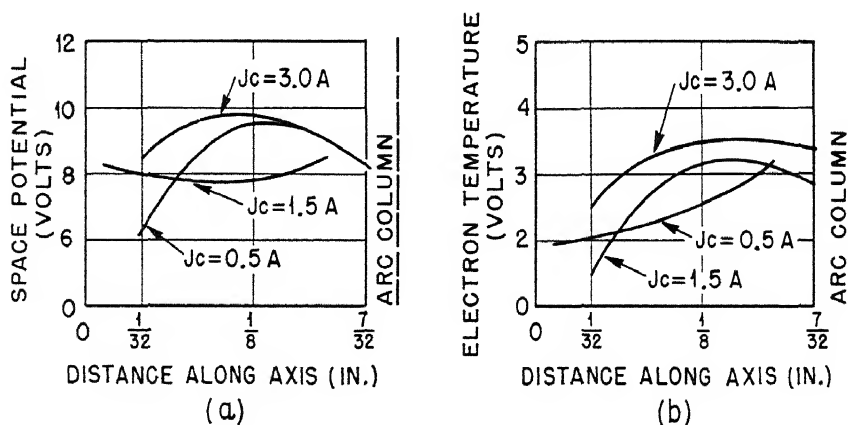


Fig. 9.85—Variation of electron temperature and space potential along central axis for small arc in argon. (a) Arc voltage 150 volts; magnetic field 3,700 gauss; pressure 8×10^{-4} mm Hg. (b) Arc voltage 150 volts; magnetic field 3,700 gauss; pressure 6×10^{-4} mm Hg.

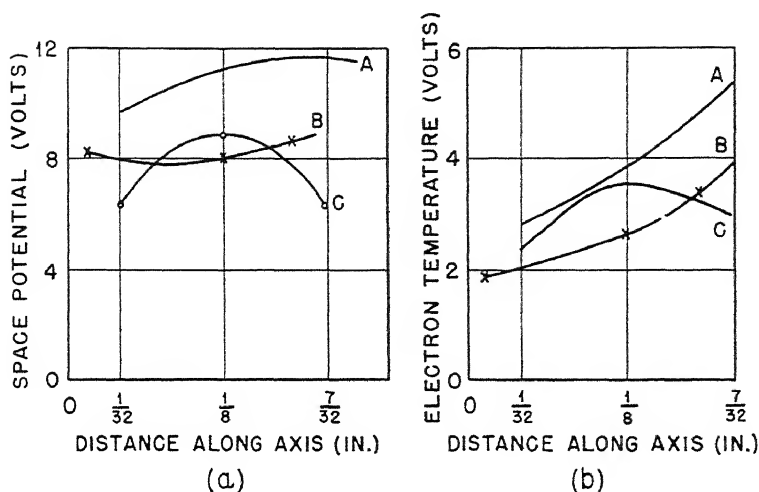


Fig. 9.86—Variation of electron temperature and space potential along central axis for small arc in argon. Curve A: pressure 0.3×10^{-3} mm Hg; magnetic field 3,700 gauss; arc voltage 300 volts; arc current 1.2 amp. Curve B: pressure 0.6×10^{-3} mm Hg; magnetic field 3,700 gauss; arc voltage 150 volts; arc current 1.5 amp. Curve C: pressure 1.4×10^{-3} mm Hg; magnetic field 3,700 gauss; arc voltage 150 volts; arc current 1.5 amp.

Table 9.11

x, in.	Space potential, volts
0	9.5
$1/32$	10.5
$3/32$	10.5
$5/32$	11.3

(1) decreases with increase of magnetic field, (2) increases with increase of arc voltage, (3) does not appear to depend markedly on arc current, and (4) decreases with increase of pressure.

Measurements of space potential using the cold-probe method were also taken in the case of the curved collimating slot for the small arc in argon for one set of conditions (0.7×10^{-3} mm Hg pressure, 3,700 gauss magnetic field, 150 volts arc potential, 1.5 amp arc current).

Table 9.11 shows the measured space potentials at different distances along the central axis in this case.

It appears that the space potential relative to the walls is 2 or 3 volts greater than for the straight symmetrical collimating slot. The measurements are so fragmentary, however, that it is difficult to say whether much weight should be placed on them.

A few space-potential measurements were taken for a chlorine arc using the small arc chamber. The results of the only systematic set taken are shown in Fig. 9.87. One feature of this distribution is that the space potential relative to the walls is somewhat lower than in the

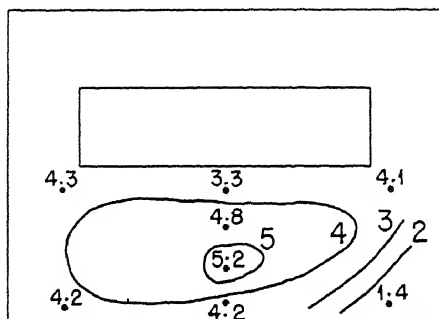


Fig. 9.87—Space potential relative to arc-chamber walls for small arc in chlorine. Pressure 1.0×10^{-3} mm Hg; magnetic field 3,700 gauss; arc voltage 150 volts; arc current 1.5 amp.

case of the argon arc, taken under similar conditions. Furthermore, the variation in the plasma itself is smaller than in the case of argon except for the one point in the right-hand bottom corner of Fig. 9.87. One might expect much smaller potential differences within the plasma in the case of chlorine since, as has been shown in an earlier section, the negative current in the chlorine arc is largely caused by negative ions. Unlike electrons, these are not more mobile than the positive ions, and thus there is no need for potential differences within the plasma to get the positive ions to the walls. Of course, since some of the negative current is still caused by electrons, the plasma still runs positive with respect to the walls, but the plasma potentials are in general smaller.

Figure 9.87 for Cl_2 should be compared with Fig. 9.72 for argon, taken under similar arc conditions except that the pressure is slightly higher in the latter case. In the case of argon the highest space potential relative to the walls is 8.8 volts; in the case of chlorine, 5.2 volts.

A few measurements were also made of space potentials in the large Cl_2 arc. In this case it was found that the maximum space potential of the plasma relative to the chamber walls under the conditions of pressure 10^{-3} mm Hg, magnetic field 3,700 gauss, arc voltage 150 volts, and arc current 1.5 amp was about 11 volts compared with about 14 volts under the same conditions in the large arc in argon.

4.3 Electron Temperature. Secondary electrons are continually being produced in the arc column by ionization of the neutral gas atoms. These electrons make collisions with electrons, ions, and neutral atoms in the plasma and are also accelerated and retarded in the oscillating fields existing in the plasma. As a result their energies become rapidly redistributed into a Maxwellian distribution. The secondary electrons produced by primary electron impact have on the average about 10 per cent of the primary electron energy. The currents of electrons and ions reaching the walls, however, carry away energy, and the electron temperature is determined by the balance between the energy gained from the primary beam and the energy lost to the walls.

One would expect the electron temperature in the plasma to increase with the arc voltage, since a voltage increase means a higher average initial energy of formation of the secondary electrons.

On the other hand, it would be expected that increase of pressure would decrease the electron temperature, since increase of pressure means a greater number of collisions between electrons and gas atoms. In the case of elastic collisions this would not produce much effect, since an electron loses very little energy in elastic collisions with a gas atom. However, an appreciable fraction of the plasma electrons will possess sufficient energy to excite and even ionize the atoms of the residual gas. It has been shown in the section on ion densities in the arc that some of the observed phenomena require the postulation of ionization by plasma electrons for their interpretation. Thus the plasma-electron temperature may be appreciably reduced by inelastic collisions.

The effect of the magnetic field on the electron temperature is primarily to reduce the effective mean free path of the electron, since, ignoring the effects of plasma oscillations, the mean free path of the electron in the plane transverse to the magnetic field is of the same order as the Larmor radius, and the importance of inelastic collisions will be increased by increase of field.

According to this view there is no obvious reason why arc current should be effective in changing the electron temperature. However,

plasma oscillations may be expected to have a marked effect on electron temperature, and the amplitude of these oscillations will probably depend on the ion density in the plasma and thus on the arc current. Accordingly it is not easy to say whether or not arc current should affect electron temperature.

The curves shown in Figs. 9.88 to 9.91 for the variation of electron temperature with arc conditions bear out these expectations. Since in these curves the electron temperature was estimated from the floating potential and the hot-probe measurement of space potential, one cannot place any reliance on the absolute value of the electron temperature given on the curves. However, the observed variation with arc conditions should be a true measure of the way in which the electron temperature varies.

Figure 9.88 shows the variation of electron temperature with magnetic field. For comparatively low magnetic fields (less than 4,000 gauss) there is seen to be a rapid decrease with increase of field, but at higher fields the electron temperature remains constant or decreases rather slowly.

Figure 9.89 illustrates the decrease of electron temperature with pressure.

Figure 9.90 shows that the variation with arc current is quite slow, although there does appear to be a small increase as the current is increased from 0.5 to 3.0 amp.

Figure 9.91 shows the variation with arc voltage. At a pressure of 0.6×10^{-3} mm Hg (Western Electric gauge) the increase with voltage appears quite marked, but it is much smaller at a pressure of 3.5×10^{-3} mm Hg.

On comparing these curves with Figs. 9.79 to 9.82, which show the variation of space potential with arc conditions, one is struck with the close correlation between the two quantities. This can be understood in terms of remarks made above, which indicate that the fall of space potential within the plasma and the drop across the sheath are determined by the electron temperature.

Figures 9.83b to 9.86b show the electron temperature under different arc conditions as determined by the cold-probe method. Unlike the hot-probe case, the absolute values of the electron temperature determined by this method should be significant. In fact, the observed electron temperatures vary between 2 to 6 volts in different cases, while the variation of space potential in the plasma does not appear to exceed about 3 volts in any case. This agrees with the expectation noted above that the variation of space potential within the plasma should not exceed about half the electron temperature.

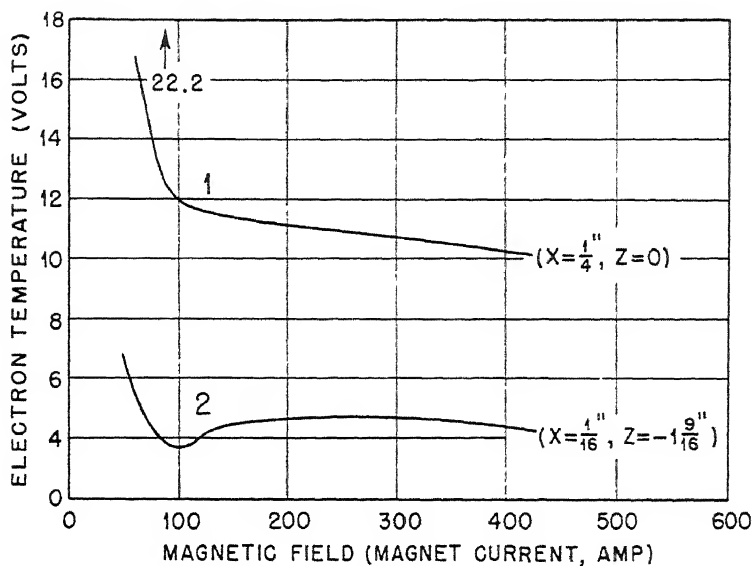


Fig. 9.88—Electron temperature vs. magnetic field. Pressure 0.6×10^{-3} mm Hg (curve 1), 3.5×10^{-3} mm Hg (curve 2); arc voltage 150 volts; arc current 1.5 amp. A magnetic current of 100 amp = magnetic field of 3,700 gauss; 400 amp = 11,000 gauss.

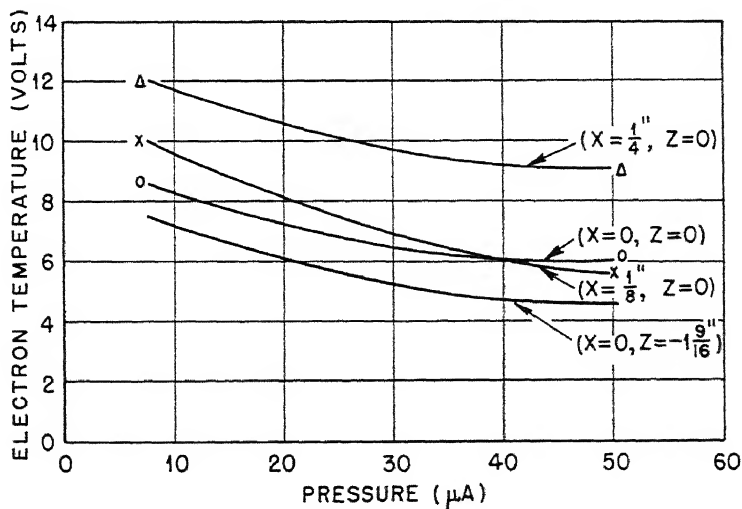


Fig. 9.89—Electron temperature vs. pressure. Magnetic field 3,700 gauss; arc voltage 150 volts; arc current 1.5 amp. $1 \mu A = 0.7 \times 10^{-4}$ mm Hg.

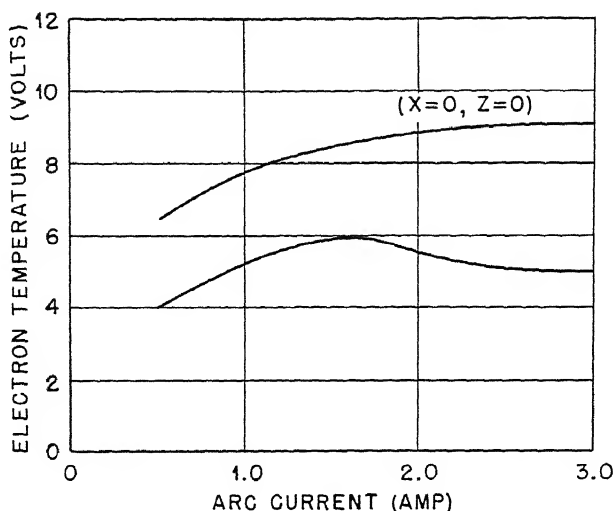


Fig. 9.90—Electron temperature as a function of arc current. Pressure 0.6×10^{-3} mm Hg (curve 1), 3.5×10^{-3} mm Hg (curve 2); magnetic field 3,700 gauss; arc voltage 150 volts.

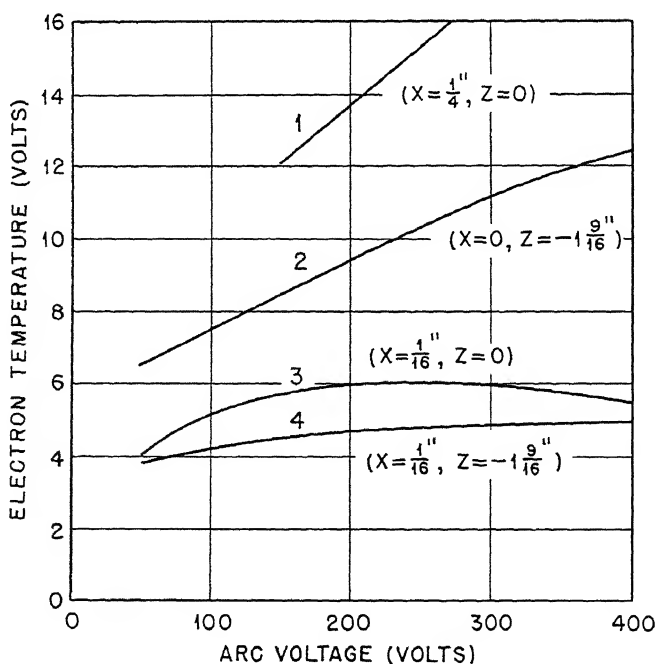


Fig. 9.91—Electron temperature as a function of arc voltage. Pressure 0.6×10^{-3} mm Hg (curves 1 and 2), 3.5×10^{-3} mm Hg (curves 3 and 4). Magnetic field 3,700 gauss; arc current 1.5 amp.

When the curves of Figs. 9.83b to 9.86b for electron temperature are compared with the corresponding curves of Figs. 9.83a to 9.86a for space potential, it is seen that a close correlation exists between the two quantities even with respect to their variation with distance from the arc column. In most discussions of electron temperature it is usually assumed that this quantity does not vary greatly throughout the plasma. However, the present work seems to indicate in general a drop of electron temperature of the order of a few volts in moving away from the arc column to the sheath edge. This variation is probably explicable, since the space potential itself, which drops by about this amount in the same distance, is such as to retard the electrons so that one might expect a corresponding drop in electron temperature.

The curves of Figs. 9.83b to 9.86b appear to bear out in general the conclusions regarding variation of electron temperature with arc conditions observed in the case of the hot probe. An exception, however, is the variation with magnetic field. Thus Fig. 9.83b indicates that for a pressure of 0.6×10^{-3} mm Hg the electron temperature in the case of a magnetic field of 11,400 gauss is slightly greater than for a field of 3,700 gauss. The reason for this apparent anomaly is difficult to understand. However, at a higher pressure (1.4×10^{-3} mm Hg) it was found that the variation of electron temperature with magnetic field was in the expected sense (i.e., it decreased with increase of field).

In the case of the chlorine arc systematic measurements of electron temperature were not carried out. A number of cold-probe characteristics were measured, but great difficulty was experienced in interpreting these owing to the presence of negative ions. In general, electron temperatures of from 1 to 4 volts were estimated from these curves, but insufficient measurements are available to justify any statement concerning the variation of electron temperature with arc conditions in chlorine.

5. HASH OBSERVATIONS

The term "hash" has come to be applied to any time variation of the electrical properties of the arc not controlled by the regulator. In practice very-high-frequency fluctuations (> 1 megacycle) are rarely observed, owing to time attenuation. In these studies no effort has been made to arrange conditions to measure the amplitudes of these high frequencies. By use of the single-sweep-oscillograph method described in Sec. 1 a good survey of the fluctuations of currents in the arc could be made over the frequency range from a few hundred cycles to 1 megacycle. These fluctuations could be observed

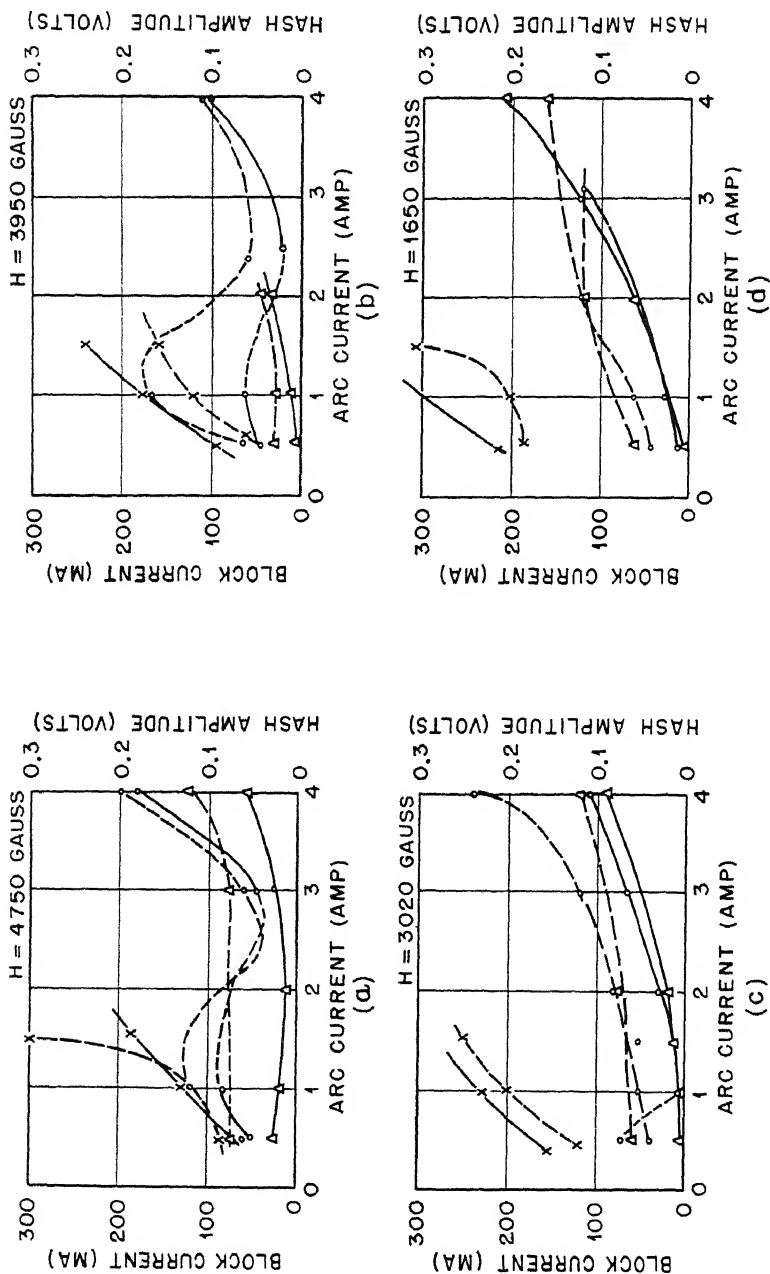


Fig. 9.92—Correlation of block current and hash amplitude in annex arc with argon. Pressure: X, 0.8×10^{-3} mm Hg; O, 1.4×10^{-3} mm Hg; Δ , 2.1×10^{-3} mm Hg; arc voltage 150 volts. Solid lines represent block current. Dashed lines represent hash amplitude.

in the arc current or in the currents to the anode, collimating-slot plate, block, any one of the probing wires over anode or slot plate, and any probe.

5.1 Relaxation Oscillations. (a) Transition Regions. In general, the observed variations could be classified as predominantly a combination of relatively few harmonic oscillations or of a form characteristic of relaxation oscillations. It is probable that, although the harmonic variations represent plasma oscillations, the relaxation effects arise from back-and-forth transitions of the arc between two states that differ in the mode of secondary-electron and ion disposal. The occurrence of transition regions between different modes can usually be closely seen on an oscillograph connected across the arc voltage in the usual way. If one of the arc-control variables is continuously varied, the appearance on this oscillograph normally varies in the following fashion:

Over wide ranges a clean trace exhibiting only low-frequency ripple (60 to 369 cycles) is observed, but at intermediate ranges of values the trace becomes strongly blurred owing to the presence of unresolved disturbances of higher frequency. This region of blurred trace is referred to as a "transition region," as the values of various arc quantities such as block current often exhibit discontinuous variation from one side to the other of such a region. This behavior is illustrated in Fig. 9.92, which exhibits the results of observations made in the Backus arc (Sec. 1.1a). Referring to Fig. 9.92a, it will be seen that with the argon pressure equal to 1.4×10^{-3} mm Hg, a magnetic field of 4,750 gauss, and an arc voltage of 150 volts the block current increases steadily with arc current up to 1 amp. At this current strong instability sets in, and this transition region persists until a current of 3.0 amp is reached. The block current is then found to have fallen to a value considerably less than that obtained on the low-current side of the transition region. The over-all amplitude of the hash exhibits a similar variation. Increase of pressure tends to smooth out the transition region (see curves of Fig. 9.92), and a decrease makes it more marked and more extensive. Reduction of magnetic field tends to reduce the extent of the transition region and also the arc current at which it sets in. The detailed circumstances attendant on transitions seem to be very sensitive to a number of conditions, many of which have not yet been resolved. They were found to occur very definitely in the large arc in argon and in greater variety in chlorine but were also present in the small arc. Examples are given in Table 9.12. These are given only by way of illustration, as it was difficult to reproduce the conditions for a particular transition region from day to day. However, an extensive study was made of the

nature of the fluctuations in the arc and other currents, using the single-sweep oscilloscope, when the conditions were approaching a transition region. It was always found that the approach to such a region was accompanied by the appearance of quite clearly marked relaxation oscillations that grew in amplitude the nearer the conditions approached those for the transition.

Table 9.12—Transition Regions Observed with Different Arcs

Type of arc	Pressure, mm Hg $\times 10^{-3}$	Magnetic field, gauss	Arc voltage, volts	Arc current, amp
Small arc in argon	3.5	11,500	150	0.5 (very narrow), 1.8–4.5
	3.5	11,500	300	0.4–2.4, > 2.8
	3.5	11,500	50	0.7 (very narrow), 1.5–2.7, 3–6
Large arc in argon	3.5	5,500	140	1.0–3.0
	1.4	3,500	200–250	1.5
	1.4	< 2,700	150	1.5
	5.6–42	11,500	150	1.5
Large arc in chlorine	1	3,500	150	0.5 (very narrow), > 2.5
Small arc in oxygen	1	3,500	150	0.4–0.6, > 1.0.

As an illustration take the case of the large arc run with argon at a pressure of 3.5×10^{-3} mm Hg in a magnetic field of 11,600 gauss with an arc voltage of 150 volts. As the arc current was increased, no relaxation oscillations were observed, using the single-sweep oscilloscope, in the arc current or any of the other currents until the arc current reached 1.4 amp. Under these conditions very definite relaxation oscillations appeared on the block and wire currents as well as the arc current. The arc-voltage oscilloscope trace revealed the effect by exhibiting a very pronounced “blurring.” A detailed examination of the arc-current relaxation oscillations showed that they consisted of a change between two states, both exhibiting approximately the same amount of hash in the 20- to 500-kc range, the changes of state occurring about five hundred times a second and the arc continuing in one state (state A) for about 80 per cent of the time. As the arc current increases, the frequency of the relaxation oscillations increases, and the proportion of time spent in the two states tends to become equal and then favors the second state (state B). Eventually the relaxations disappear when the arc current slightly exceeds 3.0

amp. At 3.0 amp they are still present with a relaxation frequency of 1,500 cycles per second, and the greater proportion of the time is spent in the state B. The relaxation oscillations remain absent as the arc current is increased to 4.0 amp.

All this suggests that, while the arc may run with comparative stability in state A until the arc current reaches 1.4 amp, it is no longer able to do so as the current is increased. Similarly, for a range of arc currents beyond 3.0 amp up to at least 4.0 amp, it is able to run stably in state B. In the current range from 1.4 to 3.0 amp no single stable region appears possible, with the result that the arc continually jumps back and forth between the two states, spending relatively more and more time in state B as the arc current increases. The nature of these two regions is not yet clear. It is of interest to notice, however, that observations of the block-current hash showed that in state A the block current was much smaller than in state B. Also the direct current to the block was observed to change sign in going through the transition region, being $+30\mu\text{a}$ at an arc current of 1.6 amp and $-52\mu\text{a}$ at 3.0 amp. This strongly suggests that state B differs markedly from state A in the mode of disposal of the secondary ionization.

Effects generally similar to the above were observed under a number of circumstances. It is of interest that in some cases the relaxations seemed to indicate that the arc was going on and off rhythmically; in others it seemed to be jumping between two different states. This was indicated by the fact that the higher-frequency hash (20 to 500 kc) could be observed in the latter cases at all parts of the cycle, though often at different amplitude in the different states, whereas in the former during the "Off" part of the cycle no such hash was apparent.

In the absence of a detailed investigation aimed at identifying the properties distinguishing the different states of the arc, it has usually not proved possible to understand the underlying details of the phenomenon. It is believed, however, that the states may differ in the degree of asymmetry, or in quality and quantity of the hash associated with transport of space charge across the magnetic field. This point should be studied in much greater detail. In the important case of low pressures and arc voltages, however, the situation is clearer and will now be described.

(b) Relaxation Oscillations at Low Pressure and Arc Voltage; Pressure and Voltage Thresholds for Stable Arc Operation. In order that an arc current equal to J_c should be supplied by the cathode it, in turn, must be fed by a positive-ion current J_+ given by

$$\frac{J_+}{J_c} \geq \alpha \sqrt{\frac{m_e}{m_+}} \quad (48)$$

where m_e and m_+ are the respective masses of electrons and positive ions and α is a number probably between 1 and 10 dependent on filament conditions. We may write

$$J_+ = \phi(J_c) \psi(J_v) p f_k \quad (49)$$

where $p\phi(J_c)\psi(J_v)$ is the rate of ion production by the electron column, f_k is the fraction of such ions reaching the filament, p is the gas pressure, and $\phi(J_c)$ represents the effect of varying J_c . For low J_c it is proportional to J_c but tends to saturation as the current is increased to such a value as to produce practically complete ionization of all neutral molecules passing through the arc column. $\psi(J_v)$ represents the effect of arc voltage due to the dependence of rate of ionization on electron energy. In general, $\psi(J_v)$ has the form illustrated in Fig. 9.93 if primary ionization alone is considered. Secondary ionization can occur if the mean energy of the secondary electrons resulting from the first ionization is sufficiently high.

Comparing Eq. 49 with 48, we see that

$$p f_k \psi(J_v) \frac{\phi(J_c)}{J_c} \geq \alpha \sqrt{\frac{m_e}{m_+}} \quad (50)$$

and for fixed J_v , J_c , and f_k it follows that the arc must go out if the pressure falls below a certain critical value p_c for which Eq. 50 becomes an equality. The running pressure may be reduced below this value if f_k increases in some way, e.g., by a change of state of the arc. Hence, if J_v and J_c are kept constant and the pressure is reduced, a condition must be reached in which the arc either goes out or changes state to one in which f_k is increased. In the latter event we may expect relaxation oscillations to set in in the intermediate region.

A somewhat similar behavior might be expected if J_v is gradually reduced, keeping p and J_c constant. Eventually $\psi(J_v)$ will fall to such a value that Eq. 50 becomes an equality. Any further reduction of J_v will cause the arc to go out or change its state. In this case the change of state may either be to one increasing f_k or increasing ψ by increasing the contribution from secondary ionization. Thus we would expect to find relaxation effects arising at sufficiently low J_v for a given p and J_c .

The behavior as regards J_c is rather different. For small J_c , relationship 50 is practically independent of J_c , but sufficient increase of J_c will lead to such reduction of $[\phi(J_c)]/J_c$ that relationship 50 can hold only if f_k or $\psi(J_v)$ is increased. Effects of this sort may well be responsible for the transitions occurring at arc currents of 1.5 amp or more as illustrated in Fig. 9.93, but the evidence on this matter is still not conclusive. A more detailed theory of these effects is given in Chap. 4, "Theoretical Considerations Regarding Minimum Pressure for Stable Arc Operation."

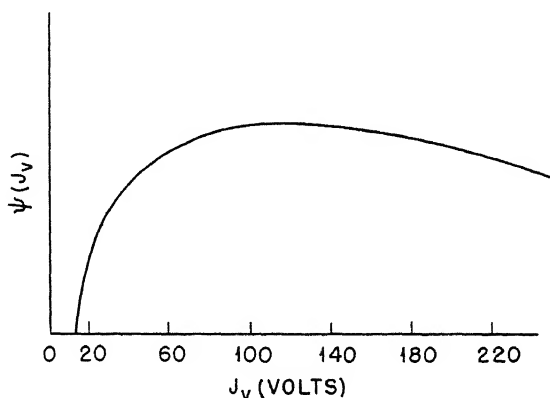


Fig. 9.93 — Behavior of $\psi(J_v)$ as function of arc voltage; primary ionization only.

In view of the above considerations a study was made of the threshold running conditions of the arc with regard to both pressure and arc voltage with the following results: With the highest magnetic field (11,500 gauss) the observed relation between threshold pressure and arc voltage for an argon arc is illustrated in Fig. 9.94. This was found by setting the pressure to a definite value and then increasing the voltage until the arc struck and yielded an arc current of 1.0 to 1.5 amp. In this range there was little dependence on current, showing that $[\phi(J_c)]/J_c$ of relationship 50 was effectively constant. A study of the stability of the arc near the threshold conditions showed that strong relaxation oscillations were present. When the conditions were adjusted so that the arc was on the point of going out, these oscillations usually seemed to correspond to rhythmical extinguishing and lighting up of the arc, no higher-frequency hash being observed during one part of the cycle. Increase of pressure or voltage above the threshold then changed the relaxation effects to jumps between two states of the arc, higher-frequency hash being observed at all parts of the cycle, though often differing in intensity in the two states.

Further increases of pressure led to complete disappearance of the relaxation oscillations.

Observations were also made of the threshold conditions at a reduced magnetic field (3,700 gauss); the results are illustrated in Fig. 9.94. It will be seen that high magnetic field favors low threshold pressure and arc voltage. This is because the quantity f_k in Eq. 49 increases with magnetic field owing to increased difficulty of diffusion of ions and electrons perpendicular to the field.

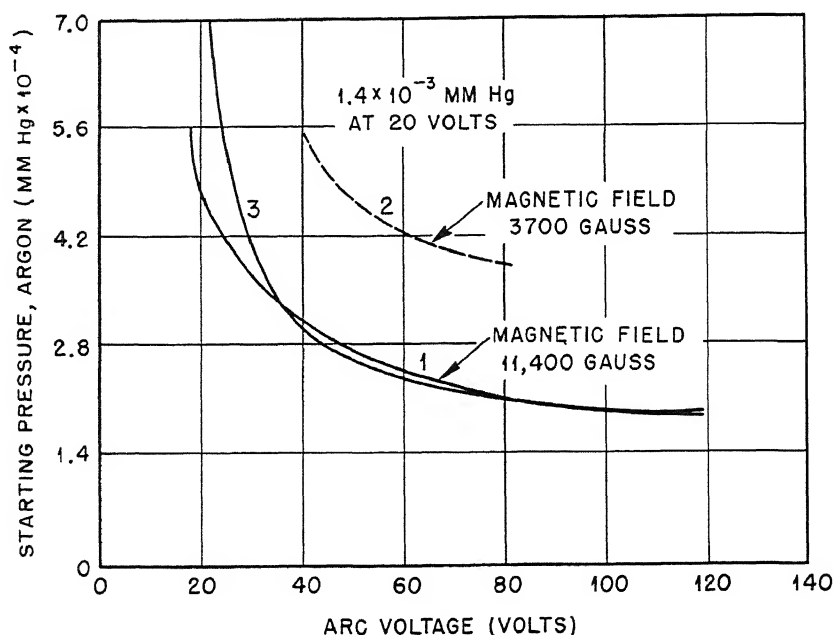


Fig. 9.94—Starting pressure of argon for small arc as function of arc voltage. Magnetic field 11,400 gauss (curve 1), 3,700 gauss (curve 2). Theoretical curve (curve 3) is based on the assumption of only primary ionization.

In obtaining curves of the type illustrated in Fig. 9.94 it is necessary to determine consistently the condition for striking the arc, not extinguishing it. Once a steady arc is running under conditions above the threshold, it is usually possible by careful operation to reduce conditions somewhat below the threshold before the arc goes out.

It is also necessary to note that, for a small range of pressure just below threshold, it was often possible to run a very pale, weak arc of current strength about 0.2 to 0.4 amp. This was usually accompanied by a rise of arc voltage and occurred frequently as a jump from a

low-voltage high-current state in which strong relaxation oscillations were apparent to a low-current high-voltage state with no such oscillations when the pressure was slightly reduced below threshold conditions. The situation is the same as that which would result if the second state, which begins to appear as the threshold is approached, could tide over the ion shortage for only a limited field of pressure. Below this state the arc current runs with current greater than a fraction of the normal current.

According to relationship 50, if f_k is constant the curves of Fig. 9.94 should be given by the equation

$$p\psi(J_v) = \text{const.} \quad (51)$$

If it may be supposed that all ionization produced is primary, then $\psi(J_v)$ must have the same form as the ionization cross section as a function of energy. Taking this to be so, using the known ionization cross sections for argon and adjusting the constant in Eq. 51 so that agreement with curve 1 of Fig. 9.94 is reached at an arc voltage of 120 volts, curve 3 would be obtained. It will be seen that the observed starting pressures are in agreement with the assumption of primary ionization except at low arc voltage. Here the arc is able to run at pressures considerably smaller than would be expected on the assumption that primary ionization alone is important. The effect is somewhat analogous to low-voltage arcs, which may be run with arc drop less than the ionization potential of the gas. In these the plasma-potential gradients are abnormally large, and consequently a considerable fraction of the electrons in the discharge have sufficient energy to produce ionization and thus maintain the discharge. It is possible that the two states involved in the relaxation oscillations that run near threshold conditions do in fact differ, in that normal low potential gradients with little secondary ionization exist in the first, which is dominant when conditions are far from the threshold, and high gradient and large secondary ionization exist in the second, which becomes more and more prominent when threshold conditions, with resulting ion scarcity, are approached.

Some observations were made of the effect of resistance in series with the arc on the relaxation oscillations that occur at low pressure and arc voltage. With the pressure at 0.56×10^{-3} mm Hg, magnetic field at 3,500 gauss, arc voltage at 40 volts, and arc current at 1.5 amp, the relaxation oscillations observed had the form shown in Fig. 9.95 when no series resistance was present. Table 9.13 shows the effect of introducing series resistances of different magnitude. The general effect of series resistance would be to maintain the arc in

operation as observed, for, as the arc current tends to drop, the voltage across the arc will tend to rise and thus help to maintain the arc.

Some observations were made in an attempt to compare threshold pressure conditions for arcs with symmetrically and unsymmetrically placed straight collimating slots and with curved collimating slots. Within the accuracy of determination, which was not high, no differences were found.

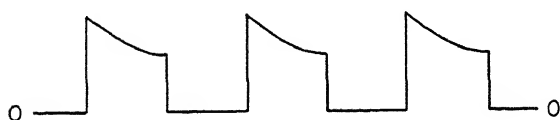


Fig. 9.95—Relaxation oscillations. Pressure 5.6×10^{-4} mm Hg; magnetic field 3,500 gauss; arc voltage 40 volts; arc current 1.5 amp. No series resistance.

Table 9.13

Series resistance, ohms	Length of complete cycle, sec $\times 10^{-4}$	Fraction of cycle during which arc is on
0-15	8.5	0.33
15	7	0.42
19	1.4	1.00
25	1.0	1.00
30-60	0.83	1.00

Form changes
to regular
oscillations

(c) Arc Starting Conditions in Chlorine. No detailed study of the threshold conditions for running the arc in chlorine was made, but it was found possible to strike the Cl_2 arc at a pressure of 8×10^{-4} mm Hg and even a little lower. In view of the lack of steadiness of conditions in these experiments, due probably to chemical actions, etc., the fact that a reasonably steady arc could be struck at these pressures indicates that there is nothing substantially different in this respect between the argon and chlorine arcs.

5.2 Plasma Oscillations. Under this heading we include all those oscillations observed with the single-sweep oscilloscope which were not obviously of relaxation form and were of frequency 20 kc or greater. Theory indicates that "electrical sound waves," consisting of ionic as distinct from simple electronic oscillations, can have frequencies from about 20 kc to 5 mc. There was evidence that some

oscillations of frequency 40 kc were of relaxation type, as they appeared as the result of continuous increase of frequency with changing conditions of true low-frequency relaxations. In any case, at these frequencies the distinction largely disappears. The major part of the investigations was concentrated on arc-current hash, but the distribution in amplitude and frequency of the hash as observed in the anode, block, and wire currents was also studied to a considerable extent. The results may be summarized as follows:

(a) Small Arc in Argon. (1) Arc-current Hash. In general it was found that this consisted of a medium-frequency region (100 to 300 kc) always present to a considerable degree with variable admixture of a lower frequency (20 to 60 kc) and higher frequency (1 to 2 mc). No extensive studies were made of the latter as its amplitude was always small, possibly because of line attenuation. The 100- to 300-kc band will be referred to henceforth as medium frequency and the 20- to 60-kc band as low frequency.

The following is a summary of the results obtained concerning the frequency and amplitude of the medium- and low-frequency hash observed in the small arc in argon with symmetrically placed collimating slots. As the observations are extremely difficult, owing to the complexity of the trace observed in many cases, some of the correlations mentioned are not sufficiently definite to be regarded as more than indications. Some of the relations are exhibited graphically in Figs. 9.96 to 9.97.

A. Medium-frequency Hash (100 to 300 kc); Variation of Frequency.

1. Tends to increase with pressure (see Fig. 9.96).
2. Passes through a minimum as the magnetic field increases, an effect more marked at the higher pressures (see Fig. 9.96).
3. At a pressure of 3.5×10^{-3} mm Hg, magnetic field of 10,500 gauss and arc current of 1.5 amp, the frequency appeared to decrease from the 200- to 300-kc region to the 100- to 200-kc region as the arc voltage increased from 50 to 300 volts. The generality of this result is unknown.

4. No correlation was found with arc current.

Variation of Amplitude. The order of magnitude may be seen from the diagrams of Figs. 9.96 and 9.97, in which the hash amplitude is given as a fraction of the direct arc current.

1. Decreases sharply as pressure increases from 2.8×10^{-3} to 5.6×10^{-3} mm Hg and then remains roughly constant (see Fig. 9.96).
2. For low magnetic fields the amplitude decreases rapidly with increasing field to a sharp minimum in the neighborhood of 3,500 gauss. For the lower arc currents it then increases steadily up to the greatest fields that could be attained (12,000 gauss). At higher cur-

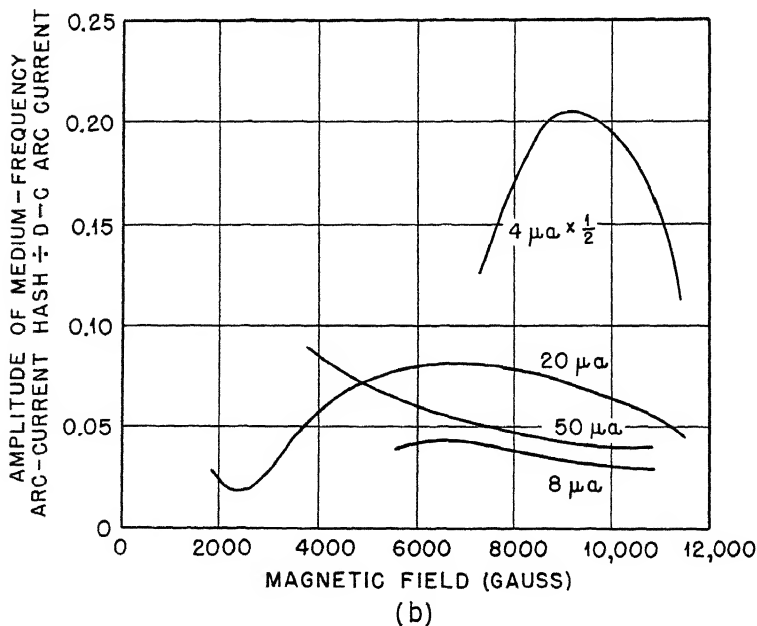
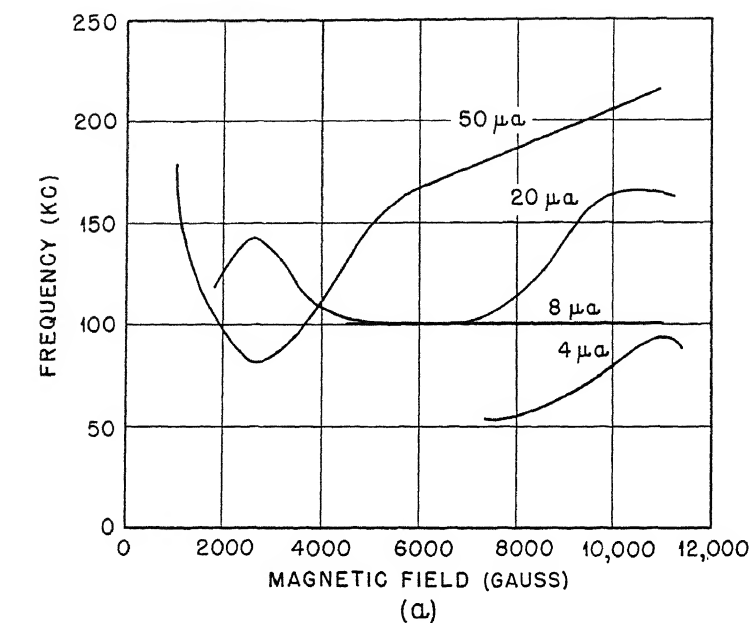
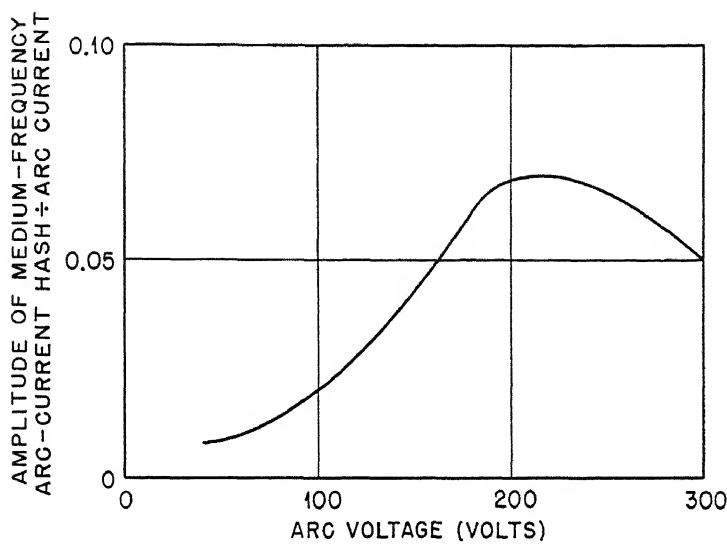
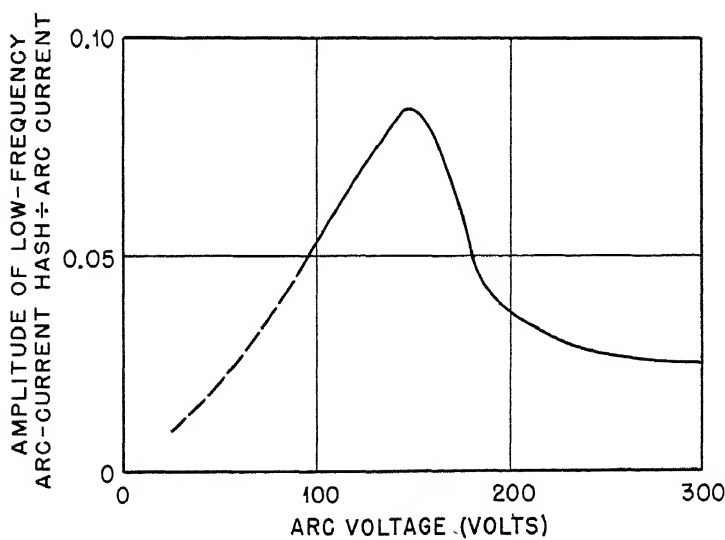


Fig. 9.96—Variation of frequency and amplitude of medium-frequency hash with magnetic field and pressure for small arc in argon. Arc voltage 150 volts; arc current 2 amp. $1 \mu\text{a} = 0.71 \times 10^{-4}$ mm Hg.



(a)



(b)

Fig. 9.97—Variation of amplitude of medium- and low-frequency hash with arc voltage for small arc in argon. Pressure 3.5×10^{-3} mm Hg; magnetic field 10,700 gauss; arc current 1.5 amp.

Table 9.14 — Distribution of Current Hash in Small Arc in Argon

Pressure, mm Hg $\times 10^{-4}$	Magnetic field, gauss	Arc voltage, volts	Arc amplitude		Anode amplitude		Block amplitude		Wire 3 amplitude		Wire 6 amplitude	
			D-c, amp	Hash, amp	D-c, amp	Hash, amp	D-c, amp	Hash, amp	D-c, ma	Hash, ma	D-c, ma	Hash, ma
Arc voltage 150 volts; arc current 1.5 amp												
5.6	3,700	150	1.5	0.045	1.38	0.023	0.30	0.018	-68	2.5	-0.4	0.15
5.6	11,800	150	1.5	0.038	1.25	0.068	0.15	0.027	-28	8.0	-2.2	1.7
14	3,700	150	1.5	0.075	1.45	0.031	0.59	0.028	-60	4.3	-0.4	1.1
14	11,800	150	1.5	0.035	1.18	0.045	0.23	0.027	-76	5.0	-2.8	3.6
Magnetic field 3,700 gauss; arc current 1.5 amp												
5.6	3,700	150	1.5	0.045	1.38	0.023	0.30	0.018	-68	2.5	-0.4	0.15
5.6	3,700	300	1.5	0.045	1.25	0.042	0.45	0.035	-81	3.4	-0.1	0.24
14	3,700	50	1.5	0.037	1.31	0.014	0.34	0.009	-68	1.2	-0.3	0.55
14	3,700	150	1.5	0.075	1.45	0.031	0.59	0.028	-60	4.3	-0.4	1.1
14	3,700	300	1.5	0.025	1.18	0.015	0.58	0.028	-86	6.0	-0.1	1.1
Magnetic field 3,700 gauss; arc voltage 150 volts												
5.6	3,700	150	0.5	0.006	0.45	0.013	0.11	0.007	-10	1.3	-0.10	0.10
5.6	3,700	150	1.5	0.045	1.38	0.023	0.30	0.018	-68	2.5	-0.4	0.15
14	3,700	150	0.5	0.008	0.5	0.014	0.22	0.014	-20	1.0	+0.15	0.02
14	3,700	150	1.5	0.075	1.45	0.031	0.59	0.028	-60	4.3	-0.4	1.1
14	3,700	150	3.0	0.180	2.55	0.043	0.85	0.036	-100	5.0	+0.55	1.5

rents it appears to reach a maximum at some intermediate field and is falling again at the highest fields.

3. Increases with arc voltage up to 200 volts, after which it slowly decreases. This has been varified in detail at one pressure (3.5×10^{-3} mm Hg) (see Fig. 9.97) but seems to hold also at lower pressures (see Table 9.14).

4. Increases roughly as the arc current, but the constants of proportionality change in passing through a region in which strong relaxation oscillations occur.

B. Low-frequency Hash (20 to 60 kc). As pointed out above, it is not at all easy to determine when oscillations in this frequency range are of relaxation character or not, and it may be that the distribution has not much meaning when the frequency falls within the range of possible plasma frequencies. For this reason we place the lower limit of frequency as 20 kc and count anything lower as relaxation in character. Observations in the small arc showed that at pressures below 1.4×10^{-3} mm Hg of argon very little low-frequency hash, defined in this way, is present in the arc current, but at higher pressures it becomes apparent. Below 1.4×10^{-3} mm Hg the low-frequency hash has such a long period as always to be counted as of relaxation type. The lower the magnetic field, the higher the pressure at which the frequency exceeds 20 kc. For example, at a pressure of 3.5×10^{-3} mm Hg with an arc voltage of 150 volts and arc current of 2.0 amp, the low frequency fell below 20 kc when the magnetic field was decreased below 3,000 gauss. Figure 9.97 illustrates the variation in amplitude of the low-frequency hash with arc voltage, the arc running at a pressure of 3.5×10^{-3} mm Hg in a magnetic field of 10,700 gauss with 1.5 amp arc current. Figure 9.98a illustrates the variation with magnetic field, the arc running at the same pressure with 150 volts arc voltage and 2 amp current. The variation with arc current is normally complicated by transitions of state in the arc, but in Fig. 9.98b a comparatively smooth variation is illustrated for a low arc voltage of 50 volts, the pressure being again 3.5×10^{-3} mm Hg and the magnetic field 10,700 gauss.

Under some conditions a very pure harmonic oscillation could be obtained in the low-frequency range, usually about 40 kc. Thus at a pressure of 3.5×10^{-3} mm Hg, an arc voltage of 50 volts, and a magnetic field of 10,700 gauss a very pure oscillation of this frequency was observed at an arc current of 3.0 amp (see Fig. 9.98b). The conditions for production of these nearly pure oscillations were very critical.

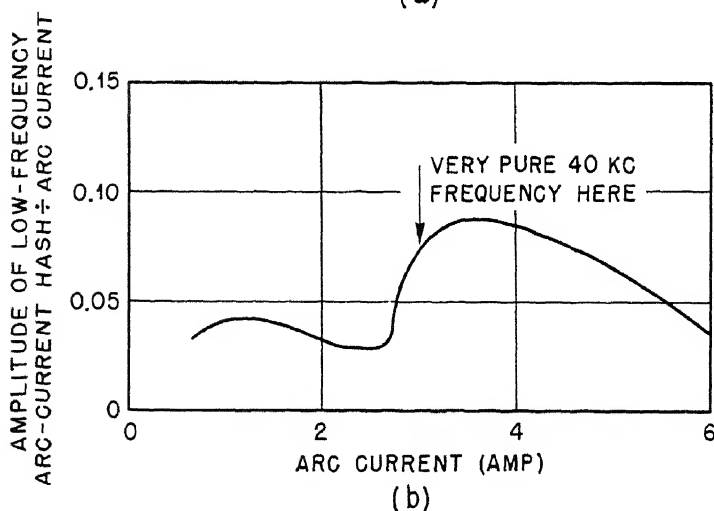
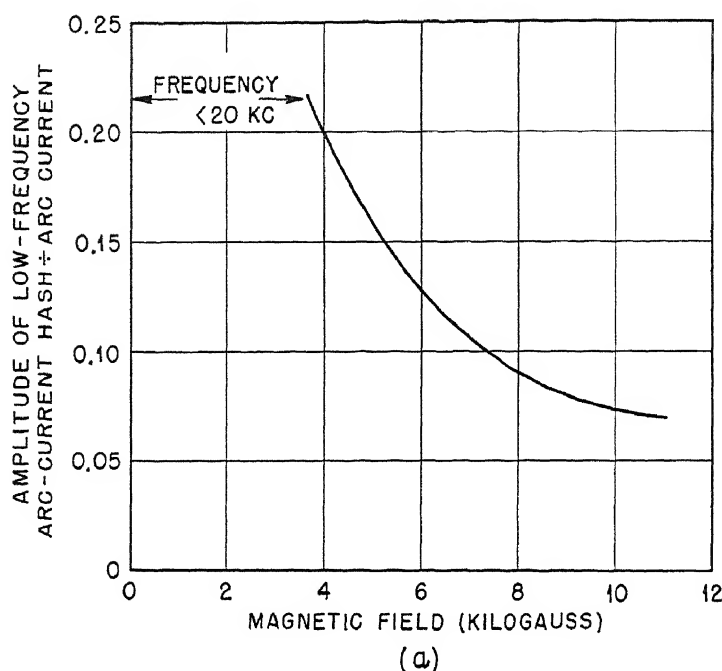


Fig. 9.98—Variation of amplitude of low-frequency hash with arc current for small arc in argon. (a) Pressure 3.5×10^{-3} mm Hg; arc voltage 150 volts; arc current 2 amp. (b) Pressure 3.5×10^{-3} mm Hg; magnetic field 10,700 gauss; arc voltage 150 volts.

(2) Distribution of Current Hash. The general conclusion from a study of the distribution of the hash among anode, block, and wire currents was as follows: The current hash on the outer wires and block currents often included quite strongly a component of frequency about twice as great as that referred to previously as medium frequency, i.e., it was in the range 400 to 600 kc. This component was occasionally observed in the anode and arc currents but very much less clearly. It seems that these higher-frequency oscillations were not present to any appreciable degree in the arc column but became important at some lateral distance from it. (See also the following section on analysis of hash distribution in large arc.)

Table 9.14 summarizes a set of observations made to determine the amplitude distribution of current hash throughout the small arc in argon under various conditions. The amplitude referred to is the over-all amplitude irrespective of frequency.

It will be seen from Table 9.14 that under all the conditions listed, which involved apparently stable arcs (no relaxation oscillations present), the amplitude of the arc-current hash was rarely more than 5 per cent of the arc current and often considerably less. A similar result was found for the hash on the anode current. Unlike the arc current, however, the anode-current hash was found to become more important at higher magnetic fields than at lower, as will be seen by reference to the upper part of Table 9.14. The same dependence on magnetic field was found for block-current hash. Thus in Table 9.14 it will be observed that at 5.6×10^{-4} mm Hg pressure the ratio of block-current hash amplitude to direct block current increases from 0.06 to 0.18 as the magnetic field increases from 3,700 to 11,800 gauss. At 1.4×10^{-3} mm Hg pressure the increase is from 0.047 to 0.12. In general, this ratio is higher than for the anode and arc currents. No very definite correlations of the hash amplitude with arc voltage or current were found.

As far as the hash observed on the current to wire probes 3 and 6 (see Fig. 9.3) is concerned, the two most striking results are: (1) the hash amplitude falls off much more slowly with distance from the arc column than does the direct current to the wires; (2) the importance of the hash increases as the magnetic field increases, particularly at low pressures on the outer wire. Again no very definite correlations with arc voltage or current were found.

It seems likely from these observations that part of the oscillations present in the arc are associated with the flow of ions and electrons normal to the magnetic field; these oscillations have a frequency of the order 400 kc and increase in amplitude to maintain the transverse

flow when the magnetic field is increased. In this connection it is of interest to note that in some conditions strong relaxation oscillations were observed in the current to the outer wires when it was hardly perceptible in the arc-current hash. This suggests that the need for disposing of the ions and electrons at the walls of the arc chamber may also be a factor important in producing relaxation effects, apart from the need for supplying the necessary ion current to maintain the double sheath at the filament (see also Sec. 5.2b). A detailed study of plasma oscillations has shown that plasma instabilities exist which may result in oscillations of the type observed and which account in order of magnitude for the observed rate of electron diffusion across the magnetic field.

(b) Large Arc in Argon. In general, the plasma oscillations observed with the large arc in argon were qualitatively similar to those with the small arc, but some effects obtained were more marked. Thus the arc-current hash included mainly the medium- and low-frequency components described for the small arc, but the 400-kc component was even less marked in the arc-current hash than with the latter arc. On the other hand, the block- and wire-current hash included this 400-kc component far more definitely in the case of the large arc, other conditions being the same. The medium frequency of about 200 kc was often almost entirely absent in these cases. Under conditions where relaxation oscillations were weak, the amplitude of the hash on the arc current never exceeded 16 per cent, but this value is somewhat higher than the corresponding one for the small arc. Therefore it may be that the large arc chamber reduces the inherent stability of the system, but insufficient data are available to establish this with certainty.

The amplitude of the hash observed on the block and wire currents is relatively large compared with the direct currents, as might be expected from the comparatively great distance ions and electrons must move perpendicular to the magnetic field before collection in these cases.

Under some conditions a clear correlation was observed between the variation with arc current of the direct block current and the amplitude of one of the main frequency components of the hash. Thus in Figs. 9.99 to 9.102 an analysis of the amplitudes observed in block and wire currents is given in terms of functions of the direct arc current. Three types of hash are distinguished: relaxation, low frequency (20 to 80 kc), and medium frequency. In a number of cases a correlation was observed between the variation with arc current of the direct current to the block or a wire and that of the amplitude of one of the main frequency components of the hash. As before, these

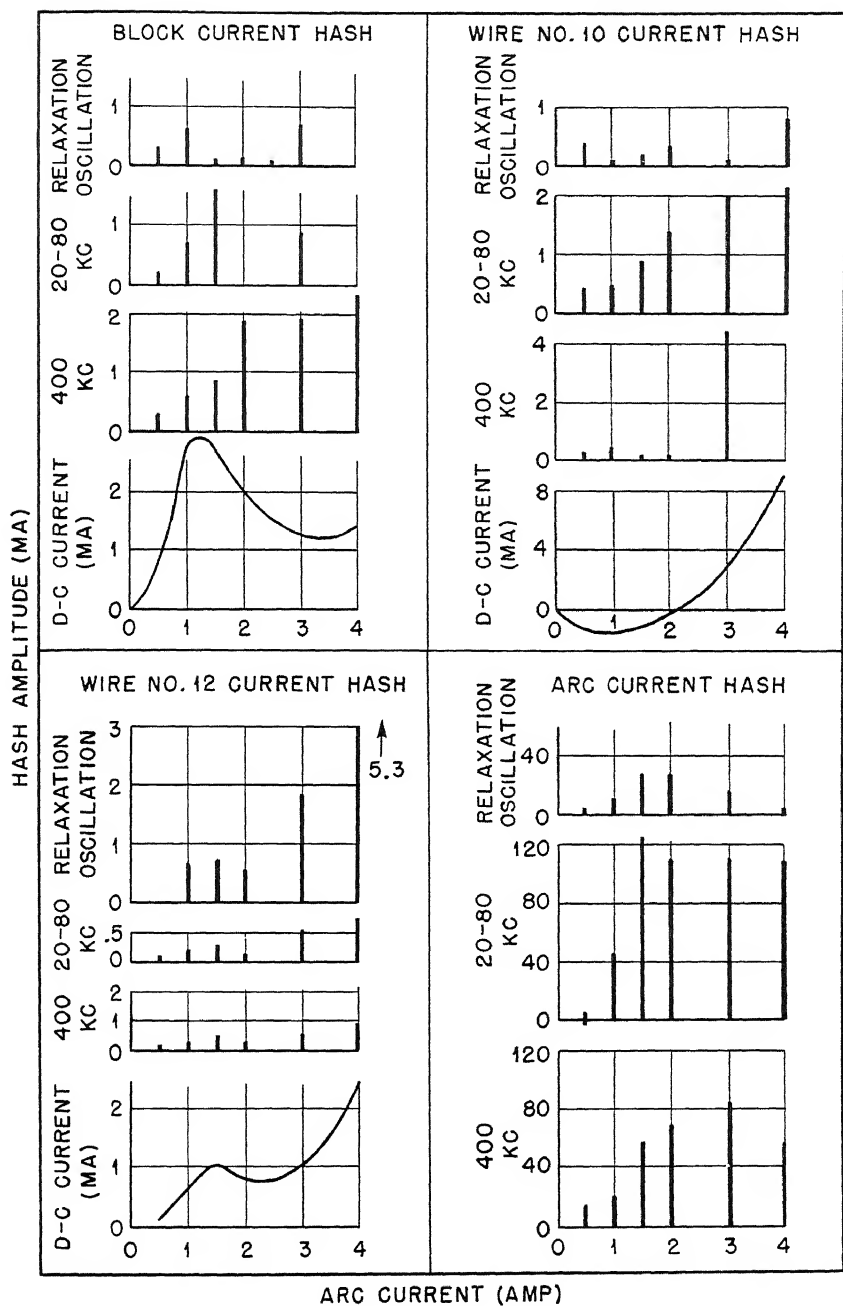


Fig. 9.99—Hash correlations for large arc in argon. Pressure 5.6×10^{-4} mm Hg; magnetic field 3,700 gauss; arc voltage 150 volts.

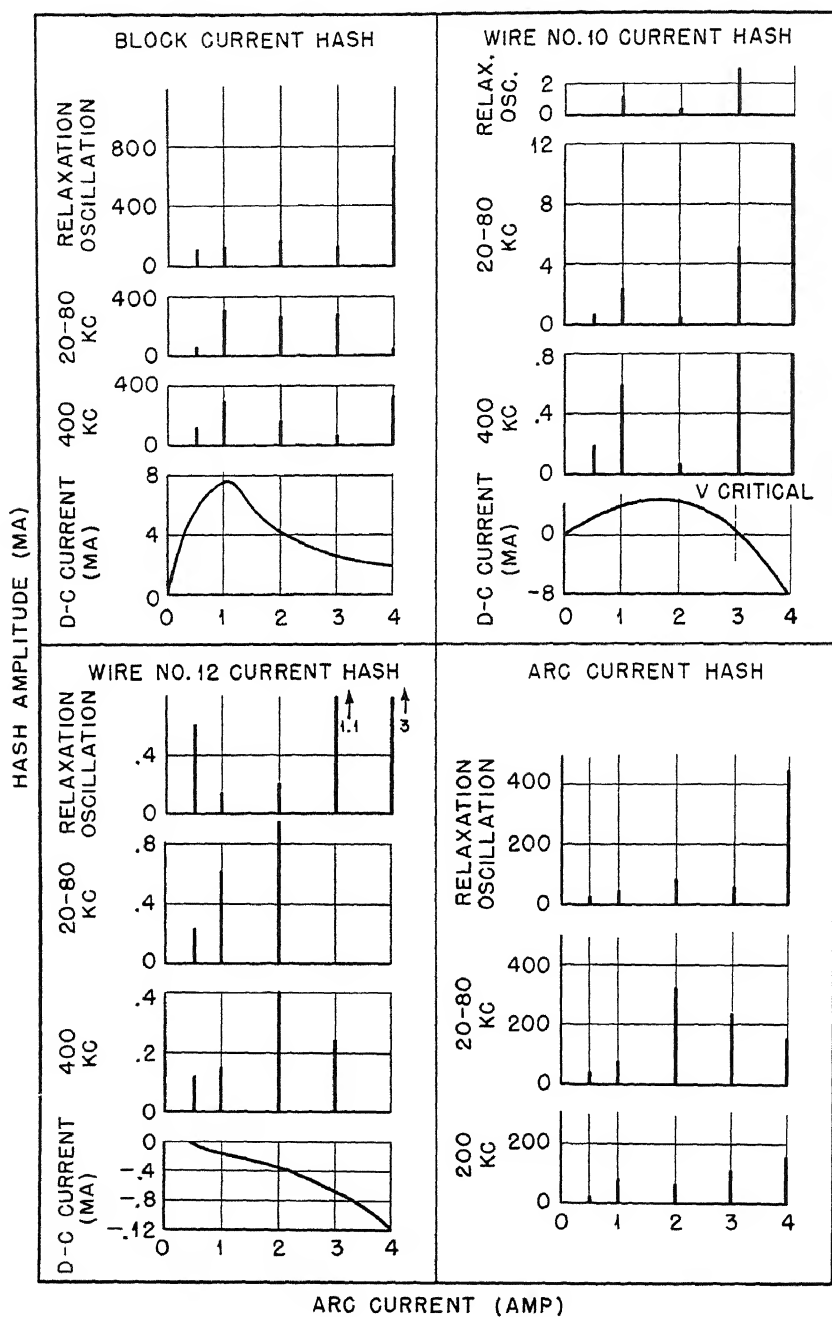


Fig. 9.100—Hash correlations for large arc in argon. Pressure 1.4×10^{-3} mm Hg; magnetic field 5,500 gauss; arc voltage 150 volts.

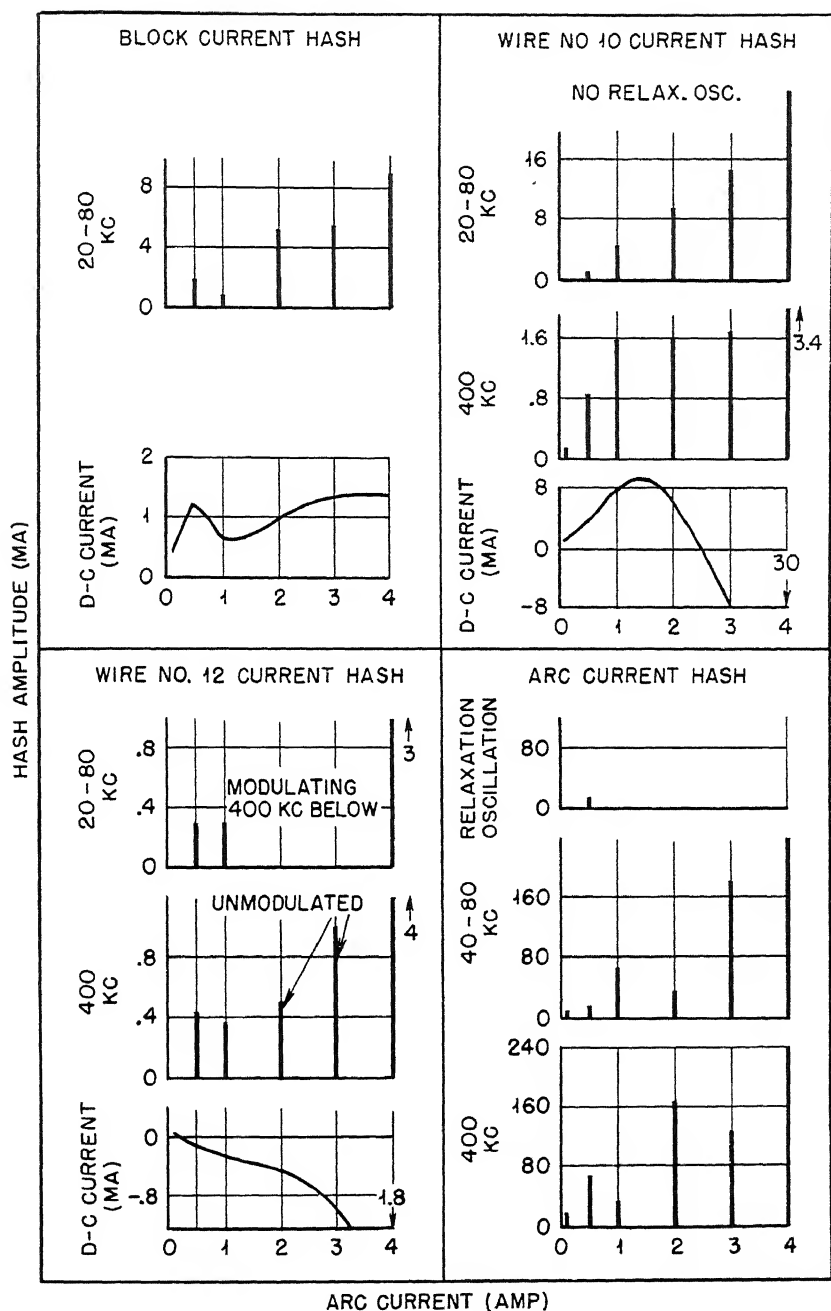


Fig. 9.101—Hash correlations for large arc in argon. Pressure 3.5×10^{-3} mm Hg; magnetic field 5,500 gauss; arc voltage 150 volts.

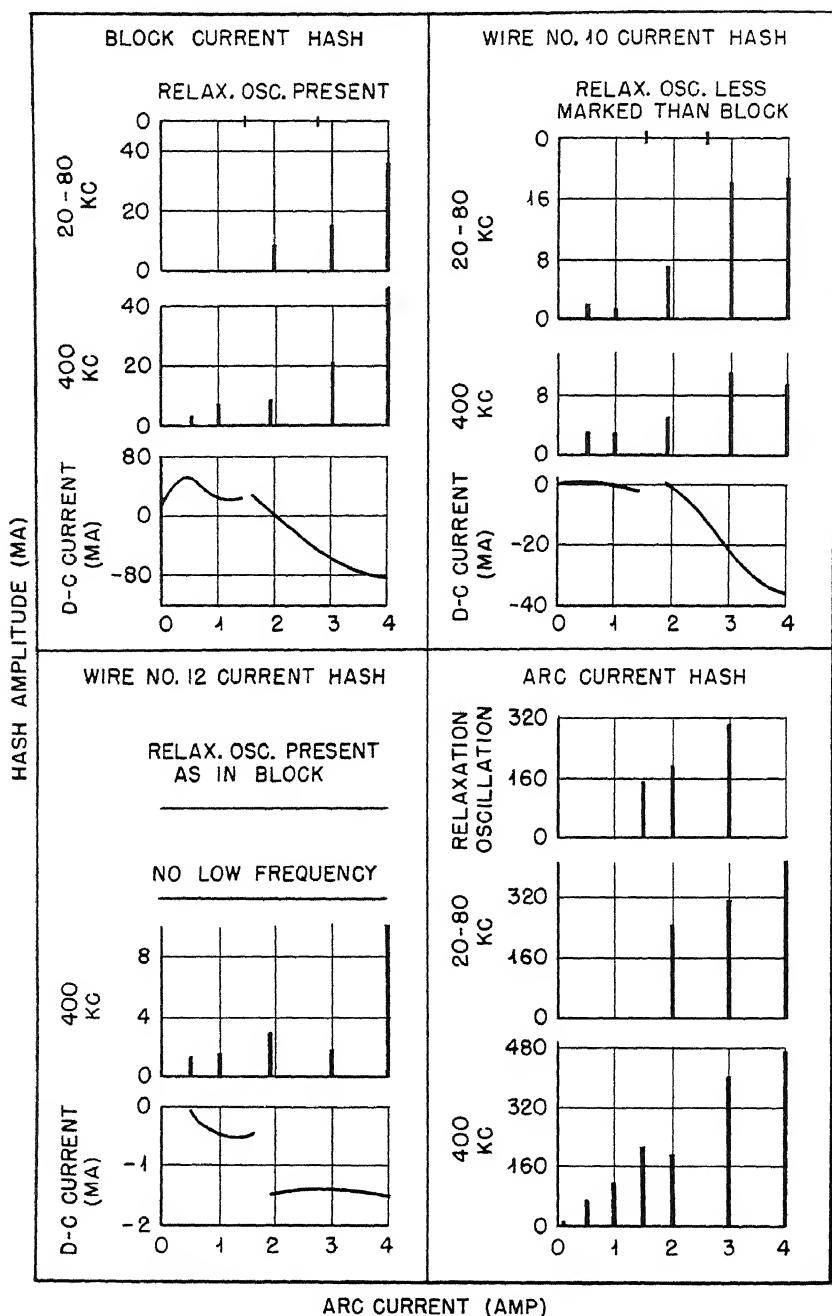


Fig. 9.102—Hash correlations for large arc in argon. Pressure 3.5×10^{-3} mm Hg; magnetic field 11,700 gauss; arc voltage 150 volts.

are distinguished as relaxation, low-frequency (20 to 80 kc), and medium-frequency (about 400 kc) types. Table 9.15 summarizes the correlations found, and Figs. 9.99 to 9.102 illustrate the data from which the table has been compiled. It appears that the low-frequency

Table 9.15—Correlations Observed between Hash Amplitude and Direct Currents to Block and Wires for Large Arc in Argon

Pressure, mm Hg $\times 10^{-3}$	Magnetic field, gauss	Arc voltage, volts	Hash amplitude correlation			Reference
			With d-c current to block	With d-c current to wire 10	With d-c current to wire 12	
0.56	3,700	150	20-80 kc	400 kc	Relaxations	Fig 9.99
1.4	5,500	150	20-80 kc	No clear cor- relation	Relaxations	Fig. 9.100
3.5	5,500	150	20-80 kc	No clear cor- relation	400 kc	Fig 9.101
3.5	11,700	150	No clear cor- relation but exhibits a discontinuity in a region of strong relaxation oscillations	As for block	Exhibits a very marked dis- continuity in the region of strong re- laxation os- cillations, correlates with 400 kc at high arc currents	Fig. 9.102

(20 to 60 kc) oscillations normally play an important role in producing current flow to the block, but it seems that the medium-frequency (400 kc) oscillations can also play a part. Similarly for the outer wire (12) a large portion of the current seems derived from relaxation oscillations. In many of the cases observed the hash amplitude considerably exceeds the direct current. The discontinuity observed, for the highest magnetic field and pressure, in the block and wire currents in going through a range of arc currents associated with strong relaxation effects is in accord with the assumption that these effects arise primarily at a transition between two states of the arc plasma differing in the mode of ion and electron disposal. The difference may be partially in the type of asymmetry of equipotentials, as discussed in Sec. 4, and partly in the type and magnitude of the 400-kc or other components of the hash, which can also move ions and electrons to the wall.

(c) Small and Large Arcs in Chlorine. The observations made on the hash distribution in arcs running with chlorine did not cover such a wide range of variables as with argon, but the results obtained for both small and large arcs showed that the same classification of hash

remained appropriate, namely, relaxation oscillations, low-frequency oscillations (20 to 60 kc), and medium-frequency oscillations (about 200 kc on arc current, higher frequency on block and outer wires). In general, there appeared to be more transition regions than with argon, but there was no evidence of a greater proportion of low- or medium-frequency hash in regions where relaxation oscillations were weak or absent than with argon. Insufficient evidence was obtained, however, to establish this definitely.

5.3 Comparison of Hash Observed with A-c and D-c Arc Supplies.

In order to determine whether the residual ripple present in rectified a-c supplies to filament and arc voltage had any effect on the quantity and quality of the hash in the arc, a direct comparison was made by arranging alternative supplies from batteries of accumulators. The arc conditions for the experiment were: pressure 4.2×10^{-3} mm Hg, magnetic field 3,700 gauss, arc voltage 140 volts, arc current 1.05 amp, and the small arc in argon. Under these conditions a strong 60-cycle component was observed on the arc-voltage scope with a-c heating. Nevertheless no difference, within the reproducibility of the experiment, could be seen between either the quality or quantity of the hash for the arcs with a-c and d-c supplies. This result was found not only for the arc-current hash but also for that on the block current or current to wire 6. A further comparison was made with the same magnetic field and arc voltage, but with pressure reduced to 9.1×10^{-4} mm Hg and arc current reduced to 0.55 amp, and again no difference was detected.

6. CONTROL OF THE ARC BY POTENTIALS APPLIED TO THE BLOCK AND WIRE ELECTRODES IN THE ARC

6.1 Application of Block Potential, General Discussion. A series of measurements was carried out on the effect of applying potential differences between the side walls (or block) of the arc chamber and the anode. Potential differences were also applied between the wire electrodes at the top and bottom of the arc chamber and the anode, and the effects were observed. In all these experiments the anode was connected to the collimating slot. Qualitatively the effects observed were as follows:

As the potential of the block was made positive relative to the anode and collimating slot, the potential of the whole plasma tended to rise with it. The potential of the plasma increased less rapidly than the block potential at first, however, so that at a block potential of about 15 volts positive relative to the anode the space potential throughout the whole plasma was about equal to the block potential.

As the block potential was raised still further, the plasma potential went slightly negative relative to it and remained a couple of volts negative relative to the block potential up to potentials above +50 volts. On the other hand, when the block voltage was made negative relative to the walls of the arc chamber, the plasma potential remained about constant. Thus the plasma potential tended to follow the potential of the most positive wall of the arc chamber.

The current to the side walls of the arc, which was positive in sign under normal conditions, rapidly decreased as the block voltage was made positive and passed through zero at about +6 volts. This, then represents the floating potential of the block. In individual cases in the small arc the floating potential of the block varied from +4 to +10 volts but generally was about +6 volts. There was no obvious correlation between floating potential and arc conditions.

The application of positive block voltage also had a marked effect on the asymmetry of the ion distribution in the arc. As has been seen above, under normal conditions with the block and anode at the same potential the ion density showed a maximum on the antidrain side of the front of the arc column. As the block potential was made positive relative to the anode, the asymmetry ratio decreased until at a block potential of about +15 volts it had disappeared. If the block voltage was raised still further, the asymmetry ratio was found to decrease below unity, corresponding to the occurrence of the maximum ion density on the drain side.

At a point on the central transverse axis of the arc chamber the application of positive block voltage had a marked effect on the absolute magnitude of the ion density. As the potential of the block was raised relative to the anode, the ion density at first increased rapidly. At a potential of about 10 volts it passed through a maximum ion density that in some cases was three times as large as the ion density when the anode and block were connected together. As the potential was raised still further, the ion density decreased again and settled down at a steady value which was usually a little greater than the ion density at zero block voltage. Negative block voltage appeared to have little effect on the ion density.

The over-all amplitude of the arc hash was also measured as a function of block voltage. At first the hash amplitude increased slowly as small positive block voltages were applied; then the rate of increase of hash with block voltage became fairly rapid, so that at a positive block potential of about 15 volts the hash amplitude was some three or four times as great as for zero block volts. Application of small negative block voltages also increased arc-hash amplitude slightly, but the effect was not so great as for positive voltages. The

hash observed in these measurements was in the frequency range of 100 to 200 kc as observed on the single-sweep scope. Figure 9.103 shows some typical curves for the variation of block current, ion density, space potential, and hash amplitude with block potential, illustrating the type of behavior discussed above. However, the form of variation of arc hash with block voltage varied in different runs. Sometimes application of a small positive voltage caused a decrease in hash amplitude, although still further increase of block voltage caused the hash amplitude to increase again. Thus the general shape of the curve of hash amplitude against block voltage is like that shown in Fig. 9.103, but the position of minimum hash amplitude is shifted over to positive block voltage. No definite correlation could be found between the arc-hash amplitude variation and arc conditions.

When the arc was operated at very low pressures the application of small positive block voltages had quite a different effect. When the conditions of operation of the arc with respect to arc current and pressure were such that violent relaxation oscillations were occurring, the application of positive block voltages had a marked steadying effect and permitted stable operation of the arc without relaxations at higher arc currents for a given pressure. Likewise the minimum running pressure of the arc was decreased by the application of positive block voltages.

Application of positive voltages to the wire electrodes at the top and bottom of the arc also had a considerable effect on the ion density throughout the arc plasma and the measured space potential near the wire. The effects in this case, however, were somewhat complicated and will be discussed in detail later.

The above observations may be understood in a qualitative fashion in terms of the general picture of the arc plasma that has been developed in earlier sections of this report. The following discussion indicates the outline of this interpretation:

As has been shown above, in the case of the normal arc, two types of region are encountered inside the arc chamber. Throughout most of the chamber there exists a plasma region in which space-charge neutralization is fairly accurately established. In this region only small potential differences of the order of magnitude of half the electron temperature can be maintained.

Near the electrodes, however, there must be a potential drop of the order of 6 or 8 volts in order to hold in the electrons. This takes place over a small sheath into which so few electrons penetrate that the sheath region can be described as one of space-charge-limited positive-ion collection. The positive-ion current crossing the sheath is simply the ion current that for any reason drifts into the sheath

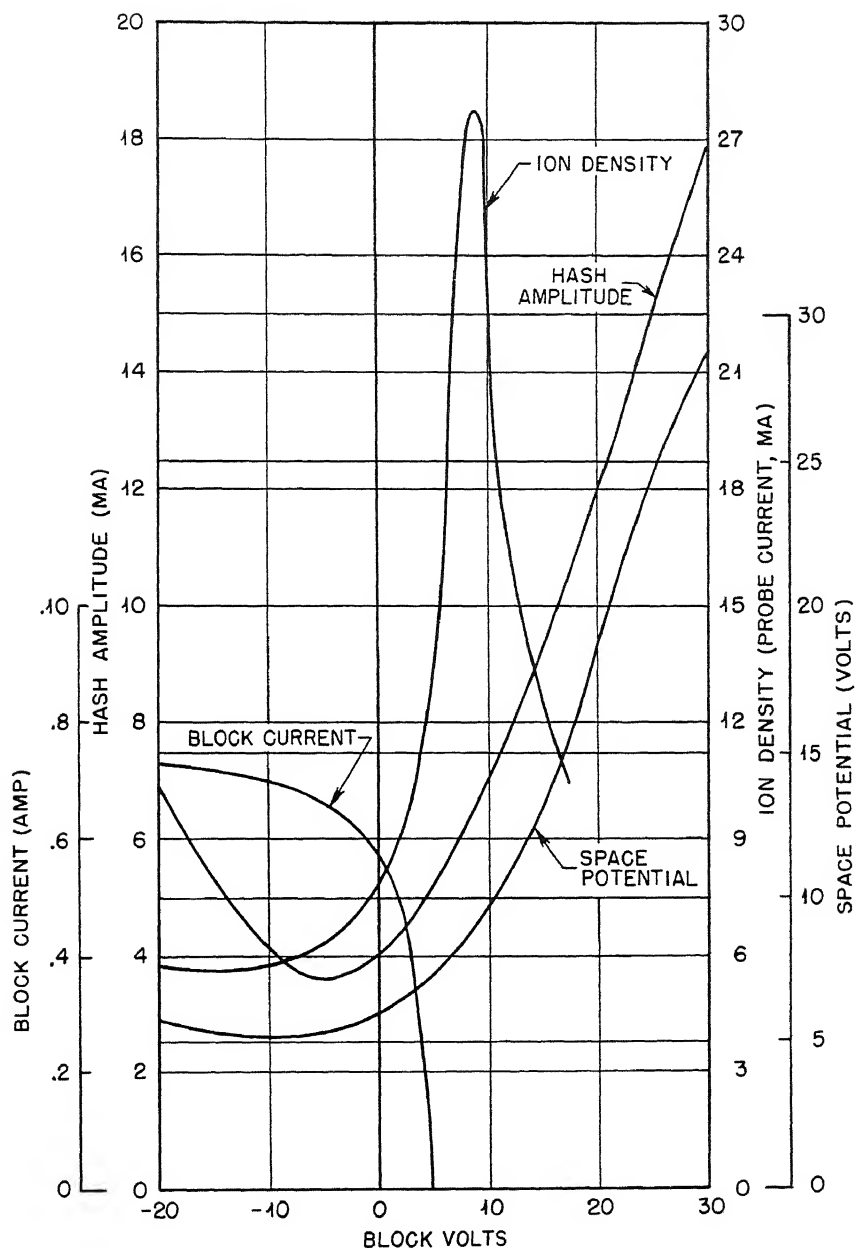


Fig. 9.103—Effect of block potential on ion density, block current, hash amplitude, and space potential in argon. Pressure 2×10^{-3} mm Hg; magnetic field 3,800 gauss; arc voltage 150 volts; arc current 1.5 amp.

edge from the plasma. The thickness of the sheath adjusts itself so that the space-charge-limited current corresponding to the voltage drop across the sheath is equal to the drift current striking the sheath.

$$d = \frac{2.32 \times 10^{-4} V^{\frac{3}{4}}}{i^{\frac{1}{2}} M^{\frac{1}{4}}}$$

where d is thickness in centimeters, V is the potential drop across the sheath in volts, i is the current density in amperes per square centimeter, and M is the atomic weight of the ion.

In most cases the sheath is very small. For example, in argon when $V = 8$ volts, $i = 0.005$ amp/sq cm, and $M = 40$, representing the kind of condition met with at the walls of the small arc in argon, $d = 0.062$ mm.

When the block is negative, it collects an inappreciable number of electrons. Thus the electrons must be collected on the anode. Because they are so mobile along the magnetic field, this increase in collection is easily attained by a slight decrease in the difference between space potential and anode potential. A positive-ion sheath shields the plasma from the block. For these two reasons the plasma is not affected much by a negative block potential.

Mechanism of Electron and Ion Diffusion across Magnetic Field. In a strong magnetic field electrons move in circles with Larmor radius $r = (c/H) (2MV/e)^{\frac{1}{2}}$, which is usually considerably less than 0.1 mm. They leave these circles either by collision with other particles or by electric fields that create rapid drain at right angles to both electric and magnetic fields (see Chap. 2). The drain of electrons in this manner is shown to be unstable, leading to plasma oscillations of frequencies of the order of 10^5 cycles. These oscillatory plasma electric fields create a more or less random drain, which causes electrons to diffuse in all directions, thus tending to fill any space available to them in spite of the constraining effect of the magnetic field. The plasma oscillations created in this way also contribute to arc hash.

Besides these random oscillatory electric fields which carry electrons across the magnetic field, the electrostatic fields may arrange themselves in such a manner as to move electrons to the wall by drain in a static fashion. For example, the equipotentials occurring in Fig. 9.104a can be shown theoretically to be consistent with plasma equations.

Evidently both electrons and ions tend to drain across the magnetic field to the wall. An essential requirement for this type of potential

distribution is that all the equipotentials crossing the ionizing column come close to the wall. This permits electrons to travel along an equipotential from the ionizing column to the wall. But if all these equipotentials come close to the wall, there must be a strong field near the wall. This means that only if the wall sheath has a fairly large potential drop can the arrangement be realized.

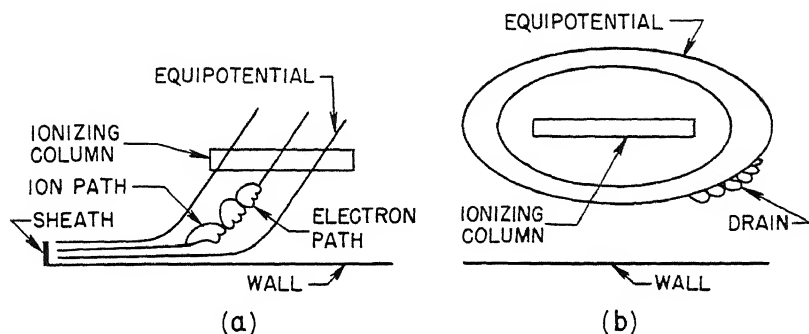


Fig. 9.104a—Equipotential arrangement permitting drain of electrons to wall.

Fig. 9.104b—Equipotential arrangement for wall at space potential.

If the arrangement can be realized, however, it provides a mechanism for removing electrons rapidly, thus keeping plasma density down. However, as the wall potential approaches space potential, the sheath disappears, and the equipotentials going through the ionizing column can no longer concentrate near the wall. Thus when the wall is at space potential the arrangement of equipotentials shown in Fig. 9.104b must be obtained, in which the equipotentials surround the ionizing column.

Because drain now results only in circulation of electrons the plasma density will tend to rise. However, the instability attending circulation by drain creates the oscillatory fields that ultimately, but more slowly, move the electrons and ions out. Hence, plasma density and hash should both increase as wall potential is increased.

When the block potential becomes more positive than space potential, several things happen. First the mobile electrons are pulled out of the plasma so rapidly that the plasma also becomes more positive. Thus the plasma potential tends to follow block potential. This makes the space so positive relative to the anode that electrons cannot collect on the anode. Thus they go to the block and make the block cur-

rent more negative. The rapid withdrawal of electrons also tends to lower the plasma density. This lowering is resisted by positive ions which can get out only at the anode. Yet, because plasma potential is now so positive relative to anode, the vertical fields penetrating into the plasma may be strong enough to pull out ions more rapidly, thus permitting the plasma density to drop in response to the more rapid collection of electrons. The existence of stronger vertical fields can be investigated by probe measurements. Furthermore these stronger vertical fields imply an increase of electron temperature when the block goes above space potential. The effect of the application of

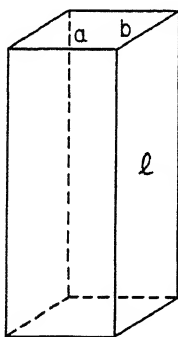


Fig. 9.105—Rectangular arc chamber of cross-sectional area ab and length l .

positive potential to the block in raising the potential of the whole plasma can be understood from the following simplified calculation:

Consider a rectangular chamber bounded by walls the lengths of whose sides are a , b , and l (see Fig. 9.105). Suppose an arc is struck in this chamber and a plasma set up, and for simplicity suppose the whole of the plasma is at a potential V_s with respect to the anode (and walls if the anode and walls are connected together). Then the whole of this drop of potential occurs across a sheath whose thickness is determined in the usual way by the fact that the total positive-ion drift current per unit area is equal to the space-charge-limited current density for the particular potential fall across the sheath. The value of the space potential is determined by the electron temperature. Thus the space potential must be sufficiently positive relative to the walls so as to allow the escape to the walls of just sufficient electrons at the upper end of the Maxwellian distribution to compensate for their rate of production in the arc column. Evidently, owing to the magnetic field, the electrons will not cross the sheath to the block

(across the field) so easily as they will cross the sheath to the anode and collimating-slot plate (parallel to the field). Let $\rho(v) dv$ be the number of electrons in unit volume having velocities between v and $v + dv$. Then the current density across any plane in the arc will be proportional to $\int_0^\infty v\rho(v) dv$.

Suppose the current density across a plane perpendicular to the field is given by $A \int_0^\infty v\rho(v) dv$ and that across a plane parallel to the field is given by $B \int_0^\infty v\rho(v) dv$. Owing to the field across the sheath repelling the electrons the total electron current to the anode and collimating slot will be given by

$$A \ 2ab \int_{\sqrt{\frac{2eV_s}{m}}}^{\infty} v\rho(v) dv$$

The total electron current to the side walls will be given by

$$B \ 2(a+b) l \int_{\sqrt{\frac{2eV_s}{m}}}^{\infty} v\rho(v) dv$$

Suppose now the side walls are raised to a positive potential V' relative to the anode and let V'_s be the potential to which the plasma is now raised. Suppose at the same time all the arc conditions and the electron temperature remain constant and that the factors A and B are also unaffected.

Then the total electron current to the anode and collimating slot now becomes

$$A \ 2ab \int_{\sqrt{\frac{2eV'_s}{m}}}^{\infty} v\rho(v) dv$$

and that collected by the side walls becomes

$$B \ 2(a+b) l \int_{\sqrt{\frac{2e(V'-V'_s)}{m}}}^{\infty} v\rho(v) dv$$

Then under these conditions it would be expected that the space potential V'_s of the plasma would adjust itself so as to make

$$2 [Aab + B(a + b)l] \int_{\sqrt{\frac{2eV_s}{m}}}^{\infty} v\rho(v) dv = 2Aab \int_{\sqrt{\frac{2eV'_s}{m}}}^{\infty} v\rho(v) dv + 2B(a + b)l \int_{\sqrt{\frac{2e(V'_s - V')}{m}}}^{\infty} v\rho(v) dv \quad (52)$$

We now write $\rho(v) = 4\pi\eta_0 \left(\frac{m}{2\pi kT}\right)^{\frac{3}{2}} v^2 e^{-mv^2/2kT} dv$

and Eq. 52 reduces to

$$[abA + (a + b)lB] \left(1 + \frac{eV_s}{kT}\right) e^{-eV_s/kT} = abA \left(1 + \frac{eV'_s}{kT}\right) e^{-eV'_s/kT} + (a + b)lB \left[1 + \frac{e(V'_s - V')}{kT}\right] e^{-e(V'_s - V')/kT} \quad (53)$$

To approximate the conditions in the small arc, make $a = b = 2$ cm, $l = 10$ cm, $V_s = 8$ volts (as measured when no block potential is applied), and $kT = 2$ ev.

For the ratio A/B we have to make a somewhat arbitrary choice. We have carried out calculations for two cases, namely, $A/B = 5$ and $A/B = 50$.

The results of the calculation are shown in Fig. 9.106.

When $A/B = 5$ the space potential tends to keep about 7 volts positive relative to the side walls up to very high wall potentials. When $A/B = 50$, however, the behavior is more like that actually observed. For block potentials between 0 and 10 volts the plasma potential scarcely changes, the space potential at 10 volts being 10.5 volts. As the block potential is increased the plasma potential rises and actually begins to fall slightly below it.

Evidently the effect of increase of magnetic field (i.e., increase of the A/B ratio) is to reduce the space potential for a given block potential. This is the kind of behavior observed in Fig. 9.109.

It is not possible to assume arbitrarily high values for A/B . For very high values it is not possible to satisfy Eq. 53. However, all this

work assumes that A , B , and T are unaffected by the block voltage. This assumption is probably only a rough approximation.

The analysis also seems to indicate that the plasma potential could not fall below the block potential by an amount in excess of the electron temperature. If this were true it would be difficult to understand the curves illustrated in Fig. 9.120 for the effect of pressure on the

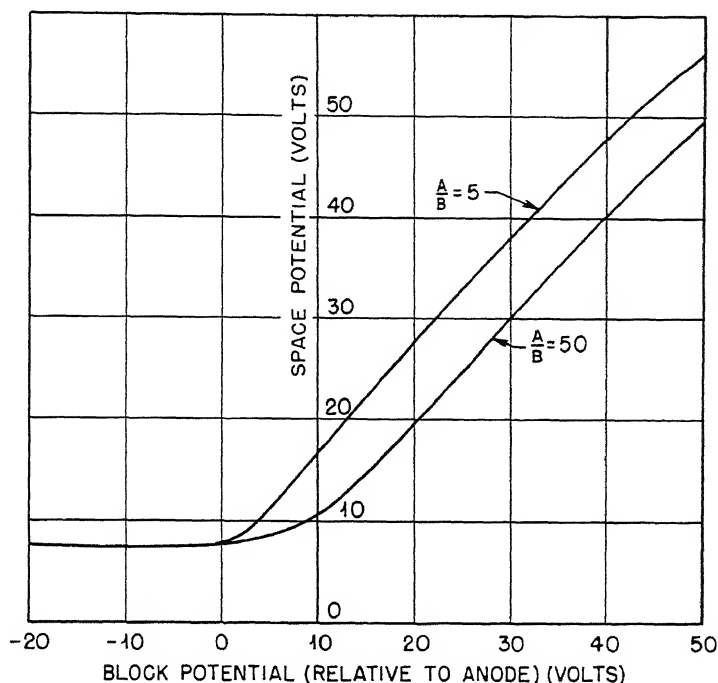


Fig. 9.106—Calculated space-potential vs. block-potential curves for $A/B = 5$ and $A/B = 50$.

space-potential variation. However, too much detail should not be expected of the analysis owing to the crudeness of the assumptions involved.

Clearly the rearrangement of equipotential surfaces, which according to the above theory accompanies changes in block potential, will have important effects on the asymmetry of the ion distribution; consequently it is not surprising that radical changes in the asymmetry are observed as the positive block potential increases. In particular, the reversal of asymmetry as the block potential is made more positive than space potential can be understood as being caused by the

reversal of drain directions attending the reversal of the plasma electric fields. A detailed discussion of the effects to be expected, however, must await further study of the equations relating to the drain diffusion of electrons and ions across the field.

6.2 Effect of Block Voltage on Ion Density, Space Potential, Electron Temperature, and Hash. We now proceed to examine in more detail the effect of arc conditions on the behavior observed when potential is applied to the side walls of the chamber relative to the anode.

(a) Effect of Magnetic Field. The effect of the magnetic field on the change of ion density with block voltage is shown in Fig. 9.107. The curves in this figure refer to the ion density at a point $x = \frac{3}{16}$ in., $z = 0$ in the same coordinate system as is used in the previous sections. Block voltage has a maximum effect on ion density at low magnetic fields. The maximum ion density decreases as the field increases, and the positive block voltage at which it occurs decreases. At a very high field (11,400 gauss) the application of block voltage causes the ion density to decrease, passing through a maximum very close to zero block volts. Figure 9.108 shows the variation of ion density with magnetic field for a number of different block voltages.

Figure 9.109 shows the variation of space potential with block voltage for different magnetic fields. As the magnetic field is increased, the space-potential difference between the plasma and the anode for a given block potential decreases. At the same time the blockpotential for which the plasma and block potentials become equal decreases. Thus from Fig. 9.109 it is seen that for a field of 2,000 gauss the plasma potential is equal to the block potential when the block potential is 17 volts. For a field of 3,700 gauss the corresponding figure is 16 volts, and for a field of 11,400 gauss it is 14 volts.

Figure 9.110 shows the variation of electron temperature with block voltage for different magnetic fields. It is seen that for the lower magnetic fields the electron temperature appears to decrease with increase of positive block voltages. However, for a high magnetic field (11,400 gauss) it shows an increasing characteristic with block voltage.

(b) Effect of Arc Current. Figure 9.111 shows the variation of ion density with block voltage at the point ($x = \frac{3}{16}$ in., $z = 0$) in the small arc for three different arc currents. The type of variation appears to be much the same for all currents. In each case the ion density passes through a maximum at about +8 volts, the maximum ion density being between three and four times the ion density for zero block volts.

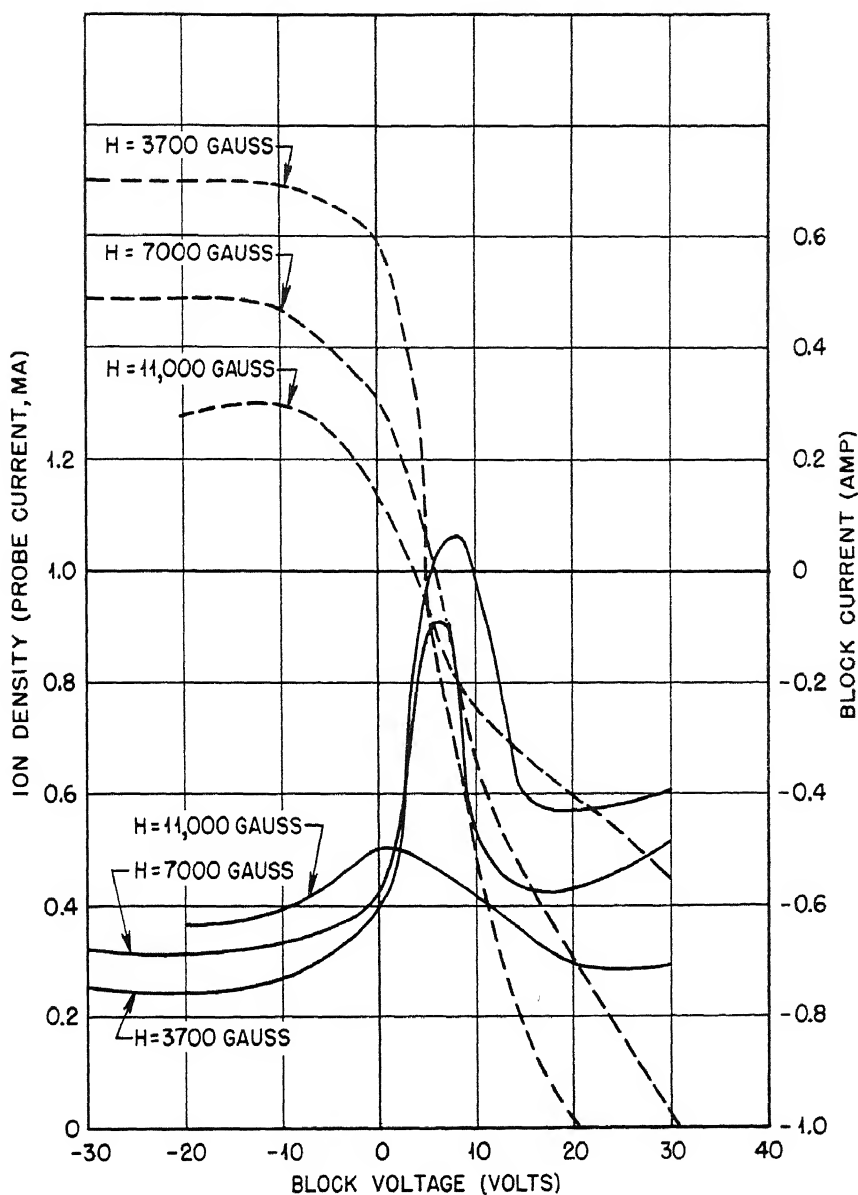


Fig. 9.107 — Effect of block voltage on ion density and block current at different magnetic fields for small arc in argon. Pressure 1.4×10^{-3} mm Hg; arc voltage 150 volts; arc current 1.5 amp; $x = \frac{3}{16}$ in.; $z = 0$. Solid lines represent ion density; dashed lines represent block current.

The main effect of increase in current appears to be to increase the absolute value of the ion density at a given block voltage a little less than proportionately with the arc current.

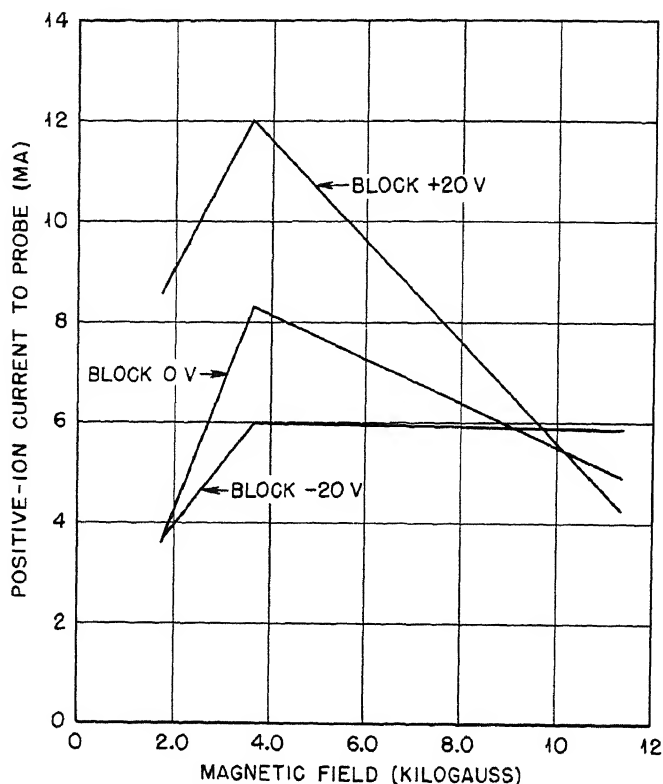


Fig. 9.108—Variation of ion density with magnetic-field strength for a number of block voltages for small arc in argon.

Figure 9.112 shows the variation of space potential with block voltage for three x positions. It is seen that the x positions have little effect on the form of variation.

Comparison of Figs. 9.103 and 9.113 shows the variation of over-all arc-hash amplitude with block voltage for two different currents. The form of curve is the same in the two cases, but the amplitude of the hash is greater in the case of larger arc current.

(c) Effect of Arc Voltage. The effect of change of arc voltage on the form of the variation of ion density with block voltage is shown in Fig. 9.114. The type of variation is the same for each of the voltages investigated. The maximum in the ion-voltage curve increases with

arc voltage, and the block voltage at which it occurs varies slightly. Thus for arc voltage of 50 volts the maximum occurs at a block voltage of +6.5 volts. For an arc voltage of 150 volts it occurs at a block voltage of 9.5 volts, and when the arc voltage is 400 volts the maximum occurs at a block voltage of 8.5 volts. Figure 9.115 shows the variation of ion density with arc voltage for different block voltages.

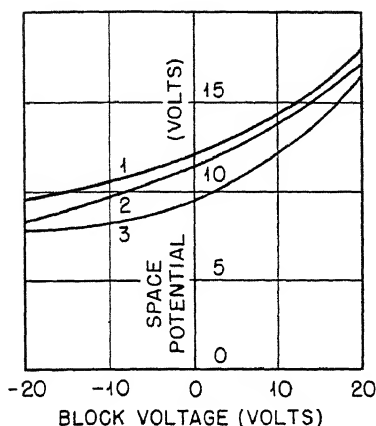


Fig. 9.109

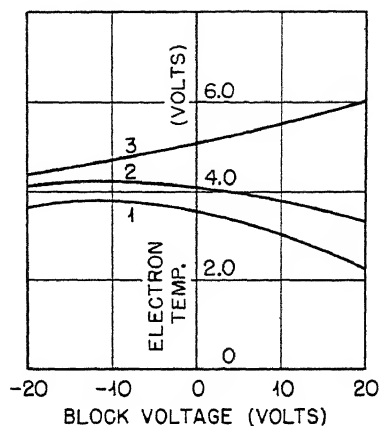


Fig. 9.110

Fig. 9.109—Effect of arc block voltage on space potential for small arc in argon. Pressure 1.4×10^{-3} mm Hg; magnetic field: curve 1 = 2,000 gauss; curve 2 = 3,700 gauss; curve 3 = 11,400 gauss; arc voltage 150 volts; arc current 1.5 amp. $x = 13/64$ in.

Fig. 9.110—Effect of arc block voltage on electron temperature for small arc in argon. Pressure 1.4×10^{-3} mm Hg; magnetic field: curve 1 = 2,000 gauss; curve 2 = 3,700 gauss; curve 3 = 11,400 gauss; arc voltage 150 volts; arc current 1.5 amp; $x = 13/64$ in.

Figure 9.116 shows the variation of space potential with block voltage for two different arc potentials. These curves appear to indicate that at the higher arc voltage the rise of space potential with block potential is less rapid than at the lower arc voltage.

The form of variation of electron temperature with block voltage for different block potentials is shown in Fig. 9.117. In both cases the electron temperature appears to increase with block voltage, and the form of variation is the same in either case.

(d) Effect of Pressure. The effect of pressure change in influencing the form of variation of ion density with block voltage is shown in Fig. 9.118. At very low pressure (3×10^{-4} mm Hg) the maximum usually occurring in the ion density at a small positive voltage seems

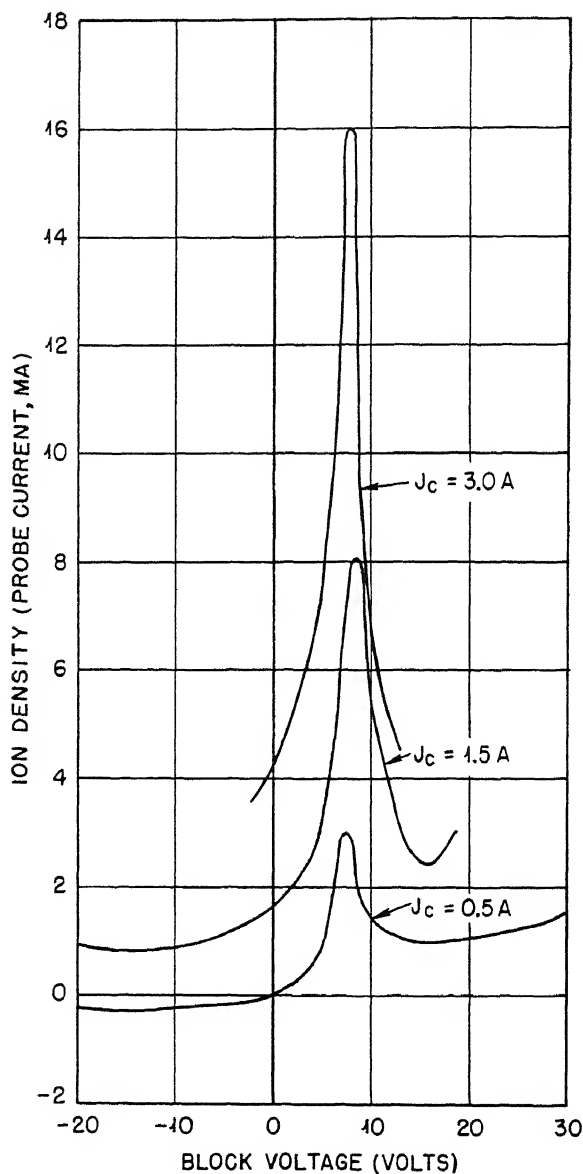


Fig. 9.111—Effect of arc block voltage on ion density at different arc currents for small arc in argon. Pressure 1.4×10^{-3} mm Hg; magnetic field 3,700 gauss; arc voltage 150 volts; $x = \frac{3}{16}$ in.; $z = 0$.

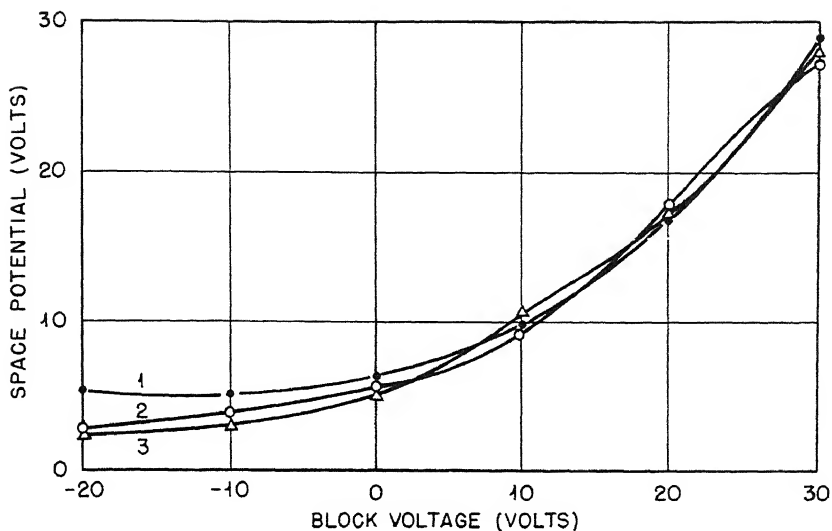


Fig. 9.112—Effect of block voltage on space potential at different positions of probe for small arc in argon. Pressure 1.4×10^{-3} mm Hg; magnetic field 3,700 gauss; arc voltage 150 volts; arc current 0.5 amp; $z = 0$; $x = \frac{1}{16}$ in. (curve 1); $x = \frac{3}{16}$ in. (curve 2); $x = \frac{5}{8}$ in. (curve 3).

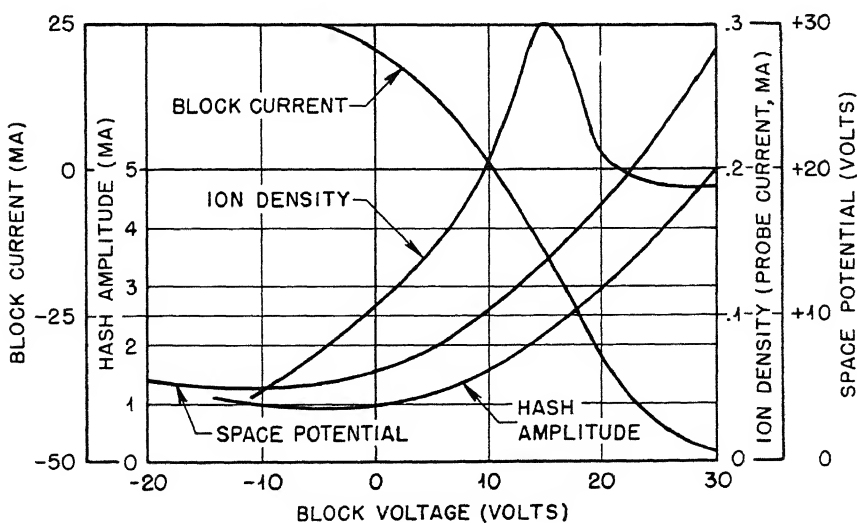


Fig. 9.113—Space potential, arc hash, ion density, and block current as function of block voltage. Pressure 1.4×10^{-3} mm Hg; magnetic field 3,700 gauss; arc voltage 150 volts; arc current 0.5 amp.

to have disappeared entirely. As the pressure is increased the maximum becomes more and more prominent. The variation of ion density with pressure for different block voltages is shown in Fig. 9.119.

Figure 9.120 shows how the space potential changes with block potential at different pressures. At low pressures the plasma potential

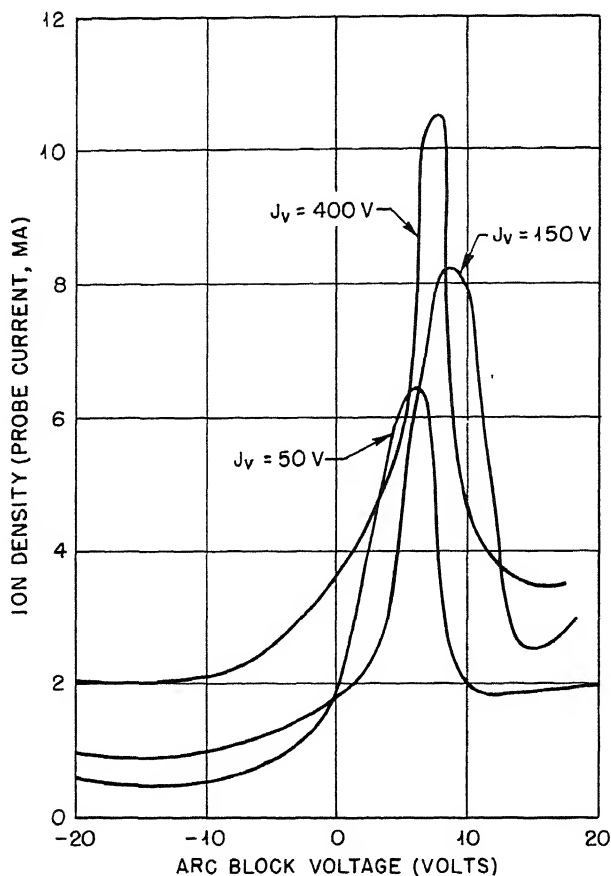


Fig. 9.114—Effect of block voltage on ion density at different arc voltages J_v for small arc in argon. Pressure 1.4×10^{-3} mm Hg; magnetic field 3,700 gauss; arc current 1.5 amp.

follows the block potential fairly closely when it is made positive. However as the pressure is increased more and more, the plasma potential is much less affected by the block potential. At a pressure of 3.5×10^{-3} mm Hg it still increases with block potential but much less rapidly than at a pressure of 0.7×10^{-3} mm Hg.

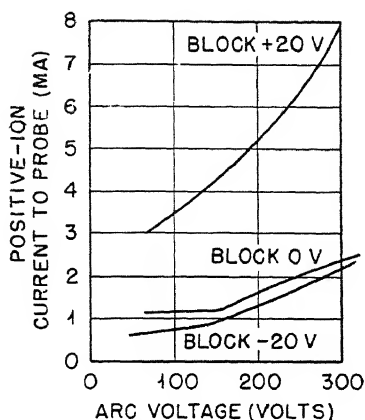


Fig. 9.115

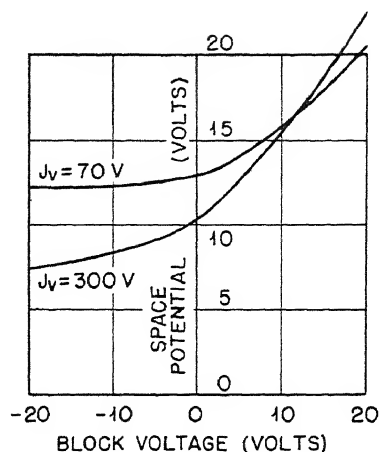


Fig. 9.116

Fig. 9.115—Variation of ion density with arc voltage for different block voltages. Pressure 1.4×10^{-3} mm Hg; magnetic field 4,100 gauss; arc current 1.0 amp; $x = \frac{3}{32}$ in.; $y = 0$; $z = 0$.

Fig. 9.116—Variation of space potential with block voltage for two values of arc voltage. Pressure 1.4×10^{-3} mm Hg; magnetic field 4,400 gauss; arc current 1.0 amp; $x = \frac{3}{32}$ in.; $z = 0$.

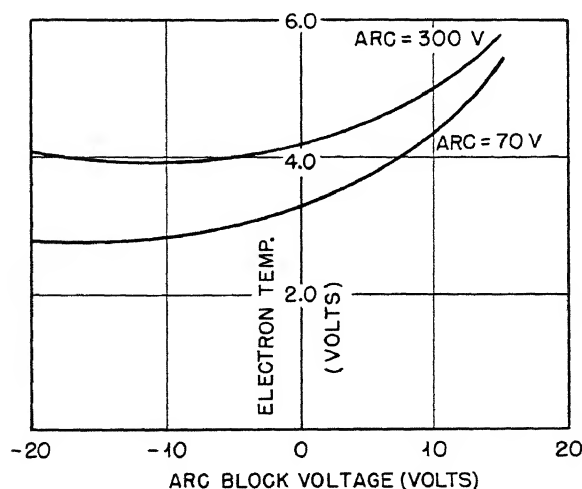


Fig. 9.117—Electron temperature as a function of arc block voltage at two arc voltages for small arc in argon. Pressure 1.4×10^{-3} mm Hg; magnetic field 4,100 gauss; arc current 1.0 amp; $x = \frac{3}{32}$ in.; $z = 0$.

Figure 9.121 shows the variation of electron temperature with block voltage for three different pressures. At low pressures the electron temperature appears to decrease with increase of block voltage, but at high pressure the variation is in the opposite direction.

(e) Effect of Block Potential at Different Positions in the Arc. Figure 9.122 shows the ion-density distribution in the arc along the line

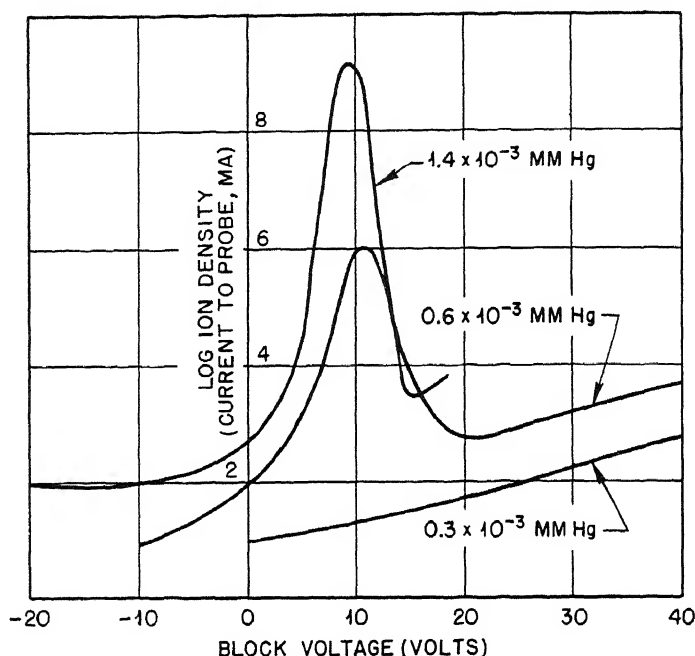


Fig. 9.118—Ion density as function of arc block potential at different pressures for small arc in argon. Magnetic field 3,700 gauss; arc voltage 150 volts; arc current 1.5 amp; $x = \frac{3}{16}$ in.

$y = 0$ in the central transverse plane ($z = 0$) for different block voltages. The effect of application of block potential on the ion density is seen to be greatest near the arc column. As one approaches the chamber wall, however, the ion density falls off more rapidly when positive block voltage is applied so that the ratio of ion density with and without positive block volts decreases.

Figure 9.123 represents the variation of space potential along the same line for different block voltages. There seems to be very little difference in the fall of potential actually occurring within the plasma

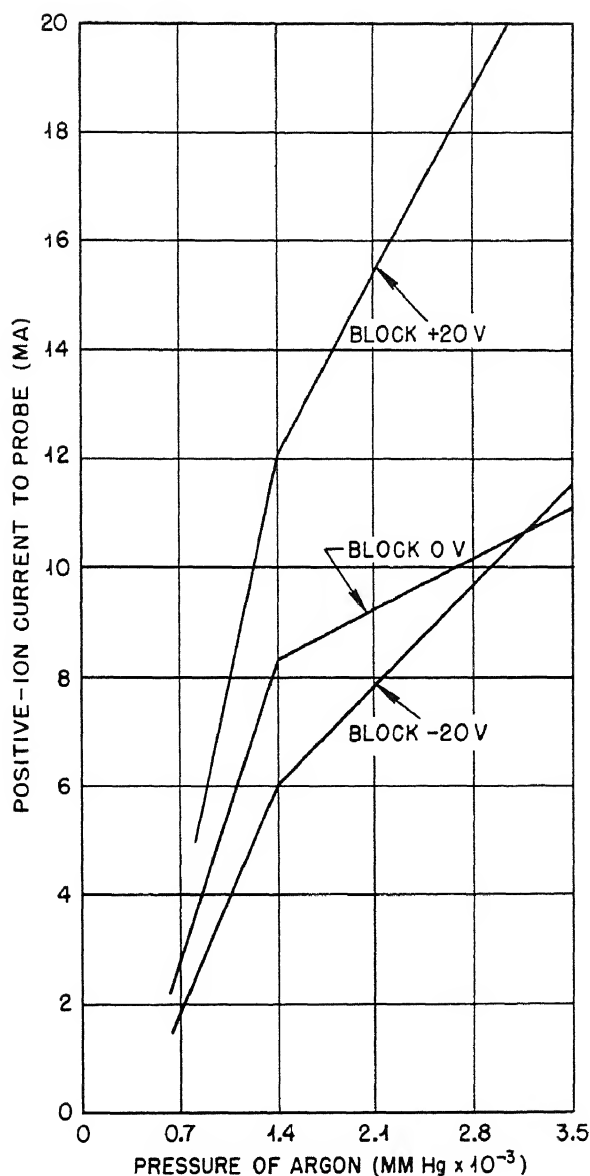


Fig. 9.119—Effect of pressure on ion density at different block potentials for small arc in argon. Magnetic field 3,700 gauss; arc voltage 150 volts; arc current 1.5 amp; $x = \frac{13}{64}$ in.; $y = 0$; $z = 0$.

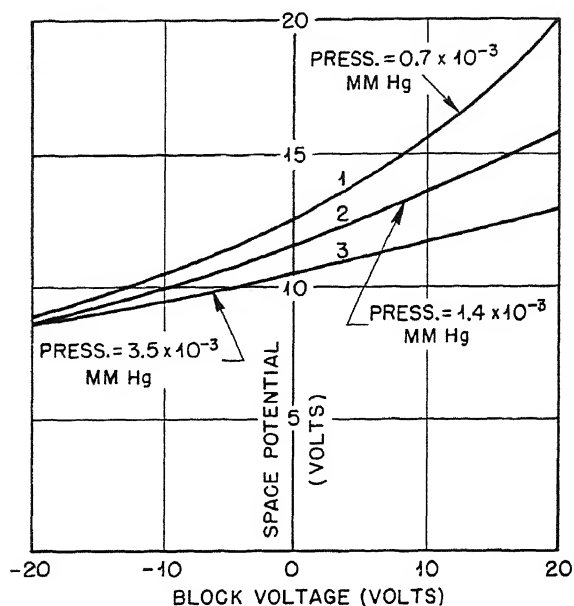


Fig. 9.120—Variation of space potential with block potential for different pressures for the small arc in argon. Pressure 0.7×10^{-3} mm Hg (curve 1), 1.4×10^{-3} mm Hg (curve 2), 3.5×10^{-3} mm Hg (curve 3); magnetic field 3,700 gauss; arc voltage 150 volts; arc current 1.5 amp; $x = \frac{13}{64}$ in.

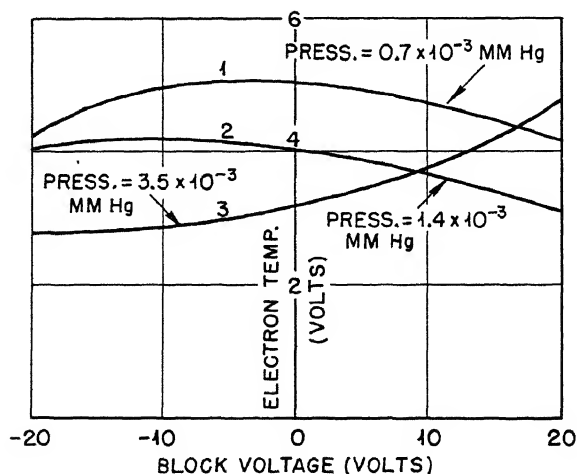


Fig. 9.121—Electron temperature vs. block potential for different pressures for the small arc in argon. Pressure 0.7×10^{-3} mm Hg (curve 1), 1.4×10^{-3} mm Hg (curve 2), 3.5×10^{-3} mm Hg (curve 3); magnetic field 3,700 gauss; arc voltage 150 volts; arc current 1.5 amp; $x = \frac{13}{64}$ in.

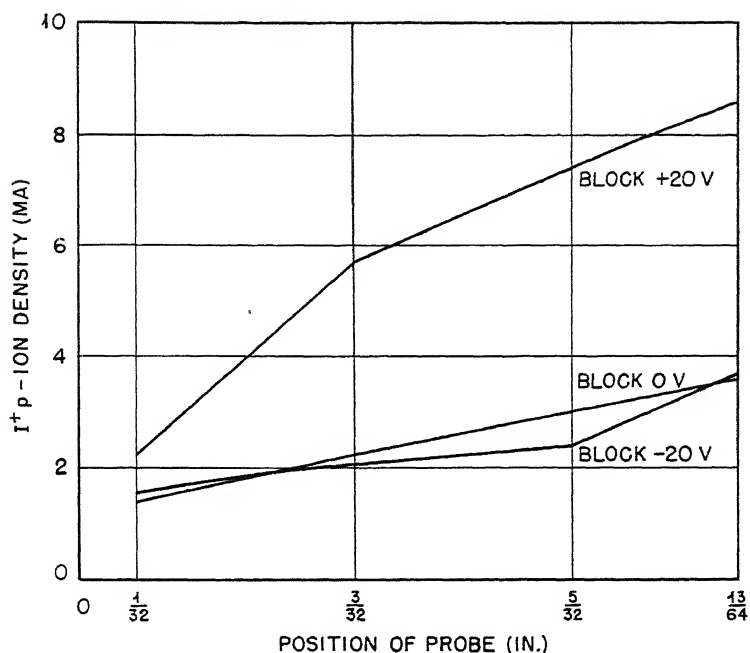


Fig. 9.122—Ion-density variation as function of position of probe for small arc in argon. Pressure 1.4×10^{-3} mm Hg; magnetic field 2,000 gauss; arc voltage 150 volts; arc current 1.5 amp.

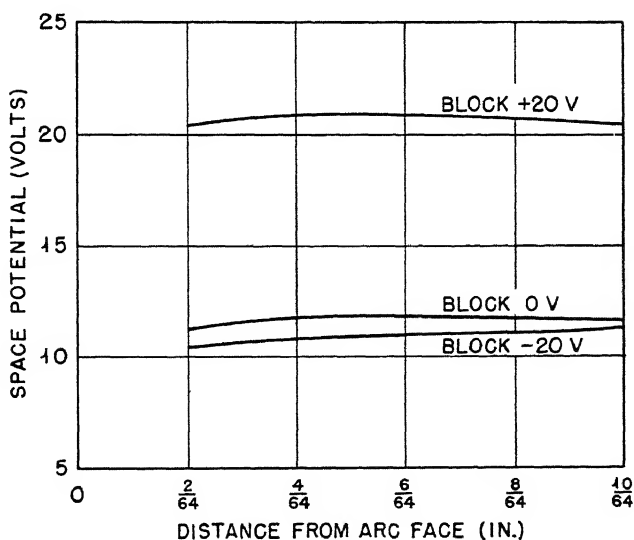


Fig. 9.123—Space potential vs. distance from arc face for small arc in argon. Pressure 1.4×10^{-3} mm Hg; magnetic field 2,000 gauss; arc voltage 150 volts; arc current 1.5 amp.

in the three cases illustrated, although there is a big difference in the fall of potential that occurs across the sheath at the side walls of the chamber. Thus at -20 volts, 0 volts, and +20 volts block voltage the fall across the sheath is 30 volts, 11 volts, and 1 volt, respectively.

Figure 9.124 shows the variation of electron temperature along the same line for three different block voltages.

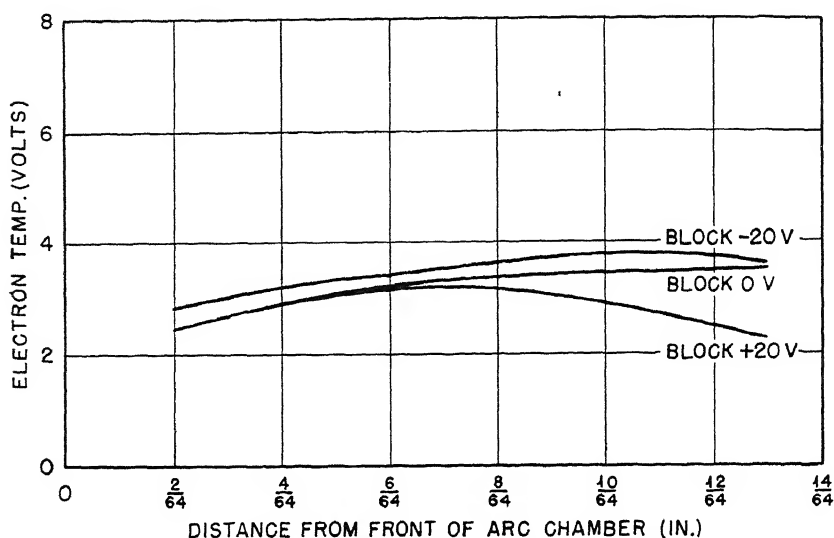


Fig. 9.124—Effect of arc potential on space variation of electron temperature. Pressure 1.4×10^{-3} mm Hg; magnetic field 3,700 gauss; arc voltage 150 volts; arc current 1.5 amp.

(f) Effect of Size of Arc Chamber. In the large arc the application of block voltage had very little effect on the ion density at fields of 3,700 gauss or greater except at points very close to the arc column. Thus Fig. 9.125 shows that the ion density measured at various points along the line $y = 0$ in the central transverse plane ($z = 0$) was almost independent of block voltage except at the point $x = 1\frac{1}{8}$ in., which is about $\frac{3}{16}$ in. in front of the arc chamber. At this point the application of small positive block voltages produced a small decrease in the positive-ion density.

When the magnetic field was decreased to 900 gauss, however, the variation of ion density with block voltage was similar in form to that observed for the small arc, the ion density first increasing and then passing through a maximum and decreasing for small positive block voltages. Further increase in block voltage produced a slight tendency

for the ion density to rise. Figure 9.125 shows the block current as a function of block voltage. It is seen that the floating potential of the block in this case also is about 5 volts.

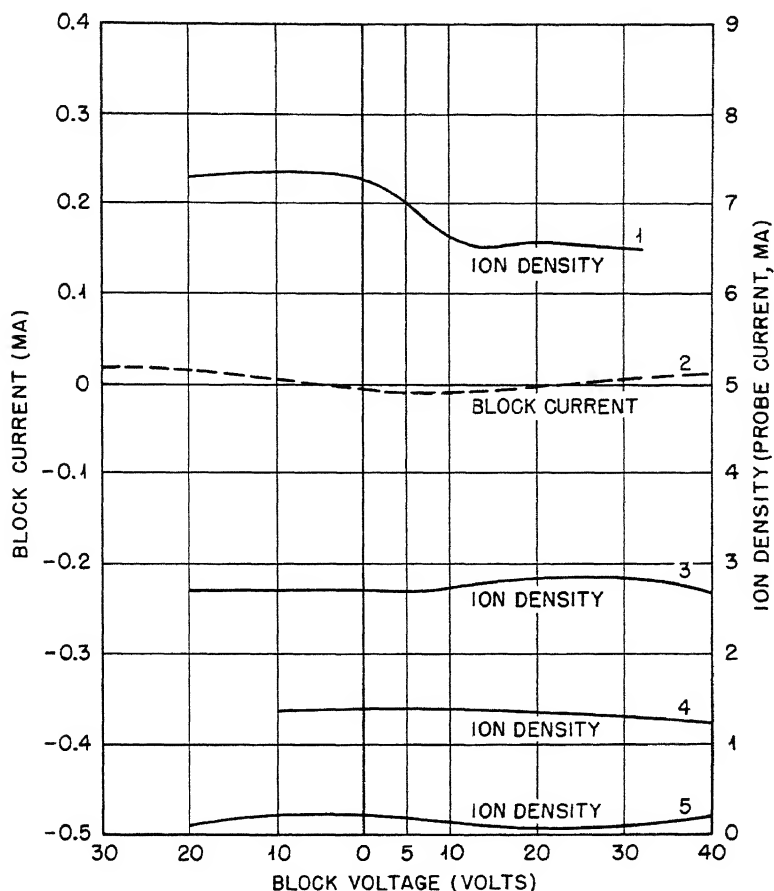


Fig. 9.125—Ion densities as a function of arc block potential for large arc in argon. Curve 1: pressure 0.6×10^{-3} mm Hg; magnetic field 3,700 gauss; arc current 1.5 amp; $x = 1\frac{1}{8}$ in. Curve 2: pressure 0.6×10^{-3} mm Hg; magnetic field 3,700 gauss; arc current 1.5 amp $x = 1\frac{1}{8}$ in. Curve 3: pressure 1.4×10^{-3} mm Hg; magnetic field 3,700 gauss; arc current 2.5 amp; $x = \frac{5}{16}$ in. Curve 4: pressure 0.6×10^{-3} mm Hg; magnetic field 3,700 gauss; arc current 1.5 amp; $x = \frac{5}{16}$ in. Curve 5: pressure 0.6×10^{-3} mm Hg; magnetic field 3,700 gauss; arc current 1.5 amp; $x = \frac{5}{16}$ in.

No measurements were made of the effect of block potentials on space potential and electron temperature in the case of the large arc.

(g) Effect of Type of Gas. All the measurements discussed above were carried out with argon in the arc chamber. Some measurements

of the same type were carried out with chlorine. In this case, measurements were made of both the positive and negative probe saturation currents to get some idea of the effect of block potential on the negative-ion densities. The results are markedly different from those in argon. In the small chlorine arc the positive-ion density first

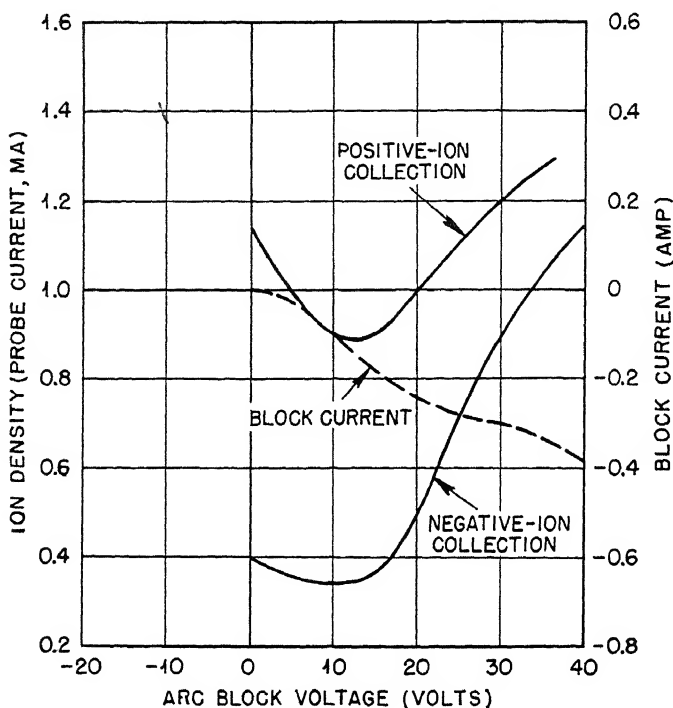


Fig. 9.126—Effect of arc block potential on positive- and negative-ion-current densities for small arc in chlorine. Pressure 1.0×10^{-3} mm Hg; magnetic field 3,700 gauss.

decreases as the block potential is raised to small positive values, reaching a broad minimum for a positive block voltage somewhere between 5 and 15 volts and then increasing slowly with further increase of block voltage. The same general type of variation was observed for the negative-ion density (as estimated from the negative saturation current). These effects are shown in Fig. 9.126.

The variation of block current with block voltage is also shown in Fig. 9.126. It is seen that in this case also the floating potential is about +5 volts.

Figure 9.127 shows the variation of ion density with block voltage in the case of the large arc in chlorine at a point distant from the

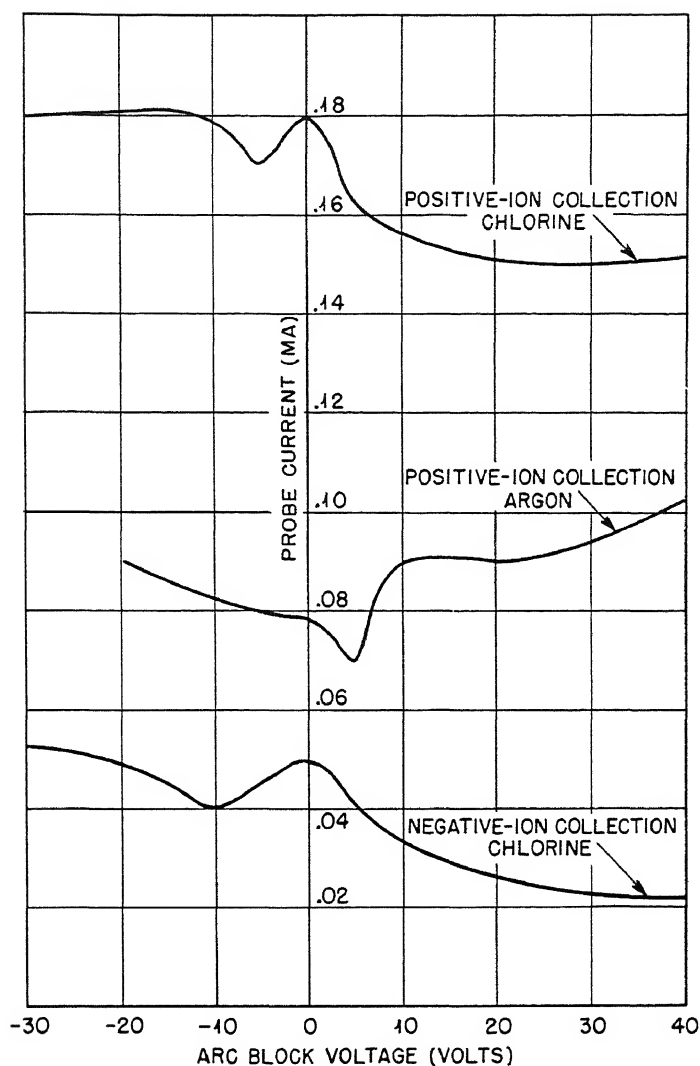


Fig. 9.127—Effect of arc block potential on positive- and negative-ion-current densities for large arc in chlorine.

arc column. For positive- and negative-ion collection the ion density appears to pass through a maximum at zero voltage and falls off slowly for small positive voltages.

No measurements were made of the influence of block voltage on space potential and electron temperature in the chlorine arc.

6.3 Effect of Application of Block Voltage on Arc Current and Minimum Arc Starting Pressure. It was found that the application of a positive block voltage had a marked effect upon the minimum running pressure and the arc current at a given running pressure for the argon arc.

For example, a small arc was run at a pressure of 0.6×10^{-3} mm Hg, a magnetic field of 2,000 gauss, an arc voltage of 150 volts, and a current of 1.5 amp with the block and anode at the same potential. The pressure was now reduced to 0.2×10^{-3} mm Hg, the arc voltage, magnetic field, and filament current being kept constant. The arc current dropped considerably. When the side walls were charged up

Table 9.16

Block voltage, volts	Arc current, amp
0	0.5
+15	2.5
+25	1.0
+40	0.5

to a potential of 40 volts positive relative to the anode, the arc current was found to attain its original value of 1.5 amp but at this greatly reduced pressure.

As another example, at a pressure of 0.3×10^{-3} mm Hg, a magnetic field of 3,700 gauss, and an arc voltage of 150 volts, the arc current varied with magnetic field as shown in Table 9.16.

Thus, without changing the filament current, arc voltage, pressure, or field, the arc current first increased with application of positive block voltage, passed through a maximum, and then fell off for higher block voltages.

Evidently the positive voltage applied to the walls causes more positive ions to go to the top and bottom of the arc and particularly sends more to the filament, thus producing additional heating of the filament and greater arc current.

Under conditions in which the arc current was undergoing violent relaxation oscillations at low pressures it was found possible by the application of a suitable positive block voltage to cause the arc to run steadily in the high-current state.

At higher pressures and magnetic fields the arc current behaved somewhat differently with increase of block potential. Thus at a pressure of 20μ a on the Western Electric gauge and at a magnetic field of 11,400 gauss the arc current dropped sharply as the block

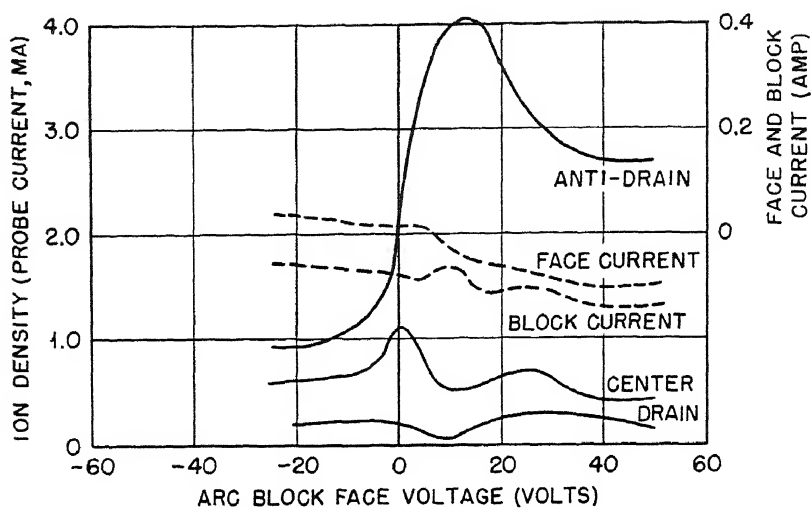
potential was increased to 10 volts. On further increase of the block voltage up to 40 volts the arc current increased slowly.

Similar effects were observed with the large arc in argon. Thus the large arc could run at a pressure of $2.5 \mu\text{a}$ (Western Electric) with 200-volt arc potential and 2 amp current, but strong relaxations were always present in the arc current. However, when a positive potential of about 5 volts was applied to the block, the arc could be made to run stably with a high current and without relaxations. When, however, the block voltage was raised above 30 volts the arc again went into violent relaxation oscillations.

6.4 Effect of Block Voltage on Asymmetry of Ion Distribution. It was found that the application of block voltage had a marked effect on the asymmetry of the ion distribution reported earlier. Measurements were made of the variation of ion density with block voltage at three points close to the arc column—one on the antidrain side, one on the drain side, and one close to the center. In general it was found that, as the block potential relative to the anode increased, the asymmetry ratio decreased and under some conditions actually reversed, causing the maximum ion density to be found on the drain side. The distribution on the antidrain side always showed the sharpest maximum in the ion density, and often a minimum occurred in the ion density on the drain side at the block potential for which the maximum ion density occurred on the antidrain side (see Fig. 9.129b).

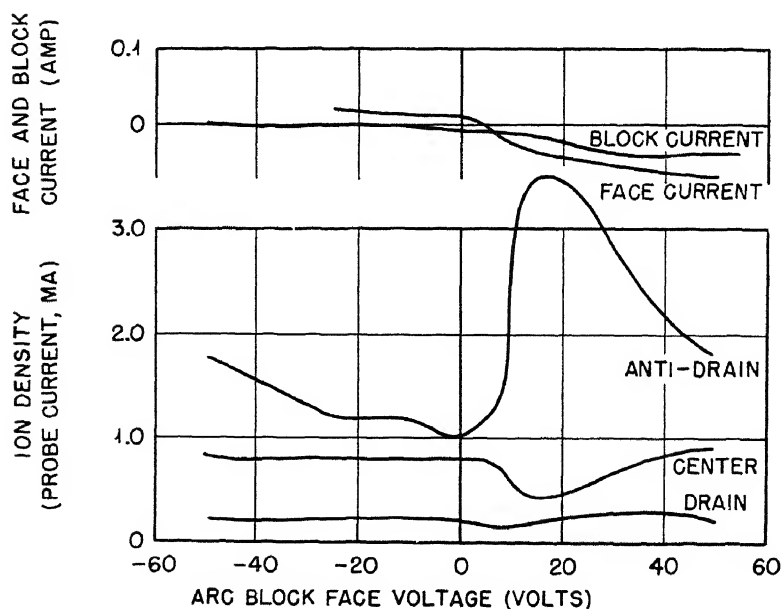
In these experiments the effect of insulating the front face of the arc block from the other side walls so that an independent potential could be placed on it was investigated. Under these conditions it was often found possible to put appropriate potentials on the front face and the remainder of the block such that the ion density was almost uniform across the whole of the plasma in front of the arc column.

Figures 9.128a to d illustrate this effect. Figure 9.128a shows the variation of ion density in the three positions with face volts when there is not voltage on the other walls of the chamber. There is seen to be a marked asymmetry at all face voltages. In Fig. 9.128b similar curves are plotted when the other walls of the arc chamber are held at +5 volts. The asymmetry is seen to have been decreased. In Fig. 9.128c, in which the other side walls have a potential of +10 volts, the asymmetry has almost completely disappeared for a small positive face voltage. In Fig. 9.128d, with +15 volts on the other side walls, the asymmetry is again very large but in the reversed sense for zero face volts, so that the maximum ion density is on the drain side. As the face voltage is increased the asymmetry decreases, until at a face voltage of about +22 volts it has almost disappeared again.



(a)

Fig. 9.128a



(b)

Fig. 9.128b

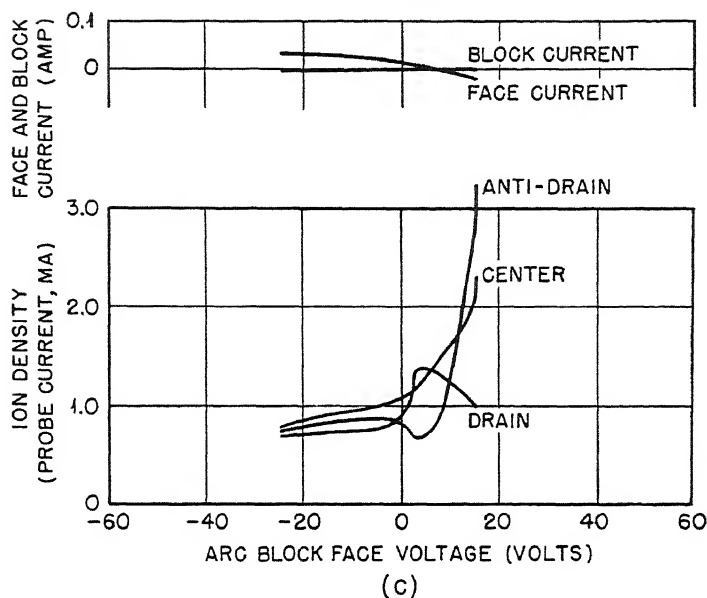


Fig. 9.128c

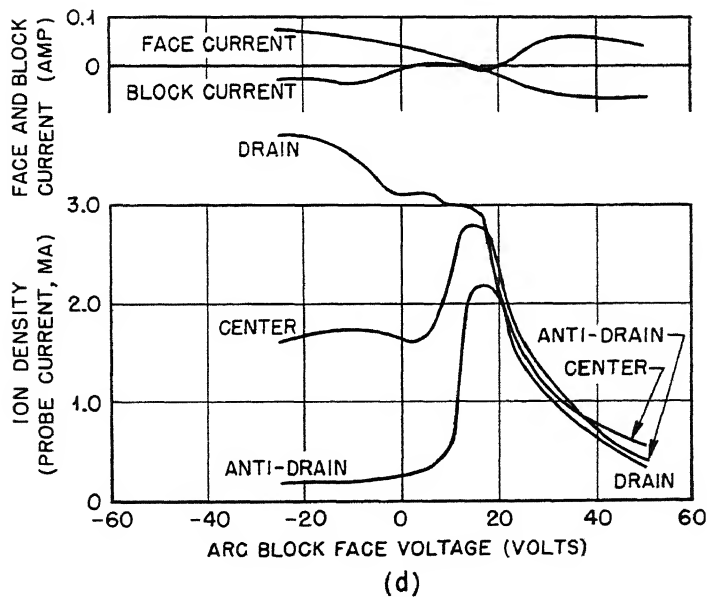


Fig. 9.128d

Fig. 9.128—Effect of applying voltage to front face of arc block on symmetry and magnitude of ion density. Pressure 0.6×10^{-3} mm Hg; magnetic field 11,400 gauss; arc voltage 150 volts; arc current 1.5 amp. (a) Solid lines represent ion density; dashed lines represent block current. (a), (b) Block voltage 0. (c) Block voltage +10 volts. (d) Block voltage +5 volts.

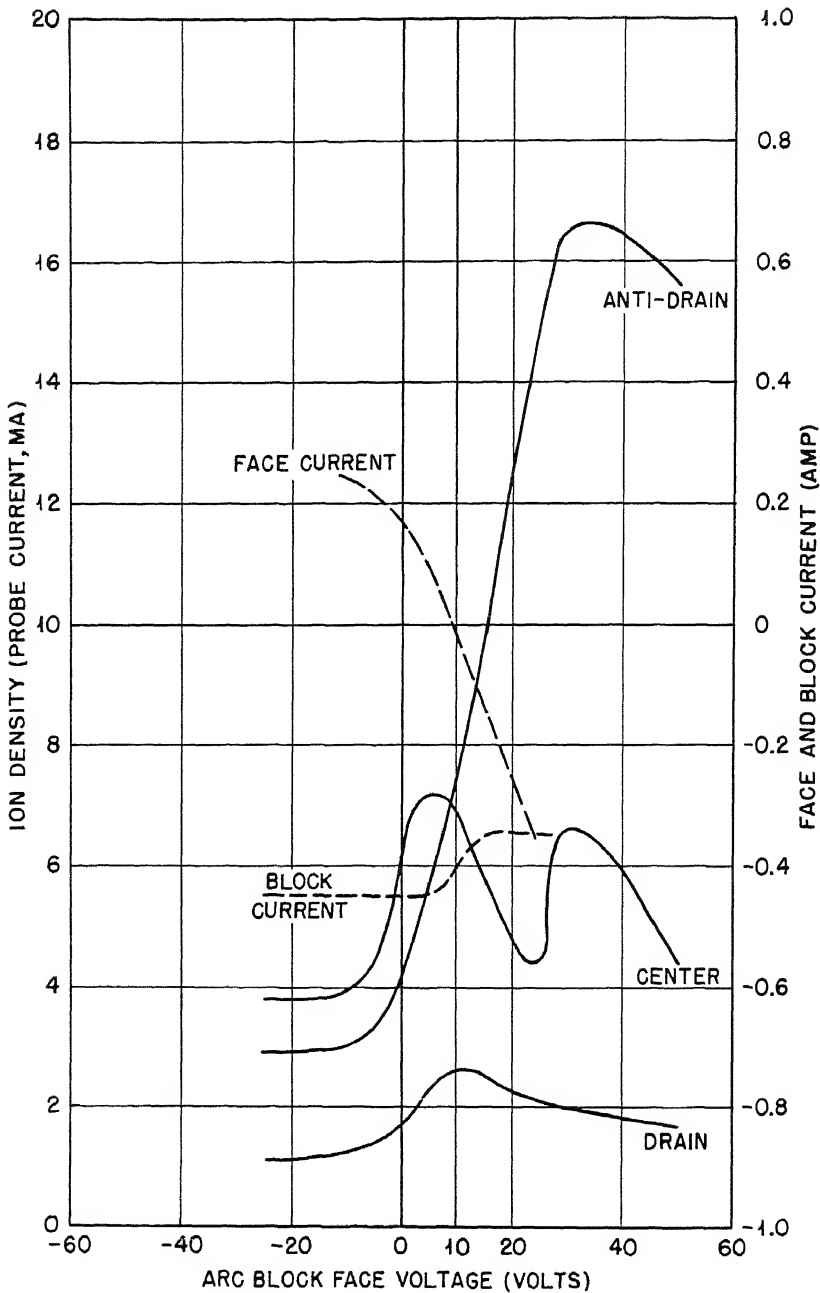


Fig. 9.129a

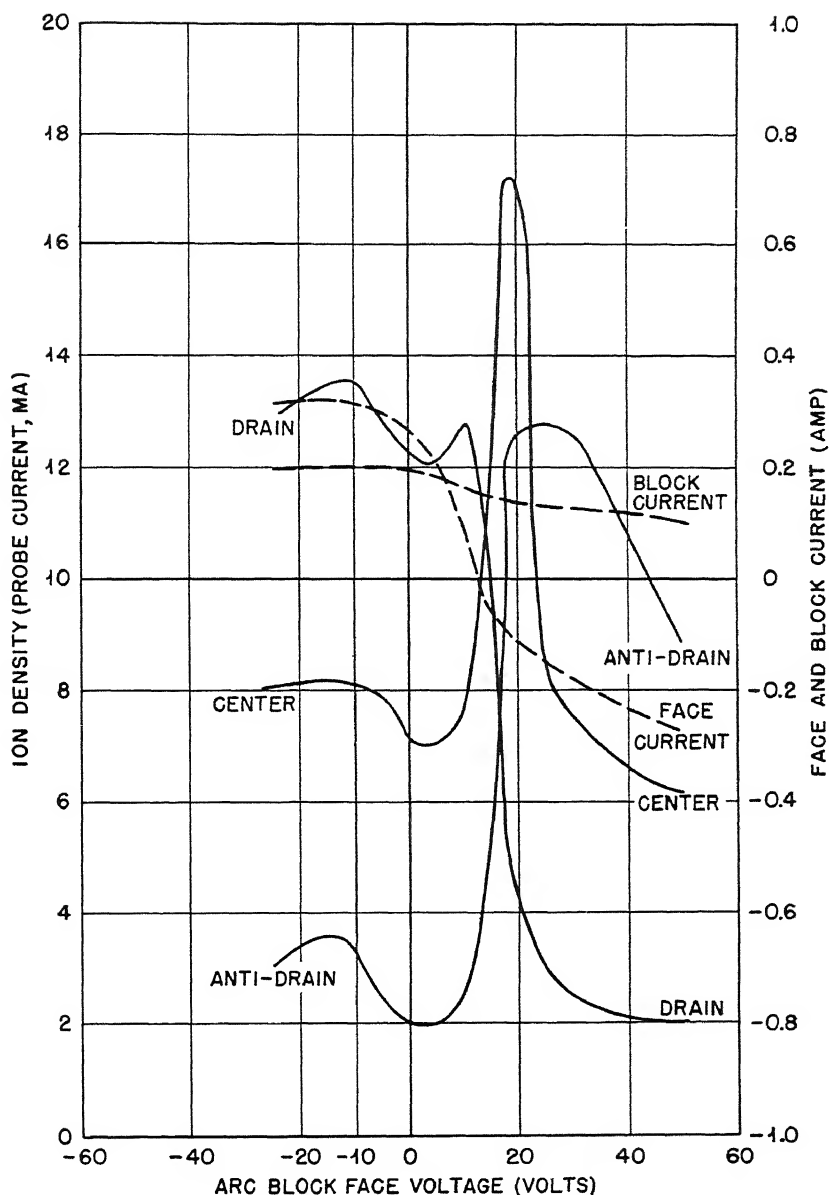


Fig. 9.129b

Fig. 9.129—Effect of applying voltage to front face of arc block on symmetry and magnitude of ion density for small arc in argon. Pressure 1.4×10^{-3} mm Hg; magnetic field 3,700 gauss; arc voltage 150 volts; arc current 1.5 amp. Solid lines represent ion density; dashed lines represent block current. (a) Block voltage 0. (b) Block voltage + 5 volts.

An interesting feature of these curves is the fact that they were taken at low pressure (6×10^{-4} mm Hg) and high magnetic field (11,400 gauss). It was reported earlier in this section that under these conditions the ion density failed to exhibit the characteristic maximum for positive block voltage when potential was applied to the whole block. Figure 9.128a shows, however, that, when potential is applied to the face of the block only, a maximum in the ion density is observed for a certain positive face voltage, but for the antidrain side only.

Figures 9.129a and 9.129b show similar curves for the variation of ion density with face voltage when the other walls are held at 0 and 15 volts positive, respectively, with a magnetic field of 3,700 gauss and a pressure of 1.4×10^{-3} mm Hg. Figure 9.129b is particularly interesting since it shows a case in which the usual asymmetry is reversed for zero face volts so that the maximum ion density is on the drain side. For face potentials above 20 volts, however, the asymmetry has reversed back to its normal sense.

6.5 Effect of Block Voltage on the Current Distribution in the Arc. Analyses were made of the magnitude and nature of the currents to the wires for one set of arc conditions without block voltage and also with a voltage of +30 volts on the block. These figures, which are produced in Table 9.17, show clearly how the effect of positive block voltage is to force positive ions to move to the ends of the arc while making it easier for electrons to reach the side walls.

6.6 Effect of Application of Potentials to Wires at Top of Arc Block. The position of the wires is shown in Fig. 9.3 of Sec. 1. The wires were numbered starting from the back of the chamber. Numbers 1, 2, and 3 were behind the arc column and 4, 5, and 6 were in front. Thus the distances of the different wires from the inside of the front surface of the chamber were, respectively, numbering from 1 to 6, $\frac{19}{32}$, $\frac{1}{2}$, $\frac{13}{32}$, $\frac{7}{32}$, $\frac{1}{8}$, and $\frac{1}{32}$ in. Potentials were applied to the various wires, and the ion densities, space potentials, and electron temperatures were measured as a function of wire potential at different points in the arc.

(a) **Effect of Wire Potentials on Ion Density.** The effect of application of wire potential on ion density depends on the particular wire to which the potential was applied and the position in the arc at which the ion density is measured. Under some circumstances the application of positive wire potential causes an increase in ion density, in other cases a decrease. Thus when positive potentials were applied to wire 6 the ion density was increased at all points on the same side of the arc column, whether these points were farther out from the column than the wire or between the wire and the column. Figure

9.130a shows a typical case of this kind. It is seen that in this case the application of wire potential caused a rise of ion density from 5.0 (in arbitrary units) without wire potential to about 8.0 when a positive potential was applied.

Table 9.17

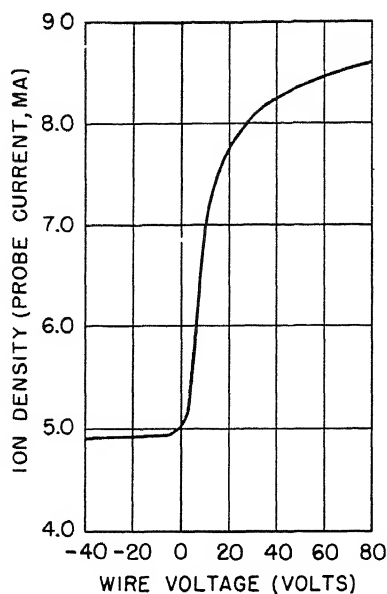
(Pressure 1.4×10^{-3} mm Hg; magnetic field 3,700 gauss; arc voltage 150 volts; arc current 0.5 amp)

Wire No.	Saturation positive-ion current, ma	Electron current when wires are held at anode potential, ma
Without block voltage*		
1	2.4	2.4
2	5.8	7.3
3	13.5	43.5
4	11.0	18.0
5	4.1	4.1
6	2.2	2.7
7	1.3	1.3
8	6.0	6.5
9	13.5	19.7
10		
11	6.4	6.4
12	2.2	2.2
With block voltage +30 volts†		
1	22.0	16.4
2	21.0	5.5
3	>50	>24
4	35.5	7.5
5	17.0	2.0
6	12.0	2.0
7	9.0	3.5
8	24.0	9.5
9	31.0	10.0
10		
11	26.0	10.5
12	13.5	2.5

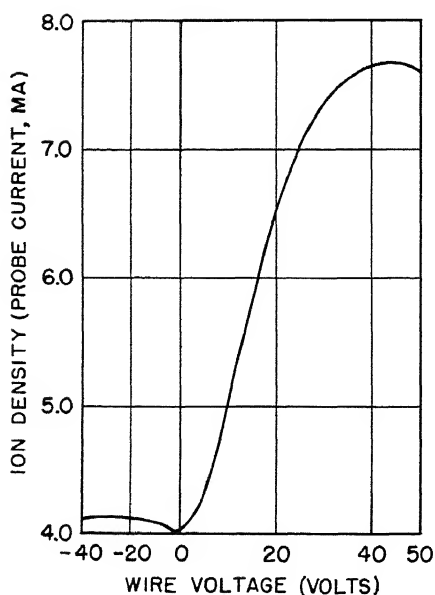
* Block current is +190 ma; it is composed of positive-ion current, 300 ma, and electron current, 110 ma.

† Block current is 700 ma.

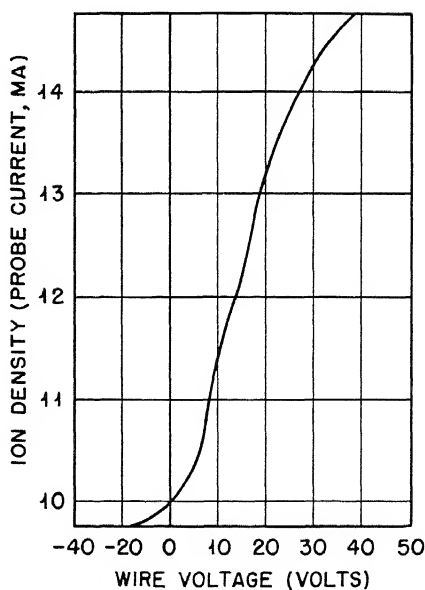
On the other hand, the application of positive potential to wire 5 (nearer the arc column than wire 6) caused a sharp drop in ion density at all points on the same side of the column. Figure 9.131 shows a typical case of this kind. Without potential on the wire the ion density



(a)



(b)



(c)

Fig. 9.130—Effect of application of potential to wire 6 across the collimating-slot plate for small arc in argon. Pressure 1.4×10^{-3} mm Hg; magnetic field 3,700 gauss; arc voltage 150 volts; arc current 0.5 amp; $x = \frac{3}{16}$ in. (a) $z = 0$. (b) $z = +1\frac{1}{16}$ in. (c) $z = -1\frac{1}{16}$ in.

(in arbitrary units) at a point between the wire and the column was about 15.0. At a wire potential of +5 volts this had increased to about 16.2. On further increase to +15 volts, however, this density dropped sharply to 9.5.

The ion-density variation with potential applied to the wire was rather different at points farther away from the arc column, in that the initial increase with small wire potentials was more pronounced. Figure 9.132 shows the variation in such a case.

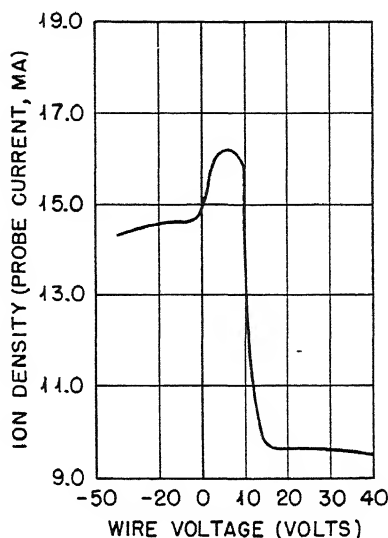


Fig. 9.131—Effect of application of potential to wire 5 across the collimating-slot plate for small arc in argon. Pressure 1.4×10^{-3} mm Hg; magnetic field 3,700 gauss; arc voltage 150 volts; arc current 0.5 amp; probe -15 volts; $z = 1\frac{1}{8}$ in.; $x = \frac{1}{4}$ in.

Measurements were also made of the effect of applying potentials to wires on the opposite side of the arc column from that in which the ion-density measurements were made. A typical curve is shown in Fig. 9.133 for the application of potential to wire 2. In every case application of positive wire potential to wires on one side of the arc column caused a rise in ion density on the other side.

Figures 9.130a, 9.130b, and 9.130c show the effect of application of wire potential (in this case to wire 6) on the ion density at different vertical positions in the arc. It is seen that the relative change in ion density produced by applying positive potentials to the curve is about the same order of magnitude at all vertical heights in the arc chamber.

The particular arc conditions under which the arc is operating do not appear to change the type of change observed when wire potential is applied. Figures 9.134a to e show the effect on ion density at the same point in the arc of applying wire potentials to wire 5 when the operating pressure, magnetic field, arc voltage, and current are varied. The form of the variation appears qualitatively much the same

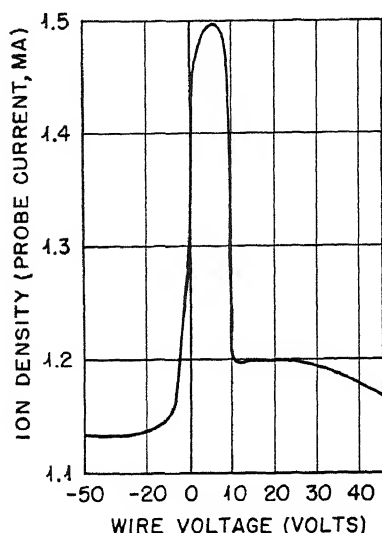


Fig. 9.132

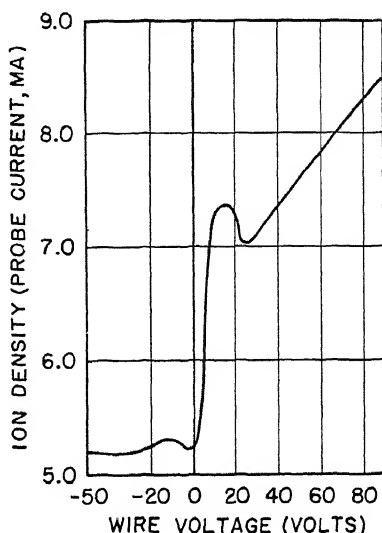


Fig. 9.133

Fig. 9.132—Effect of application of potential to wire 5 across the collimating-slot plate for small arc in argon. Pressure 1.4×10^{-3} mm Hg; magnetic field 3,700 gauss; arc voltage 150 volts; arc current 0.5 amp; probe -15 volts; $z = 1\frac{1}{8}$ in.; $x = 0$.

Fig. 9.133—Effect of application of potential to wire 2 across the collimating-slot plate for small arc in argon. Pressure 1.4×10^{-3} mm Hg; magnetic field 3,700 gauss; arc voltage 150 volts; arc current 0.5 amp; probe, -15 volts; $z = 1\frac{1}{8}$ in.; $x = \frac{1}{8}$ in.

in each case. When the pressure is low (6×10^{-4} mm Hg) the initial increase for small positive voltages has almost disappeared, and the over-all drop in density is somewhat smaller than in the other cases. On the other hand, at a high magnetic field (11,400 gauss) the initial increase in ion density is more marked than in the other cases.

(b) Effect of Wire Potentials on Space Potential. Measurements were made of the change in space potential in the arc when positive potentials were applied to one of the wires (wire 5). Table 9.18 shows the results of measurements on the space potential made by means of

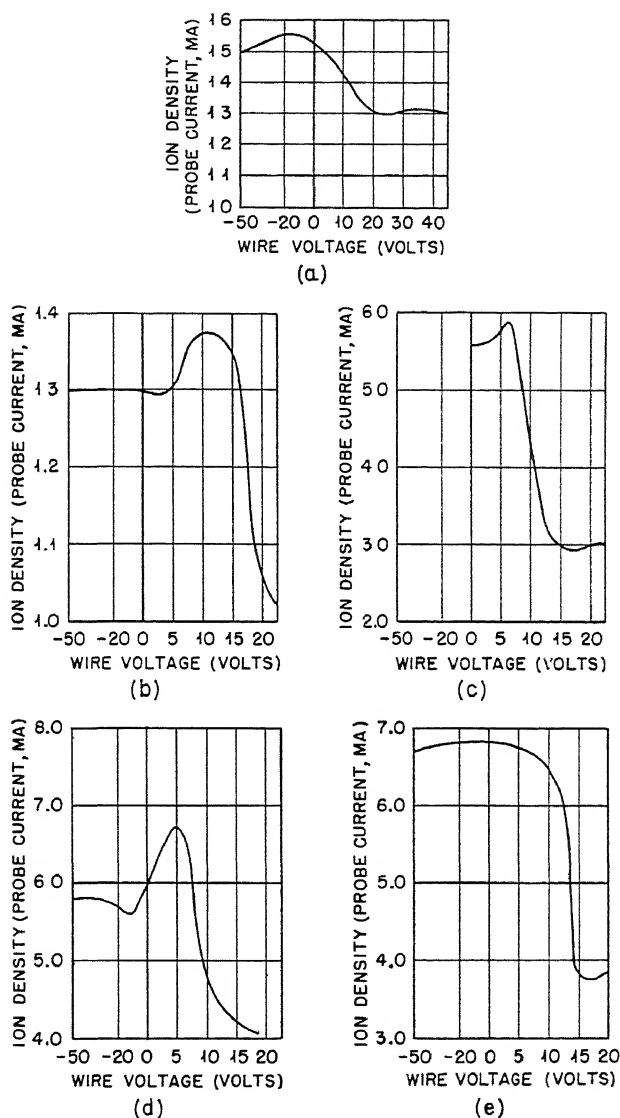


Fig. 9.134—Effect of application of potential to wire 5 across the collimating-slot plate for small arc in argon. Probe -15 volts; $x = \frac{1}{8}$ in.; $z = \frac{1}{16}$ in.; arc voltage 150 volts. (a) Pressure 0.6×10^{-3} mm Hg; magnetic field 3,700 gauss; arc current 0.5 amp. (b) Pressure 1.4×10^{-3} mm Hg; magnetic field 3,700 gauss; arc current 1.5 amp. (c) Pressure 1.4×10^{-3} mm Hg; magnetic field 3,700 gauss; arc current 0.5 amp. (d) Pressure 1.4×10^{-3} mm Hg; magnetic field 11,400 gauss; arc current 0.5 amp. (e) Pressure 1.4×10^{-3} mm Hg; magnetic field 3,700 gauss; arc voltage 300 volts; arc current 0.5 amp.

the hot probe. For each of these measurements the space potential was measured at a point in the plasma about $\frac{1}{2}$ in. directly below the wire.

Table 9.18 illustrates the results obtained for different arc conditions. It is seen that the effect of applying positive potential is to

Table 9.18

(Pressure 1.4×10^{-3} mm Hg; arc voltage 150 volts)

Wire volts (relative to anode)	Space potential (relative to anode potential), volts
-----------------------------------	---

Magnetic field 11,400 gauss; arc current 0.5 amp

0	+8.0
4.2	+7.0
6.8	+7.5
50	+14.0

Magnetic field 3,700 gauss; arc current 0.5 amp

0	+5.5
2	+5.5
8	+4.5
100	+8.0

Magnetic field 3,700 gauss; arc current 1 amp

0	+4.0
1.6	+3.5
15.5	+7.0
50	+8.0

produce a small rise in space potential in the plasma. The application of a potential of 50 volts positive on a wire relative to the anode produces a rise in the potential of the plasma of 4 or 5 volts.

A similar result was observed in measurements in which the space potential was determined by a cold-probe method. Figure 9.135 shows the space potential measured along the x axis at three different heights below wire 5, to which potential was applied. Figure 9.135a shows the space potential as a function of x when a potential of +20 volts was applied to the wire relative to the anode, and Fig. 9.135b shows the space potential when no wire potential was applied. It is seen that the effect of the application of wire potential was to raise the potential of the whole of the plasma by a few volts.

(c) Effect of Wire Potential on Hash. Some experiments were made to determine to what extent application of potential to one of probe

wires 1 to 6 affected the quality and quantity of the hash on the arc current. Detailed investigation was limited to only one set of arc conditions, namely, pressure 8×10^{-4} mm Hg, magnetic field 3,700 gauss, arc voltage 150 volts, arc current 0.5 amp, and small arc in argon.

The effects observed when voltage was applied to wire 3 (the closest to the arc column, see Fig. 9.3) are illustrated in Fig. 9.136. The

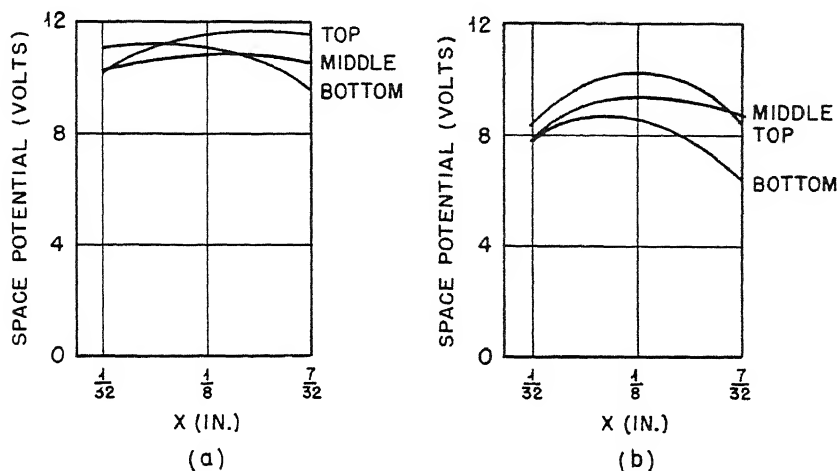


Fig. 9.135—Effect of wire voltage on space potential measured at three heights. (a) +20 volts on wire 5; $y = 0$. (b) 0 volts on wire 5; $y = 0$.

most striking result is the sudden increase in amplitude of the medium frequency (200 to 300 kc) when the wire is at a positive potential with respect to the anode of a little more than 8 volts, i.e., when the wire is at space potential. This increase persists over a range of about 20 volts, after which the amplitude settles down to a nearly steady value. Negative wire potentials have less violent effects but lead to a gradual increase in amplitude of both the relaxation and medium-frequency hash. It is noteworthy also that positive wire potential did not increase the amplitude of the relaxation oscillations.

Similar effects were found by applying potentials to the other wires, but the sharpness of the maximum in the amplitude of the medium-frequency hash when the wire is nearly at space potential becomes rapidly blurred as wires farther from the arc column are employed.

It was observed, in general, that the application of small positive potentials (a few volts) to probes within the arc gave rise to very hashy electron collection currents. On the other hand, the collection

of positive ions by small negative potentials was often nearly hash-free. However, larger negative potentials (some hundred of volts) were observed to lead in many cases to hashy conditions. The results illustrated are essentially similar, though here the hash was observed

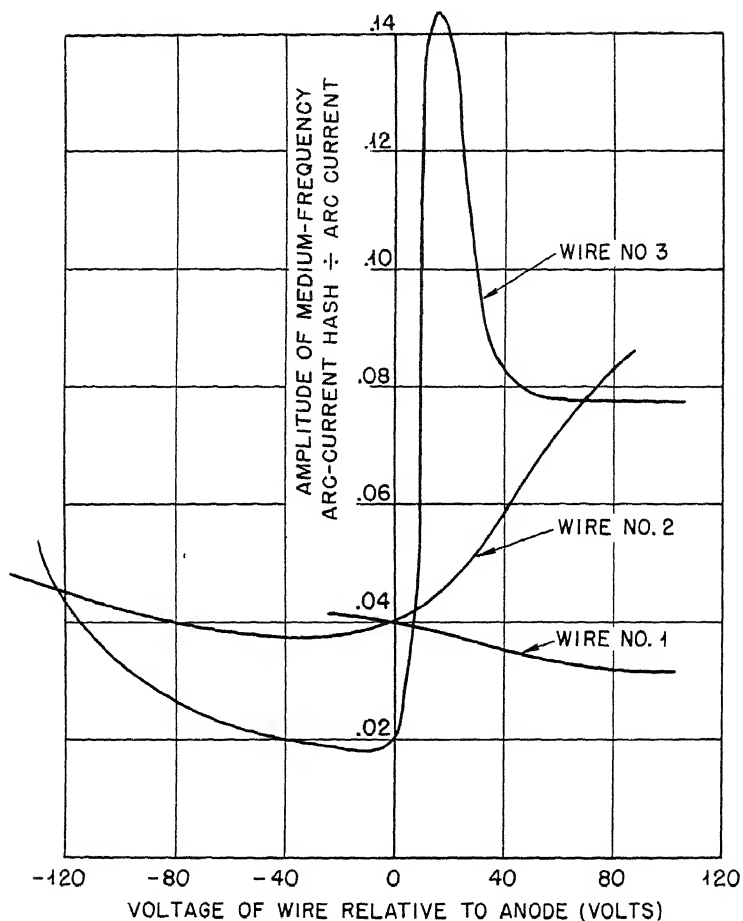


Fig. 9.136—Effect of applying voltage to wires on medium-frequency arc-current hash for small arc in argon. Pressure 5.6×10^{-4} mm Hg; magnetic field 3,700 gauss; arc voltage 150 volts; arc current 0.5 amp.

on the arc current. The increase in the effects at the innermost wire suggests that the application of small positive potentials to the anode might have considerable influence on the arc current hash, but no observations of this kind were made.

ACKNOWLEDGMENTS

The help and cooperation of the following persons made this work possible: Dr. J. Backus, who allowed the authors, in making their first measurements, to use his experimental setup in the 184-in. Annex; J. Morris and D. Stanley, who rendered technical assistance that enabled the whole program to be carried through smoothly in a very short time; Dr. L. Aller, W. D. Berkey, and Dr. J. D. Craggs, who assisted in making some of the observations; W. Baker and Dr. A. Anderson, who developed the single-sweep-oscilloscope circuit used in the hash observations; Phyllis Johnson and Mrs. Jane Jones, who analyzed the great number of probe characteristics; Mrs. Jane Jones and Mrs. J. Crittenden, who prepared the diagrams.

Chapter 10

DISCHARGE CATHODES

By William E. Parkins

This chapter describes experiments in which an attempt was made to use electrons produced in a gas discharge as a means of ionizing a vapor in a region other than that in which the discharge took place.

1. PROCESSES AVAILABLE

It is known that unlimited electron currents can be "piped" around by a suitable combination of electric and magnetic fields. This indicates that, if electrons might be produced in one of any number of special ways, they might be brought out and fed into the arcs to provide the ionizing mechanism.

Means of producing electrons are for the most part simpler than means of producing ions. Possible processes for electron production are as follows:

1. Secondary electrons from electron bombardment.
2. Secondary electrons from ion bombardment.
3. Photoelectric emission.
4. Photoionization.
5. Field emission.
6. Thermionic emission.
7. Ionization by electrons.
8. Ionization by ions.

Means of transporting the electrons may be divided into the three following classifications:

a. For \vec{E} parallel to \vec{H} , the electrons travel in the direction of $-\vec{E}$. (This scheme is especially valuable for dumping the electrons at their point of use.)

b. For \vec{E} perpendicular to \vec{H} , the electrons describe cycloids in the direction of $\vec{E} \times \vec{H}$.

been present to only a slight extent in the previously described type. The output electrons had an energy distribution indicating that almost

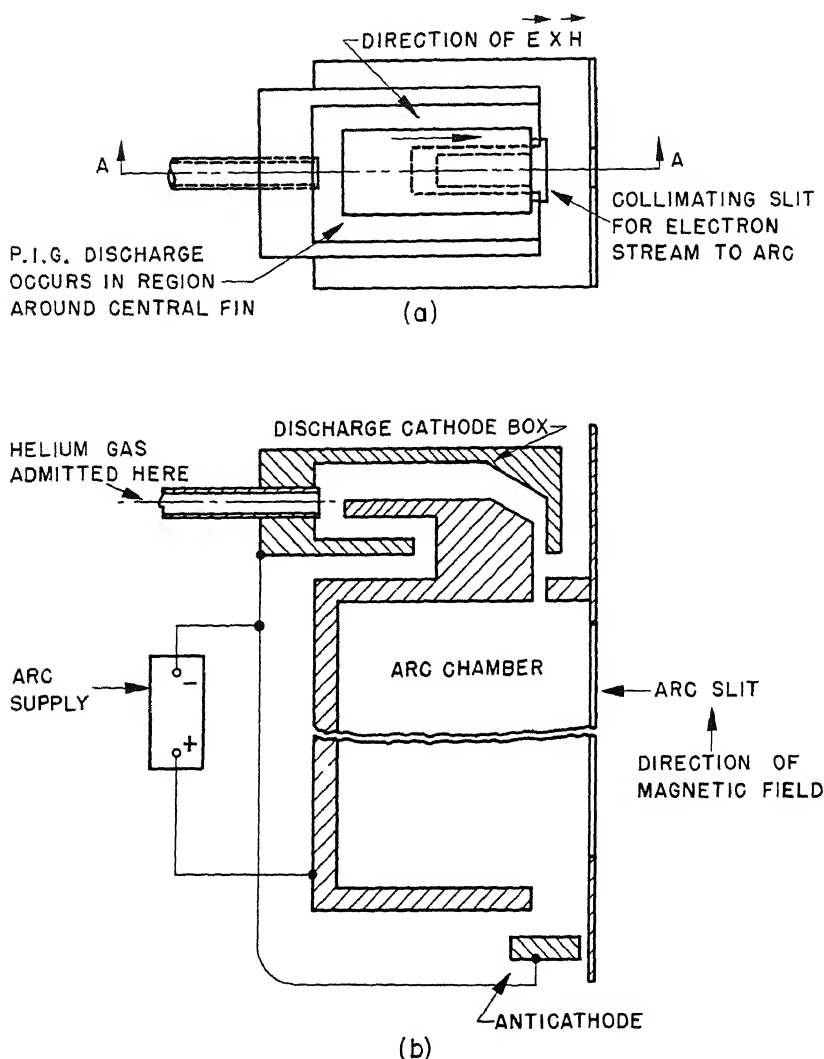


Fig. 10.1 — First discharge-type cathode and accompanying arc. (a) Top view with lid of box removed. (b) Vertical section through A-A of discharge cathode and arc chamber.

all of them were apparently produced in the plasma. Since it was questionable if the potential of the plasma of this electron source could ever be divorced from the potential of the plasma in the arc,

there was reason to doubt that such electrons could ever be effective ionizers in the final arc. It may have been that an appreciable fraction of the electrons to the collector were not produced in the plasma, but in this event their energy was reduced before they worked their way to the center where they could be used.

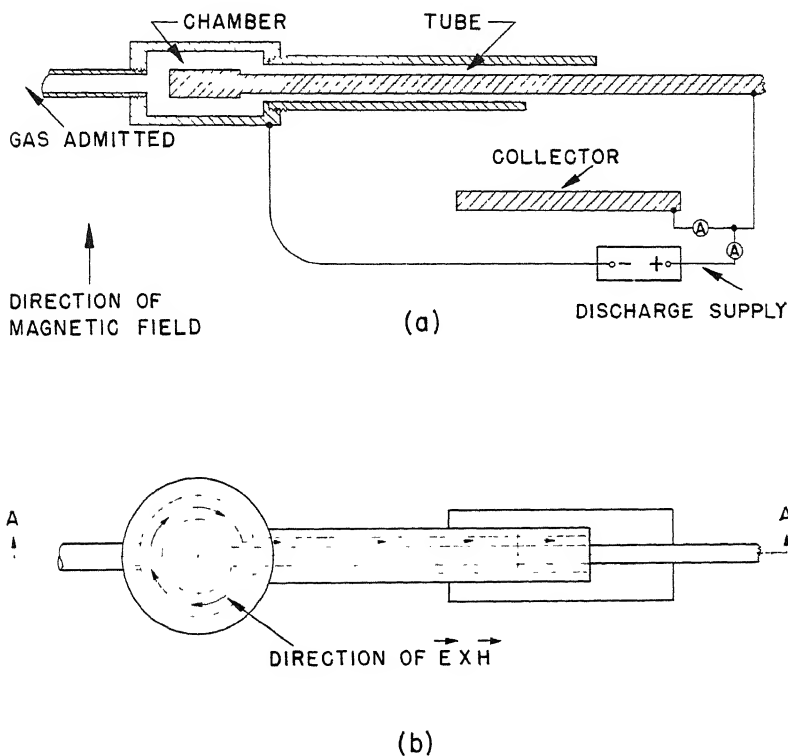


Fig. 10.2—Modified P.I.G.-discharge-type cathode. Electrons are produced in chamber, transported along tube, and dumped on collector. (a) Vertical section through A-A of P.I.G. discharge chamber and transport tube. (b) Top view.

This general method may be used to produce a high electron current of low-energy electrons. The electrons may be brought out into a lower-pressure region by the addition of a guide as shown in Fig. 10.4. Here the rod, guide, and collector may be run at the same positive potential, and the electron current will still arrive predominantly at the collector. It is interesting that the potential of the plasma apparently is controlled by the potential of the electrode receiving the electron current. If more than one electrode is drawing

the electrons and these electrodes are at different potentials, the plasma tends to assume some intermediate potential.

By a suitable change in the geometry of the electrodes, it was possible to operate in a similar manner, but the electrons were forced to drift outward instead of inward to reach the channel where they were removed.

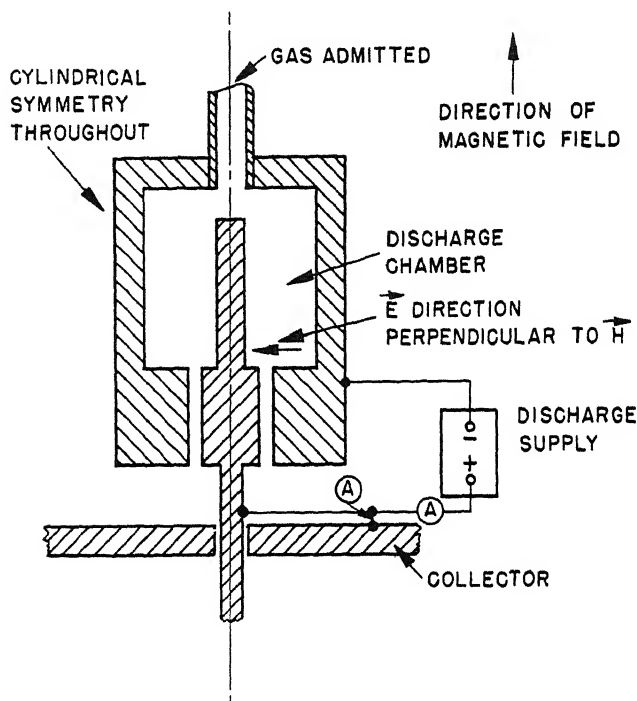


Fig. 10.3—Vertical section of P.I.G.-discharge-type chamber and collector in which electrons are transported by methods (c) and (a). Electrons dump out of slot onto collector.

1.3 Transport in the Direction of $-\vec{E}$ and Parallel to \vec{H} . Neither of the types described appeared promising, mainly because the process of transporting the electrons either lost a large fraction of them or reduced their energy to a low value. Another arrangement suggested itself and appeared to have qualities overcoming these disadvantages. Here method (a) was the only one required for the transport of electrons, but still their production made use of a P.I.G.-type discharge in a region of high pressure. The essential features of this type of discharge cathode are shown in combination with the ion-source arc chamber in Fig. 10.5.

The operation was intended as follows: Gas would be introduced at the top of a slotlike cavity, creating a relatively high pressure in this region. A high rate of ionization here would assure a large ion current flowing into the cavity walls. These ions would liberate some

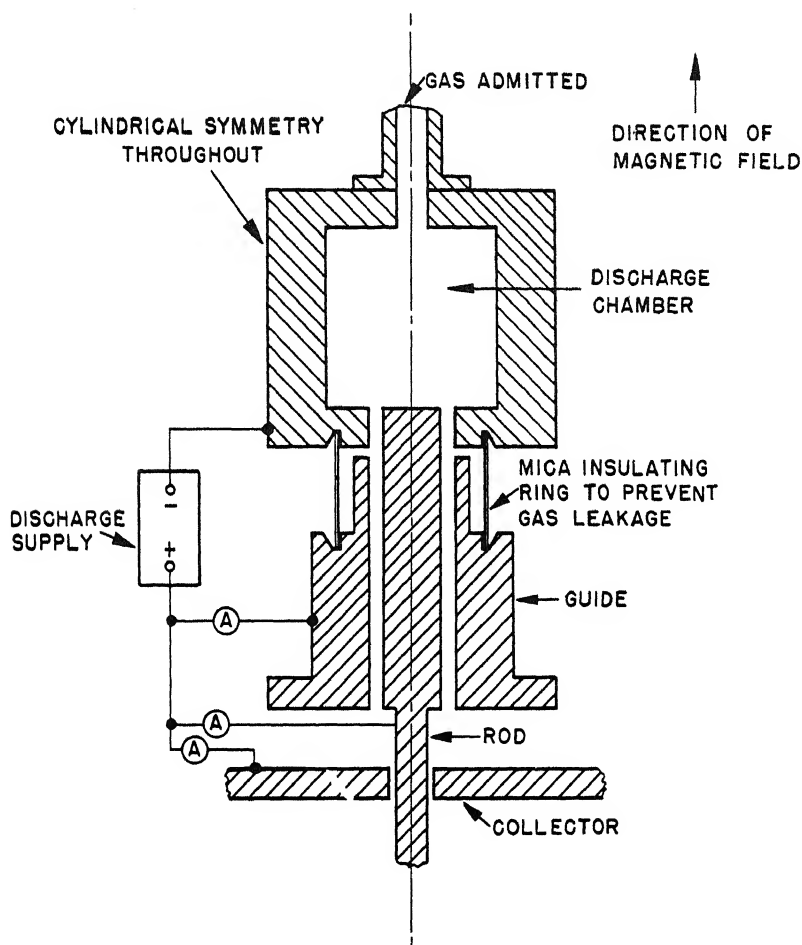


Fig. 10.4—Vertical section of discharge cathode with long channel to reduce gas flow.

electrons that would be immediately free to spiral down into the arc of the ion source. Such electrons would enter the arc with essentially full arc voltage, although only a small component of their momentum might be in the direction of the magnetic field. Few if any electrons would pass directly to the anticathode (maintained at the same potential as the cavity walls) but would be forced to oscillate along the

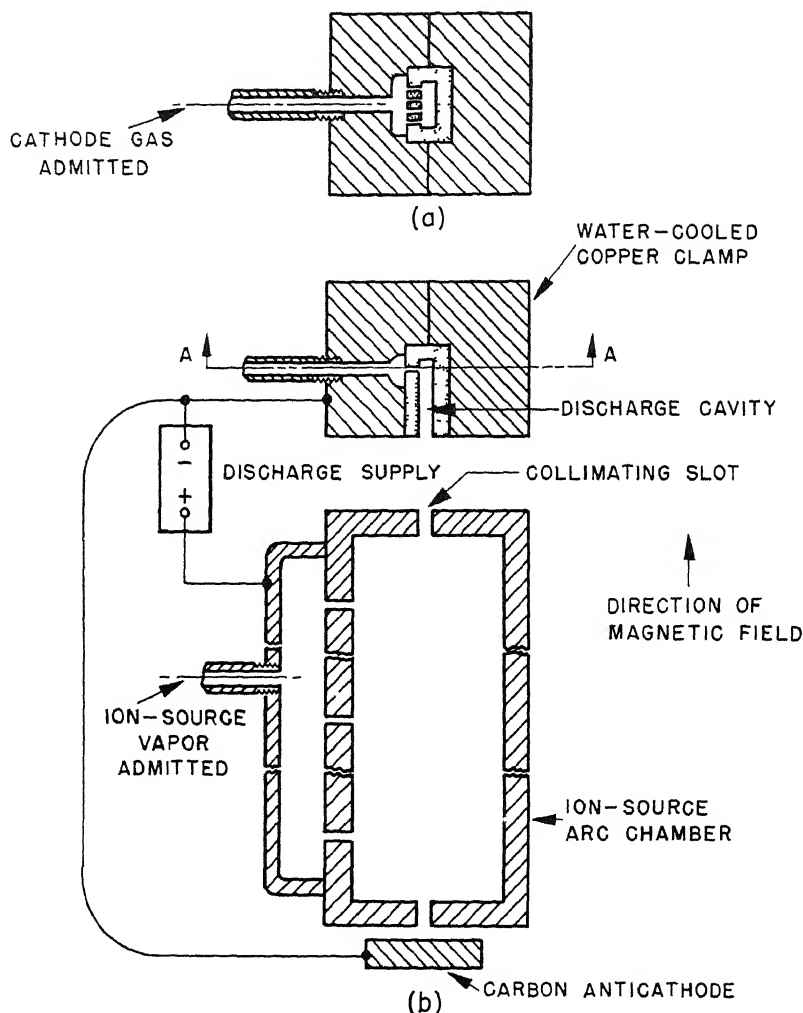


Fig. 10.5—P.I.G.-discharge-type cathode in which electrons are transported by method (a) only. (a) Horizontal section (at A-A) through center of cathode gas line. (b) Vertical section through center of cathode gas line.

magnetic-field lines until they could work their way to the walls of the arc chamber, which was to be maintained positive.

A program was pursued to determine the effects of certain refinements, including the following:

1. Use of oxygen as the cathode gas to assure an oxide coating on the cavity walls and thereby obtain a high γ (number of electrons released per incoming ion).

2. Choice of cavity material to obtain a high γ and slow sputtering rate.

3. Depth and thickness of cavity to decrease the flow of cathode gas required.

4. Use of iron in the neighborhood of the cavity to curve the magnetic-field lines there.

5. Use of cavity wall geometry, which would increase surface area or improve the ease with which electrons might escape.

To find γ the true power input to the cavity was measured by noting the change in temperature of the cooling water. This would indicate the ion current flowing to the cavity, since it was known that the plasma would assume essentially the potential of the anode. Since the total electron current was indicated by the arc-current meter, and the electron current emitted from the cathode was necessarily the total electron current minus the ion current flowing to cathode, γ could be obtained from the following formula:

$$\gamma = \frac{IV}{W_c} - 1$$

where IV is the total electrical power input, and W_c is the power absorbed by the cathode-cooling water. This formula neglects several small effects, one of them being the ion current flowing to the anti-cathode.

2. EXPERIMENTAL RESULTS ON CAVITY-TYPE DISCHARGE CATHODE

Some seventy experimental runs were made, using different cavity materials and shapes. Pure elements, certain alloys, and sintered mixtures of metals and refractory oxides were among the various materials tested. The results can be summarized briefly. Some materials, such as aluminum, beryllium, and magnesium, gave phenomenally high γ values, as high as 10 being measured in several instances. An oxide coating on the inside of the cavity, which was usually automatically provided by using oxygen for the cathode gas, invariably improved operation of the discharge and increased the γ value. The γ value increased almost linearly with voltage on the discharge, the latter being varied by changing the gas pressure. The majority of materials operated most steadily in the neighborhood of 300 to 500 volts and gave γ values varying from 0.2 to 0.6. Materials such as aluminum, beryllium, and magnesium could easily be made to operate at potentials as low as 100 volts. In all cases the discharge

could be struck by application of only a few hundred volts, provided sufficient cathode gas was flowing.

The electrons seemed to experience no difficulty in escaping from the cavity surfaces. This was inferred from the fact that no variation in the angle of tilt of the cavity surface or in the bending of the magnetic-field lines in the vicinity seemed to assure an improvement in operation.

A cavity thickness of as little as $\frac{1}{32}$ in. would work, but for steadiness and uniformity of discharge two or three times this value was much better.

In choosing a material, the sputtering rate did not seem to vary greatly and was considered a less decisive factor than certain others. Unfortunately the materials giving high γ values were unsteady in operation and seldom gave an arc of uniform intensity across its width. Beryllium and magnesium were especially bad in this respect. Also their operation was accompanied by a continual shower of small incandescent particles from the cavity walls. The explanation for this phenomenon as well as the probable explanation of the high γ values observed for the oxides of many materials was found in the work of Guntherschulze.¹

In operating a glow discharge Guntherschulze noticed that flakes of oxide particles on the surface of the cathode emitted streams of electrons. He showed further that these currents arose from a type of field emission wherein the field was set up across the oxide particles. Positive ions arriving at the cathode frequently deposited on the oxide flakes, and these flakes, being good insulators, effectively provided a strong electric field at the surface of the conducting cathode. Furthermore, if the electrical conductivity of the cathode material was sufficiently high, current concentrated so heavily in oxide particles of certain dimensions as to cause electrical breakdown in them. This process usually resulted in the particles attaining incandescence and shooting away from the cathode surface.

Inside the discharge-cathode cavity there is opportunity for similar action. The oxide surfaces probably gave high γ values as a result of the field built up across the oxide layer. Certainly no measured probabilities of electron emission upon ion bombardment at these energies have approached the better γ values found* for the oxide-coated cavities. Also in the case of beryllium and magnesium cavities, the

*Reference should be made to the recent work on this subject by Healea and Houtermans.²

conditions described above must have been present, leading to the breakdown and expulsion of oxide particles.

The cavity-type discharge cathode proved to be the most satisfactory of all those studied from the standpoint of ion production in the arc. A cavity of $\frac{3}{32}$ by $\frac{5}{8}$ in. cross section and 1 in. deep could provide the arc with amperes of energetic electrons, apparently released

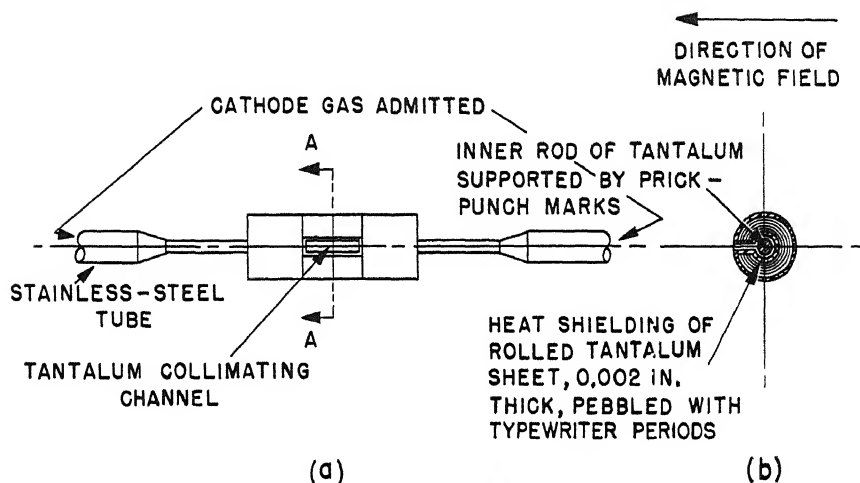


Fig. 10.6—One type of automatically heated thermionic cathode. (a) Cathode as viewed from arc collimating slot. (b) Vertical section at A-A.

from the cold cavity walls. Arc conditions could be altered by changing the vapor pressure in the arc chamber and by varying the cathode gas flow. After striking the discharge, the cathode gas flow was always reduced, but the amount of gas required to maintain the discharge was never so small as to remove objection to the cathode on this score.

3. AUTOMATICALLY HEATED THERMIONIC CATHODES

Before discontinuing experimental work along these lines an attempt was made to develop a cathode consisting of a well-heat-shielded bar of tantalum that could be kept at thermionic-emission temperatures by the ion bombardment it received. The discharge was to be started by the admission of cathode gas, but this flow was to be reduced greatly or entirely shut off when the tantalum bar was sufficiently heated. One of the more satisfactory designs is shown in

Fig. 10.6. Although these cathodes could be operated in the method described, the main difficulty lay in the fact that little control of the cathode temperature was possible. Operation of the arcs required almost continual adjustment for best results. Also an increased lifetime for this type of cathode appeared questionable.

REFERENCES

1. A. Guntherschulze, Z. Physik, 86: 778, 821 (1933).
2. M. Healea and C. Houtermans, Phys. Rev., 58: 608 (1940).

Chapter 11

THEORY AND OPERATION OF A PHILIPS IONIZATION GAUGE TYPE DISCHARGE

By John Backus

1. INTRODUCTION

The term "hash" has been used to refer to electrical fluctuations in an arc. It is applied to any time variation of the electrical properties of the arc not controlled by the regulator. A great amount of work has resulted in no real understanding of the nature of hash, as the experimental evidence obtained by probes, voltages on electrodes in the arc, etc., is chaotic and frequently contradictory. A more fundamental approach to the nature of hash involves accumulating more knowledge of the behavior of the plasma in a strong magnetic field.

The plasma in the absence of a magnetic field has been studied by Langmuir and others, and a fairly satisfactory steady-state theory developed. Until now very little has been done on a nonstatic theory of the plasma. The existence of plasma oscillations of frequency determined by the plasma density can be demonstrated theoretically, but the extent to which these oscillations exist has not been determined experimentally. It is obvious that the presence of a magnetic field will drastically alter the state of the plasma since the electron mobility perpendicular to the magnetic field is greatly reduced. An additional constraint is thus put on the plasma by the magnetic field, and therefore the steady-state solution of the continuity equations governing the plasma state in the absence of the magnetic field will not, in general, be applicable. This new constraint imposed implies that a new variable must be introduced into the equations, and the one new variable available is time. If this theory is accepted, it would be expected that the plasma in a magnetic field will not exist in a steady condition, but that the potentials, plasma densities, etc., will vary

with the time. This time variation can obviously be of great importance in defining the plasma state; all experiments should therefore be considered with this point of view in mind.

2. THE PHILIPS IONIZATION GAUGE DISCHARGE

One approach to the problem is the study of a plasma that can definitely not be steady. Such a plasma is furnished by the Philips Ionization Gauge (P.I.G.) discharge. A simple arrangement for getting this discharge is shown in Fig. 11.1. Two cathodes, K and K, are opposite

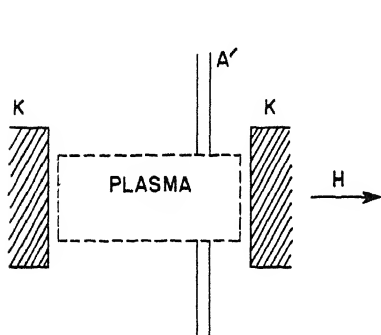


Fig. 11.1

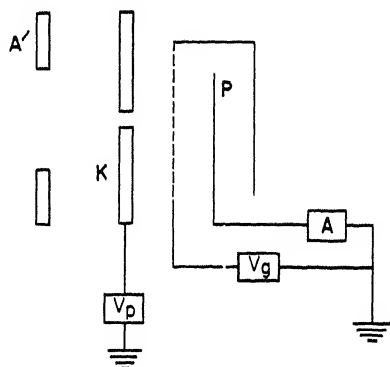


Fig. 11.2

Fig. 11.1—Arrangement producing a P.I.G. discharge.

Fig. 11.2—Arrangement of apparatus for measuring numbers of secondary electrons at the cathode.

a circular hole in a conducting metal sheet A' , which serves as the anode. A cylindrical tube with its axis along the magnetic field can be used in place of the flat sheet if desired. The direction of the magnetic field is shown by the arrow. If the anode A' is grounded and a negative voltage of a few hundred to a few thousand volts put on the cathodes, a discharge is produced which takes the form of a cylindrical column of plasma defined by the hole in the anode A' , the sides of the column following the direction of the magnetic field. The density of this plasma as well as the voltage-current characteristic of the discharge varies with the gas pressure. At a pressure of 10^{-4} mm Hg the discharge will be relatively weak; at a pressure in the neighborhood of 2×10^{-3} mm Hg it can be very strong. Ions produced in the column are accelerated to the cathodes, where they produce secondary electrons. These secondaries are accelerated back into the column,

and since their motion perpendicular to the column is restricted by the magnetic field they oscillate back and forth and produce more ions.

The existence of a continuous discharge produced in this way requires that the electrons escape as fast as they are produced; hence they must move to the anode across the magnetic field. It can be shown that, at these pressures, collisions of the electrons with neutral molecules would give a diffusion velocity across the field smaller than that observed by a factor of 1,000. Therefore another mechanism must be responsible for moving the electrons across the field. The existence of random electric fields in the plasma can produce such a motion of the electrons across the magnetic field, the electrons draining perpendicularly to both the electric and magnetic fields. It will be shown that quite reasonable electric fields can produce the required electron velocities across the magnetic field.

The column of plasma obtained as described above is quite steady and accessible for observation. Unfortunately the presence of probes disturbs the discharge considerably. For example, a 10-mil wire pushed a short distance into the discharge can put it out. Consequently the ordinary probe methods of determining ion density, electron temperatures, etc., are inapplicable. The method used here is more in the nature of a sampling method, whereby ions and electrons are drawn out of the discharge without disturbing it.

2.1 Secondary Electrons at the Cathode. One of the first points of interest is the production of the secondary electrons at the cathode by the positive ions. Measurement of the actual number of secondaries produced by air ions striking copper was made with the apparatus shown schematically in Fig. 11.2. The current to the plate P is plotted as a function of the voltages on the grid and on the plate. The curves can be analyzed to obtain the positive-ion current to the plate, the secondary electron current from the plate, and the secondary electron current produced by the positive ions bombarding the hole in the cathode K. The results are not too consistent, varying with the nature of the surface, the length of time it is bombarded, etc. Measurements taken with different magnetic fields and varying pressures show that there is no dependence of secondary emission on these variables. The number of secondaries produced per ion plotted as a function of ion voltage is shown in Fig. 11.3. The scatter of the points shows the variable nature of the secondary emission. The assumption is made here that the ions bombard the cathode with an energy equal to the voltage across the P.I.G.; this assumption will be justified later. In this experiment other gases were not tried, but since the P.I.G. be-

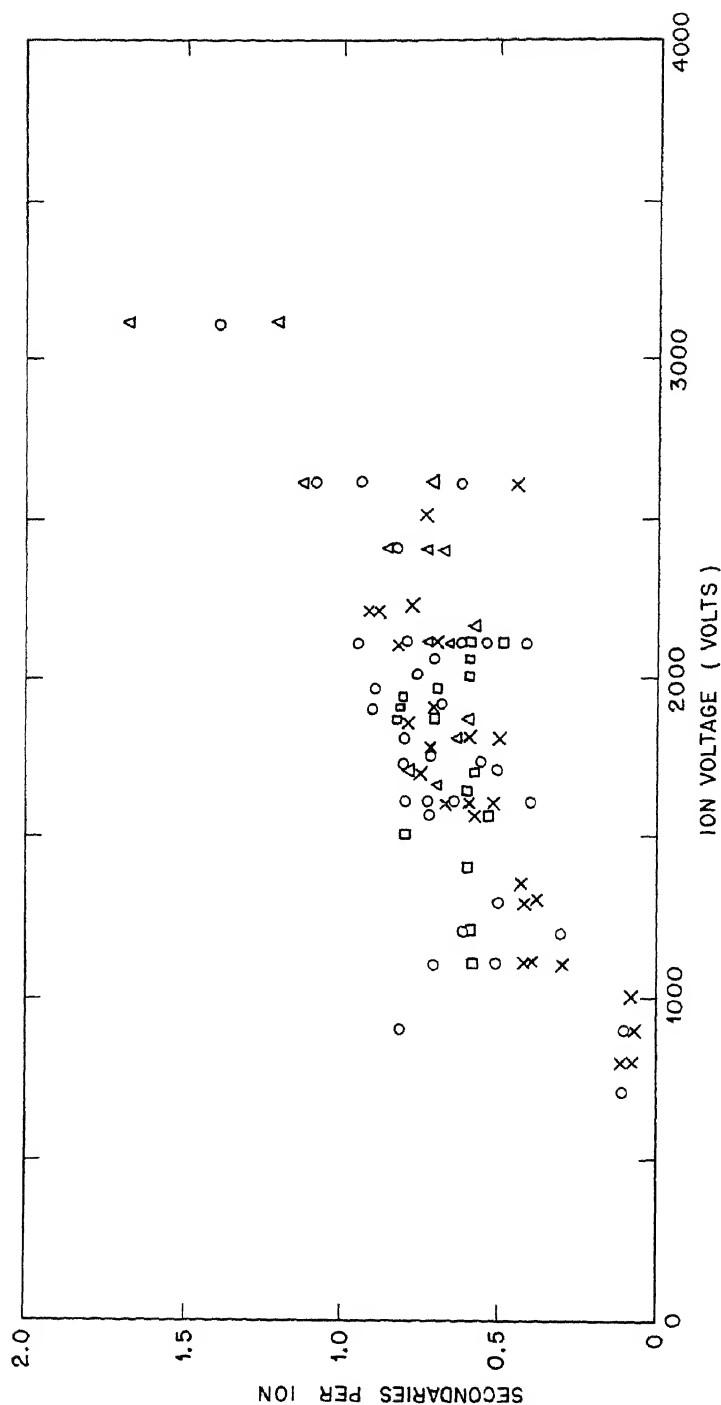


Fig. 11.3—Number of secondaries produced per ion plotted as a function of ion voltage. Cu cathode-air discharge. x represents 4,000-gauss field, o represents 2,000-gauss field, □ represents 1,000-gauss field; △ represents 500-gauss field.

haves rather similarly for different gases the secondary emission would not be expected to show great variation.

Of more interest is the effective number of secondaries produced at the cathodes. Some secondaries may move across to the opposite cathode and escape without producing ions. Also there may be some photoemission of electrons from the cathode, so that the actual number of secondaries per ion as obtained above is not the pertinent number. This effective number is obtained by measuring the wattage absorbed by the cathode, which is done by the usual method of cooling the cathode with water and measuring the water flow and temperature rise. The heating of the cathode is due to the positive-ion current i_+ striking it. The power dissipated will then be the product of this current times the P.I.G. voltage (again making the assumption that the positive-ion voltage equals P.I.G. voltage). The total watts put into the discharge is the product of the P.I.G. current times the P.I.G. voltage, and consequently the ratio of the positive-ion current to the P.I.G. current equals the ratio of the measured power to the cathode to the total power input. The P.I.G. current is equal to the sum of the positive-ion current i_+ to the cathode and the secondary electron current i_- flowing from it, and therefore the secondary electron current can be determined. One set of measurements with argon ions on copper gave a ratio i_-/i_+ in the range 0.15 to 0.2 for V in the vicinity of 1,800 to 2,000 volts and with a P.I.G. current of the order of 20 ma. Another set with a P.I.G. current of the order of 0.5 amp and the same voltage gave a ratio i_-/i_+ in the range 0.25 to 0.4. As mentioned previously, the P.I.G. behaves about the same with other common gases, and therefore the number of secondaries per ion should be similar. The experiments show that, in general, about three-fourths of the P.I.G. current is due to positive ions striking the cathode. Incidentally, a high P.I.G. current of the order of 1 amp/sq cm, which can be obtained, means that more ions than neutral molecules are striking the cathode.

2.2 Passage of Electrons through the Plasma. Experiments were tried to determine the effect of the plasma on electrons passing through it. A tungsten filament k (Fig. 11.4) is mounted opposite a small hole in one of the P.I.G. cathodes, and a grid g , consisting of a hole in a molybdenum sheet, is used to accelerate the electrons from the filament through the hole in the cathode. Another hole is drilled in the opposite cathode. Behind it is a decelerating grid G and a shielded plate P . Now if the filament is made about 200 volts negative and positive voltage is put on the accelerating grid, electrons will pass through the hole in the one cathode, traverse the discharge, pass

through the hole in the opposite cathode, go through the decelerating grid, and finally strike the plate. The current of electrons to the plate can be plotted as a function of the voltage applied to the decelerating grid. If this grid is more than 200 volts negative, no electrons can get to the plate. This plate-current variation with grid voltage is plotted with the discharge on and with the discharge off.

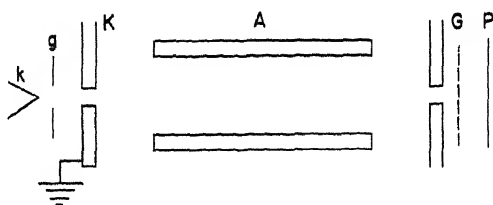


Fig. 11.4—Arrangement of apparatus for determining effect of plasma on electrons passing through it.

The results of this experiment show that the electron-energy distribution is altered by the presence of the discharge. A typical case is shown in Fig. 11.5. The curve of electron distribution with the discharge on is slightly less steep than the curve for the discharge off, indicating that the electrons have a slightly greater energy spread after passing through the P.I.G. plasma. In this particular experiment the discharge was weak, of the order of 10 ma of P.I.G. current, and consequently the effect is small.

This experiment was repeated using an ordinary hot-cathode arc run in argon, where much higher current densities could be obtained. A $\frac{1}{32}$ -in. hole was drilled in the anode directly opposite the hot cathode, and a shielded plate was placed behind it. The arc plasma projects through this hole, and electrons from the plasma strike the plate. The electron current as a function of the plate voltage can then be plotted. Now if the electrons from the cathode are unaffected by the presence of the plasma, two groups of electrons would be expected, one group consisting of electrons from the cathode and having an energy about equal to the arc voltage, and the other group consisting of plasma electrons having a few volts energy. (The anode is grounded, and the arc voltage applied to the cathode.) The actual characteristic obtained is shown in Fig. 11.6, which gives the electron current to the plate as a function of the plate voltage for a current density to the anode of about 1 amp/sq cm and arc voltages of 70 and 150 volts. The sharp drop of the curve around zero voltage is due

to the fact that low-voltage plasma electrons are repelled as the plate is made negative. The electrons from the cathode do not form a definite group, however. If they did, the characteristics in Fig. 11.6 would show a sharp drop at the points indicated by the arrows on the curves. Furthermore, some electrons reach the plate when it is more negative than the cathode even by as much as 50 volts. For example, on

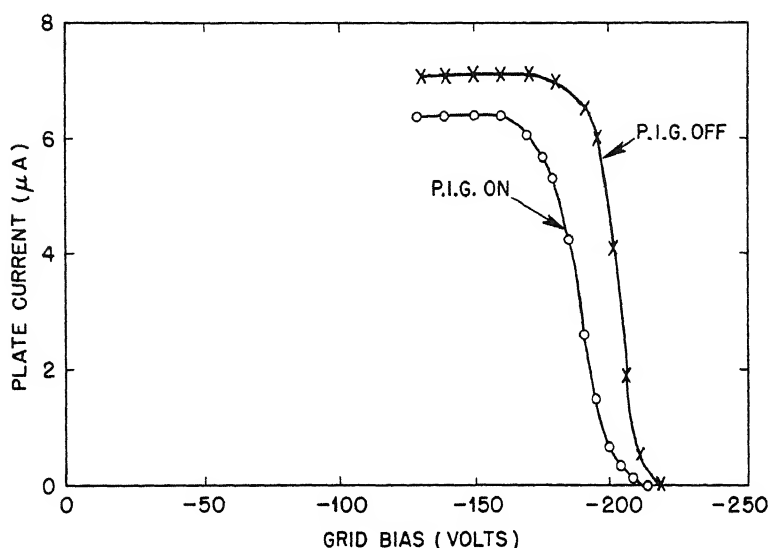


Fig. 11.5—Effect of discharge on distribution of electron energy. P.I.G. voltage 2,500 volts; current 10 ma; electron acceleration voltage 200 volts.

the 70-volt curve some electrons strike the plate when it is 120 volts negative. This means that a number of electrons from the cathode have gained energy in passing through the plasma. The dip below the axis on the 150-volt curve is due to secondary electrons produced at the plate; this region is not very reproducible, indicating probably that the character of the surface is changing. The negative values at high negative plate voltage are due to the positive-ion current from the plasma.

The distinguishing feature of these curves is the great energy spread of the cathode electrons. Some curves show no separation between cathode electrons and plasma electrons. The other feature is, as mentioned above, the presence of electrons of energy greater than the arc voltage. A theory being developed by Bohm (see Chap. 1) explains this spread in energy by the presence of plasma oscillations.

If a wave is traveling through the plasma at about the same speed as an electron from the cathode, this electron can gain or lose a considerable amount of energy; consequently the presence of plasma oscillations can result in the speeding up of some of the electrons. The theory indicates that the electrons from the cathode should excite

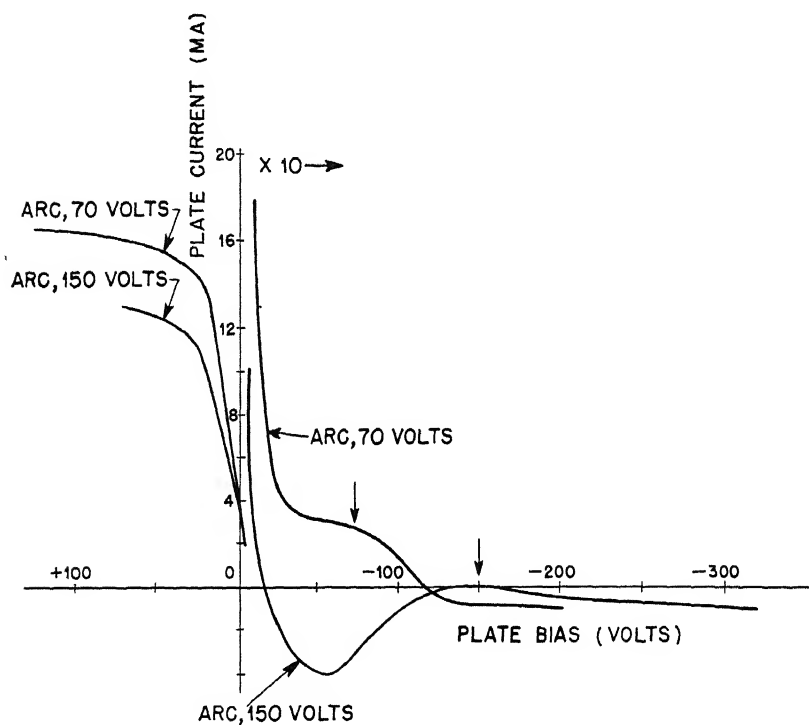


Fig. 11.6—Electron current to the plate as a function of plate voltage for arc in argon. Pressure, $40\ \mu\text{a}$; arc current, 0.5 amp. The ordinates to the right of the current axis are multiplied by 10.

these plasma waves; this results in a general spread in the energy of the electrons as they pass through the plasma. The experiment described is thus another bit of evidence that the plasma is not in a steady state.

2.3 The Energy Distribution of the Positive Ions in the Discharge. Positive ions in the discharge were studied by means of the arrangement shown schematically in Fig. 11.7. The discharge runs between the cathodes to the grounded anodes A' , which consist of coaxial holes in two copper sheets. The discharge is surrounded by a cylinder A ,

whose potential is variable by means of a power supply. Opposite a small hole in one cathode are a grid G and a plate P. The grid is biased about 90 volts negative with respect to the plate to stop emission of secondary electrons from the plate. Suppose now that A is grounded and that a discharge is run at, say, 1,500 volts. If P is negative with respect to the plasma and more than 100 volts positive with respect to the cathode, the current to it will be the sum of the

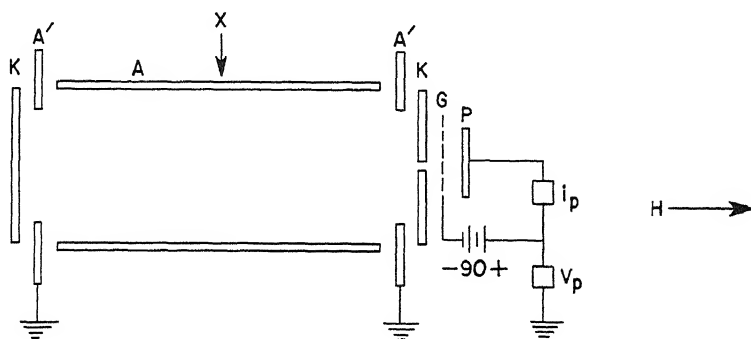


Fig. 11.7—Schematic arrangement to permit study of positive ions in the discharge.

positive-ion current from the plasma and the secondary-electron current produced by positive ions striking the sides of the hole. This electron current to the plate will be independent of the voltage of the plate as long as it is more than 100 volts positive. It is found that for the plate voltage negative the current to it is constant; as the voltage is reduced and approaches zero, the current drops and reverses sign. This indicates that the positive ions are being repelled from the plate as its potential approaches that of the anode. This drop takes place over a region of the order of 50 volts, and therefore the assumption previously made, namely, that the ions strike the cathode with an energy approximately equal to the P.I.G. voltage, is valid.

The exact form of the curves of plate current vs. voltage is quite interesting. Figure 11.8 is a typical example. Positive voltages on the plate with respect to the grounded anode give a saturation negative current; this current, as mentioned previously, is due to secondary electrons produced by positive-ion bombardment of the sides of the hole in the cathode. If the plate is made more than 100 volts negative with respect to the anode, a saturation positive-ion current is produced. Assume now that the plasma has a constant potential equal to zero and is emitting ions that have a temperature T . For a nega-

tive plate potential all ions will be collected. As the potential is made positive, slower ions will be repelled, and the current will drop. The form of curve to be expected under these conditions is shown by the dashed curve in Fig. 11.8, drawn for an ion temperature of 15 volts. We see that the actual curve differs in two respects: it lies on the

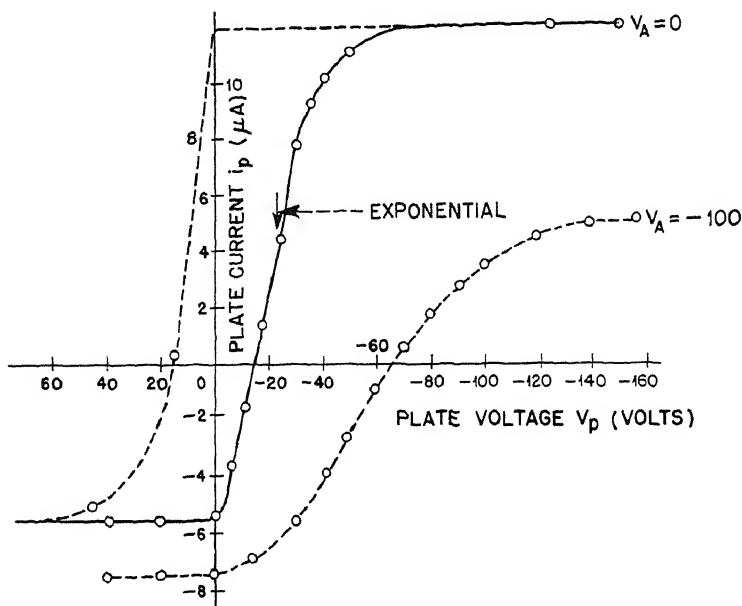


Fig. 11.8—Plate current vs. voltage, using the apparatus shown in Fig. 11.7.

wrong side of the current axis and has the opposite curvature. There exists no sudden break in the curve corresponding to a definite plasma potential. The curve actually obtained can be explained on the assumption that ions of negligible energy come from a region whose potential changes with time, being always negative. In fact, if the curve is subtracted from the dotted extrapolation shown and the differences are plotted on a semilogarithmic scale, they lie on a reasonably straight line over a good part of the curve, and therefore it may be said that the probability of finding at a particular instant a potential V at the point at which the ions are emitted is given by $V = ke^{-V/V_0}$, this being valid over the region of the curve indicated in Fig. 11.8. This fluctuation in potential would necessarily result in a fluctuation of the ion current passing through the hole in the cathode. This is corroborated by observing the ion current on an oscilloscope.

The current is not steady but comes in more or less random pulses of a frequency in the neighborhood of 50 to 250 kc. On the flat part of the curve the saturation ion current is actually the average of pulses whose amplitude may be 30 per cent of the d-c value.

The potential of the cylinder A is variable, as mentioned before, and we can study the distribution of the currents to the cylinder A, the cathodes K, and the anodes A' as the potential of the cylinder is

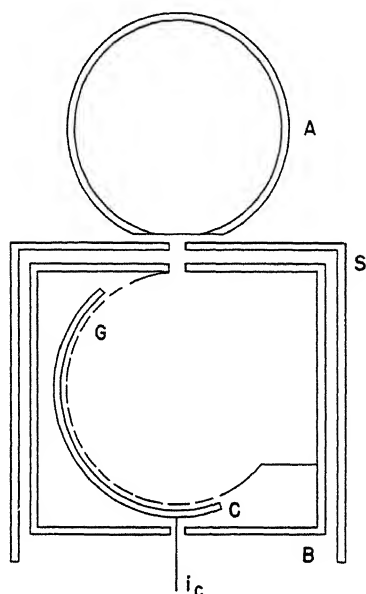


Fig. 11.9—Section through apparatus for investigating ions coming out of plasma perpendicular to the magnetic field.

varied. In particular the effect of this potential on the curve of Fig. 11.8 can be seen. If the cylinder is made positive the curve moves bodily to more positive plate voltages, its amplitude changing somewhat but not its shape. The break that shows at zero, Fig. 11.8, moves toward the left by exactly the positive voltage put on the cylinder. This is an illustration of the general principle observed before, that the plasma potential is determined by the most positive electrode in the vicinity of the plasma. If, on the other hand, the cylinder is made negative, the break at zero remains at zero but the whole curve flattens out, as shown in Fig. 11.8 by the dotted curve taken for cylinder voltage of -100 volts. This alteration in shape indicates larger fluctuations in the plasma potential for negative voltages on the cylinder.

Ions coming out of the plasma perpendicular to the magnetic field were investigated by the arrangement shown in Fig. 11.9, which shows a cross section through the apparatus at the point X in Fig. 11.7. A $\frac{1}{32}$ -by $\frac{3}{8}$ -in. slot is cut into the cylinder A. A $\frac{1}{16}$ -by $\frac{1}{2}$ -in. slot lies opposite it in the accelerating electrode S, which serves as a shield

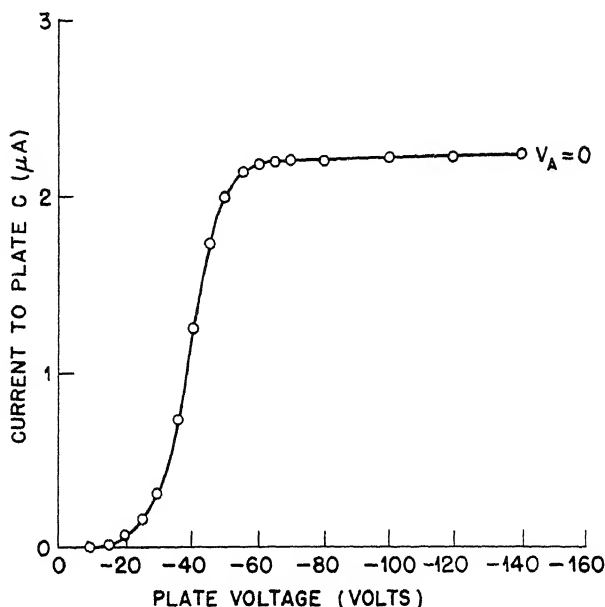


Fig. 11.10—Typical curve obtained with apparatus of Fig. 11.9.

for the box B, which also has in it a $\frac{1}{16}$ -by $\frac{1}{2}$ -in. slot as shown. A circular grid G in the box is arranged as shown so that ions from the slit will pass through it perpendicularly, regardless of their velocities and angle of entrance, and strike the plate C. Ions from the discharge will thus pass through the cylinder slit, be accelerated by the electrode S, and enter the box B with an energy given approximately by the voltage in the box. They will then move in circles in the field-free region inside the box, pass through the grid, and strike the plate. Their energy distribution can then be studied by observing the collector current as a function of the collector voltage.

Figure 11.10 shows the type of curve obtained with this apparatus. It differs from the curve of the cathode ions shown in Fig. 11.8 in having no negative part, since no secondary electrons can get to the plate; also the foot of the curve rises less abruptly from the voltage

axis than the curve of Fig. 11.8. In other respects it has similar properties. The top half of the curve has the same exponential character as the cathode ion-energy curve of Fig. 11.8, and positive-ion current is collected only with negative collector voltages. It has the additional property that the rise from the voltage axis is roughly exponential. This indicates that ions having a rather definite temperature are coming from a region whose potential is changing in time.

One significant feature of this curve is that apparently no ions can go to the cylinder A when it is grounded. All ions seemingly come from a region whose potential is negative with respect to ground. This is evidently impossible for a plasma containing electrons. The electrodes at the ends of the plasma are grounded, and, if the plasma is negative with respect to these ends, electrons can escape freely along the magnetic field, leaving an excess number of positive ions and thus bringing the potential back to a slightly positive value. This anomaly will be explained later.

The ion-distribution curve of Fig. 11.10 behaves similarly to that of Fig. 11.8 when the potential on the cylinder A is changed. If the cylinder is positive, the curve moves toward positive collector voltages by the amount that the cylinder is made positive. If the cylinder is made negative, the curve flattens in a similar manner to the cathode ion-energy curve. If the collector current is viewed on an oscilloscope, it shows the same random fluctuations as the cathode ion current.

The curves of cylinder current, anode current, and P.I.G. voltage as functions of the cylinder voltage are plotted on Fig. 11.11. The cathode current is kept constant, 8 ma for Fig. 11.11. Consider first the cylinder current. When the cylinder is positive it becomes the anode for the discharge and collects saturation electron current. At zero voltage it is collecting apparently zero current. Actually it is collecting equal positive and negative current, since the oscilloscope shows pulses of current when the d-c value is zero. For negative voltages the cylinder collects ions and shows no definite saturation as the voltage is increased. The curve for the anode current runs almost exactly parallel to that for the cylinder, being displaced from it by an amount equal to the P.I.G. current. For positive cylinder voltages the anodes collect a small positive-ion current. Since the cylinder is positive, the plasma is made positive by the same amount, and the anodes act as probes, repelling most electrons and collecting positive ions.

Consider the anode-current curve in more detail. When the cylinder is positive the anodes are collecting positive ions and some fast elec-

trons from the cathode. For a P.I.G. current of 8 ma the largest fast-electron current that will go to the anodes will be about 2 ma, as judged from the data taken on secondary emission. Since from the curve the net anode current is 1 ma, about 3 ma of positive ions are actually moving to the anodes. As the cylinder voltage approaches

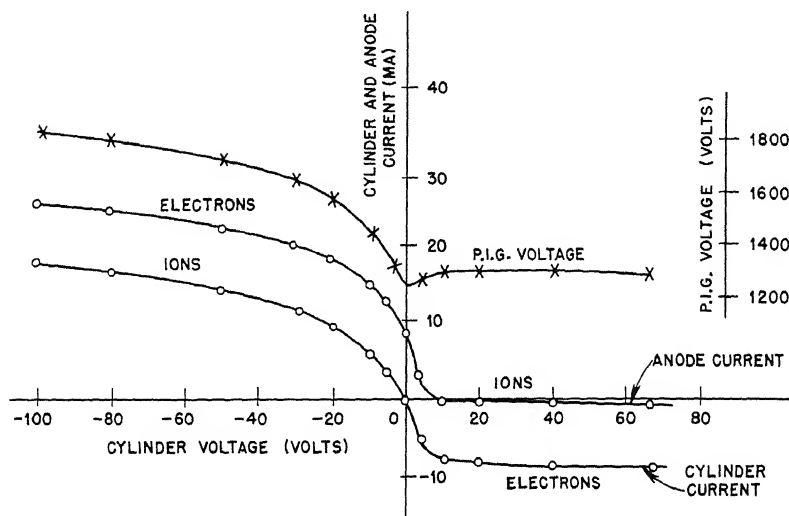


Fig. 11.11—Curves of cylinder current, anode current, and P.I.G. voltage as functions of the cylinder voltage. Cathode current, 8 ma.

zero the anode current rises to 8 ma, of which, then, at least 6 ma must be slow electrons from the plasma. Evidently, then, the rise in the cylinder current must be due to at least 6 ma of positive ions going to the cylinder, and therefore it does collect positive ions when grounded. At first sight this is incompatible with the ion curve shown in Fig. 11.10, which indicates that all ions have a negative energy with respect to the cylinder. This rise in cylinder current could perhaps be due to photoelectric emission from the cylinder. A separate experiment in which the cylinder was surrounded by a screen shows that this is not so; hence the rise in current must be due to positive ions.

To explain the curves of ion-energy distribution at the cylinder and the cathode it is thus necessary to assume that the ions come from a region whose potential fluctuates in time. Since electrons can now move freely along the magnetic field, it would be expected that there can be no very large potential difference between points along the

magnetic field, and therefore fluctuations in the potential at the two ends of the discharge should be to some extent in phase. An experiment to test this was tried. The grid-and-plate arrangement of Fig. 11.7 was used at both cathodes. One cathode was made movable in order that the holes in the cathodes could be put either in line along the magnetic field or out of line. The two plates were connected to the horizontal and vertical sweeps of an oscilloscope having identical amplifiers for each sweep. It was found that, when the two holes were in line along the magnetic field, the randomly fluctuating ion currents to the two plates were very nearly in phase, the pattern on the scope screen being a diagonal ellipse with a major axis some five to ten times the length of the minor axis. Viewed on a single-sweep oscilloscope, it was seen that the lower-frequency components were in phase, whereas the higher-frequency components were more random. As the holes were moved out of line this phase relation disappeared. In one experiment, for example, when the holes were out of line $\frac{1}{8}$ in., the ellipse on the scope widened to give a major axis only twice the minor axis; for $\frac{3}{8}$ in. out of line the phase relations were completely random. Hence the fluctuation in the ion current does not take place over the whole cross section of the discharge but it is quite localized in area perpendicular to the magnetic field. Parallel to the magnetic field the fluctuations in ion currents are about one order of magnitude less.

Using the simple discharge geometry shown in Fig. 11.1, the region outside the main plasma was studied with the probe shown in cross section in Fig. 11.12. Two tungsten wires $\frac{3}{4}$ in. apart projected $\frac{1}{16}$ in. from a grounded shield; this probe could be moved in and out of the discharge as well as rotated. The two wires were connected to the two sweeps of the oscilloscope. Outside the main column of discharge indicated by the dotted line in Fig. 11.1 the probe picks up current showing the same random fluctuations observed in ion currents previously mentioned. The currents to the two probe wires are in phase when the wires are lined up along the magnetic field; the phase relations are random when the probe is rotated 90 deg. Hence it is found that a plasma exists outside the main discharge and has the same type of fluctuations as those in the main discharge. The electrons in this plasma do not have enough energy to produce excitation in the neutral gas, and therefore this plasma is not visible.

Further experiments were performed with a hot-filament probe. An 8-mil tungsten wire was bent in the shape of a small hairpin and arranged to project about $\frac{1}{8}$ in. from a shield. This probe could be moved about in the discharge. The filament is heated to emitting temperatures. Its potential is variable, and the emission current is

observed on the oscilloscope. The filament will emit electrons when it is more negative than the surrounding region. With this arrangement it was found that the filament did not emit when more than 3 to 5 volts positive with respect to the grounded anodes. At these positive

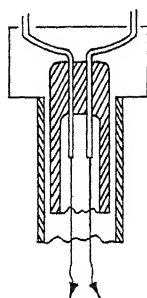


Fig. 11.12

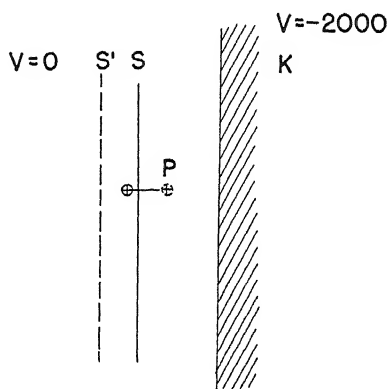


Fig. 11.13

Fig. 11.12—Probe for studying region outside the main plasma.

Fig. 11.13—Section of ion sheath at the cathode.

voltages it collected an electron current that showed the same random fluctuations previously observed in the positive-ion currents and was independent of whether the filament was off or on. If the filament was reduced in voltage below about +4 volts it emitted electrons in pulses of the same random character, the pulses being of the same kind but of greater amplitude than the pulses of the positive-ion current observed with the filament turned off. The potential at which the filament shows no emission pulses is the most positive value of the fluctuating potential of the surrounding plasma. It has a rather well-defined value in the neighborhood of +4 volts, which varies slightly with discharge conditions but is quite independent of the position of the probe outside the main discharge column. The filament cannot be pushed very far into the discharge without greatly disturbing it; however, it can project into the discharge about $\frac{1}{32}$ in. without upsetting it too much, and in this position it is found that the most positive space potential is about -2 volts. The discharge was next surrounded by a cylinder spaced everywhere about $\frac{1}{2}$ in. away from the discharge, with the tungsten filament projecting through a small opening in the cylinder. The potential on the cylinder could be varied. It was found

that, if the cylinder was made more positive than -4 volts, the most positive space potential rose so as to be always approximately equal to the cylinder potential. If the cylinder is made more negative than this value, the most positive space potential remains unchanged for any voltage to -300 volts and for all distances from the discharge, even to within 1 mm of the cylinder wall. This is surprising, since it can be calculated from the cylinder voltage and current that the positive-ion sheath should be much thicker than 1 mm; consequently it would be expected that the space potential very near the cylinder would always be negative. If the filament is made somewhat negative, say -20 volts, the emission from it consists of pulses superimposed on a direct current, i.e., the modulation is not 100 per cent. The pattern on a single-sweep oscilloscope consists of pulses of more irregular amplitudes than the currents, their amplitude being perhaps 30 per cent of the d-c value. If now the cylinder is made negative, say -50 volts, the scope pattern shows occasional longer spikes in a direction to indicate that the electron emission is momentarily interrupted; the more negative the potential on the cylinder, the greater the number of those spikes. This effect shows at distances from the cylinder several times the calculated sheath thickness. Evidently the electric field from the negatively charged cylinder at times penetrates considerable distances toward the main discharge.

3. CHARACTER OF THE P.I.G. HASH

The picture that emerges from the foregoing discussion is thus the following: Ions from the discharge fall through the potential difference across the P.I.G. and strike the cathode, liberating secondary electrons. These fall through the same potential difference, gaining energy, and produce more ions and slow electrons. By some mechanism yet to be explained, the high-speed electrons from the cathode give up energy to the plasma, building up fluctuations in plasma density and potential. Owing to the mobility of the electrons along the magnetic field, these fluctuations are two dimensional, the density and potential varying for the most part in directions perpendicular to the magnetic field. The electric fields set up are hence perpendicular to the magnetic field, and the electrons in the plasma will move across the field with the drain velocity, permitting the electrons (both fast and slow) to move to the anode and escape from the discharge. Ions in the plasma will acquire a few volts of energy from the same random electric fields, getting a sort of temperature in directions perpendicular to the magnetic field. Space-charge conditions at the

edge of the main discharge prevent the ions from escaping at will from the column, so there must be a potential barrier at the edge of the column to reflect most of the ions back into the discharge. The ions will therefore bounce back and forth in the column. Occasionally there will be collisions with neutral molecules, which will transfer some of the transverse temperature into motion along the magnetic field; consequently ions will have a certain lower temperature in the direction of the magnetic field and will escape to the cathodes. This temperature will necessarily be higher than the temperature of the neutral gas, and therefore with a discharge of high density there may be more ions than neutral molecules striking the cathode. At times a considerable number of ions may be directed toward the same point (or rather, line) on the boundary. The accumulation of positive ions in this region will raise the potential enough to prevent slow electrons from escaping along the magnetic field to the anode. A column of plasma containing ions and slow electrons will then detach itself from the main column and move away from it in some direction. As before, the escape of ions from the sides of this column will be governed by space-charge conditions, and there will be a potential barrier at the sides to hold the ions in this column. Its interior will be a few volts positive with respect to the anode at the ends. Ions can thus wander down the length of the column and escape to the anode. As they escape, the potential of the column is lowered, and electrons also are allowed to escape to the ends. The column thus disappears. As the column approaches a negative electrode, such as the cylinder described previously, space-charge conditions can then allow a considerable number of ions to escape from the sides of the column to the electrode, the electrons escaping to the ends as before. Between these columns of plasma that have detached themselves from the main discharge there may be only a very few ions, so that fields from a negative electrode can reach much farther than the simple-sheath theory would predict. Conversely, the columns themselves can be quite rich in ions, so that the potential in the near neighborhood of the negative electrode can at times be much more positive than the simple sheath theory would allow.

The anomalous nature of the curves of ion energy to the cathodes and anode can be explained on this theory. Consider Fig. 11.13, which is a small section of the ion sheath at the cathode. Assume that the plasma is at zero potential and the cathode at $-2,000$ volts. An ion approaches the sheath, which at this particular instant is at the point S, and begins to fall to the cathode. In a short time the ion will move to some point P, which might be at, say, -50 volts with respect to the plasma, with the sheath at position S. Suppose at this instant a sudden

fluctuation in the ion density of the plasma moves the sheath to a new position S' ; the potential at the point P will then be lower, say -70 volts, while the ion at P has 50 volts energy. If the sheath now stays at S' until the ion moves to the cathode, the ion will arrive with 20 volts less than the 2,000-volt drop. This argument works both ways,

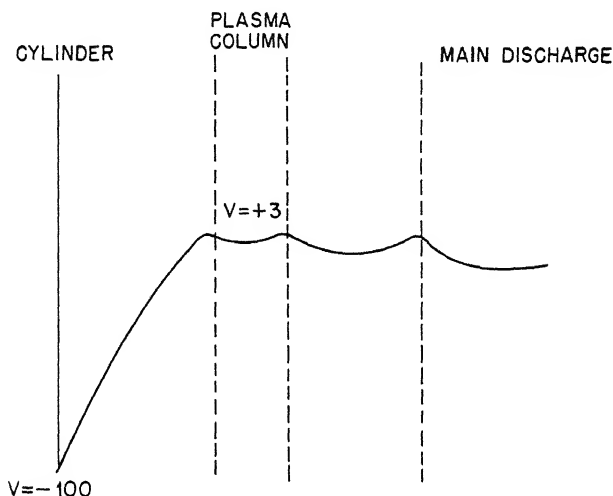


Fig. 11.14—Curve showing potential distribution across cylinder, plasma column, and main discharge.

of course. An ion can gain more energy than the total drop. The point to be brought out is that an ion going from a region at zero potential to an electrode at potential $-V$ does not necessarily have V volts energy when it arrives.

A similar situation exists for ions going to the cylinder around the discharge. Figure 11.14 is a cross section through the cylinder and the discharge with a detached plasma column somewhere in between. With the cylinder at -100 volts the momentary potential distribution might be as shown by the solid line. Suppose an ion with enough energy to get over the potential barrier starts toward the cylinder. If the potential remains steady the ion will arrive at the cylinder with 103 volts energy. However, the column is disappearing by losing ions at the ends, and therefore by the time that the ion has gone a little way toward the cylinder the column has diminished in size. By the argument given in the preceding paragraph the ion will arrive at the cylinder with less than 103 volts. This effect works only in one direction, since in the region between the discharge and the cylinder the

columns are always disappearing. If the cylinder is grounded it will be seen that ions can still reach it; the fluctuations in time of the potential distribution can reduce the energy gained by an ion in reaching a given electrode but cannot prevent it from getting there. The qualitative picture described above makes the curves discussed previously consistent with one another.

Some orders of magnitude are of interest. Suppose a P.I.G. discharge is run in argon at 350 ma and 1,600 volts, on cathodes $\frac{3}{4}$ in. in diameter. Allowing for secondaries produced at the cathodes, there will be about 150 ma of ions to each cathode, or 50 ma/sq cm. At 1,600 volts the ion density at the cathode will then be about 4×10^{10} per cubic centimeter. In the plasma, assume that the ions have about 1 volt energy along the magnetic field. The ion density will then be $\sqrt{1,600}$ times as large as the density at the cathode, or about 2×10^{12} per cubic centimeter. Electrons to the amount of 350 ma must then migrate across the magnetic field to the boundary, which might have an area in a typical case of 60 sq cm; consequently there must be an electron-current density of about 6 ma/sq cm from the plasma of density 2×10^{12} electrons per cubic centimeter. This requires an electron velocity across the magnetic field of 2×10^8 cm/sec. The drift velocity across the magnetic field is $10^8 E/H$, where E is in volts per centimeter and H is in gauss. Assuming $H = 1,000$ gauss, $E = 20$ volts/cm is found to be the order of magnitude of the random electric field necessary to move the electrons at the required rate across the magnetic field. This is a quite reasonable value. Suppose this field fluctuates at a frequency of the order of 50 kc; this is in reasonable accord with the oscilloscope observations. An argon ion in an electric field of 20 volts/cm oscillating at this frequency will then have a maximum energy of 1 volt, which again is a reasonable value. The picture described above thus gives a fairly good qualitative outline of the mechanism of the discharge.

4. HOT-CATHODE ARC

Some of the above experiments were carried out using an argon discharge run in the ordinary way with a hot cathode. The discharge could be adjusted so that the hash on the arc current was less than 1 per cent. Under these conditions a hot-filament probe used as described previously showed emission with pulses of the same general character as previously observed with the P.I.G. discharge; however, their amplitude compared with the d-c value was much less. The two-wire probe of Fig. 11.12 showed that the hash had the same two-

dimensional property as that observed in the P.I.G. discharge, the currents in the two wires being in phase when the ions were lined up along the magnetic field. A filament mounted just inside the cylinder surrounding the discharge showed that when the cylinder was made negative a sheath was produced. It can be concluded that in the ordinary arc the hash effects are an order of magnitude less than those in the P.I.G. discharge, being more in the nature of ripples superimposed on a steady flow. The magnitude of the hash on the current collected on a small probe depended greatly on the electrode potentials, changing sometimes by a factor of 10 for a change of a few volts on the arc block.

The conclusion can be drawn that in the ordinary arc a type of hash exists which is similar to the type observed in the P.I.G. discharge, i.e., fluctuations in ion density along directions perpendicular to the magnetic field. The amplitude and frequency of this hash are determined by whatever values are necessary to remove ions and electrons from the discharge at the proper rate and depend in a way not yet understood on the electrode potentials and geometric form.

5. TESTS OF MATERIALS FOR P.I.G. CATHODES

An investigation has been made of different cathode materials in P.I.G.-type arcs. Two outstanding features of this P.I.G. discharge are the high arc voltage required and the rapid wear of the cathodes. It was decided to make tests of various materials, hoping to find a material that would give a discharge at low voltage and minimum wear.

The apparatus used for the first tests is shown diagrammatically in Fig. 11.15. The material to be tested is mounted in the form of $1\frac{1}{2}$ -in. disks in holders facing holes in a copper box that serves as anode. The cathodes were 6 in. apart and $\frac{1}{8}$ in. from the surface of the box. Application of the proper voltage to the two cathodes produces a column of discharge defined by the holes in the anode box. Two such units mounted on the same faceplate were used, so that two materials could be tested under identical conditions.

The type of characteristic curve for the discharge with this geometrical form is shown in Fig. 11.16, the voltage across the P.I.G. being plotted as a function of current. The length of the curved portion and height of the flat portion of the characteristic is a function of the cathode material. Various materials were run for 1 hr at 0.5 amp current in a gas pressure of $10\ \mu\text{a}$ in argon, and the characteristic curves were taken and the amount of wear measured. The accom-

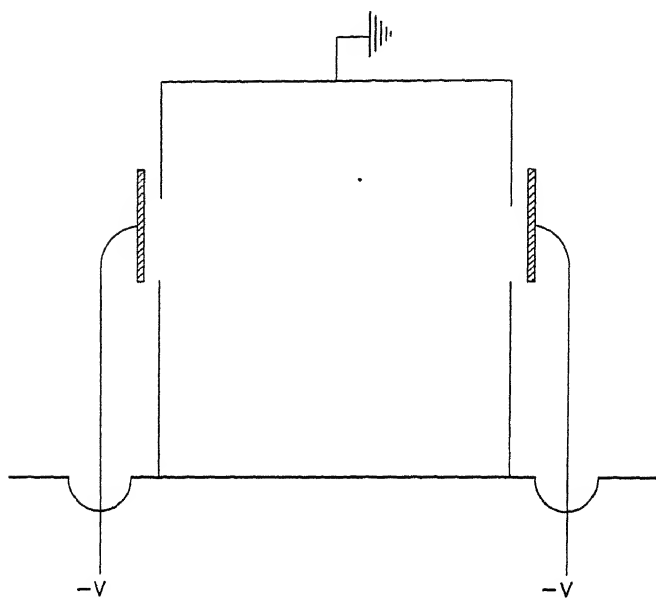


Fig. 11.15—Schematic representation of apparatus for testing P.I.G. cathodes.

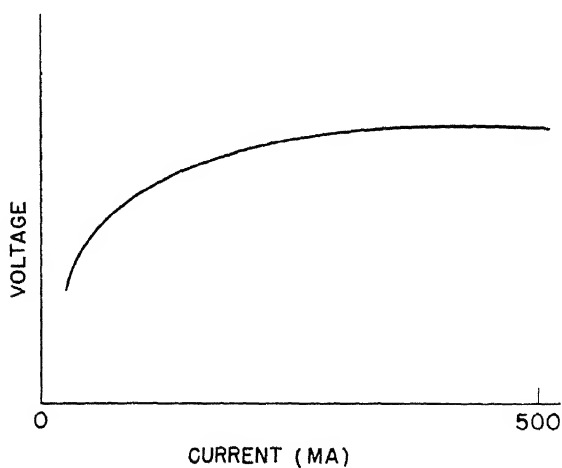


Fig. 11.16—Characteristic curve for discharge with apparatus of Fig. 11.15.

panying table summarizes the results obtained. The voltage given is that corresponding to the flat portion of the characteristic, and the wear is given in mils where it could be measured.

Material	Voltage, volts	Wear, mils
Ni	3,600	5
Zn	3,600	
Cu + 3% Be	3,600	5
Brass	2,800	9
Monel	2,800	
Cu	2,300	11
C (graphite)	2,300	1
Mo	1,800	3
Al	350	0
Be	280	0

The interesting feature about this table is the low voltage required for Al and Be. This is evidently caused by a surface layer of oxide on the metal. In the case of Al, if the gas pressure is reduced, the voltage will then rise to a value sufficient to sputter off the oxide coating; when this coating has been removed the discharge at the normal pressure of argon will require 3,500 volts. Now if air is introduced instead of argon, the voltage will fall over a period of a few minutes, until the discharge is again running at a low voltage.

Further tests on Be were then made. The cathodes in this arrangement were 2 in. apart, and the anode holes $\frac{1}{2}$ in. in diameter. Beryllium cathodes were tried in various gases at various pressures. The voltage necessary to maintain a given current is not a rapidly varying function of pressure. Starting with a low pressure and raising it causes the voltage first to fall and then to rise slowly. The voltage to maintain a 1-amp discharge at 25 μ a pressure was as follows:

Gas	Volts
O ₂	350
N ₂	470
H ₂	400

In argon a 1-amp discharge could not be maintained unless the pressure was raised to over 200 μ a; the voltage required then was 600 volts.

Various sintered mixtures furnished by the Westinghouse and General Electric companies were tried as cathodes. The materials were

pressed in the form of disks of various sizes and were mounted in water-cooled copper blocks, the geometrical form being the same as before.

A sintered mixture of osmium plus 10 mole % ThO_2 gave quite promising results at the beginning. A steady discharge of 0.7 amp at 200 volts could be maintained in argon at $10\ \mu\text{a}$ pressure. At this pressure the discharge was quite uniform. As the pressure was raised the discharge began to concentrate more in the center, until at $80\ \mu\text{a}$ it was entirely concentrated in a bright line along the axis of the P.I.G. When the discharge was turned off, it could be seen that the cathodes were at a bright-red heat. On removal it was found that they had broken into numerous pieces, evidently because of thermal expansion.

Disks of fused ThS_2 were tried. Their behavior was rather erratic. This material seems to form cathode spots rather easily, so that it was difficult to get a uniform steady discharge. A steady discharge was obtained by using a high-voltage supply with sufficient ballast resistor; this cut the maximum current that could flow down to the point where the cathode spots could not be maintained. The discharge showed a negative characteristic in argon at $30\ \mu\text{a}$ pressure, 0.1 amp would flow at 750 volts; at 0.5 amp the voltage dropped to 450 volts. The cathodes ran red hot.

A sintered mixture of molybdenum plus 10 mole % ThO_2 showed the same negative characteristic in argon, the voltage required at $60\ \mu\text{a}$ pressure falling from 800 volts at 0.4 amp to 550 volts at 1.4 amp.

A mixture of graphite plus 15 mole % ThO_2 pressed into cavities in the cathodes exhibited the same behavior as the ThS_2 cathodes. The mixture formed cathode spots very easily but would run at currents of 1 amp at about 300 volts. If the steady discharge were interrupted by the appearance of a cathode spot, it would come on again at a considerably higher voltage and decrease smoothly to the low voltage in some seconds.

Two sintered mixtures of nickel plus BeO in proportions of 10 and 25 mole %, respectively, were tried and worked very poorly. To get currents of the order of 0.5 amp required pressures of over $80\ \mu\text{a}$ and voltages of over 900 volts.

The above results show quite clearly that the low-voltage discharge is a condition in which the electrons are liberated from the cathode thermionically. Positive ions bombarding the cathode will liberate secondary electrons in insufficient number at low voltages to maintain the discharge, but, if the surface of the cathode is heated sufficiently by this bombardment, it can then liberate thermionically enough electrons to maintain the discharge. This explains both the

fall in voltage after the discharge has been started and the property of the discharge to run in a narrow line down the axis of the P.I.G., the center of the cathodes running hottest. This low-voltage discharge is quite stable under the proper conditions; most of the instability is due to the formation of cathode spots, which give a very-low-voltage discharge (less than 50 volts) but are very erratic and uncontrollable.

The conclusion from the present series of experiments is that, of the materials tried, graphite is as good as any. It shows less wear than the other metals except for aluminum and beryllium, where the high secondary electron emission is evidently due to a surface coating. The ThO_2 mixtures show some promise but need more investigation.

INDEX

A

Accumulators, 292
 Adsorption, 133, 134
 Aluminum, in P.I.G. discharge, 367
 Anode, 2
 reflecting, 105
 Anticathode, 339
 Antidrain side, 182
 Arc, argon, 17-29, 111-126, 175, 182-197
 large, 201-206, 233-234, 240, 272-273, 286-291
 small, 206, 230, 237-240, 279-286
 chlorine, 206-225, 229
 small and large, 98, 175-177, 234, 242-245, 291-292
 starting conditions of, 278
 description of apparatus for studies of, 173-180
 Backus arc, 173
 large arc, 176-177
 probes, 177-179
 small arc, 174-176, 291-292
 helium, 111-126
 hot-cathode, 364-365
 nitrogen, 17-29
 Arc chamber, 13
 construction of, 26, 173
 Arc control, 292-332
 Arc current, effect of block voltage on, 318-319
 effect on n_-/n_+ , 219
 variation with pressure, magnetic field, and arc voltage, 117
 Arc meniscus, 88, 103-105
 Arc operation, Langmuir condition for, 107
 minimum pressure for, 101-103
 Arc plasma (see Plasma)
 Arc voltages, 5
 Argon, ionization cross section, 135-143
 large arc in, 233, 240, 286-291

Argon, small arc in, 206, 230, 237-240, 279-286
 threshold pressure experiment, 111-126
 Asymmetry of ion distribution, 319
 Asymmetry factor, 182
 Atoms, electronegative, 3
 metastable, 23-24
 neutral, ionization of, 4-7

B

Backus arc chamber, 173
 Berkeley magnet, 147
 Beryllium, in P.I.G. discharge, 367
 Bias, collector, 138
 Block voltage, 292-302
 effect of, on arc current, 318-319
 on asymmetry of ion distribution, 301, 319
 on current distribution in the arc, 293, 324
 on electron temperature, 302-317
 on hash, 302-317
 on ion density, 302-317
 on minimum arc starting pressure, 318-319
 on space potential, 302-317
 Born approximation, 172
 Boyle's law, 134

C

Cathode, P.I.G., materials for, 365-369
 sintered-mixture, 367-368
 thermionic, 343-344
 Cavity, 339
 Charge bottle, 130-131, 141
 Charge-exchange process, 155, 158
 Chlorine, arc in, 206-225, 229
 interpretation of effects, 215-220
 large and small, 98, 175-177, 234, 242-245, 291-292

- Coefficient, diffusion, 200
 - longitudinal, 50
 - transverse, 15, 50, 54
 - recombination, 204-205, 216
 - Coils, Helmholtz, 27
 - Collimating slot, position of, 17
 - use of, 2
 - Collision-diffusion theory, 67-68
 - Collision parameter, 35
 - Column, central, 9-10, 12
 - Coulomb scattering, 59
 - Current, anode, variation of, 226-235, 357-358
 - with arc current, 231-234
 - with arc voltage, 234-235
 - with magnetic field, 226-227
 - with pressure, 227-231
 - block, variation of, 226-235
 - with arc current, 231-234
 - with arc voltage, 234-235
 - with magnetic field, 226-227
 - with pressure, 227-231
 - collector, 136, 143
 - collimating slot, variation of, 226-235
 - with arc current, 231-234
 - with arc voltage, 234-235
 - with magnetic field, 226-227
 - with pressure, 227-231
 - cylinder, 357
 - drift, 220
 - electron, proportion to negative ion, 211-215
 - ratio to ion saturation current, 49
 - space-charge-limited, 88
 - negative ion, 211-215
 - to probe in plasma, 13
 - positive ion, interpretation, 48-49
 - random thermal, 31
 - saturation, to wires, 247-248
 - saturation block, 245-247
 - saturation negative, 242
 - saturation probe, 13, 28
 - negative, 15
 - positive, 15
 - total probe, 52-54
 - to wires at top of arc, 235-245
 - variations of, 237-245
 - large arc in argon, 240-242
 - large arc in chlorine, 242-245
 - small arc in argon, 237-240
 - Current collection, negative, 23-29
 - parallel to magnetic field, 27-28
 - Current distribution, in arc plasma, 225-248
 - effect of block voltage on, 293, 324
 - Current flow, at sheath edge, maximum, 41
 - Cycloidal motion, 4, 8, 62
- D
- Decay distance, 3, 12
 - Density ratio, negative-ion-positive-ion, 219
 - Diffusion, 11-12, 49-50, 57-66
 - by collision, 58-62, 64
 - drain, 58, 62, 201
 - electron and ion, 29, 296-302
 - transverse to fields, 62-66, 347
 - Diffusion coefficient, for electrons, 11-12, 16, 57-58, 65, 97-98, 200
 - longitudinal, 50
 - transverse, 15, 50, 54
 - Diffusion theory, with negative ions, 220-225
 - Discharge, P.I.G., 335, 345-369
 - aluminum in, 367
 - beryllium in, 367
 - hash, 361-364
 - means of obtaining, 346-347
 - Discharge cathode, cavity-type, 341-343
 - Distribution, energy, of positive ions, 352-361
 - ion density, 180-225
 - Maxwellian, 7, 14, 41, 77, 198, 265, 298
 - potential, in the arc, 96-97
 - Drain, methods of, 62-63, 96
 - oscillatory, 96-97
 - Drain diffusion, 58, 62-63, 201
 - rate of, 65
 - theory of, 68-69
 - Drain velocity, 62-63, 96, 364
 - Drift, electron, 9
- E
- Effusion, 131-132
 - Electron, cycloidal motion of, 4, 8
 - fast, 12
 - kinetic energy of, 39, 77-78
 - passage of, through a plasma, 349-352
 - photoemission of (see Emission, photoelectric)
 - plasma, 6, 9
 - primary, 2

Electron, secondary, 5, 77, 92, 110, 347, 349
 production at cathode, 349
 thermal, 251
 thermal equilibrium of, 80
 Electron collection, 30
 in magnetic field, 49-57
 Electron current, maximum from
 double sheath, 87
 primary, 6
 proportion of, 211
 saturation, 19
 Electron density, 14
 Electron diffusion, coefficient of, 15-16
 mechanism of, 57-66
 Electron drift, cause of, 8
 direction of, 9-10
 Electron Larmor radius, 3, 15, 29
 Electron mobility, 3-4, 15
 Electron production, 334
 Electron temperature, 6, 15, 31, 57, 77-78, 95, 248, 265-269
 effect of block voltage on, 302-317
 effect of magnetic field on, 266
 Electron transportation, 334-341
 Electron velocity, 96
 Electrometer tube, 147
 Electroplating, 133
 Emission, field, 342
 photoelectric, 4, 358
 secondary, 49
 thermionic, 248
 Energy, mean random, 14
 Equation, Laplace's, 33, 52
 plasma-sheath, 78
 Poisson's, 39, 81
 Saha's, 150
 Equilibrium, thermal, of electrons, 80
 Equipotential, in the arc, 96
 central, 9-11
 plasma, 188

F

Field, electric, fluctuation in plasma, 4
 static electric field in plasma, 9
 magnetic, direction of, 2
 effect, on electrons, 2
 on electron diffusion, 29
 on ion distribution, 95-101
 on plasma-balance process, 8-12
 electron collection in, 49-57
 probe characteristics in, 17-29

Field emission, 342
 Filament, 2
 electron emission of, 87
 Flopping hash, 88, 103
 Flow, hydrodynamical, of vapor, 134
 Flowmeter, 134, 143
 Fokker-Planck-Einstein method, 60

G

Gas kinetic effects, 31-34
 Gauge, McLeod, 26, 131, 134, 143, 173, 176
 Western Electric ionization, 134, 176
 Gauss's theorem, 33
 Gradients, pressure, 131-132, 139
 temperature, 131
 Graphite, in P.I.G. discharge, 368

H

Hash, 28, 50, 269-292, 345
 with a-c and d-c arc supplies, 292
 arc current, 279-283
 distribution, 285-286
 low-frequency, 283
 medium-frequency, 279, 283
 amplitude variation, 279
 frequency variation, 279
 effect of block voltage on, 302-317
 effect on probe collection, 48
 effect of wire potential on, 330-332
 measurement of, 180
 in P.I.G. discharge, 361-364
 Helium, threshold pressure experiment
 for, 111-126
 Helmholtz coils, 27

I

Intensity, ion-beam, variation of,
 147-155
 with arc current, 150
 with arc voltage, 148, 150
 Iodine, discharge in, 15
 Ion, doubly charged, 148-158
 negative, 22, 24
 behavior in chlorine arc, 216-217
 destruction of, 216
 diffusion theory with, 220-225
 positive, collection by probes, 31-49
 effects of electric fields, 34-38
 effects of space charge, 38-49
 gas kinetic effects, 31-34

- Ion, positive, energy distribution, 352-361
 - saturation current, 353
 - production of, 4-7, 92-94
 - rate, 5, 100, 166-172
 - radii of curvature, 11
- Ion beams, appearance potential of, 153, 155, 158
 - mode of formation, 160-162
 - relative intensity of, 147-148, 155-156
 - variation of intensity, 148-153
 - with arc current, 150
 - with voltage, 148, 150
- Ion density, at arc column, 96
 - distribution, 180-225
 - transverse, 182-189
 - vertical, 189, 211
 - effect of block voltage on, 302-317
 - effect of wire potential on, 324-328
 - variation of, 69-75, 191-197
 - in argon arc, 201-206
 - with arc current, 204
 - with arc voltage, 206
 - with magnetic field, 201-204
 - with pressure, 204-206
 - in chlorine arc, 206-225
 - positive, 209-211
 - transversely, 191-197, 211-215
- Ion distribution, 7
 - asymmetry of, 182-189, 301, 319
 - effect of magnetic field on, 95-101
- Ion extraction, 124
- Ion temperature, 48-49, 353
- Ionization, by plasma electrons, 93
 - potential, 5
 - rate of, 6, 94
 - by secondary electrons, 110, 274
- Ionization cross section, 127-128
 - of argon, 5
 - measurement of, 135-143
 - variation with arc voltage, 92
- Ionization gauge, Western Electric, 135

K

- Kinetic energy, of electrons, 39, 77-78
 - of ions, 8

L

- Langmuir condition for stable arc operation, 107
- Langmuir probe, 13

- Langmuir theory, 85
- Laplace's equation, 32, 52
- Larmor radius, electron, 3, 15, 29-30, 49-50, 96
 - of positive ions, 15, 49, 128
- Leeds & Northrup potentiometer, 153

M

- McLeod gauge, 26, 131, 134, 143, 173, 176
- Magnet, Annex, 17
 - Berkeley, 147
 - cyclotron, 17
- Manometer, U-tube, 134
- Materials for cathodes, 365-369
- Maxwell-Boltzmann relation, 39
- Maxwellian distribution, 7, 14, 41, 77, 198, 265, 298
- Megavac, 26
- Meniscus, arc, 103-105
- Metastable atoms, 23-24
- Modulation, 361
- Molybdenum, 18
 - in P.I.G. discharge, 368

N

- Negative glow, length of, 2
- Neutralization, space-charge, 7, 16, 199, 251, 335
- Nitrogen, arc in, 17

O

- Oscillations, in arc, 27
 - high frequency, 28
 - plasma, 11, 29-30, 64, 250-251, 278-292, 352
 - relaxation, 271-278
 - at low pressure and arc voltage, 273-278
- Oscillatory drain, 97
- Osmium, in P.I.G. discharge, 368

P

- Parameter, collision, 35, 37, 41-42
- Photoemission of electrons (see Emission, photoelectric)
- P.I.G. discharge, 335, 345-369
 - aluminum in, 367
 - beryllium in, 367
 - osmium in, 368

- Plasma, 7, 94
 - density, 2-3, 49, 53
 - diffusion theory of, 197-201
 - in presence of negative ions, 220-225
 - distribution, 11
 - of currents, 225-248
 - effect of magnetic field on, 8-12
 - electron passage through, 349-352
 - electrons, 6, 9
 - equipotentials, 188
 - ions, 4
 - oscillations, 11, 29-30, 64, 250-251, 278-292, 354
 - penetration, 14
 - stability of, 85-86
 - turbulence, 11
 - waves, 64
- Plasma-balance process, 7-8, 94-101
 - effect of magnetic field on, 95
- Plasma-sheath equation, 78
- Poisson's equation, 39, 80, 90
- Positive-ion current density, 7, 125
- Potential, appearance, 148, 153, 155, 158-159
 - block, application to control arc, 292-302
 - collector-bias, 131
 - contact, 153
 - floating, 13, 26, 249
 - ionization, 153, 160, 162
 - probe, 248
 - repulsive, 13
 - residual, 39
 - wall, 94, 297
 - wire, 324-332
- Potential distribution in the arc, 97
- Potentiometer, Leeds & Northrup, 153
- Pressure, effect on n_-/n_+ , 219
 - gradient, 131-132, 139
 - minimum, effect of arc meniscus on, 88, 103-105
 - effect of block voltage on, 318-319
 - effect of flopping hash on, 88
 - operating, 103-106
 - threshold, theory of, 107-111
- Primary column (see Column)
- Probe, cold-disk type, 26, 177
 - collection, 17
 - current-voltage characteristics, 13, 17
 - effect of strong magnetic field on, 17-29
 - processes governing, 29-30
- Probe, effect on discharge, 347
 - effective radius of, 38
 - hot-filament type, 26, 179, 359-361
 - Langmuir type, 13
 - parallel position of, 17
 - shape, effect on collection, 54-57
 - theory of, 29-31
 - types of, 17-18
 - voltage, 34
- Probe boundary, 37
- R
- Radius, electron Larmor, 3, 15, 29
 - electronic, 2
- Regulator, Foxboro constant-temperature, 129
- Reynolds numbers, 11
- S
- Saha's equation, 150
- Seal, Wilson, 132, 163
- Sheath, 7, 95
 - double, 87-92, 107
 - size of, 38-39, 91-92
 - stability of, 8, 82
- Shuffling, 5
- Space-charge-limited electron current, 88
- Space-charge neutralization, 7, 16, 199, 251, 335
- Space potential, 13, 27-28, 248-265
 - distribution, 252
 - effect of block voltage on, 302-317
 - effect of wire potential on, 328
 - measurement of, 248-251, 263
 - variation of, with arc current, 257
 - with arc voltage, 257
 - with magnetic field, 256
 - with pressure, 256
- Spectrograph, mass, 138
- Spectrometer, mass, 146
- Spectrum, mass, 163
- Steatite, 17
- Sulfur hexafluoride, threshold pressure experiment for, 111-126
- T
- Temperature, mean electron, 31
- Thermocouple, 129, 132
- Thorium oxide, in P.I.G. discharge, 368

Thorium sulfide, in P.I.G. discharge, 368
 Threshold pressure, theory of, 107-111
 variation of, 117-120
 with arc voltage, 117-118
 with magnetic field, 118
 with type of gas, 118-120
 Trajectories, electron, 167

U

Ultraviolet rays, 29
 Uranium hexafluoride, appearance potentials of, 158
 chemical-dissociation energy, 159-160
 ion-beam intensity, 155, 158
 ionization cross section, 143
 pressure measurement, 134-135
 Uranium metal, electroplating of, 133
 ionization potential of, 164-165
 Uranium tetrachloride, appearance potentials of, 153-155
 chemical-dissociation energy, 158-159
 effusion, 131-132
 ion-beam intensity, variation of, 147-153

Uranium tetrachloride, ion-beam intensity, variation of, with arc current, 150-153
 with voltage, 148-150
 ionization cross section, 135-143
 pressure measurement, 131-133

V

Vane, defining, 147
 Velocity, drain (see Drain velocity)
 Voltage, face, 319

W

Wall potential, 94, 297
 Waves, electrical sound, 278
 Wilson seal, 132, 163
 Wire potential, effect of, 324-332
 on hash, 330-332
 on ion density, 324-328
 on space potential, 328-330

Z

Z motion, 2, 8

W

3189